Submarine channelforms and fans in the Miocene Moki and Mount Messenger formations, Taranaki Basin, New Zealand

A thesis

submitted in fulfilment

of the requirements for the degree

of

Doctor of Philosophy in Earth Sciences

at

The University of Waikato

by

Erman Kamaruzaman

THE UNIVERSITY OF
WAIKATO
Te Whare Wānanga o Waikato

2024

Abstract

Taranaki Basin (New Zealand) contains a Late Cretaceous – Cenozoic sedimentary succession up to 9 kilometres thick. Neogene strata are volumetrically a significant part of the basin fill. During the late-Middle Miocene a new sediment source, arising from the onset of uplift and erosion of the Southern Alps mountain belt, supplied the basin with copious sediment, continuing to the Recent. This resulted in the development of a northwestward prograding shelf-slope wedge within the basin. The Moki and Mount Messenger formations accumulated as sandstone strata within mudstone (Manganui Formation) and display obvious sediment conduits (i.e. canyons, channels and gullies) in seismic reflection profiles. Past studies considered that these conduits pass through submarine fans, while in reality fans occur basinward of the mouths of the sediment conduits. This thesis study leverages seismic reflection data and applies seismic stratigraphy and seismic geomorphology, integrated with analysis of wireline logs, core, and outcrops, to better understand the occurrence of sediment conduits and fans within the Moki and Mount Messenger formations. Results show that in southern Taranaki Basin, increased sediment influx resulted in steepening of the continental slope, changing the morphometrics of sediment conduits. Critical analysis of data generated here forced the dismissal of all published fans associated with these sandstone formations. Rather, two new Late Miocene submarine fans have been mapped in deep-water western Taranaki Basin towards the head of the New Caledonia Basin. New paleogeographic maps for the Middle and Late Miocene have been drawn that display the sediment conduits and new fans.

Acknowledgements

Tēnā koutou.

I extend my deepest gratitude to my esteemed supervisors, Dr Andrew La Croix and Professor Emeritus Peter Kamp, for their unwavering guidance, encouragement, and expertise throughout my research journey. The countless brainstorming sessions, meticulous paper reviews, and continuous support have been instrumental in shaping the direction of this study. Andrew, your compassion, prompt feedback, and wealth of theoretical, technical, and research skills have been invaluable. Your resourcefulness and constant challenge to elevate my research skills have significantly contributed to my growth. Peter, I appreciate your profound expertise in the subject matter, your strategic approach to the study, and your encouragement to constantly challenge ideas, fostering my development as an independent researcher. Both of you, with your unwavering toughness and high expectations, have motivated me to excel, and in challenges, your guidance has served as a crucial support system, ensuring a clear path forward. I take pride in having three of my thesis chapters published before submission, a testament to the impactful collaboration with my mentors.

I express my deepest gratitude to my wife, Dr Harizah Hariz, for her constant companionship and boundless support. I consider myself fortunate to have her by my side as we navigated this journey and worked on our PhDs together. Special thanks to my Mum, Dad, and other family members who understand and support our dreams of becoming experts in our respective areas.

I am also grateful to the University of Waikato, especially the Te Aka Mātuatua School of Science for vital support in my research. The University's commitment to a conducive academic environment and resources has been instrumental in my study. Special thanks to Dr Vicki Moon for helping fund the UAV drone operations, and to Ben Roche, Cole Dawson, and Tom Robertson for generously sharing their drone expertise.

Finally, I thank New Zealand Petroleum and Mineral (NZP&M) for generously providing seismic reflection and borehole data crucial to my study of Taranaki Basin. I also express appreciation to Schlumberger for their provision of academic licenses to the Petrel E&P software platform for geological and geophysical interpretation. A special acknowledgment goes to Cegal for providing the Blueback Petrel plugins, which enhanced my detailed seismic interpretation. Thank you Pix4D for academic licenses of Pix4Dmapper software used to construct the 3D outcrop models from UAV drones.

Table of Contents

List of Figures

List of Tables

Chapter 1

Introduction

1.1 Background

Taranaki Basin is a Cretaceous to Cenozoic depocenter situated offshore of the west coast of North Island, New Zealand, as well as onshore beneath Taranaki Peninsula (Figure 1.1). The basin spans an area of approximately 100,000 km^2 and has a stratal thickness of up to 9 km, with over half of this thickness representing deposition during the Middle Miocene to Pleistocene (King & Thrasher, 1996). A large proportion of these Middle Miocene to Pleistocene sedimentary successions are manifest as large-scale clinothems evident on seismic reflection profiles, which record north and northwestward progradation of a shelf-slope system in response to increasing sediment influx to the basin during uplift and erosion of the Southern Alps (Kamp et al., 1989; Tippett & Kamp, 1993; Ring et al., 2019). These sedimentary layers have been well studied because they are well-known examples of source-to-sink marine depositional systems responding to complex interactions at a plate boundary (Hikurangi Subduction Zone) (Inset Map; Figure 1.1). In addition, Taranaki Basin is endowed with abundant petroleum resources (King & Thrasher, 1996; NZP&M, 2018). Whereas the Pliocene to Pleistocene interval (Giant Foresets Formation) is relatively well understood in terms of environments of deposition, stratigraphic architecture, and paleogeography (Hansen & Kamp, 2002; Kamp, 2006), the Middle to Late Miocene strata (including the Moki and Mount Messenger formations) are less well-constrained.

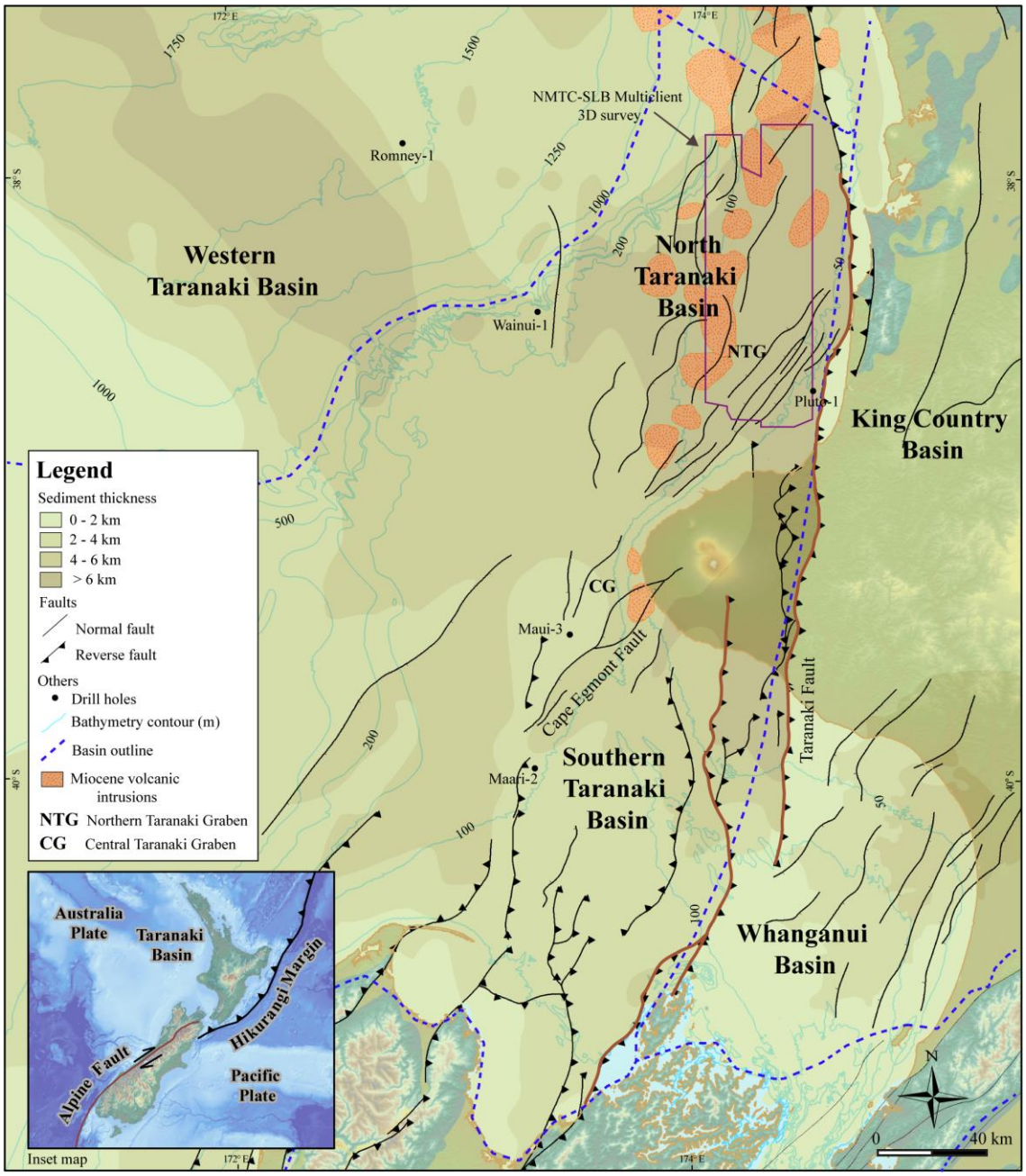

Figure 1.1: Overview map of Taranaki Basin, which shows the broad stratal thickness distribution. The map emphasizes the distinction between the northern and southern basin regions, both situated in shallow water, contrasted against the western region which occurs in deep water. Other highlighted features include Northern and Central Taranaki grabens, Taranaki and Cape Egmont Fault Zones, Miocene-age volcanic intrusions, and selected drill holes of particular interest to this study. GIS data sourced from NZP&M (2018).

Previous researchers sought to understand the regional context for these intervals and how outcrops on land, particularly of the Mount Messenger Formation in North Taranaki, link with the subsurface in terms of their sedimentary deposition (King et al., 1993; Browne & Slatt, 2002). One major limitation of these studies of the Moki and Mount Messenger formations has been the spatial disconnect between observations from seismic reflection profiles, borehole, and outcrop datasets. In the last decade, new seismic reflection data have become available and conceptual advances have been made in methods of interpreting these data (i.e. seismic geomorphology as per Posamentier et al., 2022). Moreover, new technology such as uncrewed aerial vehicle (UAV) drones provides the potential to observe and analyse previously inaccessible or poorly accessible outcrops (Laperchia, 2021).

Capitalizing on the opportunity afforded by these new data, technology, and improved interpretation techniques, this thesis has investigated the Moki and Mount Messenger formations to reveal new insights about their deep-water sedimentary systems and how they are expressed in Taranaki Basin paleogeography. The accumulation of these formations spans the start of uplift and erosion of the Southern Alps mountain belt, considered to have started at about 15 Ma (Ring et al. 2019), but became more pronounced at about 8 Ma (Tippett & Kamp 1993). The Moki Formation of Middle Miocene age (16 – 13 Ma) was not derived from the Torlesse Composite Terrane, which underlies the Southern Alps based on zircon geochronology, although the Mount Messenger Formation was derived from this terrane (pers. comm. P.J.J Kamp). The uplift of the source area is a direct result of the Pacific plate colliding obliquely with the Australian plate in South Island. Sediment from the Southern Alps was routed to Taranaki Basin via the Moutere Basin south of Nelson and via longshore drift along the Westland coastline.

The overarching aim of this study is to better understand the slope to deep-water sediment delivery systems during the Middle to Late Miocene in Taranaki Basin. In particular an aim is to test the reality of otherwise of the large Moki and Mount Messenger formation submarine fans as illustrated in paleogeographic maps by Strogen et al. (2011, 2022) and Kroeger et al. (2019). The resolution of seismic reflection data in Taranaki Basin both 2D and 3D are sufficient to identify the stratal patterns associated with submarine fans but not necessarily smaller scale features such as individual lobes. This resolution of these seismic data has also determined the fan model adopted in this study, which is based on Walker (1978). This study is a regional mapping and paleogeography study rather than a detailed mapping of fan elements of limited spatial extent. In the reassessment of the lower Mount Messenger Formation in the North Taranaki coastal section, we also rely on seismic mapping of a 3D seismic data survey area located immediately offshore, rather than undertaking a detailed facies analysis of the formation to determine its depositional environments.

In this study I have integrated seismic stratigraphy and seismic geomorphology of 2D and 3D seismic reflection datasets with well logs and borehole data, as well as with 3D digital outcrop models to: 1) quantitatively parameterize channelforms on the Middle and Late Miocene continental slope in south and central Taranaki Basin; 2) map and revise the basin paleogeography at 14 Ma, 12 Ma, and 6 Ma; and 3), re-evaluate outcrop interpretations for the world-known North Taranaki coastal section.

The thesis comprises 6 chapters, primarily written in paper format. This chapter, (Chapter 1) is the introduction to the thesis. Chapter 2 is a quantitative analysis of channelforms on the continental slope. Chapter 3 is a seismic geomorphology-driven evaluation and revision of basin paleogeography. Chapter 4 constitutes an offshore-seismic to outcrop linked study of

the coastal section in North Taranaki Basin. Chapter 5 is a description of 3D computer models of outcrops constructed using UAV drone imagery. Finally, Chapter 6 is the thesis conclusion chapter. The following sections are a brief synopsis of Chapters 2 to 5, which collectively advance understanding of the Middle to Late Miocene Moki and Mount Messenger formations.

1.2 Summary of Chapter 2: Quantitative seismic geomorphology of sediment conduits on an evolving Miocene slope in Taranaki Basin (New Zealand): The influence of increasing slope gradient through time

Submarine canyons, channels, and gullies are important sediment pathways that link sedimentary systems from source to sink (Allen, 2017). In the foreland of Taranaki Basin, situated in the hinterland of the Australia-Pacific plate boundary (Hikurangi subduction zone), prior research (e.g. Strogen et al., 2011; Kroeger et al., 2019; Bull et al., 2019) identified a Miocene progradational slope margin and documented sediment conduits along part of the paleo-shelf and slope. However, a quantitative analysis of these submarine canyons and channels, along with their morphometric relationship with the prograding slope remains unknown.

This study leveraged the techniques of seismic geomorphology to quantitatively characterize morphometric attributes of submarine canyons, channels, and gullies in southern and central Taranaki Basin. The morphometrics included cross-sectional features such as width, depth, and cross-sectional area, as well as planform characteristics such as sinuosity, meander length, and meander amplitude (Peakall et al., 2000; Deptuck et al., 2007; Gamboa et al., 2012; Qin et al., 2016; Harishidayat et al., 2018). Such quantitative insights about the evolution of sediment conduits and the factors influencing their physical attributes are a major

knowledge gap, especially in ancient/buried systems. This research was published in the journal Marine and Petroleum Geology (Kamaruzaman et al., 2023).

1.3 Summary of Chapter 3: Critical re-assessment of Middle and Late Miocene submarine fans in offshore southern and western Taranaki Basin, New Zealand, to update the paleogeography

Petroleum exploration and sedimentary basin research geoscientists globally have had a vested interest in understanding ancient deep-water sedimentary systems for several decades. However, recently this interest has been reinvigorated due to the growing availability of 3D seismic reflection datasets and advanced seismic reflection mapping methods and tools. Moreover, advancements in the field of marine geomorphology, derived from the study of Recent distributary sedimentary systems such as channel networks, submarine fans, and continental slopes, have provided new insights with potentially impactful applications to the ancient record (Stow & Mayall, 2000; Shanmugam, 2013; Mayall & Kneller, 2021; Mitchell et al., 2023). One such method, seismic amplitude extraction, is routinely used for mapping ancient depositional systems such as fans, and is a technique that is sometimes used without proper due care and attention. For example, if the data are not detuned in the target interval before amplitude signatures are mapped and interpreted, inaccurate geological interpretations might result due to thin-bed tuning effects (Bunt, 2015; Ab Fatah et al., 2016; Francis, 2016; Márquez et al., 2021).

In Chapter 3, I raised concern over the Miocene submarine fans mapped by prior researchers in southern Taranaki Basin (i.e., Grain, 2008; Baur et al., 2010; Kroeger et al., 2019) because of the observation that they do not adhere to established stratal seismic criteria

commonly used to identify ancient fans (Posamentier & Erskine, 1991). Therefore, this study has aimed to re-evaluate the Middle and Late Miocene deep-water sedimentary system in southern, central, and western offshore Taranaki Basin. The approach involved objective deconstruction of the currently accepted interpretation of submarine fans, followed by building a case for two newly described fans in distal deep-water parts of offshore western Taranaki Basin. A version of this study was published in the journal Marine and Petroleum Geology (Kamaruzaman et al., 2024a).

1.4 Summary of Chapter 4: Interpreting Environments of Deposition from Facies Analysis of Outcrop Versus Seismic Reflection Data: A Cautionary Tale from the Mount Messenger Formation, Taranaki Basin (New Zealand)

The North Taranaki coastal section (North Island, New Zealand) features well-exposed outcrops of the Late Miocene Mount Messenger Formation (King et al., 1993). Previous studies of these outcrop strata concluded that they are of basin floor (i.e. submarine) fan origin (King et al., 1993; Hansen, 1996; Browne & Slatt, 2002; Maier et al., 2010; Strogen et al., 2011; Sharman et al., 2015). Even the most recent study by Masalimova et al. (2016) viewed these outcrops of the lower Mount Messenger Formation as representing a basin floor fan (i.e. single fan with multiple lobes). Yet, despite this model permeating the literature and forming the basis for field training of petroleum geoscientists and students about deep-water sedimentary processes and submarine fan reservoir architecture (e.g., Jordan et al., 1994; Browne & Slatt, 2002; Staff, 2002; Childs et al., 2007), the basin floor fan depositional model for the lower Mount Messenger Formation has never undergone critical examination.

An opportunity to revisit and scrutinize the depositional models for the North Taranaki Basin coastal section has arisen with the 2018 release of a 3D seismic reflection dataset (Mercury-Mokau 3D seismic survey) by the New Zealand Government (NZP&M, 2018), that covers an area offshore and immediately adjacent to the outcrops. This was matched with the fact that no one has developed 3D models of the outcrops using UAV drones. The hypothesis driving the study was that if exhumed basin floor fans are indeed present in the coastal section, they should be detectable in the seismic volume just offshore and down-dip of the exposed succession in sea cliffs.

1.5 Summary of Chapter 5: Dataset of 3D computer models of Late Miocene Mount Messenger Formation outcrops in New Zealand, built with UAV drones

This paper was in support of Chapter 4, having the objective of building 3D computer models of the lower Mount Messenger Formation outcrops to aid in their analysis. The Late Miocene-aged sedimentary strata, prominently exposed along the North Taranaki coast, have previously been regarded as exemplary instances of deep-water sandstone and siltstone sediments. They have been encountered in offshore drill hole materials and seismic reflection data imagery immediately adjacent to the coast. However, past investigations of these outcrops predominantly relied on observations and measurements made in the field of outcrops of the lower Mount Messenger Formation (e.g., Hansen, 1996; Masalimova et al., 2016). This study of outcrop strata has distinguished itself from these past studies of outcrop strata by integrating UAV drone imagery to build 3D computer models and capture the sedimentary characteristics of the outcrops. The utilization of UAV drones has significantly expanded the scope of coverage, encompassing areas previously inaccessible on foot. Consequently, the geological

analysis of these deep-water sedimentary systems is markedly enhanced, particularly when examined through the prism of a 3D perspective. This analytical approach fosters a more comprehensive understanding of the ancient sedimentary system in the region, surpassing the insights offered by earlier studies. The acquired drone images underwent meticulous processing in Pix4Dmapper version 4.4.12, ensuring precise geolocation for the generation of highly detailed 3D computer models. Subsequent qualitative and quantitative stratigraphic analyses of the outcrops were meticulously conducted using ArcGIS Pro version 3.0.3 (Marques et al., 2020). A version of this study was published in the journal Data In Brief (Kamaruzaman et al., 2024b).

1.6 References

Ab Fatah, A., Mohamed, H., Hee, R. P., & Tukimin, N. (2016). Horizon Independent Detuning of Seismic Volume from Sarawak Field. *2016*(1), 1-5. https://doi.org/https://doi.org/10.3997/2214-4609.201602407

Allen PA. *Sediment Routing Systems: First Concepts. In: Sediment Routing Systems: The Fate of Sediment from Source to Sink*. Cambridge: Cambridge University Press; 2017:3-19. doi:10.1017/9781316135754.002

Baur, J. R., King, P. R., Stern, T., Leitner, B., Wood, L. J., Simo, T. T., & Rosen, N. C. (2010). Development and Seismic Geomorphology of a Miocene Slope Channel Megasystem, Offshore Taranaki Basin, New Zealand. In *Seismic Imaging of Depositional and Geomorphic Systems* (Vol. 30, pp. 0). SEPM Society for Sedimentary Geology. https://doi.org/10.5724/gcs.10.30.0618

Browne, G. H., & Slatt, R. M. (2002). Outcrop and Behind-Outcrop Characterization of a Late Miocene Slope Fan System, Mt. Messenger Formation, New Zealand. *AAPG Bulletin*, *86*(5), 841-862. https://doi.org/10.1306/61eedbb6-173e-11d7-8645000102c1865d

Bull, S., Nicol, A., Strogen, D., Kroeger, K., & Seebeck, H. S. (2019). Tectonic controls on Miocene sedimentation in the Southern Taranaki Basin and implications for New Zealand plate boundary deformation. *Basin Research*, *31*(2), 253-273. https://doi.org/10.1111/bre.12319

Bunt, R. J. W. (2015). The use of seismic attributes for fan and reservoir definition in the Sea Lion Field, North Falkland Basin. *Petroleum Geoscience*, *21*(2-3), 137-149. https://doi.org/https://doi.org/10.1144/petgeo2014-055

Childs, C., Walsh, J. J., Manzocchi, T., Strand, J., Nicol, A., Tomasso, M., Schöpfer, M. P. J., & Aplin, A. C. (2007). Definition of a fault permeability predictor from outcrop studies of a faulted turbidite sequence, Taranaki, New Zealand. *Geological Society, London, Special Publications*, *292*(1), 235-258. https://doi.org/doi:10.1144/SP292.14

Deptuck, M. E., Sylvester, Z., Pirmez, C., & O'Byrne, C. (2007). Migration–aggradation history and 3-D seismic geomorphology of submarine channels in the Pleistocene Benin-major Canyon, western Niger Delta slope. *Marine and Petroleum Geology*, *24*(6-9), 406-433. https://doi.org/10.1016/j.marpetgeo.2007.01.005

Francis, A. (2016). *Seismic Amplitudes Benefit From Seismic Trace Detuning*. https://www.hartenergy.com/exclusives/seismic-amplitudes-benefit-seismic-trace-detuning-176002#:~:text=In%20summary%2C%20seismic%20trace%20detuning%20is%20a%20significant,and%20direct%20hydrocarbon%20detection%20from%20seismic%20data.%2018

Gamboa, D., Alves, T. M., & Cartwright, J. (2012). A submarine channel confluence classification for topographically confined slopes. *Marine and Petroleum Geology*, *35*(1), 176-189. https://doi.org/10.1016/j.marpetgeo.2012.02.011

Grain, S. L. (2008). *Paleogeography of a Mid Miocene Turbidite Complex, Moki Formation, Taranaki Basin, New Zealand* Victoria University of Wellington].

Hansen, R. J. (1996). Stratigraphy, Sedimentology, and Paleomagnetism of a late Miocene Succession, Eastern Taranaki Basin Margin, unpublished MSc. thesis, Department of Earth and Ocean Sciences (Unpublished master's thesis), University of Waikato, New Zealand.

Hansen, R. J., & Kamp, P. J. J. (2002). Evolution of the Giant Foresets Formation, northern Taranaki Basin, New Zealand. Conference held at Auckland. Conference Contribution retrieved from https://hdl.handle.net/10289/3617

Harishidayat, D., Omosanya, K. O., Johansen, S. E., Eruteya, O. E., & Niyazi, Y. (2018). Morphometric analysis of sediment conduits on a bathymetric high: Implications for palaeoenvironment and hydrocarbon prospectivity [https://doi.org/10.1111/bre.12291]. *Basin Research*, *30*(5), 1015-1041. https://doi.org/https://doi.org/10.1111/bre.12291

Jordan, D. W., Schlutz, D. J., Cherng, J. A., Weimer, P., Bouma, A. H., & Perkins, B. F. (1994). Facies Architecture and Reservoir Quality of Miocene Mt. Messenger Deep-Water Deposits, Taranaki Peninsula, New Zealand. In *Submarine Fans and Turbidite Systems—Sequence Stratigraphy, Reservoir Architecture and Production Characteristics Gulf of Mexico and International* (Vol. 15, pp. 0). SEPM Society for Sedimentary Geology. https://doi.org/10.5724/gcs.94.15.0177

Kamaruzaman, E. H., La Croix, A. D., & Kamp, P. J. J. (2023). Quantitative seismic geomorphology of sediment conduits on an evolving Miocene slope in Taranaki Basin (New Zealand): The influence of increasing slope gradient through time. *Marine and Petroleum Geology*, *152*, 106233. https://doi.org/https://doi.org/10.1016/j.marpetgeo.2023.106233

Kamaruzaman, E. H., La Croix, A. D., & Kamp, P. J. J. (2024a). Critical re-assessment of Middle and Late Miocene submarine fans in offshore southern and western Taranaki Basin, New Zealand, to update the paleogeography. *Marine and Petroleum Geology*, *161*, 106664. https://doi.org/https://doi.org/10.1016/j.marpetgeo.2023.106664

Kamaruzaman, E. H., La Croix, A. D., & Kamp, P. J. J. (2024b). Dataset of 3D computer models of Late Miocene Mount Messenger Formation outcrops in New Zealand, built with UAV drones. *Data in Brief*, 110035. https://doi.org/https://doi.org/10.1016/j.dib.2024.110035

Kamp, P. J.J., Green, P., & White, S. (1989). Fission track analysis reveals character of collisional tectonics in New Zealand. *Tectonics*, *8*, 169-195. https://doi.org/10.1029/TC008i002p00169

Hansen, R. J., Kamp, P. J. J. (2006). Sequence stratigraphy and architectural elements of the Giant Foresets Formation, northern Taranaki Basin, New Zealand. New Zealand Petroleum Conference

King, P., & Thrasher, G. P. (1996). Cretaceous-Cenozoic Geology and Petroleum Systems of the Taranaki Basin, New Zealand. *Insitute of Geological and Nuclear Science Monograph*, *13*(Part 1 and 2).

King, P. R., Scott, G. H., & Robinson, P. H. (1993). *Description, Correlation and Depositional History of Miocene Sediments Outcropping Along North Taranaki Coast*.

Kroeger, K. F., Thrasher, G. P., & Sarma, M. (2019). The Evolution of a Middle Miocene Deep-water Sedimentary System in Northwestern New Zealand (Taranaki Basin):

Depositional Controls and Mechanisms. *Marine and Petroleum Geology*, *101*, 355-372. https://doi.org/10.1016/j.marpetgeo.2018.11.052

Laperchia, V. (2021). *Mapping the Inaccesible: Why Geologists Use Drones to Create 3D Models of Cliffs, Coasts and Volcanoes*. DJI Enterprise. https://enterprise-insights.dji.com/blog/why-geologists-use-drones-to-create-3d-models-of-volcanoes

Maier, K. L., Masalimova, L. U., Rotzien, J. R., Graham, S. A., & Lowe, D. R. (2010). 2010 New Zealand Guide: Deep-water deposits of the upper Miocene Mount Messenger, Urenui, and Kiore formations, Taranaki Basin, North Island, New Zealand: SPODDS Affiliates Trip Guidebook. https://spodds.stanford.edu/publications/field-guide/2010-new-zealand-guide-deep-water-deposits-upper-miocene-mount-messenger

Marques, A., Horota, R. K., de Souza, E. M., Kupssinskü, L., Rossa, P., Aires, A. S., Bachi, L., Veronez, M. R., Gonzaga, L., & Cazarin, C. L. (2020). Virtual and digital outcrops in the petroleum industry: A systematic review. *Earth-Science Reviews*, *208*. https://doi.org/10.1016/j.earscirev.2020.103260

Márquez, E., Berton, F., Stevanato, A. C., Chaves, F., Ojevan, N., & Brasil, E. (2021). New opportunities in a mature oil field: Stretching data interpretation for complex reservoir prediction.

Masalimova, L. U., Lowe, D. R., Sharman, G. R., King, P. R., & Arnot, M. J. (2016). Outcrop characterization of a submarine channel-lobe complex: The Lower Mount Messenger Formation, Taranaki Basin, New Zealand. *Marine and Petroleum Geology*, *71*, 360-390. https://doi.org/10.1016/j.marpetgeo.2016.01.004

Mayall, M., & Kneller, B. (2021). Seismic interpretation workflows for deep-water systems: A practical guide for the subsurface. *AAPG Bulletin*, *105*(11), 2127-2157. https://doi.org/10.1306/05262120094

Mitchell, W. H., Whittaker, A. C., Mayall, M., & Lonergan, L. (2023). Reconciling bathymetric and stratigraphic expressions of submarine channel geometry. *Marine Geology*, *459*, 107025. https://doi.org/https://doi.org/10.1016/j.margeo.2023.107025

NZP&M. (2018). *New Zealand Petroleum Exploration Data Pack,* New Zealand Petroleum and Minerals.

Peakall, J., McCaffrey, B., & Kneller, B. (2000). A Process Model for the Evolution, Morphology, and Architecture of Sinuous Submarine Channels. *Journal of Sedimentary Research*, *70*(3), 434-448. https://doi.org/10.1306/2dc4091c-0e47-11d7-8643000102c1865d

Posamentier, H. W., & Erskine, R. D. (1991). Seismic Expression and Recognition Criteria of Ancient Submarine Fans. In P. Weimer & M. H. Link (Eds.), *Seismic Facies and Sedimentary Processes of Submarine Fans and Turbidite Systems* (pp. 197-222). Springer New York. https://doi.org/10.1007/978-1-4684-8276-8_10

Posamentier, H. W., Paumard, V., & Lang, S. C. (2022). Principles of seismic stratigraphy and seismic geomorphology I: Extracting geologic insights from seismic data. *Earth-Science Reviews*, *228*. https://doi.org/10.1016/j.earscirev.2022.103963

Qin, Y., Alves, T. M., Constantine, J., & Gamboa, D. (2016). Quantitative seismic geomorphology of a submarine channel system in SE Brazil (Espírito Santo Basin): Scale comparison with other submarine channel systems. *Marine and Petroleum Geology*, *78*, 455-473. https://doi.org/10.1016/j.marpetgeo.2016.09.024

Ring, U., Glodny, J., Angiboust, S., Little, T., & Lang, K. A. (2019). Middle to Late Miocene Age for the End of Amphibolite-Facies Mylonitization of the Alpine Schist, New Zealand: Implications for Onset of Transpression Across the Alpine Fault. *Tectonics*, *38*(12), 4335-4359. https://doi.org/https://doi.org/10.1029/2019TC005577

Shanmugam, G. (2013). New perspectives on deep-water sandstones: Implications. *Petroleum Exploration and Development*, *40*(3), 316-324. https://doi.org/https://doi.org/10.1016/S1876-3804(13)60038-5

Sharman, G. R., Graham, S. A., Masalimova, L. U., Shumaker, L. E., & King, P. R. (2015). Spatial patterns of deformation and paleoslope estimation within the marginal and central portions of a basin-floor mass-transport deposit, Taranaki Basin, New Zealand. *Geosphere*, *11*(2), 266-306. https://doi.org/10.1130/ges01126.1

Staff, P. (2002). Reservoir Studies of Outcropping Deep Water Miocene Sequences, North Taranaki, New Zealand.

Stow, D. A. V., & Mayall, M. (2000). Deep-water sedimentary systems: New models for the 21st century. *Marine and Petroleum Geology*, *17*(2), 125-135. https://doi.org/https://doi.org/10.1016/S0264-8172(99)00064-1

Strogen, D. P., Baur, J. R., Bland, K. J., King, P. R., Vonk, A. J., & Kamp, P. J. J. (2011). *Updated paleogeographic maps for the Taranaki Basin and surrounds* (GNS Science Report 2010/53, Issue.

Tippett, J. M., & Kamp, P. J. J. (1993). Fission track analysis of the late Cenozoic vertical kinematics of continental Pacific crust, South Island, New Zealand. *Journal of Geophysical Research: Solid Earth*, *98*(B9), 16119-16148.

Walker, R. G., 1978. Deep-water sandstone facies and ancient submarine fans: Models for exploration for stratigraphic trap. AAPG Bulletin (American Association of Petroleum Geologists), 62 (6).

Chapter 2

Quantitative seismic geomorphology of sediment conduits on an evolving Miocene slope in Taranaki Basin (New Zealand): The influence of increasing slope gradient through time[1]

2.1 Introduction

Submarine canyons, channels and gullies are integral sediment conduits as parts of larger source-to-sink sedimentary systems (Allen, 2017). These systems are globally significant features at continental margins through which sediment, organic carbon, nutrients and pollutants are transported from shallow water to deep-sea environments (Field et al., 1999; Weimer & Slatt, 2004; Covault, 2011; Hughes et al., 2015; Kane et al., 2020). In the foreland Taranaki Basin, located inboard of the Australia-Pacific plate boundary (the Hikurangi subduction zone) (Figure 2.1), prior studies have documented a Miocene progradational slope margin (Bull et al., 2019) and sediment conduits across part of the paleo-shelf and in particular the related slope (Strogen et al., 2011; Kroeger et al., 2019). These submarine canyons and channels have not hitherto been quantitatively parameterised and their morphometric relationship with the prograding slope is yet to be established. The availability of high-resolution 3D seismic reflection data for the part of the basin where many of these conduits occur, enables such a study to be undertaken, in particular determination of the relationship between submarine canyon and channel geomorphology in relation to increasing slope gradient through time.

[1]A version of this chapter has been published in Marine and Petroleum Geology: Kamaruzaman, E. H., La Croix, A. D., & Kamp, P. J. J. (2023). Quantitative seismic geomorphology of sediment conduits on an evolving Miocene slope in Taranaki Basin (New Zealand): The influence of increasing slope gradient through time. Marine and Petroleum Geology, 152, 106233. https://doi.org/https://doi.org/10.1016/j.marpetgeo.2023.106233. The published version is included in Appendix A-i.

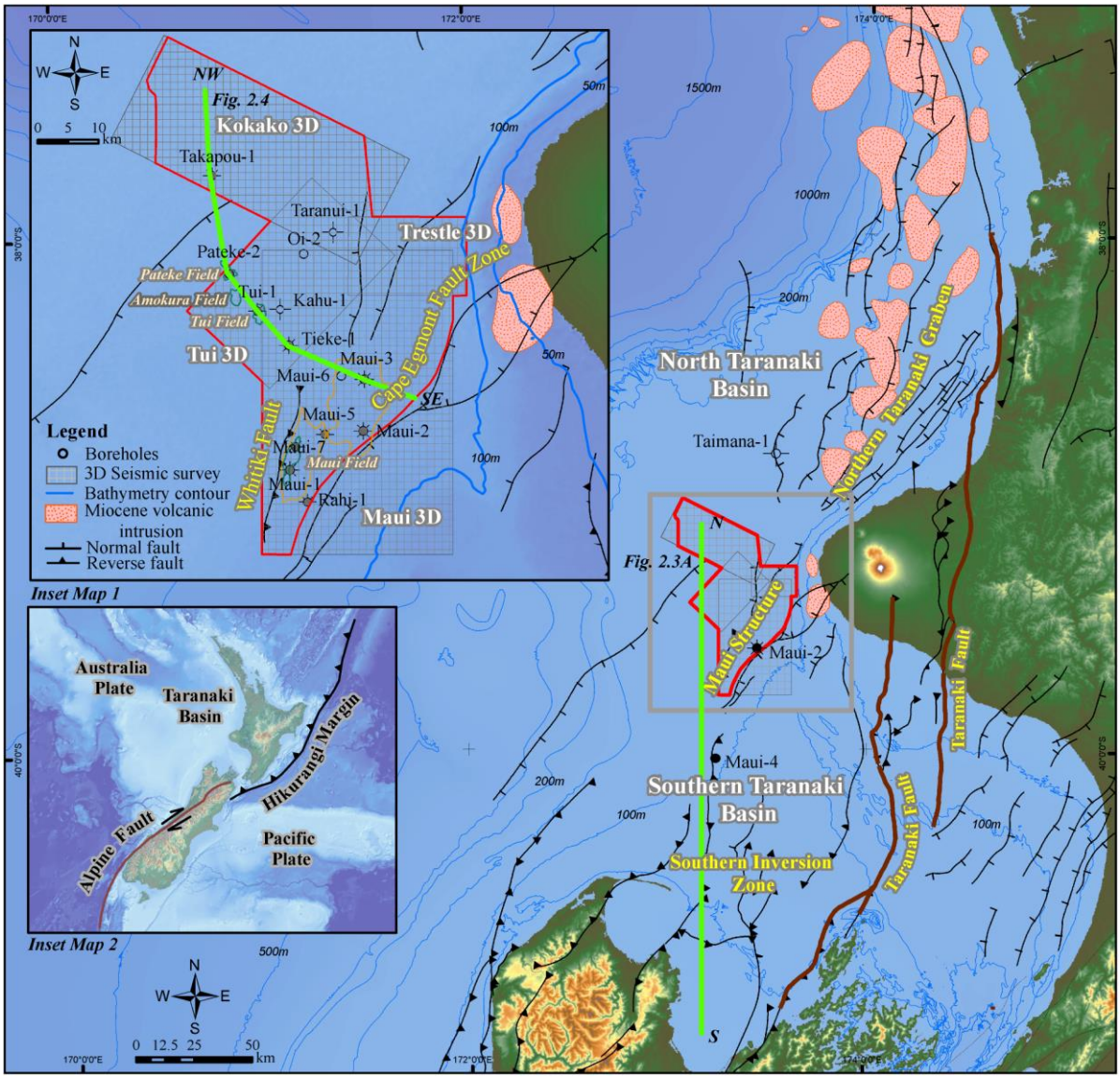

Figure 2.1: Map of Taranaki Basin located west of North Island, New Zealand, showing its main structural features. Inset Map 1 shows the outlines of the 3D seismic volumes and boreholes used in this study. The study area is marked by the red polygon bounded by the Cape Egmont Fault Zone on the eastern side. Inset Map 2 shows the boundary between the Pacific and Australia plates (Alpine Fault and Hikurangi Margin). GIS data from NZP&M (2018).

High-resolution 3D seismic reflection data allows morphometric attributes of submarine canyons, channels and gullies to be quantitatively characterised (i.e., using seismic geomorphology; Posamentier et al., 2022), including cross-sectional (width, depth and cross-sectional area) and planform (sinuosity, meander length and meander amplitude) characteristics (Peakall et al., 2000; Deptuck et al., 2007; Gamboa et al., 2012; Qin et al., 2016;

Harishidayat et al., 2018). These types of quantitative insights lead to a better understanding of sedimentary processes within slope and deep-water systems, the evolution of sediment conduits, and factors that influence their physical characteristics. However, quantitative characterisation is not always straightforward and there are challenges to morphologic interpretations using 3D seismic reflection data. The challenges include resolution limits of seismic data and variations within submarine canyons, channels and gullies due to the effects of internal (e.g., erosion within channel complexes) and external (e.g., post-depositional faulting) factors (Gamboa et al., 2012; Qin et al., 2016; Posamentier et al., 2022). Nevertheless, it is possible to document variability in the geomorphology of canyons, channels and gullies, and to link the resulting geomorphology to sediment transport across the shelf-slope system and into the deep-sea realm.

Most previous studies undertaking geomorphological analysis of submarine canyons, channels and gullies have investigated modern-day or Quaternary systems (Shumaker et al., 2018; Palm et al., 2021; Bührig et al., 2022), and there are comparatively fewer studies documenting the morphometrics of pre-Quaternary systems. In order to fill this research gap on ancient deep-water canyons, channels and gullies, this study focuses on undertaking seismic geomorphological analysis of Miocene-age examples from Taranaki Basin, New Zealand. The aim of this research is to gain insights into the sediment pathways that filled Taranaki Basin by understanding the morphometrics, evolution and distribution of canyon, channel and gully networks on the prograding slope margin as it steepened through the Miocene. In addition to understanding ancient sedimentary processes, the outcomes of this study provide numerical data that can be used for exploration and modelling of large-scale petroleum reservoirs typical of deep-water systems (Hewlett et al., 1993; Weimer & Slatt, 2004; Mayall & Kneller, 2021)

or reservoirs for CO2 and H2 geostorage (Benson & Cook, 2005; Heinemann et al., 2018; Raza et al., 2018).

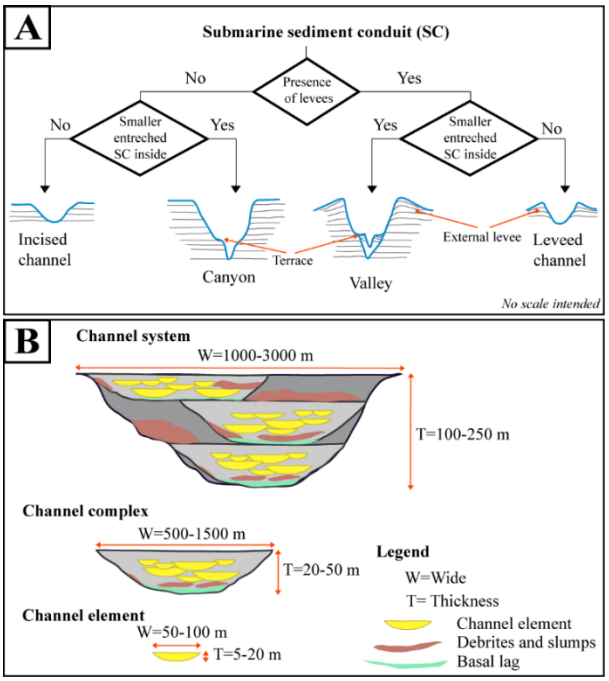

Figure 2.2: (A) Classification of submarine channels, canyons and valleys used in this study after Lemay et al. (2020). (B) Three-level hierarchy of channel bodies applied herein and modified from Mayall and Kneller (2021).

2.2 Classification of sediment conduits in the study area

No standardized criteria currently exist to differentiate between submarine canyons, channels and gullies, although the names imply there are scale differences between the different sets of terminology (Deptuck et al., 2007; Wynn et al., 2007; Shanmugam, 2016). The choice of lexicon has depended on the context of past studies (e.g., stratigraphy, sedimentological processes, basin analysis or geomorphology), and has included a wide variety of terms such as "canyon" (Harris & Whiteway, 2011; Huvenne & Davies, 2014), "valley" (Shepard, 1965; Normark et al., 1993), "canyon-channel" (Covault, 2011), "master channel" (Baur et al., 2010) and "gullies" (Shumaker et al., 2017). These differences in terminology have hindered accurate and repeatable communication of results between studies. In this context, I simplify the

description of channel-form features in my study area into three main classes: 1) submarine canyons, 2) submarine channels and 3) submarine gullies.

Submarine canyons are erosive features typically exhibiting a V-shape due to deep incision and they have limited development of external levees with heads located near the shoreline or on the shelf (Shepard, 1965; Normark et al., 1993; Wynn et al., 2007). By contrast, submarine channels are predominantly U-shape and can be either aggradational or erosional (Deptuck et al., 2007; Qin et al., 2016), and they display a wide range of flow behaviour (Peakall & Sumner, 2015). Herein I adopt the classification of canyons and channels used by Lemay et al. (2020). In this system, canyons do not have external levees whereas channels may or may not have levees (Figure 2.2A). Canyons can contain channels within their walls and most often, channels are smaller than canyons, although not exclusively (Lemay et al., 2020). In addition to differentiating channels from canyons, I adapt the channel body hierarchy system employed in Mayall and Kneller (2021) to describe the internal characteristics of stacked channels within canyons (Figure 2.2B). The hierarchical structure consists of channel systems (1-3 km wide and 100-250 m thick), channel complexes (0.5-1.5 km wide and 20-50 m thick) and channel elements (0.05-0.1 km wide and 5-20 m thick). Lastly, submarine gullies are straight, parallel, regularly spaced channelforms, commonly found on continental slopes with steep topography, especially on prograding or aggrading margins and they are an order of magnitude smaller than submarine canyons (Field et al., 1999; Amblas et al., 2018). The term Gully Complex refers to nested gullies (Shumaker et al., 2017). In terms of gully dimensions, the recorded average widths are in the 100s of m, while the average depths are in the 10s of m (Field et al., 1999; Lonergan et al., 2013) to 100s of m (Gales et al., 2013; Shumaker et al., 2017; Harishidayat et al., 2018).

2.3 Geological setting

Taranaki Basin is a Late Cretaceous to Cenozoic sedimentary basin situated mainly offshore in central-western North Island, New Zealand (Figure 2.1). It contains a sedimentary succession that is up to 9 km thick and which is variably deformed, initially by crustal extension concurrent with seafloor spreading in the Tasman Sea, and subsequently by shortening driven from the Late Oligocene – present-day Hikurangi subduction. Shortening structures are mainly evident along the eastern margin of the basin involving the Taranaki Fault System (King & Thrasher, 1996; Bull et al., 2015). During the Late Eocene to the Early Oligocene, the basin underwent a regional subsidence phase resulting in a bathymetric deepening of the basin in the northwestward direction (King & Thrasher, 1996; Strogen et al., 2011). Marine inundation of central and southern Taranaki Basin occurred during the late-Early Oligocene (29 Ma), peaking during the latest Oligocene when the central and southern parts of the basin became a foredeep due to loading by basement across the Taranaki Fault System (King & Thrasher, 1996). Marine regression began during the late-Early Miocene from southern Taranaki Basin due to an increasing supply of sediment initially from the fold-thrust belt along the eastern margin, followed during latest Middle Miocene by uplift and erosion of the Southern Alps in South Island southeast of the Alpine Fault (Kamp et al., 1989; Tippett & Kamp, 1993; Higgs & King, 2018). Bull et al. (2019) generated a series of basin models to demonstrate the increase of sediment supply into Taranaki Basin beginning in the Early Miocene (Figure 2.3A shows the 8 Ma example). King and Thrasher (1996) calculated a similar Early Miocene increase of sediment supply rate in wells using the parameters of Hayward and Wood (1989) (Figure 2.3B).

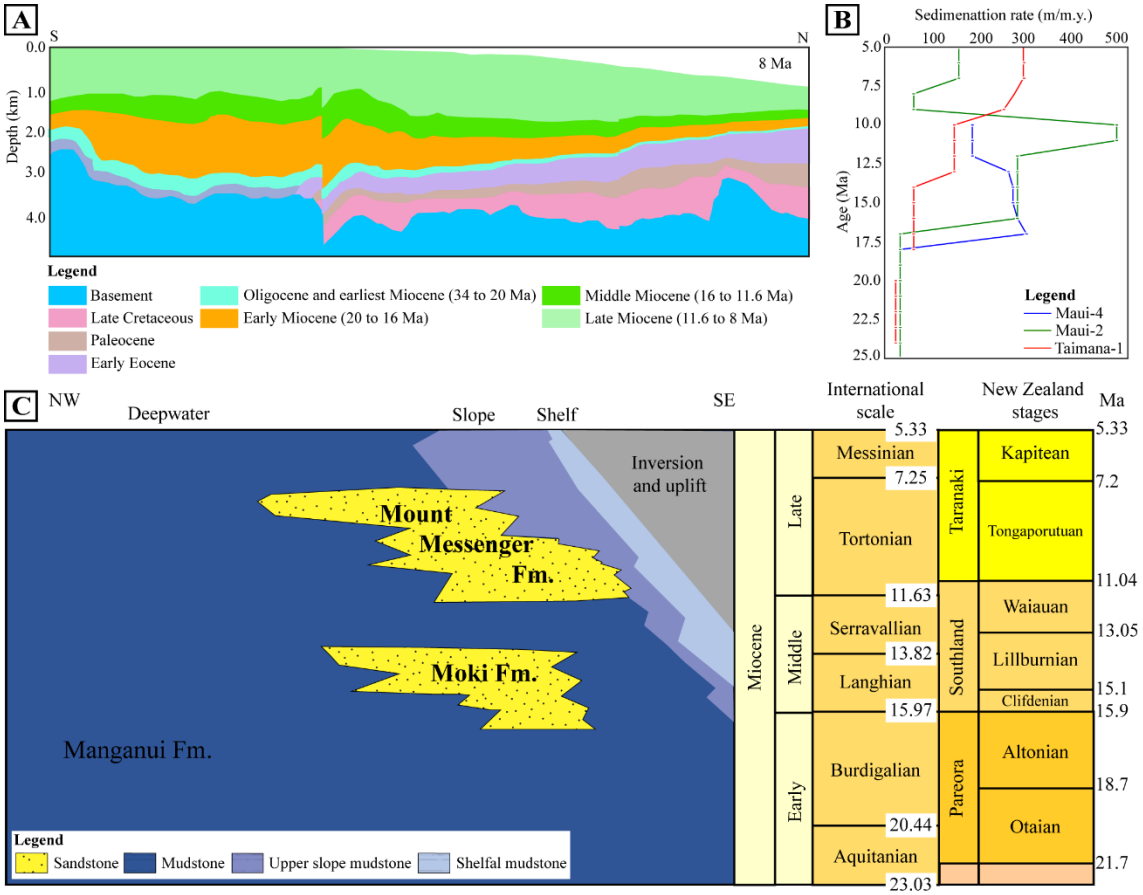

Figure 2.3: (A) The Late Cretaceous to Late Miocene (8 Ma) stratigraphy of southern Taranaki Basin shown as age intervals in a south to north section, simplified from Bull et al. (2019): See Figure 2.1 for the section location. (B) Sedimentation rate data from three boreholes from King and Thrasher (1996) based on geohistory data in Hayward and Wood (1989). See Figure 2.1 for the borehole locations. (C) Generalised Miocene stratigraphy of Taranaki Basin in a chronostratigraphic chart with the New Zealand stages shown against international stages, epochs and timescale in the chart on the right-hand side. The Moki Formation was deposited during the Early to Middle Miocene and the Mount Messenger Formation was deposited during the Middle to Late Miocene. The Manganui Formation is the background mudstone facies. Modified after Bull et al. (2019).

The Early to Middle Miocene Moki Formation represents the initial development of submarine channel networks in a defined regressive shelf-slope system that prograded across the foreland basin towards the "forebulge" area; however, the forebulge never became fully developed. Late Cretaceous – Paleocene and Late Eocene – Early Oligocene normal faults in southern Taranaki Basin were reactivated as reverse faults from 12–10 Ma, forming pronounced antiforms from the crustal shortening that migrated into the foreland basin from its

eastern margin (Kamp & Green, 1990; Crowhurst et al., 2002). The start of this phase of deformation coincided with the start of deposition of the Mount Messenger Formation (ca. 12 Ma). The majority of this sediment was sourced from the Southern Alps and a portion was sourced from erosion of the antiforms rising in the Southern Inversion Zone of southern Taranaki Basin.

North of the Maui Field, submarine canyon and channel networks developed within the lower part of the Mount Messenger Formation. Their character differs from the upper Moki Formation channel complexes, and I document these differences in this study. The phase of structural shortening of the southern Taranaki Basin ended around 6.5 Ma. The structure in which the Maui oil and gas field occurs is the most northern structure on the western side of the basin. At 6.5 Ma, the whole of southern Taranaki Basin was emergent (i.e., above sea level). During the Pliocene and Pleistocene, southern Taranaki Basin subsided again and it currently lies at shelf depths while the shelf-slope break is displaced well to the west, where the Giant Foresets Formation shelf-slope system has been prograding for the last 5 million years (Hansen & Kamp, 2002).

2.4 Study area and interval of interest

The focus of this study is the west-central portion of Taranaki Basin (Figure 2.1, Inset map 1), through which the Moki and Mount Messenger formations, which comprise interbedded sandstone and mudstone (Figure 2.3C), were routed via numerous submarine canyon and channel networks to the deep part of the basin (Strogen et al., 2011; Kroeger et al., 2019). The Manganui Formation is a time equivalent mud-prone unit that envelopes the Moki and Mount Messenger formations, and is commoly considered to comprise the “background”

sediments on the slope and in deep water (King & Thrasher, 1996). The distinction between the sand-prone Moki and Mount Messenger formations and the mud-prone Manganui Formation is based on wireline response in wells that intersect the formations (King & Thrasher, 1996; Roncaglia et al., 2013; Kroeger et al., 2019).

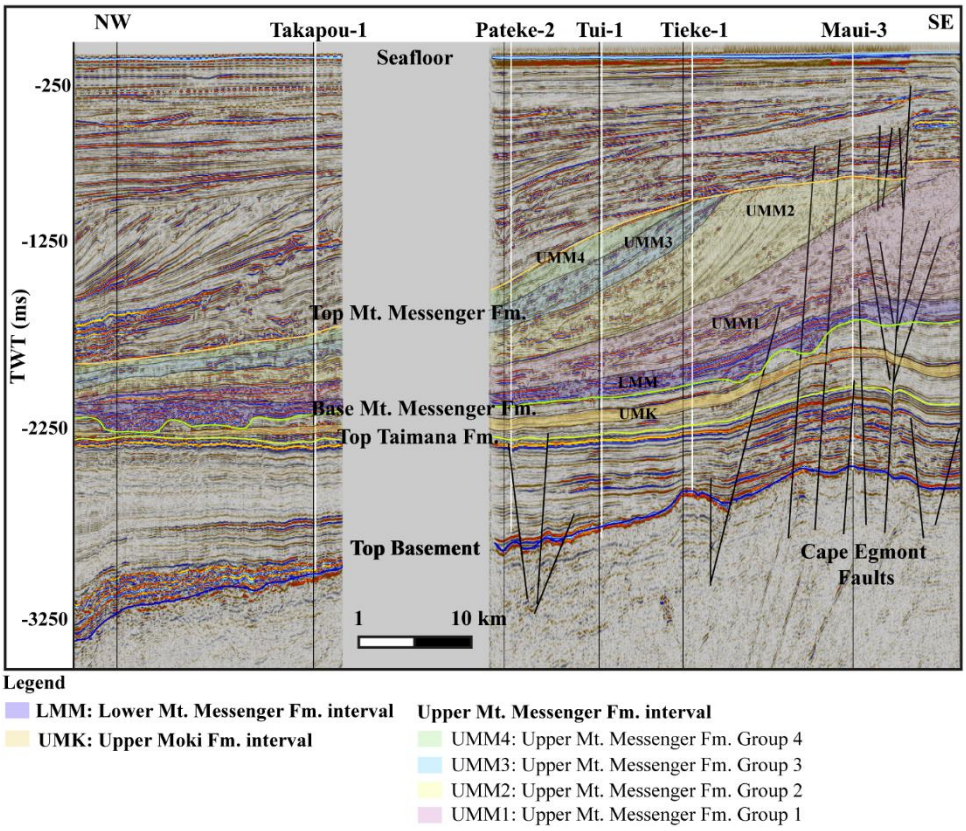

Figure 2.4: Seismic section showing clinoforms of the Moki and Mount Messenger formations dipping to the north and northwest. The regional horizons are Top Basement, Top Taimana Formation, Base Mount Messenger Formation and Top Mount Messenger Formation. The location of the transect is shown in Figure 2.1 within Inset Map 1.

The study area is broadly situated atop the Maui Field, encompassing the Maui Structure that marks the northwestern extent of the Southern Inversion Zone. The Whitiki Fault marks the western side of the study area and the eastern extent is broadly parallel to the Cape Egmont Fault Zone (Bryant et al., 1994; Bussell, 1994; Bryant & Greenstr, 1995) (Figure 2.1).

The regional orientation of prograding sediment accumulation is northwestward, as indicated by the seaward dipping clinoforms visible in seismic data (Figure 2.4).

For my analysis I subdivide the Moki and Mount Messenger formations into three intervals: (i) Upper Moki Formation (Lillburnian Stage (Sl), 16 – 13 Ma); (ii) Lower Mount Messenger Formation (Waiauan (SW) to Early Tongaporutuan, (Tt) stages, 13 – 9 Ma); and (iii) Upper Mount Messenger Formation (Middle to Late Tongaporutuan Stage, 9 – 7.2 Ma) (Figure 2.3C). The New Zealand stages, as defined by Cooper et al. (2004), are defined biostratigraphically by foraminiferal content. Stage boundaries are recorded on drill-hole well logs (Roncaglia et al., 2013) for the area of interest in this study. Selected stage boundaries have been mapped within the 3D seismic volume used in this study.

2.5 Dataset and methods

2.5.1 Seismic data

This study utilises ca. 1800 km^2 of an open-source, industry-acquired, post-stack time migrated (PSTM) 3D seismic reflection dataset, as well as wireline logs from 14 exploration drill holes accessed through the New Zealand Petroleum & Minerals database (https://data.nzpam.govt.nz). Seismic volumes have 19 m × 12.5 m bin spacing, record lengths of 4.5 to 6 s two-way travel time (TWT), vertical sampling rates of 4 ms (TWT) and a 20 to 50 Hz dominant frequency within the intervals of interest (seismic TWT: 1250-2200 ms^{-1}). Seismic volumes were merged, and amplitude was balanced in the merged volume before interpretation. A velocity model was derived for time-depth conversion using check shot data, with the average velocity for the Moki and Mount Messenger formation intervals ranging from

1800 ms^{-1} to 2500 ms^{-1}. In addition, well logs were used to aid seismic interpretation by helping identify lithological changes corresponding to seismic reflections.

Coloured Inversion (CI) was performed on the merged 3D volume to derive relative band-limited acoustic impedance, which boosts the low-frequency seismic response, and therefore increases the resolution of the data (Lancaster & Whitcombe, 2000; Maurya & Singh, 2017; Assis et al., 2018). First, synthetic logs were matched to the seismic data and used to determine the major reflection horizons while considering existing biostratigraphic data from Roncaglia et al. (2013).

Seismic attributes, including Amplitude Accentuating Attributes (e.g., Root Mean Square Amplitude; RMSA and Sweetness), Geometric Attributes (e.g., Semblance and Dip Curvature), and Spectral Decomposition, were extracted along and within the interpreted horizons to visualise the geomorphology of the submarine canyon and channel networks. These attributes were especially useful for distinguishing between sandstone beds within and along the margins of canyons and channels from the background mudstone succession (Taner, 2001; Brown, 2011; Othman et al., 2019). Importantly, attribute extraction was undertaken using horizon-parallel and/or proportional slices to reduce structural effects that might obscure images of the canyons and channels and to ensure slices were broadly time-equivalent snapshots (Zeng et al., 1998; Zeng et al., 2001; Miall, 2002; Zeng, 2013).

2.5.2 Quantitative seismic geomorphology

The seismic geomorphology of submarine canyon, channel and gully networks were quantified by using both cross-sectional and plan views of the 3D seismic volume. However, to understand the limit of seismic resolution and any potential effects of thin-bed tuning of the

data, I generated wedge models. To do so, I calculated both Rayleigh (Kallweit & Wood, 1982) and Widess (Widess, 1973; Chopra et al., 2006) (vertical) resolution limits in terms of bed thickness. The Rayleigh limit of resolution is one-quarter the wavelength of the seismic data (i.e., ƛ/4; where ƛ=wavelength), and the Widess limit of resolution is one-eighth of the wavelength (i.e., ƛ/8). The Widess thin-bed tuning effect (ƛ/4) and the onset of thin-bed tuning effect (ƛ/2) were also calculated.

Initial seismic horizon interpretation and surface generation of the sediment conduits were accomplished in Petrel, and the subsequent spatial analysis was done in both Petrel and ArcGIS. Morphometrics that primarily rely on cross-sectional views of the data include width, depth, cross-sectional area and canyon wall steepness. These were measured every 500 to 700 meters perpendicular to the orientation of sediment conduit axes, down-canyon, down-channel or down-gully (Figure 2.5). For cross-sectional morphometrics: (i) width refers to the measurement at the overspill points perpendicular to their flow directions; (ii), the depth measurements refer to the average height from the two-separate overspill points, due to asymmetrical walls; (iii) the cross-sectional area is calculated based on the digitised points within the canyons (at the base and walls) (Lemay et al., 2020); and (iv) canyon wall steepness refers to the gradient between canyon top and base at the thalweg (Bührig et al., 2022). Due to sediment compaction, the depth of the sediment conduits in this study are considered as minimum depth, and the estimation of compacted sediment cannot be calculated with high confidence due to limited well data within the varying gradient prograding slope strata.

For planform metrics of the canyons, channels and gullies: (i) sinuosity index is the ratio between the length of the lowest point of the thalweg and the overall down-system distance for a given section (a single bend wavelength) (Wynn et al., 2007); (ii) meander length

and amplitude were measured through the same stretch of canyons, channels and gullies where sinuosity index was measured; and (iii) canyon length measurements were taken along-canyon following the thalweg. In addition to cross-sectional and planform parameterisation of canyons and channels, the slope gradient, orientation and steepness (in percent rise) were also calculated at the thalweg and smoothed over a 1-2 km sliding window. In some cases, the sediment conduit incisions did not occur exactly on the mapped regional or sub-regional seismic surfaces (i.e., especially on variably steep surfaces) and in these cases, the incisions were projected onto the nearest surfaces (Shumaker et al., 2017). Finally, the width-to-depth ratio of the sediment conduits was also calculated.

Because the base and top horizons of the canyons, channels and gullies are offset by the Whitiki Fault and the Cape Egmont Fault System, the original depositional surfaces were corrected to pre- and post-faulting positions using horizon flattening and structural restoration. The base of the middle fill of canyons is measured at the base of the aggradational channel systems (Deptuck et al., 2007). Morphometric parameters were analysed using Pearson's correlation coefficient (r).

The morphometric parameters of sediment conduits in this study are based on stratigraphic surfaces. As pointed out by Strong and Paola (2008), and investigated by Sylvester et al. (2011), valleys/canyons in the rock record are not necessarily the result of Earth-surface topography at the time of deposition, they may also be a manifestation of stratigraphic processes. At the present time, no concrete criteria exist to differentiate between stratigraphic valleys and topographic valleys and I cannot be completely certain that I am not comingling the two. However, deposits observed in sediment cores and outcrop from the Moki and Mount

Messenger formations suggest that sediment was delivered to the basin via large-scale sediment conduits.

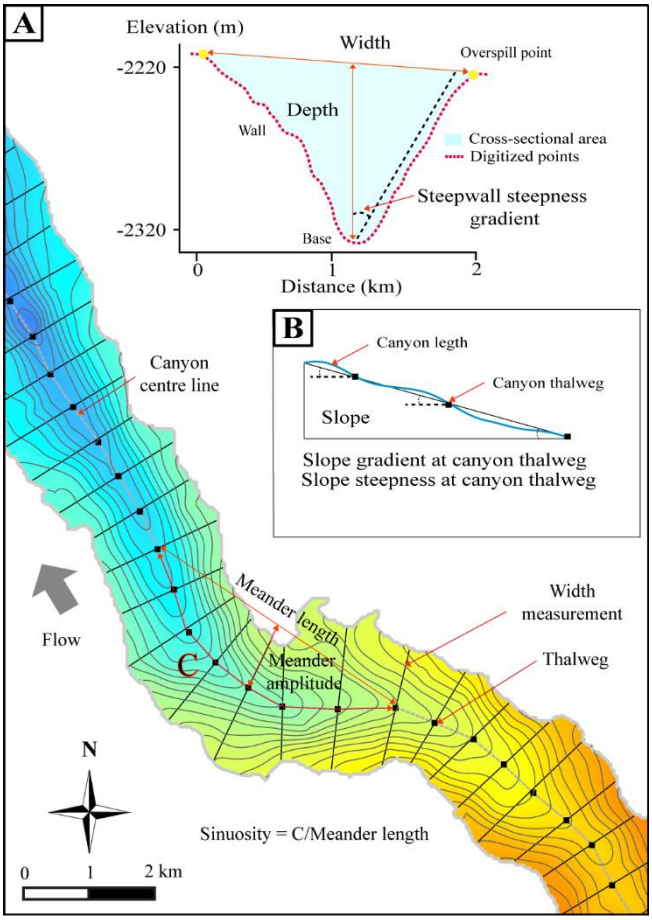

Figure 2.5: (A) The main seismic geomorphological parameters calculated in this study and their definitions, including width, depth, cross-sectional area, wall steepness, meander amplitude, meander length and sinuosity. (B) Explanation of canyon length, slope gradient and steepness parameters at thalweg.

2.6 Results

2.6.1 Resolution of seismic data

Calculation of the Widess and Rayleigh seismic resolution limits yielded a vertical resolution of 6 to 20 m within the intervals of interest (Figure 2.6; Table 2.1). Thus, the morphology of canyons, channel systems and channel complexes are resolvable on seismic data (Figure 2.2B). By contrast, the morphology of channel elements cannot be quantified with high confidence in the interval of interest because their overall dimensions fall below seismic resolution.

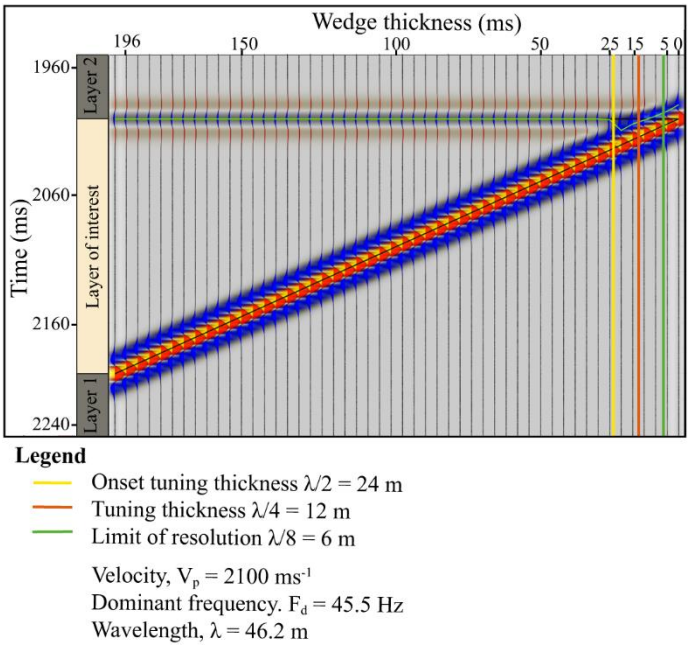

Figure 2.6: An example seismic wedge model used to determine the onset of the thin-bed tuning effect. In this case the onset of the tuning effect occurs at a bed thickness of 24 m. The tuning effect is greatest with a bed-thickness of 12 m. Finally, the limit of resolution due to the tuning effect is when bed-thickness reaches 6 m. These calculations are based on Widess (1973).

Table 2.1: Seismic data and seismic resolution parameters. The vertical seismic resolution of ƛ/4 is based on Rayleigh's Limit of Resolution, and ƛ/8 is based on Widess (1973).

Range of velocity within Miocene	Range of dominant frequency within Miocene	Rayleigh's limit of resolution ƛ/4	Widess' (1973) limit of resolution, ƛ/8
1800 ms^{-1} to 2500 ms^{-1}	40 to 50 Hz	12 to 20 m	6 to 10 m

2.6.2 Seismic geomorphology

The upper Moki Formation interval consists of sinuous channel complexes that meander from south to north with a mean sinuosity, width and depth of 2.4, 1.1 km and 67 m, respectively. The lower Mount Messenger Formation interval comprises canyon networks of highly variable dimensions with a maximum width and depth of 9 km and 350 m, respectively. These canyon networks consist of numerous medium to large U-shape channel systems (and/or channel complexes) developed within canyon walls ranging from 50 to 200 m deep. Finally, the upper Mount Messenger Formation interval is characterised by linear gully complexes oriented from southeast to northwest, with a mean sinuosity, width and depth of 1.0, 1.1 km and 116 m, respectively. Below I describe the seismic geomorphological parameters, stratigraphic interval by interval.

2.6.2.1 Upper Moki Formation

The morphology and morphometrics of the upper Moki Formation channel complexes are shown in Figures 2.7 and 2.8. The channel complex networks developed on the lower slope margin in the study area, roughly 80 km from the shelf edge and 100 km from the shoreline (Figure 2.7C) (Strogen et al., 2011). Seismic reflectors have a gentle basinward slope (i.e., the mean slope gradient is 0.2°). Channel complexes have a nearly symmetrical U-shape cross-

section, with mean width, depth, and cross-sectional area of 1.1 km, 67 m and 0.06 km^2, respectively (Figures 2.7D, E and 2.8A). Overall, the channel complexes show a significant variation in the width and depth metrics ranging from 0.5-1.80 km and 32-85 m, respectively, with such scatter in values that the correlation coefficient is small (i.e., $R^2 = 0.07$; Figure 2.8A). Planform views show that these channel complexes have a high range of sinuosity (1.3–4.34), with the range of meander amplitudes and lengths being 1.7–3.7 km and 1.4–5.5 km, respectively (Figure 2.8B, C and D). There is a lack of evidence for lateral stacking and abandoned meanders, but abrupt lateral shifts in thalweg position are observed along some channel complex margins (Figure 2.7B and E). These channel complexes also do not show levee wedge development. In seismic plan view, overbank splays and crevasse splays are not observed.

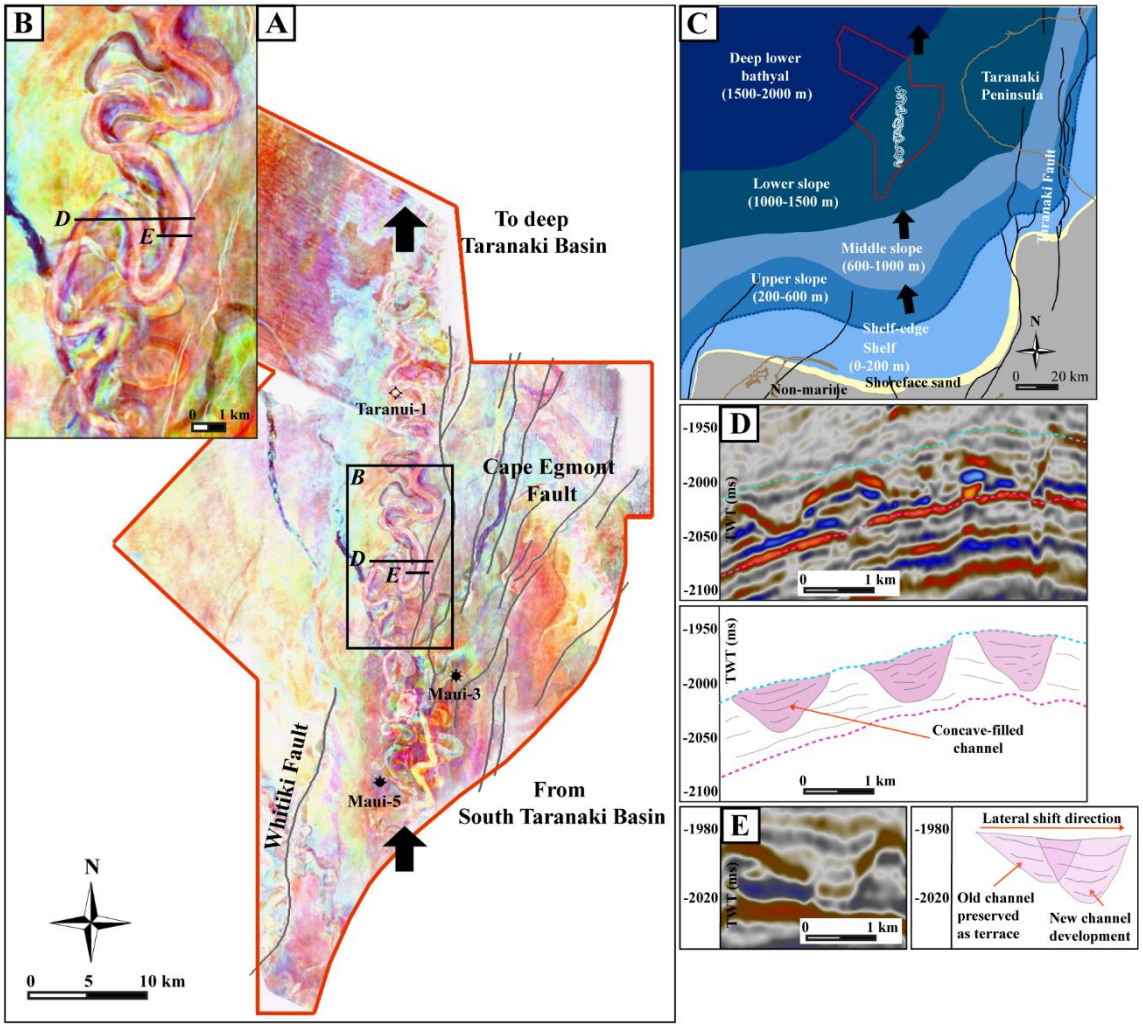

Figure 2.7: (A) Map showing the cyan-magenta-yellow (cyan: 20 Hz, magenta: 30 Hz and yellow: 40 Hz) blend of the General Spectral Decomposition (GSD) seismic attribute, which is used to highlight the geomorphology of upper Moki Formation channel complexes. The red polygon outlines the study area. (B) Close-up view of the sinuous channel complexes. (C) Paleogeographic map (modified from Strogen et al., 2011) showing the location of the upper Moki Formation channel complexes on the lower slope during the Middle Miocene (14 Ma). (D) and (E) are uninterpreted and interpreted cross-sections of the upper Moki Formation channel complexes illustrating the seismic facies of channel-infill and channel lateral shift patterns.

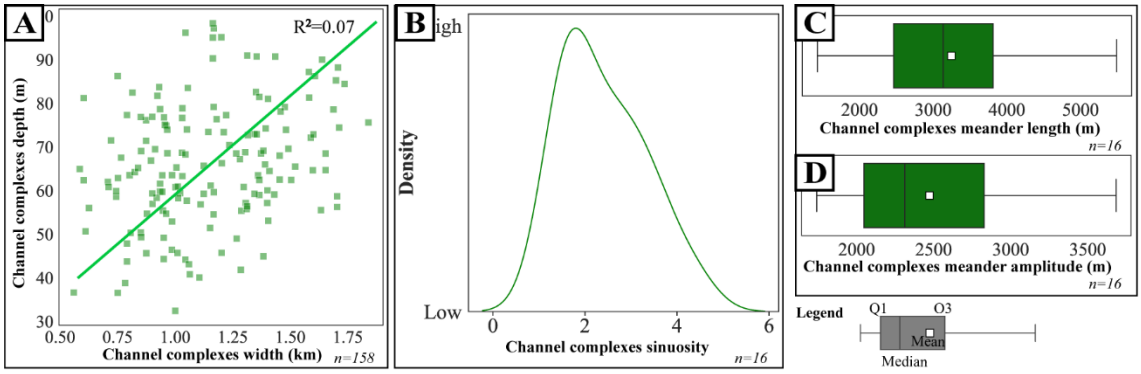

Figure 2.8: Seismic geomorphological metrics of the upper Moki Formation channel complexes. (A) Plot of the channel complexes depth versus width showing a poor correlation (R^2 = 0.07). (B) Kernel density plot of the channel complexes sinuosity. Plots of the channel complexes (C) meander length and (D) meander amplitude. n is the number of samples.

2.6.2.2 Lower Mount Messenger Formation

Figures 2.9 to 2.17 and Table 2.2 contain information about the morphology and morphometrics of the lower Mount Messenger Formation canyon networks. In total, ten canyons were identified within the interval. The canyons occur in two networks based on their geographic position and connectivity in seismic data: Group 1 (Canyons A, B, C, D, E, F, G to H) and Group 2 (Canyons I and J) (Figure 2.9A and B), and their morphometrics are summarized in Table 2.2. These canyons are the extension of larger canyon networks that originated from southern Taranaki Basin (Strogen et al., 2011) (Figure 2.9C). The canyons occur roughly 75 km from the shoreline and 50 km from the shelf-break and are situated on the lower slope margin (Figure 2.9C). In the study area, the canyons occur within the bottomsets of Manganui Formation clinoforms on a slope gradient ranging from 0.4 to 1.0° (Figure 2.10). The planform morphology of canyons is straight with a mean sinuosity, meander length and meander amplitude of 1.1, 3.3 km and 0.5 km, respectively (Figure 2.11B, C and D).

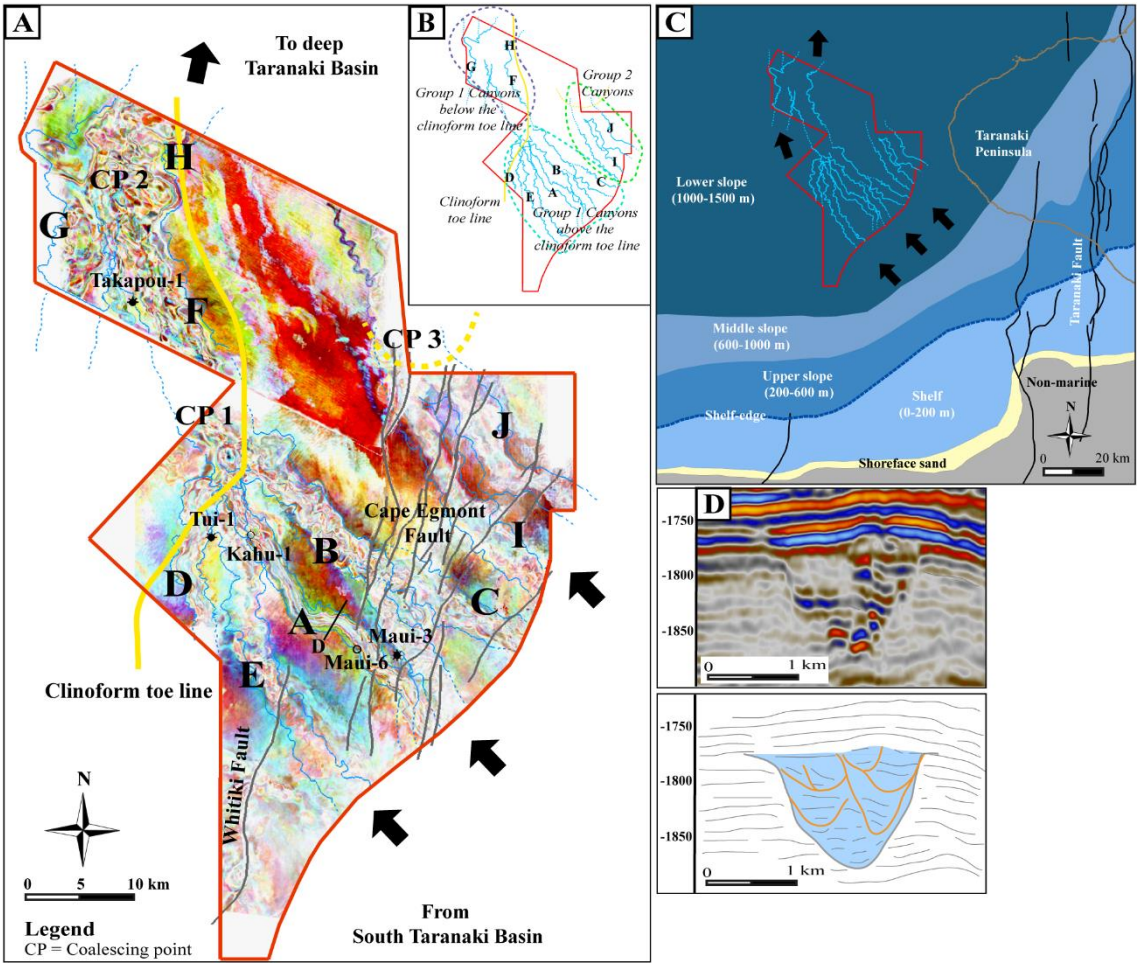

Figure 2.9: (A) Map showing the cyan-magenta-yellow (cyan: 20 Hz, magenta: 30 Hz and yellow: 40 Hz) blend of the General Spectral Decomposition (GSD) seismic attribute, highlighting the geomorphology of the lower Mount Messenger Formation canyons and channel systems. The canyons are labelled from A to J. (B) The grouping of canyons. (C) Palaeogeography map showing the location of the lower Mount Messenger Formation canyon networks in the Middle Miocene (12 Ma) in relation to the basin physiography (modified from Strogen et al., 2011), and blue outlines show the canyon networks mapped in this study. (D) Uninterpreted and interpreted cross-section of Canyon A demonstrating the predominantly sandy infill of the canyon.

2.6.2.2.1 Group 1 canyon network

The total length of the Group 1 canyon network is 78 km, with Canyon B having the longest component (36 km) and Canyon H the shortest (6 km) (Figure 2.11A). The subsurface elevation of the Group 1 canyon network ranges from -1620 m to -2980 m, the depositional

slope ranges from 0.4–1.0° and the depositional orientation is predominantly to the northwest (Figure 2.10A and B).

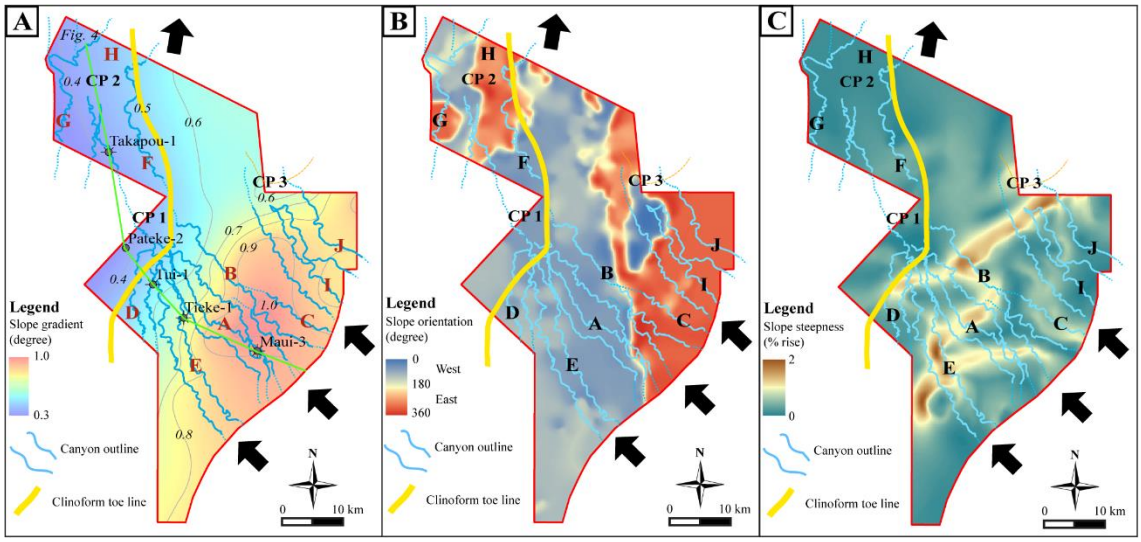

Figure 2.10: Regional maps depicting: (A) Changes in slope gradient, (B) Slope orientation and (C) slope steepness of the lower Mount Messenger Formation canyons. The canyons are labelled from A to J and the clinoform toe line is marked by the yellow line, which subdivides the steep and flat parts of the slope.

Canyon A incises the deepest of all of the canyons into the background strata of the Manganui Formation, roughly 80 ms (TWT) from its top incision surface. However, although Canyon A is the oldest it is difficult to decipher the order of incision for the younger constituent canyons because their top incision surfaces occur at or near the same stratigraphic horizon. Nonetheless, Canyons A, B and E coalesce at the base of the clinoform slope at coalescing point 1 (CP1), forming Canyon F. The base of the clinoform slope, refer in this study to the clinoform toe line (i.e. equivalent to the clinoform toe point), marking the position where the clinoform bottomsets become horizontal with the underlying surface (Pirmez et al., 1998; Patruno et al., 2015). It occurs broadly along the 0.5° slope gradient line, and it is at or below this point that all canyons coalesce (Figures 2.9 and 2.10). Canyon F coalesces with Canyon G

(originating from the south) at coalescing point 2 (CP2) to form the much larger Canyon H (Figures 2.9 and 2.10).

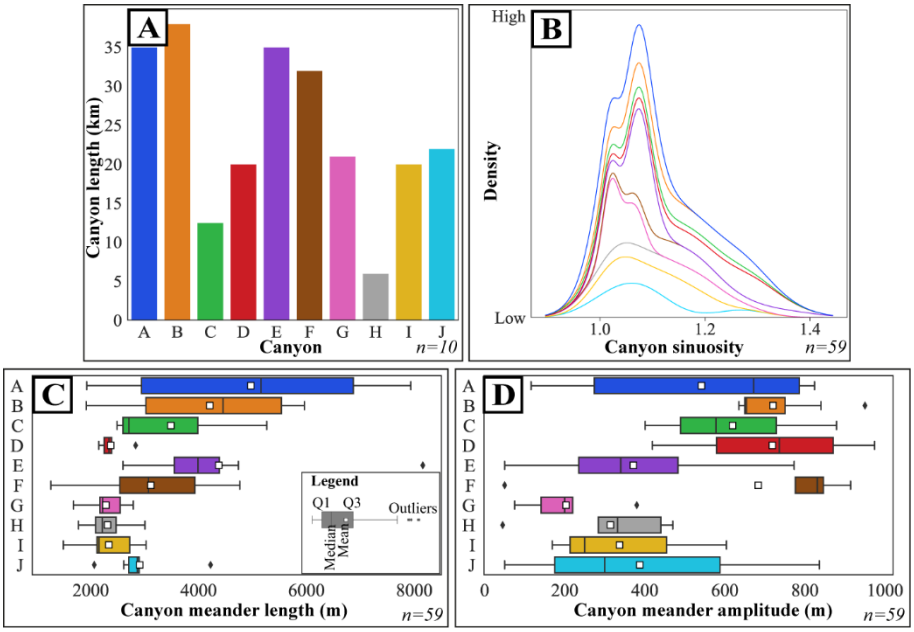

Figure 2.11: (A) Bar chart comparing the length of the lower Mount Messenger Formation canyons. (B) Kernel density plot comparing the canyons sinuosity (colour codes same as in A). Comparison of the individual canyon (C) meander length and (D) meander amplitude measurements (colour codes same as in A). n is the number of samples.

2.6.2.2.2 Morphometrics of Group 1 canyons

Calculation of the morphometrics of Group 1 canyons reveals two distinct canyon populations: (i) canyons above the clinoform toe line (Canyons A, B, C, D, E, I and J), and (ii), canyons below the clinoform toe line (Canyons F, G and H) (Figure 2.9B). Accordingly, I analysed and described them separately in the following text.

In summary, the cross-sectional morphometrics of the canyons below the clinoform toe line increase by factors of depth (1.8), width (2.4) and cross-sectional area (4.7) in comparison to the canyons above the clinoform toe line (Figure 2.12B, C and D). The mean width, depth

and cross-sectional area of the canyons above the clinoform toe line are 2.69 km, 142 m and 0.22 km^2 respectively, while the mean width, depth and cross-sectional area of the canyons below the clinoform toe line are 6.6 km, 252 m and 1.04 km^2, respectively. Correlation analyses of measured morphometric variables using Pearson's correlation are summarized in Figure 2.12G, H and I. Overall the slope gradient (at the canyon thalweg) and the canyon elevation have a strong correlation (r=0.92–0.98). The slope gradient also strongly correlates with the canyon width, depth and cross-sectional area (r=-0.71–-0.86). However, the slope steepness only displays a moderate correlation to the canyon width, depth and cross-sectional area (r=-0.28–-0.56). Lastly, canyon elevation and canyon width, depth and cross-sectional area correlate strongly with canyon wall steepness (r=-0.52–-0.77).

2.6.2.2.2.1 Group 1 canyons above the clinoform toe line

Planform morphometrics reveals that canyons above the clinoform toe line (Canyons A, B, C, D and E) are primarily straight with an average sinuosity index, meander length and amplitude of 1.1, 3.9 km, and 0.6 km, respectively (Figure 2.11). Canyon A is the straightest with a sinuosity index and maximum meander length of 1.05 and 7.9 km, respectively. In comparison, Canyon D is the most sinuous with a sinuosity index and maximum meander length of 1.2 and 2.8 km, respectively. The principal drainage axes of canyons is towards the northwest, corresponding to the dominant depositional slope orientation (Figure 2.10B) and the spacing between canyons ranges from 1 to 7 km (Figure 2.9A).

Analysis of canyon cross-sections reveals that most canyons are characterized by asymmetrical sharp V-shape incisions with a narrow base. However, in some cases parts of the canyons display U-shape incisions with a wide base. The cross-sectional elements of the canyons are shown in Figure 2.13 and mainly consist of canyon bases, walls and flanks. The

canyons have steep walls with average wall steepness of 12.5^{o} and deep indentation of the thalweg. Throughout the canyon course, the thalweg only shifts laterally by slight amounts.

2.6.2.2.2.2 Group 1 canyons below the clinoform toe line

Similar to canyons above the clinoform toe line, canyons below the clinoform toe line (Canyons F, G and H) are straight with a mean sinuosity index of 1.1 and meander length and amplitude of 2.6 km and 0.4 km, respectively (Figure 2.11). The regional slope into which Canyons F and H incise dips to the east (Figure 2.10B), which impacts canyon trajectory (toward the northeast) at the edge of the study area.

The cross-section of canyons in this region shows asymmetrical V-shape indentation with greater depth than the canyons above the clinoform toe line (Figure 2.14), and the average canyon wall steepness is 9^{o}. In general, the width and depth of the canyon measured above 5 km and 200 m, respectively. The width of the canyons increased dramatically after the canyons merged at CP2, from roughly 6 km to 8.5 km (Figure 2.12B). However, the cross-sectional metrics of Canyon G, which originated from the south, are not correlated with Canyon F and H (Figure 2.12). The canyon cross-sections also reveal that the right wall of the canyons displays more significant terrace development than the left wall due to the progressive channel incisions toward the east (Figure 2.14 C-C').

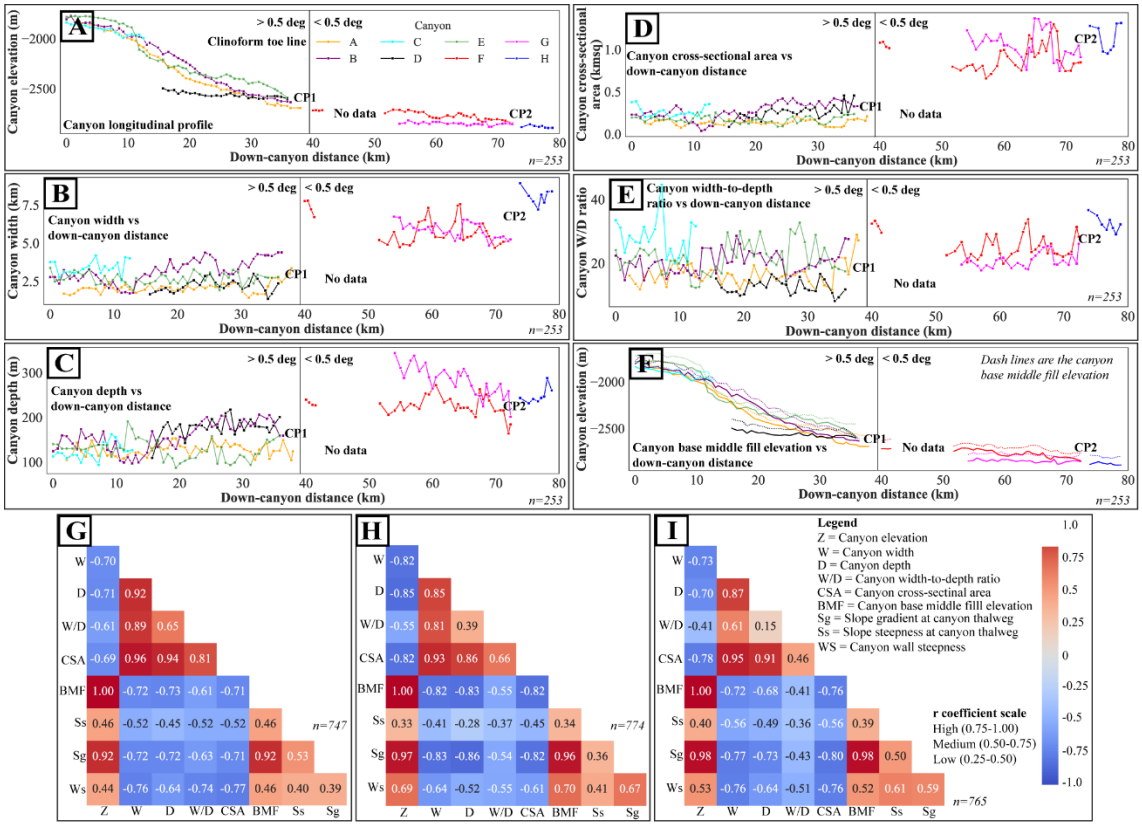

Figure 2.12: Cross-sectional morphometrics of the lower Mount Messenger Formation canyons. (A) Canyon elevation versus down-canyon distance, (B) canyon width versus down-canyon distance, (C) canyon depth versus down-canyon distance, (D) canyon cross-sectional area versus down-canyon distance, (E) canyon width-to-depth ratio versus down-canyon distance and (F) canyon elevation and base middle fill elevation versus down-canyon distance. Matrix of Pearson's correlation coefficient between the major morphometric parameters for (G) Canyons A, F and H. (H) Canyons B, F and H. (I) Canyons E, F and H. n is the number of samples.

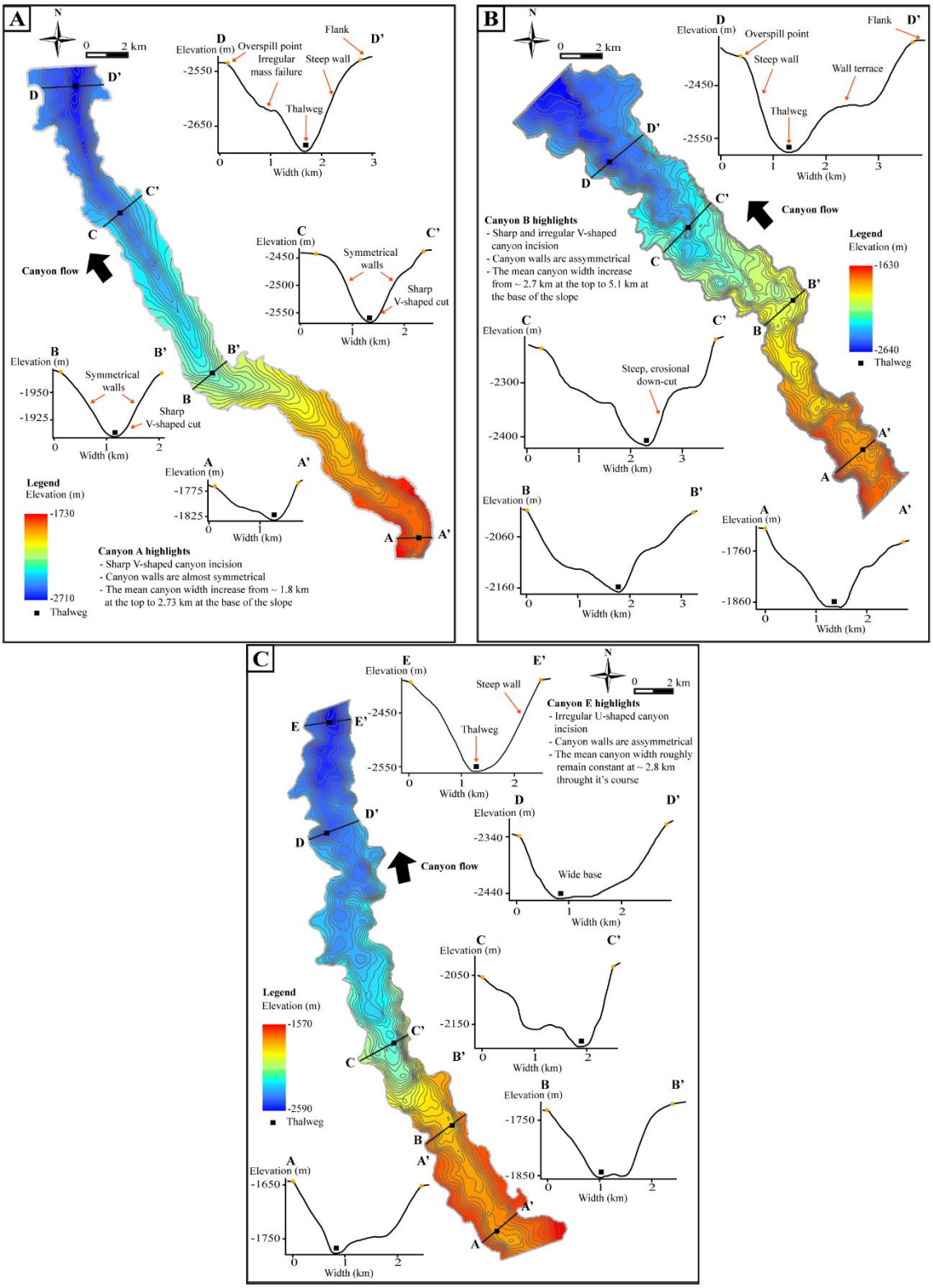

Figure 2.13: Cross-sectional views of the lower Mount Messenger Formation canyons above the clinoform toe line. (A) Canyon A, (B) Canyon B and (C) Canyon E. The main elements of the canyons are also highlighted.

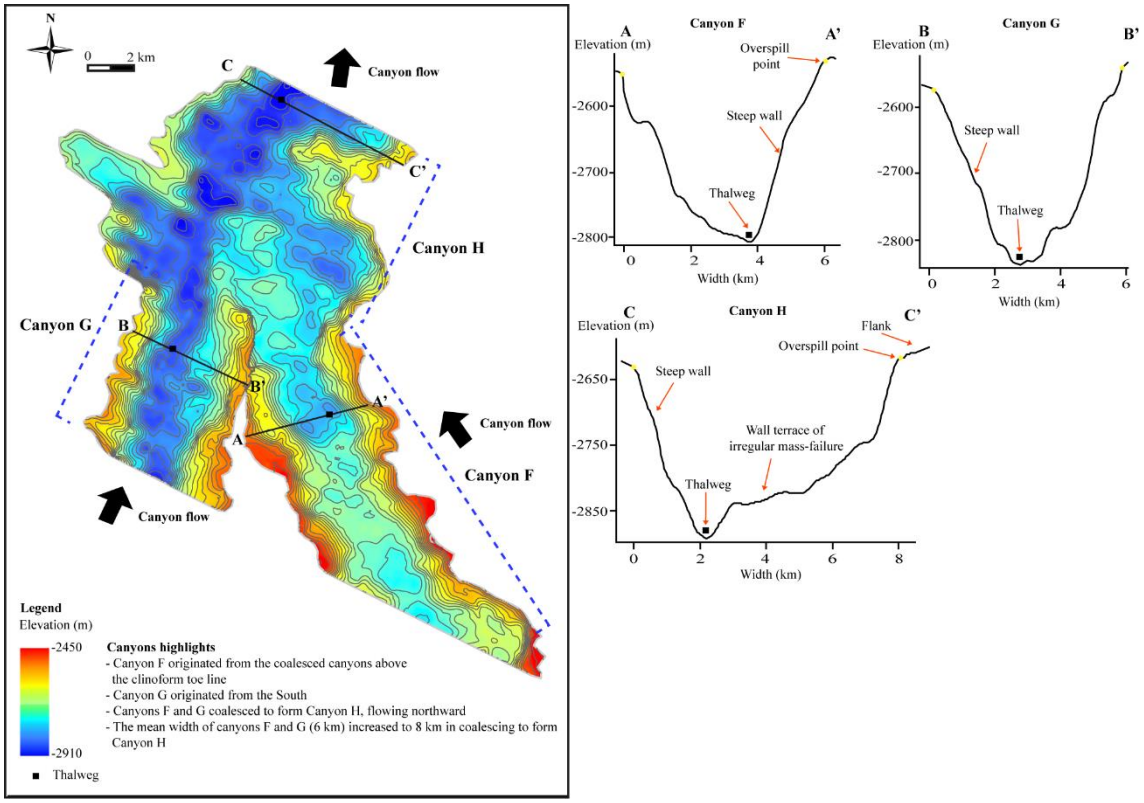

Figure 2.14: Cross-sectional views of the lower Mount Messenger Formation canyons below the clinoform toe line for Canyons F, G, and H. The main elements of the canyons are also highlighted.

2.6.2.2.3 Group 2 canyon network

The canyons in Group 2 consist of Canyons I and J, which developed on the northeastern side of the study area (Figure 2.9A). The course of the canyons cannot be fully mapped due to the limitation of the 3D seismic data coverage, however the length of each canyon within the study area is roughly 20 km (Figure 2.11A). The canyons developed on slopes ranging from 0.5 to 0.9º (Figure 2.10B). The range of elevation of the canyons is between -1800 m to -2400 m, with Canyon J formed roughly 100 m deeper than Canyon I near the beginning of the canyon course (Figure 2.15A). Based on this, I infer that Canyon J is older than Canyon I. Canyons in Group 2 merge at the clinoform toe line (at coalescing point 3; CP3) similar to canyons in Group 1 (Figure 2.9A).

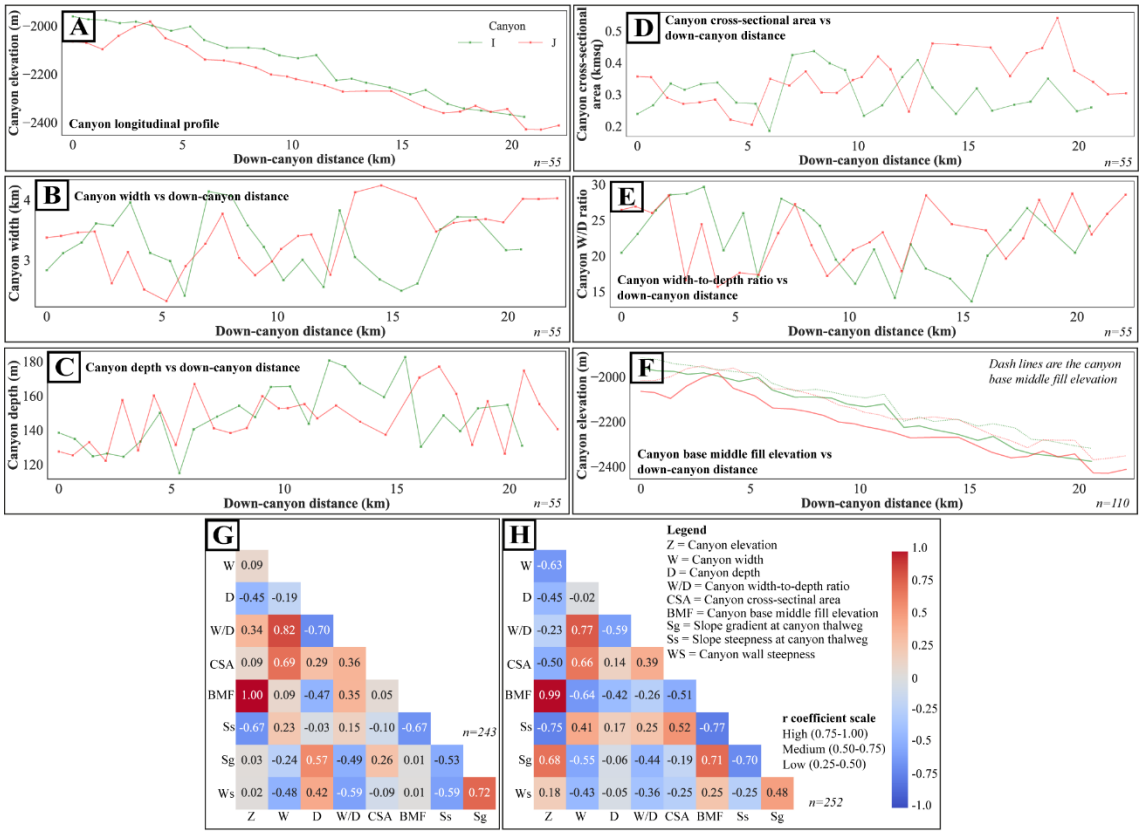

Figure 2.15: Cross-sectional metrics of the lower Mount Messenger Formation canyons are described as: (A) canyon elevation versus down-canyon distance, (B) canyon width versus down-canyon distance, (C) canyon depth versus down-canyon distance, (D) canyon cross-sectional area versus down-canyon distance, (E) canyon width-to-depth ratio versus down-canyon distance and (F) canyon elevation and base middle fill elevation versus down-canyon distance. Matrix of Pearson's correlation coefficient between the major morphometric parameters for (G) Canyon I and (H) Canyon J. n is the number of samples.

2.6.2.2.3.1 Morphometrics of Group 2 canyons

Both Canyon J and Canyon I are relatively straight, with an average sinuosity index of 1.1 (Figure 2.11B). Canyon J has slightly wider meanders than Canyon I, with a mean meander amplitude of 387 m versus 337 m (Figure 2.11D). The cross-sectional morphometrics of the canyons do not show a clear down-canyon trend (Figure 2.15B, C, D and E), while the Pearson's correlation coefficient shows mainly low to medium correlation (Figure 2.15G and

H). The cross-sectional shape of both canyons is a combination of moderate V-shape and U-shape profiles and with mean wall steepness of 10° (Figure 2.16).

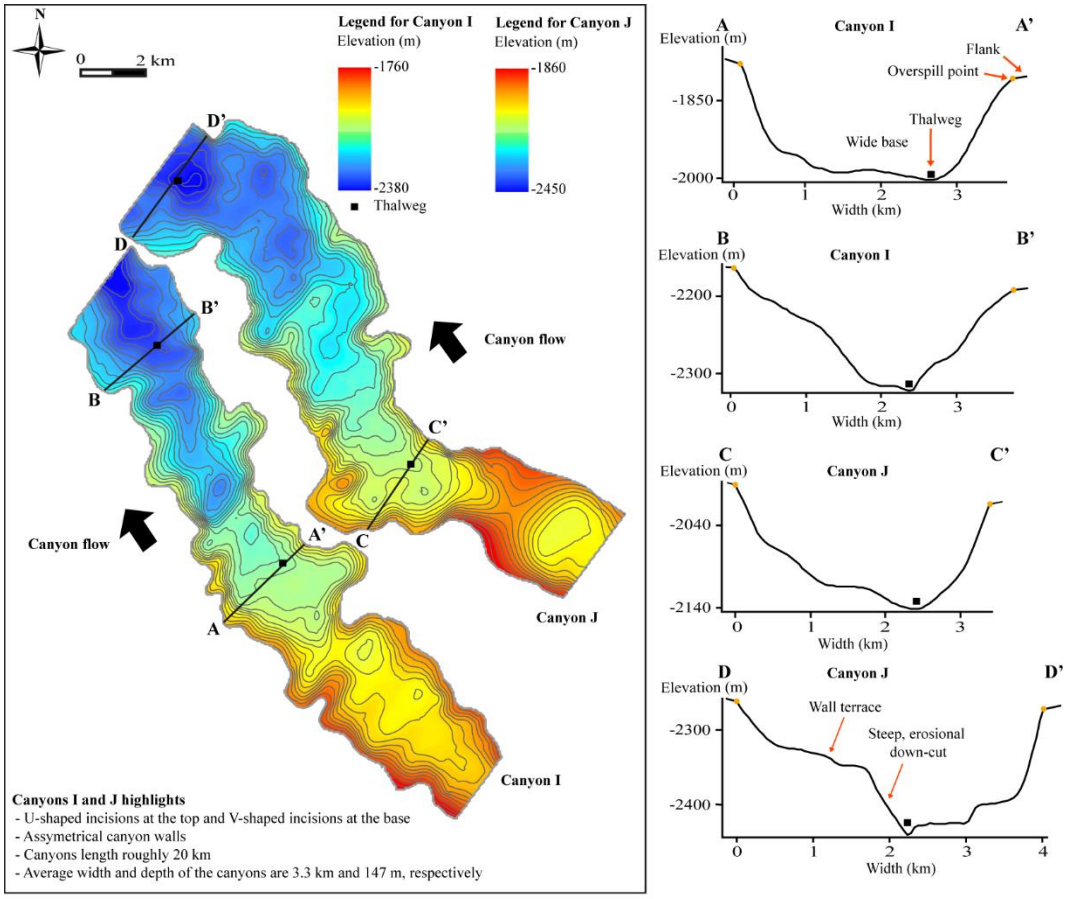

Figure 2.16: Cross-sectional geometry of the Group 2 lower Mount Messenger Formation canyons (i.e., Canyons I and J). The main elements of the canyons are also highlighted.

2.6.2.2.4 Lower canyon infill

Overall, the erosive base of the canyons displays an irregular profile due to multiple channel incisions of different magnitudes along the canyon course (Figure 2.17). Multiple re-incision surfaces were identified along the course of the canyons, but the surfaces cannot be mapped with high confidence due to the complex nature of the incisions. Below the clinoform toe line, the seismic profile of the canyons displays erosive surfaces formed through multiple

alternating canyon incision and infilling phases, which further complicates the attempt to map the incision surfaces.

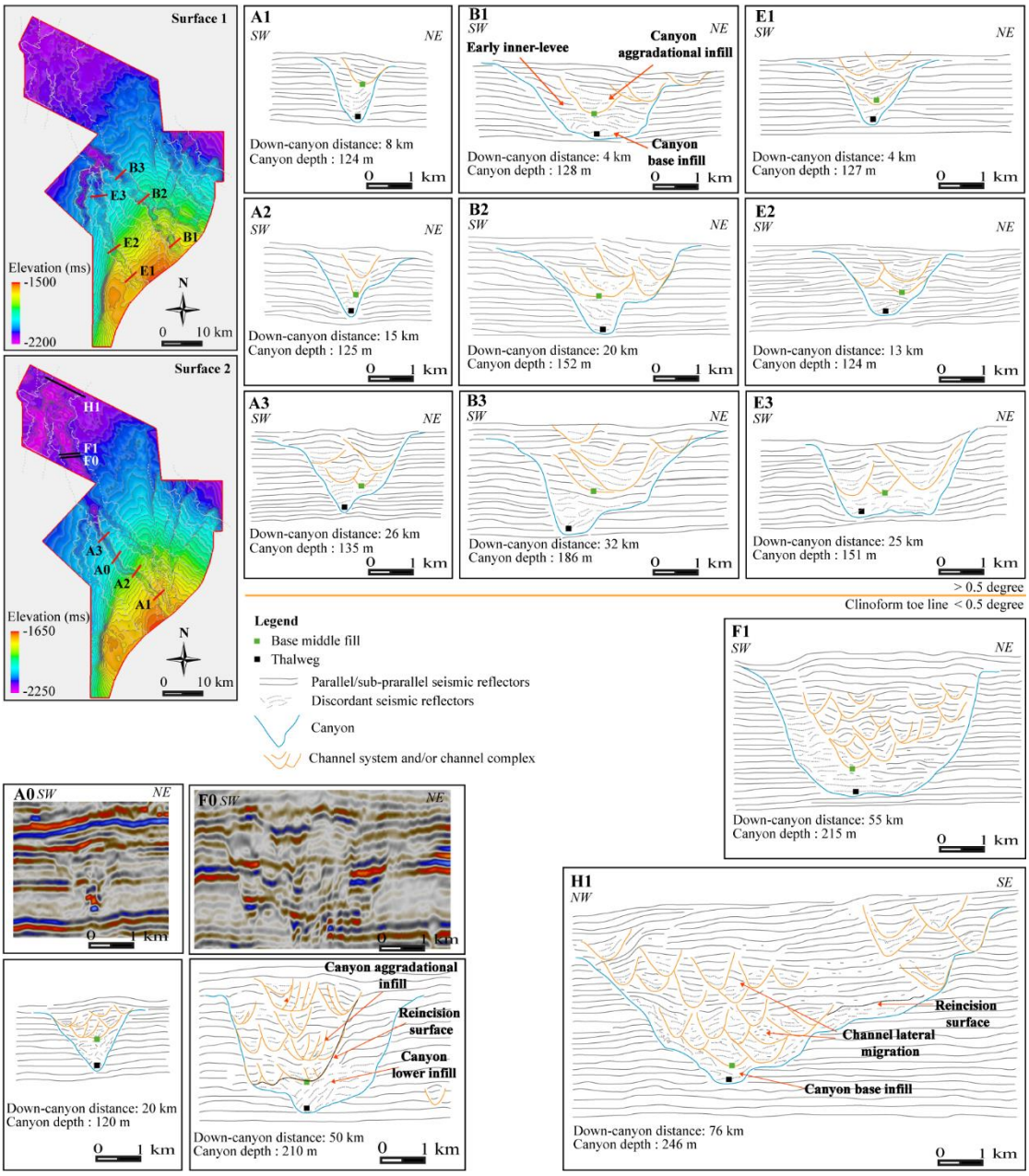

Figure 2.17: Plots showing the cross-sectional infill pattern of the lower Mount Messenger Formation canyons as well as the lower and upper infill characteristics of the canyons, based on mapping of seismic reflection surfaces.

2.6.2.2.5 Middle and upper canyon infill

The base of the middle canyon infill is marked by the onset of a mainly aggradational channel system (and/or channel complexes) formed within the canyon walls (Deptuck et al., 2007). Within lower Mount Messenger Formation canyons, numerous medium to large U-shape channels formed within the canyon walls were observed at depths ranging from 50 to 200 m (Figure 2.17). In some areas, successive channel incisions partly or entirely erode channel walls. In plan view, the canyons are flanked by extensive overbank deposits, especially the ones below the clinoform toe line. Overall, the base of the middle canyon fill profile mimics the canyon (base) longitudinal profile (Figures 2.12F and 2.15F).

2.6.2.3 Upper Mount Messenger Formation gully complex networks

The morphology and morphometrics of the upper Mount Messenger Formation slope-confined gully complexes are summarized in Figure 2.18 and Table 2.3. These complexes are enclosed in a thick prograding mudstone succession of Tongaporutuan age (~11-7.2 Ma). In the study area, the thickness of the prograding mudstone reaches roughly 700 m in Maui-3 and 430 m in Tui-1 drill holes. Throughout the Tongaporutuan, the seafloor slope increased from about 4^{o} at the base to about 11^{o} at the top of the succession. The steep clinoform (of oblique progradational pattern) is attributed to the rapid progradation of the shelf-break and reorientation of the slope, in addition to the strata thickening into the foot-walls of the reverse Cape Egmont Fault (Bull et al., 2019). In the study area, I grouped the gully complexes that formed on the steep clinoform slope in the upper Mount Messenger Formation interval into four groups (i.e., Groups 1, 2, 3 and 4) based on the major clinoform surfaces that bound them (Figure 2.4). The exact age of the surfaces cannot be determined from the available

biostratigraphic data, however for simplicity, Group 1 gully complexes are the oldest and Group 4 gully complexes are the youngest.

Gully complexes in Group 1 are bounded by the gentle slope of mainly bottomset surfaces (mean: 3.7°), and they are 0.67 – 2.62 km wide and 54 – 259 m deep. Groups 2 and 3 gully complexes developed within the foreset and bottomset sigmoidal-oblique clinoform wedges. However, some gullies in Group 2 (mean width: 1.18 km, mean depth: 108 m) developed within aggradational successions and, therefore, developed a much steeper slope surface (mean: 5.6°). Group 3 gully complexes (mean width: 1.03 km, mean depth: 105 m) formed on progradational clinoforms with less steep slopes than Group 2 (mean: 5.1°). Lastly, Group 4 gully complexes formed on steep sigmoid-shaped clinoform slopes (mean: 4.3 °) and have a width and depth range of 0.40 – 1.52 km and 20 – 158 m, respectively.

Gully networks within the upper Mount Messenger Formation are predominantly linear, sharp, symmetrical and V-shape, are oriented northwestward, and their down-slope length varies from 10 – 20 km. The sharp V-shape morphology is associated with the steep wall and flank of the gullies, and the average wall steepness angle is 20°. The spacing of the gullies ranges from 1.5 to 5 km, with most gullies spaced evenly and a few gullies exhibiting downslope convergence before transitioning to frontal splays or die out at the base of the clinoform slope.

The longitudinal profile of the gullies displays an overall very subtle concave profile as the slope gradient decreases from the topset to the bottomset of the clinofom (Figure 2.18C and D). The width and depth of individual gully complexes significantly increase sharply in the first ~2.5 km of their course. Then, the gully widths exhibit an overall gradual increase, and

the gully depth displays a decreasing trend before terminating at the base of the slope (Figure 2.18E and F).

In comparing the morphometrics of the gullies throughout the interval (from Group 1 to 4), the average gully width, depth and meander amplitude exhibit a decreasing trend from Group 1 to Group 4 (Figure 2.18E, F, H, I and Table 2.3). The correlation between the gully width and depth ranges from $R^2 = 0.06 – 0.43$ (Figure 2.18L). In seismic data, the gullies do not show significant evidence of lateral and vertical migration; instead, they display deep incisions into the background prograding mudstone. In addition, the gullies commonly display nested complexes with multiple incisions.

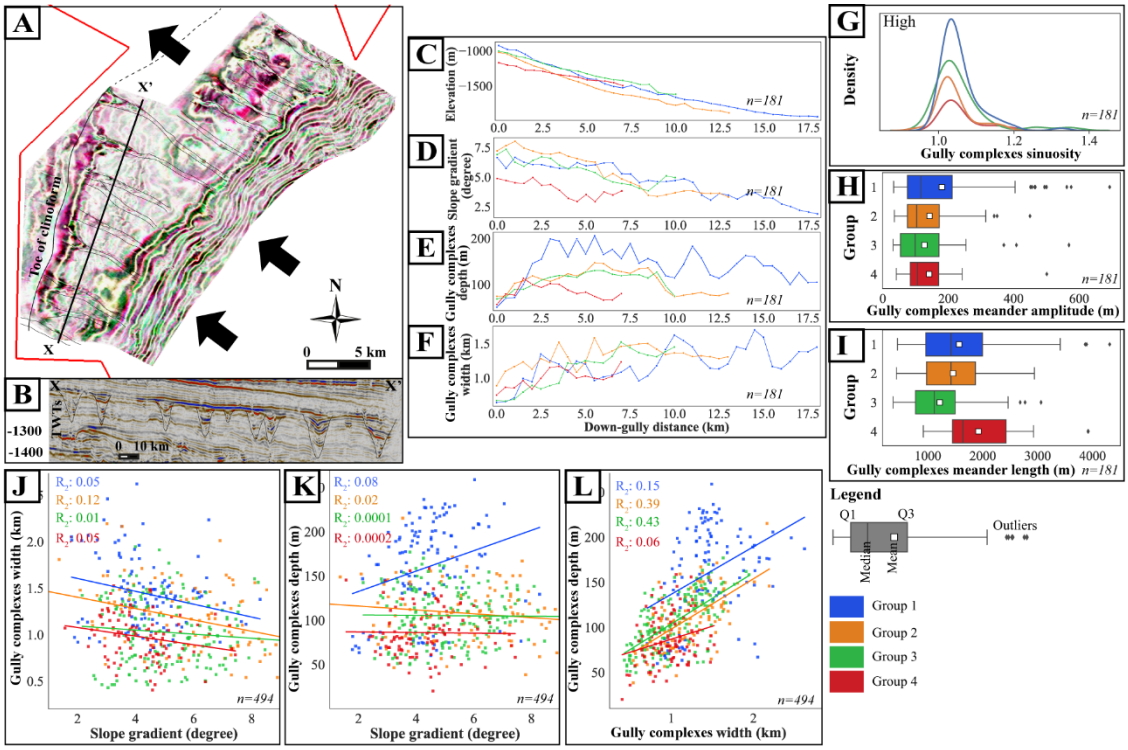

Figure 2.18: (A) and (B) An example of upper Mount Messenger Formation gully complexes on a stratigraphic horizon. (C) gully complexes longitudinal profile versus down-gully distance, (D) slope gradient at gully complexes thalweg versus down-gully distance, (E) gully complexes depth versus down-gully distance, (F) gully complexes width versus down-gully distance, (G) kernel density plot of gully complexes sinuosity, (H) gully complexes meander amplitude, (I) gully complexes meander length, (J) gully complexes width versus slope gradient, (K) gully complexes depth versus slope gradient and (L) gully complexes width versus depth. n is the number of samples.

Table 2.2: Morphometrics of lower Mount Messenger Formation canyons.

Lower Mount Messenger Fm. canyons	Width min-max, mean (km)	Depth min-max, mean (m)	Sinuosity min-max, mean	Meander length min-max, mean (m)	Meander amplitude min-max, mean (m)	Gradient at thalweg min-max, mean (°)
Group 1 canyons						
Canyon A	1.42-3.35, 2.08	104-153, 127	1.0-1.1, 1.1	1926-7935, 4970	116-824, 542	0.5-1.0, 0.8
Canyon B	1.70-4.38, 3.15	97-206, 157	1.0-1.3, 1.1	1915-5963, 4206	635-950, 720	0.5-1.0, 0.8
Canyon C	2.53-4.17, 3.39	94-162, 124	1.0-1.2, 1.1	2487-5264, 3486	401-879, 619	0.9-1.0, 0.9
Canyon D	1.35-2.98, 2.18	109-217, 177	1.1-1.3, 1.2	2149-2832, 2370	419-974, 718	0.45-0.60, 0.5
Canyon E	1.90-3.37, 2.67	87-191, 128	1.0-1.1, 1.1	2597-8158, 4373	50-773, 371	0.5-0.8, 0.7
Canyon F	4.70-7.75, 5.87	164-272, 227	1.1-1.4, 1.2	1260-4764, 3113	50-914, 683	0.4-0.5, 0.5
Canyon G	4.84-6.73, 5.83	201-344, 282	1.0-1.1, 1.0	1679-2789, 2280	75-380, 203	0.4-0.4, 0.4
Canyon H	7.19-8.92, 8.06	232-288, 249	1.0-1.2, 1.1	1771-3005, 2310	45-470, 314	0.44-0.46, 0.44
Group 2 canyons						
Canyon I	2.41-4.14, 3.23	115-183, 147	1.0-1.2, 1.1	1491-3026, 2336	169-604, 337	0.7-0.9, 0.8
Canyon J	2.32- 4.24, 3.38	122-177, 147	1.0-1.3, 1.1	2065-4222, 2908	50-836, 387	0.6-0.8, 0.8

Table 2.3: Morphometrics of upper Mount Messenger Formation gully complexes.

Upper Mount Messenger Fm. gully complexes	Width min-max, mean (km)	Depth min-max, mean (m)	Sinuosity min-max, mean	Meander length min-max, mean (m)	Meander amplitude min-max, mean (m)	Gradient at thalweg min-max, mean (degree)
Group 1	0.67-2.62, 1.30	54-259, 144	1.0-1.2, 1.1	445-3866, 1501	38-456, 142	1.1-6.0, 3.7
Group 2	0.54-2.19, 1.18	38-215, 108	1.0-1.2, 1.0	428-2940, 1459	36-450, 143	0.7-9.0, 5.6
Group 3	0.43-1.95, 1.03	50-177, 105	1.0-1.4, 1.1	368-3061, 1241	32-569, 129	2.2-9.1, 5.1
Group 4	0.40-1.52, 0.97	20-159, 86	1.0-1.2, 1.1	917-3923, 1919	41-170, 131	1.6-7.4, 4.3

2.7 Discussions

2.7.1 Synthesis of the geomorphology and morphometrics of sediment conduits in Taranaki Basin

My results show that the deposition of thick Miocene prograding wedges in Taranaki Basin is a function of high sediment supply beginning in the late-Early Miocene (Figure 2.3A and B), resulting in clinoforms with variable geometries and steepness (i.e., slope gradients). The upper Moki Formation and Mount Messenger Formation sediments both accumulated in various types of conduits, transporting the sediments to deep basin. In summary, the upper Moki Formation is dominated by small, sinuous, U-shape channel complexes in a very low-relief slope setting, whereas the lower Mount Messenger Formation is characterised by very large canyon networks in low-relief slope settings. By contrast, the upper Mount Messenger Formation consists of numerous linear, V-shape gully complexes that developed within a high-relief slope.

The variation in morphometrics between canyons, channels and gullies presented in this study mainly highlight how morphology of sediment conduits responds to changes in depositional slope gradient. By the early-Middle Miocene, sinuous upper Moki Formation channel complex networks developed, which routed sediment from south to north in the basin (Figure 2.7). At this time, the cross-sectional area and shape of channel complexes did not change significantly across the system (i.e., mean width: 1.1 km, mean depth: 67 m).

By the late-Middle Miocene, the slope began to prograde rapidly, and the dip of the regional slope reoriented to be northwest (Bull et al., 2019). During this time, the lower Mount

Messenger Formation canyon networks incised into the prograding slope surface, which had a gradient of 0.4-1.0°. At shallower slopes of less than 0.5°, canyon morphometrics are 1.8 to 4.7 times bigger than on steeper slopes of greater than 0.5° (mean width of 2.7 km, mean depth of 142 m and mean cross-sectional area of 0.22 km^2 *versus* mean width of 6.6 km and mean depth of 253 m and mean cross-sectional area of 1.04 km^2, respectively) (Figure 2.12B, C and Table 2.2). This shift in morphometrics occurs abruptly across the clinoform toe line.

Rapid slope progradation of the shelf break dominated much of the Late Miocene interval, resulting in the development of steep clinoform surfaces of up to 11° into which relatively straight upper Mount Messenger Formation gully complexes incised (Figure 2.18). The mean gully width and depth throughout the interval decreased from 1.30 to 0.97 km and 143.81 to 86 m, respectively, as the slope became steeper.

2.7.2 Slope gradient controls the morphometrics of sediment conduits

The morphology of channels in the upper Moki Formation is typical of deep-water sinuous channels (Kolla et al., 2007; Wynn et al., 2007; Posamentier et al., 2022). In seismic plan view, overbank splays and crevasse splays are not observed, implying that the sediment was contained within the incised channels with little to no avulsion and associated overtopping of the channel margins. This is likely to be a result of sediments being transported through the channels on the relatively flat slope (mean: 0.2°) and with no breaks in slope on its lower margins (Posamentier & Kolla, 2003). For similar reasons, the geometry of channel complexes did not significantly change throughout the study area in comparison with the lower Mount Messenger and upper Mount Messenger formation intervals.

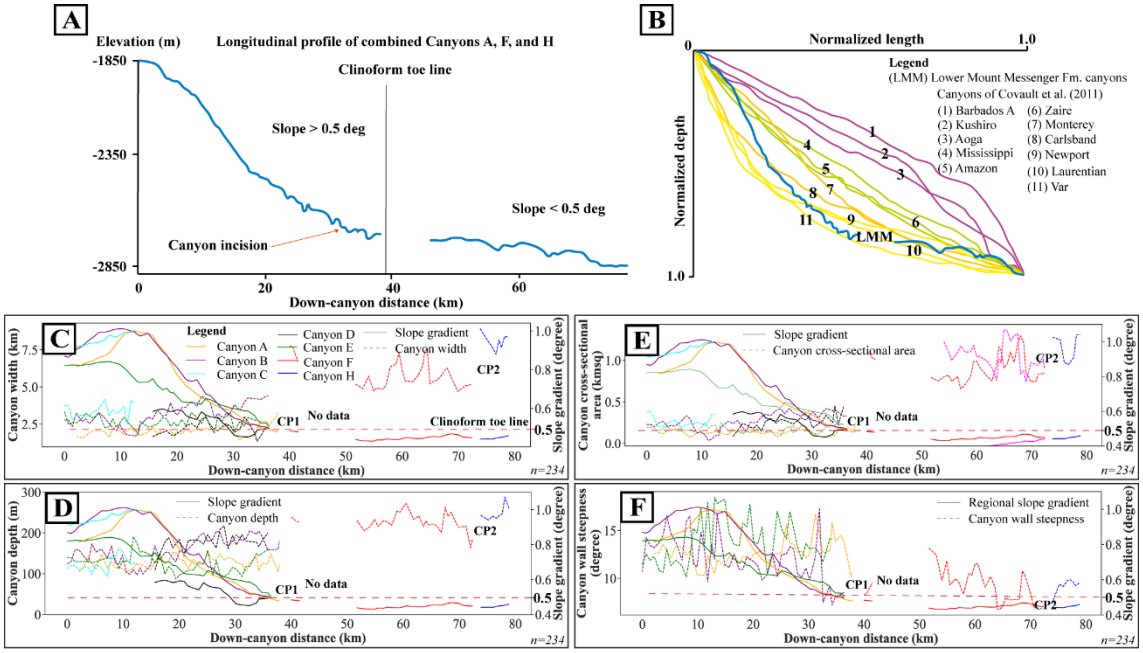

Figure 2.19: (A) Longitudinal profile of lower Mount Messenger Formation canyons showing their irregular incisions along their course. (B) Comparison between the lower Mount Messenger Formation canyons (blue) with the longitudinal profiles of other canyons globally. The lower Mount Messenger Formation canyons match the very concave profile of other canyons. The data source for the other canyons is from Covault et al. (2011). The depositional slope gradient relationship with the lower Mount Messenger Formation canyons (C) canyon width, (D) canyon depth, (E) canyon cross-sectional area and (F) canyon wall steepness. n is the number of samples.

The development of lower Mount Messenger Formation canyons on higher and more variable slope gradients due to rapid shelf progradation and reorientation is best explained by a power law of slope to distance (Mitchell, 2005; Gerber et al., 2009). In essence, the longitudinal profile of lower Mount Messenger Formation canyons displays a comparatively steep slope in proximal areas (i.e., 0.5-1.0°), and they transition to relatively flat slopes in their distal reaches (i.e., 0.4-0.5°). Such concave longitudinal profiles are similar to several modern submarine canyon and channel systems globally, such as the Laurentian and Var canyon-channel systems (Covault et al., 2011) (Figure 2.19A and B). These systems are highly erosional, with narrow shelves, steep slope gradients, and close proximity to sediment sources

with intense erosion from sediment-gravity flows (Covault et al., 2011). Very concave profiles are typical of underfilled basins. Taranaki Basin fits this definition during the Middle Miocene.

In general, the cross-sectional morphometrics of canyons increase down-slope due to an increase in frequency and acceleration of sediment gravity flows transporting granular material down-slope (Shepard et al., 1974; Shepard, 1981). This study emphasizes that the clinoform toe line (i.e., slope gradient: 0.5°) is a significant feature for controlling: (i) the spatial arrangement of canyon networks, including where they coalesce, and (ii), the position where a significant shift in the canyon cross-sectional morphometrics occurs. The position of the clinoform toe line, which is a major part of the clinoform structure, in turn, heavily influenced pre-existing topography within the basin (Lofi et al., 2003; Clairmont et al., 2020), as well as sediment supply. In the case of Taranaki Basin, regional subsidence during the Late Eocene to Early Oligocene profoundly affected the basin morphology by establishing a seafloor topography template across the basin, based on the concept in Covault et al. (2011). With bathymetric deepening towards the northwest, this resulted in the creation of vast accommodation for later sediment deposition.

The linear morphology of the upper Mount Messenger Formations gully networks is typical of gullies that form on a high gradient slope. Correspondingly, their morphometric parameters are in the range of the gullies measured by other workers e.g., Gales et al. (2013), Prélat et al. (2015), Shumaker et al. (2017) and Harishidayat et al. (2018). Morphometrics measured in this study shows that gullies form on steep slopes of over 5°, supporting the same findings of Micallef and Mountjoy (2011). The width and depth of gullies increase rapidly from their landward margins (~0-2.5 km). This is probably due to rapid incision of unconfined

sediment gravity flows accelerating down slope (Micallef & Mountjoy, 2011; Lintern et al., 2016) or slumping on the slope (Ricketts & Evenchick, 1999).

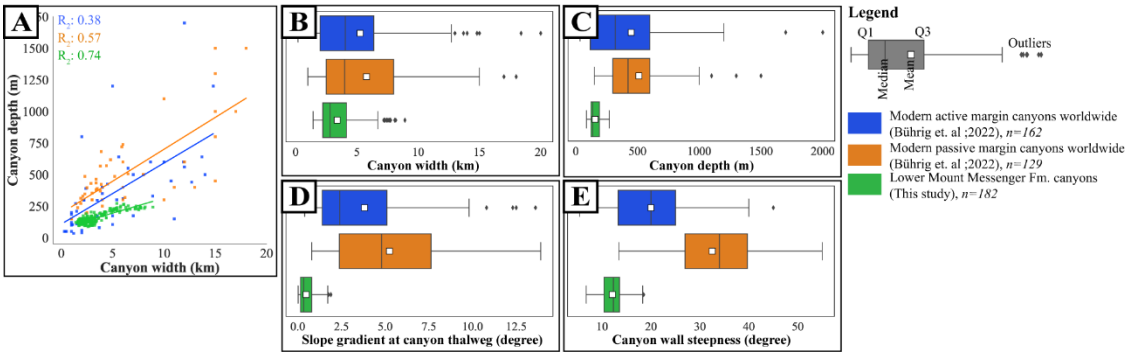

Figure 2.20: Comparison between the lower Mount Messenger Formation canyons and modern canyons globally. (A) Canyon depth versus width, (B) canyon width, (C) canyon depth, (D) slope gradient at canyon thalweg and (E) canyon wall steepness. The modern canyon morphometric measurements are from Bührig et al. (2022). n is the number of samples.

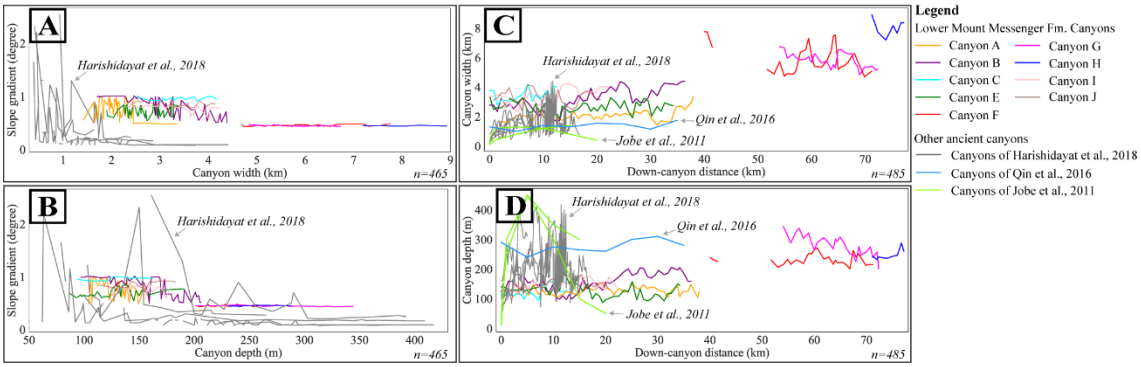

Figure 2.21: Comparison between lower Mount Messenger Formation canyons and other ancient canyon systems. (A) Slope gradient versus canyon width, (B) slope gradient versus canyon depth, (C) canyon width versus down-canyon distance and (D) canyon depth versus down-canyon distance. The down-canyon distance reflects the area of respective data. The ancient canyon morphometric measurements are from Jobe et al. (2011), Qin et al. (2016) and Harishidayat et al. (2018). n is the number of samples.

Overall, gully complexes show a trend of decreasing cross-sectional dimensions (i.e., width, depth and cross-sectional area) from Group 1 (at the base of the interval) to Group 4 (at the top of the interval) due to a depleted supply of sand. This is reflected in the transition from the sand-dominated Mount Messenger Formation to the mud-dominated Manganui Formation at the end of the Miocene (Figure 2.3C).

2.7.3 Comparison with other canyon systems globally

Canyon systems of the lower Mount Messenger Formation fall within the natural width and depth ranges of modern canyons, but their metrics sit towards the smaller end of global data with shallower cross-sectional metrics (Figure 2.20). However, correlation between width and depth within the lower Mount Messenger Formation canyons is higher than for modern canyons on both passive and active margins, with R2 values of 0.74, compared with 0.57 (passive) or 0.38 (active) (Bührig et al., 2022). The width and depth distributions of the lower Mount Messenger Formation canyons are narrow compared with modern canyons: the width range is 1.4 – 8.9 km (lower Mount Messenger Formation) versus 0.2 – 20 km (modern), and the depth range 87 – 344 m (lower Mount Messenger Formation) versus 35 – 2000 m (modern) (Figure 2.20B and C). This difference is attributed to: (i) Lower Mount Messenger Formation canyons being of Miocene age, and therefore on seismic data, sediment compaction has influenced the canyon morphometric measurements (Deptuck et al., 2007; Harishidayat et al., 2018) (modern canyons are less affected by sediment compaction) and (ii), the morphometrics of the lower Mount Messenger Formation canyons are concentrated on the lower slope margin, in contrast to other canyons for which the morphometrics are based on mean values from various basin physiographic setting. Similarly, the canyon thalweg gradient and the canyon wall steepness ranges of the lower Mount Messenger canyons are also narrow compared with

modern canyons. This variation is predominantly due to the position of the canyons being located at the clinothems terminations, where the slope gradient range is relatively minor.

In comparison to other ancient canyon systems, a significant portion of the morphometrics of the lower Mount Messenger Formation canyons are similar to the range of their counterparts (Figure 2.21). However, lower Mount Messenger Formation canyons have a higher width range and lower depth range than other ancient canyons. The range differences could be attributed to sediment properties such as grain size distribution (Hsu & Liu, 2010), flow patterns within canyons (Shepard et al., 1974), flow types within and around canyons (Talling, 2014), and flow volume (Qin et al., 2016), as well as other physical processes such as inner terrace architecture (Babonneau et al., 2004) and inner canyon erosion and mass failure (May et al., 1983; Qin et al., 2016).

In Taranaki Basin during the Middle Miocene to Late Miocene, the occurrence of numerous lower Mount Messenger Formation canyons is in tandem with the increasing sediment supply into the basin. This is not consistent with the conclusion made by Fisher et al. (2021), which suggested that canyons are associated with low to negligible sediment supply. The Taranaki Basin example I describe here may therefore be an outlier.

2.7.4 Source-to-sink environment significance

From a palaeogeography perspective, during the Miocene, the absence of canyons and large channel systems within the upper Moki Formation interval implies that sediment transport to deep Taranaki Basin was ineffective. This is due to the limited sand supply available during the early-Middle Miocene, which hindered the development of large channel complexes

(Figure 2.3C). However significant time-equivalent mudstone (Manganui Formation) was being deposited outside the channel complexes.

In contrast, the lower Mount Messenger Formation interval, having numerous canyons and channel networks, indicates the efficiency of sediment transfer to deep Taranaki Basin based on the concept in Stow and Mayall (2000) and in Posamentier and Kolla (2003). These sediments bypassed the study area as the canyons and channels routed voluminous sediment to the deeper basin towards the New Caledonia Trough (Bull et al., 2019). For the upper Mount Messenger Formation, the gully complexes died out at the base of the slope. Therefore, sediments during this interval were not delivered efficiently to the deeper parts of the basin, based on the concepts in Dalla Valle et al. (2013).

2.7.5 Reservoir exploration significance

The morphometrics of sediment conduits presented in this study have implications for understanding deep-water reservoir systems and especially the relationship between reservoir size and slope gradient. Previous reservoir exploration in the study area has focused mainly on Paleocene and Eocene strata of the Kapuni Group, which is the most significant commercial hydrocarbon reservoir system in Taranaki Basin (Bryant et al., 1994; Funnell et al., 2004), leaving the Middle Miocene interval relatively unexplored. The large cross-sectional areas of the lower Mount Messenger Formation canyon networks, including the thick interconnected aggradational channel infills show excellent reservoir characteristics, at least in terms of the size of the reservoirs (Clark & Pickering, 1996; Mayall & Kneller, 2021). Furthermore, oil and gas fields do occur in these reservoirs onshore in Taranaki Peninsula (i.e., Kaimiro, Cheal and Radnor fields). The thick prograding mudstone succession overtopping the canyons and channels acts as up-slope stratigraphic pinch-out traps for hydrocarbon accumulation in the up-

dip slope direction (McCaffrey & Kneller, 2001; Amy, 2019). Moreover, the inversion structures around the Maui Field (e.g. Manaia Anticline and Cape Egmont Fault) could assist in the migration and trapping of hydrocarbons (Seebeck et al., 2020). In other jurisdictions, high-nutrient slope facies can be source rocks due to low oxygen content along such margins (Bjorlykke, 2010).

The upper Moki and upper Mount Messenger Formation channel complexes are relatively small in comparison with the canyons and channel systems of the lower Mount Messenger Formation, and therefore their reservoir potential is limited by their smaller dimensions (Mayall & Kneller, 2021). Even though the upper Mount Messenger Formation gully networks have large dimensions, their infill is dominated by muddy deposits and therefore have low reservoir potential. My analysis offers improved data to help assess the reservoir potential of sediment conduits in Taranaki Basin.

2.8 Conclusions

Detailed seismic geomorphologic analysis of 3D seismic reflection data for the Moki and Mount Messenger formations in Taranaki Basin has enabled me to parameterize submarine canyon, channel, and gully networks within them. The results of this study show that there are robust differences between their cross-sectional and planform geomorphology. The following captures the major conclusions of this work:

1. The main sediment conduits are variable in their seismic geomorphology. The upper Moki Formation is dominated by sinuous channel complex networks. Canyon networks dominate the lower Mount Messenger Formation interval and they show numerous

aggradational channel formations. The upper Mount Messenger Formation is dominated by linear gully networks.

2. The development of the lower Mount Messenger canyons was strongly influenced by depositional slope. The clinoform toe line marks a rapid change in the cross-sectional area and shape, as well as the spatial arrangement of the canyon networks.

3. The development of the upper Moki Formation complex networks is typical of basin floor sinuous channels with high sinuosity and meander amplitude. In contrast, the development of the linear upper Mount Messenger Formation gully networks is heavily influenced by the steep prograding clinoform slope of the intervening mudstone strata.

2.9 References

Allen PA. *Sediment Routing Systems: First Concepts. In: Sediment Routing Systems: The Fate of Sediment from Source to Sink*. Cambridge: Cambridge University Press; 2017:3-19. doi:10.1017/9781316135754.002

Amblas, D., Ceramicola, S., Gerber, T. P., Canals, M., Chiocci, F. L., Dowdeswell, J. A., Harris, P. T., Huvenne, V. A. I., Lai, S. Y. J., Lastras, G., Iacono, C. L., Micallef, A., Mountjoy, J. J., Paull, C. K., Puig, P., & Sanchez-Vidal, A. (2018). Submarine Canyons and Gullies. In A. Micallef, S. Krastel, & A. Savini (Eds.), *Submarine Geomorphology* (pp. 251-272). Springer International Publishing. https://doi.org/10.1007/978-3-319-57852-1_14

Amy, L. A. (2019). A review of producing fields inferred to have upslope stratigraphically trapped turbidite reservoirs: Trapping styles (pure and combined), pinch-out formation, and depositional setting. *AAPG Bulletin*, *103*(12), 2861-2889. https://doi.org/10.1306/02251917408

Assis, C., Santos, H., & Schleicher, J. (2018). Colored and Linear Inversions to Relative Acoustic Impedance. *Geophysics*, *84*(2). https://doi.org/DOI:10.1190/geo2018-0185.1

Babonneau, N., Savoye, B., Cremer, M., & Bez, M. (2004). Multiple terraces within the deep incised Zaire Valley (ZaïAngo Project): are they confined levees? *Geological Society, London, Special Publications*, *222*(1), 91-114. https://doi.org/doi:10.1144/GSL.SP.2004.222.01.06

Baur, J. R., King, P. R., Stern, T., Leitner, B., Wood, L. J., Simo, T. T., & Rosen, N. C. (2010). Development and Seismic Geomorphology of a Miocene Slope Channel Megasystem, Offshore Taranaki Basin, New Zealand. In *Seismic Imaging of Depositional and Geomorphic Systems* (Vol. 30, pp. 0). SEPM Society for Sedimentary Geology. https://doi.org/10.5724/gcs.10.30.0618

Benson, S., & Cook, P. (2005). Underground geological storage. In G. Borm, D. Hawkins, & A. Lee (Eds.), *IPCC special report on carbon dioxide capture and storage* (pp. 197-265). Cambridge University Press.

Bjorlykke, K. (2010). *Petroleum Geoscience: From Sedimentary Environments to Rock Physics*. Springer Berlin Heidelberg. https://books.google.co.nz/books?id=bi8pd8JoTZcC

Brown, A. R. (2011). *Interpretation of three-dimensional seismic data*. Society of Exploration Geophysicists and American Association of Petroleum ….

Bryant, I. D., & Greenstr, C. W. (1995). Integrated 3-D Geological Modeling of the C1 Sands Reservoir, Maui Field, Offshore New Zealand. *AAPG Bulletin*, *79*. https://doi.org/10.1306/8d2b152a-171e-11d7-8645000102c1865d

Bryant, I. D., Marshall, M. G., Greenstreet, C. W., W.R, V., Cohen, J. M., & Stroemmen, J. F. (1994). Integrated Geological Reservoir Modelling of the Maui Field, Taranaki Basin, New Zealand. New Zealand Petroleum Conference, Wellington.

Bührig, L. H., Colombera, L., Patacci, M., Mountney, N. P., & McCaffrey, W. D. (2022). Tectonic Influence on the Geomorphology of Submarine Canyons: Implications for Deep-Water Sedimentary Systems [Original Research]. *Frontiers in Earth Science*, *10*. https://doi.org/10.3389/feart.2022.836823

Bull, S., Hill, M., Strogen, D., Arnot, M., Seebeck, H., Kroeger, K., & Zhu, H. (2015). Seismic reflection interpretation, static modelling and velocity modelling of the southern Taranaki Basin (4D Taranaki Project). *GNS Science Report*, *2*.

Bull, S., Nicol, A., Strogen, D., Kroeger, K., & Seebeck, H. S. (2019). Tectonic controls on Miocene sedimentation in the Southern Taranaki Basin and implications for New Zealand plate boundary deformation. *Basin Research*, *31*(2), 253-273. https://doi.org/10.1111/bre.12319

Bussell, M. R. (1994). Seismic interpretation of the Moki Formation on the Maui 3D survey, Taranaki Basin. New Zealand Petroleum Conference, Wellington.

Chopra, S., Castagna, J., & Portniaguine, O. (2006). Thin bed reflectivity inversion. In *SEG Technical Program Expanded Abstracts 2006* (pp. 2057-2061). Society of Exploration Geophysicists. https://doi.org/doi:10.1190/1.2369941

10.1190/1.2369941

Clairmont, R., Kolawole, F., Omale, A. P., & Bedle, H. (2020). Controls of pre-existing structures on clinoform architecture and the associated progradational system elements. *Basin Research*, *33*(2), 875-902. https://doi.org/10.1111/bre.12487

Clark, J. D., & Pickering, K. T. (1996). Architectural elements and growth patterns of submarine channels: Application to hydrocarbon exploration. *AAPG Bulletin*, *80*(2), 194-221.

Cooper, R., Agterberg, F. P., Alloway, B., Beu, A., Campbell, H., Crampton, J. S., Crouch, E., Crundwell, M., Graham, I. J., Hollis, C., Jones, C., Kamp, P., Mildenhall, D. C., Morgans, H., Naish, T. R., Raine, J. I., Roncaglia, L., Sadler, P. M., Schiøler, P., & Wilson, G. (2004). The New Zealand Geological Timescale. *Institute of Geological and Nuclear Sciences. Monograph*, 22-284.

Covault, J. A. (2011). Submarine Fans and Canyon-Channel Systems: A Review of Processes, Products, and Models. *Nature Education Knowledge*.

Covault, J. A., Fildani, A., Romans, B. W., & McHargue, T. (2011). The natural range of submarine canyon-and-channel longitudinal profiles. *Geosphere*, *7*(2), 313-332. https://doi.org/10.1130/ges00610.1

Crowhurst, P., Green, P., & Kamp, P. (2002). Appraisal of (U-Th)/He Apatite Thermochronology as a Thermal History Tool for Hydrocarbon Exploration: An Example from the Taranaki Basin, New Zealand. *AAPG Bulletin*, *86*. https://doi.org/10.1306/61EEDD82-173E-11D7-8645000102C1865D

Dalla Valle, G., Gamberi, F., Trincardi, F., Baglioni, L., Errera, A., & Rocchini, P. (2013). Contrasting slope channel styles on a prograding mud-prone margin. *Marine and Petroleum Geology*, *41*, 72-82. https://doi.org/10.1016/j.marpetgeo.2012.02.003

Deptuck, M. E., Sylvester, Z., Pirmez, C., & O'Byrne, C. (2007). Migration–aggradation history and 3-D seismic geomorphology of submarine channels in the Pleistocene Benin-major Canyon, western Niger Delta slope. *Marine and Petroleum Geology*, *24*(6-9), 406-433. https://doi.org/10.1016/j.marpetgeo.2007.01.005

Field, M. E., Gardner, J. V., & Prior, D. B. (1999). Geometry and significance of stacked gullies on the northern California slope. *Marine Geology*, *154*(1), 271-286. https://doi.org/https://doi.org/10.1016/S0025-3227(98)00118-2

Fisher, W. L., Galloway, W. E., Steel, R. J., C.Olariu, Kerans, C., & Mohrig, D. (2021). Deep-water Depositional Systems supplied by Shelf-incising Submarine Canyons: 2

Recognition and Significance in the Geologic Record. *Earth-Science Reviews*, *214*. https://doi.org///doi.org/10.1016/j.earscirev.2021.103531

Funnell, R., Stagpoole, V. M., Nicol, A., McCormack, N., & Reyes, A. G. (2004, 7th-10th March). Petroleum generation and implications for migration: a Maui Field charge study, Taranaki Basin. 2004 New Zealand Petroleum Conference Proceedings, New Zealand,

Gales, J. A., Larter, R. D., Mitchell, N. C., & Dowdeswell, J. A. (2013). Geomorphic signature of Antarctic submarine gullies: Implications for continental slope processes. *Marine Geology*, *337*, 112-124. https://doi.org/https://doi.org/10.1016/j.margeo.2013.02.003

Gamboa, D., Alves, T. M., & Cartwright, J. (2012). A submarine channel confluence classification for topographically confined slopes. *Marine and Petroleum Geology*, *35*(1), 176-189. https://doi.org/10.1016/j.marpetgeo.2012.02.011

Gerber, T. P., Amblas, D., Wolinsky, M. A., Pratson, L. F., & Canals, M. (2009). A model for the long-profile shape of submarine canyons. *Journal of Geophysical Research: Earth Surface*, *114*(F3). https://doi.org/https://doi.org/10.1029/2008JF001190

Hansen, R. J., & Kamp, P. J. J. (2002). Evolution of the Giant Foresets Formation, northern Taranaki Basin, New Zealand. Conference held at Auckland. Conference Contribution retrieved from https://hdl.handle.net/10289/3617

Harishidayat, D., Omosanya, K. O., Johansen, S. E., Eruteya, O. E., & Niyazi, Y. (2018). Morphometric analysis of sediment conduits on a bathymetric high: Implications for palaeoenvironment and hydrocarbon prospectivity [https://doi.org/10.1111/bre.12291]. *Basin Research*, *30*(5), 1015-1041. https://doi.org/https://doi.org/10.1111/bre.12291

Harris, P. T., & Whiteway, T. (2011). Global distribution of large submarine canyons: Geomorphic differences between active and passive continental margins. *Marine Geology*, *285*(1), 69-86. https://doi.org/https://doi.org/10.1016/j.margeo.2011.05.008

Hayward, B. W., & Wood, R. A. (1989). *Computer-generated geohistory plots for Taranaki drillhole sequences*. New Zealand Geological Survey.

Heinemann, N., Booth, M. G., Haszeldine, R. S., Wilkinson, M., Scafidi, J., & Edlmann, K. (2018). Hydrogen storage in porous geological formations – onshore play opportunities in the midland valley (Scotland, UK). *International Journal of Hydrogen Energy*, *43*(45), 20861-20874. https://doi.org/10.1016/j.ijhydene.2018.09.149

Hewlett, J. S., Jordan, D. W., Weimer, P., & Posamentier, H. (1993). Stratigraphic and Combination Traps Within a Seismic Sequence Framework, Miocene Stevens Turbidites, Bakersfield Arch, California. In *Siliciclastic Sequence Stratigraphy: Recent Developments and Applications* (Vol. 58, pp. 0). American Association of Petroleum Geologists. https://doi.org/10.1306/m58581c6

Higgs, K., & King, P. (2018). Sandstone provenance and sediment dispersal in a complex tectonic setting: Taranaki Basin, New Zealand. *Sedimentary Geology*, *372*. https://doi.org/10.1016/j.sedgeo.2018.05.004

Hsu, R. T., & Liu, J. T. (2010). In-situ estimations of the density and porosity of flocs of varying sizes in a submarine canyon. *Marine Geology*, *276*(1-4), 105-109. https://doi.org/10.1016/j.margeo.2010.07.003

Hughes, D. J., Shimmield, T. M., Black, K. D., & Howe, J. A. (2015). Ecological impacts of large-scale disposal of mining waste in the deep sea. *Sci Rep*, *5*, 9985. https://doi.org/10.1038/srep09985

Huvenne, V. A. I., & Davies, J. S. (2014). Towards a new and integrated approach to submarine canyon research. *Deep Sea Research Part II: Topical Studies in Oceanography*, *104*, 1-5. https://doi.org/10.1016/j.dsr2.2013.09.012

Kamp, P. J.J., Green, P., & White, S. (1989). Fission track analysis reveals character of collisional tectonics in New Zealand. *Tectonics*, *8*, 169-195. https://doi.org/10.1029/TC008i002p00169

Jobe, Z. R., Lowe, D. R., & Uchytil, S. J. (2011). Two fundamentally different types of submarine canyons along the continental margin of Equatorial Guinea. *Marine and Petroleum Geology*, *28*(3), 843-860. https://doi.org/10.1016/j.marpetgeo.2010.07.012

Kallweit, R. S., & Wood, L. C. (1982). The limits of resolution of zero-phase wavelets. *Geophysics*, *47*(7), 1035-1046. https://doi.org/10.1190/1.1441367

Kamp, P. J.J., & Green, P. (1990). Thermal and tectonic history of selected Taranaki Basin (New Zealand) wells assessed by apatite fission track analysis. *Aapg Bulletin - AAPG BULL*, *74*, 1401-1419.

Kane, I. A., Clare, M. A., Miramontes, E., Wogelius, R., Rothwell, J. J., Garreau, P., & Pohl, F. (2020). Seafloor microplastic hotspots controlled by deep-sea circulation. *Science*, *368*(6495), 1140-1145. https://doi.org/doi:10.1126/science.aba5899

King, P., & Thrasher, G. P. (1996). Cretaceous-Cenozoic Geology and Petroleum Systems of the Taranaki Basin, New Zealand. *Insitute of Geological and Nuclear Science Monograph*, *13*(Part 1 and 2).

Kroeger, K. F., Thrasher, G. P., & Sarma, M. (2019). The Evolution of a Middle Miocene Deep-water Sedimentary System in Northwestern New Zealand (Taranaki Basin): Depositional Controls and Mechanisms. *Marine and Petroleum Geology*, *101*, 355-372. https://doi.org/10.1016/j.marpetgeo.2018.11.052

Lancaster, S., & Whitcombe, D. (2000). Fast-track 'coloured' Inversion. 2000 SEG Annual Meeting,

Lemay, M., Grimaud, J.-L., Cojan, I., Rivoirard, J., & Ors, F. (2020). Geomorphic variability of submarine channelized systems along continental margins: Comparison with fluvial meandering channels. *Marine and Petroleum Geology*, *115*. https://doi.org/10.1016/j.marpetgeo.2020.104295

Lintern, D. G., Hill, P. R., & Stacey, C. (2016). Powerful unconfined turbidity current captured by cabled observatory on the Fraser River delta slope, British Columbia, Canada. *Sedimentology*, *63*(5), 1041-1064. https://doi.org/https://doi.org/10.1111/sed.12262

Lofi, J., Rabineau, M., Gorini, C., Berne, S., Clauzon, G., De Clarens, P., Tadeu Dos Reis, A., Mountain, G. S., Ryan, W. B. F., Steckler, M. S., & Fouchet, C. (2003). Plio–Quaternary prograding clinoform wedges of the western Gulf of Lion continental margin (NW Mediterranean) after the Messinian Salinity Crisis. *Marine Geology*, *198*(3-4), 289-317. https://doi.org/10.1016/s0025-3227(03)00120-8

Lonergan, L., Jamin, N. H., Jackson, C. A. L., & Johnson, H. D. (2013). U-shaped slope gully systems and sediment waves on the passive margin of Gabon (West Africa). *Marine Geology*, *337*, 80-97. https://doi.org/10.1016/j.margeo.2013.02.001

Maurya, S. P., & Singh, N. P. (2017, 30th November -01st December 2017). *Seismic Colored Inversion: A Fast Way to Estimate Rock Properties from the Seismic Data* Challenges in Petro-physical Evaluation and Rock physics Modelling of Carbonate Reservoirs, Likely Elucidations & Way Forward, Victor Menezes Convention Centre (VMCC), IIT Bombay, India.

May, J. A., Warme, J. E., Slater, R. A., Stanley, D. J., & Moore, G. T. (1983). Role of Submarine Canyons on Shelfbreak Erosion and Sedimentation: Modern and Ancient Examples. In *The Shelfbreak: Critical Interface on Continental Margins* (Vol. 33, pp. 0). SEPM Society for Sedimentary Geology. https://doi.org/10.2110/pec.83.06.0315

Mayall, M., & Kneller, B. (2021). Seismic interpretation workflows for deep-water systems: A practical guide for the subsurface. *AAPG Bulletin*, *105*(11), 2127-2157. https://doi.org/10.1306/05262120094

McCaffrey, W., & Kneller, B. (2001). Process Controls on the Development of Stratigraphic Trap Potential on the Margins of Confined Turbidite Systems and Aids to Reservoir Evaluation. *AAPG Bulletin*, *85*(6), 971-988. https://doi.org/10.1306/8626ca41-173b-11d7-8645000102c1865d

Miall, A. D. (2002). Architecture and Sequence Stratigraphy of Pleistocene Fluvial Systems in the Malay Basin, Based on Seismic Time-Slice Analysis. *AAPG Bulletin*, *86*.

Micallef, A., & Mountjoy, J. J. (2011). A topographic signature of a hydrodynamic origin for submarine gullies. *Geology*, *39*(2), 115-118. https://doi.org/10.1130/g31475.1

Mitchell, N. C. (2005). Interpreting long-profiles of canyons in the USA Atlantic continental slope. *Marine Geology*, *214*(1), 75-99. https://doi.org/https://doi.org/10.1016/j.margeo.2004.09.005

Normark, W. R., Posamentier, H., & Mutti, E. (1993). Turbidite systems: State of the art and future directions [https://doi.org/10.1029/93RG02832]. *Reviews of Geophysics*, *31*(2), 91-116. https://doi.org/https://doi.org/10.1029/93RG02832

NZP&M. (2018). *New Zealand Petroleum Exploration Data Pack,* New Zealand Petroleum and Minerals.

Othman, A. A. A., Fathy, M., & Negm, A. (2019). Identification of channel geometries applying seismic attributes and spectral decomposition techniques, Temsah Field, Offshore East Nile Delta, Egypt. *NRIAG Journal of Astronomy and Geophysics*, *7*(1), 52-61. https://doi.org/10.1016/j.nrjag.2018.04.001

Palm, F. A., Peakall, J., Hodgson, D. M., Marsset, T., Silva Jacinto, R., Dennielou, B., Babonneau, N., & Wright, T. J. (2021). Width variation around submarine channel bends: Implications for sedimentation and channel evolution. *Marine Geology*, *437*, 106504. https://doi.org/https://doi.org/10.1016/j.margeo.2021.106504

Patruno, S., Hampson, G. J., & Jackson, C. A. L. (2015). Quantitative characterisation of deltaic and subaqueous clinoforms. *Earth-Science Reviews*, *142*, 79-119. https://doi.org/https://doi.org/10.1016/j.earscirev.2015.01.004

Peakall, J., McCaffrey, B., & Kneller, B. (2000). A Process Model for the Evolution, Morphology, and Architecture of Sinuous Submarine Channels. *Journal of Sedimentary Research*, *70*(3), 434-448. https://doi.org/10.1306/2dc4091c-0e47-11d7-8643000102c1865d

Peakall, J., & Sumner, E. J. (2015). Submarine channel flow processes and deposits: A process-product perspective. *Geomorphology*, *244*, 95-120. https://doi.org/10.1016/j.geomorph.2015.03.005

Pirmez, C., Pratson, L. F., & Steckler, M. S. (1998). Clinoform development by advection-diffusion of suspended sediment: Modeling and comparison to natural systems. *Journal of Geophysical Research: Solid Earth*, *103*(B10), 24141-24157. https://doi.org/https://doi.org/10.1029/98JB01516

Posamentier, H. W., & Kolla, V. (2003). Seismic Geomorphology and Stratigraphy of Depositional Elements in Deep-Water Settings. *Journal of Sedimentary Research*, *73*(3), 367–388. https://doi.org/https://doi.org/10.1306/111302730367 (SEPM (Society for Sedimentary Geology))

Prélat, A., Pankhania, S. S., Jackson, C. A. L., & Hodgson, D. M. (2015). Slope gradient and lithology as controls on the initiation of submarine slope gullies; Insights from the North Carnarvon Basin, Offshore NW Australia. *Sedimentary Geology*, *329*, 12-17. https://doi.org/https://doi.org/10.1016/j.sedgeo.2015.08.009

Qin, Y., Alves, T. M., Constantine, J., & Gamboa, D. (2016). Quantitative seismic geomorphology of a submarine channel system in SE Brazil (Espírito Santo Basin): Scale comparison with other submarine channel systems. *Marine and Petroleum Geology*, *78*, 455-473. https://doi.org/10.1016/j.marpetgeo.2016.09.024

Raza, A., Gholami, R., Rezaee, R., Bing, C. H., Nagarajan, R., & Hamid, M. A. (2018). CO2 storage in depleted gas reservoirs: A study on the effect of residual gas saturation. *Petroleum*, *4*(1), 95-107. https://doi.org/10.1016/j.petlm.2017.05.005

Ricketts, B. D., & Evenchick, C. A. (1999). Shelfbreak gullies; products of sea-level lowstand and sediment failure; examples from Bowser Basin, northern British Columbia. *Journal of Sedimentary Research*, *69*(6), 1232-1240. https://doi.org/10.2110/jsr.69.1232

Roncaglia, M., M., P., C. M., Miko., F., & G., M. H. E. (2013). *Well log stratigraphy in the central and southern offshore area of the Taranaki Basin, New Zealand*. Lower Hutt : GNS Science.

Seebeck, H., Thrasher, G. P., & Viskovic, G. P. (2020). Inversion history of the northern Tasman Ridge, Taranaki Basin, New Zealand: implications for petroleum migration and accumulation. *New Zealand Journal of Geology and Geophysics*, *63*(3), 299-323. https://doi.org/10.1080/00288306.2019.1695633

Shanmugam, G. (2016). Submarine fans: A critical retrospective (1950–2015). *Journal of Palaeogeography*, *5*(2), 110-184. https://doi.org/10.1016/j.jop.2015.08.011

Shepard, F. P. (1965). Types of submarine valleys. *American Association of Petroleum Geologists Bulletin*, *49*(3), 304-310.

Shepard, F. P. (1981). Submarine Canyons: Multiple Causes and Long-Time Persistence1. *AAPG Bulletin*, *65*(6), 1062-1077. https://doi.org/10.1306/03b59459-16d1-11d7-8645000102c1865d

Shepard, F. P., Marshall, N. F., & McLoughlin, P. A. (1974). Currents in submarine canyons. *Deep Sea Research and Oceanographic Abstracts*, *21*(9), 691-706. https://doi.org/https://doi.org/10.1016/0011-7471(74)90077-1

Shumaker, L. E., Jobe, Z. R., & Graham, S. A. (2017). Evolution of submarine gullies on a prograding slope: Insights from 3D seismic reflection data. *Marine Geology*, *393*, 35-46. https://doi.org/10.1016/j.margeo.2016.06.006

Shumaker, L. E., Jobe, Z. R., Johnstone, S. A., Pettinga, L. A., Cai, D., & Moody, J. D. (2018). Controls on submarine channel-modifying processes identified through

morphometric scaling relationships. *Geosphere*, *14*(5), 2171-2187. https://doi.org/10.1130/ges01674.1

Stow, D. A. V., & Mayall, M. (2000). Deep-water sedimentary systems: New models for the 21st century. *Marine and Petroleum Geology*, *17*(2), 125-135. https://doi.org/https://doi.org/10.1016/S0264-8172(99)00064-1

Strogen, D. P., Baur, J. R., Bland, K. J., King, P. R., Vonk, A. J., & Kamp, P. J. J. (2011). *Updated paleogeographic maps for the Taranaki Basin and surrounds* (GNS Science Report 2010/53, Issue.

Strong, N., & Paola, C. (2008). Valleys that never were: Time surfaces versus stratigraphic surfaces. *Journal of Sedimentary Research*, *78*, 579-593. https://doi.org/10.2110/jsr.2010.007

Sylvester, Z., Pirmez, C., & Cantelli, A. (2011). A model of submarine channel-levee evolution based on channel trajectories: Implications for stratigraphic architecture. *Marine and Petroleum Geology*, *28*(3), 716-727. https://doi.org/10.1016/j.marpetgeo.2010.05.012

Talling, P. J. (2014). On the triggers, resulting flow types and frequencies of subaqueous sediment density flows in different settings. *Marine Geology*, *352*, 155-182. https://doi.org/10.1016/j.margeo.2014.02.006

Taner, M. T. (2001). Seismic Attributes. *26*(7), 48-56.

Tippett, J., & Kamp, P. J.J. (1993). Fission Track Analysis of the Late Cenozoic Vertical Kinematics of Continental Pacific Crust, South Island, New Zealand. *Journal of Geophysical Research*, *981*. https://doi.org/10.1029/92JB02115

Weimer, P., & Slatt, R. M. (2004). Petroleum Systems of Deepwater Settings. In *Petroleum Systems of Deepwater Settings* (pp. i-xviii).

Widess, M. B. (1973). How thin is a thin bed? *Geophysics*, *38*(6), 1176-1180. https://doi.org/10.1190/1.1440403

Wynn, R. B., Cronin, B. T., & Peakall, J. (2007). Sinuous deep-water channels: Genesis, geometry and architecture. *Marine and Petroleum Geology*, *24*(6-9), 341-387. https://doi.org/10.1016/j.marpetgeo.2007.06.001

Zeng, H. (2013). Stratal slice: The next generation. *The Leading Edge*.

Zeng, H., Backus, M. M., Barrow, K. T., & Tyler, N. (1998). Stratal Slicing, Part 1: Realistic 3D Seismic Model. *Geophysics*, *63*.

Zeng, H., Hentz, T. F., & Wood, L. J. (2001). Stratal Slicing of Miocene-Pliocene Sediments in Vermilion Block 50-Tiger Shoal Area, Offshore Louisiana. *The Leading Edge*.

Chapter 3

Critical re-assessment of Middle and Late Miocene submarine fans in offshore southern and western Taranaki Basin, New Zealand, to update the paleogeography[1]

3.1 Introduction

There is continuing interest amongst the petroleum exploration sector and the research community in the characteristics and distribution of ancient deepwater sedimentary systems. The increasing coverage and availability of 3D seismic reflection datasets, coupled with the availability of sophisticated seismic reflection mapping methods (e.g., Posamentier et al., 2022), have contributed to this interest. In parallel, there have been conceptual developments in the marine geomorphology of Recent distributary sedimentary systems, such as channel networks, submarine fans, and continental slope debris flows (e.g., Stow and Mayall, 2000; Shanmugam, 2013; Mayall and Kneller, 2021; Mitchell et al., 2023). One method in particular, seismic amplitude extraction, is widely used in mapping ancient depositional systems, such as fans. However it is now recognized that detuning of seismic reflection data within the interval of interest must be undertaken prior to amplitude extraction to avoid tuning-related effects that possibly result in erroneous geological interpretations, leading to inaccurate paleogeographical maps (Bunt, 2015; Francis, 2015; Ab Fatah et al., 2016; Francis, 2016; Márquez et al., 2021).

[1]A version of this chapter has been published in Marine and Petroleum Geology: Kamaruzaman, E. H., La Croix, A. D., & Kamp, P. J. J. (2024). Critical re-assessment of Middle and Late Miocene submarine fans in offshore southern and western Taranaki Basin, New Zealand, to update the paleogeography. Marine and Petroleum Geology, 161, 106664. https://doi.org/https://doi.org/10.1016/j.marpetgeo.2023.106664. The published version is included in Appendix A-ii.

In my work reported I consider this to have been the case with respect to the Miocene submarine fans mapped by prior researchers in southern Taranaki Basin (Figure 3.1) (Grain, 2008; Baur et al., 2010; Kroeger et al., 2019). The Root Mean Square (RMS) seismic attribute interpretation presented in those studies did not account for thin-bed tuning-related effects in deeply buried ancient strata (Simm & Bacon, 2014; Francis, 2016). In addition, the mapped Miocene fans do not fulfil the established stratal criteria (Posamentier & Erskine, 1991) that are commonly adapted in the identification of ancient fans. This study aims to re-evaluate the Middle and Late Miocene deep-water sedimentary system in southern, central and western offshore Taranaki Basin. I achieve this by objectively deconstructing the basis for prior mapping of submarine fans, and then I build the case for two fans in distal deep-water parts of offshore western Taranaki Basin. My results are embodied in three updated Middle and Late Miocene paleogeographic maps for Taranaki Basin. The paleogeographic maps are relevance for reservoir exploration in the deep-water parts of the basin, of which largely unexplored.

My work builds upon the results in a companion paper (Kamaruzaman et al., 2023) that fully analysed and parameterised the morphology of canyons, channels and gullies in the Middle and Late Miocene continental slope succession of offshore southern and central Taranaki Basin. That study established the importance of the increasing depositional slope angle through time upon the change in conduit type expressed within the slope succession, due to an increase in the rate of terrigenous sediment supply to the basin. I build upon that work by extending it to the deep-water occurrence and characteristics of two new submarine fans in offshore western Taranaki Basin.

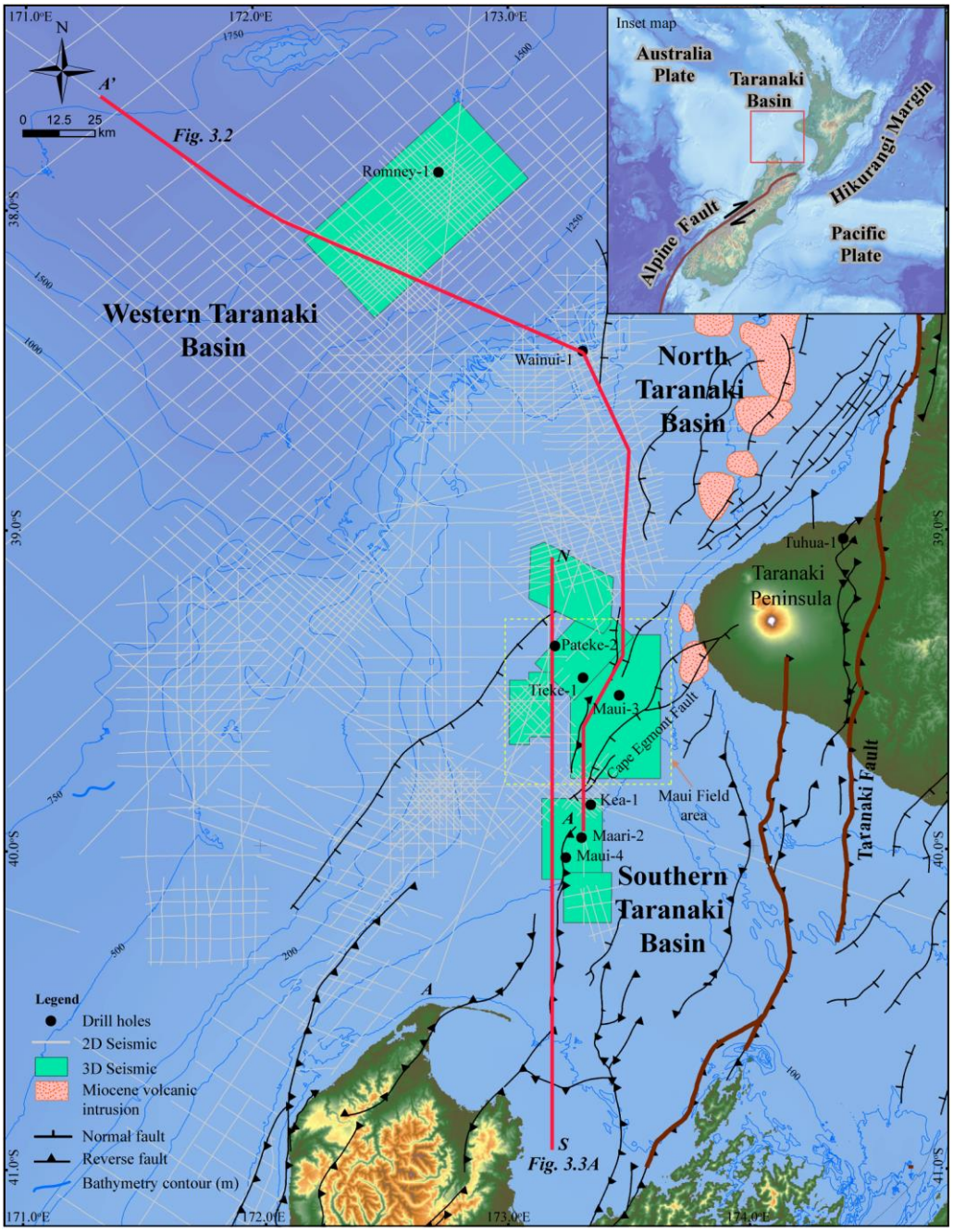

Figure 3.1: Map of the study area in Taranaki Basin, New Zealand, showing the location of 2D and 3D seismic surveys and some drill holes relevant to this study. GIS data from NZP&M (2018). Refer Figures i and ii – Appendix B for more information.

3.2 Geological setting of Taranaki Basin

Taranaki Basin is a long-lived (Late Cretaceous – Cenozoic) depocenter offshore of central-western North Island (Figure 3.1). This basin formed during three phases of crustal extension, followed by crustal shortening and then late extension (backarc to the modern Hikurangi margin subduction zone) (King & Thrasher, 1996; Strogen et al., 2022). The first phase of extension is considered to have occurred during c. 105–c. 83 Ma (Albanian – Campanian) (Strogen et al., 2017); the second occurred during 80–55 Ma (Campanian – Ypresian), concurrent with seafloor spreading in the Tasman Sea (King & Thrasher, 1996; Gaina et al., 1998; Strogen et al., 2017). The third phase of extension occurred during 38–28 Ma (Bartonian – Rupelian) and only affected southern Taranaki Basin (King & Thrasher, 1996; Strogen et al., 2014). These early extension phases set forth the bathymetric deepening of Taranaki Basin towards New Caledonia Basin (Strogen et al., 2022), affecting later sedimentation in the basin (King & Thrasher, 1996). Crustal shortening started in North Taranaki Basin during the Late Eocene to Early Oligocene, affecting central and southern Taranaki Basin during the Late Oligocene and Neogene (King & Thrasher, 1996; Campbell et al., 2003; Bierbrauer et al., 2008; Stagpoole & Nicol, 2008; Strogen et al., 2014). This shortening was focussed within the Taranaki Fault System along the eastern margin of the basin.

The structural development of Taranaki Basin is expressed in its stratigraphy (Figures 3.2 and 3.3A), as detailed by King and Thrasher (1996), which remains the most complete description of the basin and its development. Figure 3.3B shows a simplified chronostratigraphy of the Miocene succession in Taranaki Basin. Important stratigraphic elements of the Miocene succession are the dominance of mudstone facies (Manganui Formation) and the occurrence of two sandstone intervals within it (Moki and Mount

Messenger formations). Inversion of southern Taranaki Basin started around 12 Ma (Serravallian) (Kamp & Green, 1990; Crowhurst et al., 2002), involving reversal of the sense of throw on prior normal faults (King & Thrasher, 1996). This inversion resulted in erosion of the late-Early and Middle Miocene succession that had accumulated in southernmost parts of the basin. It forced progradation of the shelf-slope system northward and westward through the basin, culminating in the Pliocene – Pleistocene accumulation of the Giant Foresets Formation in North Taranaki Basin (Hansen & Kamp, 2002; Kamp et al., 2004). Most of the pre-12 Ma sediment was probably sourced from the Oligocene and Miocene thrust belt along the eastern margin of the basin and from basement along its southern margin. From 12 Ma onwards, the sediment supplied to the basin was mostly sourced from crustal shortening, uplift and erosion of basement in the Southern Alps, South Island (Kamp et al., 1989; Tippett & Kamp, 1993). Hence the Moki Formation (~16–13 Ma, Late Altonian to Early Lillburnian stages) had a different provenance to that of the Mount Messenger Formation, which started accumulating at about 12 Ma (latest Middle Miocene, ~12 Ma, Waiauan Stage) concurrent with the start of intra-basin inversion.

In this study I have analysed the upper Moki Formation (age duration ~14–13 Ma, Lillburnian Stage; Cooper et al., 2004) and the Mount Messenger Formation (age duration ~12–6 Ma, Waiauan, Tongaporutuan and Kapitean stages) (Figure 3.3B) in southern, central and western Taranaki Basin. Stage boundaries have been located on biostratigraphic criteria in drill hole sections (Roncaglia et al., 2013) and I have tied them to seismic reflection data in the study area. In this study I have adopted the spatial positions of morphological boundaries (shelf-slope break; upper, middle and lower slope) determined for the basin during its Miocene development by previous paleoecological work on drill hole samples in combination with seismic reflection mapping, as shown on the paleogeographic maps in Strogen et al. (2011) (see Table i – Appendix B). Both the Moki and Mount Messenger formations accumulated on

the continental slope at the time and in deeper water parts of the basin plain towards the New Caledonia Basin. The Miocene section thins westward towards the basin plain from a thickness of 1700 m in the vicinity of the Maui Oil Field (Maui-3 drill hole; upper slope position) to 700 m in deep Taranaki Basin (Romney-1 drill-hole) (Figure 3.2).

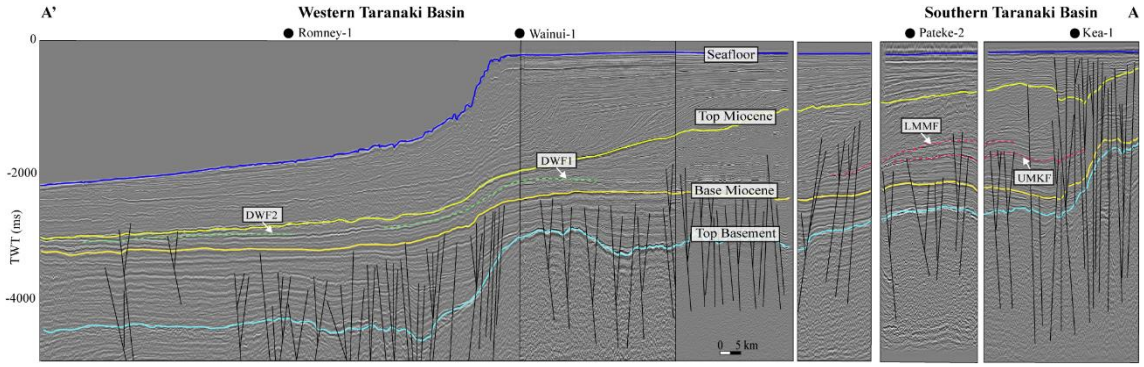

Figure 3.2: Interpreted regional composite seismic line showing the main reflectors that mark the base and top of the Miocene succession. See Figure 3.1 for the section location. The approximate location for interpreted fans by Kroeger et al (2019) are upper Moki Formation Fan (UMKF) and lower Mount Messenger Formation Fan (LMMF) in the southern Taranaki Basin region (Miocene slope). This study interpreted deep-water fans as Mount Messenger Deep Water Fan 1 (DWF1) and Deep Water Fan 2 (DWF2), located in the western Taranaki Basin region (Miocene lower slope and basin plain regions).

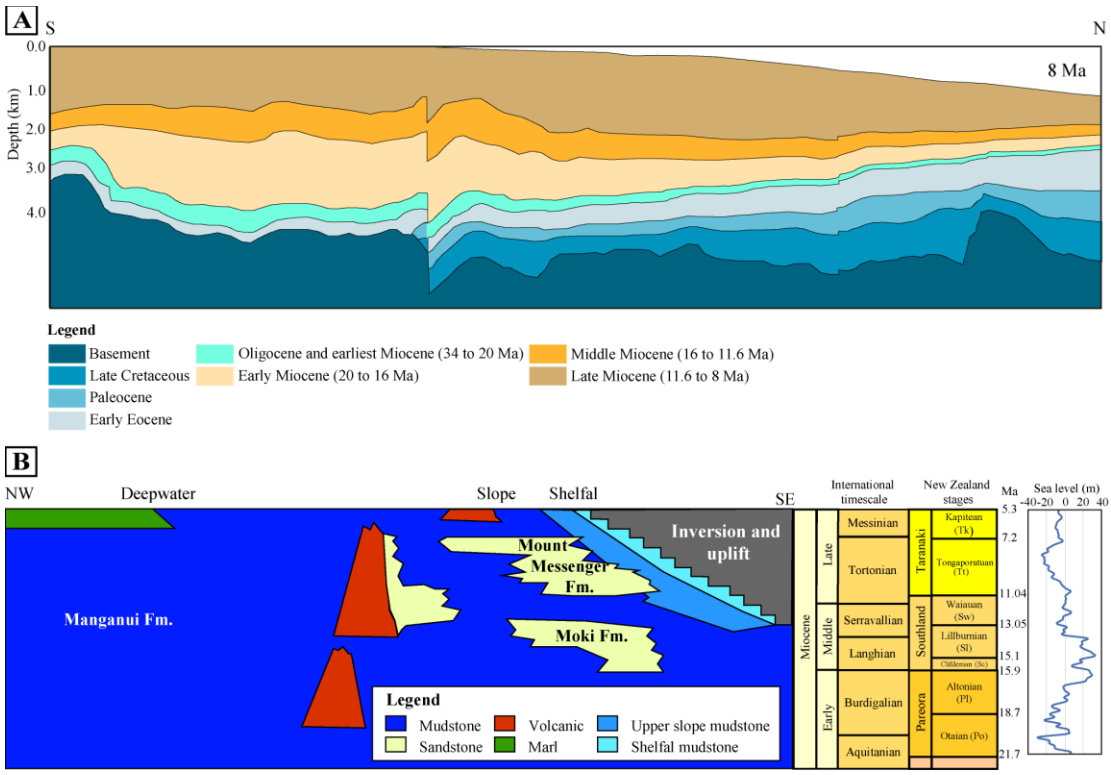

Figure 3.3: (A) South to north cross section showing the generalised Late Cretaceous to Late Miocene stratigraphy of southern Taranaki Basin at ~8 Ma, based on basin modelling (simplified from Bull et al., 2019); See Figure 3.1 for the section location. (B) Chronostratigraphic diagram and sea level curve for Taranaki Basin showing that the Moki Formation was deposited during the Early to Middle Miocene and the Mount Messenger Formation during the Late Miocene. Manganui Formation is the mudstone that encloses the Moki and Mount Messenger formations (chronostratigraphy simplified from Bull et al., 2019; sea level curve from Miller et al., 2020).

3.3 Context for my re-assessment of Miocene fans in Taranaki Basin

In my analysis I have critically re-assessed the occurrence of Miocene submarine fans in southern and central Taranaki Basin, as reported most recently by Kroeger et al. (2019) for the upper Moki Formation and for the lower Mount Messenger Formation (Figure 3.4). I do not address the lower Moki Formation fans reported by Kroeger et al. (2019) because there are no stratal patterns defining their extent and internal depositional fabric. Hence I cannot map them to demonstrate that they do not show the accepted stratal patterns of submarine fans.

Nevertheless, their study was the first to apply amplitude extraction to map the extent of Miocene submarine fans in Taranaki Basin, which was an advance upon the mapping of their extent based upon wireline log interpretations alone (e.g., Strogen et al., 2011).

The work on Miocene submarine fan occurrence in Taranaki Basin was originally undertaken by petroleum company geologists (e.g., de Bock, 1994; Bussell, 1994). The first research-based investigation of the Moki and Mount Messenger formations was undertaken by King and Thrasher (1996). They reported that these two sandstone formations were characterised by high amplitude signals in seismic reflection profiles, and based on this feature and wireline log interpretations, mapped the distribution of channels and fans. King and Thrasher's (1996) interpretations were strongly informed by down-hole tabular or blocky (spontaneous potential) SP and gamma-ray log motifs (e.g., in Maui-4 and Te Whatu-2 records). Their extensive Moki and Mount Messenger fan interpretations were reported in a series of paleogeographic maps. A second generation of paleogeographic maps showing the extent of canyons, channels and fans in the Moki and Mount Messenger formations was reported by (Strogen et al., 2011). Seven paleogeographic maps cover the interval from 16.5 to 7.2 Ma. These maps draw heavily upon the fan extents shown in King and Thrasher (1996), although they were modified to be consistent with new paleobathymetric data. Attribute mapping in selected areas and seismic facies mapping are claimed to have assisted in the remapping of these submarine fans (Strogen et al., 2011), although no details were given. The mapping of submarine fans and channels by Kroeger et al. (2019) is the most recent contribution and the first to have used amplitude extraction to map these depositional elements. Hence I refer to that work in relation to demonstrating the importance of detuning seismic reflection data within the intervals ahead of amplitude extraction and mapping. The outcome is that I dismiss all of the lobes and fans in their upper Moki and Mount Messenger formation palaeogeographic maps (Figure 3.4). Separately, I have mapped the occurrence and character

of two new distal deep-water fans in offshore western Taranaki Basin, which I attribute to lying within the lower and uppermost Mount Messenger Formation. Strogen et al. (2011) also reported the distribution of submarine fans beneath on land Taranaki Peninsula and in offshore North Taranaki Basin. They were not considered in the Kroeger et al. (2019) study. Neither have I re-assessed those "fans" here, although my investigations in eastern parts of offshore North Taranaki Basin and the well-known coastal outcrop section so far do not support their occurrence in those areas; rather, I regard the sandstone beds as slope deposits, including as channels and gully fills.

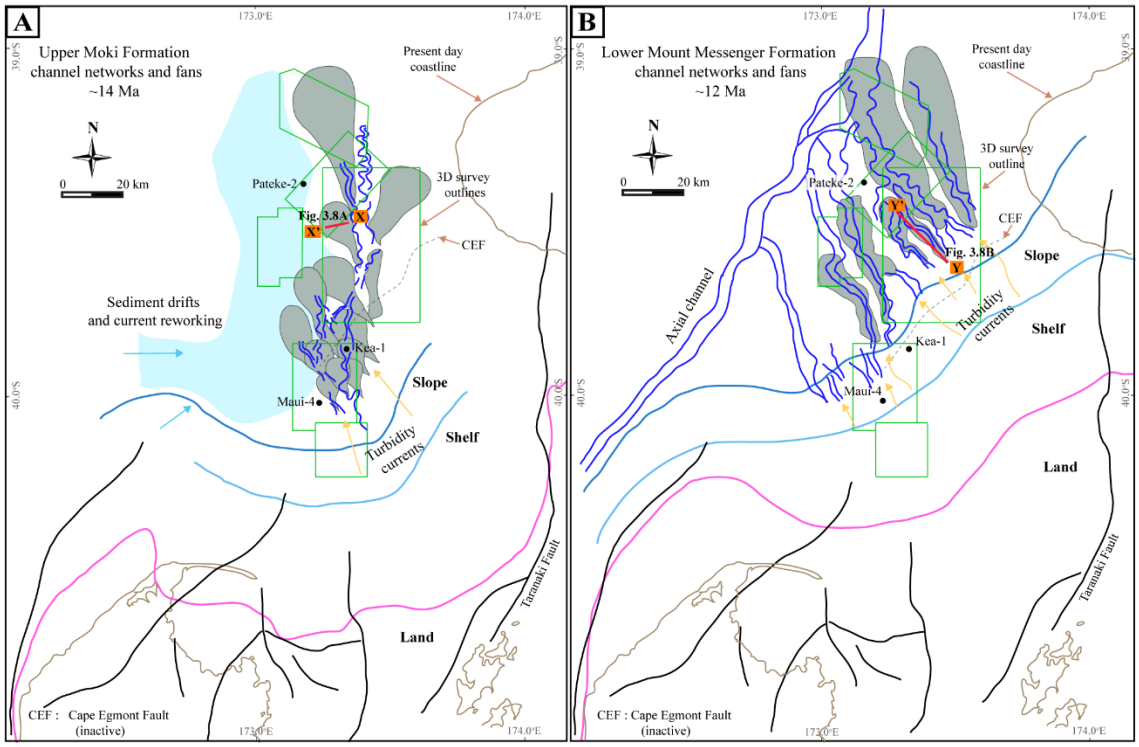

Figure 3.4: Paleogeography maps of Kroeger et al. (2019) showing the location and distribution of: (A) upper Moki Formation channels and fans (Lillburnian Stage (Sl), ~14 Ma); and (B) lower Mount Messenger Formation channels and fans (Waiauan (Sw) to Early Tongaporutuan (Tt) stages, ~13–12 Ma) in southern and central Taranaki Basin. The approximate location of the upper Moki Formation Fan (UMKF) and lower Mount Messenger Formation Fan (LMMF) are shown in Figure 3.2.

3.4 Data and methods

This study utilises 6550 km^2 of 3D and 24,000 km of 2D seismic reflection data as well as petrophysical well log data for 14 drill holes (see Table ii – Appendix B) accessed through the New Zealand Petroleum and Minerals database (https://www.data.nzpam.govt.nz) (Figure 3.1). The quality of the 2D and 3D seismic data (see Table iii – Appendix B) is good to excellent. These data were examined using integrated methodologies that leverage several key disciplines, including seismic interpretation, seismic stratigraphy, seismic attributes analysis, well log interpretation and seismic geomorphology.

Coloured inversion was implemented to the 3D seismic volumes to boost the low-frequency seismic response, thereby increasing the resolution of the seismic data in the intervals of interest (Lancaster & Whitcombe, 2000; Maurya & Singh, 2017; Assis et al., 2018). Synthetic seismographs were then aligned with the seismic data to guide the mapping of regional horizons, while incorporating biostratigraphy markers from Roncaglia et al. (2013). For time-depth conversion, a regional velocity model was constructed using drill hole checkshot data. The average seismic velocity of the Miocene interval ranged from 1200 to 3000 ms^{-1}, with a mean value of 2200 ms^{-1}.

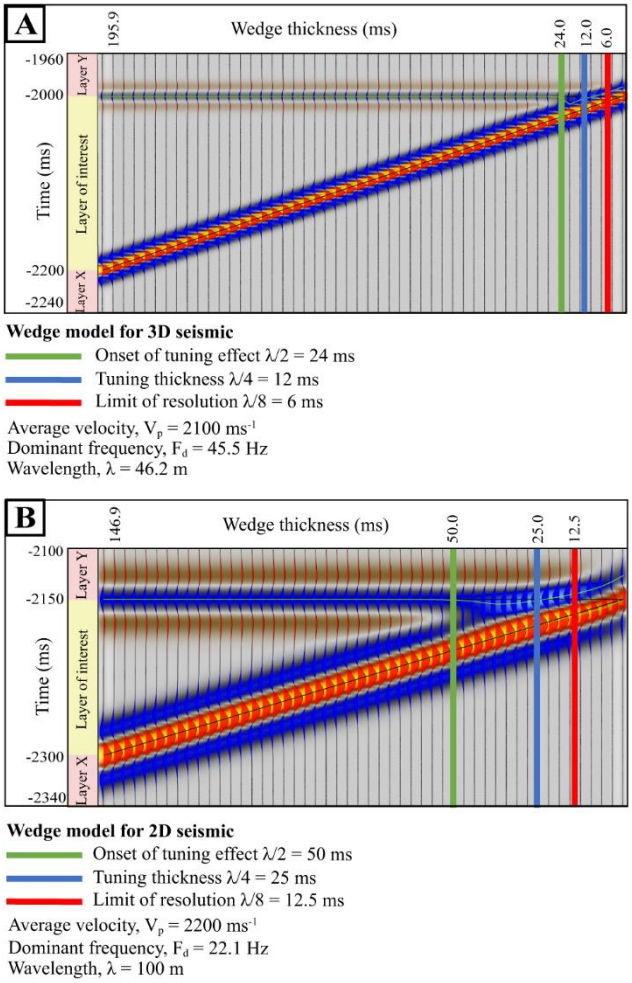

Figure 3.5: Example wedge models for (A) 2D seismic data and (B) 3D seismic data from Taranaki Basin. Each example model uses a different velocity and frequency. The models show the thickness at the onset of the tuning effect (24 ms in A and 50 ms in B), the tuning thickness (12 ms in A and 25 ms in B), and the limit of resolution (6 ms in A and 12.5 ms in B). Calculations are based on Widess (1973).

The effects of thin-bed tuning on seismic data due to constructive and destructive interference (Simm & Bacon, 2014), were assessed using wedge models analysed in the Cegal Blueback plugin for Petrel (https://www.cegal.com/en/software) (Figure 3.5). A process of seismic amplitude detuning was carried out to leave only meaningful seismic amplitudes in the data (Brown et al., 1986; Bunt, 2015; Francis, 2015; Guo et al., 2015; Ab Fatah et al., 2016).

Mapping geomorphological elements began with identifying and mapping major canyon and channel networks because they are the sediment conduits necessary to build submarine fans. Their mouths are where fans are expected to develop (Posamentier & Erskine, 1991; Covault et al., 2012; Deptuck & Sylvester, 2018; Fildani et al., 2021). Next, I compared the seismic reflection patterns in the interval of interest against specific seismic stratal pattern criteria developed by previous workers for identifying submarine fans (e.g., Sarg and Skjold, 1982; Mitchum et al., 1985; Posamentier and Erskine, 1991) (Table 3.1). These criteria include: (i) pinch out of reflectors against high paleo-seafloor topography, (ii) continuous high-amplitude reflectors that onlap basin margins, (iii) the occurrence of bidirectional downlapping reflectors within fans or lobes, and (iv), subtle low-relief external mounding of any upper bounding surface/reflector of a fan. During this comparison I considered both Widess' (1/4 λ; Chopra et al., 2006) and Rayleigh's (1/2 λ; Kallweit and Wood, 1982) vertical seismic resolution limits to determine the range of geobody thickness that would be resolvable in my data. This is because seismic stratal pattern recognition depends upon vertical seismic resolution as a function of velocity, frequency, and wavelength (Widess, 1973; Kallweit and Wood, 1982; Posamentier et al., 2022).

In addition to mapping seismic reflector geometry, I also applied seismic geomorphological concepts to seismic attributes extracted from the interpreted horizons using the Root Mean Square (RMS) amplitude and variance (e.g., coherence and curvature) attributes (Miller & Stuart, 1992; Sømme et al., 2013; Bunt, 2015). These attributes are important for distinguishing Moki and Mount Messenger formation sandstone beds from the background mudstone of the Manganui Formation. Detuned seismic attribute analysis was based on the concepts of Connolly (2007) and Simm (2009). During analysis of seismic amplitude attribute maps, I picked base and top horizons for each interval as well as additional horizons within the interval to sub-divided my analysis. Extra horizons were inspected to constrain amplitude

analysis using relatively small time-windows (i.e., ~30 ms for the upper Moki Formation and ~40 ms for the lower Mount Messenger Formation). To constrain the amplitude in the upper Moki Formation I used two sub-intervals (i.e., UMK 1 and UMK 2) and in the lower Mount Messenger I used three sub-intervals (i.e., LMM 1, LMM 2 and LMM 3). Finally, horizons were flattened and structural balancing was applied to the 3D seismic data to measure the gradient of the slope. Slope gradient was smoothed using a window of roughly 10–50 km^2 to remove the effects of seafloor irregularities.

Table 3.1: List of stratal patterns used to identify fans in seismic data, as outlined by Posamentier and Erskine (1991)

1. Reflectors pinch out against high seafloor topography.
2. Continuous high-amplitude reflectors onlap basin margin.
3. Bidirectional downlap reflectors within the fans or lobes.
4. External mounding on the fan top bounding surface.

3.5 Terminology

3.5.1 Submarine-fan subdivision

There are numerous models of submarine fans in the literature (Bouma, 1962; Walker, 1978; Mitchum et al., 1985; Vail, 1987). These models generally subdivide fans into feeder canyon-channels, upper fan, middle fan, and lower fan components (Figure 3.6A), based on the following criteria: (i) geometry, morphology and organisation of channel complexes within a fan, (ii) longitudinal (i.e., down dip) seismic facies variations, (iii) channel depth and fan thickness, and (iv), seafloor slope gradient where a fan may have developed (Mutti & Ricci-Lucchi, 1972; Walker, 1978; Droz & Bellaiche, 1991; Weimer & Link, 1991; Escutia et al., 2000; Curray et al., 2002). However, due to limitations in the interpretation of fan elements in

2D seismic data, I describe Taranaki Basin Miocene fans using a simplified tripartite scheme consisting of (i) feeder canyon and distributary channels, (ii) upper fan segment, and (iii), lower fan segment.

With regard to the findings of previous studies, submarine fan divisions can be distinguished by their key characteristics, and in parts, I use these key characteristics to guide my fan system interpretation. On the continental slope at gradients of ~2–5°, feeder canyon-channels are generally narrow with steep walls (Droz & Bellaiche, 1991; Cronin et al., 2005; Kamaruzaman et al., 2023). They widen significantly as they become less confined towards the basin plain, where depositional gradients decrease to the range ~0–2°. The upper fan segment typically shows low-relief external mounding on upper seismic reflectors compared with lower fan segments (Posamentier & Erskine, 1991; Lee et al., 1996). Seismic facies of the upper fan show medium to high-amplitude reflectors indicative of the presence of sand-prone strata (Walker, 1978; Weimer, 1990; McHargue, 1991; Deptuck et al., 2003). In contrast, the lower fan region typically displays mainly low-amplitude reflectors representing mud-prone deposits. The basal bounding surface of the upper fan exhibits prominent erosional effects, while the erosional basal bounding surface in the lower fan is hardly recognisable on seismic data. The upper fan is narrower than the lower fan as the fan widens towards the lower slope and basin plain (Figure 3.6A) (Walker, 1978). The number of distributary channels also differs between the upper fan and lower fan segments; there are more channels in upper versus lower parts of a fan (Normark & Gutmacher, 1983; Flood & Damuth, 1987). This study focuses on mapping the fan systems rather than describing their internal hierarchy and therefore I have chosen to refrain from applying any fan hierarchical models.

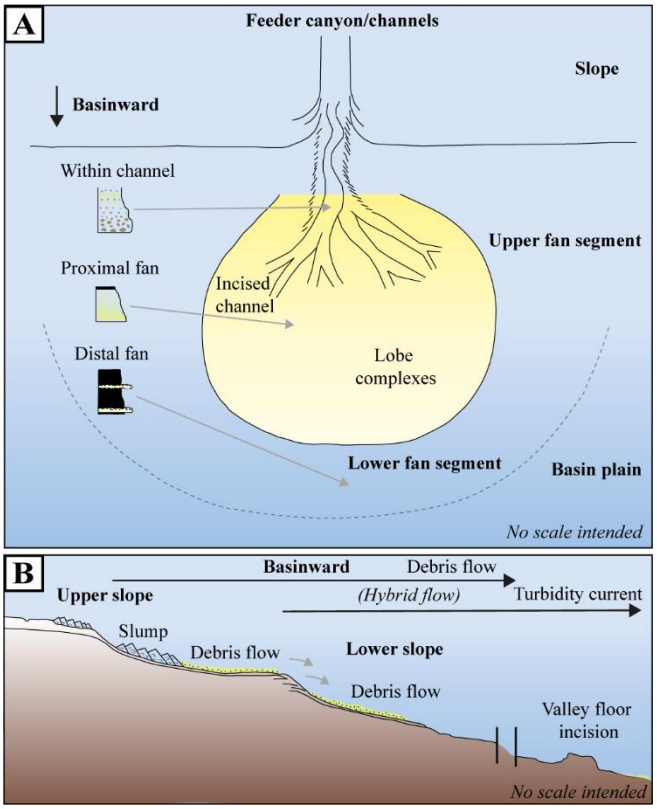

Figure 3.6: (A) Conceptual model of an ancient fan system used in this study that demonstrates the fan system comprises an upper fan segment, including feeder and distributary channels and a lower fan segment on a shallower slope gradient of the basin plain (modified from Walker, 1978). This study adapted this fan model to map the Miocene fans' divisions and the associate feeder canyons and/or channel networks on continental slope. (B) Conceptual model of sandy debris flows that develop on slope margins. Debris flows occur due to the down-slope evolution of a mass-slumping event, i.e., the 1929 Grand Banks earthquake (modified from Piper et al., 1999).

3.5.2 Sedimentary processes and deposits

A range of depositional mechanisms are inferred for continental slopes and on basin floors, resulting in a confusing lexicon in the literature (Talling, 2013; Shanmugam, 2016). To standardize my terminology, I have adopted the Gani (2004) model of gravity flow deposits (Figure 3.7). I have applied this model to the interpretation of wireline log records for drill holes investigated in the study area, following (Bernhardt et al., 2012; Shanmugam & Wang, 2015; Fudol et al., 2019). This has involved focussing on differentiating blocky gamma-ray log

motifs with sharp upper and lower contacts (debris flow deposits) from bell-shaped (i.e., gamma-ray increasing upwards) log motifs (turbidity current deposits). A conceptual example is shown in Figure 3.7 exhibiting debrites, densites and turbidites. Densites in particular, represent hybrid deposits consisting commonly of a lower debrite and an upper turbidite without developing any bedding plane in between, originated by bipartite sediment gravity flows (Gani, 2004). These deposits originated by flow transformation, or simultaneous or retrogressive release of co-genetic debris flows and turbidity currents, and belong to the class of hybrid event beds (Davis et al., 2009; Haughton et al., 2009; Talling, 2013). I chose this model (Figure 3.7) in my study because I want to objectively distinguish the resultant sandstone bodies of sediment gravity flow processes. These processes can also produce mud-dominated deposits such as muddy debrites and turbidites (Amy & Talling, 2006; Shan et al., 2019; Patacci et al., 2020), however they are not the focus of this study. Where available, I have used drill cores to distinguish amongst gravity flow deposits.

While submarine fans can be constructed by a variety of sediment gravity flow deposit types, including debrites, densites and turbidites (Middleton & Hampton, 1973; Lowe, 1982; Shanmugam, 2000; Davis et al., 2009; Haughton et al., 2009), these deposits are not exclusive to fan systems. For example, sediment gravity flow deposits also occur in relation to submarine mass movement such as on the continental slope (Lee et al., 2007; Micallef et al., 2007; Parsons et al., 2007; Talling et al., 2007; Shanmugam, 2009; Fudol et al., 2019) (Figure 3.6B). This distinction is relevant to the arguments I set forth later in this paper.

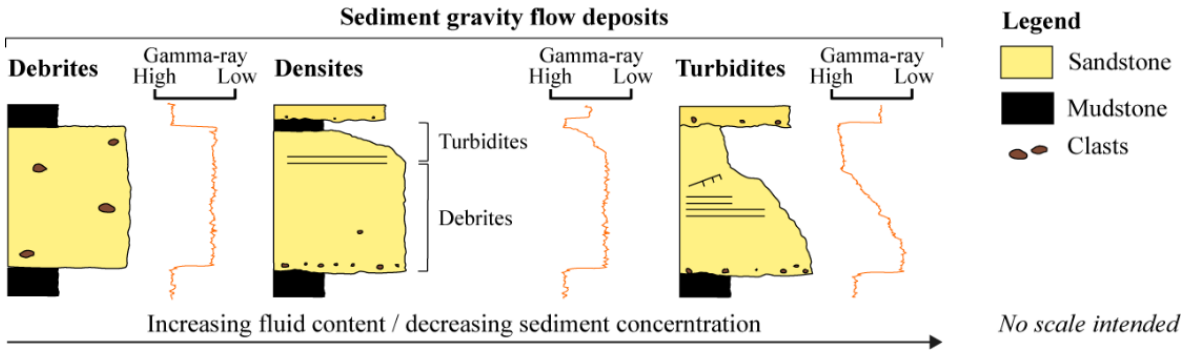

Figure 3.7: Example facies characteristics of debrites, densites and turbidites, alongside typical gamma-ray lot motifs. Debrites are characterised by blocky sandstone bodies with abrupt lower and upper contacts, densites show a more subtly transitional upper contact, and turbidites have a very gradational profile from their base to top. Note the presence of mud clasts in debrites and their absence from turbidites (modified from Gani, 2004).

3.6 Results

3.6.1 Resolution of seismic data

Calculation of the Widess and Rayleigh seismic resolution limits yielded a vertical resolution ranging from 6 to 16 ms within the stratigraphic intervals of interest on both 2D and 3D seismic data, respectively, from the study area, depending on the dominant frequency range (Table 3.2). This calculation also gives the thin bed tuning thickness and the thickness at which the onset of tuning occurs. Calculation of seismic resolution limits of the data means that not all fan elements are detectable. For example, individual lobes and/or lobe complexes may not be resolvable.

Table 3.2: Seismic data parameters and their calculated resolution. Parameters are based on Widess (1973).

Seismic data type	Dominant frequency within interval of interest (Hz)	Thickness at onset of tuning effect ƛ/2 (ms)	Tuning thickness ƛ/4 (ms)	Resolution limit ƛ/8 (ms)
2D	20 to 35	50 to 64	25 to 32	12.5 to 16
3D	40 to 50	24 to 40	12 to 20	6 to 10

3.6.2 Part I: Objective evaluation of previous interpretations of Moki and Mount Messenger formation submarine fans

3.6.2.1 Upper Moki Formation

Objective comparison of the parameters outlined in Table 3.1 against the Kroeger et al. (2019; that is, their Figure 6C) map for the upper Moki Formation demonstrates that (1) only one of the five Posamentier and Erskine (1991) seismic reflection criteria for submarine fans is met; specifically, the presence of continuous high amplitude reflectors throughout the interval. Seismic section Figure 3.8A, which crosses the Kroeger et al. (2019) upper Moki Formation fan, shows this point. (2) Further interrogation of the locations of high seismic amplitude locations on the map in Figure 3.9A and B shows that there are significant differences between the RMS amplitude attribute extraction and the detuned amplitude attribute extraction. The amplitude extraction maps of Kroeger et al. (2019) (their Figures 12A and B) used proportional slices. They did not specify if the maps show RMS or average amplitude, and therefore, I could not reproduce the maps exactly. As a result, in this study I take the maps as RMS amplitude and demonstrate the effect of seismic tuning on it. Comparison between their amplitude extraction and my detuned amplitude attribute extraction for one of the sub-intervals (Figure 3.10) shows a significant reduction in the area of high-

amplitude (Figure 3.9A and B; see Figure iii – Appendix B). Furthermore, the distribution of high amplitude in the detuned map does not show a lobate morphology as would be expected of fans, but instead displays a patchy (isolated) pattern. (3) A third aspect of the Kroeger et al. (2019) submarine fan interpretation for the upper Moki Formation is the presence of low gamma-ray signatures in drill hole logs. The gamma-ray log motifs show blocky profiles with sharp basal and upper contacts (Figure 3.10B), which they interpreted as imaging turbidites. However, I note that such gamma-ray log motifs are equivocal and may also be interpreted as amalgamated sandy debris flow deposits (see examples in Bernhardt et al., 2012; Shanmugam and Wang, 2015; Fudol et al., 2019). (4) A final aspect that questions the interpretation made by Kroeger et al. (2019) for the fan-like character of the upper Moki Formation, is that they did not clearly define a fan morphology (i.e., the upper, middle and lower fan regions), which precludes objective seismic interrogation of their mapped fan systems. When taken together and in context, my results demonstrate that there is insufficient evidence to support the interpretation and occurrence of widespread submarine fan systems in the upper Moki Formation within southern Taranaki Basin.

3.6.2.2 Lower Mount Messenger Formation

As with the upper Moki Formation interval, I compared the parameters outlined in Table 3.1 against the lower Mount Messenger Formation fans mapped by Kroeger et al. (2019; that is, their Figure 6D). My results show that the only Posamentier and Erskine (1991) criteria possibly defining their inferred submarine fan system is the occurrence of continuous high amplitude reflectors throughout the lower Mount Messenger Formation interval (Figure 3.8B). Comparison between their RMS amplitude extraction versus my detuned amplitude extraction shows a significant reduction in the area of high amplitude (Figure 3.9C and D; see Figure iv

in Supplementary Data for complete sub-intervals). However, in the detuned amplitude map an area of high amplitude remains in the northern part of the map, which Kroeger et al. (2019) referred to as the "SW Sands".

Finally, gamma-ray log motifs of the sandstone bedsets in the lower Mount Messenger Formation display mainly blocky profiles with sharp basal and top contacts (Figure 3.10B), which, Kroeger et al. (2019) infer to be turbidite fans. However, the morphology of their mapped fans is not clearly defined in terms of upper, middle, and lower fan zones and their inferred fans (high amplitude areas) are located marginal to what I map as through-going channel margins (but which Kroeger et al. (2019) map as fans atop channels). Based on these observations, I simply do not find enough evidence to support the interpretation of fan systems occurring within the lower Mount Messenger Formation interval where they have been mapped by Kroeger et al. (2019).

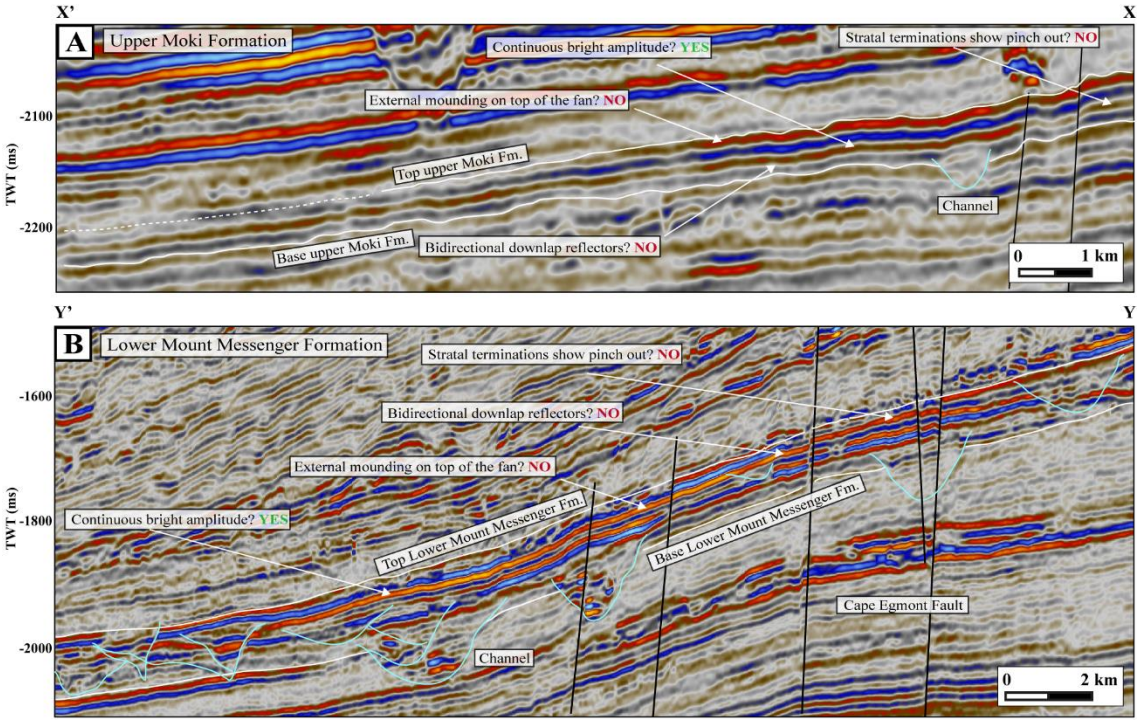

Figure 3.8: Seismic cross-sections intersecting the interpreted "fans" of Kroeger et al. (2019) compared with the recognition parameters outlined in Posamentier and Erskine (1991) (Table 3.1). (A) Upper Moki Formation showing continuous high amplitude reflectors but (i) without pinchout of reflectors against the paleo-sea floor, (ii) bidirectional downlap of reflectors within fans, or (iii), external mounding of reflectors at the top of the fan. (B) Lower Mount Messenger Formation that does show continuous high amplitude reflectors but does not show pinchout of reflectors against the paleo-sea floor, bidirectional downlap of reflectors within fans, or external mounding of reflectors at the top of the fan. Refer Figure 3.4 for transect lines location.

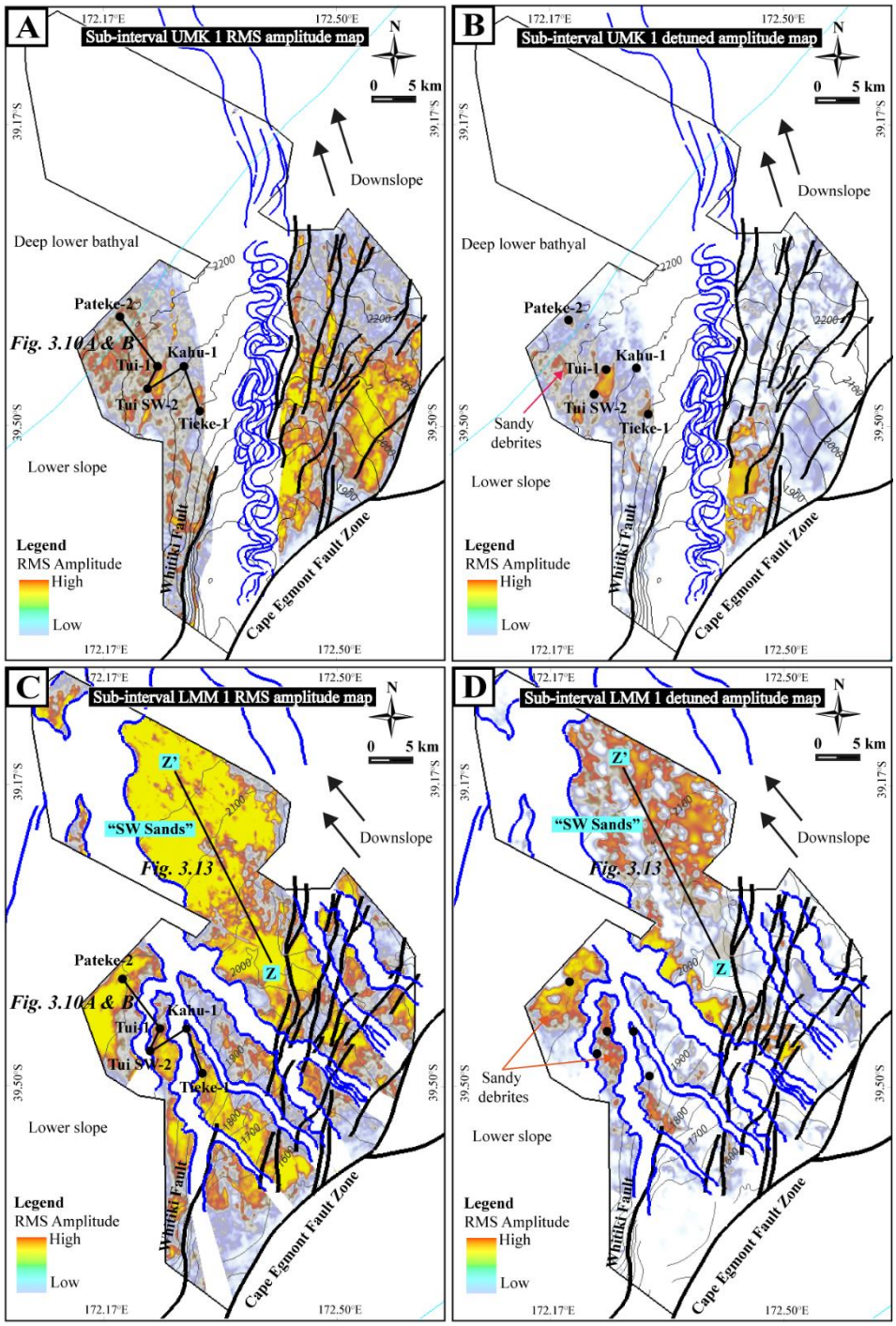

Figure 3.9: Root mean squared (RMS) amplitude and detuned amplitude maps for the Moki and Mount Messenger formations (A) upper Moki Formation RMS amplitude and B) upper Moki Formation detuned amplitude. (C) Lower Mount Messenger Formation RMS amplitude and (D) lower Mount Messenger Formation detuned amplitude. Note how much of the high amplitude area was reduced during the detuning process. Most of the remaining high amplitude areas are interpreted as sandy debris flow deposits, although there is uncertainty in interpreting high amplitude areas away from well control. The underlain contour maps are in TWT (ms). Refer to Figure iii and iv – Appendix B for complete set of maps for each sub-interval.

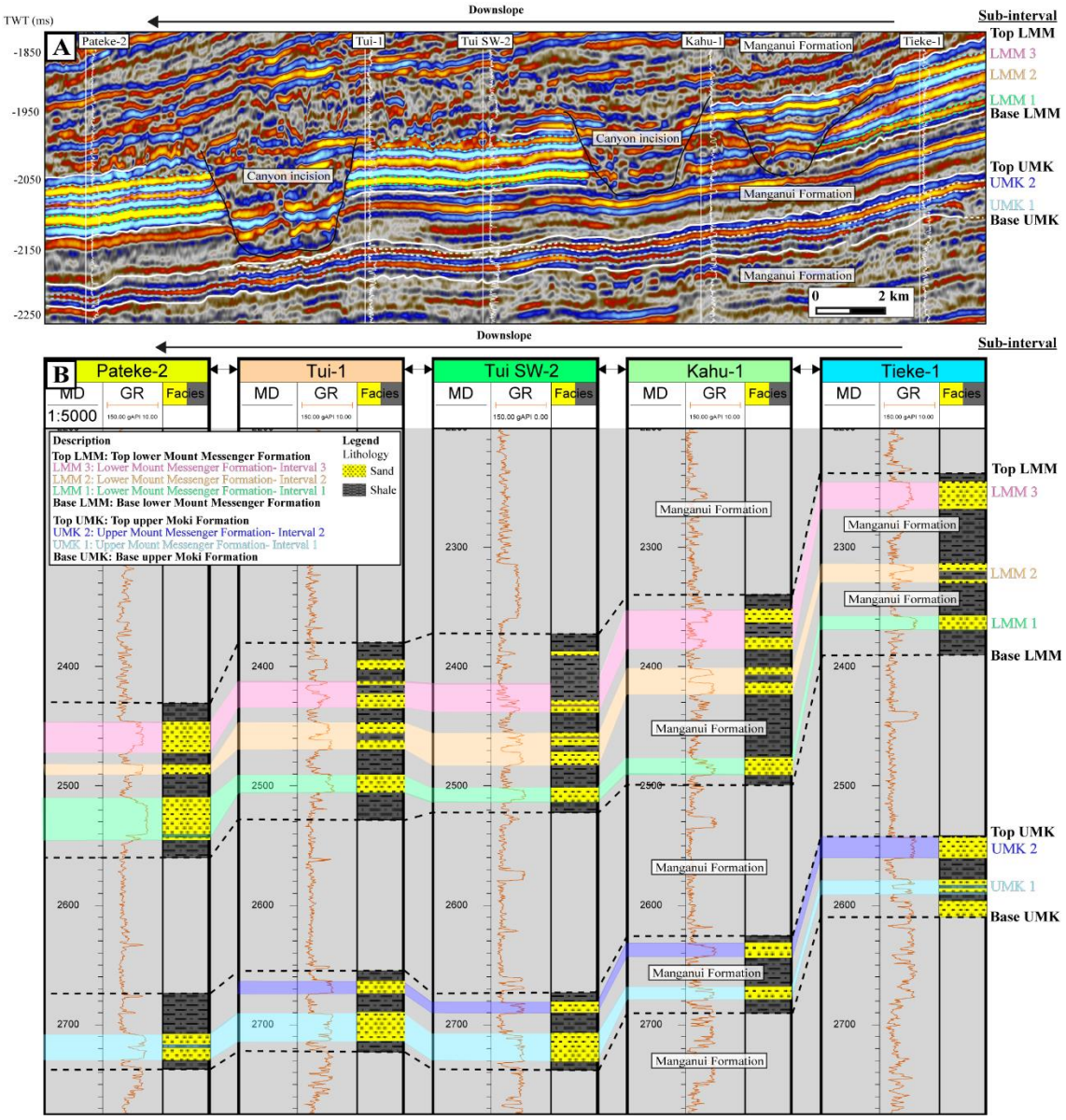

Figure 3.10: (A) Seismic cross-section and (B) well correlation panel showing the sub-intervals within the upper Moki Formation and lower Mount Messenger Formation used during the seismic detuning process. The upper Moki Formation is split into the UMK 1 and UMK 2 intervals. The lower Mount Messenger Formation is divided into the LMM 1, LMM 2 and LMM 3 intervals). Refer to Figure 3.9A and C for the location of the cross-section and drill holes.

3.6.3 Revised mapping of Moki and Mount Messenger formations

In this section I revisit the same dataset used by Kroeger et al. (2019) and more seismic data to the north and west of it, and propose an alternate interpretation for the deep-water sedimentary systems in the Moki and Mount Messenger formations in offshore southern Taranaki Basin.

3.6.3.1 Upper Moki Formation

3.6.3.1.1 Channel complex networks

Mapping of the channel complex in the upper Moki Formation in southern Taranaki Basin demonstrates that it is oriented south to north (Figure 3.11A), crossing middle and lower slope regions, roughly 30 km north of the shelf edge and about 50 km north of the contemporary (Lillburnian, ~14 Ma) shoreline. Incised channel complexes drained northward normal to obliquely across a smooth slope with gradients ranging from 0.2 to 0.5° (Figure 3.11A). The channel complexes within the middle slope region (mean slope gradient: 0.4°) are mainly aggradational, straight to slightly sinuous (mean sinuosity index: 1.1), with a maximum width of 2.5 km. In contrast, on the lower slope region (mean slope gradient: 0.2°), individual channels within the prominent channel complex are highly sinuous (mean sinuosity index: 2.4) and their maximum width decreased to approximately 1.2 km (Kamaruzaman et al., 2023) (Figure 3.11A).

3.6.3.1.2 Gravity flow deposits on the slope

As shown in the previous section, detuned seismic amplitude maps display high amplitudes mainly within the slope region and they have a patchy distribution (Figure 3.9B). The gamma-ray log response in the drill holes that intersect the high-amplitude area have blocky log motifs with sharp basal and upper contacts (Figures 3.10B and 3.12A). Furthermore, these low gamma-ray intervals (sandstone bedsets) are not readily correlated between neighbouring drill holes (i.e., distance between drill holes ranges from ~1 to 6 km). The thickest sandstone intervals are up to 40 m thick in the Maari- 2 drill hole located within the middle slope (Figure 3.12A). In the Tui-1 drill hole, situated within the lower slope region, sandstone intervals get as thick as 28 m (Figure 3.10B). Analysis of core data extracted from these intervals shows that they consist of massive (predominantly fine-grained) sandstone beds with mud clasts with long axes of up to 10 cm (Figure 3.12B–F).

I interpret the patchy high (detuned) amplitude seismic distributions (Figure 3.9B) to represent localised slope sandstone deposits (i.e., not lobate fans), and this is supported by the fact that sandstone intervals cannot be correlated on wireline logs between neighbouring drill holes (Figures 3.9B and 3.12A). Nevertheless, due to the complexity of deep-water sedimentary systems (Shanmugam, 2000; Stow & Mayall, 2000), the localised sandstone deposits could also be reworked by contourite drifts (Kroeger et al., 2019). In addition, blocky gamma-ray log motifs, the massive internal nature of sandstone beds, including the presence of mud clasts (Figure 3.12B–F), suggests that these deposits were generated by gravity flows with high sediment concentrations, low Reynolds numbers (i.e., laminar), and a relatively strong matrix strength (Gani, 2004). Hence, the deposits of the upper Moki Formation on the depositional slope margin are interpreted here to be amalgamated sandy debrites following

Gani (2004) and other publications (e.g., Talling et al., 2007; Haughton et al., 2009; Shanmugam et al., 2009; Jin et al., 2021) (Figure 3.7).

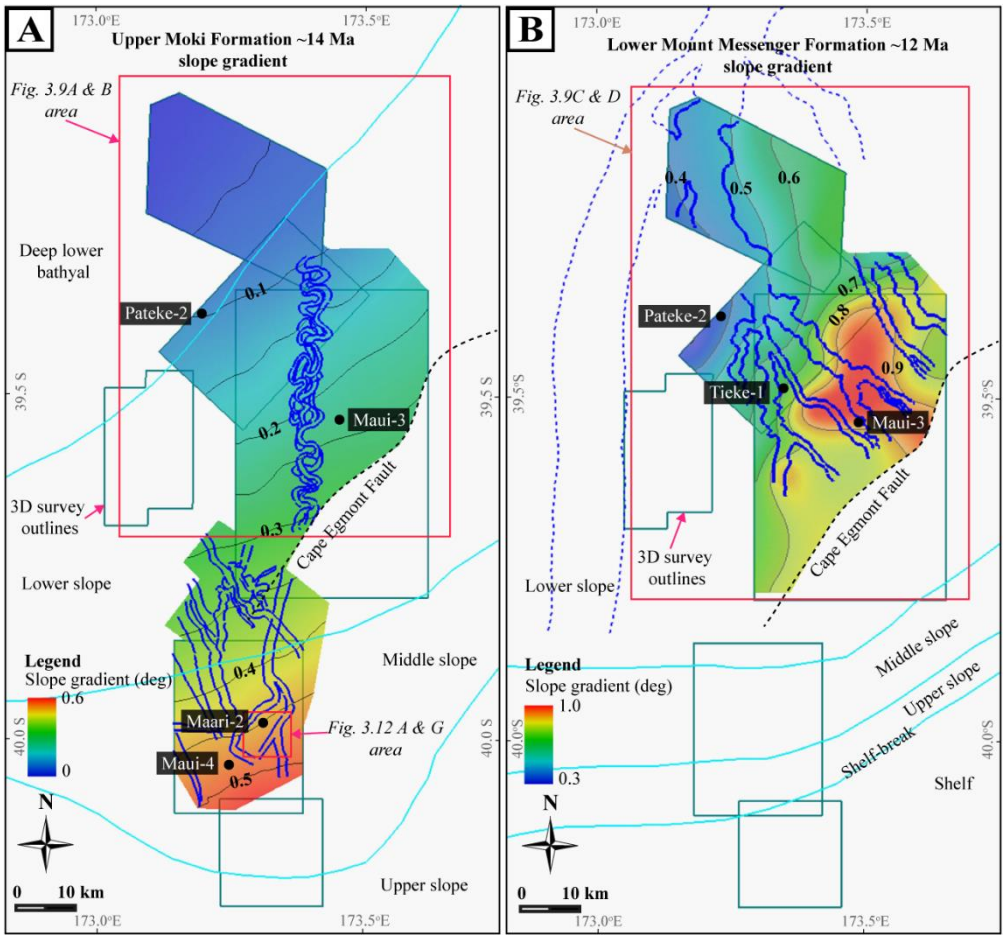

Figure 3.11: Slope gradient map of (A) upper Moki Formation and (B) lower Mount Messenger Formation in southern Taranaki Basin showing a trend of decreasing gradient to the north and northwest. Slope gradients range from <0.1 to <0.6◦ in the upper Moki Formation and from 0.3 to 1.0◦ in the lower Mount Messenger Formation. The lower Mount Messenger slope gradient is adapted from Kamaruzaman et al. (2023).

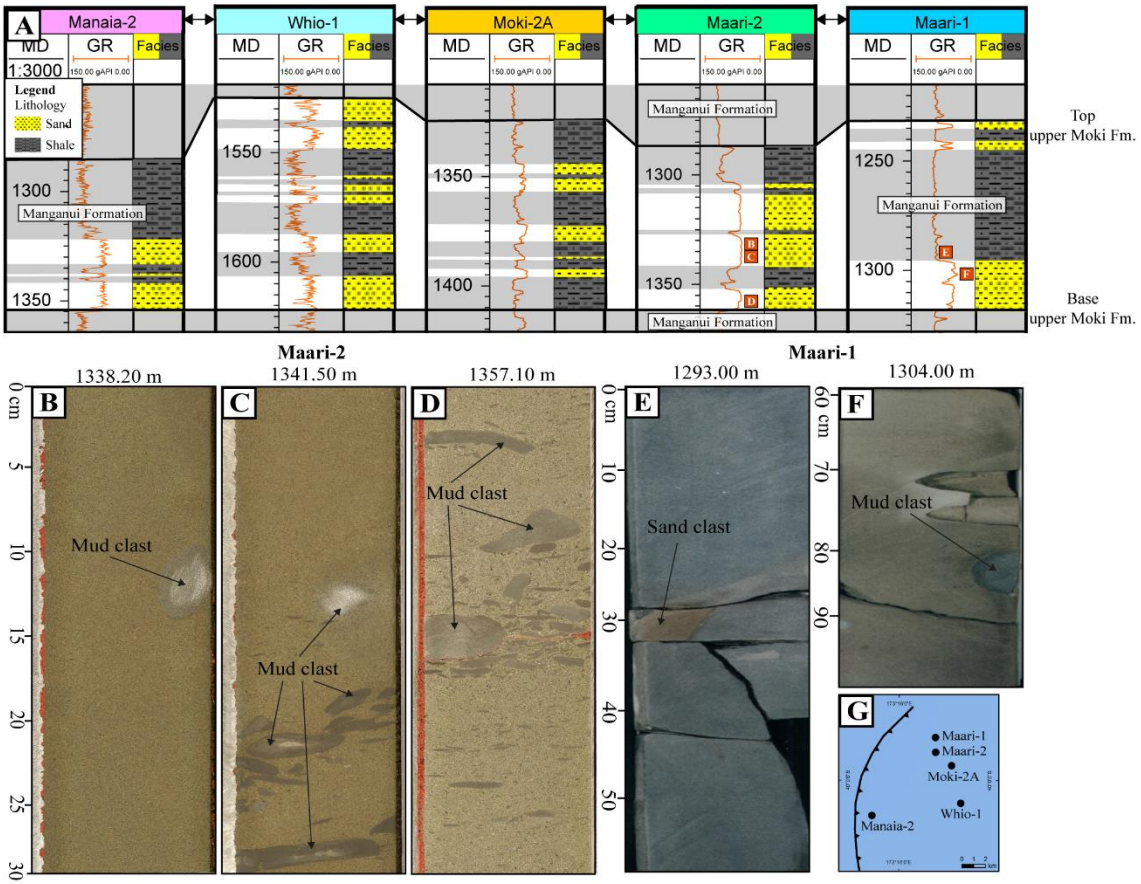

Figure 3.12: (A) Gamma-ray log motifs for the upper Moki Formation interval in the upper slope region from selected drill holes. (B) to (D) core photographs from Maari- 2 through interpreted sandy debris flow deposits showing floating mudstone clasts. (E) Core photograph from Maari-1 showing sandstone within mudstone. (F) Core photograph from Maari-1 showing a mudstone clast within an ungraded sandstone. The sandy deposits are considered debrites. (G) Location of drill holes, refer Figure 3.11A for the location of the area.

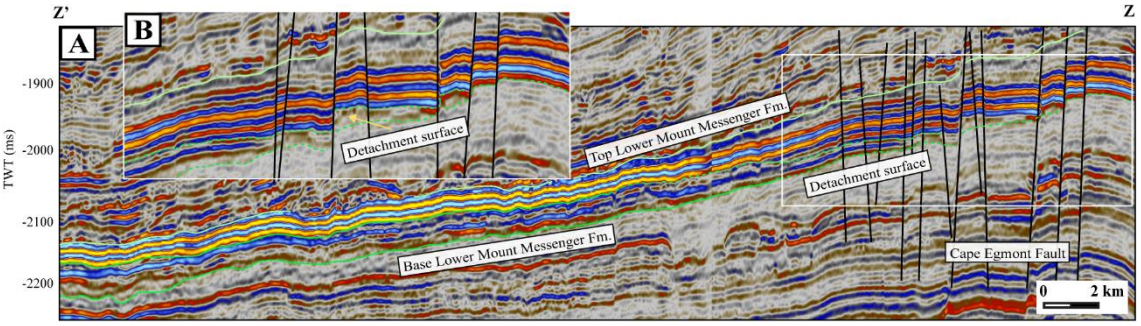

Figure 3.13: (A) Seismic cross-section showing a detachment surface at the base of sandy debris flow deposits in the lower Mount Messenger Formation. (B) A close-up view of the detachment surface. See Figure 3.9D for location.

3.6.3.2 Lower Mount Messenger Formation

3.6.3.2.1 Channel complex networks

The lower Mount Messenger Formation canyon-channel networks originated from, and lie within, southern Taranaki Basin, roughly 16–22 km from the contemporary (Waiauan, ~12 Ma) shoreline (Figure 3.11B). The canyons reached 9 km wide on the lower slope (Figure 3.9C and D). The canyon-channels directed sediment in a SE-NW direction, incising into the lower slope margin in the vicinity of the Maui Field (Figure 3.1).

Numerous lower Mount Messenger Formation canyon-channels are observed incised into thick sandy strata forming a network. The canyon-channels developed on a smooth slope gradient of 0.4◦ to 1◦ (Figure 3.11B) along the bottomset of sigmoidal clinoforms (Kamaruzaman et al., 2023). Seismic profiles reveal that asymmetrical V- and U-shape incisions, which are narrow at their base, are the dominant type of canyon incision (Figure 3.10A). Internal seismic configuration within the canyons shows high amplitude discordant seismic reflectors at the base. The canyons are filled with vertical and lateral stacked U-shape channel complexes of 50–200 m thickness (Kamaruzaman et al., 2023). These channel complexes are manifest as a combination of parallel to sub-parallel and divergent low to medium amplitude seismic reflectors, dipping at low angles toward channel thalwegs.

3.6.3.2.2 Gravity flow deposits on the slope

The detuned seismic amplitude map for the lower Mount Messenger Formation shows high amplitude patches on the lower slope (Figure 3.9C and D; "SW Sands"). Further investigation of the seismic facies occurring within these patches show sudden changes from continuous, parallel and high amplitude reflectors to discontinuous, discordant and mixed low to medium amplitude reflectors at the base of the interval (Figure 3.13A and B). Notably, no feeder channels are observed at the stratigraphic interval where these seismic facies change as described above. Furthermore, extraction of the curvature seismic attribute along the base horizon (i.e., detachment surface) displays a rugose pattern within the area where the "SW Sands" occur as opposed to a smooth surface in other areas on the map (Figure 3.14).

Wireline log cross-sections show a general basinward thickening of sandstone bedsets represented by overall blocky and narrow-spiky gamma-ray log motifs (Figure 3.9B). The sandstone beds are poorly consolidated and comprised of very fine to fine sand (New Zealand Overseas Petroleum Ltd, 2004). The thickest sandstone interval is ~50 m, recorded in the Pateke-2 drill hole. However, these sandstone intervals cannot be individually correlated down dip.

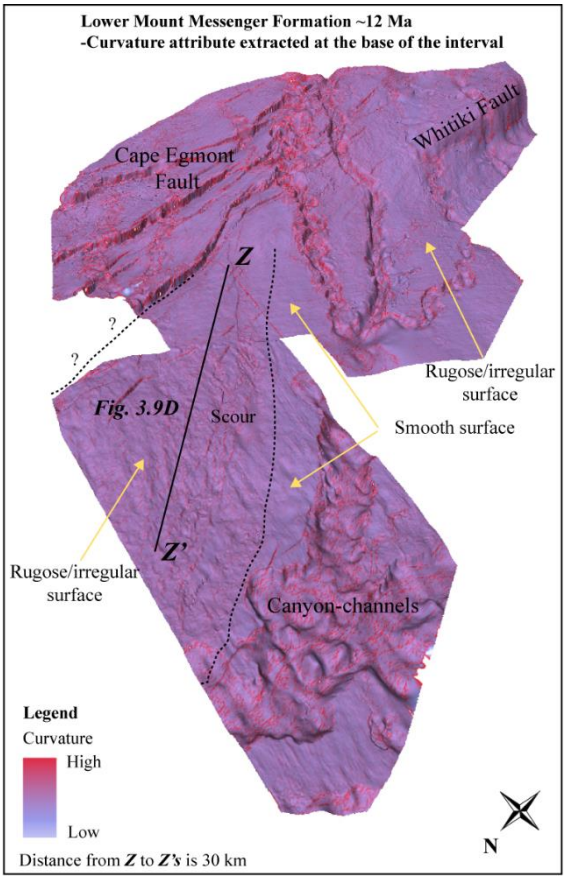

Figure 3.14: Curvature seismic attribute extraction from the base of an interval (+10 ms) characterised by sandy debris flows in the lower Mount Messenger Formation. The surface is characterised by rugose topography, and is interpreted as a debris flow detachment surface.

Based on the distribution of high-amplitude regions in detuned amplitude maps, the lack of feeder channel mouths and the blocky gamma-ray log characteristics with poor lateral and down-dip continuity, I interpret the Mount Messenger Formation interval in the area, as analysed by Kroeger et al. (2019), to be dominated by amalgamated sandy debris flow beds separated by mudstone. These debrites would have been deposited on the lower slope by flows with high sediment concentration, a low Reynolds number (i.e., laminar flow), and a relatively high matrix strength (Figure 3.7). This interpretation is further supported by seismic reflection profiles that show down-dip (towards the NW, parallel to slope orientation) changes in their coherence, amplitude and vertical stacking, which I take to represent a detachment surface at the base of a sandy debris flow interval (Figure 3.13). The rough surface identified at the base

of the lower Mount Messenger Formation (Figure 3.14) is attributed to the scouring of debris flows into the underlying mudstone strata ahead of the actual deposition from the debris flow (Figure 3.13). The analogue to this interpretation (debris flows) is presented in publications (e.g., Piper et al., 1985; Sohn, 2000; Pareschi et al., 2000).

3.6.4 Part II: New insights into the Taranaki Basin deep-water fan systems

I further investigated here the Mount Messenger Formation fan systems in deep-water Taranaki Basin beyond the contemporary depositional slope. This mapping and interpretation were carried out using the fan criteria of Posamentier and Erskine (1991), as outlined in Table 3.1. The results show that in offshore western Taranaki Basin there are two main deep-water fan systems: (i) a Middle Miocene Deep Water Fan System 1 (~13–12 Ma; Waiauan Stage), and (ii) a Late Miocene Deep Water Fan System 2 (~7–6 Ma; Kapitean Stage), both of which are characterised by a terminal submarine fan (Figure 3.15). The pathway for the older of the two fan systems originated from the southeast part of the basin and propagated through the Maui Field area, routing sediment in a southeast to northwest direction to deep Taranaki Basin. The younger sediment pathway (Late Miocene Deep Water Fan System) originated in the south and flowed directly northward to the deep-water basin plain. Here, i describe both deepwater fan systems appealing to a simplified tripartite scheme consisting of (i) feeder canyon-channel networks, (ii) upper fan segment, and (iii) lower fan segment.

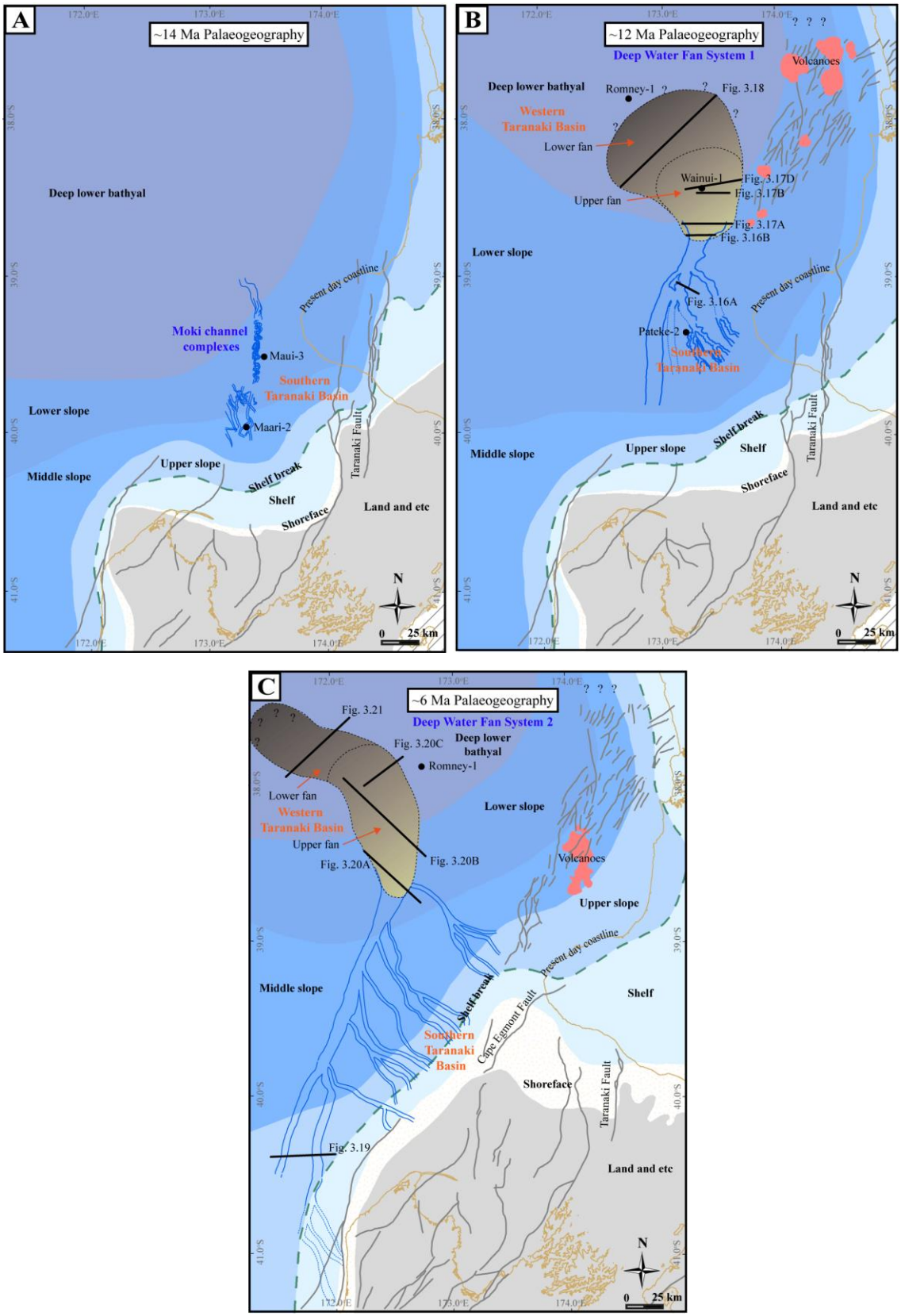

Figure 3.15: Revised paleogeography maps of: (A) upper Moki Formation (~14 Ma), Mount Messenger Formation (B) Deep Water Fan System 1 (labelled DWF1 in Figure 3.2) and (C) Deep Water Fan System 2 (labelled DWF2 in Figure 3.2). Note that I remove fans from the paleogeography maps in southern and central Taranaki Basin entirely in all intervals, but depict new fans in deep Taranaki Basin in the western part of the basin (i.e., in B and C). The paleobathymetry, active faults and volcanoes are adapted from Strogen et al. (2011)

3.6.4.1 Deep water fan system 1 (Middle Miocene)

3.6.4.1.1 Feeder canyon-channel networks

The Mid-Miocene feeder canyon-channel is located on the lower slope and can be divided into upper and lower parts, which together form a network. The upper part of the feeder canyon-channel displays prominent convex-upward bulges with highly asymmetry canyon walls (Figure 3.16A). The canyons contain dense multi-storey (stacked) lateral channel complexes. The canyons have an average width of 8 km and an average depth of 215 m. The confined channel complexes have lesser widths and depths that range from 0.5 to 2 km and 20 to 120 m, respectively (Kamaruzaman et al., 2023). In map view, these internal channels are linear to sinuous. The slope gradient in the region ranges from 0.3 to 0.5^{o}.

The lower part of this canyon-channel network passes basinward into the main feeder channel where it becomes less confined and has nearly symmetric walls (Figure 3.16B). Wall steepness decreases significantly as the main channel broadens across the lower slope with a gradient less than 0.2^{o}. A convex-up surface at the top of the channel complex is observed throughout the region, even though the convex-up surface is less conspicuous than in the upper feeder canyon-channel region. The width of the main channel increases from ~12.5 to ~15 km basinward. As with the upper feeder canyon-channel (Figure 3.16A), the lower feeder channel (Figure 3.16B) is also composed of numerous superimposed channels within the complex with average widths between 1.0 and 2.5 km and average depths between 40 and 80 m. In contrast to the densely stacked channel complex in the upper feeder canyon-channel region, the channel complex of the lower feeder channel region displays less multi-storey stacking and has a more lateral (adjacent) offlapping arrangement. Channel networks in this region are sinuous to meandering.

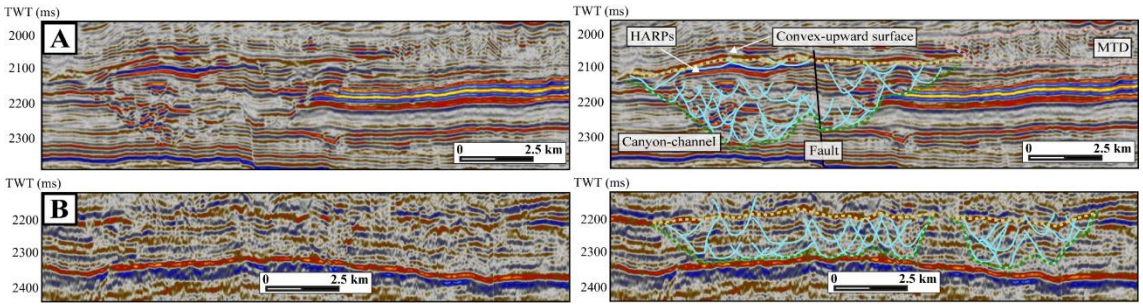

Figure 3.16: Uninterpreted and interpreted (A) upper (inline 1080, Kokako 3D) and (B) lower (2D seismic line BO_81 nm-204–1018) parts of feeder canyon-channels in the Mount Messenger Formation Deep Water Fan System 1 (~12 Ma). Refer to Figure 3.15B for cross-section location.

3.6.4.1.2 Upper fan segment

An upper fan segment can be observed immediately basinward of the mouth of the primary feeder channel, and it extends outward across a slope of approximately 0.4°, with a width ranging from 32.5 to 50 km (Figure 3.17). The upper surface of the fan exhibits subtle low-relief mounding, characterized by a convex-up morphology and high-amplitude reflections along its upper bounding surface. Above this top surface, the fan is overlain by an interval of chaotic and low-amplitude reflectors.

Within the upper fan, a combination of stratified and discontinuous medium to high-amplitude reflections can be distinguished from the low-amplitude reflections in underlying strata (Figure 3.17D). Subtle bidirectional pinch-out of reflectors and multiple channel incisions with concave-upward infill patterns are also observed. The maximum width of channel systems within the region is approximately 2.5 km. The basal bounding surface of the fan is identified by truncation of reflectors against the underlying strata, and the surface is depressed at the centre of the fan and rises towards the flanks before pinching out beneath overlying strata (Figure 3.17B). Gamma-ray log responses from the appropriate Wainui-1 drill

hole level reveals that the fan is approximately 100 m thick with the gamma-ray log showing an alternate increasing and decreasing signal upward through the fan succession (Figure 3.17C).

I interpret the presence of a subtle low-relief mounding surface at the top of the fan to indicate rapid sedimentation and associated fan build up within the vicinity of the mouth of feeder channels, generally in the centre of the fan (Figure 3.17A). This feature is subtle in cross-sectional images. However, well completion reports for the Wainui-1 drill hole indicate that the fan strata are overlain by Mohakatino Formation strata (Shell BP Todd Oil Services Ltd, 1982) (Figure 3.17C), which I interpret as a 250–350 m thick mass transport deposit (MTD) because of its chaotic and low amplitude reflectors. The occurrence of bidirectional reflector pinch-out and concave-upward channel incision suggests lateral migration of channels and switching of lobe complexes (Figure 3.17B). Bidirectional downlapping reflectors at the edge of the fan are not clearly observed, as the late-Middle Miocene seafloor slope in the region was very low, with a mean gradient of only 0.4^{o}. Depression at the base and centre of the fan complex is attributed to compaction subsidence of the fan into the underlying Manganui Formation mudstone (Figure 3.17B). The gamma-ray log motif corresponds to alternating coarsening (very fine sand) upward and fining (mud) upward successions indicating switching of lobe complexes as the fan built upward (Figure 3.17C).

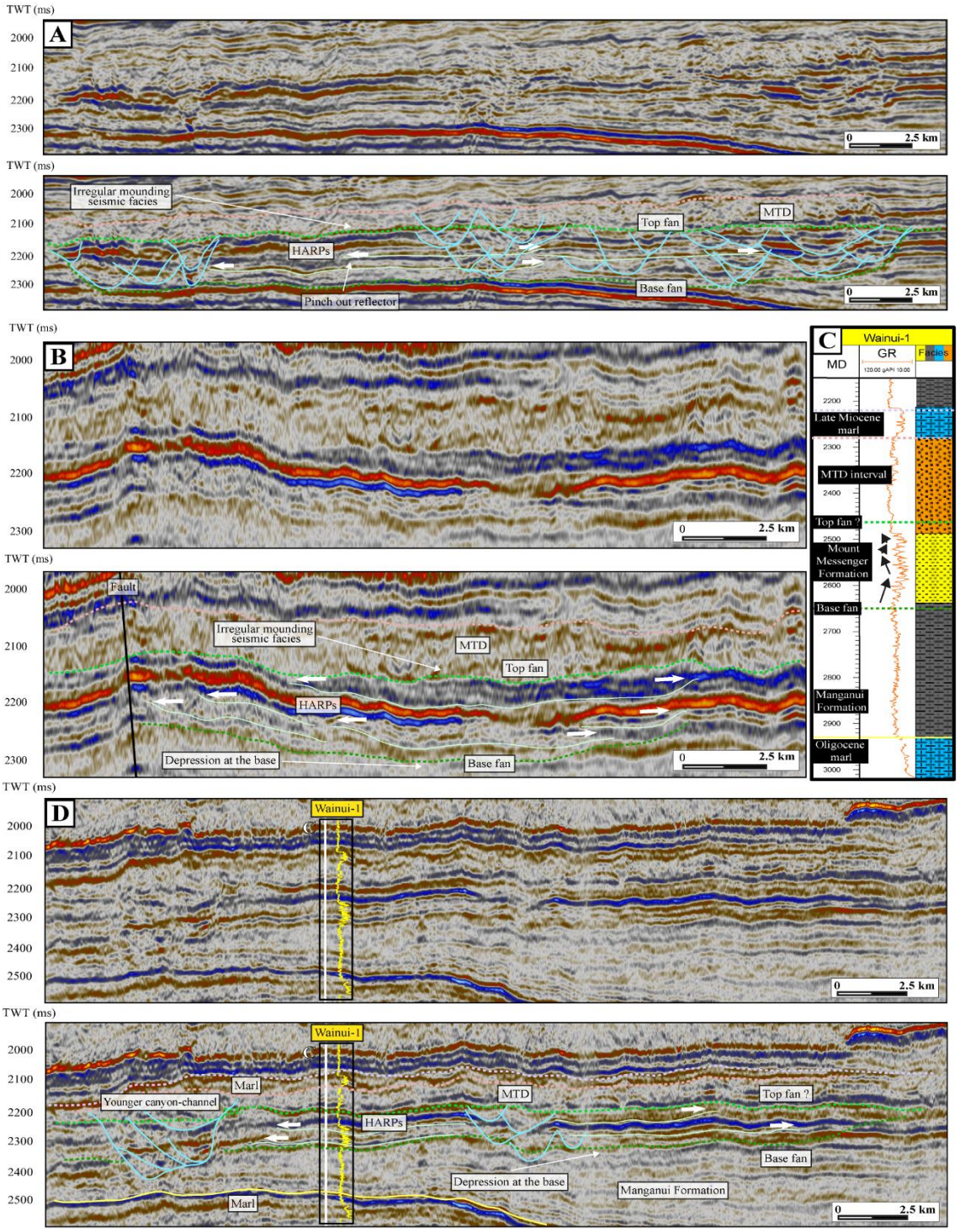

Figure 3.17: Uninterpreted and interpreted seismic sections of upper fan segment in the Mount Messenger Formation Deep Water Fan System 1 (~12 Ma): 2D seismic (A) line BO_ar90-445-110-1628, (B) line BO_ar89-446-106-1475 and (D) line ar89-446-108-1475. Refer to Figure 3.15B for cross-sections location. (C) Gamma-ray motifs and associated lithology from Wainui-1 drill hole.

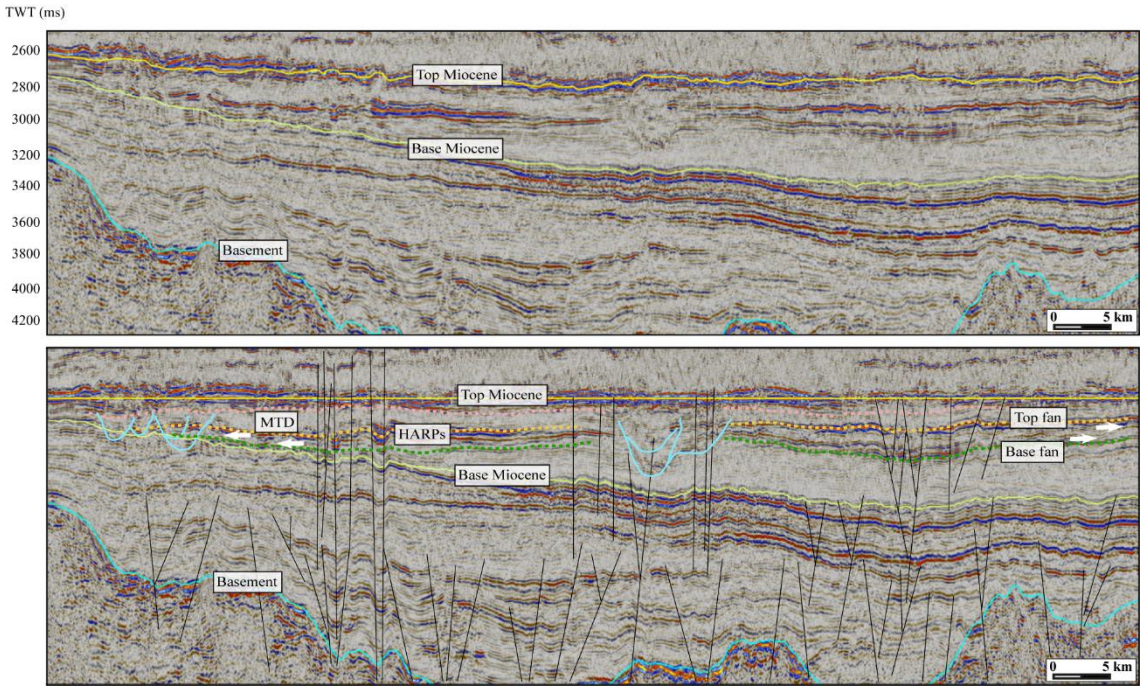

Figure 3.18: Uninterpreted and interpreted lower fan segment in the Mount Messenger Formation Deep Water Fan System 1 (~12 Ma), 2D seismic line BO_DTB01-26- 2847. Refer to Figure 3.15B for cross-section location.

3.6.4.1.3 Lower fan segment

The lower fan segment is situated on the basin floor where the slope is ~0.2°. This portion of the fan extends for approximately 75 km laterally (Figure 3.18). While high amplitude continuous reflectors mark its upper bounding surface, stratal truncation along the basal bounding surface is not observed. Fan strata primarily onlap the high sloping margins of the basin floor along its southwestern side, which demarcates the southwestern boundary of the fan. There is no channel incision into the lower fan segment originating from the southeast. The lower fan blanketed the prior flat seafloor profile with sheet-like deposits. There may be a volcanic ash component within the upper part of the fan as Mohakatino volcanic edifices occur nearby to the northwest (Figure 3.15B). The base of the fan is identified by a contrast in seismic facies with low amplitude reflectors of Manganui Formation mudstone, contrasting with medium amplitude reflectors of the lowermost fan facies. Stratal onlap of sloping portions of

the basin floor implies that pre-existing seafloor topography influenced the distribution of the fan and its depositional trajectory towards the head of the New Caledonia Basin (also known as the Aotea Basin). A northern boundary of the fan has not been identified. A channel system that incises this fan segment from the west is associated with a younger sediment routing system.

3.6.4.2 Deep water fan system 2 (Late Miocene)

3.6.4.2.1 Feeder canyon-channel networks

The sediment pathway system at ~7–6 Ma includes a feeder canyon-channel network that supplied sediment to a fan in lower bathyal water depths (Figure 3.15C). The canyon network originated from the south, with the main branch having a width of 4.2 km and symmetrical walls and the other branch being 8 km wide with asymmetrical walls (Figure 3.19). The average depth of both channels was about 260 m. Both channels were directed basinward across a slope with an average gradient of ~1.5°. The infill of the channels is a combination of stratified and discordant low to medium-amplitude reflectors and they display a predominantly concave-upward pattern. The internal organisation of the channel systems is one of predominantly multi-storey (i.e., stacked) sediment accumulation.

3.6.4.2.2 Upper fan segment

The upper fan occurs immediately basinward of the feeder canyon-channel network, on a slope gradient of ~1° (Figures 3.15C and 3.20). The upper fan is approximately 40 km wide in the immediate vicinity of the feeder canyon-channel mouth and 70 km wide where it

transitions into the lower fan segment. The base of the fan is recognized by the contrast between low amplitude reflectors of Manganui Formation mudstone and higher amplitude reflectors of the overlying fan (Figure 3.20B). The top of the fan is demarcated by high-amplitude reflectors. The lateral boundaries of the fan are identified by stratal onlap onto the underlying topography (Figure 3.20A). A channel system across the upper fan segment has an average width of 3.5 km and an average depth of 100 m.

The upper fan developed outside and west of the canyon-channel network due to it being less confined on the lower slope and basin plan region. Bidirectional pinch-out of reflectors and concave-upward channel incisions have been identified (Figure 3.20), indicative of lateral migration of the channel and switching of the lobe complex across the fan. However, evidence for bidirectional downlapping of fan reflectors against the seafloor is difficult to identify because the seafloor was so flat (~0.1^{o}). One challenge to clearly identifying the upper bounding surface of the fan was to differentiate its continuous high-amplitude reflectors from similar reflectors of the overlying Ariki Formation marl, which has similar characteristics.

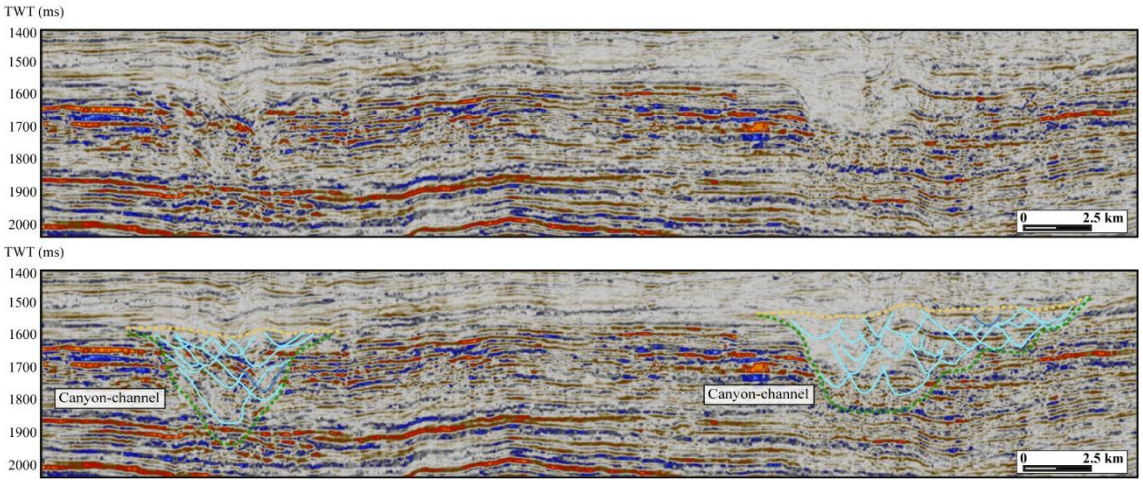

Figure 3.19: Uninterpreted and interpreted canyon-channel networks in the Mount Messenger Formation Deep Water Fan System 2 (~6 Ma), 2D seismic line BO_HZT82C_AWE_1_106. Refer to Figure 3.15C for cross-section location.

3.6.4.2.3 Lower fan segment

The lower fan segment is marked by stratified medium to high-amplitude reflectors that onlap the underlying topography (Figure 3.21). Away from these margins, and in the middle of the lower fan segment, reflectors are more or less continuous and have low amplitude.

The underlying topography expressed as structural highs in the region extends into the New Caledonia Basin. These highs controlled the initial morphology of the fan and its depositional trajectory. However, in the lower fan segment it is challenging to differentiate the fan from background Manganui Formation mudstone strata due to both being expressed as amplitude reflectors, possibly signifying that the lower fan is mud-prone. Incising into the top of the fan are younger canyon-channels heading towards New Caledonia Basin.

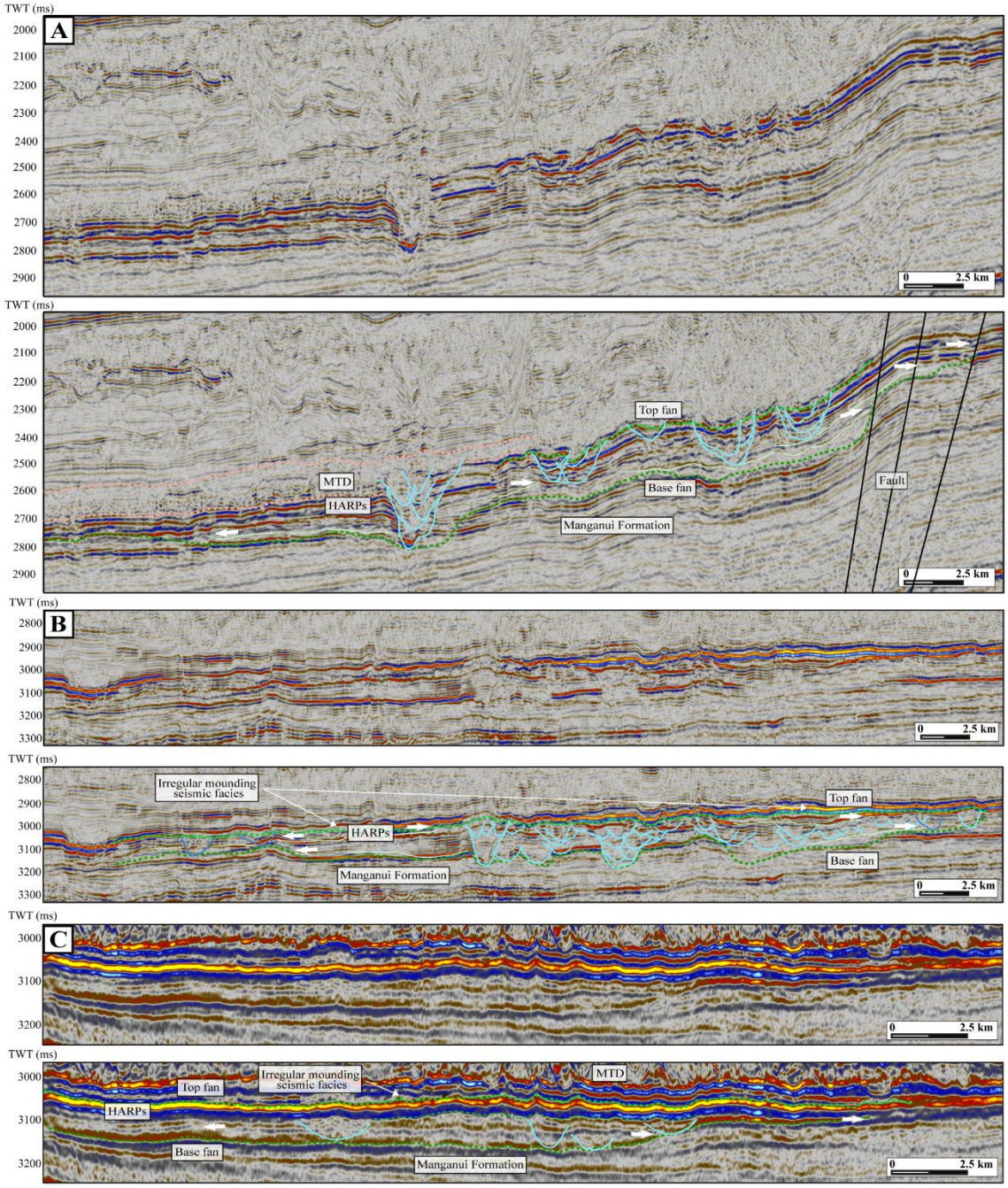

Figure 3.20: (A) 2D seismic line BO_DTB01-21-2847, (B) 2D seismic line BO_DTB01-19-2847 and (C) Inline 2150, Romney 3D, uninterpreted and interpreted upper fan segment in the Mount Messenger Formation Deep Water Fan System 2 (~6 Ma). Refer to Figure 3.15C for cross-section location.

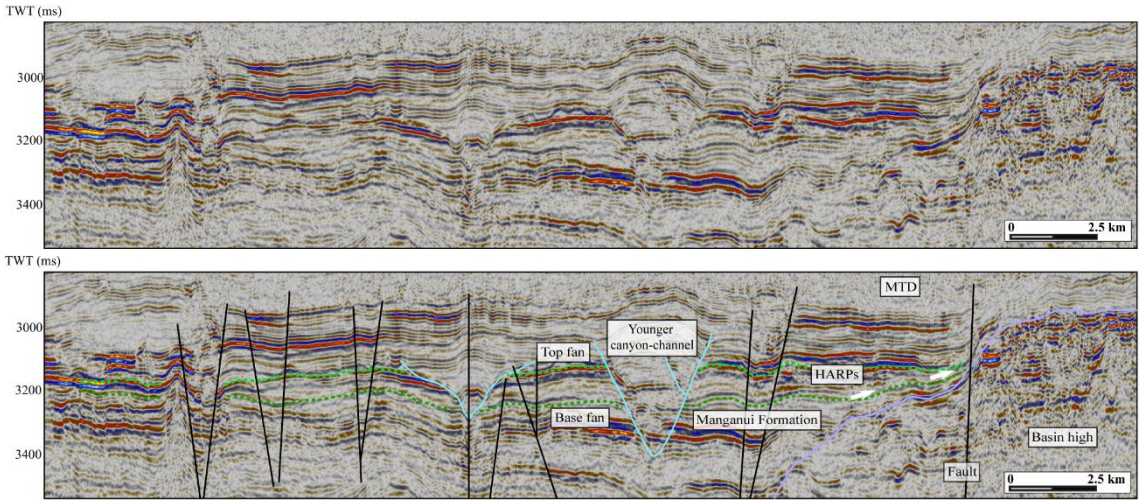

Figure 3.21: Uninterpreted and interpreted lower fan segment in the Mount Messenger Formation Deep Water Fan System 2 (~6 Ma), 2D seismic line BO_DTB01-08- 2847. Refer to Figure 3.15C for cross-section location.

3.7 Discussion

3.7.1 Dismissal of middle Miocene fan systems in southern and central Taranaki Basin

Submarine channels in southern and central Taranaki Basin have been described in several papers (e.g., King and Thrasher, 1996; Baur et al., 2010; Strogen et al., 2011; Kroeger et al., 2019), but in none of them provided explicit documentation of where the mouth of a feeder channel has transitioned into a fan. For example, in the paleogeographic maps in Kroeger et al. (2019) (see Figure 3.4) most of the submarine channels cross fans along their whole down-slope length; that is, the mouths of feeder channels do not transition into fans, but rather pass through them. I think that this highly atypical stratal arrangement is incorrect and arises from two incorrect interpretations. (1) The high amplitude slope strata adjacent to channels have been interpreted to represent turbidite beds or bedsets and hence are considered to have accumulated as submarine fans. (2) High amplitude continuous reflectors on the flanks of channels define submarine fan geometry. My detuning of the southern and central Taranaki Basin seismic reflection within the interval of interest ahead of amplitude extraction, has resulted in removal of the high amplitude signal in most areas where fans have previously been defined (Figure 3.9), including adjacent to channels, meaning that the inferred fan geometry is an artifact of bed thickness; that is, those fans do not exist in reality. In the one area where high-amplitude remained after detuning, which was named the ”SW Sands” by Kroeger et al. (2019) (Figure 3.9C and D), curvature seismic attribute extraction shows a rugose surface at its base (Figure 3.14), which resulted from seafloor scouring typical of the base of debris flows (Costard et al., 2001; Micallef et al., 2007; Nomikou et al., 2009; Posamentier et al., 2011). Hence, the patchy amplitude distribution in the area of “SW Sands” better fits a model of patchy base of slope deposition of thick isolated and discontinuous sandy debris flows amongst muddy

strata (Zampetti et al., 2004; Bernhardt et al., 2012; Liu et al., 2023), rather than the deposition of lowstand turbidite fans as in Kroeger et al. (2019). Accordingly, I have interpreted the upper Moki and lower Mount Messenger formation strata showing high amplitude reflections adjacent to channels as representing upper to middle slope debris flow deposits (debrites). In addition, the fans inferred by Kroeger et al. (2019) and others do not meet the criteria for fan systems as outlined in Tables 3.1 and 3.3, which are widely applied to (fully or partially) recognise fan systems in deep water settings using seismic reflection data (Mitchum et al., 1985; Posamentier & Erskine, 1991; Jager et al., 1993; Radovich et al., 2002; Pickering & Corregidor, 2005; Saller et al., 2008; Covault & Romans, 2009; Vesely, 2016; Park et al., 2021). In seismic reflection lines across the inferred Kroeger et al. (2019) fans, the only seismic criteria that could potentially support them is the presence of high amplitude reflectors (Figure 3.8; Table 3.3). However, the continuous high amplitude reflectors adjacent to channels are repeated in sections with thicknesses of 20–40 ms, rather than being limited to the upper bounding surface. This contradicts observations of fan systems by other workers (e.g., McHargue, 1991; Flood et al., 1991; Gong et al., 2022; Maier et al., 2020). Hence, I have dismissed interpretations about the occurrence of submarine fans in the Moki and Mount Messenger formations in southern and central Taranaki Basin as reported in King and Thrasher (1996), Grain (2008), Baur et al. (2010), Strogen et al. (2011) and Kroeger et al. (2019).

3.7.2 New deep water fan systems in the Mount Messenger Formation

Mapping of canyon and channel networks in offshore western Taranaki Basin reveals two major Mount Messenger Formation fan systems (i.e., a Middle Miocene Deep Water Fan System 1: DWF1 and a Late Miocene Deep Water Fan System 2: DWF2 in Figure 3.2) and associated sediment routing pathways (Figure 3.15B and C). I have included both of these fan systems in the Mount Messenger Formation, even though the older one is of Waiauan age

(about 13–11 Ma) and about 1–2 million years older than the 11 Ma age of the base of this formation as defined in the coastal North Taranaki outcrop section (King et al., 1993). The Middle Miocene Deep Water Fan System 1 fan has previously been attributed to the Mohakatino Formation in the well completion report for Wainui-1 (Shell BP Todd Oil Services Ltd, 1982). While some volcanic ash is recorded in the fan interval, this fan is best included in the Mount Messenger Formation as it represents diachronous outbuilding of sediment sourced from the south, as for other parts of this formation. These two newly identified fan systems were identified from analysis of seismic reflection data using the stratal patterns summarised in Table 3.1. They also fulfil most of the submarine fan criteria presented in Table 3.3. Both of these submarine fans occur at the terminus of channel mouths and lie on the outer parts of the lower slope and basin plain. This contrasts with the King and Thrasher (1996), Strogen et al. (2011) and Kroeger et al. (2019) fan locations higher up on the continental slope. New paleogeographic maps including the two new fans are shown in Figure 3.15B and C.

Table 3.3: Assessment of recognition criteria for fans in southern and central Taranaki Basin versus western Taranaki Basin for the upper Moki and lower Mount Messenger formations based on seismic and well log data. Criteria after Posamentier and Erskine (1991) but expanded upon.

Aspect	Criteria	Southern Taranaki Basin		Western Taranaki Basin	
		Upper Moki Fm. (~14 Ma)	Lower Mt. Messenger Fm. (~12 Ma)	Mt. Messenger Fm. Deep Water Fan System 1 (~12 Ma)	Mt. Messenger Fm. Deep Water Fan System 2 (~6 Ma)
Physiography of fan systems	The mouth of the feeder canyon-channels can be located				
	The segments of the fans (i.e., upper and lower) can be identified				
Seismic stratigraphic interpretation	Continuous high-amplitude reflectors (usually at top fans) onlap basin margin				
	Bidirectional downlap reflectors within fan				
	Stratal terminations show pinchout				
	External mounding on the fan upper bounding surface				
Seismic amplitude analysis	Detuned seismic maps show regions of high amplitude that resemble fans				
Gamma-ray log signature	Overall trend of Gamma-ray log leaning towards fan depositions				

Legend

High confidence Low confidence No confidence

Cannot be accessed

3.7.2.1 Factors controlling fan development

A revised southern Taranaki paleogeographic map for the 14 Ma interval (Figure 3.15A) shows the main channel of the Moki Formation does not connect with a submarine fan. This arises because there was insufficient terrigenous sediment supply to form a fan. Sandstone is markedly subordinate to mudstone in the Early and Middle Miocene succession of Taranaki Basin. Sandstone became more common during the Late Miocene when uplift and erosion of the basement underlying the Southern Alps started along the continent-continent plate boundary in South Island (Kamp et al., 1989; Tippett and Kamp, 1993; Ring et al., 2019). Zircon U-Pb ages for two samples from the Moki Formation in Kea-1 (southern Taranaki Basin) have age distributions suggesting a source from Cretaceous basement in northwest Nelson immediately south of Taranaki Basin (unpublished data, 2023). The zircon ages are not similar to the distinctive age distribution of the Permian and Triassic age peaks in Torlesse Complex sandstone and schist that underlies the Southern Alps. Insufficient sand was supplied to the Moki channels to build a submarine fan beyond the sand that accumulated within the channels. A revised paleogeography is shown in Figure 3.15A.

The rate of terrigenous sediment supply to Taranaki Basin increased rapidly from about 12 Ma and particularly from 11 Ma (Tongaporutuan Stage), as expressed in the voluminous accumulation (e.g., 510 m thick in Tuhua-1; Figure 3.1) of the Mount Messenger Formation, both in Taranaki Basin and across the King Country Basin to the east of Taranaki Basin (Kamp et al., 2004), which markedly prograded the shelf-slope margin to the northwest within the Taranaki foreland basin (Bull et al., 2019). This coincides with the age of early uplift of the Southern Alps (Kamp et al., 1989; Tippett and Kamp, 1993; Ring et al., 2019), and with the start of inversion in southern Taranaki Basin (Kamp and Green, 1990; Crowhurst et al., 2002), which enhanced progradation of the shelf-slope margin to the north into the Taranaki Peninsula

area and northwest into deeper parts of the basin. These factors help explain why there is no submarine fan associated with the Moki channels, yet fans accumulated in deep water to the west and north in the Mount Messenger Formation. The Middle Miocene Deep Water Fan System 1 (~13–12 Ma) coincides with the timing of a global drop in sea level (sea-level curve of Miller et al., 2020, Figure 3.3B). While sea level change is considered to influence deep water sedimentation processes (e.g., Posamentier and Erskine, 1991; Xiong et al., 2004; Saller et al., 2004) the mechanism by which this occurs in the case of channel and fan development in Taranaki Basin is difficult to substantiate. The Late Miocene Deep Water Fan System 2 (~7–6 Ma) in deep water Taranaki Basin shows little correlation with a fall in sea level (less than 10 m) on the Miller et al. (2020) sea-level curve (Figure 3.3B). Many workers (e.g., Covault and Graham, 2010; Dixon et al., 2012; Harris et al., 2018) have argued that deep water sedimentation can occur at any phase of a sea level cycle where submarine sediment routing systems remain connected to their sediment source areas, which may also have been the case for Taranaki Basin (Maier et al., 2013).

Research efforts to date have shown that the Moki Formation channels were relatively stable in their locations. From the late-Middle Miocene (Waiauan Stage) onwards, the shelf-slope margin in Taranaki Basin became increasingly rich in gullies as the depositional slope became steeper (Kamaruzaman et al., 2023). In the Mount Messenger Formation, the gullies were captured by feeder canyon-channels, which in turn fed sediment to two fans of different age (~13–12 Ma and ~7–6 Ma). However the rate of sediment supply to the depositional slope during the Late Miocene also resulted in the retention of a proportion of the material in the gully network, with frequent burial of gullies and formation of new ones as the slope rapidly prograded to the north and west (Kamaruzaman et al., 2023). The retention of material on the slope can partly explain the enigma that although there was copious supply of sediment to the

basin during the Late Miocene, so far only two Mount Messenger Formation submarine fans have been documented outboard of the depositional slope (c.f., Fisher et al., 2021).

3.7.2.2 Modern analogue

As noted above, the newly mapped Middle and Late Miocene deep-water fans in western Taranaki Basin are mudstone-dominated. Despite the Wainui-1 drill hole containing intervals of sandstone in the upper fan part of the ~13–12 Ma fan (Figure 3.17C), the maximum width (10 km) of the main feeder canyon-channels and the distance of the fans from the contemporary shelf-slope break (~150 km) support this notion. The principal source rock area (Torlesse Complex in the Southern Alps) for the two fans is comprised of greywacke and schist, which breaks down by weathering and attrition to fine sand and mud. The closest analogue to the conditions that led to the Late Miocene fan accumulations in Taranaki Basin is the fan that has formed at the mouth of the Hikurangi Channel east of North Island (Figure 3.22) (Grahame, 2015). Sediment entering the Hikurangi Channel is fed by the very steep Kaikoura Canyon offshore of the northern end of the Southern Alps and by canyons at the eastern end of Cook Strait (Figure 3.22). The sediment routed via the Cook Strait canyons followed a pathway from the western face of the Southern Alps via longshore drift to the northwestern tip of South Island (Farewell Spit) and hence into Cook Strait. The Hikurangi Channel mostly lies at 3000–5000 m water depth east of the Hikurangi subduction zone. It traverses the Hikurangi Plateau (thickened oceanic crust) northward before turning sharply east and then north upon reaching the Southwest Pacific Abyssal Plain, where sediment transport and the depositional trajectory are strongly controlled by the Ocean Conveyor Current (Hikurangi Fan-drift; Lewis, 1994; Carter et al., 2004). At the terminus of the channel the sediment has accumulated in a mud-dominated basin floor fan called the Hikurangi Fan, which started accumulating during the late

Neogene (Figure 3.22) (Lewis et al., 2013; Mountjoy et al., 2018). Common features of the Hikurangi Fan and the Late Miocene fans in the Mount Messenger Formation are, (i) that their sediments derived from the same source area, (ii) they lie at the mouths of prominent channels, (iii) the sediments comprising the fans are mudstone, and (iv), they have similar plan shapes. In addition, the respective fans are small in size and volume compared with the volumes of material eroded from the Southern Alps during the late Neogene.

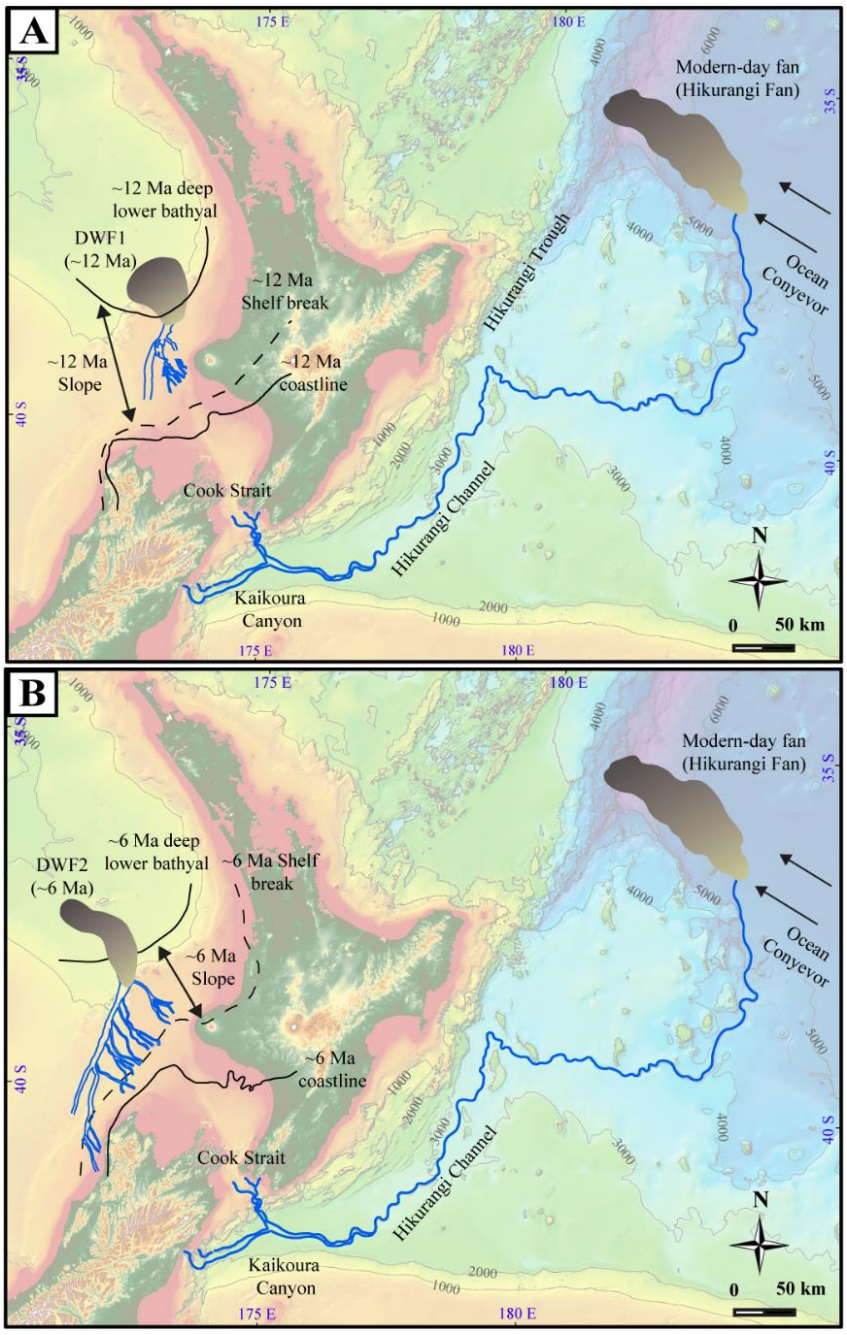

Figure 3.22: Comparison between the newly interpreted (A) the Mount Messenger Formation Deep Water Fan System 1: DWF1 (~12 Ma) and (B) the Mount Messenger Formation Deep Water Fan System 2: DWF2 (~6 Ma) with the late Neogene fan (Hikurangi Fan) at the terminus of the Hikurangi Channel. Subdivision between the paleo-coastline, shelf-break (at 200 m water depth) and deep lower bathyal (>1500 m water depth) for ~12 Ma and ~6 Ma are also shown. The modern Hikurangi Channel and fan outlines are adapted from (Lewis et al., 2013), and modern seafloor bathymetry data (water depth in meter) are from NZP&M (2018).

3.7.2.3 Significance of newly mapped deep water Mount Messenger formation fan systems for resource exploration

The significance of Moki Formation channels for petroleum exploration and production has been well described by Engbers et al. (2000) and Engbers (2002). The two newly mapped Mount Messenger submarine fans occur on the Western Stable Platform, a structural province built upon Palaeozoic basement, overlain in places by Late Cretaceous-Paleocene sediments, sometimes in half-grabens. The province is onlapped by Eocene-Recent strata disrupted by few faults (King and Thrasher, 1996). The Top Eocene surface forms a monocline dipping east, in part arising from flexure associated with Oligocene-Miocene foreland basin subsidence to the east (Holt & Stern, 1994). Oligocene and Miocene sediments onlap the monocline, including the two new fans described here. This structural and stratigraphic setting differs from that in the Taranaki oil and gas fields, which arises from structural traps. These either formed through shortening within the Taranaki Fault System or shortening in the southern Taranaki Inversion Zone, where antiforms formed from the inversion on pre-existing normal faults. The antiforms represent migration of shortening from the Taranaki Fault System into the foreland basin during the Late Miocene. Hence the two fans lie in frontier parts of Taranaki Basin and should oil and/or gas occur there, it is likely to be in stratigraphic traps. The presence of high-amplitude reflectors within the proximal upper fan segments, probably images continuous sheet sandstone beds (Shanmugam & Moiola, 1988; Nagatomo & Archer, 2015; Mayall & Kneller, 2021). This differs from the distal lower fan segments, which appear to be muddier, as shown by lower seismic amplitude (Reading & Richards, 1994; Bouma & Stone, 2000; Fildani et al., 2021). The mud-rich sediment calibre of the two fans and the inclusion of volcanic ash in the younger one will likely be challenges for reservoir quality. Seal may not be an issue. Given that only one drill hole (Wainui-1) has been located over one of the fans means that source rock distribution and composition are poorly known. Maturation of organic matter in either of the

two fans will be an issue (VR of 0.58% in the coal measure beds in Wainui-1) to charge stratigraphic traps within the fans. Hence migration pathways from deeper organic horizons will need to be considered in any exploration proposal. To further access the petroleum potential of the fans, high-resolution 3D seismic volumes and seep analysis will likely be required ahead of drilling to gain some confidence about the presence or otherwise of mobile thermogenic hydrocarbons in the Mount Messenger Formation within the vicinity of the documented fans.

3.8 Conclusions

1. Submarine channels in the Middle Miocene Moki Formation are standalone features on the continental slope in southern Taranaki Basin and do not transition down-slope into submarine fans. Detuning of 3D seismic data coverage has removed the RMS high amplitude extracted attribute signal from which the previously published Moki Formation fans have been inferred. Published late-Middle Miocene submarine fans located on the continental slope in the lower Mount Messenger Formation (southern and central Taranaki Basin) have also been dismissed on the same basis as well as not displaying well-established stratal criteria for the identification of fan systems (Table 3.3).

2. Two new submarine fan systems in the Mount Messenger Formation do, however, occur in deeper parts of western Taranaki Basin, one of late-Middle Miocene age and the other of Late Miocene age. They have been mapped and verified on established submarine fan stratal criteria.

3. A marked increase in terrigenous sediment supply at about 12 Ma, sourced from uplift and erosion of the Southern Alps, resulted in rapid progradation of the Late Middle to Late Miocene continental slope in Taranaki Basin. Most sediment rapidly accumulated on the slope. Consequently, its angle increased and gullies became prolific, incising, infilling, re-incising and being buried. A few channels are mapped on the lower slope passing into a fan on the basin plain. A second fan with similar attributes and 7–6 Ma age accumulated above the first, extending farther out towards the New Caledonia Basin. Both fans are mud-dominated. Their volume is minor compared with the volume of sediment delivered to the basin during the Late Miocene and hence submarine fans are much less volumetrically significant than the slope as depositional surfaces. The Hikurangi Fan outboard of the Hikurangi subduction zone is a modern analogue for the two new fans documented here for western Taranaki Basin.

3.9 References

Ab Fatah, A., Mohamed, H., Hee, R. P., & Tukimin, N. (2016). Horizon Independent Detuning of Seismic Volume from Sarawak Field. *2016*(1), 1-5. https://doi.org/https://doi.org/10.3997/2214-4609.201602407

Amy, L. A., & Talling, P. J. (2006). Anatomy of turbidites and linked debrites based on long distance (120 × 30 km) bed correlation, Marnoso Arenacea Formation, Northern Apennines, Italy. *Sedimentology*, *53*(1), 161-212. https://doi.org/https://doi.org/10.1111/j.1365-3091.2005.00756.x

Assis, C., Santos, H., & Schleicher, J. (2018). Colored and Linear Inversions to Relative Acoustic Impedance. *Geophysics*, *84*(2). https://doi.org/DOI:10.1190/geo2018-0185.1

Baur, J. R., King, P. R., Stern, T., Leitner, B., Wood, L. J., Simo, T. T., & Rosen, N. C. (2010). Development and Seismic Geomorphology of a Miocene Slope Channel Megasystem, Offshore Taranaki Basin, New Zealand. In *Seismic Imaging of Depositional and Geomorphic Systems* (Vol. 30, pp. 0). SEPM Society for Sedimentary Geology. https://doi.org/10.5724/gcs.10.30.0618

Bernhardt, A., Stright, L., & Lowe, D. R. (2012). Channelized debris-flow deposits and their impact on turbidity currents: The Puchkirchen axial channel belt in the Austrian Molasse Basin. *Sedimentology*, *59*(7), 2042-2070. https://doi.org/https://doi.org/10.1111/j.1365-3091.2012.01334.x

Bierbrauer, K., Herdy, T., Rek, A., & Mills, K. (2008). Exploring the Greater Taranaki Basin north of the established hydrocarbon fairway.

Bouma, A. H. (1962). *Sedimentology of some flysch deposits: A graphical approach to facies interpretation*. New York: Elsevier.

Bouma, A. H., & Stone, C. (2000). Fine-grained, mud-rich turbidite systems: model and comparison with coarse-grained, sand-rich systems. *Special Publication-SEPM*, *68*, 9-20.

Brown, A. R., Wright, R. M., Burkart, K. D., Abriel, W. L., & McBeath, R. G. (1986). Tuning effects, lithological effects and depositional effects in the seismic response of gas reservoirs. *Geophysical Prospecting*, *34*(5), 623-647. https://doi.org/https://doi.org/10.1111/j.1365-2478.1986.tb00485.x

Bunt, R. J. W. (2015). The use of seismic attributes for fan and reservoir definition in the Sea Lion Field, North Falkland Basin. *Petroleum Geoscience*, *21*(2-3), 137-149. https://doi.org/https://doi.org/10.1144/petgeo2014-055

Campbell, H. J., Mortimer, N., & Turnbull, I. M. (2003). Murihiku Supergroup, New Zealand: Redefined. *Journal of the Royal Society of New Zealand*, *33*(1), 85-95. https://doi.org/10.1080/03014223.2003.9517722

Connolly, P. (2007). A simple, robust algorithm for seismic net pay estimation. *The Leading Edge*, *26*(10), 1278-1282. https://doi.org/10.1190/1.2794386

Costard, F., Forget, F., Mangold, N., Mercier, D., & Peulvast, J.-P. (2001). Debris Flows on Mars: Analogy with Terrestrial Periglacial Environment and Climatic Implications.

Covault, J. A., & Romans, B. W. (2009). Growth patterns of deep-sea fans revisited: Turbidite-system morphology in confined basins, examples from the California

Borderland. *Marine Geology*, *265*(1), 51-66. https://doi.org/https://doi.org/10.1016/j.margeo.2009.06.016

Covault, J. A., Shelef, E., Traer, M., Hubbard, S. M., Romans, B. W., & Fildani, A. (2012). Deep-Water Channel Run-Out Length: Insights from Seafloor Geomorphology. *Journal of Sedimentary Research*, *82*(1), 21-36. https://doi.org/10.2110/jsr.2012.2

Cronin, B. T., Akhmetzhanov, A. M., Mazzini, A., Akhmanov, G., Ivanov, M., & Kenyon, N. H. (2005). Morphology, evolution and fill: Implications for sand and mud distribution in filling deep-water canyons and slope channel complexes. *Sedimentary Geology*, *179*(1), 71-97. https://doi.org/https://doi.org/10.1016/j.sedgeo.2005.04.013

Crowhurst, P., Green, P., & Kamp, P. (2002). Appraisal of (U-Th)/He Apatite Thermochronology as a Thermal History Tool for Hydrocarbon Exploration: An Example from the Taranaki Basin, New Zealand. *AAPG Bulletin*, *86*. https://doi.org/10.1306/61EEDD82-173E-11D7-8645000102C1865D

Curray, J. R., Emmel, F. J., & Moore, D. G. (2002). The Bengal Fan: morphology, geometry, stratigraphy, history and processes. *Marine and Petroleum Geology*, *19*(10), 1191-1223. https://doi.org/https://doi.org/10.1016/S0264-8172(03)00035-7

Davis, C., Haughton, P., McCaffrey, W., Scott, E., Hogg, N., & Kitching, D. (2009). Character and distribution of hybrid sediment gravity flow deposits from the outer Forties Fan, Palaeocene Central North Sea, UKCS. *Marine and Petroleum Geology*, *26*(10), 1919-1939. https://doi.org/https://doi.org/10.1016/j.marpetgeo.2009.02.015

Deptuck, M. E., Steffens, G. S., Barton, M., & Pirmez, C. (2003). Architecture and evolution of upper fan channel-belts on the Niger Delta slope and in the Arabian Sea. *Marine and Petroleum Geology*, *20*(6-8), 649-676. https://doi.org/10.1016/j.marpetgeo.2003.01.004

Deptuck, M. E., & Sylvester, Z. (2018). Submarine Fans and Their Channels, Levees, and Lobes. In *Submarine Geomorphology* (pp. 273-299). https://doi.org/10.1007/978-3-319-57852-1_15

Droz, L., & Bellaiche, G. (1991). Seismic Facies and Geologic Evolution of the Central Portion of the Indus Fan. In P. Weimer & M. H. Link (Eds.), *Seismic Facies and Sedimentary Processes of Submarine Fans and Turbidite Systems* (pp. 383-402). Springer New York. https://doi.org/10.1007/978-1-4684-8276-8_21

Engbers, P. (2002). Evaluation of Moki sands prospectivity in Maui PML. 1989 New Zealand Oil Exploration Conference proceedings,

Engbers, P., Adams, S., Farmer, R., Mathers, R., & Soek, H. (2000). Whaarangi; Prospect Potential Resolved. SPE Asia Pacific Oil and Gas Conference and Exhibition,

Escutia, C., Eittreim, S. L., Cooper, A. K., & Nelson, C. H. (2000). Morphology and Acoustic Character of the Antarctic Wilkes Land Turbidite Systems: Ice-Sheet-Sourced Versus River-Sourced Fans. *Journal of Sedimentary Research*, *70*(1), 84-93. https://doi.org/10.1306/2dc40900-0e47-11d7-8643000102c1865d

Fildani, A., Kostic, S., Covault, J. A., Maier, K. L., Caress, D. W., & Paull, C. K. (2021). Exploring a new breadth of cyclic steps on distal submarine fans. *Sedimentology*, *68*(4), 1378-1399. https://doi.org/https://doi.org/10.1111/sed.12803

Flood, R. D., & Damuth, J. E. (1987). Quantitative characteristics of sinuous distributary channels on the Amazon Deep-Sea Fan. *GSA Bulletin*, *98*(6), 728-738. https://doi.org/10.1130/0016-7606(1987)98<728:QCOSDC>2.0.CO;2

Francis, A. (2015). Geophysics: A Simple Guide to Seismic Amplitudes and Detuning. *GeoExPro*, *12*. https://www.geoexpro.com/articles/2015/11/geophysics-a-simple-guide-to-seismic-amplitudes-and-detuning

Francis, A. (2016). *Seismic Amplitudes Benefit From Seismic Trace Detuning*. https://www.hartenergy.com/exclusives/seismic-amplitudes-benefit-seismic-trace-detuning-176002#:~:text=In%20summary%2C%20seismic%20trace%20detuning%20is%20a%20significant,and%20direct%20hydrocarbon%20detection%20from%20seismic%20data.%2018

Fudol, Y. A. H., Zhao, Y., Liu, H., Zhou, S., Li, Y., & Li, X. (2019). Origin and reservoir properties of deep-water gravity flow sediments in the Upper Triassic Ch6–Ch7 members of the Yanchang Formation in the Jinghe Oilfield, the Southern Ordos Basin, China. *ENERGY EXPLORATION & EXPLOITATION*, *37*(4), 1227-1252. https://doi.org/10.1177/0144598719832066

Gaina, C., Müller, D. R., Royer, J.-Y., Stock, J., Hardebeck, J., & Symonds, P. (1998). The tectonic history of the Tasman Sea: A puzzle with 13 pieces. *Journal of Geophysical Research: Solid Earth*, *103*(B6), 12413-12433. https://doi.org/https://doi.org/10.1029/98JB00386

Gani, M. R. (2004). From turbid to lucid: a straightforward approach to sediment gravity flows and their deposits. *The Sedimentary Record*(2(3)), 4-8. https://doi.org/https://doi.org/10.2110/sedred.2004.3.4

Grahame, J. (2015). Deepwater Taranaki Basin, New Zealand - New Interpretation and Modelling Results for Large Scale Neogene Channel and Fan Systems: Implications for Hydrocarbon Prospectivity. AAPG/SEG International Conference & Exhibition, Melbourne, Australia.

Grain, S. L. (2008). *Paleogeography of a Mid Miocene Turbidite Complex, Moki Formation, Taranaki Basin, New Zealand* Victoria University of Wellington].

Guo, Q., Islam, N., & Pennington, W. D. (2015). Tuning of flat spots with overlying bright spots, dim spots, and polarity reversals. *Interpretation: SEG*, *3*(3), SS37-SS48.

Hansen, R. J., & Kamp, P. J. J. (2002). Evolution of the Giant Foresets Formation, northern Taranaki Basin, New Zealand. Conference held at Auckland. Conference Contribution retrieved from https://hdl.handle.net/10289/3617

Haughton, P., Davis, C., McCaffrey, W., & Barker, S. (2009). Hybrid sediment gravity flow deposits – Classification, origin and significance. *Marine and Petroleum Geology*, *26*(10), 1900-1918. https://doi.org/https://doi.org/10.1016/j.marpetgeo.2009.02.012

Holt, W. E., & Stern, T. (1994). Subduction, platform subsidence, and foreland thrust loading: The late Tertiary development of Taranaki Basin, New Zealand. *Tectonics*, *13*, 1068-1092.

Jager, D. D. H., Giles, M. R., & Griffiths, G. R. (1993). Evolution of Paleogene submarine fans of the North Sea in space and time. *Geological Society, London, Petroleum Geology Conference Series*, *4*(1), 59-71. https://doi.org/doi:10.1144/0040059

Kamaruzaman, E. H., La Croix, A. D., & Kamp, P. J. J. (2023). Quantitative seismic geomorphology of sediment conduits on an evolving Miocene slope in Taranaki Basin (New Zealand): The influence of increasing slope gradient through time. *Marine and Petroleum Geology*, *152*, 106233. https://doi.org/https://doi.org/10.1016/j.marpetgeo.2023.106233

Kamp, P. J.J., & Green, P. (1990). Thermal and tectonic history of selected Taranaki Basin (New Zealand) wells assessed by apatite fission track analysis. *Aapg Bulletin - AAPG BULL*, *74*, 1401-1419.

Kamp, P. J.J., Green, P., & White, S. (1989). Fission track analysis reveals character of collisional tectonics in New Zealand. *Tectonics*, *8*, 169-195. https://doi.org/10.1029/TC008i002p00169

Kamp, P. J.J., Vonk, A. J., Nelson, C. S., Hansen, R. J., Tripathi, A. R. P., Hood, S. D., Nagati, M., & Hendy, A. J. W. (2004, 2004-03-07 to 2004-03-10). *Constraints on the evolution of Taranaki Fault from thermochronology and basin analysis: Implications for the Taranaki Fault play* [Conference Contribution]. Conference held at Wellington. https://hdl.handle.net/10289/3613

King, P., & Thrasher, G. P. (1996). Cretaceous-Cenozoic Geology and Petroleum Systems of the Taranaki Basin, New Zealand. *Insitute of Geological and Nuclear Science Monograph*, *13*(Part 1 and 2).

Kroeger, K. F., Thrasher, G. P., & Sarma, M. (2019). The Evolution of a Middle Miocene Deep-water Sedimentary System in Northwestern New Zealand (Taranaki Basin): Depositional Controls and Mechanisms. *Marine and Petroleum Geology*, *101*, 355-372. https://doi.org/10.1016/j.marpetgeo.2018.11.052

Lancaster, S., & Whitcombe, D. (2000). Fast‐track ‘coloured’ inversion. In *SEG Technical Program Expanded Abstracts 2000* (pp. 1572-1575). https://doi.org/10.1190/1.1815711

Lee, G. H., Watkins, J. S., & Bryant, W. R. (1996). Bryant Canyon Fan System: An Unconfined, Large River-Sourced System in the Northwestern Gulf of Mexico1. *AAPG Bulletin*, *80*(3), 340-357. https://doi.org/10.1306/64ED87DC-1724-11D7-8645000102C1865D

Lee, H. J., Locat, J., Desgagnés, P., Parsons, J. D., McAdoo, B. G., Orange, D. L., Puig, P., Wong, F. L., Dartnell, P., & Boulanger, E. (2007). Submarine mass movements on continental margins. In *Continental margin sedimentation: from sediment transport to sequence stratigraphy* (Vol. 37, pp. 213-274). Citeseer.

Lewis, K., Carter, L., & Nodder, S. D. (2013). *Sea floor geology: New Zealand sea-floor sediment, Te Ara: the Encyclopedia of New Zealand*. http://www.TeAra.govt.nz/en/map/5624/hikurangi-channel.

Liu, C., Xie, X., Yu, X., Huang, L., He, Y., Chen, H., Tian, D., Mi, H., Li, M., & Zhang, H. (2023). Kinematics and Sediment Dispersal Pattern of Multi-Stage Mass Transport Deposits on a Stepped Slope with Numerous Elliptical Depressions, Northwestern South China Sea.

Lowe, D. R. (1982). Sediment gravity flows; II, Depositional models with special reference to the deposits of high-density turbidity currents. *Journal of Sedimentary Research*, *52*(1), 279-297. https://doi.org/10.1306/212f7f31-2b24-11d7-8648000102c1865d

Maier, K. L., M.A., C., S.A., G., P., K., G.H., B., M.J., A., & M.P., C. (2013). Provenance and Paleogeographic Reconstruction of a Progradational Deep-water Slope Succession in the Late Miocene Taranaki Basin, North Island, New Zealand. *Geological Society of America Abstracts with Programs*, *v. 45/7*, p.604.

Márquez, E., Berton, F., Stevanato, A. C., Chaves, F., Ojevan, N., & Brasil, E. (2021). New opportunities in a mature oil field: Stretching data interpretation for complex reservoir prediction.

Maurya, S. P., & Singh, N. P. (2017, 30th November -01st December 2017). *Seismic Colored Inversion: A Fast Way to Estimate Rock Properties from the Seismic Data* Challenges in Petro-physical Evaluation and Rock physics Modelling of Carbonate Reservoirs, Likely Elucidations & Way Forward, Victor Menezes Convention Centre (VMCC), IIT Bombay, India.

Mayall, M., & Kneller, B. (2021). Seismic interpretation workflows for deep-water systems: A practical guide for the subsurface. *AAPG Bulletin*, *105*(11), 2127-2157. https://doi.org/10.1306/05262120094

McHargue, T. R. (1991). Seismic Facies, Processes, and Evolution of Miocene Inner Fan Channels, Indus Submarine Fan. In P. Weimer & M. H. Link (Eds.), *Seismic Facies and Sedimentary Processes of Submarine Fans and Turbidite Systems* (pp. 403-413). Springer New York. https://doi.org/10.1007/978-1-4684-8276-8_22

Micallef, A., Berndt, C., Masson, D. G., & Stow, D. A. V. (2007). A technique for the morphological characterization of submarine landscapes as exemplified by debris flows of the Storegga Slide. *Journal of Geophysical Research: Earth Surface*, *112*(F2). https://doi.org/https://doi.org/10.1029/2006JF000505

Middleton, G. V., & Hampton, M. A. (1973). Part I. Sediment Gravity Flows: Mechanics of Flow and Deposition.

Miller, L. R., & Stuart, W. J. (1992). SEISMIC STRATIGRAPHIC EVALUATION OF A NEOCOMIAN SUBMARINE FAN SYSTEM, BROWSE BASIN, NORTH WEST SHELF. *The APPEA Journal*, *32*, 171-182.

Mitchum, R. M., Jr., Berg, O. R., & Woolverton, D. G. (1985). Seismic Stratigraphic Expression of Submarine Fans. In *Seismic Stratigraphy II: An Integrated Approach to Hydrocarbon Exploration* (Vol. 39, pp. 0). American Association of Petroleum Geologists. https://doi.org/10.1306/m39449c7

Mountjoy, J. J., Howarth, J. D., Orpin, A. R., Barnes, P. M., Bowden, D. A., Rowden, A. A., Schimel, A. C. G., Holden, C., Horgan, H. J., Nodder, S. D., Patton, J. R., Lamarche, G., Gerstenberger, M., Micallef, A., Pallentin, A., & Kane, T. (2018). Earthquakes drive large-scale submarine canyon development and sediment supply to deep-ocean basins. *Science Advances*, *4*(3), eaar3748. https://doi.org/doi:10.1126/sciadv.aar3748

Mutti, E., & Ricci-Lucchi, F. (1972). Turbidites of the northern Apennines. *A.G.I. Reprint Ser.*, *3*, 125-166. https://www.scopus.com/inward/record.uri?eid=2-s2.0-84912716413&partnerID=40&md5=21f6ea550aad24f5bc0104da731a25b6

Nagatomo, A., & Archer, S. (2015). Termination geometries and reservoir properties of the Forties Sandstone pinch-out, East Central Graben, UK North Sea. *Geological Society, London, Special Publications*, *403*(1), 133-155. https://doi.org/doi:10.1144/SP403.14

Nomikou, P., Tibaldi, A., Pasquaré Mariotto, F., & Papanikolaou, D. (2009). Submarine morphological analysis based on multibeam data of a huge collapse at the SE flank of Nisyros volcano. *Rendiconti Online Societa Geologica Italiana*, *7*, 177-179.

Normark, W. R., & Gutmacher, C. E. (1983). Delgada Fan: Preliminary interpretation of channel development. *Geo-Marine Letters*, *3*(2), 79-83. https://doi.org/10.1007/BF02462451

NZP&M. (2018). *New Zealand Petroleum Exploration Data Pack,* New Zealand Petroleum and Minerals.

Park, Y., Yoo, D., Kang, N., Yi, B., & Kim, B. (2021). Tectonic control on mass‐transport deposit and canyon‐fed fan system in the Ulleung Basin, East Sea (Sea of Japan). *Basin Research*, *33*(2), 991-1016. https://doi.org/https://doi.org/10.1111/bre.12501

Parsons, J. D., Friedrichs, C. T., Traykovski, P. A., Mohrig, D., Imran, J., Syvitski, J. P. M., Parker, G., Puig, P., Buttles, J. L., & García, M. H. (2007). The Mechanics of Marine Sediment Gravity Flows. In *Continental Margin Sedimentation* (pp. 275-337). https://doi.org/https://doi.org/10.1002/9781444304398.ch6

Patacci, M., Marini, M., Felletti, F., Di Giulio, A., Setti, M., & McCaffrey, W. (2020). Origin of mud in turbidites and hybrid event beds: Insight from ponded mudstone caps of the Castagnola turbidite system (north-west Italy). *Sedimentology*, *67*(5), 2625-2644. https://doi.org/https://doi.org/10.1111/sed.12713

Pickering, K. T., & Corregidor, J. (2005). Mass-Transport Complexes (MTCs) and Tectonic Control on Basin-Floor Submarine Fans, Middle Eocene, South Spanish Pyrenees. *Journal of Sedimentary Research*, *75*(5), 761-783. https://doi.org/10.2110/jsr.2005.062

Posamentier, H. W., & Erskine, R. D. (1991). Seismic Expression and Recognition Criteria of Ancient Submarine Fans. In P. Weimer & M. H. Link (Eds.), *Seismic Facies and Sedimentary Processes of Submarine Fans and Turbidite Systems* (pp. 197-222). Springer New York. https://doi.org/10.1007/978-1-4684-8276-8_10

Posamentier, H. W., Martinsen, O. J., Shipp, R. C., Weimer, P., & Posamentier, H. W. (2011). The Character and Genesis of Submarine Mass-Transport Deposits: Insights from Outcrop and 3D Seismic Data. In *Mass-Transport Deposits in Deepwater Settings* (Vol. 96, pp. 0). SEPM Society for Sedimentary Geology. https://doi.org/10.2110/sepmsp.096.007

Radovich, B. J., Armentrout, J. M., & Rosen, N. C. (2002). Cyclic Attributes on Seismic Data and Sequence Stratigraphy—New Criteria for Exploration, New Interpretation Styles. In *Sequence Stratigraphic Models for Exploration and Production: Evolving Methodology, Emerging Models and Application Histories* (Vol. 22, pp. 0). SEPM Society for Sedimentary Geology.

Reading, H. G., & Richards, M. (1994). Turbidite Systems in Deep-Water Basin Margins Classified by Grain Size and Feeder System 1. *AAPG Bulletin*, *78*(5), 792-822. https://doi.org/10.1306/a25fe3bf-171b-11d7-8645000102c1865d

Roncaglia, M., M., P., C. M., Miko., F., & G., M. H. E. (2013). *Well log stratigraphy in the central and southern offshore area of the Taranaki Basin, New Zealand*. Lower Hutt : GNS Science.

Saller, A., Werner, K., Sugiaman, F., Cebastiant, A., May, R., Glenn, D., & Barker, C. (2008). Characteristics of Pleistocene deep-water fan lobes and their application to an upper Miocene reservoir model, offshore East Kalimantan, Indonesia. *AAPG Bulletin*, *92*(7), 919-949. https://doi.org/10.1306/03310807110

Shan, X., Shi, X., Qiao, S., Jin, L., Otharán, G. A., Zavala, C., Liu, J., Zhang, Y., Zhang, D., Xu, T., & Fu, C. (2019). The fluid mud flow deposits represent mud caps of Holocene hybrid event beds from the widest and gentlest shelf. *Marine Geology*, *415*, 105959. https://doi.org/https://doi.org/10.1016/j.margeo.2019.06.004

Shanmugam, G. (2000). 50 years of the turbidite paradigm (1950s—1990s): deep-water processes and facies models—a critical perspective. *Marine and Petroleum Geology*, *17*(2), 285-342. https://doi.org/https://doi.org/10.1016/S0264-8172(99)00011-2

Shanmugam, G. (2009). Slides, Slumps, Debris Flows, and Turbidity Currents. In J. H. Steele (Ed.), *Encyclopedia of Ocean Sciences (Second Edition)* (pp. 447-467). Academic Press. https://doi.org/https://doi.org/10.1016/B978-012374473-9.00669-X

Shanmugam, G. (2016). Submarine fans: A critical retrospective (1950–2015). *Journal of Palaeogeography*, *5*(2), 110-184. https://doi.org/10.1016/j.jop.2015.08.011

Shanmugam, G., & Moiola, R. J. (1988). Submarine fans: Characteristics, models, classification, and reservoir potential. *Earth-Science Reviews*, *24*(6), 383-428. https://doi.org/https://doi.org/10.1016/0012-8252(88)90064-5

Shanmugam, G., & Wang, Y. (2015). The landslide problem. *Journal of Palaeogeography*, *4*(2), 109-166. https://doi.org/https://doi.org/10.3724/SP.J.1261.2015.00071

Simm, R., & Bacon, M. (2014). *Seismic Amplitude: An Interpreter's Handbook*. Cambridge University Press. https://doi.org/DOI: 10.1017/CBO9780511984501

Simm, R. W. (2009). Simple net pay estimation from seismic: a modelling study. *First Break*, *27*, 45-53.

Sømme, T. O., Jackson, C. A. L., & Vaksdal, M. (2013). Source‐to‐sink analysis of ancient sedimentary systems using a subsurface case study from the Møre‐Trøndelag area of southern Norway: Part 1 – depositional setting and fan evolution. *Basin Research*, *25*(5), 489-511. https://doi.org/https://doi.org/10.1111/bre.12013

Stagpoole, V., & Nicol, A. (2008). Regional structure and kinematic history of a large subduction back thrust: Taranaki Fault, New Zealand. *Journal of Geophysical Research: Solid Earth*, *113*(B1).

Stow, D. A. V., & Mayall, M. (2000). Deep-water sedimentary systems: New models for the 21st century. *Marine and Petroleum Geology*, *17*(2), 125-135. https://doi.org/https://doi.org/10.1016/S0264-8172(99)00064-1

Strogen, D. P., Seebeck, H., Nicol, A., & King, P. R. (2017). Two-phase Cretaceous–Paleocene rifting in the Taranaki Basin region, New Zealand; implications for Gondwana break-up. Journal of the Geological Society, 174(5), 929-946. doi:10.1144/jgs2016-160

Strogen, D. P., Baur, J. R., Bland, K. J., King, P. R., Vonk, A. J., & Kamp, P. J. J. (2011). *Updated paleogeographic maps for the Taranaki Basin and surrounds* (GNS Science Report 2010/53, Issue.

Strogen, D. P., Bland, K. J., Nicol, A., & King, P. R. (2014). Paleogeography of the Taranaki Basin Region during the Latest Eocene–Early Miocene and Implications for the 'Total Drowning' of Zealandia. *New Zealand Journal of Geology and Geophysics*, *57*(2), 110-127. https://doi.org/10.1080/00288306.2014.901231

Strogen, D. P., Seebeck, H., Hines, B. R., Bland, K. J., & Crampton, J. S. (2022). Palaeogeographic evolution of Zealandia: mid-Cretaceous to present. *New Zealand Journal of Geology and Geophysics*, 1-30. https://doi.org/10.1080/00288306.2022.2115520

Talling, P. J. (2013). Hybrid submarine flows comprising turbidity current and cohesive debris flow: Deposits, theoretical and experimental analyses, and generalized models. *Geosphere*, *9*(3), 460-488. https://doi.org/10.1130/ges00793.1

Talling, P. J., Wynn, R. B., Masson, D. G., Frenz, M., Cronin, B. T., Schiebel, R., Akhmetzhanov, A. M., Dallmeier-Tiessen, S., Benetti, S., Weaver, P. P. E., Georgiopoulou, A., Zühlsdorff, C., & Amy, L. A. (2007). Onset of submarine debris

flow deposition far from original giant landslide. *Nature*, *450*(7169), 541-544. https://doi.org/10.1038/nature06313

Tippett, J. M., & Kamp, P. J. (1993). Fission track analysis of the late Cenozoic vertical kinematics of continental Pacific crust, South Island, New Zealand. *Journal of Geophysical Research: Solid Earth*, *98*(B9), 16119-16148.

Vail, P. R. (1987). Seismic Stratigraphy Interpretation Using Sequence Stratigraphy: Part 1: Seismic Stratigraphy Interpretation Procedure.

Vesely, F. F. (2016). Seismic expression of depositional elements associated with a strongly progradational shelf margin: northern Santos Basin, southeastern Brazil. *Brazilian Journal of Geology*, *46*, 585-603.

Walker, R. G. (1978). Deep-water sandstone facies and ancient submarine fans: Models for exploration for stratigraphic trap. *AAPG Bulletin (American Association of Petroleum Geologists)*, *62*(6).

Weimer, P. (1990). Sequence Stratigraphy, Facies Geometries, and Depositional History of the Mississippi Fan, Gulf of Mexico1. *AAPG Bulletin*, *74*(4), 425-453. https://doi.org/10.1306/0C9B2321-1710-11D7-8645000102C1865D

Weimer, P., & Link, M. H. (1991). Global Petroleum Occurrences in Submarine Fans and Turbidite Systems. In P. Weimer & M. H. Link (Eds.), *Seismic Facies and Sedimentary Processes of Submarine Fans and Turbidite Systems* (pp. 9-67). Springer New York. https://doi.org/10.1007/978-1-4684-8276-8_2

Widess, M. B. (1973). How thin is a thin bed? *Geophysics*, *38*(6), 1176-1180. https://doi.org/10.1190/1.1440403

Zampetti, V., Schlager, W., van Konijnenburg, J.-H., & Everts, A.-J. (2004). 3-D Seismic Characterization of Submarine Landslides on a Miocene Carbonate Platform (Luconia Province, Malaysia). *Journal of Sedimentary Research*, *74*(6), 817-830. https://doi.org/10.1306/040604740817

Chapter 4

Interpreting Environments of Deposition from Facies Analysis of Outcrop Versus Seismic Reflection Data: A Cautionary Tale from the Mount Messenger Formation, Taranaki Basin (New Zealand)

4.1 Introduction

There are a myriad of techniques for interpreting depositional environments from ancient strata, which fall into two broad categories: 1) those focussing on the physical characteristics of the strata (e.g. lithology, physical and biogenic sedimentary structures, fossil and trace fossil content) and 2), those that rely on the geophysical response of the strata (e.g. wireline log signature, seismic reflection response). From these two categories, two leading methods have emerged which are widely applied to obtain accurate and repeatable characterization: facies analysis and seismic geomorphology.

Facies analysis has proven to be an exceptional tool for interpreting the genesis of ancient strata, both in outcrop and in the subsurface (Middleton 1973; Walker 1976; Walker 1992; Posamentier & Walker 2006; Strachan & Alsop 2006; James & Dalrymple 2010). It relies on the concept of Walther's Law–that sediments deposited adjacent to one another in space are represented as strata stacked atop each other through time (Walther 1893-1894) – and focuses on subdividing sedimentary successions into fundamental building blocks (facies) to interpret the depositional environments in which sediments accumulated. Facies analysis relies on facies models developed through observation and distillation of the pertinent aspects of similar sedimentary successions of all geological ages and with a global distribution

(Dalrymple 2010). The strength of facies analysis is its ability to synthesize data acquired from various parts of a sedimentary environment and use these to reconstruct the broader context of the deposits. However, facies analysis is limited when 3D views of the strata are unavailable, and it therefore, requires inference of the geometry of geobodies using a time-for-space substitution to establish the distribution of depositional elements.

Seismic geomorphology is a more recent advancement, which builds on the success of seismic stratigraphy in accomplishing paleoenvironmental interpretation of strata by organizing depositional successions into sequences based on their seismic reflection geometries and stratal architectures (Mitchum et al. 1977a; Mitchum et al. 1977b). The seismic geomorphological approach relies on the extraction of seismic attributes from 3D seismic reflection datasets and uses these to obtain meaningful geological and geomorphological insights from section and plan views (Bischoff et al. 2021; Posamentier et al. 2022). The advantage of seismic geomorphology is the 3D perspectives seismic reflection datasets provide and the high level of detail that can be obtained about the geometry of depositional elements and hence the depositional setting.

Whether interpretations of sedimentary environments are based on 2D facies analysis or 3D seismic geomorphology, careful observation of stratal relationships (e.g., onlap, offlap, truncation, pinch out) is essential to arrive at accurate and precise inferences that can build robust paleogeographic conceptualizations. In our research, we have found this not always to be the case, such as in the recent example of Masalimova et al. (2016), who used facies analysis of 2D outcrops to interpret the depositional setting of the Miocene Mount Messenger Formation in North Taranaki Basin, New Zealand, as representing deposition in a basin floor submarine fan. Their study built on three decades of research along this 25 km of exposed outcrop that

also concluded that it accumulated as a succession of basin floor fans (King et al. 1993; King et al. 1994; Browne & Slatt 2002; Maier et al. 2010; Strogen et al. 2011). Outcrops of the Mount Messenger Formation along the North Taranaki coast were considered to be among the best analogue examples of fine-grained submarine fan systems, along with the Brushy Canyon Formation of West Texas, and the Tanqua Fan Complex in South Africa (Masalimova et al. 2016).

The interpretation of basin floor fan deposits in the lower part of the Mount Messenger Formation has, however, never been critically examined. The opportunity for critical re-examination has arisen from the 2018 release of the Mercury-Mokau 3D seismic survey for an area immediately offshore of the North Taranaki coastal section (Figure 4.1). The main aim of the Masalimova et al. (2016) study was to "provide a concrete link between flow mechanics and processes of sedimentation and the development of the larger-scale architectural elements", which had not previously been established. We argue that if the coastal outcrop exposure represents exhumed large basin floor fans, they ought to be present and imaged in the seismic volume immediately offshore and down-dip of the succession. This paper, therefore, focuses on undertaking seismic geomorphology of this offshore seismic volume and compares those interpretations with newly gathered information about channels in the Mount Messenger Formation strata exposed in the coastal section acquired using UAV drones.

This paper is the third in a triplet, two of which have been published in Marine and Petroleum Geology on the nature of sediment conduits on the paleo continental slope in southern and western Taranaki Basin (Mount Messenger Formation) and their spatial relationship to submarine fans (Kamaruzaman et al. 2023; Kamaruzaman et al. 2024a). In the second paper we demonstrated that submarine fans considered to exist on the paleo continental

slope within lower Mount Messenger Formation in southern Taranaki Basin do not exist. Rather, we have shown that basin floor fans do occur within this formation at lower bathyal depths in western Taranaki Basin, beyond the continental slope and some 130 km distant from the contemporary shelf edge (Figure 4.2) (Kamaruzaman et al. 2024a). The focus of this paper is to critically re-assess interpretations of the depositional environment for the lower Mount Messenger Formation based on facies analysis of outcrop, primarily using 3D seismic stratigraphy and seismic geomorphology. In doing so, we reveal that the outcrop strata did not accumulate as basin floor fans, but rather as deposits on the slope. The broader implications of this study are the need to re-evaluate palaeogeographic conceptualisations of Taranaki Basin for the Miocene, such as those published by Strogen et al. (2011, 2022).

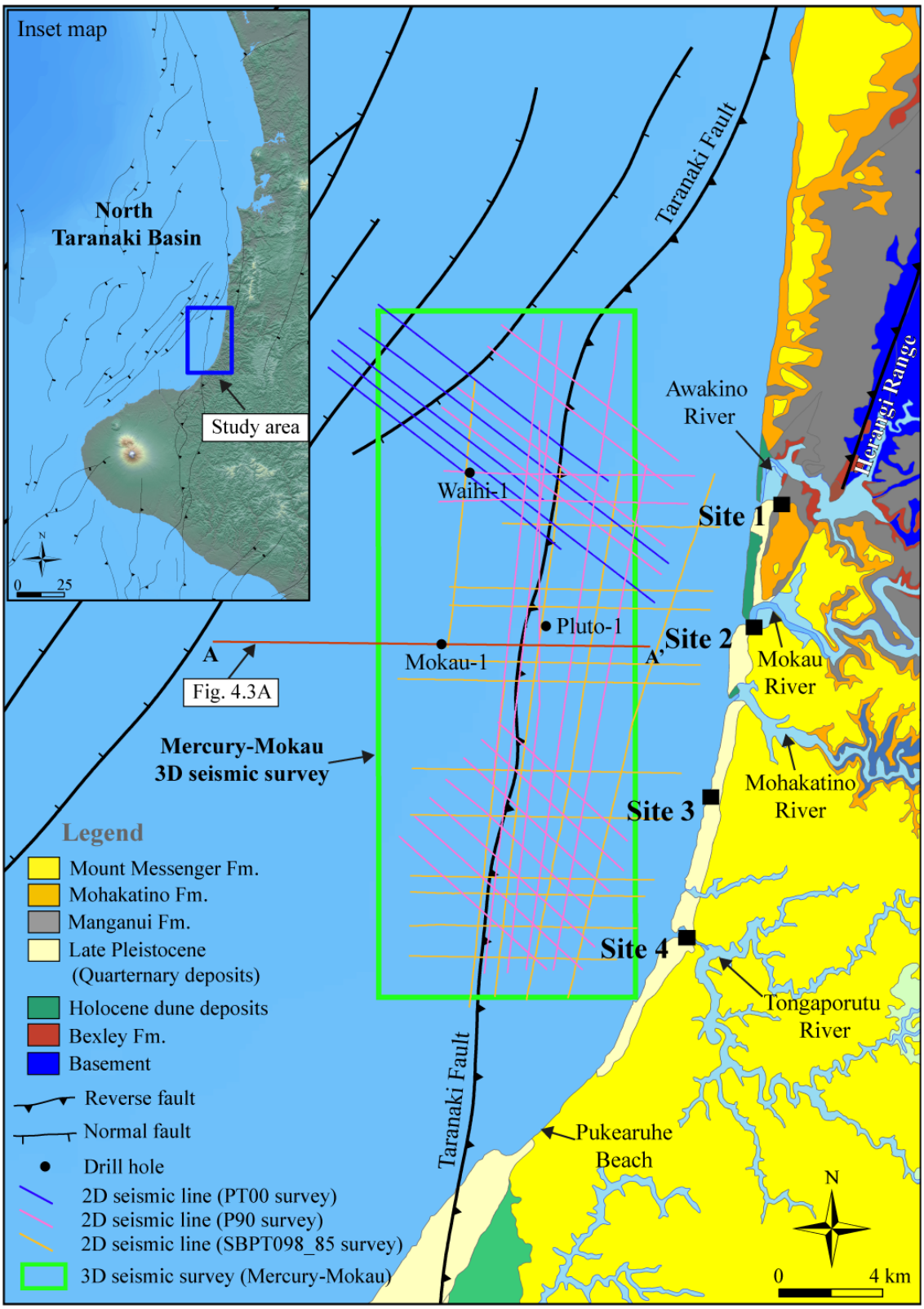

Figure 4.1: Map of the North Taranaki Basin area, showing the study area, including the four UAV drone survey locations from which outcrop models were built, the Mercury-Mokau 3D seismic reflection survey, and other relevant 2D seismic reflection lines, and drill holes in the offshore area. GIS data from NZP&M (2018).

4.2 Geological setting

4.2.1 Tectonic context

Taranaki Basin is a long-lived basin that accumulated Late Cretaceous and Cenozoic sediments (Figure 4.3) (King & Thrasher 1996). At present, most of the basin succession remains below sea level. Middle and Late Miocene marine sediments are exposed in a narrow coastal strip along the eastern margin of the basin in North Taranaki (Edbrooke 2005). These Miocene sediments young from north to south and were exhumed during the Late Pliocene and Pleistocene by doming of central-western North Island preceding the outbreak of Pleistocene volcanism within the Taupo Volcanic Zone (Figure 4.4) (Kamp et al. 2004).

King and Thrasher (1996) remains the most comprehensive basin-wide reference for the stratigraphy and structure of Taranaki Basin. The context for the Late Miocene Mount Messenger Formation is the extensive Neogene succession in the basin (e.g. Figure 4.3). This succession mostly comprises basin wide siltstone (Manganui Formation). Sandstone facies that interfinger with Manganui Formation include the Middle Miocene Moki Formation and the Late Miocene Mount Messenger Formation (King & Thrasher 1996). Overall, the Manganui Formation and the two main sandstone units constitute a 25 million-year-long regressive shelf-slope wedge about 2 km thick, representing infilling of a foredeep. Flexural subsidence of the basin resulted from westward overthrusting of basement (Murihiku Supergroup) across the Taranaki Fault Zone along the eastern margin of the basin, which started during the Late Oligocene (King & Thrasher 1996). This overthrusting switched-off from north to south along the Taranaki Fault Zone (Stagpoole & Nicol 2008). Along the North Taranaki Basin section of the Taranaki Fault Zone, the basement thrusting ended during the Early Miocene at about 20

Ma. By 19 Ma the thrust belt (the structural high known as the Herangi High) had started to subside below sea level, which resulted in marine onlap of coastal and inner shelf deposits (Bexley Sandstone) upon the former thrust belt and beyond to the east within the King Country Basin (Kamp et al. 2004; Edbrooke 2005) (Figure 4). The Bexley Sandstone is conformably overlain by a regressive coal measure succession (Maryville Coal Measures), its most western occurrence being about 6 km east of the present-day coastline. Manganui Formation accumulated conformably above the Bexley Sandstone between the thrust front of the Taranaki Fault Zone and about 6 km inland of the modern coastline, followed by rapid deepening to upper bathyal depths with a thickness of approximately 150 m (Kamp et al. 2004) (Figure 4.3).

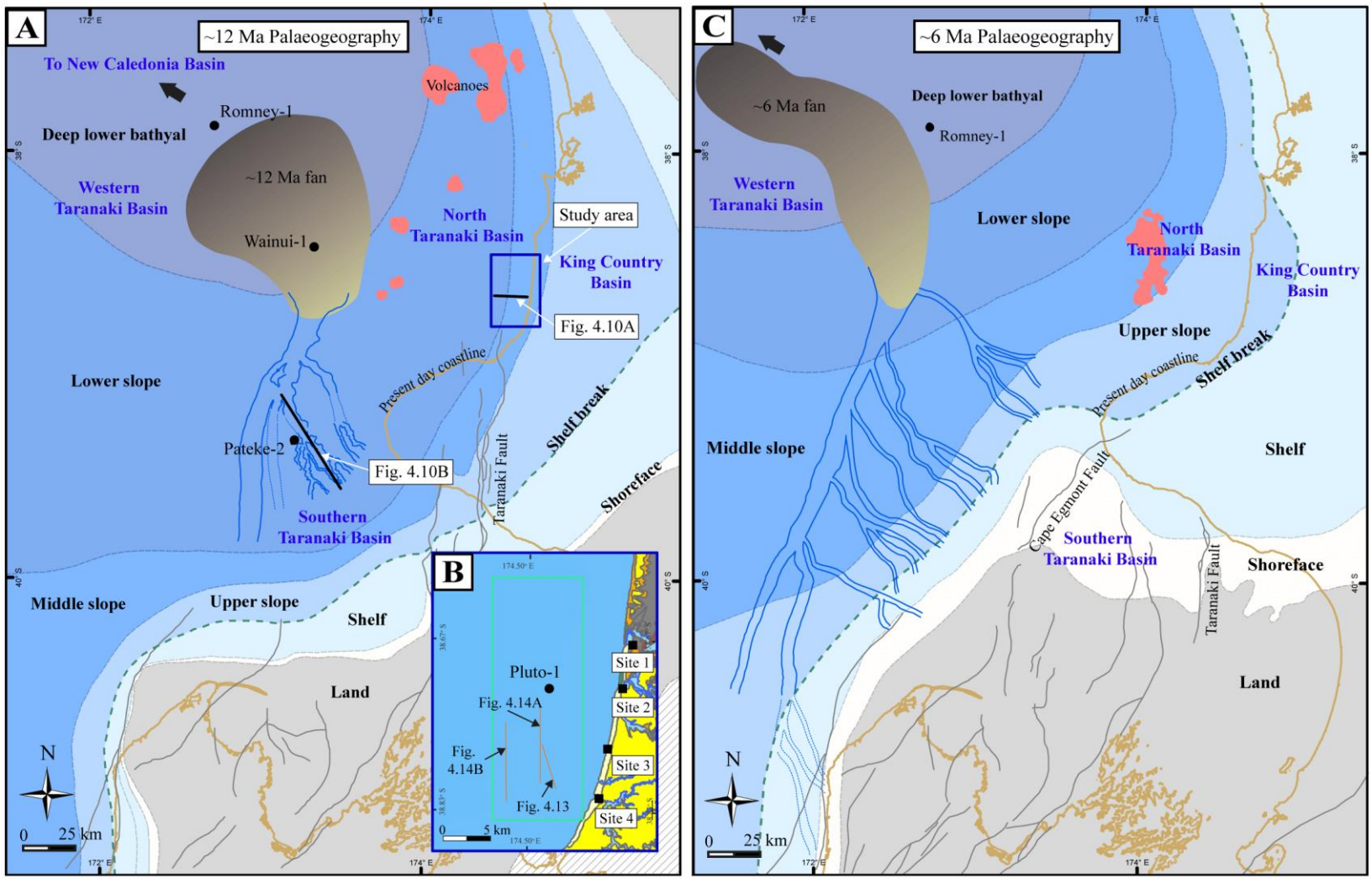

Figure 4.2: (A) Paleogeographic map of Taranaki Basin at ~12 Ma with the study area shown in blue box, and (B) close-up of the study area. (C) Paleogeographic map of Taranaki Basin at ~6 Ma. Both A and C are modified from Kamaruzaman et al. (2024a).

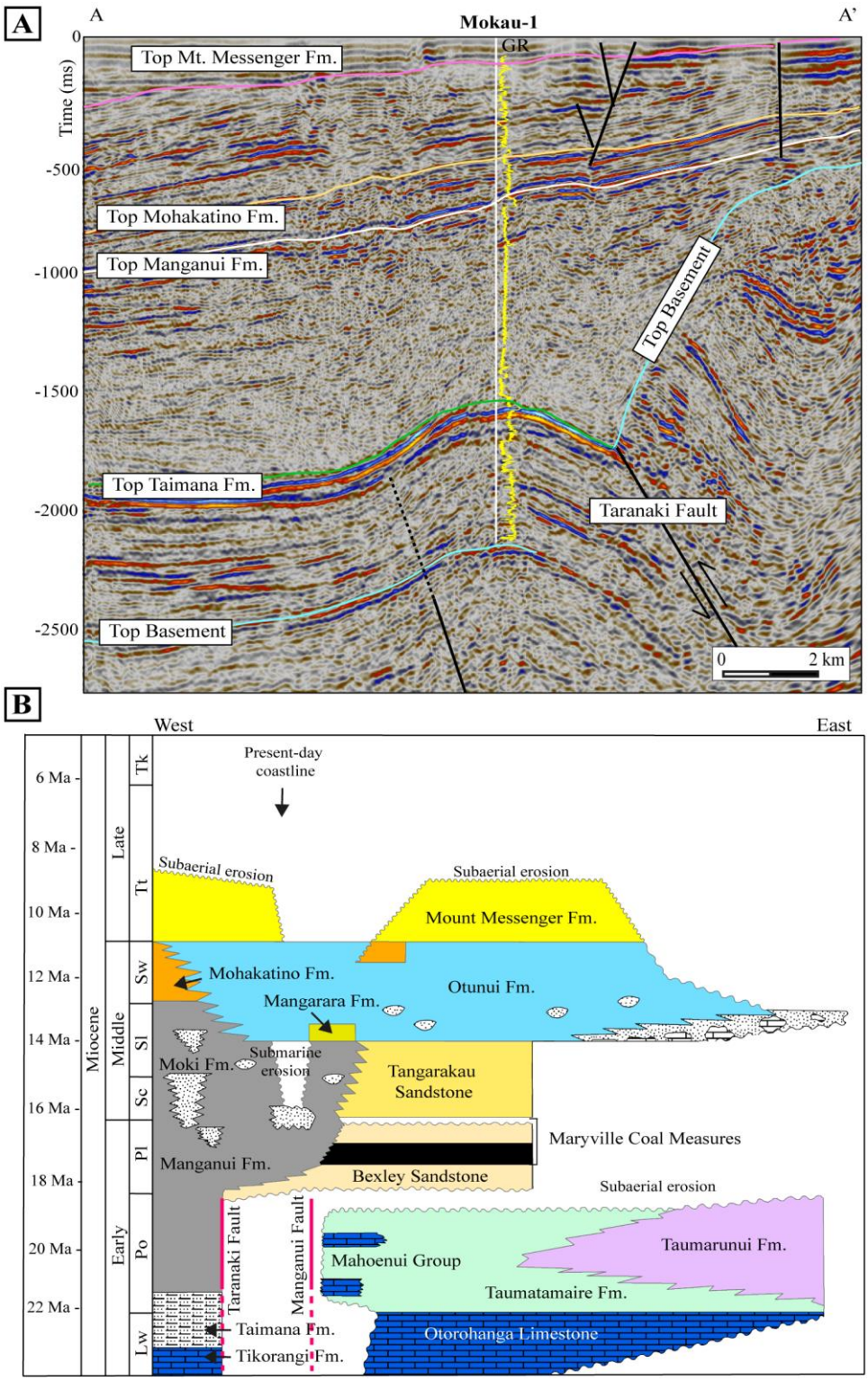

Figure 4.3: Stratigraphic context of the study area. (A) 2D seismic line (BO_hzt82b-124-geosphere) passing west-east through Mokau-1 drillhole. Note the formation boundaries, including the Mount Messenger Formation, and the gamma ray log for this hole. Adapted from Hansen (2005) (B) Chronostratigraphic panel for the Middle and Late Miocene strata in North Taranaki, both offshore and on land (present-day coastline marked by arrow), simplified from Kamp et al. (2004). The location of A shown in Figure 4.1.

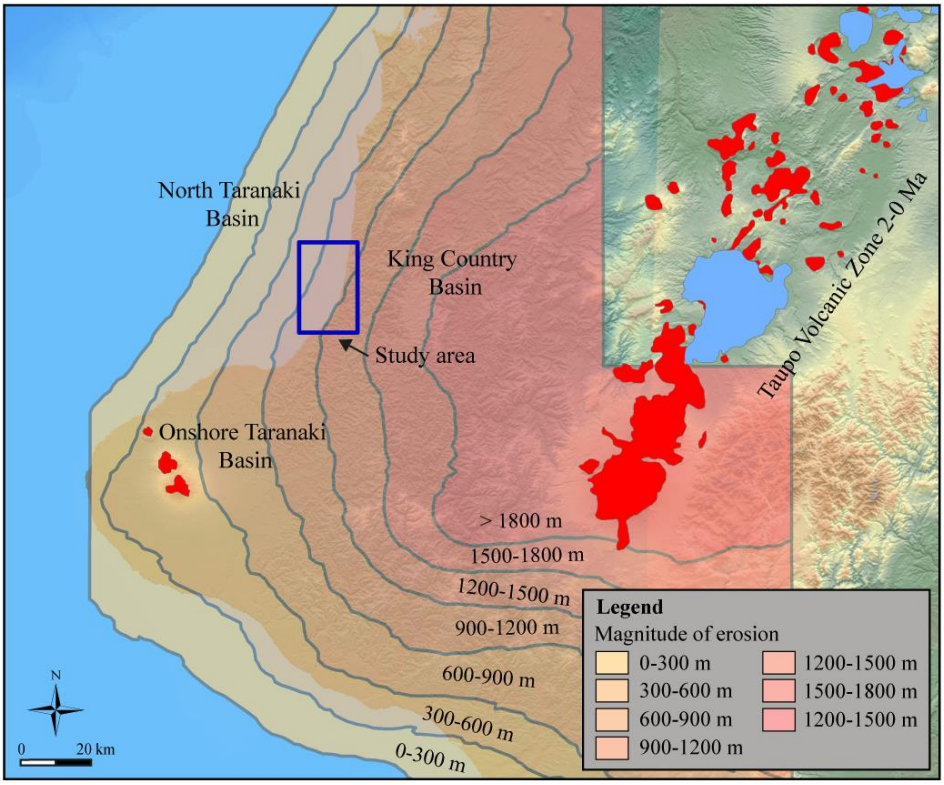

Figure 4.4: Map showing the magnitude of erosion across the central-western North Island due to Pliocene-Pleistocene doming (redrawn from Kamp et al., 2004 with volcanic products shown in red). The extent of the study area is shown in the blue box.

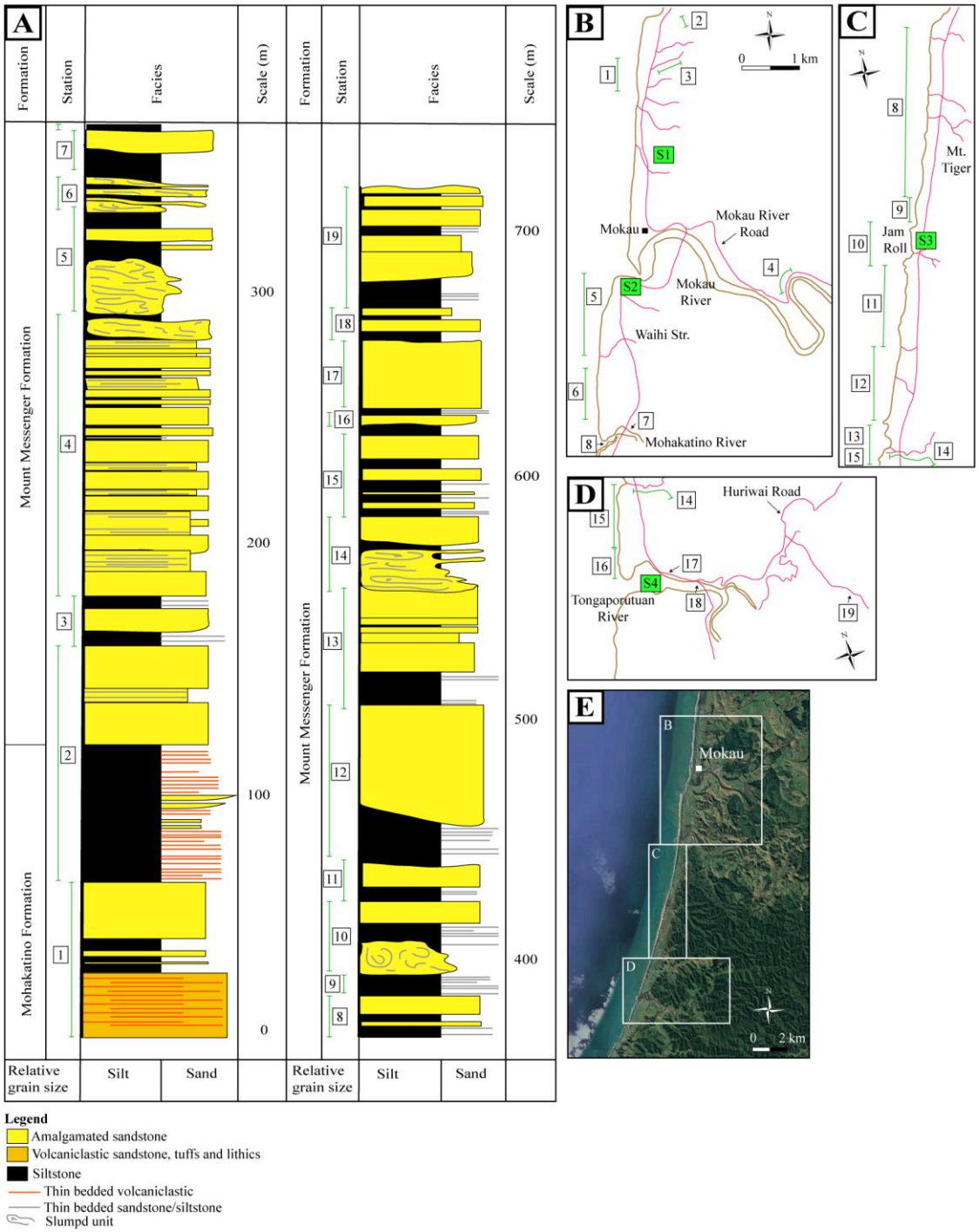

Figure 4.5: Composite stratigraphic column for the coastal exposure of the lower Mount Messenger Formation from the Awakino River to the Tongaporutu River (Refer to Figure 4.1 for these locations). Simplified from Hansen (1996). The maps B,C,D and E relate station locations to facies in the column. The outcrop site locations examined in this study are labelled as S1, S2, S3 and S4 in light green boxes in B,C and D.

4.2.2 Stratigraphic context

The Middle Miocene stratigraphy east of the modern coastline is different north and south of the Mokau River Valley (Figure 4.1). To the south in the Mohakatino River Valley, Manganui Formation is conformably overlain by Moki Formation of lower Lillburnian age (15 – 14 Ma), which comprises a succession of more than 70 m of fine-grained (very fine sandstone and siltstone) turbidites that probably accumulated on levees adjacent to channels (Kamp et al. 2004). Moki Formation is unconformably overlain by Mangarara Formation, comprising Lillburnian, 2 to 5 m-thick channelised calcareous sandstone and limestone (Puga-Bernabéu et al. 2009). In the Tongaporutu River Valley (Figure 4.1), Moki Formation consists of a more than 50 m thick turbidite succession. Its contact with the underlying Manganui Formation is not exposed as it lies in the subsurface due to the SW regional dip direction. In the Awakino and Mokau river valleys (Figure 4.1), Moki Formation does not occur in the stratigraphy. Rather, Manganui Formation is unconformably overlain by Mangarara Formation, where it is also channelised, as in the Mohakatino and Mokau river valleys (Puga-Bernabéu et al. 2009). The unconformity between Manganui and Mangarara formations lies between upper Altonian (17 – 16 Ma) and lower Lillburnian (15 – 14 Ma), implying an interval of significant submarine erosion (King et al. 1993).

During the early Middle Miocene (Clifdenian – lower Lillburnian; 16 – 14 Ma), the shelf was only about 10 km wide, as inner shelf sandstone facies (Tangarakau Formation), which conformably overlies Maryville Coal Measures (Figure 4.3B), are age equivalent to the upper part of the Manganui Formation, the Moki Formation and the Mangarara Formation (Kamp et al. 2004; Edbrooke 2005). This suggests that the upper part of the Manganui, the Moki and the Mangarara formations likely accumulated in upper bathyal depths upon the upper continental slope. The narrow shelf only some 6 km east of Moki Formation outcrops in the

Tongaporutu River Valley, is not consistent with Moki Formation having accumulated at the base of the continental slope.

The Otunui Formation of late-Middle Miocene age (upper Lillburnian and Waiauan stages; 14 – c.11 Ma) is a calcareous siltstone about 200 m thick, which is widespread in the King Country Basin east of North Taranaki Basin and within Taranaki Basin (Kamp et al. 2004; Edbrooke 2005; Townsend et al. 2008). The unit crops out in the upper reaches of the Mohakatino Valley and within the Tongaporutu Valley (Figure 4.1), but not quite as far west as the modern coastline due to the regional dip taking it into the subsurface. The Otunui Formation is part of a progradational succession that accumulated at neritic to upper bathyal depths in King Country (Kamp et al. 2004). In the Tongaporutu River Valley, Otunui Formation downlaps onto the Moki Formation as sandy siltstone and silty fine sandstone beds with diffuse boundaries due to pervasive bioturbation (Kamp 2019). It probably accumulated at upper bathyal depths on the upper slope. In North Taranaki well completion reports, Otunui Formation is not differentiated from the Mohakatino Formation or the Manganui Formation.

The Mohakatino Formation of latest Middle Miocene age comprises mass-emplaced volcaniclastic sandstone beds, which are best exposed and 100 m-thick north of Awakino, whereas they are only 15 m-thick along the coastal section between the mouths of the Awakino and Mokau rivers (Figure 4.1). These sediments were sourced from contemporary andesitic volcanoes in North Taranaki Basin and dispersed by dense flows outwards from the volcanoes, including toward the east and southeast (i.e. the modern coastline) (Nodder et al. 1990) (Figure 4.2). The modern distribution of the marine Mohakatino Formation on land is limited to a strip 5 to 7 km wide within and east of the present-day coastline (Edbrooke 2005). As this formation mostly comprises mass-emplaced sediments (Nodder et al. 1990; Sharman et al. 2015), its

limited distribution to the east reflects the runout of mass flows part-way up the contemporary continental slope that had formed initially during the accumulation of the Manganui to Otunui formations (Kamp et al. 2004).

The Mount Messenger Formation conformably overlies Otunui Formation in both the King Country Basin and within North Taranaki Basin (Figure 4.3B). In both basins, the rate of sediment accumulation increased markedly from the Otunui Formation into the Mount Messenger Formation (Bull et al. 2019). This resulted from the development of a new sediment source area – the Southern Alps, which is a mountain belt located in South Island (New Zealand), immediately southeast of the Alpine Fault. Exhumation within the Southern Alps started at about 15 Ma due to oblique continent-continent convergence across the Alpine Fault, which is part of the Australia-Pacific plate boundary zone through New Zealand (Ring et al. 2019). Fission track thermochronology data for numerous sites within the Southern Alps indicate that exhumation of basement and its erosion became marked during the Late Miocene (Kamp et al. 1989; Tippett & Kamp 1993), probably following the development of considerable topography. The Mount Messenger Formation started to accumulate during the latest Middle Miocene at ~12 Ma (Waiauan Stage) in southern Taranaki Basin and slightly later at ~11 Ma (lower part of the Tongaporutuan Stage) in the King Country and North Taranaki basins, which are farther from the sediment source. The net result of the appearance of a new sediment source area along the plate boundary and accumulation of this material in Taranaki and King Country basins was the start of marked northwestward progradation of a shelf-slope wedge within the southern and northern parts of these basins (King & Thrasher 1996; Bull et al. 2019). A difference between these two parts of Taranaki Basin is that the King Country Basin trapped some of the Late Miocene sediment from passing through it into North Taranaki

Basin, which is reflected in a less substantial wedge of slope sediments there compared with southern Taranaki Basin.

The part of the Mount Messenger Formation exposed along the North Taranaki coastal section between the Tongaporutu and Awakino rivers (Figure 4.1), is comprised of its lower part; the upper part of the formation occurs south of the Tongaporutu River to Pukearuhe (King et al. 1993; King et al. 1994). The lower part of the formation has an aggregated thickness of approximately 750 m (Hansen 1996) (Figure 4.5), although this is an aggregated estimate from the thickness of beds exposed along the coastal section and is probably an overestimate (King et al. 2007). The lower Mount Messenger Formation comprises sandstone beds up to 30 m thick, interstratified siltstone and four discrete intervals of slumped beds.

4.2.3 Paleogeographic context

The paleogeography of Taranaki Basin during the accumulation of the late-Middle Miocene (Waiauan Stage; 12.7 – 10.92 Ma) and Late Miocene (Tongaporutuan Stage; 10.92 – 6.5 Ma) Mount Messenger Formation provides important context for re-assessment of the basin-floor fan model, as applied to the North Taranaki coastal section (King et al. 1994). The initial understanding of the basin-wide paleogeography for this Neogene interval was reported by King and Thrasher (1996) and more recently by Strogen et al. (2011, 2022). The basin floor fans depicted on their Late Miocene map in the vicinity of the present-day coastal section, are some 30 to 50 km northwest of the contemporary shelf edge, within mid-bathyal water depths of about 400 – 600 m; that is, on the middle continental slope. Kamaruzaman et al. (2024a) recently published new early-Middle and Late Miocene paleogeographic maps for Taranaki Basin, based on new seismic reflection mapping and wireline log interpretation (Figure 4.2).

That work showed that prominent canyons and channel complexes within continental slope sediments (Mount Messenger Formation) in southern Taranaki Basin supplied sediment successively to each of two deep water basin floor fans in western Taranaki Basin, some 130 km from the contemporary shelf edge (Figure 4.2). The Kamaruzaman et al. (2024a) study hence disproved the existence of previously interpreted submarine fans in the Mount Messenger Formation in southern Taranaki Basin (c.f., Strogen et al. 2011; Kroeger et al. 2019). Our revised paleogeographic maps did not include the extensive Mount Messenger Formation submarine fans depicted by Strogen et al. (2011, 2022) on the parts of their paleogeographic maps across the middle slope in the Taranaki Peninsula and North Taranaki parts of the basin. These submarine fans were excluded in the maps shown in Figure 4.2 as it was already evident during our mapping of the Mercury-Mokau 3D seismic survey area in North Taranaki Basin that the Strogen et al. (2011, 2022) submarine fans did not exist there (North Taranaki Basin).

In a relatively recent detailed facies analysis study, Masalimova et al. (2016) interpreted the Mount Messenger Formation as a basin floor fan with three lobes oriented south to north (Figure 4.6). As a whole, the fan interpreted in Masalimova et al. (2016) is of considerable size (width: ~30 km, length: ~50 km and unspecified thickness). Because the description and interpretation of facies were made exclusively from strata exposed in the coastal section, necessarily, the study required a time-for-space substitution to place the facies associations into the spatial context of a submarine fan system. In this contribution, we map the 3D seismic reflection dataset that covers much of the area inferred as a basin floor fan by Masalimova et al. (2016) (Figure 4.6), and use this new mapping to test the validity of the time-for-space substitution used in their facies analysis. Our approach directly targets the shortcomings of

facies analysis in the absence of 3D views of the strata by applying 3D spatial analysis of the Mount Messenger Formation using seismic reflection data and outcrop photogrammetry.

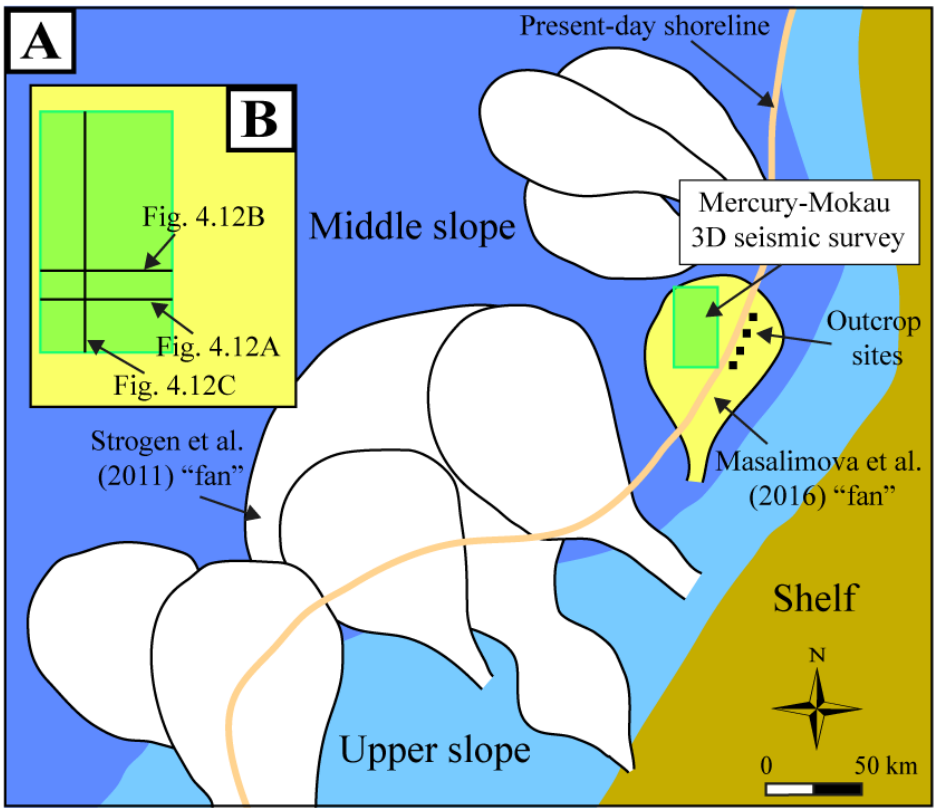

Figure 4.6: (A) Late Miocene (~10 Ma) paleogeographic map simplified from Strogen et al. (2011). The Masalimova et al. (2016) "fan" interpretation (shown in bright yellow) is overlain onto the Mercury-Mokau 3D seismic survey area, the extent of which is shown with a green rectangle. The four outcrop sites are shown in black dots adjacent to the seismic. (B) Close-up view of the 3D survey, showing seismic lines interpreted here in Figure 4.12A-C. The "fans" mapped by Strogen et al. (2011) are in white.

4.3 Nomenclature

Although their dimensions and architectures vary widely, all submarine channel systems comprise a range of sub-environments and associated deposits, including channel complexes, channel elements, thick sandstone channel fills with intervening siltstone layers, and mass-transport deposits (MTDs) (Figure 4.7) (Mayall et al. 2006). We use the channelform

models presented in Figure 4.7 to communicate our results and interpretations of both outcrop and seismic reflection data. The term "channel system" refers to very large features (i.e. widths of 1000 - 3000 m and thicknesses of 100 - 250 m) usually resolvable in seismic reflection data. In contrast, "channel elements" occur within channel systems and are much smaller in their dimensions (i.e. width < 250 m and thickness < 25 m) (Figure 4.7B). Correspondingly, channel elements may or may not be resolvable on seismic reflection data but they are generally mappable within outcrop strata (Hubbard et al. 2014; Stright 2014). Overall, channel elements are partitioned into margin and axis regions (Figure 4.7B).

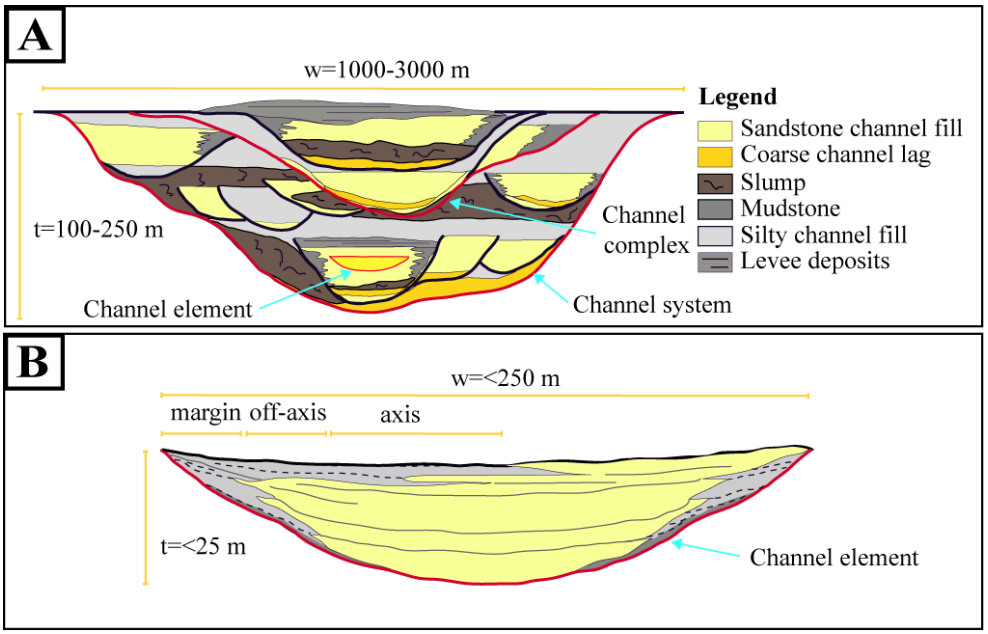

Figure 4.7: Submarine channelform models used in this paper to clarify terminology. (A) Definition of channel system, channel complex, and channel element showing their nested characteristic. The scale range of channel system varies from 1000-3000 m wide and from 100-250 m thick. They are, therefore, typically resolvable in seismic data (Modified from Mayall et al., 2006). (B) Definition of a channel element, which has a width less than 250 m and a thickness less than 25 m. The scale of channel elements means that they are observable in outcrop but seldom resolved in seismic data. Modified from Fildani et al. (2013).

4.4 Data and Methods

This study primarily used two main methods and datasets: 1) seismic stratigraphy and seismic geomorphology of the Mercury-Mokau 3D seismic volume and 2), photogrammetric analysis of outcrops. The seismic stratigraphy and seismic geomorphology were broad-scale tools used to determine the 3D distribution and architecture of reflection packages, while the photogrammetric analysis of outcrops was used to link the offshore seismic data to the on-land distribution of strata exposed along the coast. To remain objective with our analysis and interpretation of the seismic reflection data we use the criteria of Posamentier and Erskine (1991) for the recognition and mapping of submarine fans (Table 4.1). Our outcrop analysis focused on establishing whether or not sediment conduits of the type mapped in southern Taranaki Basin by Kamaruzaman et al. (2023) occur, and if so, to measure their geometry and the stratal characteristics of their infill. The analysis of strata in outcrop can be made at the scale of beds and even laminae, which is a much finer scale than possible in the mapping of elements in a seismic reflection dataset. Therefore in this study, we do not undertake a comprehensive facies analysis of strata exposed in the coastal section at the bed and laminae-scale as this information has already been published (i.e., King et al. 1993; Hansen 1996; King et al. 2007; Masalimova et al. 2016).

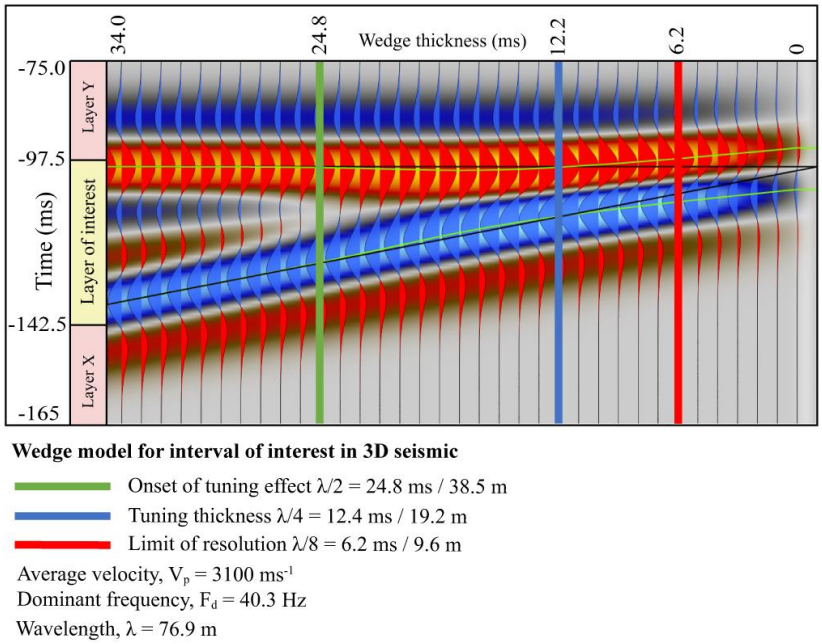

Figure 4.8: Wedge model for the Mount Messenger Formation interval in the Mercury-Mokau 3D seismic survey showing the limit of resolution, tuning thickness and onset of the tuning effect. Calculations are based on Widess (1973).

4.4.1 Seismic Stratigraphy

This study utilized the Mercury-Mokau 3D seismic volume, which covers an area of 239 km^2, together with 500 line-km of 2D seismic reflection data in the same area acquired during earlier petroleum exploration (Figure 4.1). In the Mercury-Mokau 3D seismic volume, the Mount Messenger Formation occurs between -100 to -800 ms TWT. The quality of the 3D seismic data in the Mount Messenger Formation interval varies from poor to good. This partly reflects the fact that the data was acquired to image and characterize an interval much lower in the stratigraphy, and hence the seismic processing was not optimized in the Mount Messenger interval. The presence of gas chimneys also compromises the quality of seismic images (Loyz NZ Ventures Ltd, 2014), and this poses challenges in mapping strata and sediment conduits in some areas (Figures i - iv – Appendix C).

Coloured inversion was performed on the 3D seismic volumes to boost the low-frequency seismic response, hence increasing the resolution of the data in the Mount Messenger Formation interval (Lancaster & Whitcombe 2000). One limitation of the analysis was the fact that no detuning process could be carried out on the interval of interest (lower Mount Messenger Formation) because there are no continuous bright-amplitude reflectors within this interval and there are few wireline log datasets available. However, wedge models were constructed to understand the vertical resolution of seismic reflections in the Mount Messenger Formation interval while considering the tuning effect using the Widess (Widess 1973) and Rayleigh methods (Kallweit & Wood 1982) (Figure 4.8). With this information, regional horizons described in well-completion reports (e.g., Pluto-1: Shell Todd Oil Services Ltd, 1991) were picked, followed by mapping sediment conduits and searching for stratal patterns indicative of submarine fans. Borehole checkshots were used for time-depth conversion. The average seismic velocity of the Mount Messenger Formation interval is 1300 ms^{-1}.

4.4.2 Outcrop Photogrammetry

Three thousand UAV drone images were captured from four outcrop locations using a DJI Phantom 4 drone connected to a real-time kinetic (RTK) global positioning system (GPS) for accurate geolocation. Drone surveying of the four sites used pre-programmed flight paths using the WGS 84 UTM 60S coordinate reference system, and EGM 96 geoid (Figure 4.9). The focal length of the drone camera is 24 mm with a 20-megapixel resolution, which captures outcrop images at an average of 3-8 cm Ground Sampling Distance (GSD). Survey images were overlapped by 80%. Drone images were processed using Pix4Dmapper software to generate dense 3D point clouds, digital surface models (DSMs), digital terrain models (DTMs), triangle meshes, and orthomosaic images of the outcrops (i.e., 3D models). Once 3D models of outcrop were constructed, they were imported into ArcGIS Pro as scene layer packages.

We used the outcrop images chiefly to map the occurrence of discontinuities in the lower Mount Messenger Formation at each site, in particular, possible channel features and evidence for stratal terminations that might be consistent with the characteristics of submarine fans (Posamentier & Erskine 1991). We also mapped outcrops at the bedset scale for which the 3D outcrop models had the optimal resolution (20 cm to 1 m). This resulted in ~200 bedset "horizons" across the four sites. From each of these bedsets, the thickness, dip and dip direction were calculated, and lithologs of each site were drawn based on the models. Accuracy was ensured by using sample points of well-exposed rock, avoiding weathered and vegetated strata. Ground truth assessment of measurements verified the calculated parameters. The length of bedsets could not be quantified accurately because some areas along the outcrops are covered by vegetation or obscured by Late Pleistocene deposits. However, the estimated length of bedsets is presented in the results section. The drone models are described in more detail in Kamaruzaman et al. (2024b). In addition to UAV drone images, photographs were also taken to help describe sandstone beds.

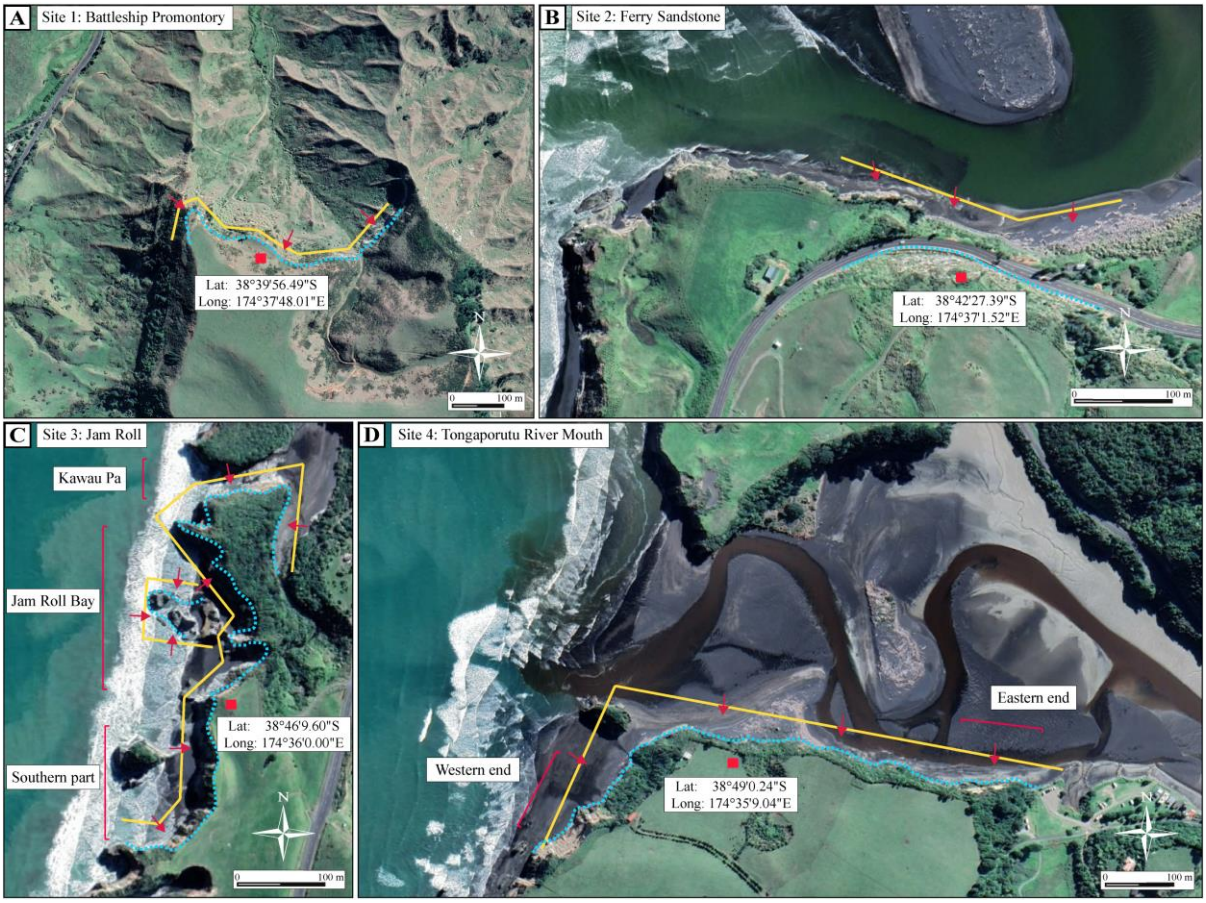

Figure 4.9: Map showing the four locations for which outcrop models were built. Outcrops are outlined with cyan dashed lines. The yellow lines represent UAV drone flight paths, and the red arrows indicate the direction the UAV drone camera was facing. The location of the sites is shown in Figure 4.1.

Table 4.1: List of stratal patterns used to identify fans in seismic data, as outlined by Posamentier and Erskine (1991).

1. Reflectors pinch out against high seafloor topography.
2. Continuous high-amplitude reflectors onlap basin margin.
3. Bidirectional downlap reflectors within the fans or lobes.
4. External mounding on the fan top bounding surface.

4.5 Results and Interpretation

4.5.1 Seismic Resolution

The wedge model shows that in the interval of interest, the vertical seismic resolution (λ/8) is 9.6 m, the tuning thickness (λ/4) is 19.2 m, and the onset of the tuning effect (λ/2) occurs at a thickness of 38.5 m (Figure 4.8), based on Widess (1973). Given this resolution limit, channel systems and channel complexes can be imaged in the seismic data, whereas individual channel elements approaching the scale of seismic resolution are not always visualized. In comparison, the outcrop models have a resolution of between 20 cm and 1 m (Section 4.4.2), and the outcrop models are generally of the channel element scale (Figure 4.7).

4.5.2 Seismic Stratigraphy

The continental slope in Taranaki Basin during the late-Middle and Late Miocene interval regionally trended southwest to northeast (Figure 4.2A). In northern Taranaki offshore from the coastal section the slope trended north to south. The two seismic reflection profiles in Figure 4.10 image the Mount Messenger Formation and enclosing formations in North Taranaki Basin (Figure 4.10A) and in southern Taranaki Basin (Figure 4.10B), both oriented down-dip. In both areas there are differences in the strata between the lower and upper Mount Messenger Formation (separated by light green coloured horizon). In southern Taranaki Basin (Figure 10B), the lower Mount Messenger Formation strata (below the light green horizon) are represented by parallel and moderately continuous reflectors, with some high amplitude areas, and low dip (~0.5^{o}). The upper Mount Messenger Formation strata (above the light green horizon) shows clinoform reflectors that progressively steepen upward and are truncated, and are onlapped by Pliocene-Pleistocene strata (above the pink horizon). In North Taranaki Basin

(Figure 4.10A) there is a similar structure except that the image captures a more upslope section. The lower Mount Messenger Formation reflectors are parallel, although their continuity is disrupted, and they are overlain by clinoform reflectors that steepen upwards, followed by truncation and onlap of Pliocene-Pleistocene strata. These reflection profiles are representative of areas approximately 120 km apart on the continental slope (Figure 4.2A).

The seismic reflection profiles (Figure 4.10) clearly show that the sediments accumulated on a continental slope. Clinothem progradation resulted from a late-Middle and Late Miocene increase in the rate of sediment supply to the margin from the uplifted and erosion of the Southern Alps. In both locations (Figure 4.10A and B), the strata imaged as reflectors have been steepened by post-Mount Messenger Formation tectonic tilting, the amount indicated by the dip of the overlying erosion surfaces. The lower Mount Messenger Formation had a slope of 0.5 - 1^{o} (Figure 4.10B) and accumulated on the lower slope (Figure 4.2), whereas in North Taranaki the slope for the corresponding part of the formation is 2 - 4^{o} (Figure 4.10A) and the sediment accumulated on the middle slope region (Figure 4.2A). In neither region did the lower Mount Messenger Formation sediments accumulate on a basin floor. The partitioning of the slope into upper, middle and lower parts, as shown in Figure 4.2, has been adopted from Strogen et al. (2011, 2022).

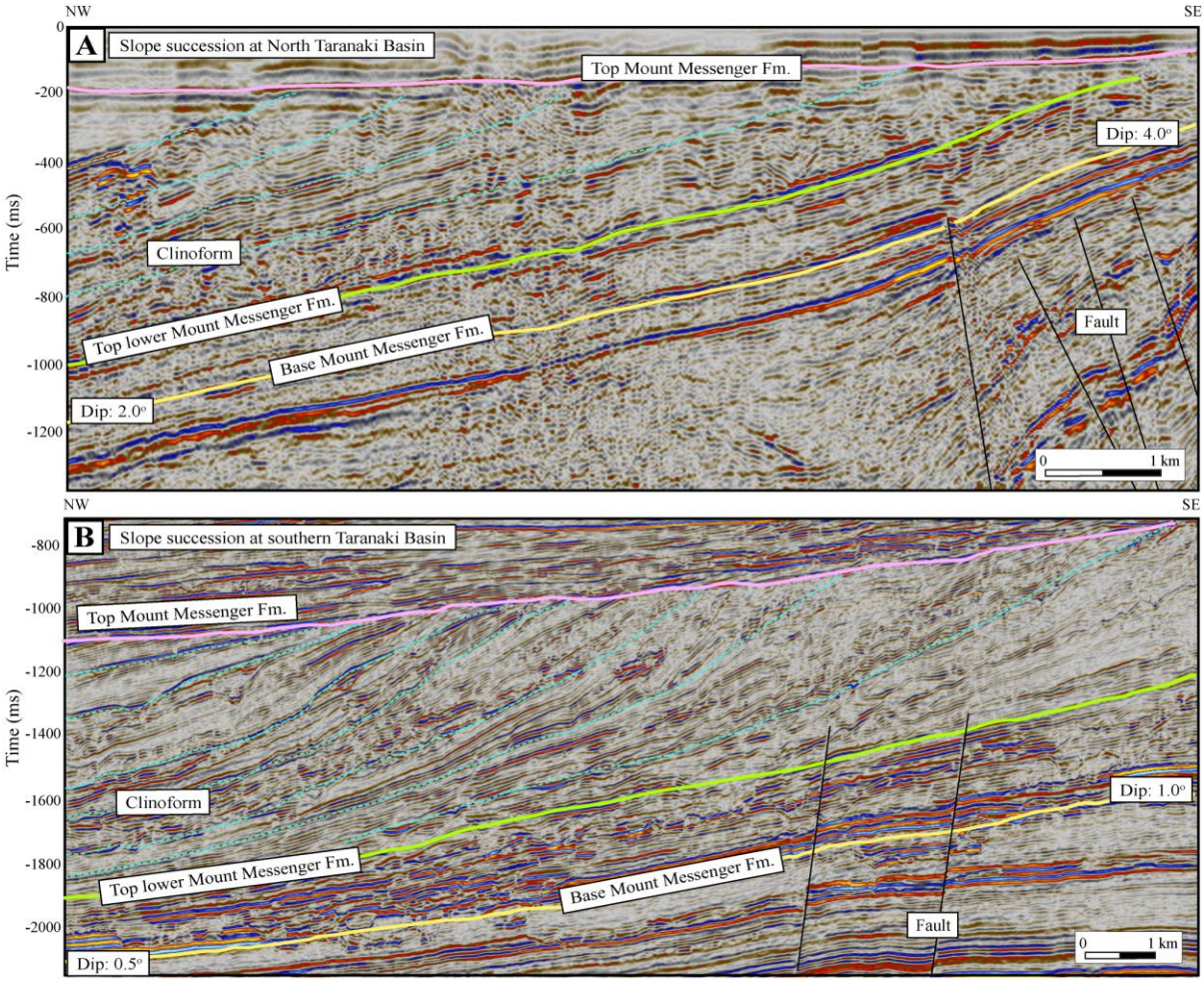

Figure 4.10: Seismic reflection profiles showing the slope succession and major regional horizons for (A) North Taranaki Basin (study area) with slope dip ranging from 2 to 4º, and (B) southern Taranaki Basin with slope ranging from 0.5 to 1º. The succession immediately above the base of the Mount Messenger Formation horizon was used to determine slope angle. Light green horizon approximately separates the lower and upper parts of the Mount Messenger Formation. Refer to Figure 4.2A for the seismic line locations (A: 2D seismic line BO_hzt82b-114 and B: arbitrary line from Maui – Kokako 3D merge seismic surveys). Refer to Figure v in Appendix C for channelform features interpretation on the seismic sections, and Figure vi in Appendix C for the uninterpreted seismic sections.

4.5.3 Structure Contour, Isopach Thickness and Dip Mapping

Structure contour and isopach thickness maps of the base and top of the Mount Messenger Formation in North Taranaki Basin interpreted in Mercury-Mokau 3D seismic (Figure 4.11A-C), show that (truncated) thickness increases uniformly from 80 m to ~700 m orthogonally to the west-southwest away from the eastern edge of the 3D seismic survey area and the coastline, along the whole north-south length of the survey area. Dip and dip-direction maps of the contact separating the lower Mount Messenger Formation from the upper Mount Messenger Formation indicate a regional dip of ~3.6^{o} and a dip direction of 259^{o} (southwestward) (Figure 4.11D-E). These trends are consistent with the pattern observed in the isopach thickness map (Figure 4.11C).

The very simple thickness pattern observed in the isopach maps is largely a function of the erosional truncation of sediments arising from Pliocene-Pleistocene uplift (Figure 4.4) and erosion of the basin succession preferentially along its eastern margin during doming of central-western North Island (Kamp et al. 2004). The western margin of the erosion surface coincides with the western margin of the survey area. The trends observed in the regional dip maps are a function of the angle of the depositional surface at the time of deposition as well as post-depositional tectonic tilt.

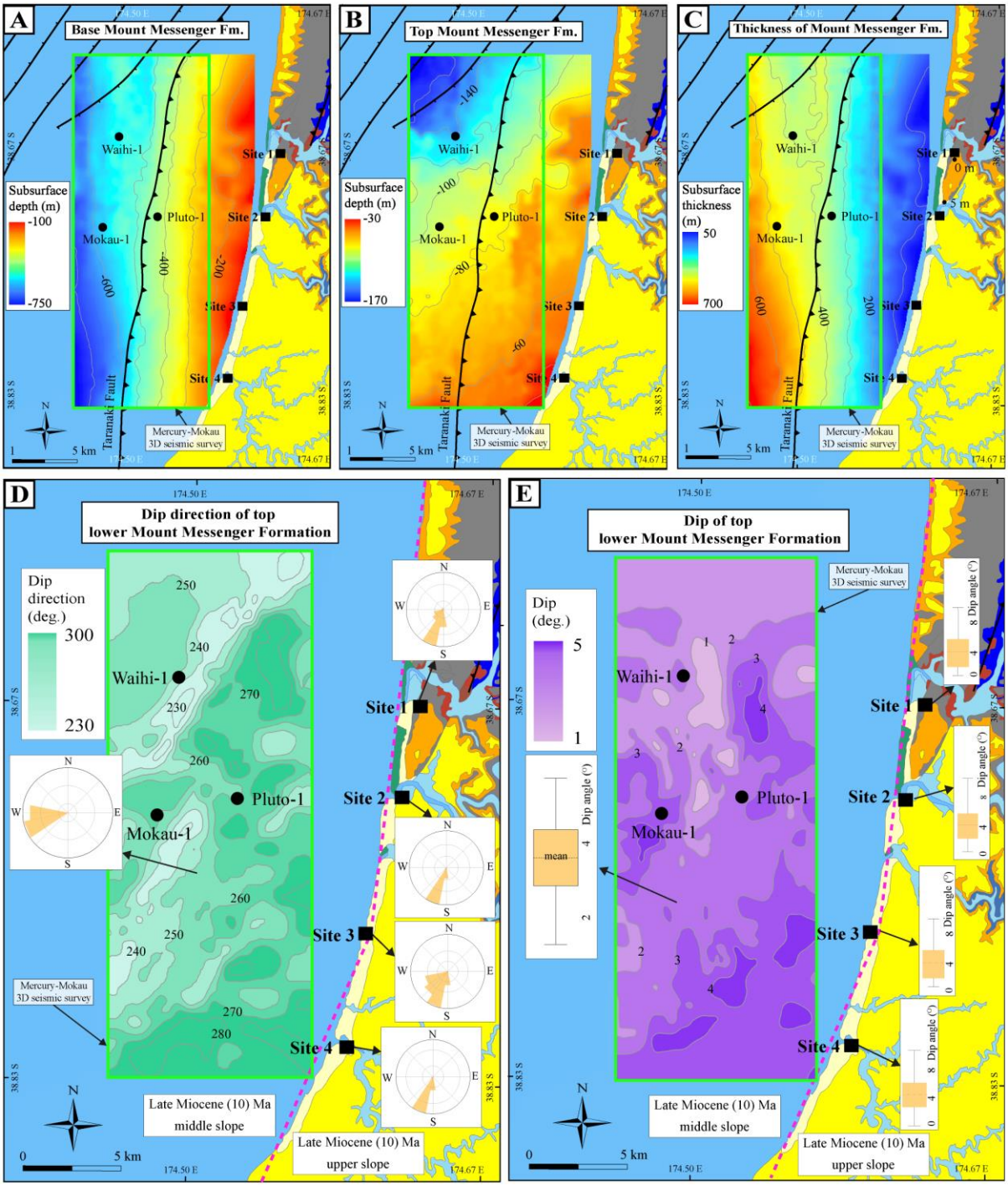

Figure 4.11: Maps the Mount Messenger Formation based on interpretation of 2D and 3D seismic data. (A) Structure contour map of the base of the Mount Messenger Formation. (B) Structure contour map of the top the Mount Messenger Formation (also referred to as the top of the Mohakatino Formation). (C) Thickness map of Mount Messenger Formation. (D) Dip direction and (E) Dip of a surface within the lower Mount Messenger Formation. The maps also show the distribution of the lower Mount Messenger Formation onshore (yellow). Overall, the onshore strata dip southwest with a mean angle of 3.6°. The division between the Late Miocene (~10 Ma) upper and middle slope is marked with a red dashed line. Refer to the legend in Figure 4.1 for more information.

4.5.4 Seismic Geomorphology

The Mercury-Mokau 3D seismic survey was searched for the stratal patterns outlined by Posamentier and Erskine (1991) as indicative of buried submarine fans (Table 4.1). Figure 4.12 shows annotated representative seismic reflection profiles showing where there is the presence of, or absence of, those stratal features. This is also summarized in Table 4.2. The analysis shows clearly how stratal pinch-out does not occur within the lower Mount Messenger Formation interval, a feature highly characteristic of submarine fans. Similarly, bidirectional pinch-out of strata that resemble outward build-up of lobes is not observed. There is no evidence in the seismic data for stratal mounding, which usually indicates the presence of vertical build-up on the top-middle region of fans. These features should be discernible in the dataset given the seismic resolution limit of 9.6 m (Figure 4.8).

In the Mercury-Mokau 3D seismic volume there are high-amplitude reflectors within the Mount Messenger Formation interval, but their occurrence is primarily limited to the upper Mount Messenger Formation and areas of the data affected by gas chimneys, faults, or otherwise low-quality data. Moreover, these reflectors are not smooth and continuous but rather appear highly disrupted. This is similar to the patterns demonstrated for the continental slope in southern Taranaki Basin where channelforms incising into the slope caused reflector disruption (e.g. Kamaruzaman et al., 2023; 2024a). In the absence of other Posamentier and Erskine (1991) stratal criteria, it is highly unlikely that these high-amplitude reflectors represent submarine fan(s). It is more plausible that they represent sandstone beds that accumulated on the continental slope or within channel complexes incised into the slope.

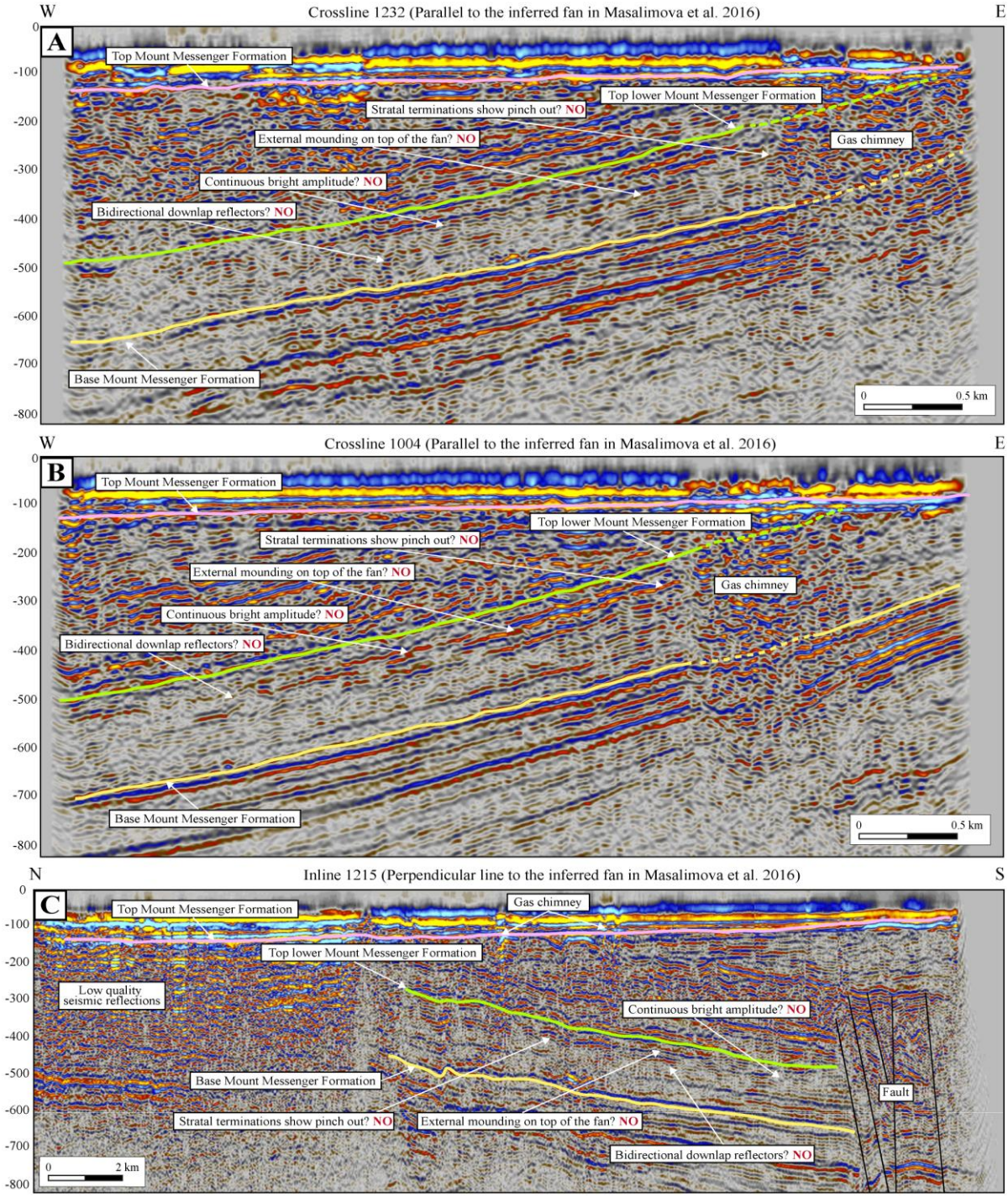

Figure 4.12: (A), (B) and (C) are selected seismic reflection lines from the Mercury-Mokau 3D seismic survey area in offshore North Taranaki Basin, showing that the Posamentier and Erskine (1991) criteria (Table 1) for the identification of submarine fans are not met in any of these lines (and other lines in the seismic dataset), meaning that the fan inferred by Masalimova et al. (2016) does not exist. Refer to Figures 4.6B and 4.21A for seismic line locations. Refer to Figure vii – xi in Appendix C for more seismic sections.

Table 4.2: Assessment of the Posamentier and Erskine (1991) criteria for identifying submarine fans in seismic reflection in the Mercury-Mokau 3D seismic data shown in Figure 4.12. The criteria are expanded from those listed in (Table 4.1).

Aspect	Criteria	Masalimova et al. (2016) inferred fan
Physiography of fan systems	The mouth of the feeder canyon-channels can be located	
	The segments of the fans (i.e., upper and lower) can be identified	
Seismic stratigraphic interpretation	Continuous high-amplitude reflectors (usually at top fans) onlap basin margin	
	Bidirectional downlap reflectors within fan	
	Stratal terminations show pinch out	
	External mounding on the fan upper bounding surface	

Legend

High confidence Low confidence No confidence Cannot be accessed

4.5.5 Sediment Channelforms Mapping

Due to the quality of seismic data within the interval of interest, we have conservatively mapped the occurrence of channels on selective and representative seismic reflection images of the lower Mount Messenger Formation in the Mercury-Mokau 3D seismic survey area (Figures 4.13 - 4.14). Channels are objectively identified based on: (i) trough-like or U-shaped reflector geometry, (ii) prominent truncation of underlying reflectors, (iii) truncated reflectors within the interpreted channelforms and (iv), concave and/or convex-upward reflectors within the interpreted channelforms.

The density of channels increases upwards within the formation and channels dominate the upper part. This is not unexpected, as channels are well-known structures in outcrop sections of the upper Mount Messenger Formation (Browne & Slatt 2002; King et al. 2007; Rotzien et al. 2014). Figure 4.14 illustrates our mapped channels in the lower part of the Mount Messenger Formation. The occurrence of channel systems ~100 m high and ~1 km wide are recognized by their erosional bases. These channel systems consist of multiple channel complexes and channel elements, exhibiting diverse dimensions and architecture. Channel complexes, in particular, are characterised by an erosional down-cut surface, where seismic reflectors are truncated. The thickness and width of channel complexes are typically ~60 m and < 0.5 km, respectively. In contrast, channel elements are challenging to identify and map as they approach the limit of seismic resolution within the interval, as their typical dimensions are ~20 m high and < 150 m wide.

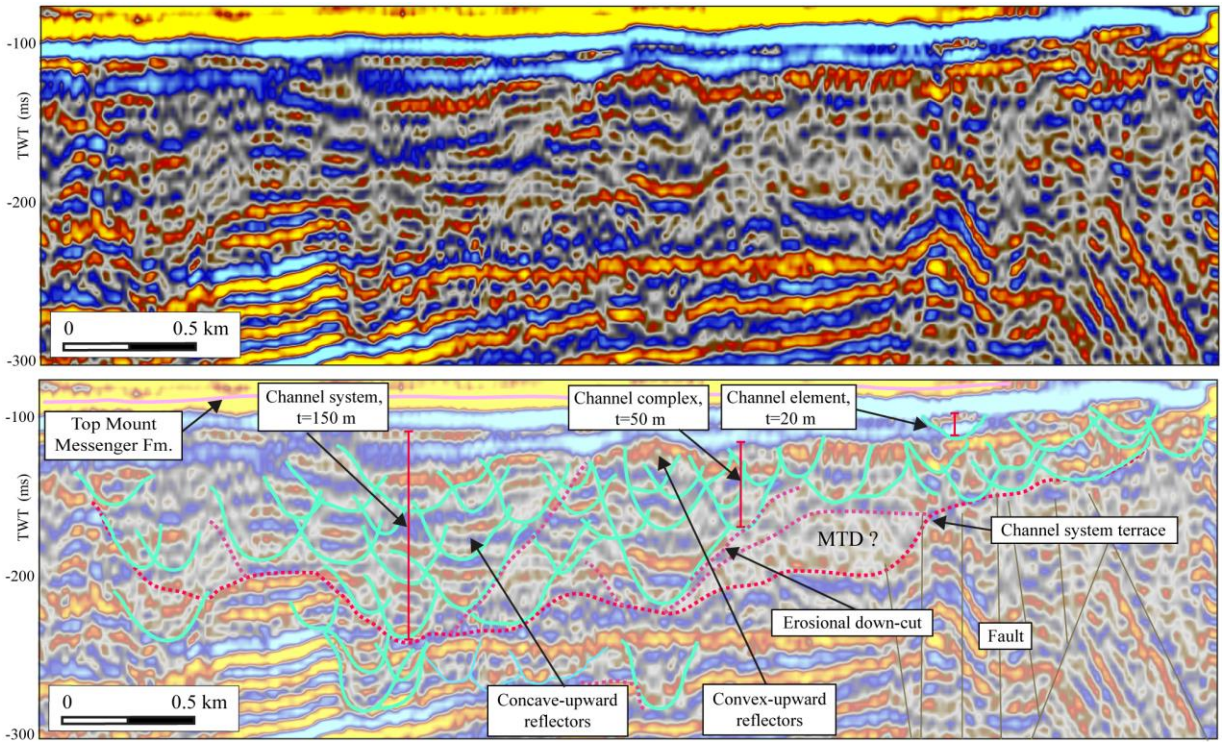

Figure 4.13: An uninterpreted and interpreted seismic reflection profile showing channelform features, including channel systems, channel complexes and channel elements in the upper Mount Messenger Formation interval. Note the channel system width and thickness measured at 1 km and 150 m, respectively. Refer to Figures 4.2B and 4.21B for the location of the seismic line.

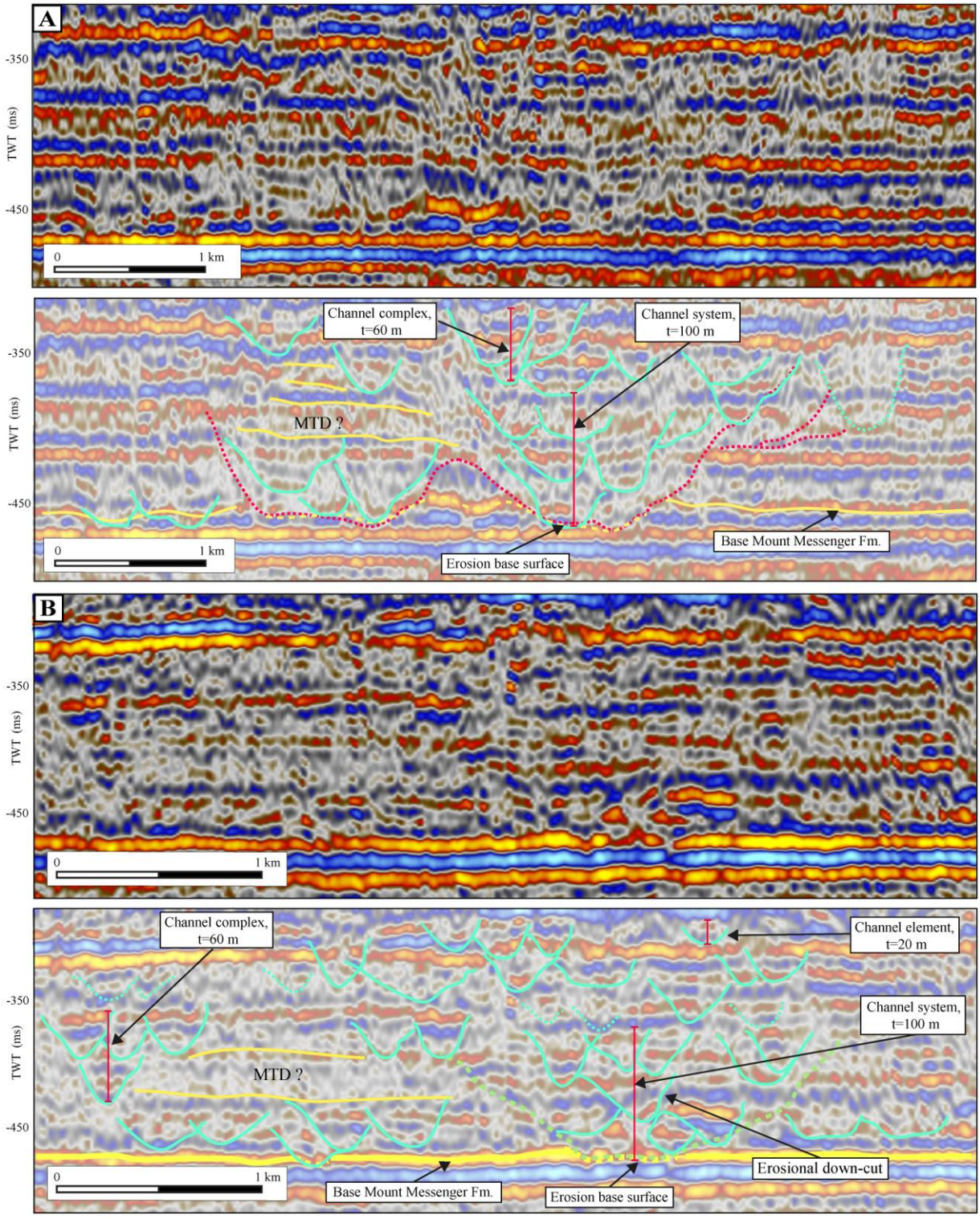

Figure 4.14: (A) and (B) are uninterpreted and interpreted seismic reflection lines from the Mercury-Mokau 3D seismic survey area showing channelform features, including channel systems, channel complexes and channel elements in the lower Mount Messenger Formation interval. The channel system is approximately 100 m thick and 1 km wide, while the channel complex is 60 m thick and less than 500 m wide. Channel elements approach the resolution of the seismic data, with a thickness of ~20 m and width of less than ~200 m. Refer to Figures 4.2B and 4.21B for seismic line locations.

4.5.6 Outcrop Photogrammetry

4.5.6.1 Site 1: Battleship Promontory Section

The Battleship Promontory site includes what appears to be a conformable contact between the Mount Messenger Formation and the underlying Mohakatino Formation, and about 10 m of the lower Mount Messenger Formation (which itself accumulated on a slope) (Figure xii - Appendix C). The outcrop model for this site extends over ~900 m along the formation at elevations between 145 m and 210 m above sea level. It covers a ground area of approximately 0.20 km^2, with the outcrop primarily facing north (Figure 4.9A).

At this location, the lower Mount Messenger Formation shows parallel beds of massive to wavy laminated sandstone (Figure 4.15A-B). The beds have sharp and planar contacts with no evidence of erosion or pinch-out of strata as observed in outcrop drone model. Channel-shaped margins are not evident in this section. The beds dip at 4.4º to the southwest (Figure 4.15C-D). Within the measured sections, bedset thickness ranges from 0.3 to 5.2 m, with a mean of 1.2 m (Figure xiii - Appendix C).

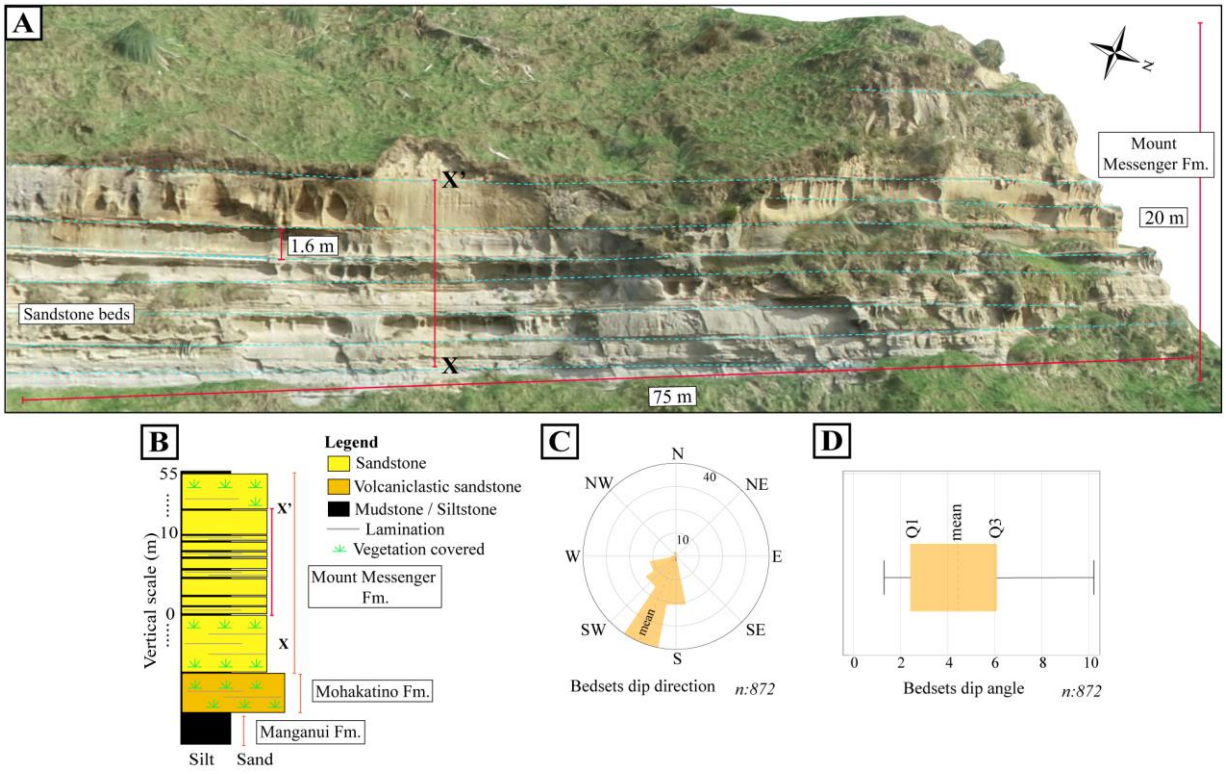

Figure 4.15: (A) Interpreted outcrop image of lower Mount Messenger Formation bedsets at Site 1, Battleship Promontory. (B) Litholog of the area marked X-X' in A. (C) Rose plot of dip direction of bedsets. (D) Range of dip for bedsets. Refer to Figure xii in Appendix C for the outcrop location, and Figure xiv in Appendix C for the uninterpreted version of the outcrop image.

4.5.6.2 Site 2: Ferry Sandstone Section

The Ferry Sandstone section forms a steep outcrop on the south side of the Mokau River estuary. The base of the outcrop is within a few 10s of m of the base of the Mount Messenger Formation. The outcrop model for this site is ~250 m long and 80 m high (Figure 4.9B) and it faces north along State Highway 3. The lowermost part of this section comprises ~12 m of undeformed siltstone beds, overlain by a ~53 m-thick succession of massive to wavy-laminated sandstone beds, with bedset thickness ranging from 0.3 – 5.2 m, with a mean of 2.1 m (Figure xv - Appendix C). An erosion surface occurs in the middle portion of the section, recognized by notches (incisions) and beds that terminate against the surface (Figure 4.16A-B). This erosion surface is interpreted to represent an irregular shaped channel margin, which slopes at 10^{o} towards the southwest. The channel truncates a ~4 m-thick sandstone bedset and is overlain by 20 m of sandstone beds with conformable contacts, which appear to onlap the channel margin. A ~9 m-thick siltstone beds overlie the channel fill (Figure 4.16A). The beds dip into the outcrop at 4.5^{o} southwest (Figure 4.16C-D).

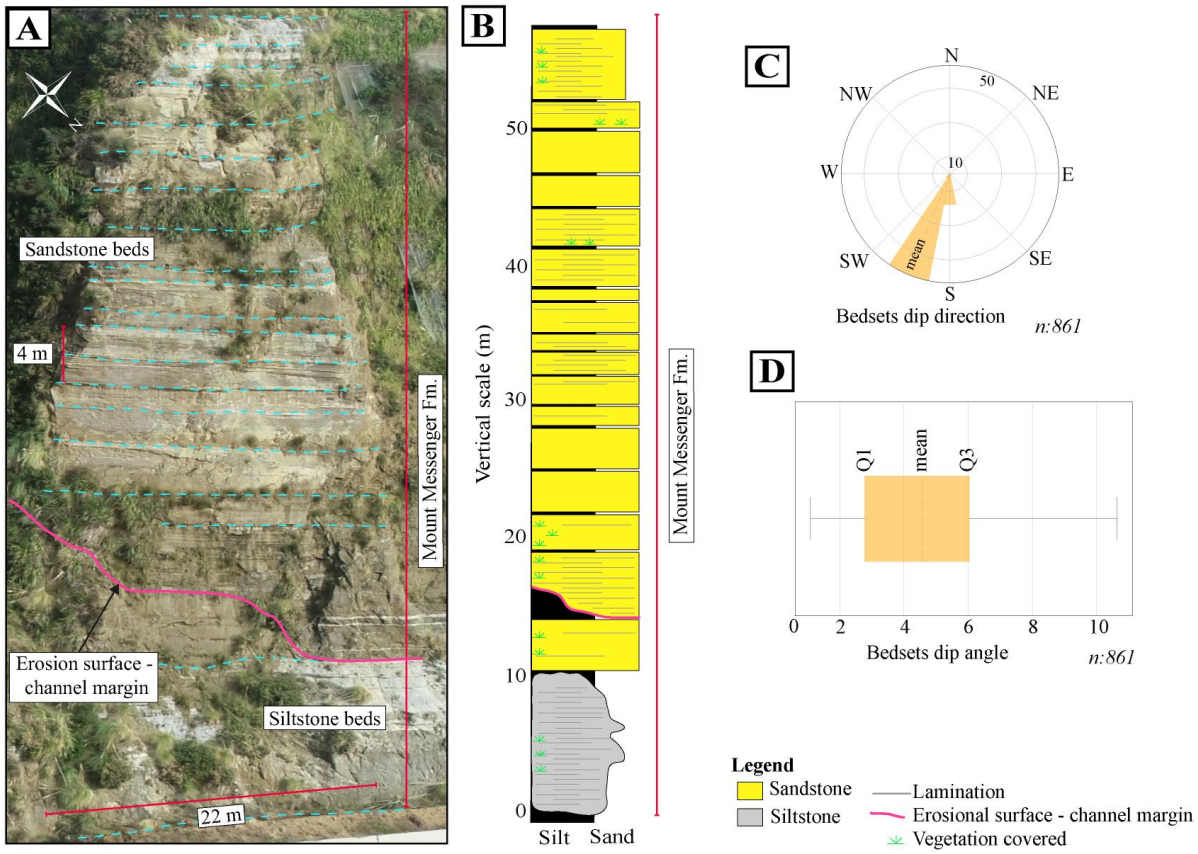

Figure 4.16: (A) Interpreted outcrop image of lower Mount Messenger Formation bedsets at Site 2, Ferry Sandstone. (B) Litholog of the outcrop. (C) Rose plot of dip direction of bedsets. (D) Range of dip for bedsets. Refer to Figure xvi in Appendix C for the uninterpreted version of the outcrop image.

4.5.6.3 Site 3: Jam Roll Section

Site 3 lies 300 m above the base of the Mount Messenger Formation and a little below the middle of the lower Mount Messenger Formation (Figure 4.5). This is a structurally complicated section, particularly in the bay hosting the Jam Roll structure (Figures 4.17 and 4.18). The outcrop model of the lower Mount Messenger Formation stretches over ~3 km in length, where the coastal cliffs are between sea level and 22 m above sea level. The site mainly faces west to the Tasman Sea (Figure 4.9C). Analysis of Site 3 focused on discontinuities between beds and the juxtaposition of blocks that have no stratigraphic relationships to each other.

On the northern side of Site 3 (Figure 4.9C: Kawau Pa), the best exposures are the cliffs on the south side of the stream (Figure 4.17A) as well as the break in outcrop that trends north-south at the end of the first north-facing cliff. Figure 4.17A displays a sharp, erosional and sloping surface separating a ~6 m-thick siltstone beds from overlying sandstone beds ~8 m thick that we interpret as the margin of a channel element. This surface is ~220 m long from north to south and slopes at 5^{o} to the southwest. The same surface also continues to the west (seaward) of the break in outcrop for another 200 m and separates siltstone and sandstone units with 5 m of relief.

Figure 4.18A is a view along the coastal section of Jam Roll Bay (Figure 4.9C), which is the central part of Site 3. The feature labelled C in Figure 4.18A is a 7 m-high and 3 m-wide body of sandstone. Its eastern (inland) margin is a deeply eroded contact into an 8 m-thick exposure of steeply dipping and bedded siltstone that dips west (seaward). The western side of the sandstone body is also eroded (by 7 m) into a massive siltstone that dips at 20^{o} to the west. These siltstone units are not correlative with one another. The top of the sandstone body is

truncated by a wave-cut surface. We interpret the sandstone body as the fill of a narrow channel, but the deformation of the sandstone suggests that there was subsequent shortening within it, involving the siltstone units on either side.

The feature labelled D in Figure 4.18 is a sandstone package 10 m thick comprising 12 m conformable sandstone beds, some with thin (cm-scale) intervening siltstone, in places deformed into rip-up structures. A separate 0.7 m-thick massive sandstone bed lies within the underlying massive and bioturbated siltstone, and it is clear that the sandstone and underlying massive siltstone are part of the same original stratigraphic succession. The steep dip of this stratigraphic section, which is much greater than the regional dip, suggests that it was part of a synsedimentary slide.

The block labelled E in Figure 4.18 comprises 6 m of bedded siltstone, which is very similar to the siltstone on the eastern side labelled D. It passes upward into a highly disharmonically deformed siltstone. Figure 4.18F shows a folded sandstone bed 9 m thick that is capped by siltstone. We interpret blocks D, E and F as representing deformation during synsedimentary slumping of partially consolidated sediments beneath the sea floor soon after their deposition.

The Jam Roll structure in Figure 4.18G comprises recumbent folded strata, which is in situ relative to the underlying strata. Multiple water ejection or liquefaction structures involving mini sand “volcanoes” occur at the top of this block, suggesting that the sediments were folded when they were partly consolidated, but the sandstone beds were not completely dewatered. This implies that the failure of the seafloor involved deep-seated strata. The same style of

deformation is evident in the coastal cliff immediately east of the Jam Roll, indicating that it was part of a larger slide or slumps of relatively coherent sandstone beds.

Another large channel margin erosional surface is evident at the southern part (Figure 4.9C) of the Site 3 outcrop (Figure 4.17B). The erosional surface is 180 m long and it dips at 4.5^{o} to the southwest, separating a ~9.5 m-thick sandstone bed from the underlying ~7 m-thick siltstone bed. The upper part of the lower Mount Messenger Formation beds is truncated by the Late Pleistocene wave-planned surface.

In summary, Site 3 shows a complex arrangement of channels incising into underlying bedding, beds with dips steeper than the regional dip, juxtaposition of blocks with contrasting lithology, disharmonic synsedimentary slump folded strata, and slides.

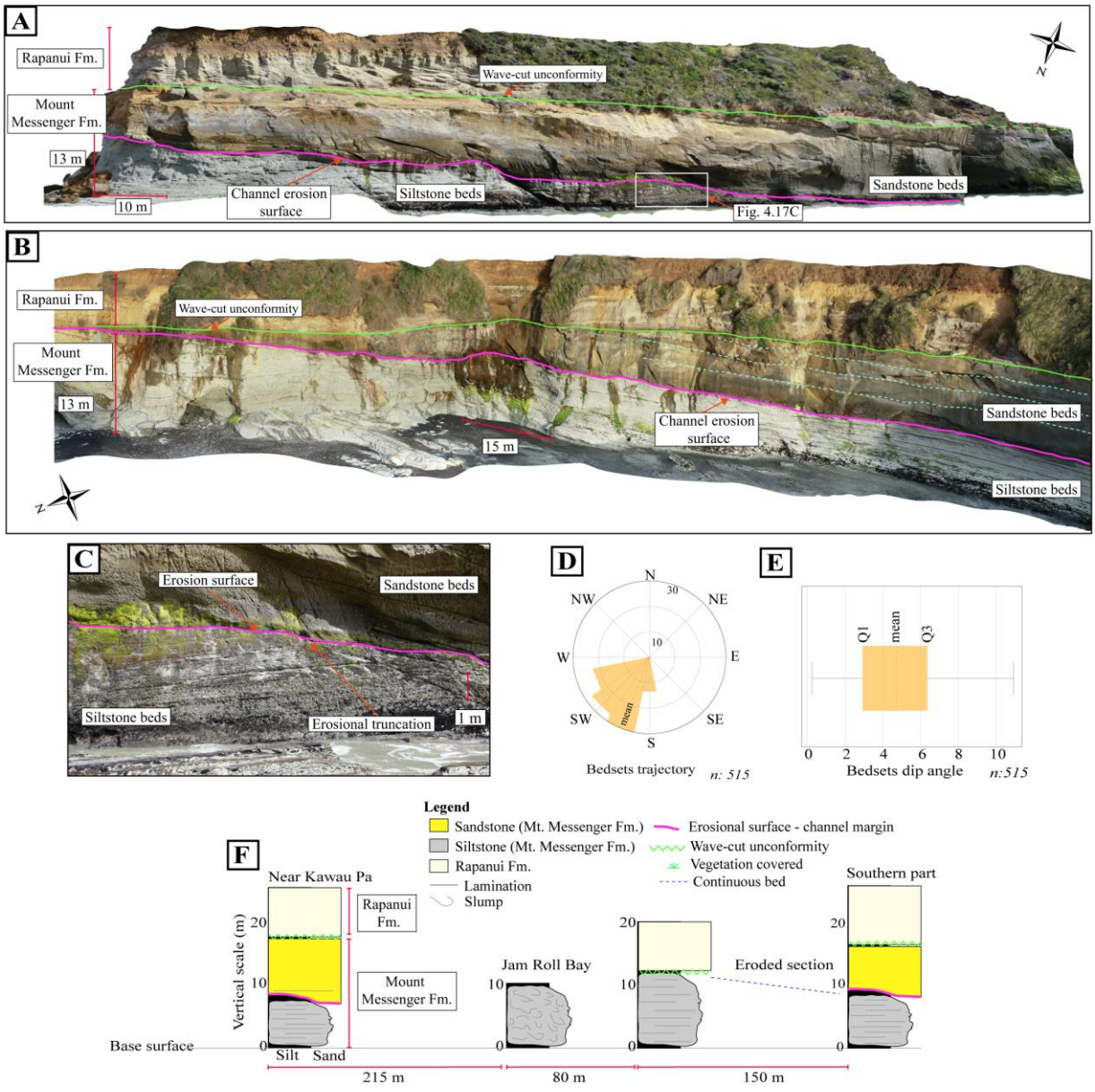

Figure 4.17: Lower Mount Messenger Formation outcrops at Site 3. (A) The area near the Kawau Pa and (B) the area to the south, showing channel erosion surface. (C) Close-up view of the erosion surface, of which the siltstone beds are truncated by the overlying sandstone beds. (D) Rose plot of dip direction of bedsets. (E) Range of dip for bedsets. (F) Lithologs for various parts of the lower Mount Messenger Formation outcrop a Site 3, emphasizing how the beds cannot be correlated. Refer to Figures xvii - xix in Appendix C for the uninterpreted version of the outcrop images.

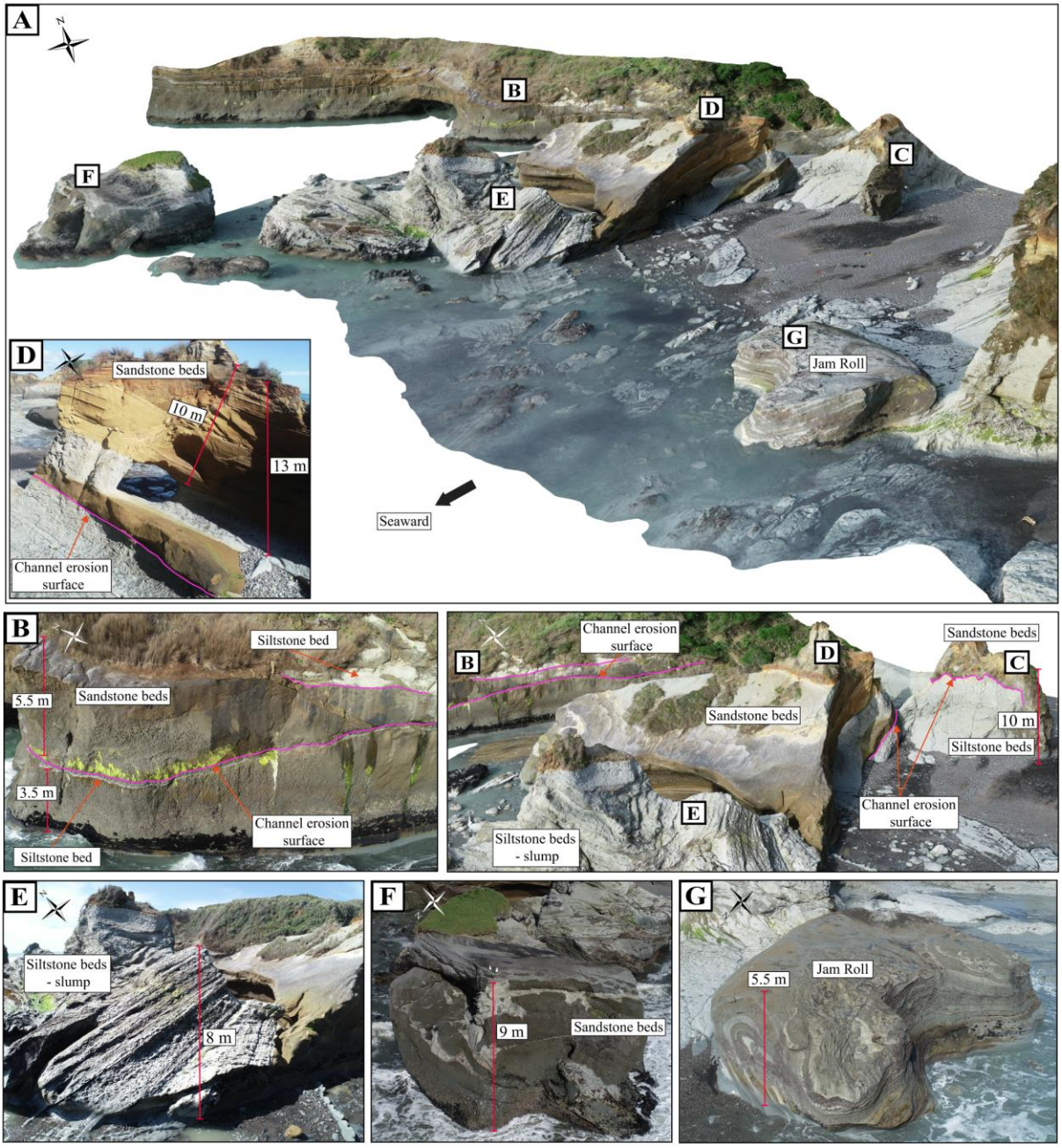

Figure 4.18: (A) Overview of the area at Site 3, Jam Roll Bay, consisting of structurally complex sediment blocks. (B) Sandstone unit that shows erosion surface, that is disconnected from the other sediment blocks. (C) and (D) Sediment blocks of massive, sandstone that represent channel fill. (E) and (F) Sediment blocks of mainly deformed siltstone. (G) Recumbent fold known as the "Jam Roll" structure.

4.5.6.4 Site 4: Tongaporutu River Mouth Section

The lower Mount Messenger Formation outcrop exposed on the southern side of the Tongaporutu River mouth (Site 4) is ~900 m in length, and trends west-east oblique to the SW regional dip direction. The height of the cliff section is 25 m above sea level, including 20 metres of lower Mount Messenger Formation (Figure 4.9D). This site corresponds to the upper part of the lower Mount Messenger Formation.

Photogrammetric mapping identified two erosional surfaces within an otherwise conformable succession of mainly sandstone beds (Figure 4.19A, E). The erosion surface at the eastern end of the section is mapped in Figure 4.19A as far as possible before it is obscured by vegetation cover. The surface has been mapped between sandstone beds with different bed thicknesses – medium bedded beneath the surface and very thick bedded above the surface, but variable in thickness, suggestive of onlap onto the surface at higher elevation towards its western (sea) end. At the eastern end (Figure 4.9D) of the outcrop, part of a slump-fold is exposed beneath an overlying thick sandstone bed. The second erosional surface has been mapped at the western end (Figure 4.9D) of the outcrop where it faces the open ocean (Figure 4.19E). The erosion surface may be related to incision by channelized deposits of the Rapanui Formation.

Overall, the beds at Site 4 dip at 5.2^{o} to the southwest (Figure 4.20A-B). The thickness range of beds varies from 4 to 22 m (mean: 4.1 m), and the bedsets tend to thin upward.

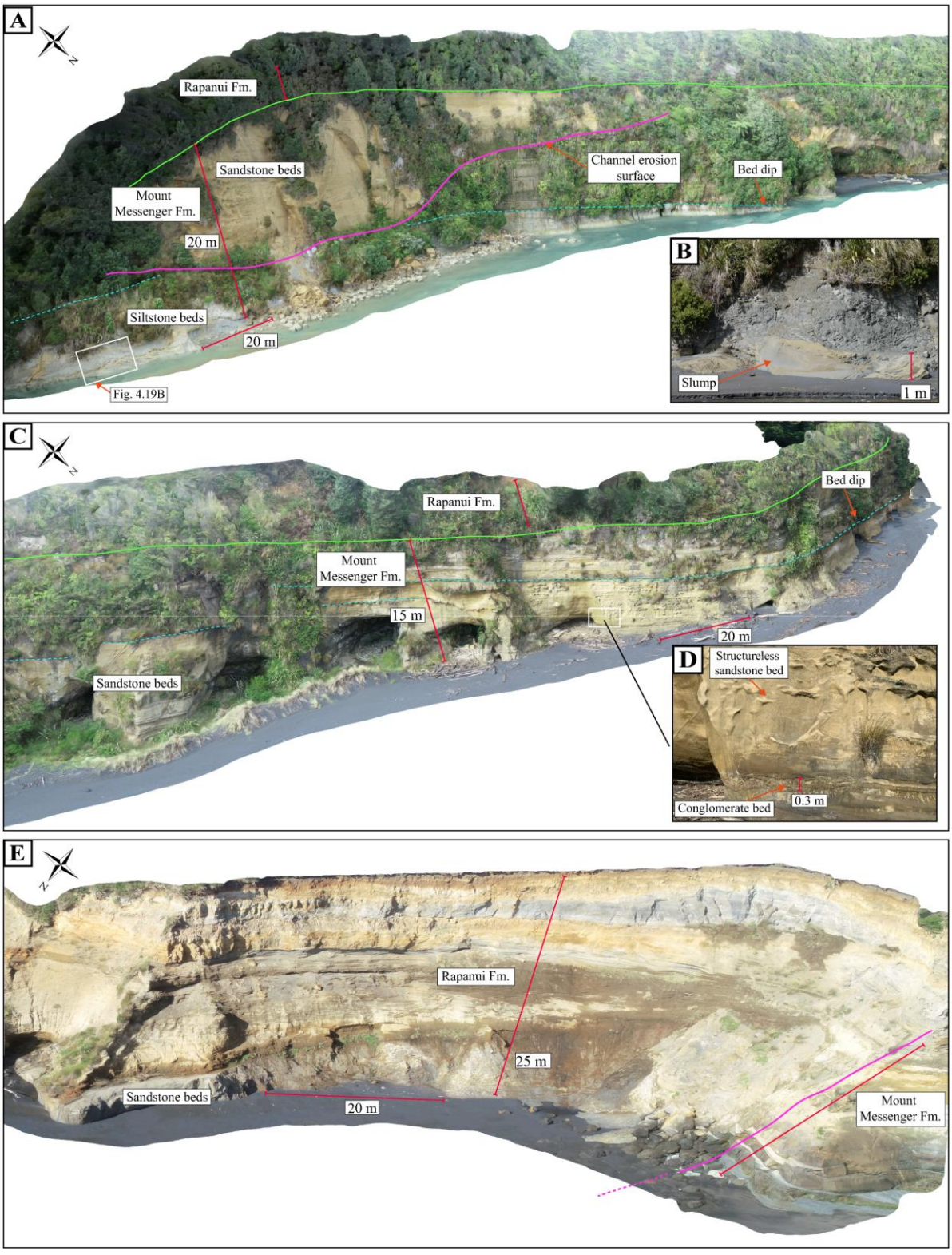

Figure 4.19: ((A), (C) and (E) are interpreted outcrop sections of the lower Mount Messenger Formation outcrop at Site 4: Tongaporutu River Mouth. (B) A close-up view of slump deposits, and (D) a close-up view of the structureless sandstone and conglomerate beds. Refer to Figures xxi - xxiii in Appendix C for the uninterpreted version of the outcrop.

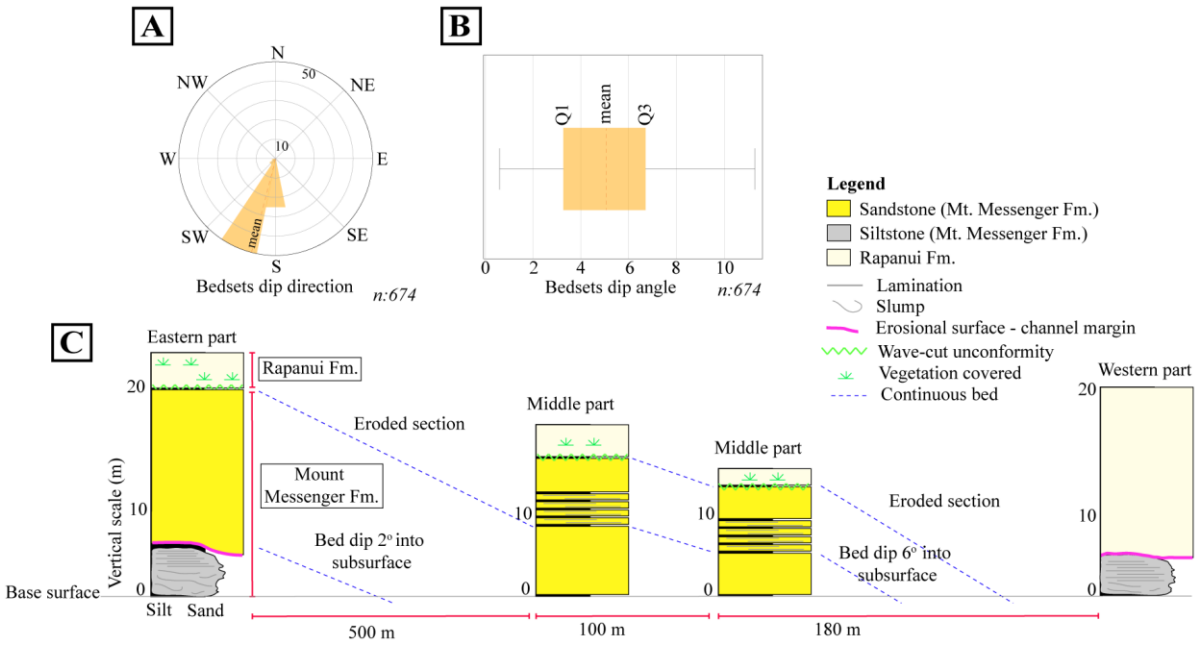

Figure 4.20: Figure 20: Overall measurement of the bedsets at Site 4, Tongaporutu River Mouth. (A) Rose plot of dip direction of bedsets. (B) Range of measured dips of bedsets. (C) Lithologs of the outcrop emphasizing uncorrelated beds. Refer to Figure xiv in Appendix C for bedset thickness measurement.

4.6 Discussion

The results of the analysis of seismic stratigraphy, seismic geomorphology, and photogrammetry from UAV drone images furnish a new picture of the depositional setting for the Mount Messenger Formation along the North Taranaki coastal section. The following text outlines four main aspects of the data that strongly support the new interpretation that the outcrops represent exhumed upper slope deposits (and not submarine fans of any significant scale). These aspects include: 1) the stratigraphic context of the stratigraphy leading into the Mount Messenger Formation, 2) the observed stratal patterns as mapped in offshore seismic data, 3) the lack of objective criteria in seismic data indicating submarine fan sedimentary environments and 4), the dominance of channelforms in the Mount Messenger Formation strata. We complete the discussion by issuing a cautionary perspective on facies analysis in the absence of 3D views of the strata and summarize the implications of our new findings for reservoir exploration and production in offshore Taranaki Basin.

4.6.1 Stratigraphic Context Supports Continental Slope Deposition for the Mount Messenger Formation

The stratigraphy and associated depositional settings of the Early to Middle Miocene formations exposed on land immediately east of the North Taranaki coastal section provide important context for understanding the deposition of the Mount Messenger Formation (Figure 4.3B). In particular, the Early Miocene (Otaian and Altonian) Manganui Formation was deposited on the upper continental slope (upper bathyal water depths), and is laterally equivalent in its lower part to the Bexley Sandstone shoreline facies, and in its upper part to

the terrestrial to nearshore Maryville Coal Measures (Kamp et al. 2004; Edbrooke 2005). Above the Manganui Formation during the Middle Miocene (Clifdenian and lower Lillburnian), the Moki Formation was deposited by sediment gravity flows, and includes levee deposits, as well as channelised calcareous sandstone of the Mangarara Formation (Kamp et al. 2004; Puga-Bernabéu et al. 2009). We interpret these units as upper slope deposits, adjacent to a very narrow shelf represented by the Tangarakau Formation. Prograding across the Moki Formation, the Otunui Formation is inferred to have accumulated in upper bathyal conditions in an upper slope setting immediately inland of the North Taranaki Basin coastal section (Figure 4.3B) (Kamp et al. 2004). The Mohakatino Formation overlies the Otunui Formation (on the slope) with apparent conformity but the Mohakatino Formation only occurs for 5 – 7 km inland of the modern coast. Finally, the Mount Messenger Formation conformably overlies the Otunui Formation in both King Country and Taranaki basins, showing bathymetric deepening concurrent with a new sediment source derived from the newly emergent Southern Alps (King & Thrasher 1996). However, wholesale subsidence of North Taranaki Basin and the area beneath the coastal section to lower bathyal base-of-continental slope depth (i.e. to basin floor depth and setting) is not envisaged.

4.6.2 Stratal Patterns Across Taranaki Basin Consistent with a Continental Slope Setting

Our comparison of seismic profiles from southern Taranaki Basin and North Taranaki Basin (Figure 4.10), demonstrate that the same continental slope trend was present across large parts of Taranaki Basin during the Miocene (Strogen et al. 2011). In both regions, the upper Mount Messenger Formation steepens upward, reflecting progradation of the shelf-slope wedge. This steepening is more marked in southern compared with North Taranaki Basin, due to a higher contemporary flux of sediment resulting from some trapping of sediment from source to sink in King Country Basin. Kamaruzaman et al. (2024a) showed that the lower Mount Messenger Formation in southern Taranaki Basin accumulated on a continental slope and it is reasonable to infer that this was also the case for North Taranaki Basin, although the depositional slope angle is difficult to isolate from the post-Mount Messenger tectonic tilt. By contrast, it has been argued by others that the lower Mount Messenger Formation exposed in the North Taranaki coastal section accumulated on a basin floor, and that the progradation observed upwards through this formation reflected progradation of slope deposits across an initial basin floor fan succession (King et al. 1993, Hansen 1996; Browne & Slatt 2002; Masalimova et al. 2016). We deny this claim and suggest that the stratigraphy underlying the Mount Messenger Formation (which therefore set the stage for its deposition), as well paleogeographic interpretations of Kamaruzaman et al. (2024a) prove that the lower Mount Messenger Formation accumulated on the continental slope.

4.6.3 Lack of Objective Criteria for Submarine Fans

If the lower Mount Messenger Formation within the North Taranaki coastal section accumulated as a succession of basin floor fans or as a submarine fan (e.g. King and Thrasher, 1996; Strogen et al., 2011; Masalimova et. al., 2016), and as the 3D seismic survey area lies within the extent of the fan mapped by Masalimova et. al. (2016), then this should be evident in the stratal patterns imaged by seismic reflectors. The submarine fan hypothesis put forth by Masalimova et al. (2016) is of a large enough scale (Figures 4.6 and 4.21A) that it would be imaged in the seismic data. Our considered analysis of the Mercury-Mokau 3D seismic survey and adjacent 2D reflection profiles did not reveal any of the objective stratal patterns defined by Posamentier and Erskine (1991) as characteristic of submarine fans in seismic reflection data (Figure 4.12 and in Table 4.2) and therefore the interpretation of submarine fans is inconsistent with the data.

4.6.4 Dominance of Channelforms in the Mount Messenger Formation Interval

Kamaruzaman et al. (2024a) mapped canyons and channel complexes in the lower Mount Messenger Formation in 3D seismic reflection data for southern Taranaki Basin and demonstrated two fans of different ages in the deep-water area of western Taranaki Basin that each lies at the mouth of distinct channels (Figure 4.2). This linkage of fan to feeder channels or canyons is a basic characteristic of deep-water sedimentary systems (Normark 1978; Posamentier et al. 1991; Shanmugam 2016). It follows that canyon and channel complexes lie upslope of submarine fans and that their occurrence is a strong indicator of a continental slope. Demonstration of abundant channelforms in the lower Mount Messenger Formation within the

Mercury-Mokau 3D seismic survey leads us to conclude that any submarine fans present in the Mount Messenger Formation must lie paleo-seaward of the North Taranaki coastal section, certainly beyond the extent of the lobe complex mapped by Masalimova et al. (2016) (Figures 4.6 and 4.21), and most likely beyond the fans mapped by Strogen et al. (2011, 2022). As there was significant amounts of sediment supplied to North Taranaki Basin during the Late Miocene, submarine fans may lie farther offshore than the Mokau-Mercury 3D seismic survey area and in deeper-water parts of Taranaki Basin. Indeed, two Late Miocene fans have been mapped there (Kamaruzaman et al. 2024a) (Figure 4.2), although they are at the end of one or more of the channels mapped on the slope in southern Taranaki Basin. It is unlikely that channelforms in the North Taranaki Basin investigated here will connect to those fans. Channels become more common in the seismic reflection data for the upper part of the Mount Messenger Formation in the Mokau-Mercury 3D seismic survey area, which is consistent with observations from the upper part of the Mount Messenger Formation in outcrop (e.g. King et al. 1993; Rotzien et al., 2014; Masalimova et. al., 2016).

Photogrammetric mapping of selected sites in the coastal section identified several channelforms within the lower Mount Messenger Formation. The scale of these channelforms corresponds to channel elements, which may be below resolution in the Mercury-Mokau 3D seismic survey (Figure 4.8). Site 3 is a ‘graveyard” of juxtaposed blocks of different internal lithology and structure that we interpret as a combination of slide blocks (e.g., coherent stratigraphy dipping much steeper than the post-depositional regional dip) and disharmonic slump blocks (e.g. the Jam Roll structure) (Figure 4.18). We envisage that these blocks accumulated within a slope channel, rather than being part of a much more extensive mass transport deposit at the base of a slope as interpreted by King et al. (2007). The scarcity of

obvious channels within exposures of the lower Mount Messenger Formation, compared with the offshore seismic data probably reflects a more upslope position of the coastal section relative to the offshore location of the seismic reflection survey area.

When the stratigraphic context of underlying units, seismic stratigraphy, and seismic geomorphology in the offshore area, and photogrammetric mapping of outcrops are taken together, the most parsimonious interpretation for the lower Mount Messenger Formation in the North Taranaki coastal section is that it was deposited on the continental slope in a position directly comparable to the situation in southern Taranaki Basin (c.f., Kamaruzaman et al. 2024a).

While our results support a channelform dominated continental slope setting, we cannot completely discount the potential that the packets of sandstone bodies (10 – 20 m thick) in the coastal section, which initially lead to the interpretation of basin floor fans (King et al. 1994), might also represent other sheet-like sandstone bodies of limited spatial extent that accumulated in subtle depressions on the continental slope. The dip of these strata and hence their lateral extent, precludes the mapping of these sandstone packets for more than 100 – 200 m along the section, which make it's difficult to distinguish their depositional setting between wide channels or other small-scale depressions on the slope.

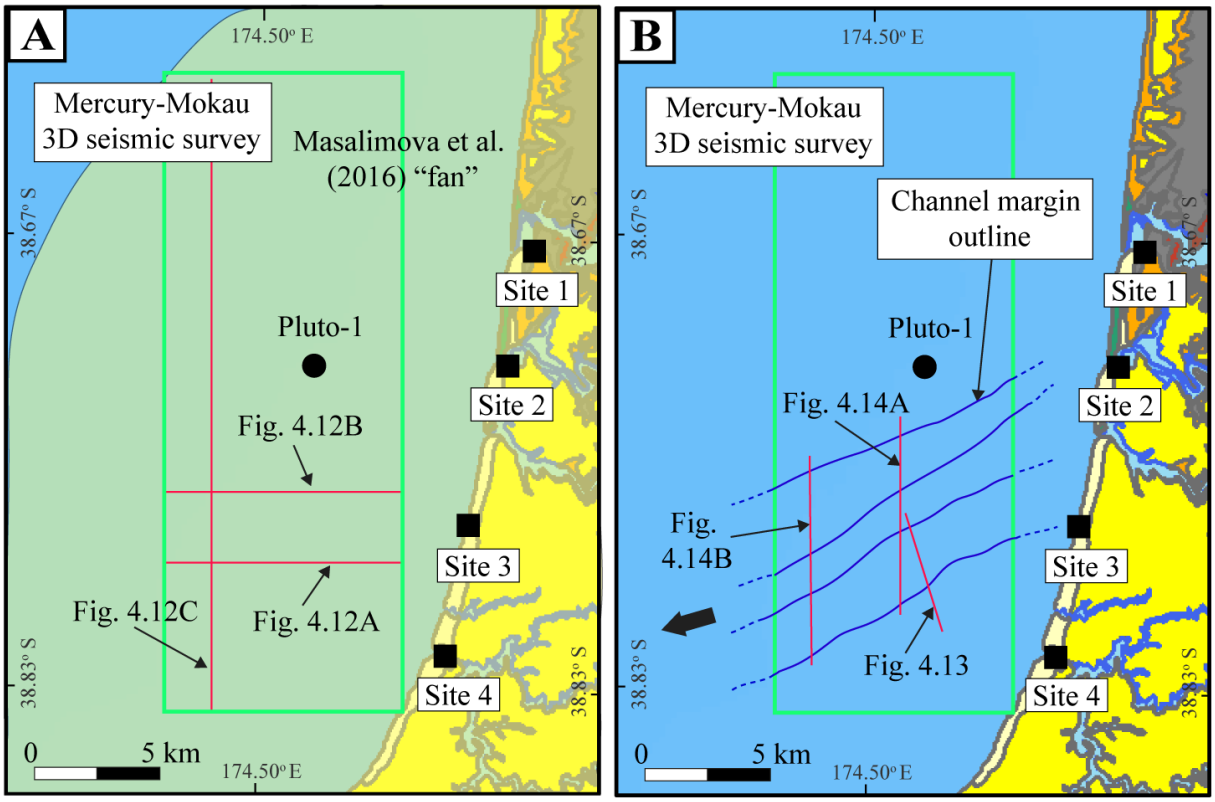

Figure 4.21: (A) Paleogeographic map of Masalimova et al. (2016), where the inferred fan (shown in green) covers the coastal outcrops (sites 1-4) and 3D seismic data offshore. (B) Paleogeographic map of this study showcases channel system outlines of a southwestward trajectory towards deep Taranaki Basin in the western part of the Taranaki Basin. The on-land extent of the Mount Messenger Formation is shown in yellow (in B) and this formation also underlies the offshore area shown in blue. In both on land and offshore areas, this formation accumulated on a continental slope. Refer to legend in Figure 4.1 for more information.

4.6.5 A Cautionary Tale for Facies Analysis of Outcrop

Based in part on observations from outcrop examples, the diagnostic features of submarine fans have been summarised into a variety of facies models (Bouma 1962; Walker 1978; Vail 1987). These models generally subdivide fan systems into feeder canyon-channels, as well as upper, middle and lower fan components based upon: (i) geometry, morphology and organization of channel complexes within fans, (ii) longitudinal facies variations, (iii) channel depth and fan thickness and (iv), seafloor slope gradient across which fans develop (Mutti & Ricci Lucchi 1978; Walker 1978; Droz & Bellaiche 1991; Weimer & Link 1991; Escutia et al. 2000; Curray et al. 2002). Each of these components of submarine fan systems, therefore, comprises a specific set of architectural elements and facies stacking patterns preserved in their stratigraphic record, which can be observed in seismic, core, or outcrop (Mutti & Normark 1987). However, owing to the similarity of processes, individual facies types may be present within more than one of the architectural elements of submarine fan systems. For example, massive sandstone facies may be formed from different flow types ranging from high-density turbidity currents (Lowe 1982) to sandy debris flows (Shanmugam 1996; Shanmugam 2000; Wang et al., 2024), which may be observed operating in several submarine-fan components (see Shanmugam 2016).

Due to the non-unique nature of any particular facies type, facies analysis in the absence of extensive 3D perspectives of the strata is problematic, as is the case for the lower Mount Messenger Formation in the North Taranaki coastal section. Although Masalimova et al. (2016) described and interpreted five facies associations, which varied from lobes and lobe complexes to channels and splays, as well as mass transport deposits, these interpretations are equivocal.

To qualify as a submarine fan, and more specifically as a basin floor submarine fan, the outcrop strata and their adjacent equivalents must display at least some of the 3D characteristics of submarine fan systems (Table 4.1), which have been chiefly developed from seismic reflection observations (e.g., Sarg & Skjold 1982; Mitchum 1985; Posamentier & Erskine 1991). These criteria are as applicable in principle to facies analysis of strata in outcrop as for strata imaged in seismic reflection analysis.

The facies analysis by Masalimova et al. (2016) gives little, if any, attention to stratal patterns to help interpret the lower Mount Messenger Formation exposed in the coastal section as having accumulated as a submarine fan. The lack of any geometrical or morphological control in their facies analysis means that it must invoke a time-for-space substitution in drawing the basin floor fan interpretation of the facies associations and complexes. This study has the advantage of access to both 2D seismic and 3D seismic reflection datasets that cover the area of the Mount Messenger fan inferred by Masalimova et al. (2016). That no fan depositional structure occurs within the seismic reflection survey area means that the time-for-space substitution is invalid. The lower Mount Messenger Formation and indeed the upper part, as included in the interpretation by Masalimova et al. (2016), must be discounted. Additionally, Masalimova et al. (2016) posited the presence of significant local confinement on the slope, attributing it to the loading by volcanic sediments that altered the seafloor, thereby purportedly creating accommodation for fan deposition. However, our seismic mapping in the study area does not show a paleo seafloor influenced by a volcanic terrain or volcaniclastic fans (Figure 4.10A and Figures i - xi in Appendix C). The only volcanic materials in the Mount Messenger Formation in the coastal section are volcanic ash beds 5 – 10 cm thick.

The Mount Messenger Formation accumulated on a continental slope dominated by channelforms. This paper is a cautionary tale about interpreting depositional environments, particularly submarine fans, based on outcrop exposures alone.

4.6.6 Significance for Reservoir Exploration

Our work has shown that Late Miocene basin floor fans are most unlikely to have been developed in the Mount Messenger Formation in the North Taranaki coastal section and immediately west of the present day coastline. Deep water submarine fans within the Mount Messenger Formation have however been mapped in deep-water western parts of Taranaki Basin (Kamaruzaman et al. 2024a), but it is unlikley at this stage that the sediment conduits on the slope in this formation in North Taranaki Basin connected to those deep water fans. Seismic reflection mapping offshore in North Taranaki Basin is complicated by the latest Miocene formation of the North Taranaki Graben.

Channel complexes are well known to be excellent hydrocarbon reservoirs (Clark & Pickering 1996; Pringle et al. 2004; Falivene et al. 2006; Atlas et al. 2023). It follows that those identified here in the Mercury-Mokau 3D seismic survey area may also be potential hydrocarbon reservoirs (Figures 4.13 - 4.14 and 4.21B). Mapping of these complexes would be greatly enhanced by reprocessing the seismic reflection data to enhance the signal and thus provide better resolution in the Mount Messenger Formation interval. One potential issue impacting the exploration potential for the Mount Messenger Formation channel complexes is the lack of closure structures to host reservoirs, which is a significant consideration given that most hydrocarbon reservoirs in Taranaki Basin are hosted within structural traps (Shell Todd

Oil Services Ltd, 1991). However, there are oil and gas fields in the Taranaki Peninsula, some of which are producing from the Mount Messenger Formation interval, such as the Ngatoro and Kaimiro fields (NZPM, 2018). Deeper oil and gas accumulations are hosted in complex stratigraphic-structural traps (Reymond et al. 2001).

The parameterization of sandstone beds within selected outcrops in this study provides a set of analogues useful for modelling submarine channel reservoirs (Pringle et al. 2004; Falivene et al. 2006; Atlas et al. 2023). For example, the measured thickness and dip direction of the bedsets in the outcrops can be used to estimate reservoir net-to-gross volumes and paleo-flow directions (e.g., Hubbard 2005; Li et al. 2016; Mayall & Kneller 2021). Secondly, the massive to wavy laminated sandstone units in the coastal section suggest that resulting reservoirs may exhibit medium to high lateral (i.e. updip and downdip) and vertical continuity (i.e. are well-connected) for porosity, permeability and fluid flow (Clark & Pickering 1996; Dam & Sønderholm 2021). Field (2005) used Miocene-aged sandstone outcrops in New Zealand to predict reservoir parameters and concluded that individual sandstone beds could have average porosity in the range of 14.5 %. Combined with the average net-to-gross of 74%, the resultant bulk porosity could be approximately 10% (Browne & Slatt 2002).

Even though the coastal outcrops show some lateral and vertical continuity locally, their aerial extent is relatively small compared with the usual well spacing in producing hydrocarbon fields, and therefore reservoir heterogeneity is expected in large-scale reservoir modelling (Miall 1988; Grammer et al. 2004). For example, the contacts between channel complexes (Figures 4.13 - 4.14) could impact reservoir connectivity (Larue & Hovadik 2006; Stright 2006).

4.7 Conclusions

In this study, we have critically assessed the long-standing depositional model that the lower Mount Messenger Formation in the North Taranaki coastal section is part of a basin floor fan and found this not to be the case. Rather, the Mount Messenger Formation in the study area comprises channel complexes on a continental slope. This study is an extension of a comparable study of the Mount Messenger Formation in southern Taranaki Basin in which it was shown that submarine fans did not exist on the continental slope there either (Kamaruzaman et al. 2024a), despite multiple prior studies that had inferred the occurrence of submarine fan accumulations.

This study differs in that the focus is on the lower Mount Messenger Formation strata exposed in coastal cliffs, from which the basin floor fan model was developed (King et al., 1993; King & Thrasher, 1996). More recently, a detailed facies analysis of the Mount Messenger Formation, based exclusively on the strata exposed in the coastal section by Masalimova et al. (2016), reached the same conclusion as those earlier studies. Critically, and because facies analysis was focused on examinations of the outcrop in the absence of holistic 3D views of the strata, a time-for-space substitution was used to derive the spatial extent and character of a basin floor fan. We refute this interpretation of the Mount Messenger Formation outcrops and put forth a cautionary tale for the use of facies analysis in the absence of spatial context. The main points that support our interpretations include:

1. Strata underlying the Late Miocene Mount Messenger Formation, including the underlying Early and Middle Miocene marine sediments accumulated on a continental slope sedimentary environment.
2. Examination of seismic reflection profiles throughout the Mercury-Mokau 3D seismic reflection survey, which is located immediately offshore of the North Taranaki coastal section, showed no objective stratal patterns for the identification and definition of submarine fans.
3. The 3D seismic dataset, however, reveals abundant channel complexes, which are well-known features of continental slope settings.
4. Photogrammetry using images from UAV drones of selected locations along the coastal section of the lower Mount Messenger Formation shows the occurrence of some channels, but they are of a lower density than those mapped in profiles of the Mercury-Mokau 3D seismic survey. This suggests that the coastal section accumulated in a more upslope position on the continental slope.
5. Abundant channels imaged in the offshore 3D seismic reflection dataset together with the absence of seismic stratal criteria for submarine fans, are internally consistent with each other. This is because channels merge into major sediment conduits, the mouth of which links to the apex of a submarine fan. If the slope wedge of the Mount Messenger Formation in North Taranaki Basin had sufficient sediment supply, a major sediment conduit might be expected to link to a submarine fan, but this would occur in deep water (lower bathyal) western Taranaki Basin, as demonstrated for sediment conduits in southern Taranaki Basin (Kamaruzaman et al. 2024a).

4.8 References

Atlas, C. E., Morris, E. A., Johnson, C. L., & Wroblewski, A. F. J., 2023. New approaches to the architectural analysis of deltaic outcrops: Implications for subsurface reservoir characterization and paleoenvironmental reconstruction. Sedimentologika, 1 (1). https://doi.org/10.57035/journals/sdk.2023.e11.1051

Bischoff, A., Planke, S., Holford, S. P., & Nicol, A. (2021). Seismic Geomorphology, Architecture and Stratigraphy of Volcanoes Buried in Sedimentary Basins. Updates in Volcanology - Transdisciplinary Nature of Volcano Science.

Bouma, A. H., Kuenen, P. H., & Shepard, F. P., 1962. Sedimentology of some Flysch deposits : a graphic approach to facies interpretation. Elsevier Pub. Co.

Browne, G. H., & Slatt, R. M., 2002. Outcrop and Behind-Outcrop Characterization of a Late Miocene Slope Fan System, Mt. Messenger Formation, New Zealand. AAPG Bulletin, 86(5), 841-862. https://doi.org/10.1306/61eedbb6-173e-11d7-8645000102c1865d

Bull, S., Nicol, A., Strogen, D., Kroeger, K., & Seebeck, H. S., 2019. Tectonic controls on Miocene sedimentation in the Southern Taranaki Basin and implications for New Zealand plate boundary deformation. Basin Research, 31 (2), 253-273. https://doi.org/10.1111/bre.12319

Clark, J. D., & Pickering, K. T., 1996. Architectural elements and growth patterns of submarine channels: Application to hydrocarbon exploration. AAPG Bulletin, 80 (2), 194-221.

Curray, J. R., Emmel, F. J., & Moore, D. G., 2002. The Bengal Fan: morphology, geometry, stratigraphy, history and processes. Marine and Petroleum Geology, 19 (10), 1191-1223. https://doi.org/10.1016/S0264-8172(03)00035-7

Dalrymple, R. W., 2010, 'Interpreting sedimentary successions: facies, facies analysis and facies models', in N. P. James & R. W. Dalrymple (ed.), Facies Models 4, Geological Association of Canada, St. John's, Newfoundland and Labrador, Canada, pp. 3-18.

Dam, G., & Sønderholm, M., 2021. Tectonostratigraphic evolution, palaeogeography and main petroleum plays of the Nuussuaq Basin: An outcrop analogue for the Cretaceous–Palaeogene rift basins offshore West Greenland. Marine and Petroleum Geology, 129, 105047. https://doi.org/10.1016/j.marpetgeo.2021.105047

Droz, L., & Bellaiche, G., 1991. Seismic Facies and Geologic Evolution of the Central Portion of the Indus Fan. In P. Weimer & M. H. Link (Eds.), Seismic Facies and Sedimentary Processes of Submarine Fans and Turbidite Systems (pp. 383-402). Springer New York. https://doi.org/10.1007/978-1-4684-8276-8_21

Edbrooke, S. W. c., 2005, Geology of the Waikato area, Institute of Geological and Nuclear Sciences Limited, Lower Hutt, New Zealand.

Escutia, C., Eittreim, S. L., Cooper, A. K., & Nelson, C. H., 2000. Morphology and Acoustic Character of the Antarctic Wilkes Land Turbidite Systems: Ice-Sheet-Sourced Versus

River-Sourced Fans. Journal of Sedimentary Research, 70 (1), 84-93. https://doi.org/10.1306/2dc40900-0e47-11d7-8643000102c1865d

Falivene, O., Arbués, P., Gardiner, A., Pickup, G., Muñoz, J. A., & Cabrera, L. s., 2006. Best practice stochastic facies modeling from a channel-fill turbidite sandstone analog (the Quarry outcrop, Eocene Ainsa basin, northeast Spain). AAPG Bulletin, 90 (7), 1003-1029. https://doi.org/10.1306/02070605112

Field, B. D., 2005. Cyclicity in turbidites of the Miocene Whakataki Formation, Castlepoint, North Island, and implications for hydrocarbon reservoir modelling. New Zealand Journal of Geology and Geophysics, 48, 135 - 146.

Fildani, A., Hubbard, S. M., Covault, J. A., Maier, K. L., Romans, B. W., Traer, M., & Rowland, J. C., 2013. Erosion at inception of deep-sea channels. Marine and Petroleum Geology, 41, 48-61. https://doi.org/10.1016/j.marpetgeo.2012.03.006

Grammer, G. M., Harris, P. M. M., & Eberli, G. P., 2004. Integration of outcrop and modern analogs in reservoir modeling: Overview with examples from the Bahamas.

Hansen, R. J., 1996. Stratigraphy, Sedimentology, and Paleomagnetism of a late Miocene Succession, Eastern Taranaki Basin Margin University of Waikato. Unpublished.

Hansen, R. J. (2005). Seismic interpretation in the North Taranaki Basin, offshore Awakino. In Sedimentary class at the University of Waikato.

Hubbard, S. M., 2005. Utilizing outcrop analogs to improve subsurface mapping of natural gas-bearing strata in the Puchkirchen Formation, Molasse Basin, Upper Austria.

Hubbard, S. M., Covault, J. A., Fildani, A., & Romans, B. W., 2014. Sediment transfer and deposition in slope channels: Deciphering the record of enigmatic deep-sea processes from outcrop. GSA Bulletin, 126 (5-6), 857-871. https://doi.org/10.1130/b30996.1

James, N. P. & Dalrymple, R. W., 2010, Facies Models IV, Geological Association of Canada, St. John's, Newfoundland and Labrador.

Kallweit, R. S., & Wood, L. C., 1982. The limits of resolution of zero-phase wavelets. Geophysics, 47 (7), 1035-1046. https://doi.org/10.1190/1.1441367

Kamaruzaman, E. H., La Croix, A. D., & Kamp, P. J. J., 2023. Quantitative seismic geomorphology of sediment conduits on an evolving Miocene slope in Taranaki Basin (New Zealand): The influence of increasing slope gradient through time. Marine and Petroleum Geology, 152, 106233. https://doi.org/https://doi.org/10.1016/j.marpetgeo.2023.106233

Kamaruzaman, E. H., La Croix, A. D., & Kamp, P. J. J., 2024a. Critical re-assessment of Middle and Late Miocene submarine fans in offshore southern and western Taranaki Basin, New Zealand, to update the paleogeography. Marine and Petroleum Geology, 161, 106664. https://doi.org/10.1016/j.marpetgeo.2023.106664

Kamaruzaman, E. H., La Croix, A. D., & Kamp, P. J. J., 2024b. Dataset of 3D computer models of Late Miocene Mount Messenger Formation outcrops in New Zealand, built with UAV drones. Data in Brief, 110035. https://doi.org/10.1016/j.dib.2024.110035

Kamp, P.J.J, Green, P., & White, S., 1989. Fission track analysis reveals character of collisional tectonics in New Zealand. Tectonics, 8, 169-195. https://doi.org/10.1029/TC008i002p00169

Kamp, P. J. J., 2019. King Country Basin: Oligocene and Miocene Structure, Stratigraphy and Depositional Systems. 2019 Conference of the Geoscience Society of New Zealand, Hamilton, New Zealand.

King, P.R., & Thrasher, G. P., 1996. Cretaceous-Cenozoic Geology and Petroleum Systems of the Taranaki Basin, New Zealand. Insitute of Geological and Nuclear Science Monograph, 13 (Part 1 and 2).

King, P. R., Browne, G. H., Malcolm, J. A., & Martin, P. C., 2007. A 2-D, Oblique-dip Outcrop Transect through a Third-order, Progradational, Deep-water Clastic Succession, Urenui–Mount Messenger Formations, New Zealand. The American Association of Petroleum Geologists (56). https://doi.org/DOI: 10.1306/12401023St563302

King, P. R., Browne, G. H., Slatt, R. M., Weimer, P., Bouma, A. H., & Perkins, B. F., 1994. Sequence Architectural of Exposed Late Miocene Basin Floor Fan and Channel-Levee Complexes (Mount Messenger Formation), Taranaki Basin, New Zealand. In Submarine Fans and Turbidite Systems—Sequence Stratigraphy, Reservoir Architecture and Production Characteristics Gulf of Mexico and International (15). SEPM Society for Sedimentary Geology. https://doi.org/10.5724/gcs.94.15.0209

King, P. R., Scott, G. H., & Robinson, P. H., 1993. Description, Correlation and Depositional History of Miocene Sediments Outcropping Along North Taranaki Coast.

Kroeger, K. F., Thrasher, G. P., & Sarma, M., 2019. The Evolution of a Middle Miocene Deep-water Sedimentary System in Northwestern New Zealand (Taranaki Basin): Depositional Controls and Mechanisms. Marine and Petroleum Geology, 101, 355-372. https://doi.org/10.1016/j.marpetgeo.2018.11.052

Lancaster, S., & Whitcombe, D., 2000. Fast-track ‘coloured’ inversion. In SEG Technical Program Expanded Abstracts 2000 (pp. 1572-1575). https://doi.org/10.1190/1.1815711

Larue, D. K., & Hovadik, J., 2006. Connectivity of channelized reservoirs: a modelling approach. Petroleum Geoscience, 12 (4), 291-308. https://doi.org/10.1144/1354-079306-699

Li, P., Kneller, B. C., Hansen, L., & Kane, I. A., 2016. The classical turbidite outcrop at San Clemente, California revisited: An example of sandy submarine channels with asymmetric facies architecture. Sedimentary Geology, 346, 1-16. https://doi.org/https://doi.org/10.1016/j.sedgeo.2016.10.001

Lowe, D. R., 1982. Sediment gravity flows; II, Depositional models with special reference to the deposits of high-density turbidity currents. Journal of Sedimentary Research, 52 (1), 279-297. https://doi.org/10.1306/212f7f31-2b24-11d7-8648000102c1865d

Loyz NZ Ventures Ltd., 2014. Mokau-Mercury-Kahu (MMK) 3D Interpretation Report, Petroleum Report Series - PR4973.

Shell BP Todd Oil Services Ltd., 1982. Well Resume Wainui-1, PPL 38049,offshore North Taranaki, New Zealand, Petroleum Report Series PR 869.

Shell Todd Oil Services Ltd, 1991, Well resume Pluto-1, PPL 38098/PPL38453, offshore North Taranaki, New Zealand, Petroleum Report Series PR 1766.

Stagpoole, V. & Nicol, A., 2008. 'Regional structure and kinematic history of a large subduction back thrust: Taranaki Fault, New Zealand', Journal of Geophysical Research: Solid Earth 113 (B1).

Masalimova, L. U., Lowe, D. R., Sharman, G. R., King, P. R., & Arnot, M. J., 2016. Outcrop characterization of a submarine channel-lobe complex: The Lower Mount Messenger Formation, Taranaki Basin, New Zealand. Marine and Petroleum Geology, 71, 360-390. https://doi.org/10.1016/j.marpetgeo.2016.01.004

Mayall, M., Jones, E., & Casey, M., 2006. Turbidite channel reservoirs—Key elements in facies prediction and effective development. Marine and Petroleum Geology, 23 (8), 821-841. https://doi.org/10.1016/j.marpetgeo.2006.08.001

Mayall, M., & Kneller, B., 2021. Seismic interpretation workflows for deep-water systems: A practical guide for the subsurface. AAPG Bulletin, 105 (11), 2127-2157. https://doi.org/10.1306/05262120094

Miall, A. D., 1988. Reservoir Heterogeneities in Fluvial Sandstones: Lessons from Outcrop Studies1. AAPG Bulletin, 72 (6), 682-697. https://doi.org/10.1306/703C8F01-1707-11D7-8645000102C1865D

Middleton, G. V., & Hampton, M. A., 1973. Part I. Sediment Gravity Flows: Mechanics of Flow and Deposition.

Mitchum, R. M., Jr., Berg, O. R., & Woolverton, D. G., 1985. Seismic Stratigraphic Expression of Submarine Fans. In Seismic Stratigraphy II: An Integrated Approach to Hydrocarbon Exploration (39). American Association of Petroleum Geologists. https://doi.org/10.1306/m39449c7

Mitchum R. M., J., Vail, P. R., & Sangree, J. B.,1977. Seismic Stratigraphy and Global Changes of Sea Level, Part 6: Stratigraphic Interpretation of Seismic Reflection Patterns in Depositional Sequences (26). (American Association of Petroleum Geologists)

Mutti, E., & Ricci-Lucchi, F., 1972. Turbidites of the northern Apennines. A.G.I. Reprint Ser., 3, 125-166. https://www.scopus.com/inward/record.uri?eid=2-s2.0-84912716413&partnerID=40&md5=21f6ea550aad24f5bc0104da731a25b6

Nodder, S. D., Nelson, C. S., & Kamp, P. J. J., 1990. Mass-emplaced siliciclastic-volcaniclastic-carbonate sediments in Middle Miocene shelf-to-slope environments at Waikawau, northern Taranaki, and some implications for Taranaki Basin development. New Zealand Journal of Geology and Geophysics, 33(4), 599-615. https://doi.org/10.1080/00288306.1990.10421378

Normark, W. R., 1978. Fan Valleys, Channels, and Depositional Lobes on Modern Submarine Fans: Characters for Recognition of Sandy Turbidite Environments.

AAPG Bulletin, 62 (6), 912-931. https://doi.org/10.1306/c1ea4f72-16c9-11d7-8645000102c1865d

Posamentier, H. W., & Erskine, R. D., 1991. Seismic Expression and Recognition Criteria of Ancient Submarine Fans. In P. Weimer & M. H. Link (Eds.), Seismic Facies and Sedimentary Processes of Submarine Fans and Turbidite Systems (pp. 197-222). Springer New York. https://doi.org/10.1007/978-1-4684-8276-8_10

Posamentier, H. W., Erskine, R. D., & Mitchum, R. M., 1991. Models for Submarine-Fan Deposition within a Sequence-Stratigraphic Framework. In P. Weimer & M. H. Link (Eds.), Seismic Facies and Sedimentary Processes of Submarine Fans and Turbidite Systems (pp. 127-136). Springer New York. https://doi.org/10.1007/978-1-4684-8276-8_6

Posamentier, H. W., Paumard, V., & Lang, S. C., 2022. Principles of seismic stratigraphy and seismic geomorphology I: Extracting geologic insights from seismic data. Earth-Science Reviews, 228. https://doi.org/10.1016/j.earscirev.2022.103963

Posamentier, H. W. & Walker, R. G. 2006, Facies Models Revisited, SEPM Society for Sedimentary Geology, Tulsa, OK.

Pringle, J. K., Westerman, A. R., Clark, J. D., Drinkwater, N. J., & Gardiner, A. R., 2004. 3D high-resolution digital models of outcrop analogue study sites to constrain reservoir model uncertainty: an example from Alport Castles, Derbyshire, UK. Petroleum Geoscience, 10 (4), 343-352. https://doi.org/10.1144/1354-079303-617

Puga-Bernabéu, Á., Vonk, A. J., Nelson, C. S., & Kamp, P. J. J., 2009. Mangarara Formation: Exhumed remnants of a middle Miocene, temperate carbonate, submarine channel-fan system on the eastern margin of Taranaki Basin, New Zealand. New Zealand Journal of Geology and Geophysics, 52 (2), 73-93. https://doi.org/10.1080/00288300909509880

Ring, U., Glodny, J., Angiboust, S., Little, T., & Lang, K. A., 2019. Middle to Late Miocene Age for the End of Amphibolite-Facies Mylonitization of the Alpine Schist, New Zealand: Implications for Onset of Transpression Across the Alpine Fault. Tectonics, 38 (12), 4335-4359. https://doi.org/https://doi.org/10.1029/2019TC005577

Rotzien, J. R., Lowe, D. R., King, P. R., & Browne, G. H., 2014. Stratigraphic architecture and evolution of a deep-water slope channel-levee and overbank apron: The Upper Miocene Upper Mount Messenger Formation, Taranaki Basin. Marine and Petroleum Geology, 52, 22-41. https://doi.org/10.1016/j.marpetgeo.2014.01.006

Sarg, J. F., & Skjold, L. J., 1982. Stratigraphic traps in Paleocene sands in the Balder area, North Sea. The Deliberate Search for the Subtle Trap, 32, 197-206. https://www.scopus.com/inward/record.uri?eid=2-s2.0-0013282272&partnerID=40&md5=6b708ac5cc42e6dc16a3dbfaf7d6849a

Shanmugam, G., 1996. High-density turbidity currents; are they sandy debris flows? Journal of Sedimentary Research, 66 (1), 2-10. https://doi.org/10.1306/d426828e-2b26-11d7-8648000102c1865d

Shanmugam, G., 2000. 50 years of the turbidite paradigm (1950s—1990s): deep-water processes and facies models - a critical perspective. Marine and Petroleum Geology, 17 (2), 285-342. https://doi.org/https://doi.org/10.1016/S0264-8172(99)00011-2

Shanmugam, G., 2016. Submarine fans: A critical retrospective (1950–2015). Journal of Palaeogeography, 5 (2), 110-184. https://doi.org/10.1016/j.jop.2015.08.011

Sharman, G. R., Graham, S. A., Masalimova, L. U., Shumaker, L. E., & King, P. R., 2015. Spatial patterns of deformation and paleoslope estimation within the marginal and central portions of a basin-floor mass-transport deposit, Taranaki Basin, New Zealand. Geosphere, 11 (2), 266-306. https://doi.org/10.1130/ges01126.1

Stagpoole, V., & Nicol, A., 2008. Regional structure and kinematic history of a large subduction back thrust: Taranaki Fault, New Zealand. Journal of Geophysical Research: Solid Earth, 113(B1).

Strachan, L. J., & Alsop, G. I. (2006). Slump folds as estimators of palaeoslope: a case study from the Fisherstreet Slump of County Clare, Ireland. Basin Research, 18 (4), 451-470. https://doi.org/https://doi.org/10.1111/j.1365-2117.2006.00302.x

Stright, L., 2014. Seismic Modelling of Deepwater Channel Elements. http://sites.warnercnr.colostate.edu/lisastright/2020/05/06/seismic-modeling-of-deepwater-channel-elements/

Strogen, D. P., Baur, J. R., Bland, K. J., King, P. R., Vonk, A. J., & Kamp, P. J. J., 2011. Updated paleogeographic maps for the Taranaki Basin and surrounds (GNS Science Report 2010/53, Issue.

Strogen, D. P., Seebeck, H., Hines, B. R., Bland, K. J., & Crampton, J. S., 2022. Palaeogeographic evolution of Zealandia: mid-Cretaceous to present. New Zealand Journal of Geology and Geophysics, 1-30. https://doi.org/10.1080/00288306.2022.2115520

Tippett, J. M., & Kamp, P. J., 1993. Fission track analysis of the late Cenozoic vertical kinematics of continental Pacific crust, South Island, New Zealand. Journal of Geophysical Research: Solid Earth, 98 (B9), 16119-16148.

Townsend, D., et al., 2008. Geology of the Taranaki area, Institute of Geological and Nuclear Sciences Limited, Lower Hutt, New Zealand.

Vail, P. R., 1987. Seismic Stratigraphy Interpretation Using Sequence Stratigraphy: Part 1: Seismic Stratigraphy Interpretation Procedure.

Walker, R. G., 1978. Deep-water sandstone facies and ancient submarine fans: Models for exploration for stratigraphic trap. AAPG Bulletin (American Association of Petroleum Geologists), 62 (6).

Walther, J., 1893-1894, Einleitung in die Geologie als historische Wissenschaft, Verlag von Gustav Fischer, Jena.

Wang, J., La Croix, A.D., Wang, H., Pang, X. and Liu, B., 2024. Flume experiments of gravity flows: Transformation from sandy debris flows to turbidity currents with clay matrix separation. Sedimentary Geology, 461: 106576. doi.org/https://doi.org/10.1016/j.sedgeo.2023.106576.

Weimer, P., 1991. Seismic Facies, Characteristics, and Variations in Channel Evolution, Mississippi Fan (Plio-Pleistocene), Gulf of Mexico. In P. Weimer & M. H. Link (Eds.), Seismic Facies and Sedimentary Processes of Submarine Fans and Turbidite Systems (pp. 323-347). Springer New York. https://doi.org/10.1007/978-1-4684-8276-8-18

Widess, M. B., 1973. How thin is a thin bed? Geophysics, 38 (6), 1176-1180. https://doi.org/10.1190/1.1440403

Chapter 5

Dataset of 3D computer models of Late Miocene Mount Messenger Formation outcrops in New Zealand, built with UAV drones[1]

5.1 Background

The aim of constructing 3D computer models of geological outcrops of the lower Mount Messenger Formation was to better understand ancient deep-water sedimentary systems in Taranaki Basin. The Late Miocene-aged sedimentary strata that outcrop along the north Taranaki coast (Figures 5.1 and 5.2) are excellent examples of deep-water sandstone and siltstone layers that are also present in offshore drill hole materials are imaged in seismic reflection data (King et al., 1993; Browne & Slatt, 2002). While previous studies (Hansen, 1996; Masalimova et al., 2016) of these outcrops mainly used photographs, this study is the first to introduce UAV drone imagery to capture their sedimentary characteristics. Incorporating drones in this study allowed a broader coverage of areas than previously possible, including areas inaccessible by foot. Therefore, geological analysis of these deep-water sedimentary systems is improved, especially when viewed from a 3D perspective. This analysis yields a more holistic understanding of the ancient sedimentary system in the region, surpassing the insights provided by earlier studies.

[1]A version of this paper has been published in Data in Brief: Kamaruzaman, E. H., La Croix, A. D., & Kamp, P. J. J. (2024). Dataset of 3D computer models of Late Miocene Mount Messenger Formation outcrops in New Zealand, built with UAV drones. Data in Brief, 110035. https://doi.org/https://doi.org/10.1016/j.dib.2024.110035. The published version is included in Appendix A-iii.

The drone images were processed in Pix4Dmapper version 4.4.12 with precise geolocation to generate the 3D computer models. Then, qualitative and quantitative stratigraphic analyses of the outcrops were carried out using ArcGIS Pro version 3.0.3 (Marques et al., 2020).

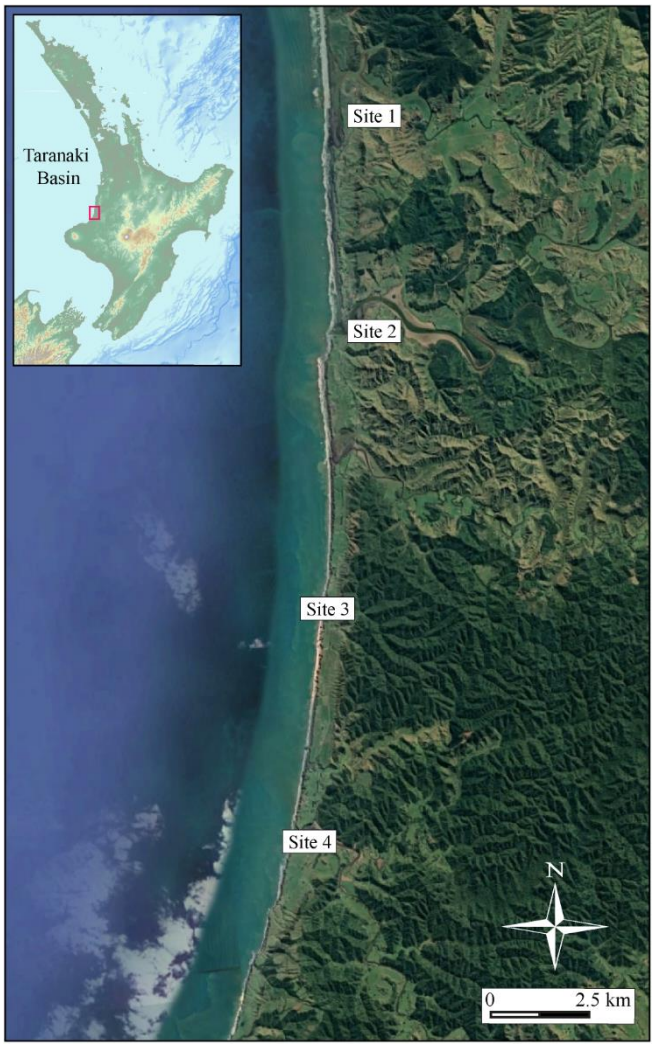

Figure 5.1: Overview map of the drone survey areas. The inset map shows the locations along the North Taranaki Coast, North Island, New Zealand (red polygon). The coordinates of the sites are shown in Figure 5.2.

5.2 Dataset description

The 3D computer models rock outcrops along the North Taranaki coast, New Zealand, were built using UAV drones to capture images of the sedimentary characteristics of the Late Miocene lower Mount Messenger Formation beds. Each 3D computer model allows the geometric analysis of sandstone and siltstone layers to be calculated, including bed thickness, bed orientation, as well as stratal stacking patterns (e.g., comfortable and erosional) and related structural deformation (e.g., faulting and folding). The present-day elevation, aerial extent, length and camera-facing direction of the outcrops are displayed in Table 5.1. The dataset are stored in a public research database: doi:10.7910/DVN/I0C6X3 (Kamaruzaman et al., 2023).

Table 5.1: Outcrop site elevation ranges and estimated length and aerial extent.

Site	Elevation range (mean sea level)	~ Length	~ Aerial extent
Site 1	145 – 210 m	900 m	0.20 km^2
Site 2	7 – 80 m	370 m	0.035 km^2
Site 3	0.5 and 22 m	800 m	0.092 km^2
Site 4	2 to 25 m	900 m	0.052 km^2

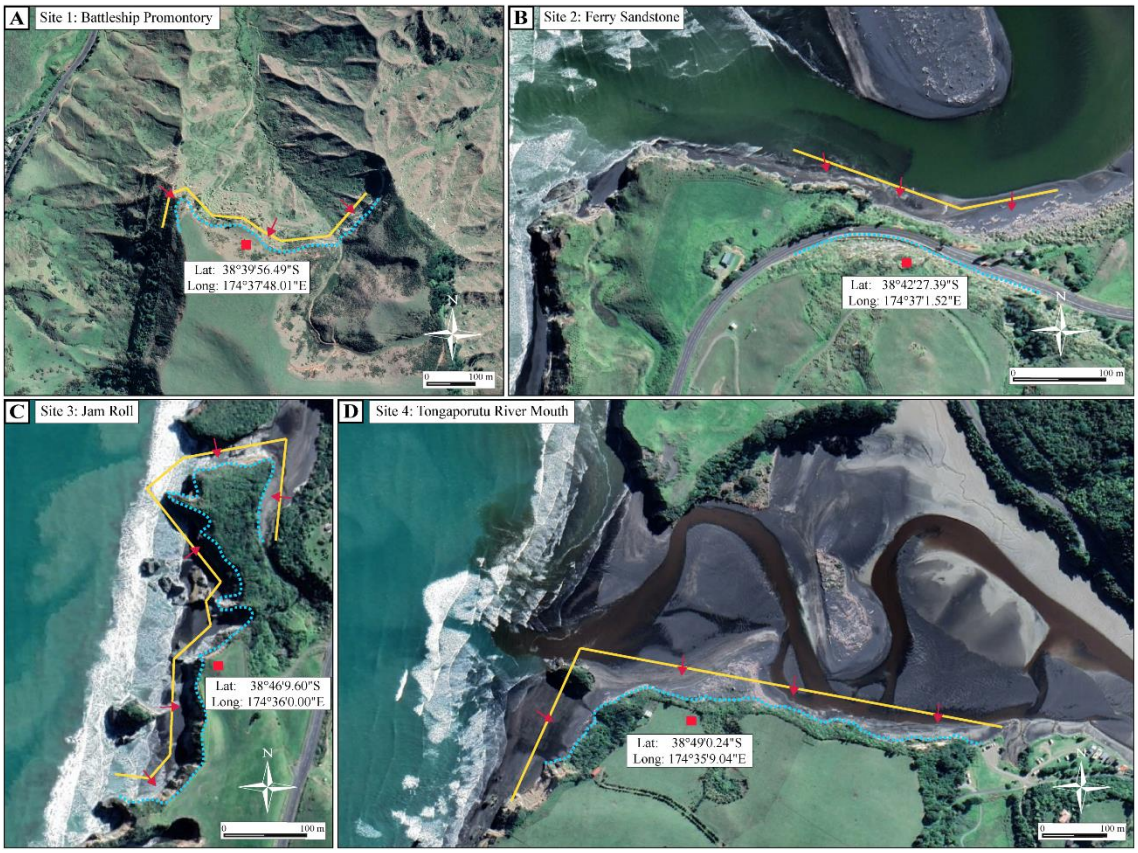

Figure 5.2: Close-up of the study areas : (A) Site 1 Battleship Promontory, (B) Site 2 Ferry Sandstone, (C) Site 3 Jam Roll and (D) Site 4 Tongaporutu River Mouth. The yellow lines are the drone flight paths, and the red arrow represents the drone camera facing direction.

Seven 3D computer models of geological outcrops are stored in ArcGIS Scene Layer Package format (i.e., Site 1 Battleship Promontory.slpk, Site 2 Ferry Sandstone.slpk, Site 3 Jam Roll Part 1.slpk, Site 3 Jam Roll Part 2.slpk, Site 4 Tongaporutu River Mouth Part 1.slpk and Site 4 Tongaporutu River Mouth Part 1.slpk). Scene layer package (.slpk) format was chosen to optimize the large file size of these 3D models. The corresponding ASCII files (.xyz format) of the computer models have the coordinates (horizontal) and elevation (vertical) information originating from the Digital Surface Model (DSM). The application of these ASCII files is extremely flexible and can be imported into many standard spatial-based software. The

resolution of the 3D models and the DSM are based on the density of the point cloud during their generation in Pix4Dmapper software, which ranged from 20 to 50 cm.

The companion ArcGIS Pro project package (.ppkx format) contains all four 3D computer models. Scientists and students, primarily geologists, can import individual models (.slpk) into their own ArcGIS Pro project, or can directly use the companion ArcGIS Pro project. The summary of the dataset is presented in Tables 5.2 and 5.3. The drone models use the WGS 84 UTM 60S coordinate reference system. When opening the ArcGIS project, users must have sufficient high-end computer capacity to display the drone models and import the ASCII files for Digital Surface Model generation.

The 3D computer models generated herein are extremely valuable as they enhance the analysis potential of large-scale geological layers, which offers more precise and detailed representations of strata compared to traditional 2D photographs and field observations. This will aid geologists, geophysicists, and engineers in gaining a better understanding of the stratigraphic and structural characteristics of formations deposited by ancient deep-water sedimentary systems. Furthermore, the data's utility extends to facilitating virtual fieldwork and field trips by researchers and students, which is advantageous for analyzing areas that are challenging to access due to high elevation, rugged terrain, or locations prone to periodic submersion during high tides. Particularly, these 3D models become invaluable in situations where travel restrictions, such as due to COVID-19, or physical constraints prevent traditional fieldwork from being undertaken.

In addition to the dataset's value for analysis and access, it is also especially important for the digital preservation of geological data and observations. The 3D computer models serve as enduring digital records of these globally significant geological outcrops, which is crucial for the Mount Messenger Formation along the west coast of the North Island of New Zealand, given their vulnerability to coastal erosion and substantial vegetation cover.

Beyond the primary users, this dataset also proves beneficial for other scientists and students engaged in sedimentology, stratigraphy, and sediment basin analysis of paleo deep-water sedimentary deposits. Researchers and industry practitioners may also find utility in this dataset for flow modeling of aquifers, petroleum reservoirs, and carbon capture and geostorage intervals. The 3D computer models function as analogs to similar reservoir systems globally, aiding in estimating flow properties such as porosity and permeability distributions.

Finally, this dataset can be used to support coastal geological and geomorphological research, offering insights into the development of coastal erosion over time. For example, outcrops at specific sites along the coast experience constant erosion from marine processes, impacting the landscape between visits. Beyond coastal studies, the dataset is versatile, applying to environmental and geotechnical analyses. The outcrop models contribute to studies of landslides, exemplified by the outcrop at a specific site adjacent to State Highway 3, an area prone to landslides and rock falls with consequential environmental, safety, and road closure implications.

Table 5.2: Specification of the 3D computer dataset

Item	Description
Subject	Earth and Planetary Sciences / Geology
Specific subject area	Construction of 3D computer model dataset based on geolocated UAV drone images of Mount Messenger Formation outcrops on coastal sections of Taranaki Basin, North Island, New Zealand.
Data format	Raw
Type of data	.slpk files (Scene Layer Packages) .xyz files (ASCII data with X,Y and Z coordinates) .ppkx files (ArcGIS Pro Project Packages)
Data collection	Approximately three thousand photographs were captured using UAV drones at four geological outcrop locations along the North Taranaki coast, North Island, New Zealand (Figures 5.1 and 5.2). Images were captured using a DJI Phantom 4 drone connected to a real-time kinetic (RTK) global positioning system (GPS) for accurate geolocation. In addition to the RTK GPS, I also used a Leica GPS system for precise ground geolocation. Drone surveys of the four sites used programmed flight paths operating on the WGS 84 coordinate reference system and EGM 96 Geoid. The focal length of the drone camera was 24 mm with a 20-megapixel resolution. The images captured outcrop at an average of 3-10 cm Ground Sampling Distance (GSD). Survey images were overlapped by 80-90%.

	Once the surveys were completed, drone images were processed using Pix4Dmapper version 4.4.12 to generate dense 3D point clouds, digital surface models (DSMs), triangle meshes, and orthomosaic images of the outcrops (i.e., 3D models). Once 3D outcrop models were built, they were exported out of Pix4Dmapper in Scene Layer Package format, and then imported into ArcGIS Pro version 3.0.3. Drone surveys were conducted on relatively fair-weather days where cloud cover was minimal and with wind speeds below 32 kilometers per hour to ensure sufficient exposure on the outcrops for good quality photographs. Permission from the Department of Conservation (New Zealand Government) and a private landowner were obtained prior to conducting the surveys. Licensed drone operators were in charge of surveys, which were flown on the 16th- 17th of June, 12th of August, and 28th-29th of October 2023.
Data source location	The location of the sites where drone surveys were conducted are as follow: Site 1 - Latitude: 38°39'56.49"S, Longitude: 174°37'48.01"E Site 2 - Latitude: 38°42'27.39"S, Longitude: 174°37'1.52"E Site 3 - Latitude: 38°46'9.60"S, Longitude: 174°36'0.00"E Site 4 - Latitude: 38°49'0.24"S, Longitude: 174°35'9.04"E These locations are situated on the west coast of New Zealand's North Island (Figures 5.1 and 5.2).
Data accessibility	Repository name: Harvard Dataverse 2023 Data identification number: https://doi.org/10.7910/DVN/I0C6X3

	Direct URL to data: 3D drone outcrop models of the Mount Messenger Formation, New Zealand - Harvard Dataverse Instructions for accessing these data: Log in to the database using your credentials and download the data.

5.3 Value of the dataset

(i) This dataset is valuable because it can be used to enhance visualization of large-scale geological layers. The 3D models provide a more precise and detailed representation of geological strata compared with photographs and hand-drawn sketches, which are historically how geological field observations have been recorded. This enhanced vizualisation helps geologists, geophysicists and engineers better understand the stratigraphic and structural characteristics of strata in outcrops that were deposited in ancient deep-water sedimentary environments.

(ii) The value of the data also lies in its capacity to facilitate virtual fieldwork or field trips. The 3D models enable researchers and students to conduct digital field analysis of the geological layers. Many sections of the lower Mount Messenger Formation outcrop are inaccessible due to their location at high elevation above ground level, occurrence in rugged and steep terrane, as well as coastal areas that may be periodically submerged during high tides. Moreover, UAV drone surveys require permission from landowners, which may limit access to field locations. The 3D models of rock outcrops are of particular use for scientists and students conducting research when travel is not

permitted (e.g., during the COVID-19 lockdown), or if they are physically unable to undertake fieldwork.

(iii) This dataset is valuable because it digitally preserves geological data and observations. The 3D computer models are digital records of the geological outcrops and preserve this for use indefinitely into the future. This is particularly important for the Mount Messenger Formation rock outcrops along the west coast of the North Island of New Zealand because they are prone to coastal erosion and significant vegetation cover.

(iv) This dataset can be used by other scientists and students for research and education relating to sedimentology, stratigraphy, and sediment basin analysis of paleo deep-water sedimentary deposits.

(v) This dataset can be used by researchers and industry practitioners for flow modelling of aquifers, petroleum reservoirs, and carbon capture and geostorage intervals. The 3D computer models are analogues to other reservoir systems globally that were deposited by deep-water sedimentary systems and can be used to estimate flow properties such as porosity and permeability distributions.

(vi) This dataset can be used for coastal geological and geomorphological research. The models will help me understand how coastal erosion develops over time. For instance, outcrops at Sites 3 and 4 are situated along the coast and are subject to constant erosion from marine processes (Figure 5.2C and D). Throughout my multiple visits to the sites to conduct drone surveys, I noticed parts of the outcrops had collapsed and eroded

between visits. Apart from coastal studies, this dataset can be used by other researchers for environmental and geotechnical analysis. The outcrop models can assist researchers in studies of landslides. For example, the outcrop at Site 2 (Figure 5.2B) is adjacent to State Highway 3 (i.e., Mokau Road). Landslides and rock falls are common in this area and cause serious environmental and safety issues and road closures.

Table 5.3: Description of the dataset

Item	Description
3D computer models – scene layer packages	
1. Site 1 Battleship Promontory Close up.slpk	3D computer model of Site 1 – close up view
2. Site 1 Battleship Promontory Overview.slpk	3D model of Site 1 - overview
3.Site 2 Ferry Sandstone.slpk	3D model of Site 2
4.Site 3 Jam Roll part 1.slpk	3D model of Site 3 - first part
5. Site 3 Jam Roll part 2.slpk	3D model of Site 3 - second part
6. Site 4 Tongaporutu River Mouth part 1.slpk	3D model of Site 4 - first part
7. Site 4 Tongaporutu River Mouth part 2.slpk	3D model of Site 4 - second part
Digital Surface Model (DSM) – ASCII xyz	
1. Site 1 Battleship Promontory Close up_i.xyz	DSM for Site 1 - close up view part 1
2. Site 1 Battleship Promontory Close up_ii.xyz	DSM for Site 1 - close up view part 2
3. Site 1 Battleship Promontory Overview.xyz	DSM for Site 1 - overview
4. Site 2 Ferry Sandstone.xyz	DSM for Site 2
5. Site 3 Jam Roll part 1_i.xyz	DSM for Site 3 - part 1
6. Site 3 Jam Roll part 1_ii.xyz	DSM for Site 3 - part 1 continue
7. Site 3 Jam Roll part 2.xyz	DSM for Site 3 - part 2
8. Site 4 Tongaporutu River Mouth part 1_i.xyz	DSM for Site 4 – part 1
9. Site 4 Tongaporutu River Mouth part 1_ii.xyz	DSM for Site 4 - part 1 continue
10.Site 4 Tongaporutu River Mouth part 2.xyz	DSM for Site 4 - part 2
ArcGIS Pro (version 3.0.3) project packages	
1. Sites 1 and 2 3D computer models	ArcGIS Pro project of the 3D computer model for Sites 1 and 2
2. Sites 3 and 4 3D computer models	ArcGIS Pro project of the 3D computer model for Sites 3 and 4

5.4 Experimental design, materials and methods

The acquisition of the dataset was divided into three stages:

(i) Planning:

Planning the drone surveys involved a pre-survey reconnaissance trip to the outcrop sites to assess the feasibility of conducting drone survey operations at the proposed locations. The reconnaissance was carried out in April 2023. Once the drone survey operations were deemed feasible, the drone survey routes and specific locations were planned and necessary permissions from the Department of Conservation, the New Zealand Government, and a private landowner were sought. Once permissions were granted, drone operations were scheduled to account for weather, daylight, and tidal conditions at coastal locations (Sites 3 and 4; Figure 5.1).

(ii) Drone survey:

Drone surveys were conducted on the 16th and 17th of June, 12th of August, and 28th and 29th of October 2023. Drone images were captured using programmed flight paths operating on the WGS 84 UTM coordinate reference system and EGM 96 Geoid. RTK and Leica GPS systems were linked to the drone for precise geolocation. The GPS accuracy ranged from 10 to 30 cm. The flight paths were planned to front-face the outcrops, and the distance from the outcrops at Sites 1, 3 and 4 was kept in the range of approximately 3-7 m. However, the drone distance from the outcrop at Site 2 (Figure 5.2B) was kept at approximately 15-20 m due to proximity to the road. Due to access permissions, at Site 3, the drone was not allowed to fly over the outcrops, except along

the beach section (Figure 5.2C). The focal length of the drone camera is 24 mm and images have 20-megapixel resolution. Survey images overlap by 80-90%. Drone survey operations were conducted per the rules and regulations of the Aviation Security Service, New Zealand, and the University of Waikato.

(iii) 3D outcrop model construction

Approximately three thousand drone images (in jpeg format) were captured during drone surveys. Quality checks of the images ensured that they adequately captured the areas of interest. Minimum preprocessing of images was undertaken, such as colour correction and contrast enhancement. However, 95% of the drone images did not require preprocessing.

The 3D outcrop drone models were constructed in Pix4Dmapper (version 4.4.12) (Figure 5.3). At each outcrop site, the software was used to generate dense 3D point clouds, digital surface models (DSMs), digital terrain models (DTMs), triangle meshes, and orthomosaic images of the outcrops (i.e., 3D models). Constructing individual 3D models took roughly 3-5 hours to complete. Once the 3D outcrop models were constructed, they were exported out of Pix4Dmapper in ArcGIS Pro (version 3.0.3) Scene Layer Package format (.slpk) and loaded into ArcGIS Pro for further geological analysis. An example of the 3D outcrop model is shown in Figure 5.4. Accordingly, the corresponding Digital Surface Models are exported to ASCII (.xyz format).

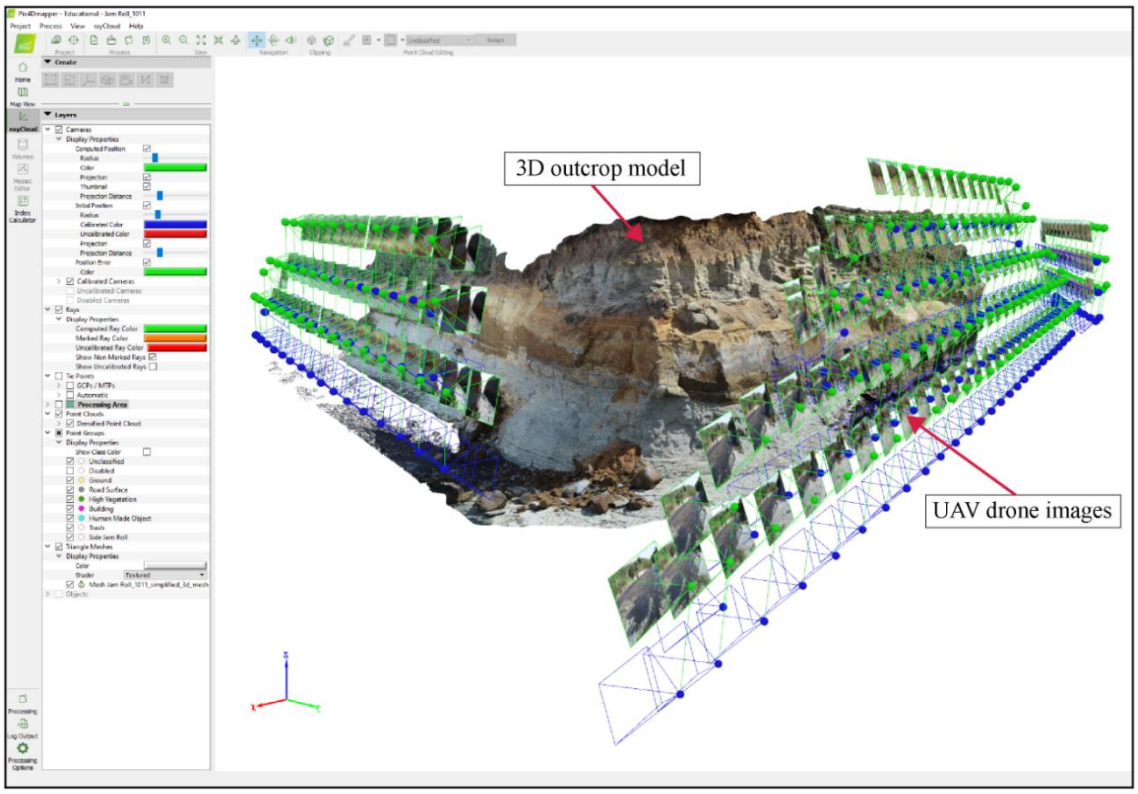

Figure 5.3: Outcrop 3D computer model generation in Pix4Dmapper. The geolocated UAV drone images are >80% overlapped to create dense point cloud to generate the outcrop model.

Figure 5.4: An example of the 3D outcrop model for a part of Site 3: Jam Roll section.

5.5 Limitations

Limitations of 3D computer models built using UAV drone imagery are primarily a function of drone image resolution and their associated models (which in this case ranges from 20 to 50 cm), based on the density of point clouds at certain locations within the models. The GPS accuracy recorded in the field ranged from 10 to 30 cm.

Weather conditions were another limiting factor, especially in terms of adequate sun exposure to capture clear imagery. For example, small parts of the outcrop were not illuminated by the sun to a satisfactory level. However, this did not hinder my objective to conduct geological analysis because the sandstone beds are relatively easy to identify, even under low lighting. Other limitations for drone images resulted from them being captured on different days and times of day, leaving sun-exposure intensity sometimes inconsistent.

5.6 References

Browne, G. H., & Slatt, R. M. (2002). Outcrop and Behind-Outcrop Characterization of a Late Miocene Slope Fan System, Mt. Messenger Formation, New Zealand. *AAPG Bulletin*, *86*(5), 841-862. https://doi.org/10.1306/61eedbb6-173e-11d7-8645000102c1865d

Hansen, R. J. (1996). Stratigraphy, Sedimentology, and Paleomagnetism of a late Miocene Succession, Eastern Taranaki Basin Margin, unpublished MSc. thesis, Department of Earth and Ocean Sciences (Unpublished master's thesis). University of Waikato, New Zealand.

Kamaruzaman, E., La Croix, A., & Kamp, P. J. J. (2023). *3D drone outcrop models of the Mount Messenger Formation, New Zealand* Version V1) Harvard Dataverse. https://doi.org/doi:10.7910/DVN/I0C6X3

King, P. R., Scott, G. H., & Robinson, P. H. (1993). *Description, Correlation and Depositional History of Miocene Sediments Outcropping Along North Taranaki Coast*.

Marques, A., Horota, R. K., de Souza, E. M., Kupssinskü, L., Rossa, P., Aires, A. S., Bachi, L., Veronez, M. R., Gonzaga, L., & Cazarin, C. L. (2020). Virtual and digital outcrops in the petroleum industry: A systematic review. *Earth-Science Reviews*, *208*. https://doi.org/10.1016/j.earscirev.2020.103260

Masalimova, L. U., Lowe, D. R., Sharman, G. R., King, P. R., & Arnot, M. J. (2016). Outcrop characterization of a submarine channel-lobe complex: The Lower Mount Messenger Formation, Taranaki Basin, New Zealand. *Marine and Petroleum Geology*, *71*, 360-390. https://doi.org/10.1016/j.marpetgeo.2016.01.004

Chapter 6

Conclusions

The studies compiled in this thesis reveal new insights into the Miocene deep-water sedimentary systems of Taranaki Basin that leveraged new seismic data, employed the most up-to-date tools and methods of analysis, and integrated these findings using state-of-the-art software. In particular, the research contained herein provided a quantitative parameterization of channelforms in the southern portion of the basin, put forth new paleogeographic conceptualizations of the south and western parts of Taranaki Basin, and integrated offshore seismic data with observations from outcrop to challenge current interpretations of the environments of deposition. Below, I briefly comment about each of these scientific contributions to highlight the novelty of the major outcomes.

As indicated at the start of each main chapter, three out of the four chapters of the study have been published in peer-reviewed international journals. The corresponding publications are attached to this thesis and can be found in Appendices A.

6.1 Quantification of submarine sediment conduits on an evolving Miocene slope

Chapter 2 provided new understanding about the morphometric evolution of submarine sediment conduits (i.e., canyons, channels, and gully networks) on the Miocene continental slope in southern and central parts of Taranaki Basin. The study undertook a comprehensive

quantitative examination of the morphology of the main sediment conduits (i.e. canyon, channel, and gully networks) within the Moki and Mount Messenger formation intervals situated on the Miocene (continental) slope.

The major outcome of this paper was demonstration how the development of complex sediment conduit networks in the upper Moki Formation (~16-13 Ma) are similar to the characteristics of basin floor sinuous channels, having high sinuosity and meander amplitude. As the Miocene slope prograded basinward (i.e. to the northwest), the occurrence of numerous canyon networks in the lower Mount Messenger Formation (~13-9 Ma) was clearly influenced by the depositional dynamics of the slope. Specifically, the clinoform toe line served as a key marker, indicating a rapid transformation in cross-sectional area, shape, and spatial arrangement of canyons. Later in time, during the upper Mount Messenger Formation (9-7.2 Ma), linear gully networks developed within an otherwise mudstone-dominated interval, which were influenced by the steep prograding clinoform slope.

6.2 Evaluation and revision of Taranaki Basin paleogeography during the Miocene

Chapter 3 built upon the findings presented in Chapter 2, extending the understanding of sediment delivery systems in the Moki and Mount Messenger formations to deep Taranaki Basin. The study critically assessed the occurrence of previously published Miocene submarine fans in the southern and west-central parts of the basin, particularly those inferred to occur on the continental slope region. By employing the latest detuning methods on 3D seismic data and

applying seismic stratal criteria from the literature to search for and identify ancient submarine fans, previously inferred fans on the paleo-continental slope were dismissed.

The second part of the study showed that two newly identified submarine fan systems in the Mount Messenger Formation occur in the deeper part of Taranaki Basin (i.e. western Taranaki Basin). One of these fans is of late-Middle Miocene age (~12 Ma) and the other is of Late Miocene age (~6 Ma). These fans in the deep basin are the manifestation of an increase in terrigenous sediment supply at ~12 Ma, sourced from uplift and erosion of the Southern Alps, resulting in rapid progradation of the Late Middle to Late Miocene continental slope in Taranaki Basin (Kamp et al., 1989; Tippett & Kamp, 1993; Ring et al., 2019). Most sediment rapidly accumulated on the slope. Consequently, its angle increased and gullies became prolific, incising, infilling, re-incising and being buried. A few coalesced channels are mapped on the lower slope passing into a fan on the basin plain. A second fan with similar attributes and ~7–6 Ma age accumulated above the first, extending farther towards the New Caledonia Basin.

6.3 Assessment of the offshore-seismic to outcrop linkage study for the coastal section in north Taranaki Basin

Chapter 4 challenges the widely accepted model of the occurrence of basin floor fans in lower Mount Messenger Formation, outcrops exposed in sea cliffs along the North Taranaki coast. The study involves building upon the findings in Chapter 3, which found that submarine fans were absent in the Mount Messenger Formation on the prograding continental slope in

southern Taranaki Basin (Kamaruzaman et al. 2024a). The methodology employed in Chapter 4 diverged from previous approaches (e.g., King et al., 1993; Hansen, 1996; Browne & Slatt, 2002), which primarily centred on facies analysis. In particular, we focussed upon a recent comprehensive facies analysis undertaken by Masalimova et al. (2016), which utilized the concept of space-for-time substitution to derive a basin floor fan model for the lower Mount Messenger Formation exposed in the North Taranaki coastal section. Instead, standard published stratal criteria for identifying ancient fan systems in seismic data were applied to the Mercury-Mokau 3D seismic volume, a dataset situated immediately offshore and down-dip from the coastal section. We applied the stratal criteria of Posamentier & Erskine (1991) in our assessment of the reality, or otherwise, of the occurrence of basin floor fans in the lower Mount Messenger Formation. In addition, UAV drone surveys were conducted to capture 3D visualizations of strata in outcrop to compare channel features with those expressed in the offshore seismic data.

Contrary to expectations, the seismic data did not show any evidence of the presence of submarine fans. Instead, the seismic reflections illustrated a prevalence of channel systems incising a slope succession, a pattern analogous to that observed in southern Taranaki Basin. These interpretations were supported by 3D computer models built using UAV drones that captured the juxtaposition of different facies and erosive channel bases in some outcrops. Ultimately, the new interpretations were captured in a new paleogeographic conceptualization of North Taranaki Basin.

6.4 3D computer models of outcrops

Chapter 5 describes in detail the acquisition of UAV drone images and the construction of 3D computer models of the Late Miocene lower Mount Messenger Formation on the North Taranaki coast. Using the newest technology (i.e., DJI Phantom 4 with RTK GPS) large areas of the outcrops were studied. The 3D models were constructed using the latest industry and academic standard software (i.e., Pix4Dmapper v 4.4.12 and ArcGIS Pro v 3.0.3), which provided precise geoprocessing tools for visualisation and geometrical analysis. The dataset is stored in commonly used spatial formats (ArcGIS .slpk) and ASCII plain text (.xyz for Digital Surface Model generation), and uploaded into a public research database (i.e. Harvard Dataverse) for public access. The models give a 3D perspective of continental slope sedimentary successions, serving as a valuable resource for virtual fieldwork and teaching fundamental geological concepts, including sedimentology and stratigraphy. Additionally, the dataset is made available for use by other researchers with diverse interests ranging from reservoir analysis to coastal erosion and landslide modelling.

6.5 Relevant Application and Direction of Future Research

The papers contained within this thesis put forward new ideas about the depositional processes and paleogeography of the Miocene-age Moki and Mount Messenger formations in Taranaki Basin, New Zealand. These studies are the first to emphasise the distinction between proximal (continental) prograding slope and distal deep-water basin sedimentation in the Miocene of Taranaki Basin. Previously, fan systems were mapped on the Miocene continental

slope margin, but this mapping was primarily based on analysis of borehole data (e.g., Strogen et al., 2011). In contrast, this thesis reveals that Miocene fan systems developed much farther offshore in deep water (western part of Taranaki Basin), with sediment routing following the main axis of the basin at the time. While the continental slope is capable of trapping a significant volume of coarse sediments through processes such as debris flows and turbidity currents, this research highlights the complexity of sedimentary systems on the continental slope and underscores the importance of thorough integration and analysis of seismic and borehole data to obtain robust interpretations (Mayall & Kneller, 2021; Posamentier et al., 2022).

From an energy exploration perspective, the new paleogeographic maps in this thesis can be used to update and improve exploration prospecting and strategies. I suggest that future efforts should focus on better understanding deep Taranaki Basin in the west, which is largely unexplored with only one drill hole (i.e. Romney-1) compared to the ~700 drill holes situated in the shallow-water and onshore areas of Taranaki Basin (NZP&M, 2018). Submarine fan plays are well known to be prolific with more than 80 sedimentary basins worldwide producing from various structural, stratigraphic, or combined traps (Weimer & Link, 1991).

This research highlights the fact that future research on Taranaki Basin should focus on better understanding the paleogeography of the Miocene interval, which could be enhanced by acquiring and/or analysing additional seismic and borehole data. For example, the 2013 NMTC-SLB Multiclient seismic data in North Taranaki Basin has not yet been released to the public (Figure 1.1) (NZP&M, 2018). This seismic volume covers an area of 4151 km^2 across

the Miocene slope region, and thus has significant potential benefit for the identification of large-scale deep-water sedimentary systems.

Other future research efforts could focus on improving and expanding upon 3D outcrop model data for the Late Miocene lower Mount Messenger Formation along the North Taranaki coastal section for facies analysis of exposed slope strata. UAV drones equipped with high-definition cameras are recommended for such work. Ideally, these cameras should be able to resolve small-scale features and bed thicknesses below 30 cm to increase the density of point clouds in 3D model generation. This enhancement would contribute to a more detailed facies analysis of slope strata and identification of the processes involved in their accumulation.

6.6 References

Kamp, P., Green, P., & White, S. (1989). Fission track analysis reveals character of collisional tectonics in New Zealand. *Tectonics*, *8*, 169-195. https://doi.org/10.1029/TC008i002p00169

Kroeger, K. F., Thrasher, G. P., & Sarma, M. (2019). The Evolution of a Middle Miocene Deep-water Sedimentary System in Northwestern New Zealand (Taranaki Basin): Depositional Controls and Mechanisms. *Marine and Petroleum Geology*, *101*, 355-372. https://doi.org/10.1016/j.marpetgeo.2018.11.052

Mayall, M., & Kneller, B. (2021). Seismic interpretation workflows for deep-water systems: A practical guide for the subsurface. *AAPG Bulletin*, *105*(11), 2127-2157. https://doi.org/10.1306/05262120094

NZP&M. (2018). *New Zealand Petroleum Exploration Data Pack,* New Zealand Petroleum and Minerals.

Posamentier, H. W., Paumard, V., & Lang, S. C. (2022). Principles of seismic stratigraphy and seismic geomorphology I: Extracting geologic insights from seismic data. *Earth-Science Reviews*, *228*. https://doi.org/10.1016/j.earscirev.2022.103963

Ring, U., Glodny, J., Angiboust, S., Little, T., & Lang, K. A. (2019). Middle to Late Miocene Age for the End of Amphibolite-Facies Mylonitization of the Alpine Schist, New Zealand: Implications for Onset of Transpression Across the Alpine Fault. *Tectonics*, *38*(12), 4335-4359. https://doi.org/https://doi.org/10.1029/2019TC005577

Strogen, D. P., Baur, J. R., Bland, K. J., King, P. R., Vonk, A. J., & Kamp, P. J. J. (2011). *Updated paleogeographic maps for the Taranaki Basin and surrounds* (GNS Science Report 2010/53, Issue.

Tippett, J. M., & Kamp, P. J. J. (1993). Fission track analysis of the late Cenozoic vertical kinematics of continental Pacific crust, South Island, New Zealand. *Journal of Geophysical Research: Solid Earth*, *98*(B9), 16119-16148.

Weimer, P., & Link, M. H. (1991). Global Petroleum Occurrences in Submarine Fans and Turbidite Systems. In P. Weimer & M. H. Link (Eds.), *Seismic Facies and Sedimentary Processes of Submarine Fans and Turbidite Systems* (pp. 9-67). Springer New York. https://doi.org/10.1007/978-1-4684-8276-8_2

Appendix A

Appendix A consists of the three published papers derived from this thesis research:

i. Paper from Chapter 2
Kamaruzaman, E. H., La Croix, A. D., & Kamp, P. J. J. (2023). Quantitative seismic geomorphology of sediment conduits on an evolving Miocene slope in Taranaki Basin (New Zealand): The influence of increasing slope gradient through time. Marine and Petroleum Geology, 152, 106233. https://doi.org/https://doi.org/10.1016/j.marpetgeo.2023.106233

ii. Paper from Chapter 3
Kamaruzaman, E. H., La Croix, A. D., & Kamp, P. J. J. (2024). Critical re-assessment of Middle and Late Miocene submarine fans in offshore southern and western Taranaki Basin, New Zealand, to update the paleogeography. Marine and Petroleum Geology, 161, 106664. https://doi.org/https://doi.org/10.1016/j.marpetgeo.2023.106664

iii. Paper from Chapter 5
Kamaruzaman, E. H., La Croix, A. D., & Kamp, P. J. J. (2024). Dataset of 3D computer models of Late Miocene Mount Messenger Formation outcrops in New Zealand, built with UAV drones. Data in Brief, 110035. https://doi.org/https://doi.org/10.1016/j.dib.2024.110035

Marine and Petroleum Geology 152 (2023) 106233

Contents lists available at ScienceDirect

Marine and Petroleum Geology

journal homepage: www.elsevier.com/locate/marpetgeo

Quantitative seismic geomorphology of sediment conduits on an evolving Miocene slope in Taranaki Basin (New Zealand): The influence of increasing slope gradient through time

Erman H. Kamaruzaman *, Andrew D. La Croix, Peter J.J. Kamp

Sedimentary Environments and Analogues Research Group, Earth and Environmental Sciences, School of Science, University of Waikato, Private Bag 3105, Hamilton, 3240, New Zealand

ARTICLE INFO

Keywords:
Seismic geomorphology
Submarine canyons
Progradational slope systems
Miocene
New Zealand
Moki Formation
Mount Messenger Formation
Taranaki Basin
Submarine channels and gullies

ABSTRACT

Submarine canyons, channels and gullies are conduits that transport sediments across shelf-slope margins to deep water. In South Taranaki Basin, an increase in sediment supply through the Miocene resulted in progradation and significant steepening of the slope system. Previous studies have identified numerous sediment conduits developed within this system, however their morphology and morphometric relationships with the depositional slope have not been considered. Here we apply seismic geomorphology to establish the statistical relationships between the metrics of sediment conduits at three stratigraphic intervals between which the slope gradient progressively increased. In the early-Middle Miocene, sinuous upper Moki Formation channel complexes with an average width of 1.1 km developed on a slope with an average gradient of 0.2°, routing sediment from south to north. By the late-Middle Miocene, the slope began to prograde rapidly, concurrent with a regional reorientation of the slope to the northwest, on which the lower Mount Messenger Formation canyon networks developed with a slope gradient of 0.4–1.0°. At shallow slopes of less than 0.5°, canyon morphometrics (mean width 6.6 km) are 1.8–4.7 times larger than on related upper slopes with gradients steeper than 0.5° (mean canyon width of 2.7 km). This significant shift in morphometrics occurs abruptly across the clinoform toe line. Rapid Late Miocene slope progradation resulted in the development of steep clinoform slope surfaces up to 9°, into which linear upper Mount Messenger Formation gully complexes incised. The mean gully width throughout the Middle to Late Miocene interval decreased from 1.3 km to 1.0 km as the slope gradient became steeper. This study documents how the morphology and morphometrics of sediment conduits on the South Taranaki Basin slope system changed through time in relation to changes in depositional slope gradients.

1. Introduction

Submarine canyons, channels and gullies are integral sediment conduits as parts of larger source-to-sink sedimentary systems (Allen, 2017). These systems are globally significant features at continental margins through which sediment, organic carbon, nutrients and pollutants are transported from shallow water to deep-sea environments (Field et al., 1999; Weimer and Slatt, 2004; Covault, 2011; Hughes et al., 2015; Kane et al., 2020). In the foreland Taranaki Basin, located inboard of the Australia-Pacific plate boundary (the Hikurangi subduction zone) (Fig. 1), prior studies have documented a Miocene progradational slope margin (Bull et al., 2019) and sediment conduits across part of the paleo-shelf, and in particular the related slope (Strogen et al., 2011; Kroeger et al., 2019). These submarine canyons and channels have not hitherto been quantitatively parameterised and their morphometric relationship with the prograding slope is yet to be established. The availability of high-resolution 3D seismic reflection data for the part of the basin where many of these conduits occur, enables such a study to be undertaken, in particular determination of the relationship between submarine canyon and channel geomorphology in relation to increasing slope gradient through time.

High-resolution 3D seismic reflection data allows morphometric attributes of submarine canyons, channels and gullies to be quantitatively characterised (i.e., using seismic geomorphology; Posamentier et al., 2022), including cross-sectional (width, depth and cross-sectional area) and planform (sinuosity, meander length and meander amplitude)

* Corresponding author.
E-mail address: ek100@students.waikato.ac.nz (E.H. Kamaruzaman).

https://doi.org/10.1016/j.marpetgeo.2023.106233
Received 19 December 2022; Received in revised form 12 February 2023; Accepted 19 March 2023
Available online 30 March 2023

characteristics (Peakall et al., 2000; Deptuck et al., 2007; Gamboa et al., 2012; Qin et al., 2016; Harishidayat et al., 2018). These types of quantitative insights lead to a better understanding of sedimentary processes within slope and deep-water systems, the evolution of sediment conduits, and factors that influence their physical characteristics. However, quantitative characterization is not always straightforward and there are challenges to morphologic interpretations using 3D seismic reflection data. The challenges include resolution limits of seismic data and variations within submarine canyons, channels and gullies due to the effects of internal (e.g., erosion within channel complexes) and external (e.g., post-depositional faulting) factors (Gamboa et al., 2012; Qin et al., 2016; Posamentier et al., 2022). Nevertheless, it is possible to document variability in the geomorphology of canyons, channels and gullies, and to link the resulting geomorphology to sediment transport across the shelf-slope system and into the deep-sea realm.

Most previous studies undertaking geomorphological analysis of submarine canyons, channels and gullies have investigated modern-day or Quaternary systems (Shumaker et al., 2018; Palm et al., 2021; Bührig et al., 2022), and there are comparatively fewer studies documenting the morphometrics of pre-Quaternary systems. In order to fill this research gap on ancient deep-water canyons, channels and gullies, this study focuses on undertaking seismic geomorphological analysis of Miocene-age examples from Taranaki Basin, New Zealand. The aim of this research is to gain insights into the sediment pathways that filled Taranaki Basin by understanding the morphometrics, evolution and distribution of canyon, channel and gully networks on the prograding slope margin as it steepened through the Miocene. In addition to understanding ancient sedimentary processes, the outcomes of this study provide numerical data that can be used for exploration and modelling of large-scale petroleum reservoirs typical of deep-water systems (Hewlett et al., 1993; Weimer and Slatt, 2004; Mayall and Kneller, 2021) or reservoirs for CO_2 and H_2 geostorage (Benson and Cook, 2005; Heinemann et al., 2018; Raza et al., 2018).

1.1. Classification of sediment conduits in the study area

No standardized criteria currently exist to differentiate between submarine canyons, channels and gullies, although the names imply there are scale differences between the different sets of terminology (Deptuck et al., 2007; Wynn et al., 2007; Shanmugam, 2016). The choice

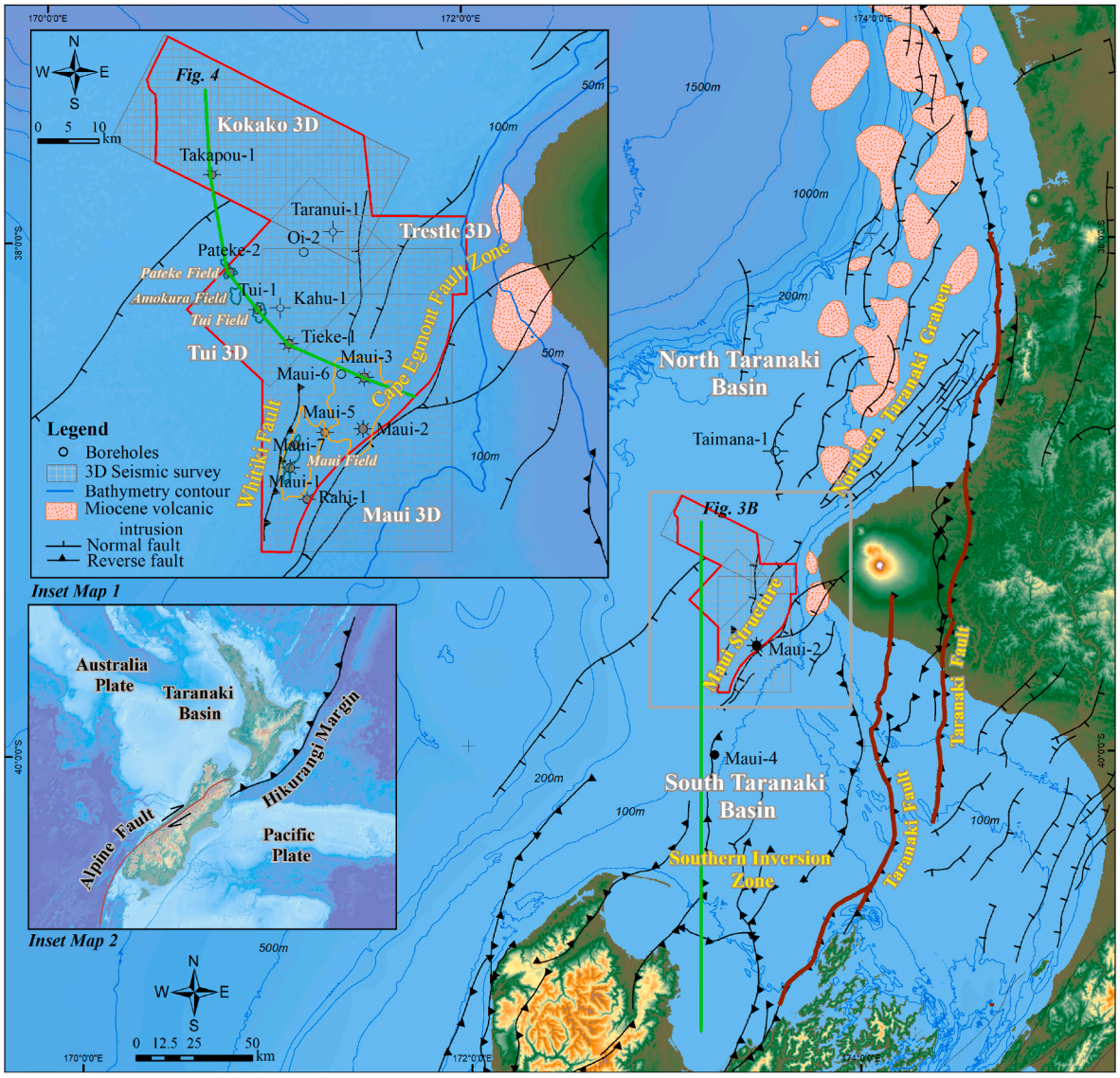

Fig. 1. Map of Taranaki Basin located west of North Island, New Zealand, showing its main structural features. Inset Map 1 shows the outlines of the seismic 3D volumes and boreholes used in this study. The study area is marked by the red polygon bounded by the Cape Egmont Fault Zone on the eastern side. Inset Map 2 shows the boundary between the Pacific and Australia plates (Alpine Fault and Hikurangi Margin). GIS data from NZP&M (2018).

of lexicon has depended on the context of past studies (e.g., stratigraphy, sedimentological processes, basin analysis or geomorphology), and has included a wide variety of terms such as "canyon" (Harris and Whiteway, 2011; Huvenne and Davies, 2014), "valley" (Shepard, 1965; Normark et al., 1993), "canyon-channel" (Covault, 2011), "master channel" (Baur et al., 2010) and "gullies" (Shumaker et al., 2017). These differences in terminology have hindered accurate and repeatable communication of results between studies. In this context, we simplify the description of channel-form features in our study area into three main classes: 1) submarine canyons, 2) submarine channels and 3) submarine gullies.

Submarine canyons are erosive features typically exhibiting a V-shape due to deep incision and they have limited development of external levees with heads located near the shoreline or on the shelf (Shepard, 1965; Normark et al., 1993; Wynn et al., 2007). By contrast, submarine channels are predominantly U-shape and can be either aggradational or erosional (Deptuck et al., 2007; Qin et al., 2016), and they display a wide range of flow behaviour (Peakall and Sumner, 2015). Herein we adopt the classification of canyons and channels used by Lemay et al. (2020). In this system, canyons do not have external levees whereas channels may or may not have levees (Fig. 2A). Canyons can contain channels within their walls and most often, channels are smaller than canyons, although not exclusively (Lemay et al., 2020). In addition to differentiating channels from canyons, we adapt the channel body hierarchy system employed in Mayall and Kneller (2021) to describe the internal characteristics of stacked channels within canyons (Fig. 2B). The hierarchical structure consists of channel systems (1–3 km wide and 100–250 m thick), channel complexes (0.5–1.5 km wide and 20–50 m thick) and channel elements (0.05–0.1 km wide and 5–20 m thick). Lastly, submarine gullies are straight, parallel, regularly spaced channel-forms, commonly found on continental slopes with steep topography, especially on prograding or aggrading margins and they are an order of magnitude smaller than submarine canyons (Field et al., 1999; Amblas et al., 2018). The term Gully Complex refers to nested gullies (Shumaker et al., 2017). In terms of gully dimensions, the recorded average widths are in the 100s of m, while the average depths are in the 10s of m (Field et al., 1999; Lonergan et al., 2013) to 100s of m (Gales et al., 2013; Shumaker et al., 2017; Harishidayat et al., 2018).

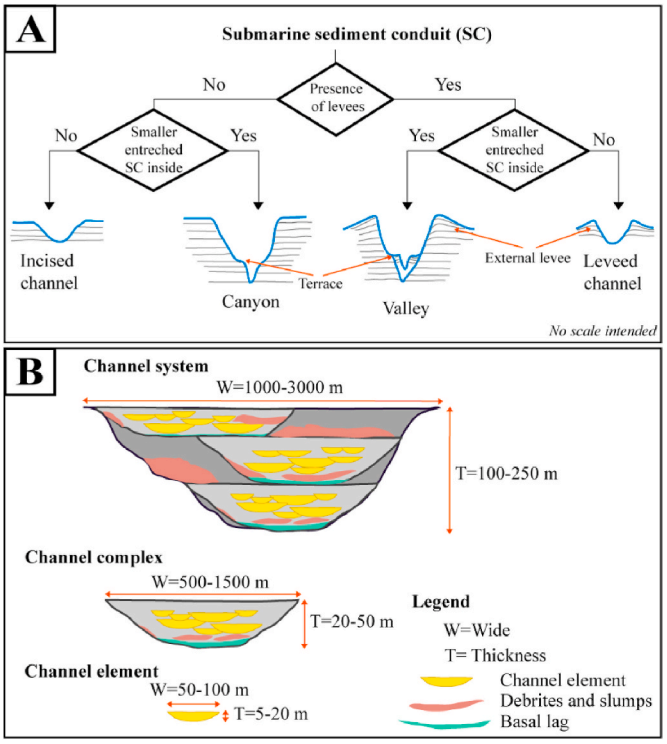

Fig. 2. (A) Classification of submarine channels, canyons and valleys used in this study after Lemay et al. (2020). (B) Three-level hierarchy of channel bodies applied herein and modified from Mayall and Kneller (2021).

2. Geological setting

Taranaki Basin is a Late Cretaceous to Cenozoic sedimentary basin situated mainly offshore in central-western North Island, New Zealand (Fig. 1). It contains a sedimentary succession that is up to 8 km thick and which is variably deformed, initially by crustal extension concurrent with seafloor spreading in the Tasman Sea, and subsequently by shortening driven from the Late Oligocene – present-day Hikurangi subduction. Shortening structures are mainly evident along the eastern margin of the basin involving the Taranaki Fault System (King and Thrasher, 1996; Bull et al., 2015). During the Late Eocene to the Early Oligocene, the basin underwent a regional subsidence phase resulting in a bathymetric deepening of the basin in the northwestward diection (King and Thrasher, 1996; Strogen et al., 2011). Marine inundation of central and southern Taranaki Basin occurred during the late-Early Oligocene (29 Ma), peaking during the latest Oligocene when the central and southern parts of the basin became a foredeep due to loading by basement across the Taranaki Fault System (King and Thrasher, 1996). Marine regression began during the late-Early Miocene from southern Taranaki Basin due to an increasing supply of sediment initially from the fold-thrust belt along the eastern margin, followed during latest Middle Miocene by uplift and erosion of the Southern Alps in South Island southeast of the Alpine Fault (Kamp et al., 1989; Tippett and Kamp, 1993; Higgs and King, 2018). Bull et al. (2019) generated a series of basin models to demonstrate the increase of sediment supply into Taranaki Basin beginning in the Early Miocene (Fig. 3A shows the 8 Ma example). King and Thrasher (1996) calculated a similar Early Miocene increase of sediment supply rate in wells using the parameters of Hayward and Wood (1989) (Fig. 3B).

The Early to Middle Miocene Moki Formation represents the initial development of submarine channel networks in a defined regressive shelf-slope system that prograded across the foreland basin towards the "forebulge" area; however, the forebulge never became fully developed. Late Cretaceous – Paleocene and Late Eocene – Early Oligocene normal faults in southern Taranaki Basin were reactivated as reverse faults from 12 to 10 Ma, forming pronounced antiforms from the crustal shortening that migrated into the foreland basin from its eastern margin (Kamp and Green, 1990; Crowhurst et al., 2002). The start of this phase of deformation coincided with the start of deposition of the Mount Messenger Formation (ca. 12 Ma). The majority of this sediment was sourced from the Southern Alps and a portion was sourced from erosion of the antiforms rising in the Southern Inversion Zone of South Taranaki Basin.

North of the Maui Field, submarine canyon and channel networks developed within the lower part of the Mount Messenger Formation. Their character differs from the upper Moki Formation channel complexes, and we document these differences in this study. The phase of structural shortening of the southern Taranaki Basin ended around 6.5 Ma. The structure in which the Maui oil and gas field occurs is the most northern structure on the western side of the basin. At 6.5 Ma, the whole of southern Taranaki Basin was emergent (i.e., above sea level). During the Pliocene and Pleistocene, southern Taranaki Basin subsided again and it currently lies at shelf depths while the shelf-slope break is displaced well to the west, where the Giant Foresets Formation shelf-slope system has been prograding for the last 5 million years (Hansen and Kamp, 2002).

3. Study area and interval of interest

The focus of this study is the west-central portion of Taranaki Basin (Fig. 1, Inset map 1), through which the Moki and Mount Messenger formations, which comprise interbedded sandstone and mudstone

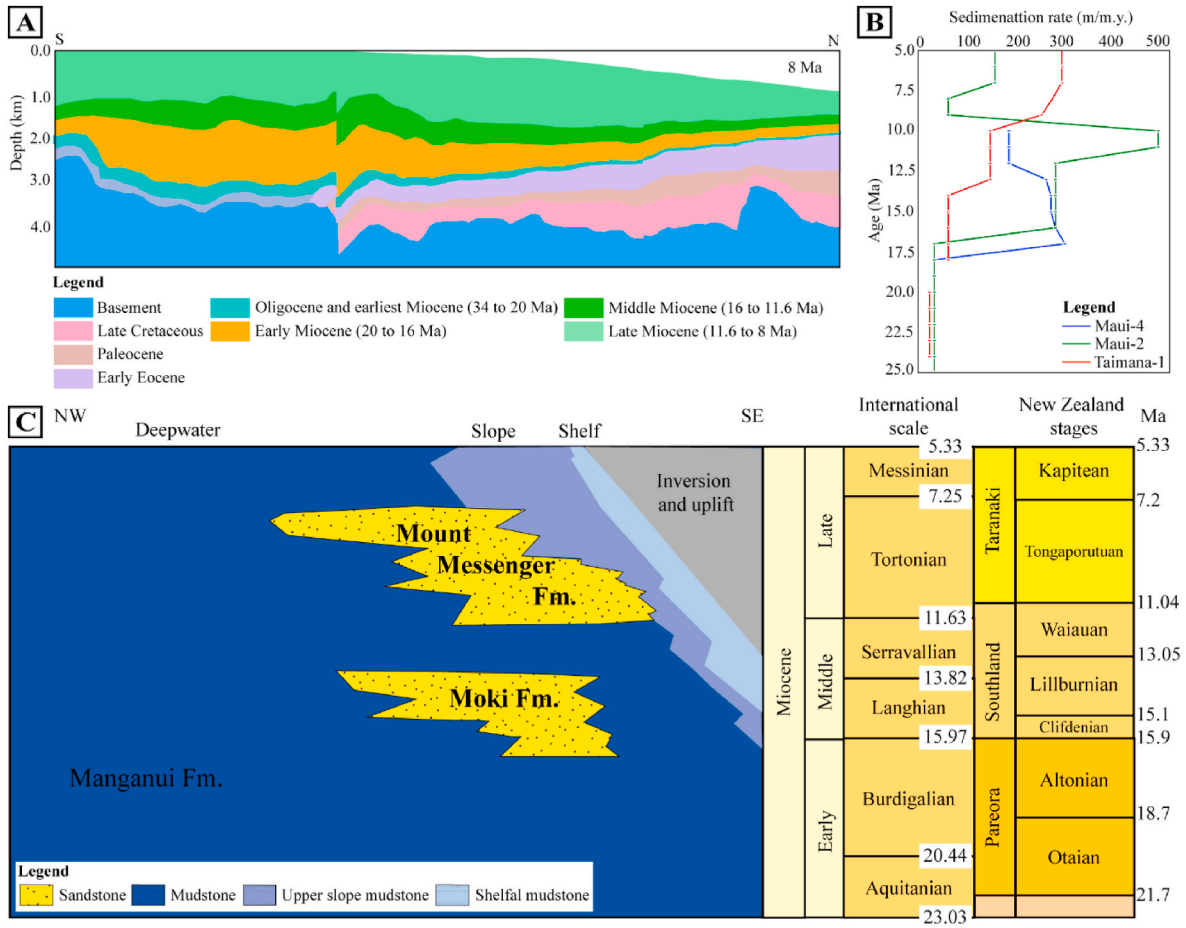

Fig. 3. (A) The Late Cretaceous to Late Miocene (8 Ma) stratigraphy of Southern Taranaki Basin shown as age intervals in a south to north section, simplified from Bull et al. (2019): See Fig. 1 for the section location. (B) Sedimentation rate data from three boreholes from King and Thrasher (1996) based on geohistory data in Hayward and Wood (1989). See Fig. 1 for the borehole locations. (C) Generalised Miocene stratigraphy of Taranaki Basin in a chronostratigraphic chart with the New Zealand stages shown against international stages, epochs and timescale in the chart on the right hand side. The Moki Formation was deposited during the Early to Middle Miocene and the Mount Messenger Formation was deposited during the Middle to Late Miocene. The Manganui Formation is the background mudstone facies. Modified after Bull et al. (2019).

(Fig. 3C), were routed via numerous submarine canyon and channel networks to the deep part of the basin (Strogen et al., 2011; Kroeger et al., 2019). The Manganui Formation is a time equivalent mud-prone unit that envelopes the Moki and Mount Messenger formations, and is commoly considered to comprise the "background" sediments on the slope and in deep water (King and Thrasher, 1996). The distinction between the sand-prone Moki and Mount Messenger formations and the mud-prone Manganui Formation is based on wireline response in wells that intersect the formations (King and Thrasher, 1996; Roncaglia et al., 2013; Kroeger et al., 2019).

The study area is broadly situated atop the Maui Field, encompassing the Maui structure that marks the northwestern extent of the Southern Inversion Zone. The Whitiki Fault marks the western side of the study area and the eastern extent is broadly parallel to the Cape Egmont Fault Zone (Bryant et al., 1994; Bussell, 1994; Bryant and Greenstr, 1995) (Fig. 1). The regional orientation of prograding sediment accumulation is northwestward, as indicated by the seaward dipping clinoforms visible in seismic data (Fig. 4).

For our analysis we subdivide the Moki and Mount Messenger formations into three intervals: (i) Upper Moki Formation (Lillburnian Stage (Sl), 16–13 Ma); (ii) Lower Mount Messenger Formation (Waiauan (SW) to Early Tongaporutuan, (Tt) stages, 13–9 Ma); and (iii) Upper Mount Messenger Formation (Middle to Late Tongaporutuan Stage, 9–7.2 Ma) (Fig. 3C). The New Zealand stages, as defined by Cooper et al. (2004), are defined biostratigraphically by foraminiferal content. Stage boundaries are recorded on drill-hole well logs (Roncaglia et al., 2013) for the area of interest in this study. Selected stage boundaries have been mapped within the 3D seismic volume used in this study.

4. Dataset and methods

4.1. Seismic data

This study utilises ca. 1800 km^2 of an open-source, industry-acquired, post-stack time migrated (PSTM) 3D seismic reflection dataset, as well as wireline logs from 14 exploration drill holes accessed through the New Zealand Petroleum & Minerals database (https://data.nzpam.govt.nz). Seismic volumes have 19 m × 12.5 m bin spacing, record lengths of 4.5–6 s two-way travel time (TWT), vertical sampling rates of 4 ms (TWT) and a 20–50 Hz dominant frequency within the intervals of interest (seismic TWT: 1250-2200 ms^{-1}). Seismic volumes were merged, and amplitude was balanced in the merged volume before interpretation. A velocity model was derived for time-depth conversion using check shot data, with the average velocity for the Moki and Mount Messenger formation intervals ranging from 1800 ms^{-1} to 2500 ms^{-1}. In addition, well logs were used to aid seismic interpretation by helping identify lithological changes corresponding to seismic reflections.

Coloured Inversion (CI) was performed on the merged 3D volume to derive relative band-limited acoustic impedance, which boosts the low-frequency seismic response, and therefore increases the resolution of the

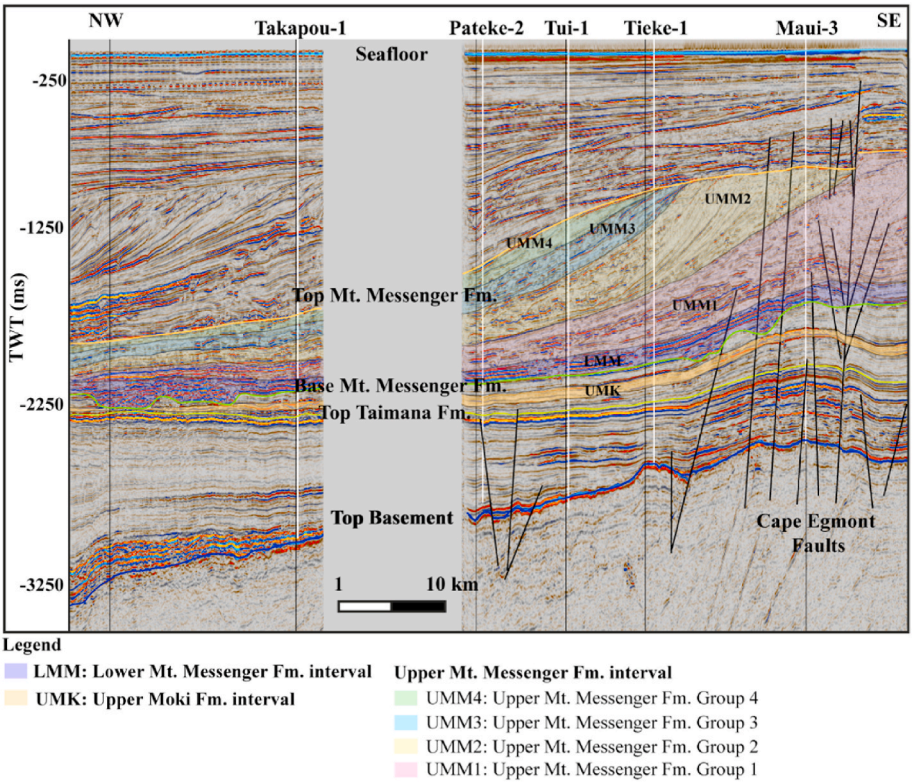

Fig. 4. Seismic section showing clinoforms of the Moki and Mount Messenger formations dipping to the north and northwest. The regional horizons are Top Basement, Top Taimana Formation, Base Mount Messenger Formation and Top Mount Messenger Formation. The location of the transect is shown in Fig. 1 within Inset Map 1.

data (Lancaster and Whitcombe, 2000; Maurya and Singh, 2017; Assis et al., 2018). First, synthetic logs were matched to the seismic data and used to determine the major reflection horizons while considering existing biostratigraphic data from Roncaglia et al. (2013).

Seismic attributes, including Amplitude Accentuating Attributes (e.g., Root Mean Square Amplitude (RMSA) and Sweetness), Geometric Attributes (e.g., Semblance and Dip Curvature), and Spectral Decomposition, were extracted along and within the interpreted horizons to visualise the geomorphology of the submarine canyon and channel networks. These attributes were especially useful for distinguishing between sandstone beds within and along the margins of canyons and channels from the background mudstone succession (Taner, 2001; Brown, 2011; Othman et al., 2019). Importantly, attribute extraction was undertaken using horizon-parallel and/or proportional slices to reduce structural effects that might obscure images of the canyons and channels and to ensure slices were broadly time-equivalent snapshots (Zeng et al., 1998, 2001; Miall, 2002; Zeng, 2013).

4.2. Quantitative seismic geomorphology

The seismic geomorphology of submarine canyon, channel and gully networks were quantified by using both cross-sectional and plan views of the 3D seismic volume. However, to understand the limit of seismic resolution and any potential effects of thin-bed tuning of the data, we generated wedge models. To do so, we calculated both Rayleigh (Kallweit and Wood, 1982) and Widess (Widess, 1973; Chopra et al., 2006) (vertical) resolution limits in terms of bed thickness. The Rayleigh limit of resolution is one-quarter the wavelength of the seismic data (i.e., $\lambda/4$; where λ = wavelength), and the Widess limit of resolution is one-eighth of the wavelength (i.e., $\lambda/8$). The Widess thin-bed tuning effect ($\lambda/4$) and the onset of thin-bed tuning effect ($\lambda/2$) were also calculated.

Initial seismic horizon interpretation and surface generation of the sediment conduits were accomplished in Petrel, and the subsequent spatial analysis was done in both Petrel and ArcGIS. Morphometrics that primarily rely on cross-sectional views of the data include width, depth, cross-sectional area and canyon wall steepness. These were measured every 500–700 m perpendicular to the orientation of sediment conduit axes, down-canyon, down-channel or down-gully (Fig. 5). For cross-sectional morphometrics: (i) width refers to the measurement at the overspill points perpendicular to their flow directions; (ii), the depth measurements refer to the average height from the two-separate overspill points, due to asymmetrical walls; (iii) the cross-sectional area is calculated based on the digitised points within the canyons (at the base and walls) (Lemay et al., 2020); and (iv) canyon wall steepness refers to the gradient between canyon top and base at the thalweg (Bührig et al., 2022). Due to sediment compaction, the depth of the sediment conduits in this study are considered as minimum depth, and the estimation of compacted sediment cannot be calculated with high confidence due to limited well data within the varying gradient prograding slope strata.

For planform metrics of the canyons, channels and gullies: (i) sinuosity index is the ratio between the length of the lowest point of the thalweg and the overall down-system distance for a given section (a single bend wavelength) (Wynn et al., 2007); (ii) meander length and amplitude were measured through the same stretch of canyons, channels and gullies where sinuosity index was measured; and (iii) canyon length measurements were taken along-canyon following the thalweg. In addition to cross-sectional and planform parameterisation of canyons and channels, the slope gradient, orientation and steepness (in percent rise) were also calculated at the thalweg and smoothed over a 1–2 km sliding window. In some cases, the sediment conduit incisions did not occur exactly on the mapped regional or sub-regional seismic surfaces (i.e., especially on variably steep surfaces) and in these cases, the incisions were projected onto the nearest surfaces (Shumaker et al., 2017). Finally, the width-to-depth ratio of the sediment conduits was also calculated.

Because the base and top horizons of the canyons, channels and

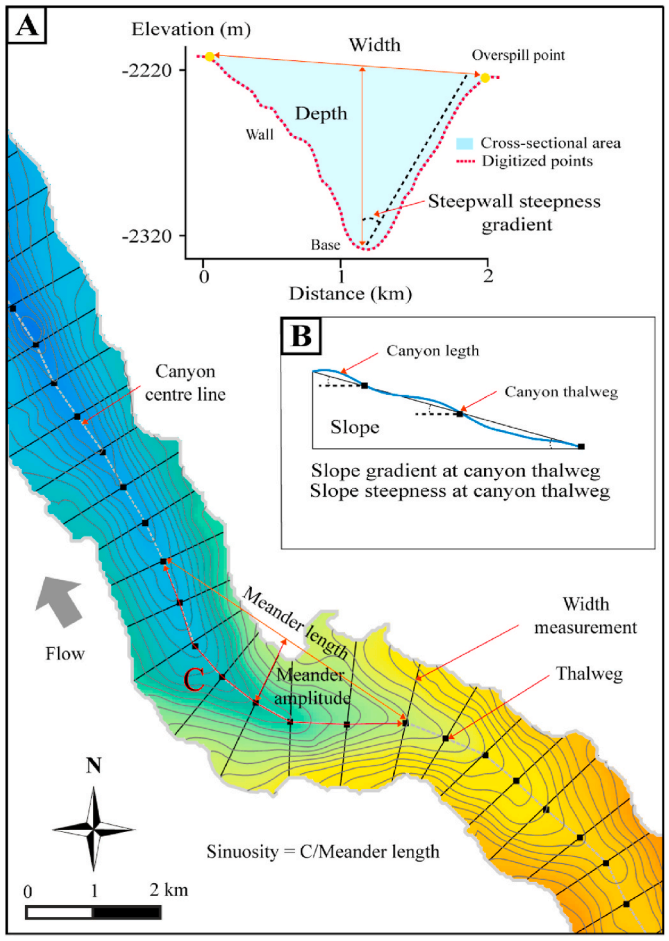

Fig. 5. (A) The main seismic geomorphological parameters calculated in this study and their definitions, including width, depth, cross-sectional area, wall steepness, meander amplitude, meander length and sinuosity. (B) Explanation of canyon length, slope gradient and steepness parameters at thalweg.

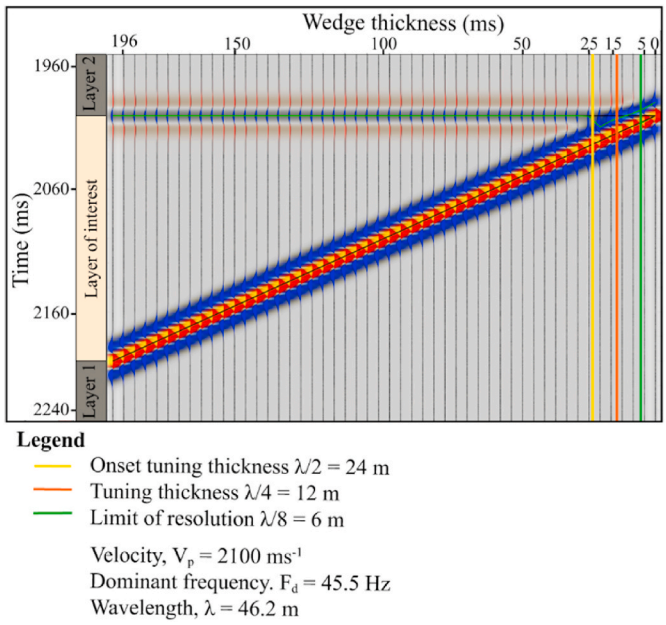

Fig. 6. An example seismic wedge model used to determine the onset of the thin-bed tuning effect. In this case the onset of the tuning effect occurs at a bed thickness of 24 m. The tuning effect is greatest with a bed-thickness of 12 m. Finally, the limit of resolution due to the tuning effect is when bed-thickness reaches 6 m. These calculations are based on Widess (1973).

Table 1
Seismic data and seismic resolution parameters. The vertical seismic resolution of λ/4 is based on Rayleigh's Limit of Resolution, and λ/8 is based on Widess (1973).

Range of velocity within Miocene	Range of dominant frequency within Miocene	Rayleigh's limit of resolution λ/4	Widess (1973) limit of resolution, λ/8
1800 ms^{-1} to 2500 ms^{-1}	40–50 Hz	12–20 m	6–10 m

gullies are offset by the Whitiki Fault and the Cape Egmont Fault System, the original depositional surfaces were corrected to pre- and post-faulting positions using horizon flattening and structural restoration. The base of the middle fill of canyons is measured at the base of the aggradational channel systems (Deptuck et al., 2007). Morphometric parameters were analysed using Pearson's correlation coefficient (r).

The morphometric parameters of sediment conduits in this study are based on stratigraphic surfaces. As pointed out by Strong and Paola (2008), and investigated by Sylvester et al. (2011), valleys/canyons in the rock record are not necessarily the result of Earth-surface topography at the time of deposition, they may also be a manifestations of stratigraphic processes. At the present time, no concrete criteria exist to differentiate between stratigraphic valleys and topographic valleys and we cannot be completely certain that we are not comingling the two. However, deposits observed in sediment cores and outcrop from the Moki and Mount Messenger formations suggest that sediment was delivered to the basin via large-scale sediment conduits.

5. Results

5.1. Resolution of seismic data

Calculation of the Widess and Rayleigh seismic resolution limits yielded a vertical resolution of 6–20 m within the intervals of interest (Fig. 6; Table 1). Thus, the morphology of canyons, channel systems and channel complexes are resolvable on seismic data. By contrast, the morphology of channel elements cannot be quantified with high confidence in the interval of interest because their overall dimensions fall below seismic resolution.

5.2. Seismic geomorphology

The upper Moki Formation interval consists of sinuous channel complexes that meander from south to north with a mean sinuosity, width and depth of 2.4, 1.1 km and 67 m, respectively. The lower Mount Messenger Formation interval comprises canyon networks of highly variable dimensions with a maximum width and depth of 9 km and 350 m, respectively. These canyon networks consist of numerous medium to large U-shaped channel systems (and/or channel complexes) developed within canyon walls ranging from 50 to 200 m deep. Finally, the upper Mount Messenger Formation are characterised by linear gully complexes oriented from southeast to northwest, with a mean sinuosity, width and depth of 1.0, 1.1 km and 116 m, respectively. Below we describe the seismic geomorphological parameters, stratigraphic interval by interval.

5.2.1. Upper Moki Formation

The morphology and morphometrics of the upper Moki Formation channel complexes are shown in Figs. 7 and 8. The channel complex networks developed on the lower slope margin in the study area, roughly 80 km from the shelf edge and 100 km from the shoreline (Fig. 7C) (Strogen et al., 2011). Seismic reflectors have a gentle basinward slope (i.e., the mean slope gradient is 0.2°).

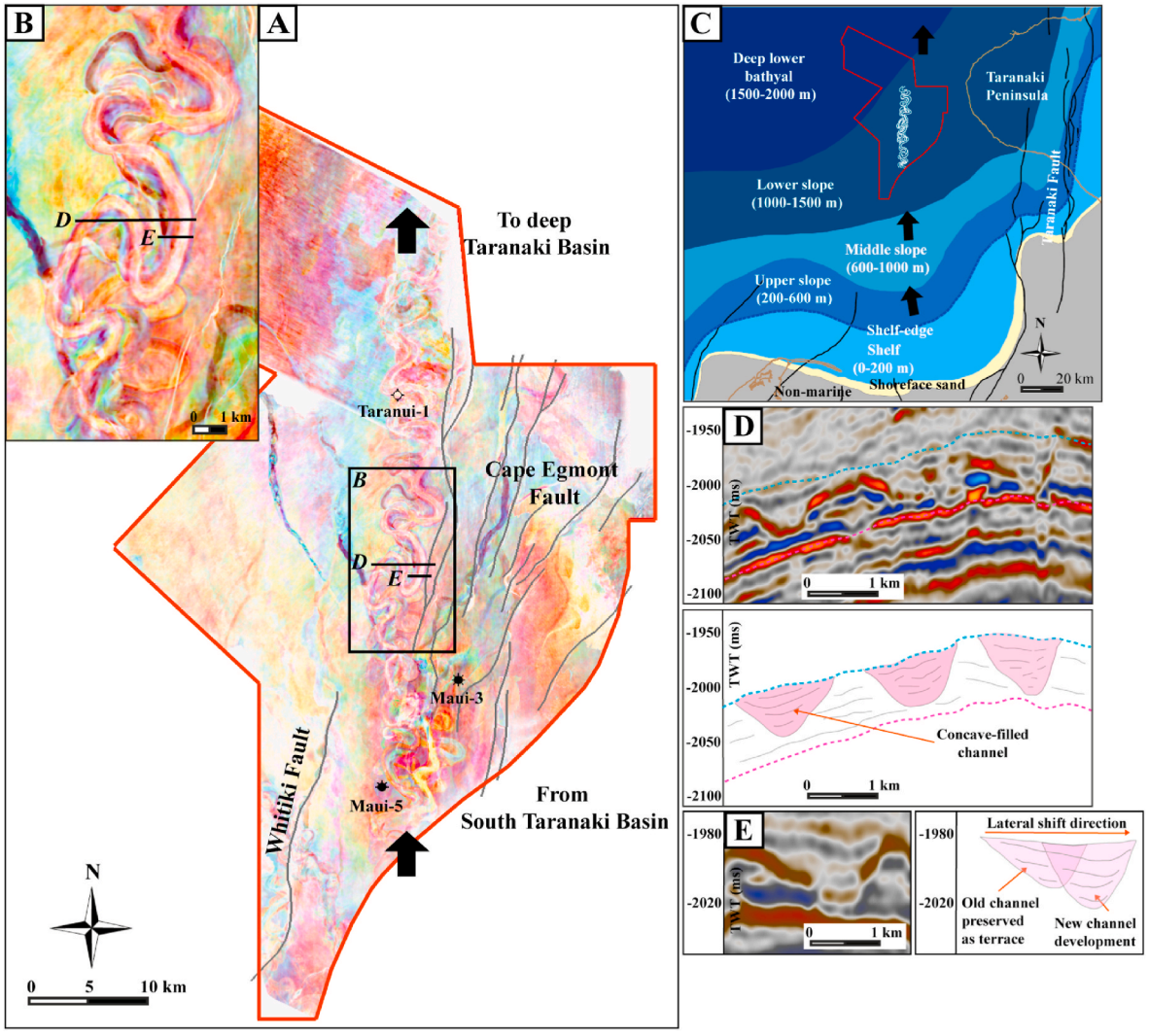

Fig. 7. (A) Map showing the cyan-magenta-yellow (cyan: 20 Hz, magenta: 30 Hz and yellow: 40 Hz) blend of the General Spectral Decomposition (GSD) seismic attribute, which is used to highlight the geomorphology of upper Moki Formation channel complexes. The red polygon outlines the study area. (B) Close-up view of the sinuous channel complexes. (C) Paleogeographic map (modified from Strogen et al., 2011) showing the location of the upper Moki Formation channel complexes on the lower slope during the Middle Miocene (14 Ma). (D) and (E) are uninterpreted and interpreted cross-sections of the upper Moki Formation channel complexes illustrating the seismic facies of channel-infill and channel lateral shift pattern.

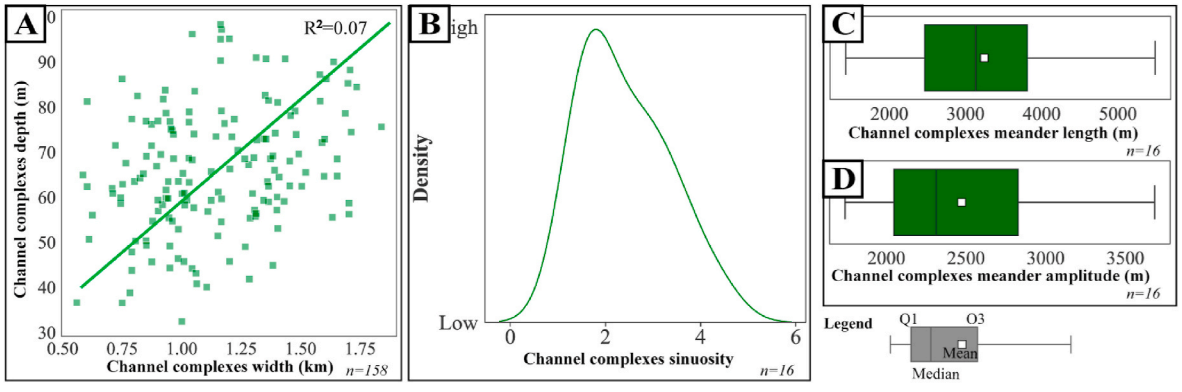

Fig. 8. Seismic geomorphological metrics of the upper Moki Formation channel complexes. (A) Plot of the channel complexes depth versus width showing a poor correlation ($R^2 = 0.07$). (B) Kernel density plot of the channel complexes sinuosity. Plots of the channel complexes (C) meander length and (D) meander amplitude. n is the number of samples.

Channel complexes have a nearly symmetrical U-shape cross-section, with mean width, depth, and cross-sectional area of 1.1 km, 67 m and 0.06 km^2, respectively (Fig. 7D and E and 8A). Overall, the channel complexes show a significant variation in the width and depth metrics ranging from 0.5 to 1.80 km and 32–85 m, respectively, with such scatter in values that the correlation coefficient is small (i.e., $R^2 = 0.07$; Fig. 8A). Planform views show that these channel complexes have a high range of sinuosity (1.3–4.34), with the range of meander amplitudes and lengths being 1.7–3.7 km and 1.4–5.5 km, respectively (Fig. 8B, C and D). There is a lack of evidence for lateral stacking and abandoned meanders, but abrupt lateral shifts in thalweg position are observed along some channel complex margins (Fig. 7B and E). These channel complexes also do not show levee wedge development. In seismic plan view, overbank splays and crevasse splays are not observed.

5.2.2. Lower Mount Messenger Formation

Figs. 9–17 and Table 2 contain information about the morphology and morphometrics of the lower Mount Messenger Formation canyon networks. In total, ten canyons were identified within the interval. The canyons occur in two networks based on their geographic position and connectivity in seismic data: Group 1 (Canyons A, B, C, D, E, F, G to H) and Group 2 (Canyons I and J) (Fig. 9A and B), and their morphometrics are summarized in Table 2. These canyons are the extension of larger canyon networks that originated from South Taranaki Basin (Strogen et al., 2011) (Fig. 9C). The canyons occur roughly 75 km from the shoreline and 50 km from the shelf-break and are situated on the lower slope margin (Fig. 9C). In the study area, the canyons occur within the bottomsets of Manganui Formation clinoforms on a slope gradient ranging from 0.4 to 1.0° (Fig. 10). The planform morphology of canyons is straight with a mean sinuosity, meander length and meander amplitude of 1.1, 3.3 km and 0.5 km, respectively (Fig. 11B, C and D).

5.2.2.1. Group 1 canyon network. The total length of the Group 1 canyon network is 78 km, with Canyon B having the longest component (36 km) and Canyon H the shortest (6 km) (Fig. 11A). The subsurface elevation of the Group 1 canyon network ranges from −1620 m to −2980 m, the depositional slope ranges from 0.4 to 1.0° and the depositional orientation is predominantly to the northwest (Fig. 10A and B).

Canyon A incises the deepest of all of the canyons into the background strata of the Manganui Formation, roughly 80 ms (TWT) from its top incision surface. However, although Canyon A is the oldest it is difficult to decipher the order of incision for the younger constituent canyons because their top incision surfaces occur at or near the same stratigraphic horizon. Nonetheless, Canyons A, B and E coalesce at the base of the clinoform slope at coalescing point 1 (CP1), forming Canyon F. The base of the clinoform slope, refer in this study to the clinoform toe

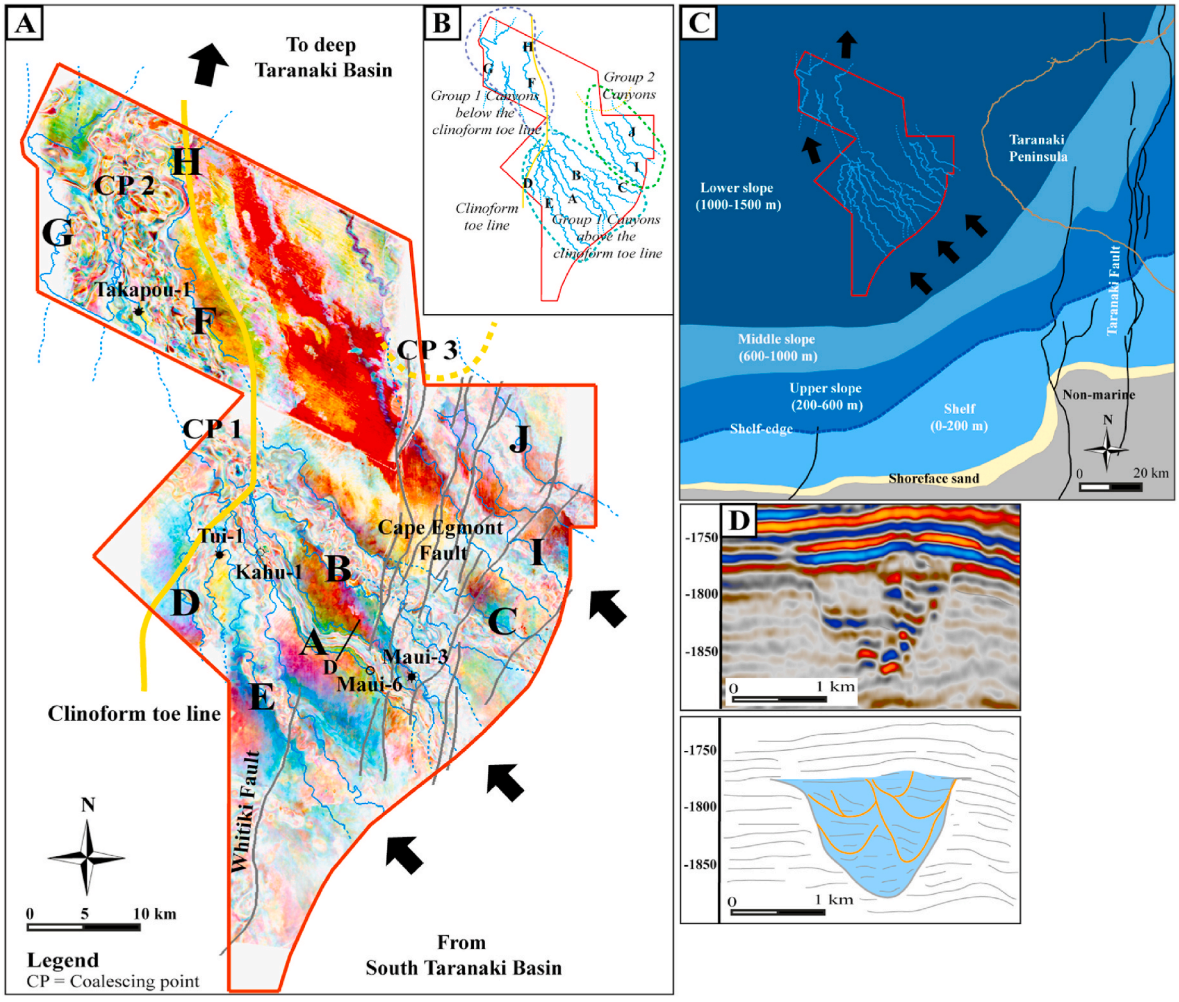

Fig. 9. (A) Map showing the cyan-magenta-yellow (cyan: 20 Hz, magenta: 30 Hz and yellow: 40 Hz) blend of the General Spectral Decomposition (GSD) seismic attribute, highlighting the geomorphology of the lower Mount Messenger Formation canyons and channel systems. The canyons are labelled from A to J. (B) The grouping of canyons. (C) Palaeogeography map showing the location of the lower Mount Messenger Formation canyon networks in the Middle Miocene (12 Ma) in relation to the basin physiography (modified from Strogen et al., 2011), and blue outlines show the canyon networks mapped in this study. (D) Uninterpreted and interpreted cross-section of Canyon A demonstrating the predominantly sandy infill of the canyon.

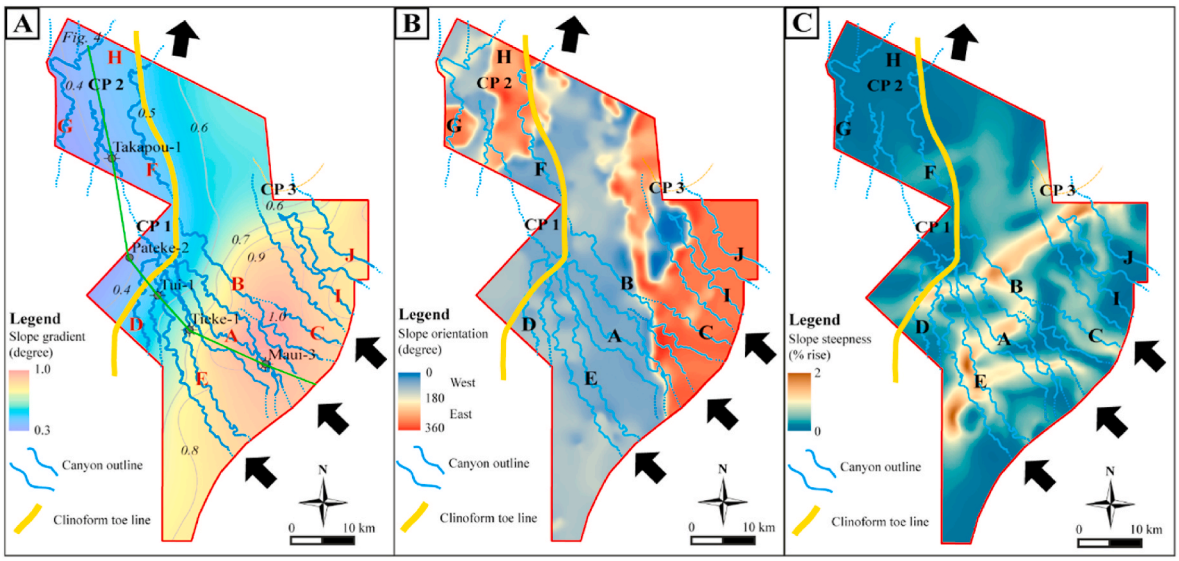

Fig. 10. Regional maps depicting: (A) Changes in slope gradient, (B) Slope orientation and (C) slope steepness of the lower Mount Messenger Formation canyons. The canyons are labelled from A to J and the clinoform toe line is marked by the yellow line, which subdivides the steep and flat parts of the slope.

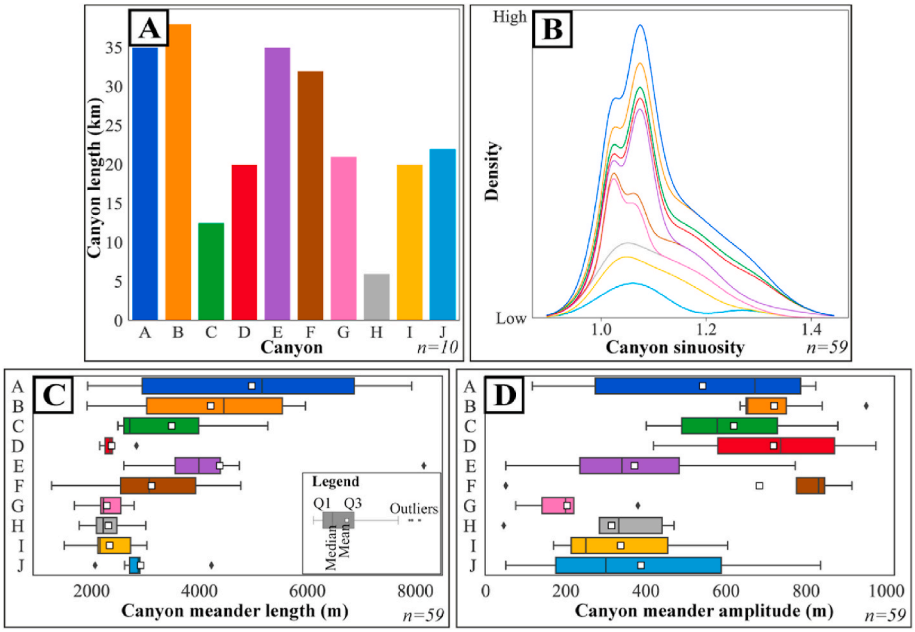

Fig. 11. (A) Bar chart comparing the length of the lower Mount Messenger Formation canyons. (B) Kernel density plot comparing the canyons sinuosity (colour codes same as in A). Comparison of the individual canyon (C) meander length and (D) meander amplitude measurements (colour codes same as in A). n is the number of samples.

line (i.e. equivalent to the clinoform toe point), marking the position where the clinoform bottomsets become horizontal with the underlying surface (Pirmez et al., 1998; Patruno et al., 2015). It occurs broadly along the 0.5° slope gradient line, and it is at or below this point that all canyons coalesce (Figs. 9 and 10). Canyon F coalesces with Canyon G (originating from the south) at coalescing point 2 (CP2) to form the much larger Canyon H (Figs. 9 and 10).

5.2.2.2. Morphometrics of group 1 canyons. Calculation of the morphometrics of Group 1 canyons reveals two distinct canyon populations: (i) canyons above the clinoform toe line (Canyons A, B, C, D, E, I and J), and (ii), canyons below the clinoform toe line (Canyons F, G and H) (Fig. 9B). Accordingly, we analysed and describe them separately in the following text.

In summary, the cross-sectional morphometrics of the canyons below the clinoform toe line increase by factors of depth (1.8), width (2.4) and cross-sectional area (4.7) in comparison to the canyons above the clinoform toe line (Fig. 12B, C and D). The mean width, depth and cross-sectional area of the canyons above the clinoform toe line are 2.69 km, 142 m and 0.22 km^2 respectively, while the mean width, depth and cross-sectional area of the canyons below the clinoform toe line are 6.6 km, 252 m and 1.04 km^2, respectively. Correlation analyses of measured morphometric variables using Pearson's correlation are summarized in Fig. 12G–I. Overall the slope gradient (at the canyon thalweg) and the canyon elevation have a strong correlation (r = 0.92–0.98). The slope gradient also strongly correlates with the canyon width, depth and cross-sectional area (r = -0.71–-0.86). However, the slope steepness only displays a moderate correlation to the canyon width, depth and cross-

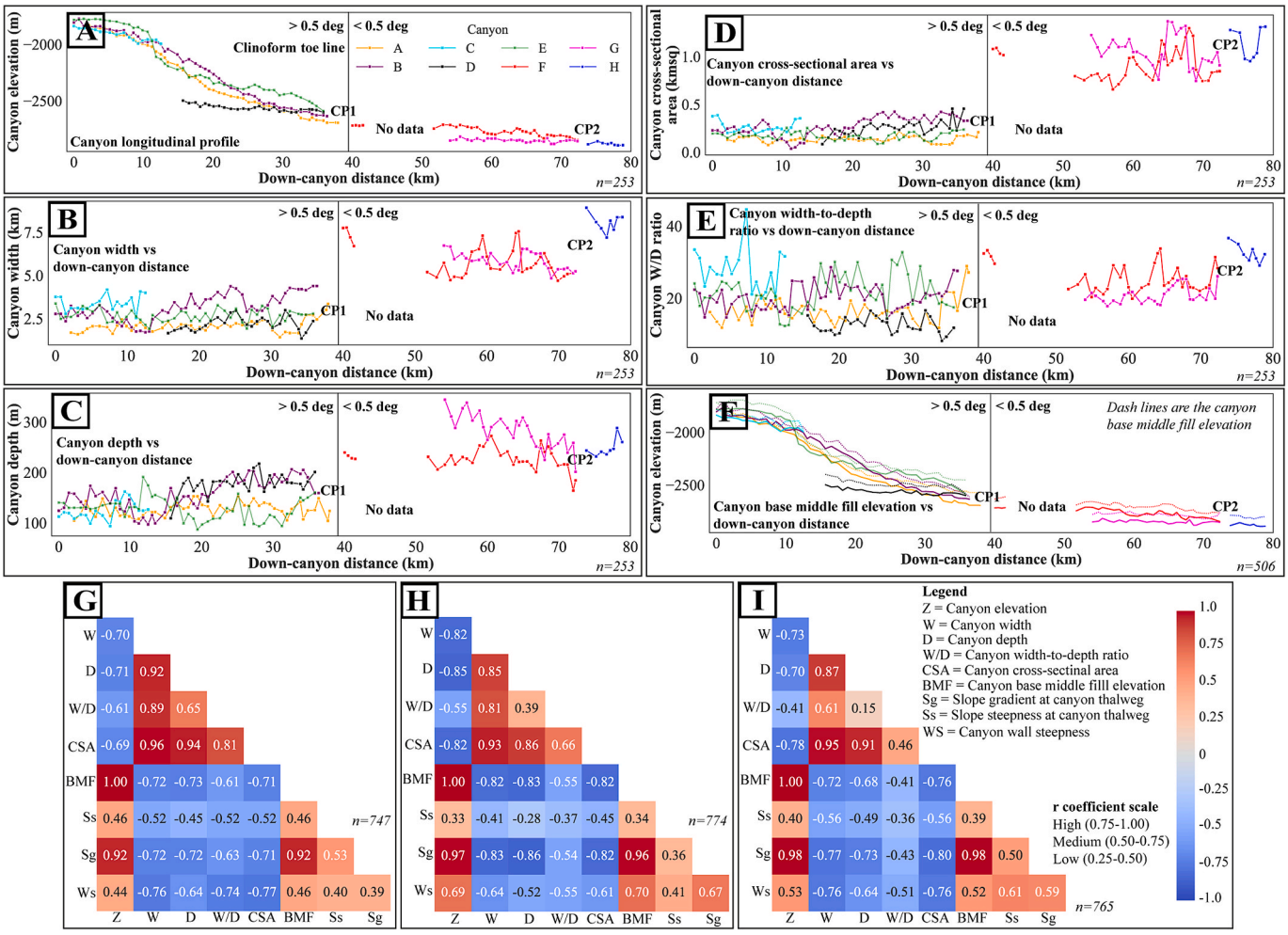

Fig. 12. Cross-sectional morphometrics of the lower Mount Messenger Formation canyons. (A) Canyon elevation versus down-canyon distance, (B) canyon width versus down-canyon distance, (C) canyon depth versus down-canyon distance, (D) canyon cross-sectional area versus down-canyon distance, (E) canyon width-to-depth ratio versus down-canyon distance and (F) canyon elevation and base middle fill elevation versus down-canyon distance. Matrix of Pearson's correlation coefficient between the major morphometric parameters for (G) Canyons A, F and H. (H) Canyons B, F and H. (I) Canyons E, F and H. n is the number of samples.

sectional area (r = -0.28–-0.56). Lastly, canyon elevation and canyon width, depth and cross-sectional area correlate strongly with canyon wall steepness (r = -0.52–-0.77).

5.2.2.2.1. Group 1 canyons above the clinoform toe line. Planform morphometrics reveal that canyons above the clinoform toe line (Canyons A, B, C, D and E) are primarily straight with an average sinuosity index, meander length and amplitude of 1.1, 3.9 km, and 0.6 km, respectively (Fig. 11). Canyon A is the straightest with a sinuosity index and maximum meander length of 1.05 and 7.9 km, respectively. In comparison, Canyon D is the most sinuous with a sinuosity index and maximum meander length of 1.2 and 2.8 km, respectively. The principal drainage axes of canyons is towards the northwest, corresponding to the dominant depositional slope orientation (Fig. 10B) and the spacing between canyons ranges from 1 to 7 km (Fig. 9A).

Analysis of canyon cross-sections reveals that most canyons are characterised by asymmetrical sharp V-shape incisions with a narrow base. However, in some cases parts of the canyons display U-shape incisions with a wide base. The cross-sectional elements of the canyons are shown in Fig. 13 and mainly consist of canyon bases, walls and flanks. The canyons have steep walls with average wall steepness of 12.5° and deep indentation of the thalweg. Throughout the canyon course, the thalweg only shifts laterally by slight amounts.

5.2.2.2.2. Group 1 canyons below the clinoform toe line. Similar to canyons above the clinoform toe line, canyons below the clinoform toe line (Canyons F, G and H) are straight with a mean sinuosity index of 1.1 and meander length and amplitude of 2.6 km and 0.4 km, respectively (Fig. 11). The regional slope into which Canyons F and H incise dips to the east (Fig. 10B), which impacts canyon trajectory (toward the northeast) at the edge of the study area.

The cross-section of canyons in this region shows asymmetrical V-shaped indentation with greater depth than the canyons above the clinoform toe line (Fig. 14), and the average canyon wall steepness is 9°. In general, the width and depth of the canyon measured above 5 km and 200 m, respectively. The width of the canyons increased dramatically after the canyons merged at CP2, from roughly 6 km–8.5 km (Fig. 12B). However, the cross-sectional metrics of Canyon G, which originated from the south, are not correlated with Canyon F and H (Fig. 12). The canyon cross-sections also reveal that the right wall of the canyons displays more significant terrace development than the left wall due to the progressive channel incisions toward the east (Fig. 14 C–C').

5.2.3. Group 2 canyon network

The canyons in Group 2 consist of Canyons I and J, which developed on the northeastern side of the study area (Fig. 9A). The course of the canyons cannot be fully mapped due to the limitation of the 3D seismic data coverage, however the length of each canyon within the study area is roughly 20 km (Fig. 11A). The canyons developed on slopes ranging from 0.5 to 0.9° (Fig. 10B). The range of elevation of the canyons is

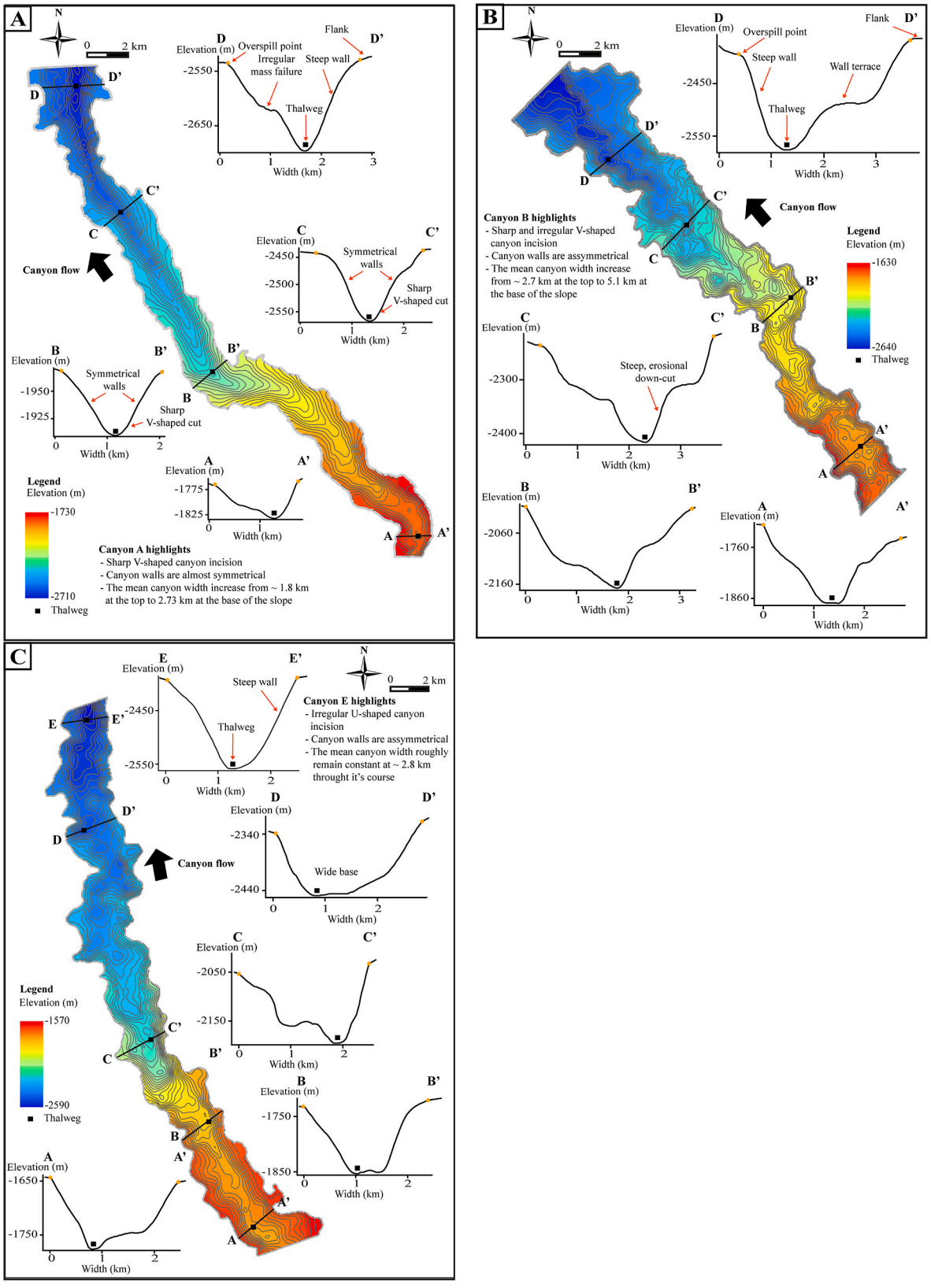

Fig. 13. Cross-sectional views of the lower Mount Messenger Formation canyons above the clinoform toe line. (A) Canyon A, (B) Canyon B and (C) Canyon E. The main elements of the canyons are also highlighted.

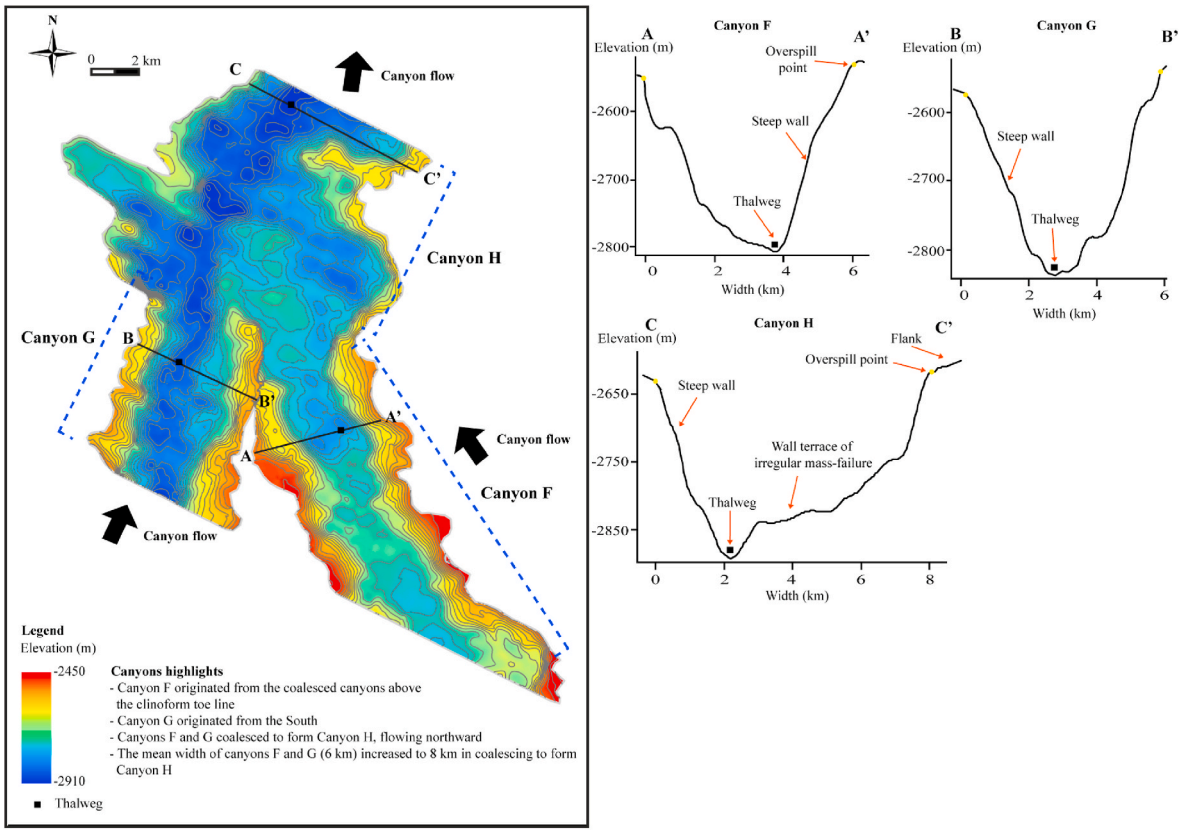

Fig. 14. Cross-sectional views of the lower Mount Messenger Formation canyons below the clinoform toe line for Canyons F, G, and H. The main elements of the canyons are also highlighted.

between −1800 m and −2400 m, with Canyon J formed roughly 100 m deeper than Canyon I near the beginning of the canyon course (Fig. 15A). Based on this, we infer that Canyon J is older than Canyon I. Canyons in Group 2 merge at the clinoform toe line (at coalescing point 3; CP3) similar to canyons in Group 1 (Fig. 9A).

5.2.3.1. Morphometrics of group 2 canyons. Both Canyon J and Canyon I are relatively straight, with an average sinuosity index of 1.1 (Fig. 11B). Canyon J has slightly wider meanders than Canyon I, with a mean meander amplitude of 387 m versus 337 m (Fig. 11D). The cross-sectional morphometrics of the canyons do not show a clear down-canyon trend (Fig. 15B, C, D and E), while the Pearson's correlation coefficient shows mainly low to medium correlation (Fig. 15G and H). The cross-sectional shape of both canyons is a combination of moderate V-shape and U-shape profiles and with mean wall steepness of 10° (Fig. 16).

5.2.4. Lower canyon infill

Overall, the erosive base of the canyons displays an irregular profile due to multiple channel incisions of different magnitudes along the canyon course (Fig. 17). Multiple re-incision surfaces were identified along the course of the canyons, but the surfaces cannot be mapped with high confidence due to the complex nature of the incisions. Below the clinoform toe line, the seismic profile of the canyons displays erosive surfaces formed through multiple alternating canyon incision and infilling phases, which further complicates the attempt to map the incision surfaces.

5.2.5. Middle and upper canyon infill

The base of the middle canyon infill is marked by the onset of a mainly aggradational channel system (and/or channel complexes) formed within the canyon walls (Deptuck et al., 2007). Within lower Mount Messenger Formation canyons, numerous medium to large U-shaped channels formed within the canyon walls were observed at depths ranging from 50 to 200 m (Fig. 17). In some areas, successive channel incisions partly or entirely erode channel walls. In plan view, the canyons are flanked by extensive overbank deposits, especially the ones below the clinoform toe line. Overall, the base of the middle canyon fill profile mimics the canyon (base) longitudinal profile (Figs. 12F and 15F).

5.3. Upper Mount Messenger Formation gully complex networks

The morphology and morphometrics of the upper Mount Messenger Formation slope-confined gully complexes are summarized in Fig. 18 and Table 3. These complexes are enclosed in a thick prograding mudstone succession of Tongaporutuan age (~11–7.2 Ma). In the study area, the thickness of the prograding mudstone reaches roughly 700 m in Maui-3 and 430 m in Tui-1 drill-holes. Throughout the Tongaporutuan, the seafloor slope increased from about 4° at the base to about 11° at the top of the succession. The steep clinoform (of oblique progradational pattern) is attributed to the rapid progradation of the shelf-break and reorientation of the slope, in addition to the strata thickening into the foot-walls of the reverse Cape Egmont Fault (Bull et al., 2019). In the study area, we grouped the gully complexes that formed on the steep clinoform slope in the upper Mount Messenger Formation interval into four groups (i.e., Group 1, 2, 3 and 4) based on the major clinoform surfaces that bound them (Fig. 4). The exact age of the surfaces cannot be determined from the available biostratigraphic data, however for simplicity, Group 1 gully complexes are the oldest and Group 4 gully complexes are the youngest.

Gully complexes in Group 1 are bounded by the gentle slope of mainly bottomset surfaces (mean: 3.7°), and they are 0.67–2.62 km wide and 54–259 m deep. Groups 2 and 3 gully complexes developed within

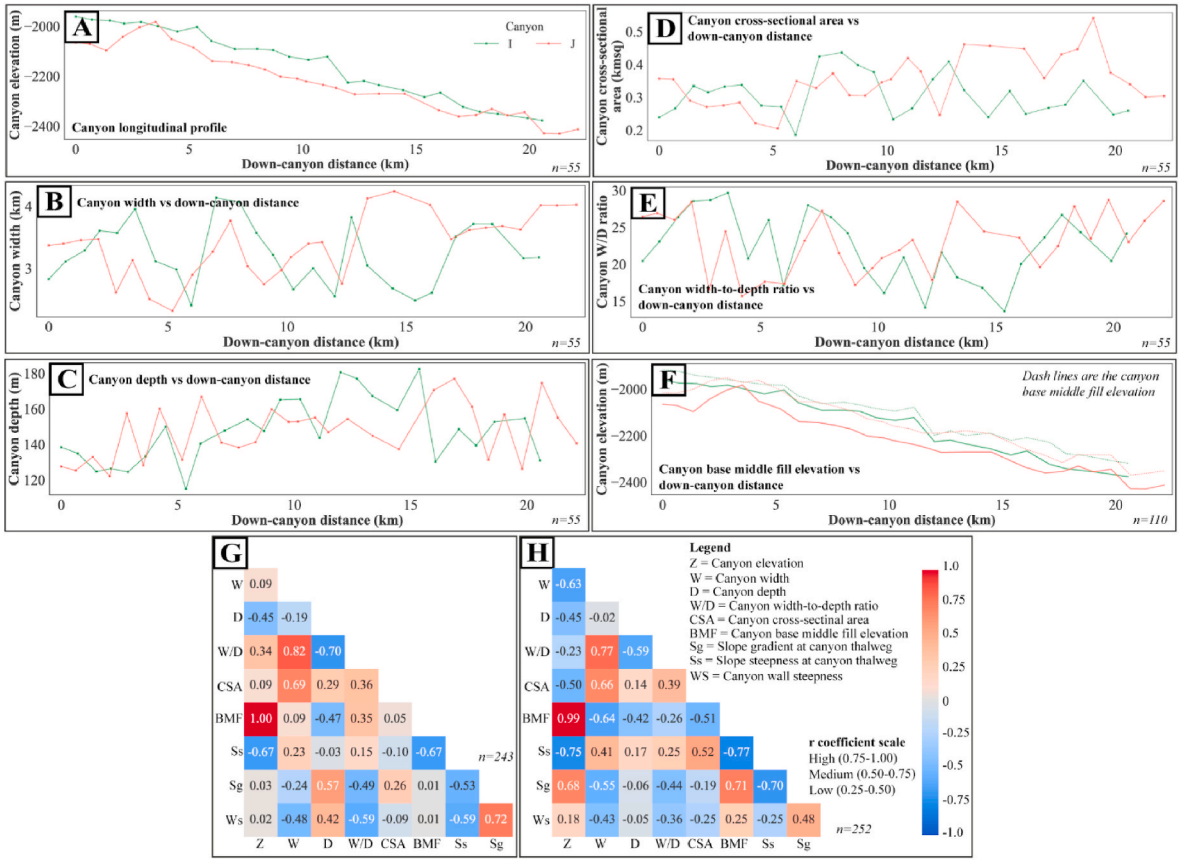

Fig. 15. Cross-sectional metrics of the lower Mount Messenger Formation canyons are described as: (A) canyon elevation versus down-canyon distance, (B) canyon width versus down-canyon distance, (C) canyon depth versus down-canyon distance, (D) canyon cross-sectional area versus down-canyon distance, (E) canyon width-to-depth ratio versus down-canyon distance and (F) canyon elevation and base middle fill elevation versus down-canyon distance. Matrix of Pearson's correlation coefficient between the major morphometric parameters for (G) Canyon I and (H) Canyon J. n is the number of samples.

the foreset and bottomset sigmoidal-oblique clinoform wedges. However, some gullies in Group 2 (mean width: 1.18 km, mean depth: 108 m) developed within aggradational successions and, therefore, developed a much steeper slope surface (mean: 5.6°). Group 3 gully complexes (mean width: 1.03 km, mean depth: 105 m) formed on progradational clinoforms with less steep slopes than Group 2 (mean: 5.1°). Lastly, Group 4 gully complexes formed on steep sigmoid-shaped clinoform slopes (mean: 4.3°) and have a width and depth range of 0.40–1.52 km and 20–158 m, respectively.

Gully networks within the upper Mount Messenger Formation are predominantly linear, sharp, symmetrical and V-shaped, are oriented northwestward, and their down-slope length varies from 10 to 20 km. The sharp V-shaped morphology is associated with the steep wall and flank of the gullies, and the average wall steepness angle is 20°. The spacing of the gullies ranges from 1.5 to 5 km, with most gullies spaced evenly and a few gullies exhibiting downslope convergence before transitioning to frontal splays or die out at the base of the clinoform slope.

The longitudinal profile of the gullies displays an overall very subtle concave profile as the slope gradient decreases from the topset to the bottomset of the clinofom (Fig. 18C and D). The width and depth of individual gully complexes significantly increases sharply in the first ~2.5 km of their course. Then, the gully widths exhibit an overall gradual increase, and the gully depth displays a decreasing trend before terminating at the base of the slope (Fig. 18E and F).

In comparing the morphometrics of the gullies throughout the interval (from Group 1 to 4), the average gully width, depth and meander amplitude exhibit a decreasing trend from Group 1 to Group 4 (Fig. 18E, F, H, I and Table 3). The correlation between the gully width and depth ranges from $R^2 = 0.06–0.43$ (Fig. 18L). On seismic data, the gullies do not show significant evidence of lateral and vertical migration; instead, they display deep incisions into the background prograding mudstone. In addition, the gullies commonly display nested complexes with multiple incisions.

6. Discussion

6.1. Synthesis of the geomorphology and morphometrics of sediment conduits in Taranaki Basin

Our results show that the deposition of thick Miocene prograding wedges in Taranaki Basin is a function of high sediment supply beginning in the late-Early Miocene (Fig. 3A and B), resulting in clinoforms with variable geometries and steepness (i.e., slope gradients). The upper Moki Formation and Mount Messenger Formation sediments both accumulated in various types of conduits, transporting the sediments to deep basin. In summary, the upper Moki Formation is dominated by small, sinuous, U-shaped channel complexes in a very low-relief slope setting, whereas the lower Mount Messenger Formation is characterised by very large canyon networks in low-relief slope settings. By contrast, the upper Mount Messenger Formation consists of numerous linear, V-shaped gully complexes that developed within a high-relief slope.

The variation in morphometrics between canyons, channels and gullies presented in this study mainly highlight how morphology of sediment conduits respond to changes in depositional slope gradient. By the early-Middle Miocene, sinuous upper Moki Formation channel complex networks developed, which routed sediment from south to north in the basin (Fig. 7). At this time, the cross-sectional area and

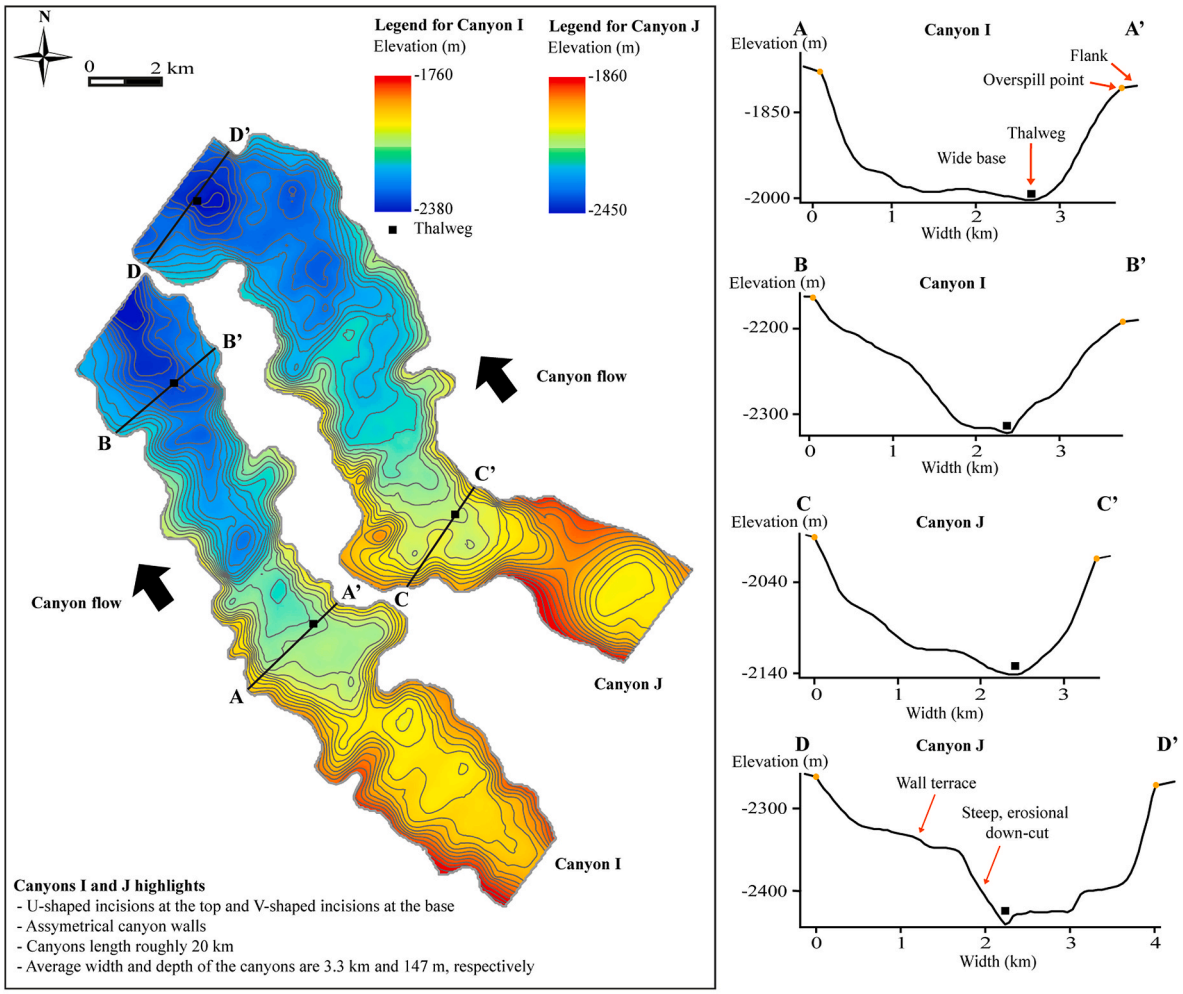

Fig. 16. Cross-sectional geometry of the Group 2 lower Mount Messenger Formation canyons (i.e., Canyons I and J). The main elements of the canyons are also highlighted.

shape of channel complexes did not change significantly across the system (i.e., mean width: 1.1 km, mean depth: 67 m).

By the late-Middle Miocene, the slope began to prograde rapidly, and the dip of the regional slope reoriented to be northwest (Bull et al., 2019). During this time, the lower Mount Messenger Formation canyon networks incised into the prograding slope surface, which had a gradient of 0.4–1.0°. At shallower slopes of less than 0.5°, canyon morphometrics are 1.8–4.7 times bigger than on steeper slopes of greater than 0.5° (mean width of 2.7 km, mean depth of 142 m and mean cross-sectional area of 0.22 km^2 *versus* mean width of 6.6 km and mean depth of 253 m and mean cross-sectional area of 1.04 km^2, respectively) (Fig. 12B and C and Table 2). This shift in morphometrics occurs abruptly across the clinoform toe line.

Rapid slope progradation of the shelf break dominated much of the Late Miocene interval, resulting in the development of steep clinoform surfaces of up to 9° into which relatively straight upper Mount Messenger Formation gully complexes incised (Fig. 18). The mean gully width and depth throughout the interval decreased from 1.30 to 0.97 km and 143.81 to 86 m, respectively, as the slope became steeper.

6.2. Slope gradient controls the morphometrics of sediment conduits

The morphology of channels in the upper Moki Formation is typical of deep water sinuous channels (Kolla et al., 2007; Wynn et al., 2007; Posamentier et al., 2022). In seismic plan view, overbank splays and crevasse splays are not observed, implying that the sediment was contained within the incised channels with little to no avulsion and associated overtopping of the channel margins. This is likely to be a result of sediments being transported through the channels on the relatively flat slope (mean: 0.2°) and with no breaks in slope on its lower margins (Posamentier and Kolla, 2003). For similar reasons, the geometry of channel complexes did not significantly change throughout the study area in comparison with the lower Mount Messenger and upper Mount Messenger formation intervals.

The development of lower Mount Messenger Formation canyons on higher and more variable slope gradients due to rapid shelf progradation and reorientation is best explained by a power law of slope to distance (Mitchell, 2005; Gerber et al., 2009). In essence, the longitudinal profile of lower Mount Messenger Formation canyons displays a comparatively steep slope in proximal areas (i.e., 0.5–1.0°), and they transition to relatively flat slopes in their distal reaches (i.e., 0.4–0.5°). Such concave longitudinal profiles are similar to several modern submarine canyon and channel systems globally, such as the Laurentian and Var canyon-channel systems (Covault et al., 2011) (Fig. 19A and B). These systems are highly erosional, with narrow shelves, steep slope gradients, and close proximity to sediment sources with intense erosion from sediment-gravity flows (Covault et al., 2011). Very concave profiles are typical of underfilled basins. Taranaki Basin fits this definition during the Middle Miocene.

In general, the cross-sectional morphometrics of canyons increase

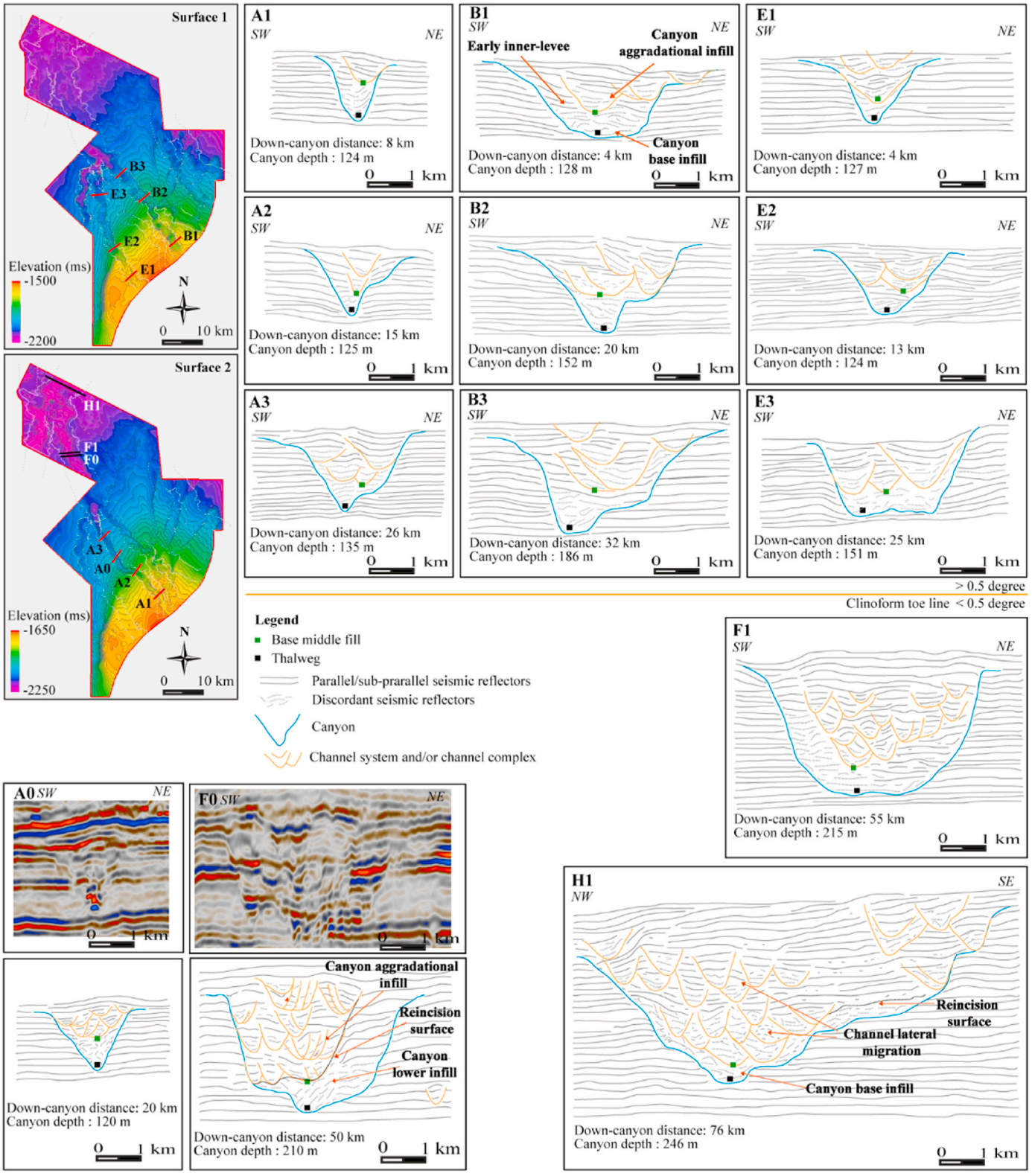

Fig. 17. Plots showing the cross-sectional infill pattern of the lower Mount Messenger Formation canyons as well as the lower and upper infill characteristics of the canyons, based on mapping of seismic reflection surfaces.

down-slope due to an increase in frequency and acceleration of sediment gravity flows transporting granular material down-slope (Shepard et al., 1974); Shepard, 1981). This study emphasizes that the clinoform toe line (i.e., slope gradient: 0.5°) is a significant feature for controlling: (i) the spatial arrangement of canyon networks, including where they coalesce, and (ii), the position where a significant shift in the canyon cross-sectional morphometrics occurs. The position of the clinoform toe line, which is a major part of the clinoform structure, in turn, heavily influenced pre-existing topography within the basin (Lofi et al., 2003; Clairmont et al., 2020), as well as sediment supply. In the case of

Table 2
Morphometrics of lower Mount Messenger Formation canyons.

Lower Mount Messenger Fm. canyons	Width min-max, mean (km)	Depth min-max, mean (m)	Sinuosity min-max, mean	Meander length min-max, mean (m)	Meander amplitude min-max, mean (m)	Gradient at thalweg min-max, mean (°)
Group 1 canyons						
Canyon A	1.42–3.35, 2.08	104-153, 127	1.0–1.1, 1.1	1926-7935, 4970	116-824, 542	0.5–1.0, 0.8
Canyon B	1.70–4.38, 3.15	97-206, 157	1.0–1.3, 1.1	1915-5963, 4206	635-950, 720	0.5–1.0, 0.8
Canyon C	2.53–4.17, 3.39	94-162, 124	1.0–1.2, 1.1	2487-5264, 3486	401-879, 619	0.9–1.0, 0.9
Canyon D	1.35–2.98, 2.18	109-217, 177	1.1–1.3, 1.2	2149-2832, 2370	419-974, 718	0.45–0.60, 0.5
Canyon E	1.90–3.37, 2.67	87-191, 128	1.0–1.1, 1.1	2597-8158, 4373	50-773, 371	0.5–0.8, 0.7
Canyon F	4.70–7.75, 5.87	164-272, 227	1.1–1.4, 1.2	1260-4764, 3113	50-914, 683	0.4–0.5, 0.5
Canyon G	4.84–6.73, 5.83	201-344, 282	1.0–1.1, 1.0	1679-2789, 2280	75-380, 203	0.4–0.4, 0.4
Canyon H	7.19–8.92, 8.06	232-288, 249	1.0–1.2, 1.1	1771-3005, 2310	45-470, 314	0.44–0.46, 0.44
Group 2 canyons						
Canyon I	2.41–4.14, 3.23	115-183, 147	1.0–1.2, 1.1	1491-3026, 2336	169-604, 337	0.7–0.9, 0.8
Canyon J	2.32–4.24, 3.38	122-177, 147	1.0–1.3, 1.1	2065-4222, 2908	50-836, 387	0.6–0.8, 0.8

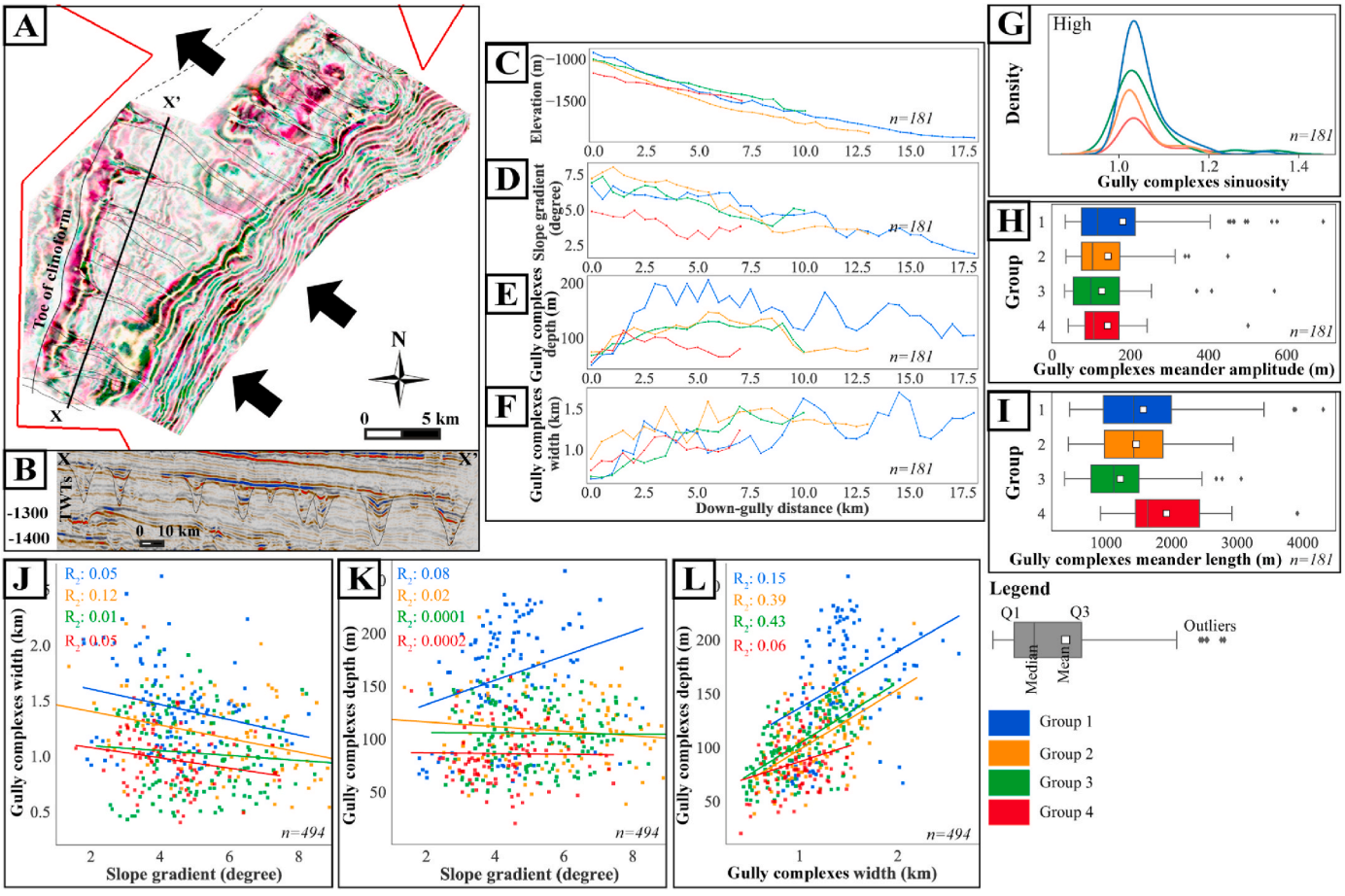

Fig. 18. (A) and (B) An example of upper Mount Messenger Formation gully complexes on a stratigraphic horizon. (C) gully complexes longitudinal profile versus down-gully distance, (D) slope gradient at gully complexes thalweg versus down-gully distance, (E) gully complexes depth versus down-gully distance, (F) gully complexes width versus down-gully distance, (G) kernel density plot of gully complexes sinuosity, (H) gully complexes meander amplitude, (I) gully complexes meander length, (J) gully complexes width versus slope gradient, (K) gully complexes depth versus slope gradient and (L) gully complexes depth versus depth. n is the number of samples.

Table 3
Morphometrics of upper Mount Messenger Formation gully complexes.

Upper Mount Messenger Fm. gully complexes	Width min-max, mean (km)	Depth min-max, mean (m)	Sinuosity min-max, mean	Meander length min-max, mean (m)	Meander amplitude min-max, mean (m)	Gradient at thalweg min-max, mean (degree)
Group 1	0.67–2.62, 1.30	54-259, 144	1.0–1.2, 1.1	445-3866, 1501	38-456, 142	1.1–6.0, 3.7
Group 2	0.54–2.19, 1.18	38-215, 108	1.0–1.2, 1.0	428-2940, 1459	36-450, 143	0.7–9.0, 5.6
Group 3	0.43–1.95, 1.03	50-177, 105	1.0–1.4, 1.1	368-3061, 1241	32-569, 129	2.2–9.1, 5.1
Group 4	0.40–1.52, 0.97	20-159, 86	1.0–1.2, 1.1	917-3923, 1919	41-170, 131	1.6–7.4, 4.3

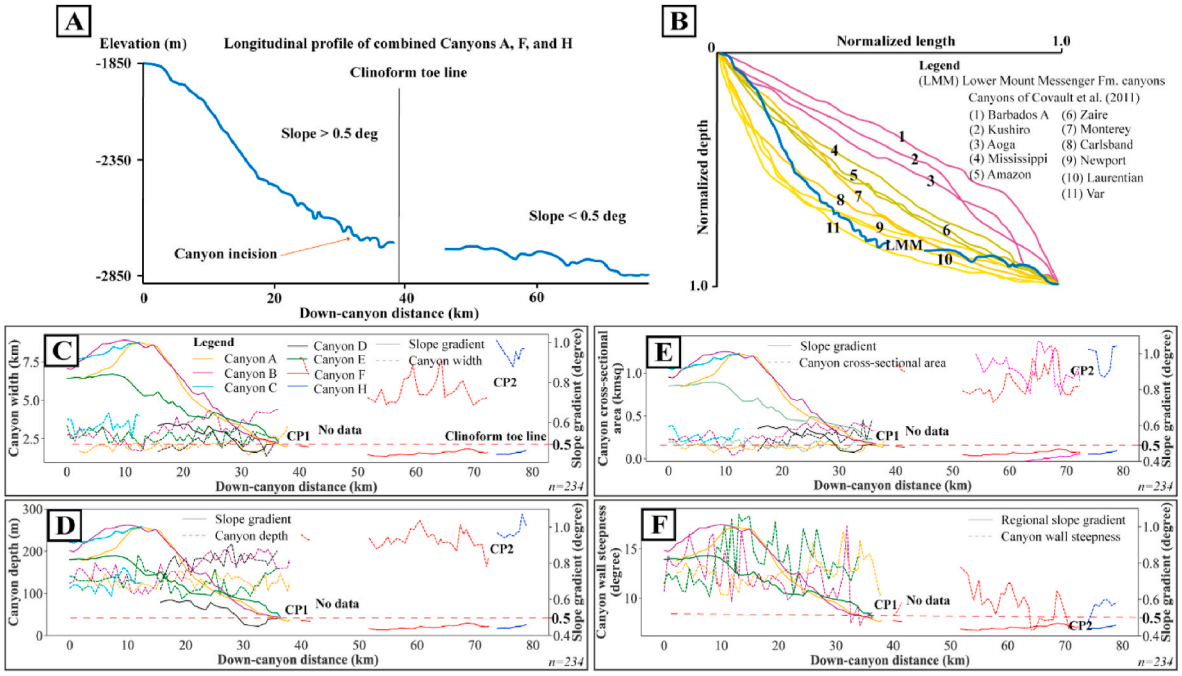

Fig. 19. (A) Longitudinal profile of lower Mount Messenger Formation canyons showing their irregular incisions along their course. (B) Comparison between the lower Mount Messenger Formation canyons (blue) with the longitudinal profiles of other canyons globally. The lower Mount Messenger Formation canyons match the very concave profile of other canyons. The data source for the other canyons is from Covault et al. (2011). The depositional slope gradient relationship with the lower Mount Messenger Formation canyons (C) canyon width, (D) canyon depth, (E) canyon cross-sectional area and (F) canyon wall steepness. n is the number of samples.

Taranaki Basin, regional subsidence during the Late Eocene to Early Oligocene profoundly affected the basin morphology by establishing a seafloor topography template across the basin, based on the concept in Covault et al. (2011). With bathymetric deepening towards the northwest, this resulted in the creation of vast accommodation for later sediment deposition.

The linear morphology of the upper Mount Messenger Formations gully networks is typical of gullies that form on a high gradient slope. Correspondingly, their morphometric parameters are in the range of the gullies measured by other workers e.g., Gales et al. (2013), Prélat et al. (2015), Shumaker et al. (2017) and Harishidayat et al. (2018). Morphometrics measured in this study shows that gullies form on steep

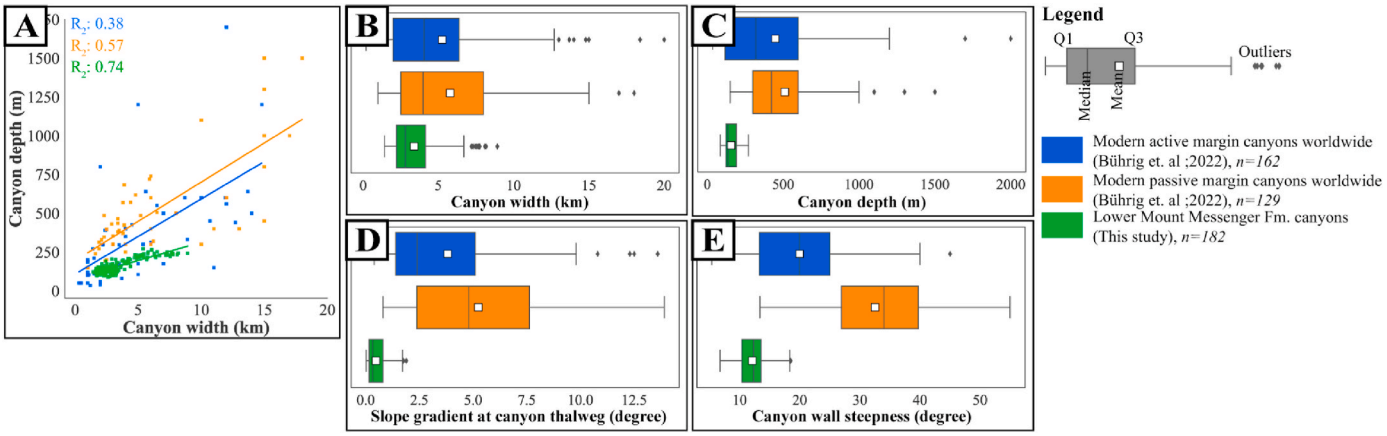

Fig. 20. Comparison between the lower Mount Messenger Formation canyons and modern canyons globally. (A) Canyon depth versus width, (B) canyon width, (C) canyon depth, (D) slope gradient at canyon thalweg and (E) canyon wall steepness. The modern canyon morphometric measurements are from Bührig et al. (2022). n is the number of samples.

slopes of over 5°, supporting the same findings of Micallef and Mountjoy (2011). The width and depth of gullies increases rapidly from their landward margins (~0–2.5 km). This is probably due to rapid incision of unconfined sediment gravity flows accelerating down slope (Micallef and Mountjoy, 2011; Lintern et al., 2016) or slumping on the slope (Ricketts and Evenchick, 1999).

Overall, gully complexes show a trend of decreasing cross-sectional dimensions (i.e., width, depth and cross-sectional area) from Group 1 (at the base of the interval) to Group 4 (at the top of the interval) due to a depleted supply of sand. This is reflected in the transition from the sand-dominated Mount Messenger Formation to the mud-dominated Manganui Formation at the end of the Miocene (Fig. 3C).

6.3. Comparison with other canyon systems globally

Canyon systems of the lower Mount Messenger Formation fall within the natural width and depth ranges of modern canyons, but their metrics sit towards the smaller end of global data with shallower cross-sectional metrics (Fig. 20). However, correlation between width and depth within the lower Mount Messenger Formation canyons is higher than for modern canyons on both passive and active margins, with R^2 values of 0.74, compared with 0.57 (passive) or 0.38 (active) (Bührig et al., 2022). The width and depth distributions of the lower Mount Messenger Formation canyons are narrow compared with modern canyons: the width range is 1.4–8.9 km (lower Mount Messenger Formation) versus 0.2–20 km (modern), and the depth range 87–344 m (lower Mount Messenger Formation) versus 35–2000 m (modern) (Fig. 20B and C). This difference is attributed to: (i) Lower Mount Messenger Formation canyons being of Miocene age, and therefore on seismic data, sediment compaction has influenced the canyon morphometric measurements (Deptuck et al., 2007; Harishidayat et al., 2018) (modern canyons are less affected by sediment compaction) and (ii), the morphometrics of the lower Mount Messenger Formation canyons are concentrated on the lower slope margin, in contrast to other canyons for which the morphometrics are based on mean values from various basin physiographic setting. Similarly, the canyon thalweg gradient and the canyon wall steepness ranges of the lower Mount Messenger canyons are also narrow compared with modern canyons. This variation is predominantly due to the position of the canyons being located at the clinothems terminations, where the slope gradient range is relatively minor.

In comparison to other ancient canyon systems, a significant portion of the morphometrics of the lower Mount Messenger Formation canyons are similar to the range of their counterparts (Fig. 21). However, lower Mount Messenger Formation canyons have a higher width range and lower depth range than other ancient canyons. The range differences could be attributed to sediment properties such as grain size distribution (Hsu and Liu, 2010), flow patterns within canyons (Shepard et al., 1974), flow types within and around canyons (Talling, 2014), and flow volume (Qin et al., 2016), as well as other physical processes such as inner terrace architecture (Babonneau et al., 2004) and inner canyon erosion and mass failure (May et al., 1983; Qin et al., 2016).

In Taranaki Basin during the Middle Miocene to Late Miocene, the occurrence of numerous lower Mount Messenger Formation canyons is in tandem with the increasing sediment supply into the basin. This is not consistent with the conclusion made by Fisher et al. (2021), which suggested that canyons are associated with low to negligible sediment supply. The Taranaki Basin example we describe here may therefore be an outlier.

6.4. Source-to-sink environment significance

From a palaeogeography perspective, during the Miocene, the absence of canyons and large channel systems within the upper Moki Formation interval implies that sediment transport to deep Taranaki Basin was ineffective. This is due to the limited sand supply available during the early-Middle Miocene, which hinderered the development of large channel complexes (Fig. 3C). However significant time-equivalent mudstone (Manganui Formation) was being deposited outside the channel complexes.

In contrast, the lower Mount Messenger Formation interval, having numerous canyons and channel networks, indicates the efficiency of sediment transfer to deep Taranaki Basin based on the concept in Stow and Mayall (2000) and in Posamentier and Kolla (2003). These sediments bypassed the study area as the canyons and channels routed voluminous sediment to the deeper basin towards the New Caledonia Trough (Bull et al., 2019). For the upper Mount Messenger Formation, the gully complexes died out at the base of the slope. Therefore, sediments during this interval were not delivered efficiently to the deeper parts of the basin, based on the concepts in Dalla Valle et al. (2013).

6.5. Reservoir exploration significance

The morphometrics of sediment conduits presented in this study have implications for understanding deep-water reservoir systems and especially the relationship between reservoir size and slope gradient. Previous reservoir exploration in the study area has focused mainly on Paleocene and Eocene strata of the Kapuni Group, which is the most significant commercial hydrocarbon reservoir system in Taranaki Basin (Bryant et al., 1994; Funnell et al., 2004), leaving the Middle Miocene interval relatively unexplored. The large cross-sectional areas of the lower Mount Messenger Formation canyon networks, including the thick interconnected aggradational channel infills show excellent

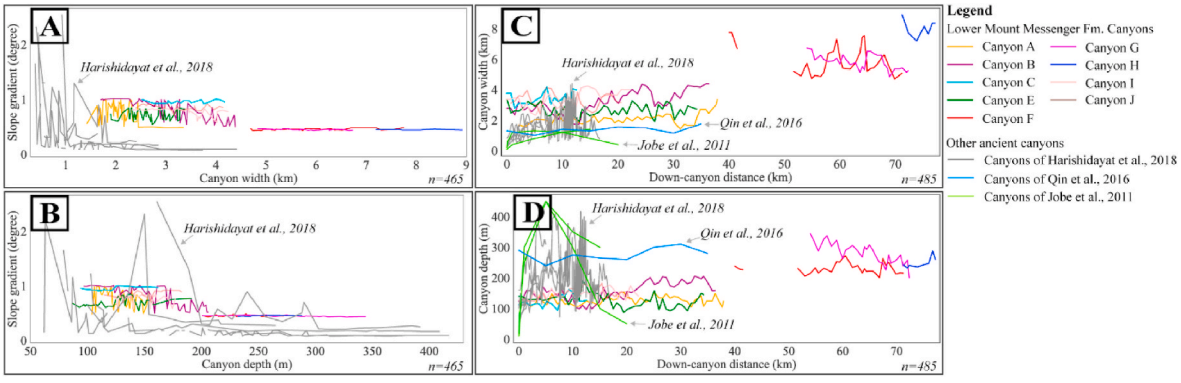

Fig. 21. Comparison between lower Mount Messenger Formation canyons and other ancient canyon systems. (A) Slope gradient versus canyon width, (B) slope gradient versus canyon depth, (C) canyon width versus down-canyon distance and (D) canyon depth versus down-canyon distance. The down-canyon distance reflects the area of respective data. The ancient canyon morphometric measurements are from Jobe et al. (2011), Qin et al. (2016) and Harishidayat et al. (2018). n is the number of samples.

reservoir characteristics, at least in terms of the size of the reservoirs (Clark and Pickering, 1996; Mayall and Kneller, 2021). Furthermore, oil and gas fields do occur in these reservoirs onshore in Taranaki Peninsula (i.e., Kaimiro, Cheal and Radnor fields). The thick prograding mudstone succession overtopping the canyons and channels acts as up-slope stratigraphic pinch-out traps for hydrocarbon accumulation in the up-dip slope direction (McCaffrey and Kneller, 2001; Amy, 2019). Moreover, the inversion structures around the Maui Field (e.g. Manaia Anticline and Cape Egmont Fault) could assist in the migration and trapping of hydrocarbons (Seebeck et al., 2020). In other jurisdictions, high-nutrient slope facies can be source rocks due to low oxygen content along such margins (Bjorlykke, 2010).

The upper Moki and upper Mount Messenger Formation channel complexes are relatively small in comparison with the canyons and channel systems of the lower Mount Messenger Formation, and therefore their reservoir potential is limited by their smaller dimensions (Mayall and Kneller, 2021). Even though the upper Mount Messenger gully networks have large dimensions, their infill is dominated by muddy deposits and therefore have low reservoir potential. Our analysis offers improved data to help assess the reservoir potential of sediment conduits in Taranaki Basin.

7. Conclusions

Detailed seismic geomorphologic analysis of 3D seismic reflection data for the Moki and Mount Messenger formations in Taranaki Basin has enabled us to parameterize submarine canyon, channel, and gully networks within them. The results of this study show that there are robust differences between their cross-sectional and planform geomorphology. The following captures the major conclusions of this work:

1. The main sediment conduits are variable in their seismic geomorphology. The upper Moki Formation is dominated by sinuous channel complex networks. Canyon networks dominate the lower Mount Messenger Formation interval and they show numerous aggradational channel formations. The upper Mount Messenger Formation is dominated by linear gully networks.
2. The development of the lower Mount Messenger canyons was strongly influenced by depositional slope. The clinoform toe line marks a rapid change in the cross-sectional area and shape, as well as the spatial arrangement of the canyon networks.
3. The development of the upper Moki Formation complex networks is typical of basin floor sinuous channels with high sinuosity and meander amplitude. In contrast, the development of the linear upper Mount Messenger Formation gully networks is heavily influenced by the steep prograding clinoform slope of the intervening mudstone strata.

8. CRediT authorship contribution statement

This paper constitutes a chapter of the PhD thesis of the primary author. Erman H. Kamaruzaman: Conceptualization, Methodology, Visualization, Investigation, Software, Validation, and Writing - Original Draft. Andrew D. La Croix and Peter J.J. Kamp: Supervision, Conceptualization, Methodology, Writing - Review & Editing.

Declaration of competing interest

The authors declare that they have no known competing financial interests or personal relationships that could have appeared to influence the work reported in this paper.

Data availability

Data will be made available on request.

10.0 Acknowledgements

We thank Schlumberger for access to Petrel software and for access to Cegal for the Marina “Blueback" plugin used for seismic and well log interpretations made here. We also acknowledge New Zealand Petroleum and Minerals (Ministry of Business, Innovation and Employment) for access to their compilation of seismic reflection and well data for Taranaki Basin. Thanks to reviewers Jeff Peakall, Mike Mayall, Brad Prather and an anonymous reviewer. Thank you to the handling editor Francisco José Lobo.

Appendix A. Supplementary data

Supplementary data to this article can be found online at https://doi.org/10.1016/j.marpetgeo.2023.106233.

References

Allen, P.A., 2017. *Sediment Routing Systems: the Fate of Sediment from Source to Sink*. Cambridge University Press. https://doi.org/10.1017/9781316135754.

Amblas, D., Ceramicola, S., Gerber, T.P., Canals, M., Chiocci, F.L., Dowdeswell, J.A., Harris, P.T., Huvenne, V.A.I., Lai, S.Y.J., Lastras, G., Iacono, C.L., Micallef, A., Mountjoy, J.J., Paull, C.K., Puig, P., Sanchez-Vidal, A., 2018. Submarine canyons and gullies. In: Micallef, A., Krastel, S., Savini, A. (Eds.), Submarine Geomorphology. Springer International Publishing, pp. 251–272. https://doi.org/10.1007/978-3-319-57852-1_14.

Amy, L.A., 2019. A review of producing fields inferred to have upslope stratigraphically trapped turbidite reservoirs: trapping styles (pure and combined), pinch-out formation, and depositional setting. AAPG (Am. Assoc. Pet. Geol.) Bull. 103 (12), 2861–2889. https://doi.org/10.1306/02251917408.

Assis, C., Santos, H., Schleicher, J., 2018. Colored and linear inversions to relative acoustic impedance. Geophysics 84 (2). https://doi.org/10.1190/geo2018-0185.1.

Babonneau, N., Savoye, B., Cremer, M., Bez, M., 2004. Multiple terraces within the deep incised Zaire Valley (ZaïAngo Project): are they confined levees? Geol. Soc. Lond. Special Publ. 222 (1), 91–114. https://doi.org/10.1144/GSL.SP.2004.222.01.06.

Baur, J.R., King, P.R., Stern, T., Leitner, B., Wood, L.J., Simo, T.T., Rosen, N.C., 2010. Development and seismic geomorphology of a Miocene slope channel megasystem, offshore Taranaki Basin, New Zealand. In: Seismic Imaging of Depositional and Geomorphic Systems, 30. https://doi.org/10.5724/gcs.10.30.0618. SEPM Society for Sedimentary Geology.

Benson, S., Cook, P., 2005. Underground geological storage. In: Borm, G., Hawkins, D., Lee, A. (Eds.), IPCC Special Report on Carbon Dioxide Capture and Storage. Cambridge University Press, pp. 197–265.

Bjorlykke, K., 2010. *Petroleum geoscience: From sedimentary environments to rock physics*. Springer Science & Business Media.

Brown, A.R., 2011. Interpretation of Three-Dimensional Seismic Data. American Association of Petroleum Geologists. https://doi.org/10.1306/m4271346.

Bryant, I.D., Greenstr, C.W., 1995. Integrated 3-D geological modeling of the C1 sands reservoir, Maui field, offshore New Zealand. AAPG (Am. Assoc. Pet. Geol.) Bull. 79 https://doi.org/10.1306/8d2b152a-171e-11d7-8645000102c1865d.

Bryant, I.D., Marshall, M.G., Greenstreet, C.W., V, W.R, Cohen, J.M., Stroemmen, J.F., 1994. Integrated Geological Reservoir Modelling of the Maui Field, Taranaki Basin, New Zealand. New Zealand Petroleum Conference, Wellington, New Zealand.

Bührig, L.H., Colombera, L., Patacci, M., Mountney, N.P., McCaffrey, W.D., 2022. Tectonic influence on the geomorphology of submarine canyons: implications for deep-water sedimentary systems [original research]. Front. Earth Sci. 10 https://doi.org/10.3389/feart.2022.836823.

Bull, S., Hill, M., Strogen, D., Arnot, M., Seebeck, H., Kroeger, K., Zhu, H., 2015. Seismic Reflection Interpretation, Static Modelling and Velocity Modelling of the Southern Taranaki Basin (4D Taranaki Project), vol. 2. GNS Science Report.

Bull, S., Nicol, A., Strogen, D., Kroeger, K., Seebeck, H.S., 2019. Tectonic controls on Miocene sedimentation in the Southern Taranaki Basin and implications for New Zealand plate boundary deformation. Basin Res. 31 (2), 253–273. https://doi.org/10.1111/bre.12319.

Bussell, M.R., 1994. Seismic Interpretation of the Moki Formation on the Maui 3D Survey, Taranaki Basin. New Zealand Petroleum Conference, Wellington, New Zealand.

Chopra, S., Castagna, J., Portniaguine, O., 2006. Thin bed reflectivity inversion. In: SEG Technical Program Expanded Abstracts 2006. Society of Exploration Geophysicists, pp. 2057–2061, 10.1190/1.236994110.1190/1.2369941.

Clairmont, R., Kolawole, F., Omale, A.P., Bedle, H., 2020. Controls of pre-existing structures on clinoform architecture and the associated progradational system elements. Basin Res. 33 (2), 875–902. https://doi.org/10.1111/bre.12487.

Clark, J.D., Pickering, K.T., 1996. Architectural elements and growth patterns of submarine channels: application to hydrocarbon exploration. AAPG (Am. Assoc. Pet. Geol.) Bull. 80 (2), 194–221.

Cooper, R., Agterberg, F.P., Alloway, B., Beu, A., Campbell, H., Crampton, J.S., Crouch, E., Crundwell, M., Graham, I.J., Hollis, C., Jones, C., Kamp, P., Mildenhall, D.C., Morgans, H., Naish, T.R., Raine, J.I., Roncaglia, L., Sadler, P.M., Schiøler, P., Wilson, G., 2004. The New Zealand Geological Timescale. Institute of Geological and Nuclear Sciences, Monograph, pp. 22–284.

Covault, J.A., 2011. Submarine fans and canyon-channel systems: A review of processes, products, and models. Nat. Educ. Knowl. 3, 4.
Covault, J.A., Fildani, A., Romans, B.W., McHargue, T., 2011. The natural range of submarine canyon-and-channel longitudinal profiles. Geosphere 7 (2), 313–332. https://doi.org/10.1130/ges00610.1.
Crowhurst, P., Green, P., Kamp, P., 2002. Appraisal of (U-Th)/He apatite thermochronology as a thermal history tool for hydrocarbon exploration: an example from the Taranaki Basin, New Zealand. AAPG (Am. Assoc. Pet. Geol.) Bull. 86 https://doi.org/10.1306/61EEDD82-173E-11D7-8645000102C1865D.
Dalla Valle, G., Gamberi, F., Trincardi, F., Baglioni, L., Errera, A., Rocchini, P., 2013. Contrasting slope channel styles on a prograding mud-prone margin. Mar. Petrol. Geol. 41, 72–82. https://doi.org/10.1016/j.marpetgeo.2012.02.003.
Deptuck, M.E., Sylvester, Z., Pirmez, C., O'Byrne, C., 2007. Migration–aggradation history and 3-D seismic geomorphology of submarine channels in the Pleistocene Benin-major Canyon, western Niger Delta slope. Mar. Petrol. Geol. 24 (6–9), 406–433. https://doi.org/10.1016/j.marpetgeo.2007.01.005.
Field, M.E., Gardner, J.V., Prior, D.B., 1999. Geometry and significance of stacked gullies on the northern California slope. Mar. Geol. 154 (1), 271–286. https://doi.org/10.1016/S0025-3227(98)00118-2.
Fisher, W.L., Galloway, W.E., Steel, R.J., Olariu, C., Kerans, C., Mohrig, D., 2021. Deep-water depositional systems supplied by shelf-incising submarine canyons: 2 recognition and significance in the geologic record. Earth Sci. Rev. 214 https://doi.org/10.1016/j.earscirev.2021.103531.
Funnell, R., Stagpoole, V.M., Nicol, A., McCormack, N., Reyes, A.G., 2004. Petroleum generation and implications for migration: a Maui Field charge study, Taranaki Basin. 2004. In: New Zealand Petroleum Conference Proceedings, New Zealand.
Gales, J.A., Larter, R.D., Mitchell, N.C., Dowdeswell, J.A., 2013. Geomorphic signature of Antarctic submarine gullies: implications for continental slope processes. Mar. Geol. 337, 112–124. https://doi.org/10.1016/j.margeo.2013.02.003.
Gamboa, D., Alves, T.M., Cartwright, J., 2012. A submarine channel confluence classification for topographically confined slopes. Mar. Petrol. Geol. 35 (1), 176–189. https://doi.org/10.1016/j.marpetgeo.2012.02.011.
Gerber, T.P., Amblas, D., Wolinsky, M.A., Pratson, L.F., Canals, M., 2009. A model for the long-profile shape of submarine canyons. J. Geophys. Res.: Earth Surf. 114 (F3) https://doi.org/10.1029/2008JF001190.
Hansen, R.J., Kamp, P.J., 2002. Evolution of the Giant Foresets Formation, northern Taranaki Basin, New Zealand. In: New Zealand Petroleum Conference Proceedings, New Zealand.
Harishidayat, D., Omosanya, K.O., Johansen, S.E., Eruteya, O.E., Niyazi, Y., 2018. Morphometric analysis of sediment conduits on a bathymetric high: implications for palaeoenvironment and hydrocarbon prospectivity. Basin Res. 30 (5), 1015–1041. https://doi.org/10.1111/bre.12291, 10.1111/bre.12291.
Harris, P.T., Whiteway, T., 2011. Global distribution of large submarine canyons: geomorphic differences between active and passive continental margins. Mar. Geol. 285 (1), 69–86. https://doi.org/10.1016/j.margeo.2011.05.008.
Hayward, B.W., Wood, R.A., 1989. Computer-generated geohistory plots for Taranaki drillhole sequences. N.Z. Geol. Surv. Rep. PAL 147.
Heinemann, N., Booth, M.G., Haszeldine, R.S., Wilkinson, M., Scafidi, J., Edlmann, K., 2018. Hydrogen storage in porous geological formations – onshore play opportunities in the midland valley (Scotland, UK). Int. J. Hydrogen Energy 43 (45), 20861–20874. https://doi.org/10.1016/j.ijhydene.2018.09.149.
Hewlett, J.S., Jordan, D.W., Weimer, P., Posamentier, H., 1993. Stratigraphic and combination traps within a seismic sequence framework, Miocene stevens turbidites, bakersfield arch, California. In: Siliciclastic Sequence Stratigraphy: Recent Developments and Applications, 58. https://doi.org/10.1306/m58581c6. American Association of Petroleum Geologists.
Higgs, K., King, P., 2018. Sandstone provenance and sediment dispersal in a complex tectonic setting: Taranaki Basin, New Zealand. Sediment. Geol. 372 https://doi.org/10.1016/j.sedgeo.2018.05.004.
Hsu, R.T., Liu, J.T., 2010. In-situ estimations of the density and porosity of flocs of varying sizes in a submarine canyon. Mar. Geol. 276 (1–4), 105–109. https://doi.org/10.1016/j.margeo.2010.07.003.
Hughes, D.J., Shimmield, T.M., Black, K.D., Howe, J.A., 2015. Ecological impacts of large-scale disposal of mining waste in the deep sea. Sci. Rep. 5, 9985. https://doi.org/10.1038/srep09985.
Huvenne, V.A.I., Davies, J.S., 2014. Towards a new and integrated approach to submarine canyon research. Deep Sea Res. Part II Top. Stud. Oceanogr. 104, 1–5. https://doi.org/10.1016/j.dsr2.2013.09.012.
Jobe, Z.R., Lowe, D.R., Uchytil, S.J., 2011. Two fundamentally different types of submarine canyons along the continental margin of Equatorial Guinea. Marine and Petroleum Geology 28 (3), 843–860. https://doi.org/10.1016/j.marpetgeo.2010.07.012.
Kallweit, R.S., Wood, L.C., 1982. The limits of resolution of zero-phase wavelets. Geophysics 47 (7), 1035–1046. https://doi.org/10.1190/1.1441367.
Kamp, P., Green, P., 1990. Thermal and tectonic history of selected Taranaki Basin (New Zealand) wells assessed by apatite fission track analysis. Aapg Bulletin - AAPG BULL 74, 1401–1419.
Kamp, P., Green, P., White, S., 1989. Fission track analysis reveals character of collisional tectonics in New Zealand. Tectonics 8, 169–195. https://doi.org/10.1029/TC008i002p00169.
Kane, I.A., Clare, M.A., Miramontes, E., Wogelius, R., Rothwell, J.J., Garreau, P., Pohl, F., 2020. Seafloor microplastic hotspots controlled by deep-sea circulation. Science 368 (6495), 1140–1145. https://doi.org/10.1126/science.aba5899.
King, P., Thrasher, G.P., 1996. Cretaceous-cenozoic geology and petroleum systems of the Taranaki Basin, New Zealand. Inst. Geol. Nucl. Sci. Monogr. 13 (Part 1 and 2).
Kolla, V., Posamentier, H.W., Wood, L.J., 2007. Deep-water and fluvial sinuous channels—characteristics, similarities and dissimilarities, and modes of formation. Mar. Petrol. Geol. 24 (6), 388–405. https://doi.org/10.1016/j.marpetgeo.2007.01.007.
Kroeger, K.F., Thrasher, G.P., Sarma, M., 2019. The evolution of a middle Miocene deep-water sedimentary system in northwestern New Zealand (Taranaki Basin): depositional controls and mechanisms. Mar. Petrol. Geol. 101, 355–372. https://doi.org/10.1016/j.marpetgeo.2018.11.052.
Lancaster, S., & Whitcombe, D. (2000). Fast-track 'coloured' inversion. In *SEG Technical Program Expanded Abstracts 2000* (pp. 1572-1575). https://doi.org/10.1190/1.1815711Lancaster, S., Whitcombe, D., 2000. Fast-track 'coloured' Inversion. SEG Annual Meeting 2000.
Lemay, M., Grimaud, J.-L., Cojan, I., Rivoirard, J., Ors, F., 2020. Geomorphic variability of submarine channelized systems along continental margins: comparison with fluvial meandering channels. Mar. Petrol. Geol. 115 https://doi.org/10.1016/j.marpetgeo.2020.104295.
Lintern, D.G., Hill, P.R., Stacey, C., 2016. Powerful unconfined turbidity current captured by cabled observatory on the Fraser River delta slope, British Columbia, Canada. Sedimentology 63 (5), 1041–1064. https://doi.org/10.1111/sed.12262.
Lofi, J., Rabineau, M., Gorini, C., Berne, S., Clauzon, G., De Clarens, P., Tadeu Dos Reis, A., Mountain, G.S., Ryan, W.B.F., Steckler, M.S., Fouchet, C., 2003. Plio–quaternary prograding clinoform wedges of the western gulf of lion continental margin (NW mediterranean) after the messinian salinity crisis. Mar. Geol. 198 (3–4), 289–317. https://doi.org/10.1016/s0025-3227(03)00120-8.
Lonergan, L., Jamin, N.H., Jackson, C.A.L., Johnson, H.D., 2013. U-shaped slope gully systems and sediment waves on the passive margin of Gabon (West Africa). Mar. Geol. 337, 80–97. https://doi.org/10.1016/j.margeo.2013.02.001.
Maurya, S.P., Singh, N.P., 2017. *Seismic Colored Inversion: A Fast Way to Estimate Rock Properties from the Seismic Data* Challenges in Petro-Physical Evaluation and Rock Physics Modelling of Carbonate Reservoirs. Likely Elucidations & Way Forward, Victor Menezes Convention Centre (VMCC), IIT Bombay, India, 30th November -01st December 2017).
May, J.A., Warme, J.E., Slater, R.A., Stanley, D.J., Moore, G.T., 1983. Role of submarine canyons on shelfbreak erosion and sedimentation: modern and ancient examples. In: The Shelfbreak: Critical Interface on Continental Margins, 33. https://doi.org/10.2110/pec.83.06.0315. SEPM Society for Sedimentary Geology.
Mayall, M., Kneller, B., 2021. Seismic interpretation workflows for deep-water systems: a practical guide for the subsurface. AAPG (Am. Assoc. Pet. Geol.) Bull. 105 (11), 2127–2157. https://doi.org/10.1306/05262120094.
McCaffrey, W., Kneller, B., 2001. Process controls on the development of stratigraphic trap potential on the margins of confined turbidite systems and aids to reservoir evaluation. AAPG (Am. Assoc. Pet. Geol.) Bull. 85 (6), 971–988. https://doi.org/10.1306/8626ca41-173b-11d7-8645000102c1865d.
Miall, A.D., 2002. Architecture and sequence stratigraphy of Pleistocene fluvial systems in the Malay Basin, based on seismic time-slice analysis. AAPG (Am. Assoc. Pet. Geol.) Bull. 86.
Micallef, A., Mountjoy, J.J., 2011. A topographic signature of a hydrodynamic origin for submarine gullies. Geology 39 (2), 115–118. https://doi.org/10.1130/g31475.1.
Mitchell, N.C., 2005. Interpreting long-profiles of canyons in the USA Atlantic continental slope. Mar. Geol. 214 (1), 75–99. https://doi.org/10.1016/j.margeo.2004.09.005.
Normark, W.R., Posamentier, H., Mutti, E., 1993. Turbidite systems: state of the art and future directions. Rev. Geophys. 31 (2), 91–116. https://doi.org/10.1029/93RG02832, 10.1029/93RG02832.
New Zealand Petroleum Exploration Data Pack, New Zealand Petroleum and Minerals, 2018.
Othman, A.A.A., Fathy, M., Negm, A., 2019. Identification of channel geometries applying seismic attributes and spectral decomposition techniques, Temsah Field, Offshore East Nile Delta, Egypt. NRIAG J. Astronomy Geophys. 7 (1), 52–61. https://doi.org/10.1016/j.nrjag.2018.04.001.
Palm, F.A., Peakall, J., Hodgson, D.M., Marsset, T., Silva Jacinto, R., Dennielou, B., Babonneau, N., Wright, T.J., 2021. Width variation around submarine channel bends: implications for sedimentation and channel evolution. Mar. Geol. 437, 106504 https://doi.org/10.1016/j.margeo.2021.106504.
Patruno, S., Hampson, G.J., Jackson, C.A.L., 2015. Quantitative characterisation of deltaic and subaqueous clinoforms. Earth Sci. Rev. 142, 79–119. https://doi.org/10.1016/j.earscirev.2015.01.004.
Peakall, J., McCaffrey, B., Kneller, B., 2000. A process model for the evolution, morphology, and architecture of sinuous submarine channels. J. Sediment. Res. 70 (3), 434–448. https://doi.org/10.1306/2dc4091c-0e47-11d7-8643000102c1865d.
Peakall, J., Sumner, E.J., 2015. Submarine channel flow processes and deposits: a process-product perspective. Geomorphology 244, 95–120. https://doi.org/10.1016/j.geomorph.2015.03.005.
Pirmez, C., Pratson, L.F., Steckler, M.S., 1998. Clinoform development by advection-diffusion of suspended sediment: modeling and comparison to natural systems. J. Geophys. Res. Solid Earth 103 (B10), 24141–24157. https://doi.org/10.1029/98JB01516.
Posamentier, H.W., Kolla, V., 2003. Seismic geomorphology and stratigraphy of depositional elements in deep-water settings. J. Sediment. Res. 73 (3), 367–388. https://doi.org/10.1306/111302730367 (SEPM (Society for Sedimentary Geology)).
Posamentier, H.W., Paumard, V., Lang, S.C., 2022. Principles of seismic stratigraphy and seismic geomorphology I: extracting geologic insights from seismic data. Earth Sci. Rev. 228 https://doi.org/10.1016/j.earscirev.2022.103963.
Prélat, A., Pankhania, S.S., Jackson, C.A.L., Hodgson, D.M., 2015. Slope gradient and lithology as controls on the initiation of submarine slope gullies; Insights from the

North Carnarvon Basin, Offshore NW Australia. Sediment. Geol. 329, 12–17. https://doi.org/10.1016/j.sedgeo.2015.08.009.
Qin, Y., Alves, T.M., Constantine, J., Gamboa, D., 2016. Quantitative seismic geomorphology of a submarine channel system in SE Brazil (Espírito Santo Basin): scale comparison with other submarine channel systems. Mar. Petrol. Geol. 78, 455–473. https://doi.org/10.1016/j.marpetgeo.2016.09.024.
Raza, A., Gholami, R., Rezaee, R., Bing, C.H., Nagarajan, R., Hamid, M.A., 2018. CO2 storage in depleted gas reservoirs: a study on the effect of residual gas saturation. Petroleum 4 (1), 95–107. https://doi.org/10.1016/j.petlm.2017.05.005.
Ricketts, B.D., Evenchick, C.A., 1999. Shelfbreak gullies; products of sea-level lowstand and sediment failure; examples from Bowser Basin, northern British Columbia. J. Sediment. Res. 69 (6), 1232–1240. https://doi.org/10.2110/jsr.69.1232.
Roncaglia, L., M. M, Crundwell, M.P., Miko, Fohrmann, Morgans, H.E.G., 2013. Well Log Stratigraphy in the Central and Southern Offshore Area of the Taranaki Basin, New Zealand. Lower Hutt : GNS Science.
Seebeck, H., Thrasher, G.P., Viskovic, G.P., 2020. Inversion history of the northern Tasman Ridge, Taranaki Basin, New Zealand: implications for petroleum migration and accumulation. N. Z. J. Geol. Geophys. 63 (3), 299–323. https://doi.org/10.1080/00288306.2019.1695633.
Shanmugam, G., 2016. Submarine fans: a critical retrospective (1950–2015). J. Palaeogeogr. 5 (2), 110–184. https://doi.org/10.1016/j.jop.2015.08.011.
Shepard, F.P., 1965. Types of submarine valleys. AAPG Bulletin 49 (3), 304–310.
Shepard, F.P., 1981. Submarine canyons: multiple causes and long-time Persistence1. AAPG (Am. Assoc. Pet. Geol.) Bull. 65 (6), 1062–1077. https://doi.org/10.1306/03b59459-16d1-11d7-8645000102c1865d.
Shepard, F.P., Marshall, N.F., McLoughlin, P.A., 1974. Currents in submarine canyons. Deep Sea Research and Oceanographic Abstracts 21 (9), 691–706. https://doi.org/10.1016/0011-7471(74)90077-1.
Shumaker, L.E., Jobe, Z.R., Graham, S.A., 2017. Evolution of submarine gullies on a prograding slope: insights from 3D seismic reflection data. Mar. Geol. 393, 35–46. https://doi.org/10.1016/j.margeo.2016.06.006.
Shumaker, L.E., Jobe, Z.R., Johnstone, S.A., Pettinga, L.A., Cai, D., Moody, J.D., 2018. Controls on submarine channel-modifying processes identified through morphometric scaling relationships. Geosphere 14 (5), 2171–2187. https://doi.org/10.1130/ges01674.1.
Stow, D.A.V., Mayall, M., 2000. Deep-water sedimentary systems: new models for the 21st century. Mar. Petrol. Geol. 17 (2), 125–135. https://doi.org/10.1016/S0264-8172(99)00064-1.
Strogen, D.P., Baur, J.R., Bland, K.J., King, P.R., Vonk, A.J., Kamp, P.J.J., 2011. Updated Paleogeographic Maps for the Taranaki Basin and Surrounds. GNS Science, Issue. Report 2010/53.
Strong, N., Paola, C., 2008. Valleys that never were: time surfaces versus stratigraphic surfaces. J. Sediment. Res. 78 (8), 579–593.
Sylvester, Z., Pirmez, C., Cantelli, A., 2011. A model of submarine channel-levee evolution based on channel trajectories: implications for stratigraphic architecture. Mar. Petrol. Geol. 28 (3), 716–727. https://doi.org/10.1016/j.marpetgeo.2010.05.012.
Talling, P.J., 2014. On the triggers, resulting flow types and frequencies of subaqueous sediment density flows in different settings. Mar. Geol. 352, 155–182. https://doi.org/10.1016/j.margeo.2014.02.006.
Taner, M.T., 2001. Seismic attributes. CSEG Recorder 26 (7), 48–56.
Tippett, J.M., Kamp, P.J., 1993. Fission track analysis of the late Cenozoic vertical kinematics of continental Pacific crust, South Island, New Zealand. J. Geophys. Res.: Sol. Earth 98 (B9), 16119–16148.
Weimer, P., Slatt, R.M., 2004. Petroleum Systems of Deepwater Settings. In: *Petroleum Systems of Deepwater Settings*, pp. i–xviii.
Widess, M.B., 1973. How thin is a thin bed? Geophysics 38 (6), 1176–1180. https://doi.org/10.1190/1.1440403.
Wynn, R.B., Cronin, B.T., Peakall, J., 2007. Sinuous deep-water channels: genesis, geometry and architecture. Mar. Petrol. Geol. 24 (6–9), 341–387. https://doi.org/10.1016/j.marpetgeo.2007.06.001.
Zeng, H., 2013. Stratal slice: The next generation. Leading Edge 32 (2), 140–144.
Zeng, H., Backus, M.M., Barrow, K.T., Tyler, N., 1998. Stratal slicing; Part 1, Realistic 3-D seismic model. Geophysics 63 (2), 502–513.
Zeng, H., Hentz, T.F., Wood, L.J., 2001. Stratal slicing of Miocene-Pliocene sediments in Vermilion block 50-Tiger Shoal area, offshore Louisiana. Leading Edge 20 (4), 408–418.

Marine and Petroleum Geology 161 (2024) 106664

Contents lists available at ScienceDirect

Marine and Petroleum Geology

journal homepage: www.elsevier.com/locate/marpetgeo

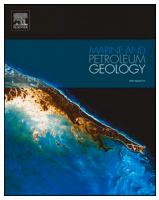

Critical re-assessment of Middle and Late Miocene submarine fans in offshore southern and western Taranaki Basin, New Zealand, to update the paleogeography

Erman H. Kamaruzaman *, Andrew D. La Croix, Peter J.J. Kamp

Sedimentary Environments and Analogues Research Group, Earth and Environmental Sciences, School of Science, University of Waikato, Private Bag 3105, Hamilton, 3240, New Zealand

ARTICLE INFO

Keywords:
Moki Formation
Mount Messenger Formation
Taranaki Basin
Miocene
Paleogeography
Deep-water sedimentary systems
New Zealand

ABSTRACT

The purpose of this paper is (i) to re-assess the presence of submarine fan systems of Middle and Late Miocene age (Moki and Mount Messenger formations) previously mapped on the continental slope in offshore southern and central Taranaki Basin, New Zealand, and (ii), to demonstrate the occurrence of two newly mapped Late Miocene submarine fans in the deep-water part of offshore western Taranaki Basin, based on accepted seismic stratigraphic criteria for submarine fans. In our work we have found that the fans previously mapped amongst canyons and channels in the Moki and Mount Messenger formations on the upper and middle continental slope in southern and central Taranaki Basin do not fulfil established stratal criteria for submarine fan deposits. Moreover, detuning of 3D seismic reflection volumes for the Moki and Mount Messenger formation intervals ahead of amplitude attribute extraction, shows that the strata previously mapped as submarine fans based on amplitude alone, are merely artifacts of bed thickness. The two new fans systems of Late Miocene age that we map here, both attributed to the Mount Messenger Formation, principally comprise mudstone and represent a minor proportion of the Late Miocene succession that accumulated in southern and central parts of the basin. Our remapping of slope canyons and channels in the southern part of the basin and the identification of the two new fan systems in the western part of the basin are embodied in three new paloegeographic maps for the Middle and Late Miocene development of Taranaki Basin. A modern analogue for the two new Late Miocene fans in Taranaki Basin is the Hikurangi Fan at the terminus of the Hikurangi Channel, located outboard of the modern subduction zone of the Hikurangi margin along Eastern North Island. The new Taranaki Basin deep-water fans documented here, may have significance for hydrocarbon exploration in deep water parts of Taranaki Basin, which is largely unexplored.

1. Introduction

There is continuing interest amongst the petroleum exploration sector and the research community in the characteristics and distribution of ancient deepwater sedimentary systems. The increasing coverage and availability of 3D seismic reflection datasets, coupled with the availability of sophisticated seismic reflection mapping methods (e.g., Posamentier et al., 2022), have contributed to this interest. In parallel, there have been conceptual developments in the marine geomorphology of Recent distributary sedimentary systems, such as channel networks, submarine fans, and continental slope debris flows (e.g., Stow and Mayall, 2000; Shanmugam, 2013; Mayall and Kneller, 2021; Mitchell et al., 2023). One method in particular, seismic amplitude extraction, is widely used in mapping ancient depositional systems, such as fans. However it is now recognized that detuning of seismic reflection data within the interval of interest must be undertaken prior to amplitude extraction to avoid tuning-related effects that possibly result in erroneous geological interpretations, leading to inaccurate paleogeographical maps (Bunt, 2015; Francis, 2015, 2016; Ab Fatah et al., 2016; Márquez et al., 2021).

In our work reported here, we consider this to have been the case with respect to the Miocene submarine fans mapped by prior researchers in southern Taranaki Basin (Fig. 1) (Grain, 2008; Baur et al., 2010; Kroeger et al., 2019). The Root Mean Square (RMS) seismic attribute

* Corresponding author.
E-mail address: ek100@students.waikato.ac.nz (E.H. Kamaruzaman).

https://doi.org/10.1016/j.marpetgeo.2023.106664
Received 17 May 2023; Received in revised form 5 December 2023; Accepted 20 December 2023
Available online 27 December 2023

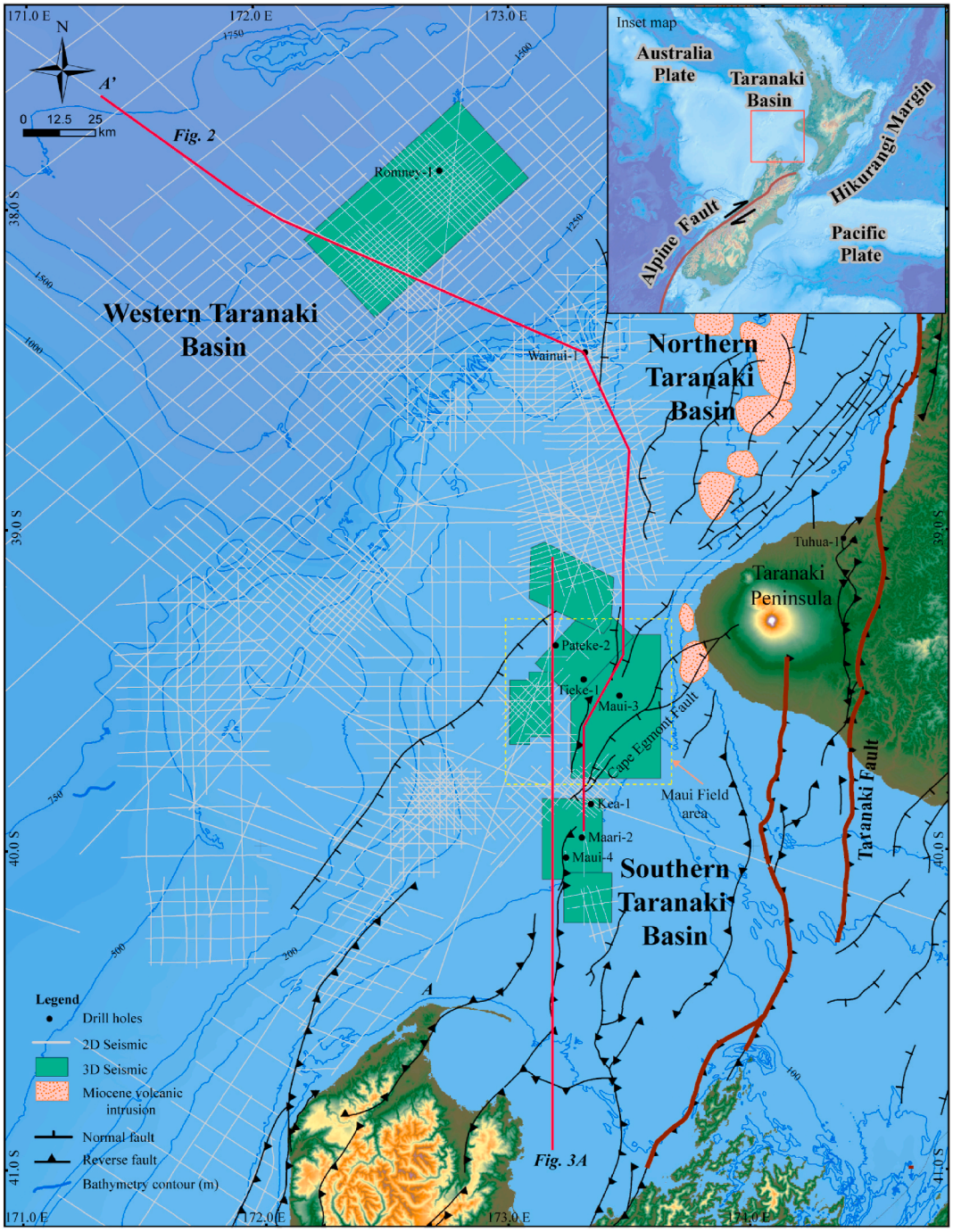

Fig. 1. Map of the study area in Taranaki Basin, New Zealand, showing the location of 2D and 3D seismic surveys and some drill holes relevant to this study. GIS data from NZP&M (20182). Refer Figure i in Supplementary Data for more information.

interpretation presented in those studies did not account for thin-bed tuning-related effects in deeply buried ancient strata (Simm and Bacon, 2014; Francis, 2016). In addition, the mapped Miocene fans do not fulfil the established stratal criteria (Posamentier and Erskine, 1991) that are commonly adapted in the identification of ancient fans. This study aims to re-evaluate the Middle and Late Miocene deep-water sedimentary system in southern, central and western offshore Taranaki Basin. We achieve this by objectively deconstructing the basis for prior mapping of submarine fans, and then we build the case for two fans in distal deep-water parts of offshore western Taranaki Basin. Our results are embodied in three updated Middle and Late Miocene paleogeographic maps for Taranaki Basin. The paleogeographic maps are relevance for reservoir exploration in the deep-water parts of the basin, of which largely unexplored.

Our work builds upon the results in a companion paper (Kamaruzaman et al., 2023) that fully analysed and parameterised the morphology of canyons, channels and gullies in the Middle and Late Miocene continental slope succession of offshore southern and central Taranaki Basin. That study established the importance of the increasing depositional slope angle through time upon the change in conduit type expressed within the slope succession, due to an increase in the rate of terrigenous sediment supply to the basin. We build upon that work by extending it to the deep water occurrence and characteristics of two new submarine fans in offshore western Taranaki Basin.

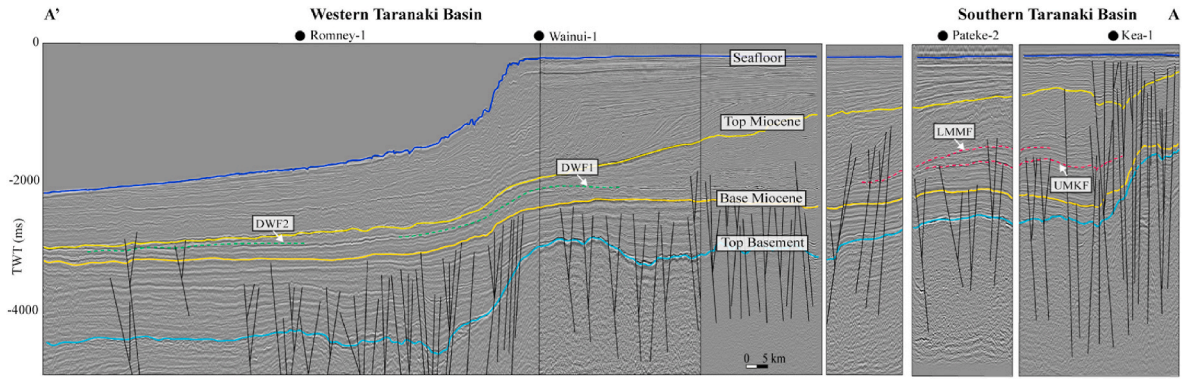

Fig. 2. Interpreted regional composite seismic line showing the main reflectors that mark the base and top of the Miocene succession. See Fig. 1 for the section location. The approximate location for interpreted fans by Kroeger et al., 2019) are upper Moki Formation Fan (UMKF) and lower Mount Messenger Formation Fan (LMMF) in the Southern Taranaki Basin region (Miocene slope). This study interpreted deep-water fans as Mount Messenger Deep Water Fan 1 (DWF1) and Deep Water Fan 2 (DWF2), located in the Western Taranaki Basin region (Miocene lower slope and basin plain).

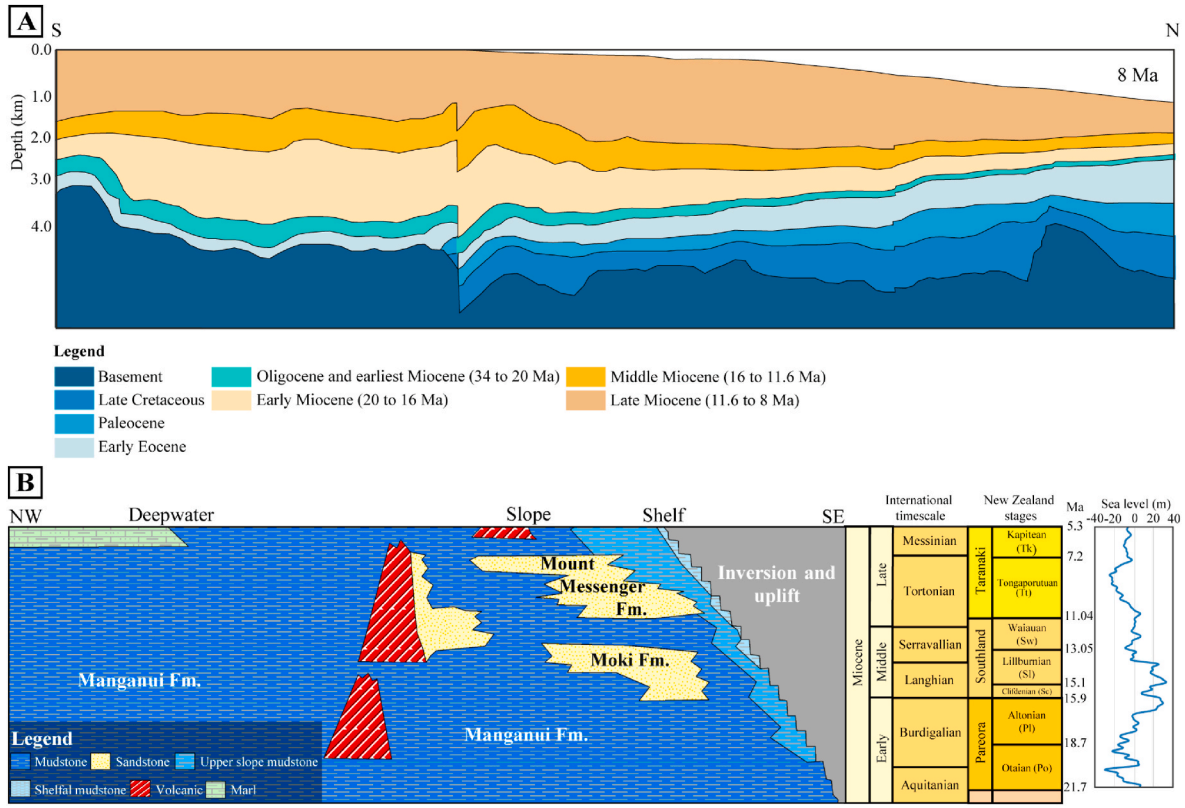

Fig. 3. (A) South to north cross section showing the generalised Late Cretaceous to Late Miocene stratigraphy of southern Taranaki Basin at ~8 Ma, based on basin modelling (simplified from Bull et al., 2019); See Fig. 1 for the section location. (B) Chronostratigraphic diagram and sea level curve for Taranaki Basin showing that the Moki Formation was deposited during the Early to Middle Miocene and the Mount Messenger Formation during the Late Miocene. Manganui Formation is the mudstone that encloses the Moki and Mount Messenger formations (chronostratigraphy simplified from Bull et al., 2019; sea level curve from Miller et al., 2020).

2. Geological setting of Taranaki Basin

Taranaki Basin is a long-lived (Late Cretaceous – Cenozoic) depocenter offshore of central-western North Island (Fig. 1). This basin formed during three phases of crustal extension, followed by crustal shortening and then late extension (backarc to the modern Hikurangi margin subduction zone) (King and Thrasher, 1996; Strogen et al., 2022). The first phase of extension is considered to have occurred during c. 105–c. 83 Ma (Albanian – Campanian) (Strogen et al., 2017); the second occurred during 80–55 Ma (Campanian – Ypresian), concurrent with seafloor spreading in the Tasman Sea (King and Thrasher, 1996; Gaina et al., 1998; Strogen et al., 2017). The third phase of extension occurred during 38–28 Ma (Bartonian – Rupelian) and only affected southern Taranaki Basin (King and Thrasher, 1996; Strogen et al., 2014). These early extension phases set forth the bathymetric deepening of Taranaki Basin towards New Caledonia Basin (Strogen et al., 2022), affecting later sedimentation in the basin (King and Thrasher, 1996). Crustal shortening started in North Taranaki Basin during the Late Eocene to Early Oligocene, affecting central and southern Taranaki Basin during the Late Oligocene and Neogene (King and Thrasher, 1996; Campbell et al., 2003; Stagpoole and Nicol, 2008; Bierbrauer et al., 2008; Strogen et al., 2014). This shortening was focussed within the

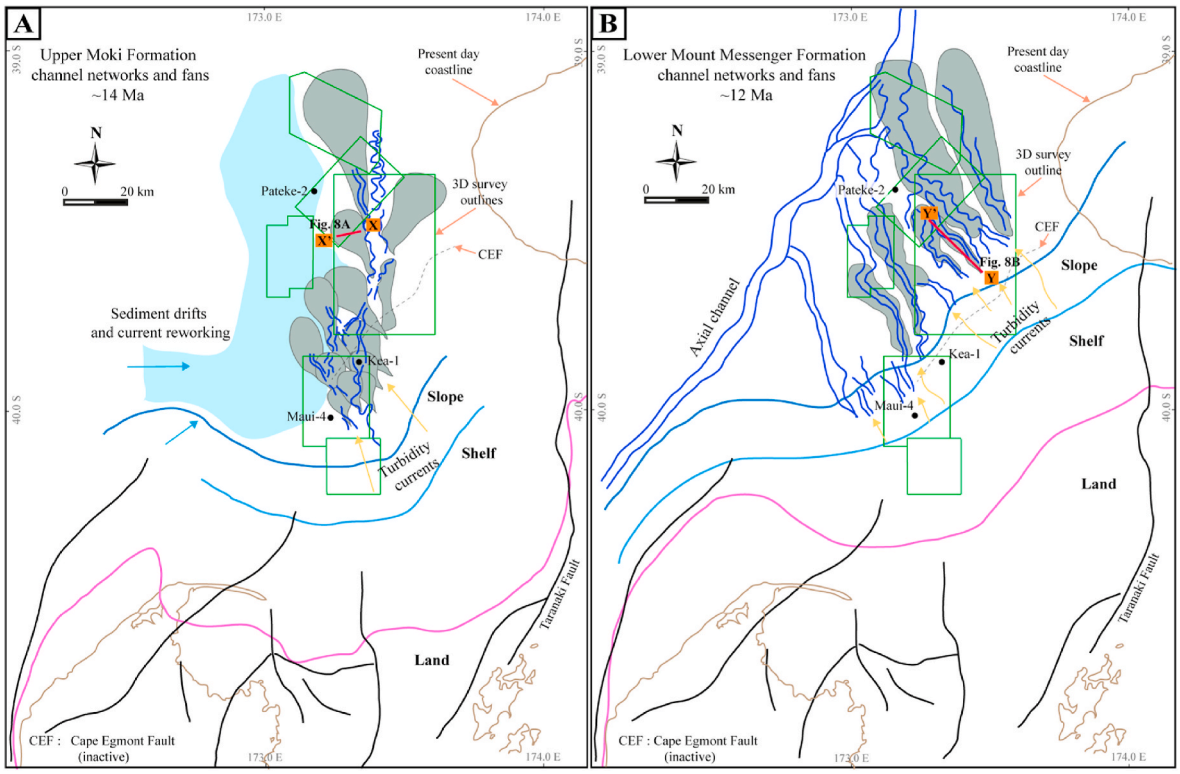

Fig. 4. Paleogeography maps of Kroeger et al. (2019) showing the location and distribution of: (A) upper Moki Formation channels and fans (Lillburnian Stage (Sl), ~14 Ma); and (B) lower Mount Messenger Formation channels and fans (Waiauan (Sw) to Early Tongaporutuan (Tt) stages, ~13–12 Ma) in southern and central Taranaki Basin. The approximate location of the upper Moki Formation Fan (UMKF) and lower Mount Messenger Formation Fan (LMMF) are shown in Fig. 2.

Taranaki Fault System along the eastern margin of the basin.

The structural development of Taranaki Basin is expressed in its stratigraphy (Figs. 2 and 3A), as detailed by King and Thrasher (1996), which remains the most complete description of the basin and its development. Fig. 3B shows a simplified chronostratigraphy of the Miocene succession in Taranaki Basin. Important stratigraphic elements of the Miocene succession are the dominance of mudstone facies (Manganui Formation) and the occurrence of two sandstone intervals within it (Moki and Mount Messenger formations). Inversion of southern Taranaki Basin started around 12 Ma (Serravallian) (Kamp and Green, 1990; Crowhurst et al., 2002), involving reversal of the sense of throw on prior normal faults (King and Thrasher, 1996). This inversion resulted in erosion of the late-Early and Middle Miocene succession that had accumulated in southernmost parts of the basin. It forced progradation of the shelf-slope system northward and westward through the basin, culminating in the Pliocene – Pleistocene accumulation of the Giant Foresets Formation in North Taranaki Basin (Fig. 2) (Hansen and Kamp, 2002; Kamp et al., 2004). Most of the pre-12 Ma sediment was probably sourced from the Oligocene and Miocene thrust belt along the eastern margin of the basin and from basement along its southern margin. From 12 Ma onwards, the sediment supplied to the basin was mostly sourced from crustal shortening, uplift and erosion of basement in the Southern Alps, South Island (Kamp et al., 1989; Tippett and Kamp, 1993). Hence the Moki Formation (~16–13 Ma, Late Altonian to Early Lillburnian stages) had a different provenance to that of the Mount Messenger Formation, which started accumulating at about 12 Ma (latest Middle Miocene, ~12 Ma, Waiauan Stage) concurrent with the start of intra-basin inversion.

In this study we have analysed the upper Moki Formation (age duration ~14–13 Ma, Lillburnian Stage; Cooper et al., 2004) and the Mount Messenger Formation (age duration ~12–6 Ma, Waiauan, Tongaporutuan and Kapitean stages) (Fig. 3A) in southern, central and western Taranaki Basin. Stage boundaries have been located on biostratigraphic criteria in drill hole sections (Roncaglia et al., 2013) and we have tied them to seismic reflection data in the study area. In this study we have adopted the spatial positions of morphological boundaries (shelf-slope break; upper, middle and lower slope) determined for the basin during its Miocene development by previous paleoecological work on drill hole samples in combination with seismic reflection mapping, as shown on the paleogeographic maps in Strogen et al. (2011) (see Table i in Supplementary Data). Both the Moki and Mount Messenger formations accumulated on the continental slope at the time and in deeper water parts of the basin plain towards the New Caledonia Basin. The Miocene section thins westward towards the basin plain from a thickness of 1700 m in the vicinity of the Maui Oil Field (Maui-3 drill hole; upper slope position) to 700 m in deep Taranaki Basin (Romney-1 drill-hole) (Fig. 1).

3. Context for our re-assessment of Miocene fans in Taranaki Basin

In our analysis we have critically re-assessed the occurrence of Miocene submarine fans in southern and central Taranaki Basin, as reported most recently by Kroeger et al. (2019) for the upper Moki Formation and for the lower Mount Messenger Formation (Fig. 4). We do not address the lower Moki Formation fans reported by Kroeger et al. (2019) because there are no stratal patterns defining their extent and internal depositional fabric. Hence we cannot map them to demonstrate that they do not show the accepted stratal patterns of submarine fans. Nevertheless, their study was the first to apply amplitude extraction to map the extent of Miocene submarine fans in Taranaki Basin, which was an advance upon the mapping of their extent based upon wireline log interpretations alone (e.g., Strogen et al., 2011).

The work on Miocene submarine fan occurrence in Taranaki Basin was originally undertaken by petroleum company geologists (e.g., de Bock, 1994; Bussell, 1994). The first research-based investigation of the

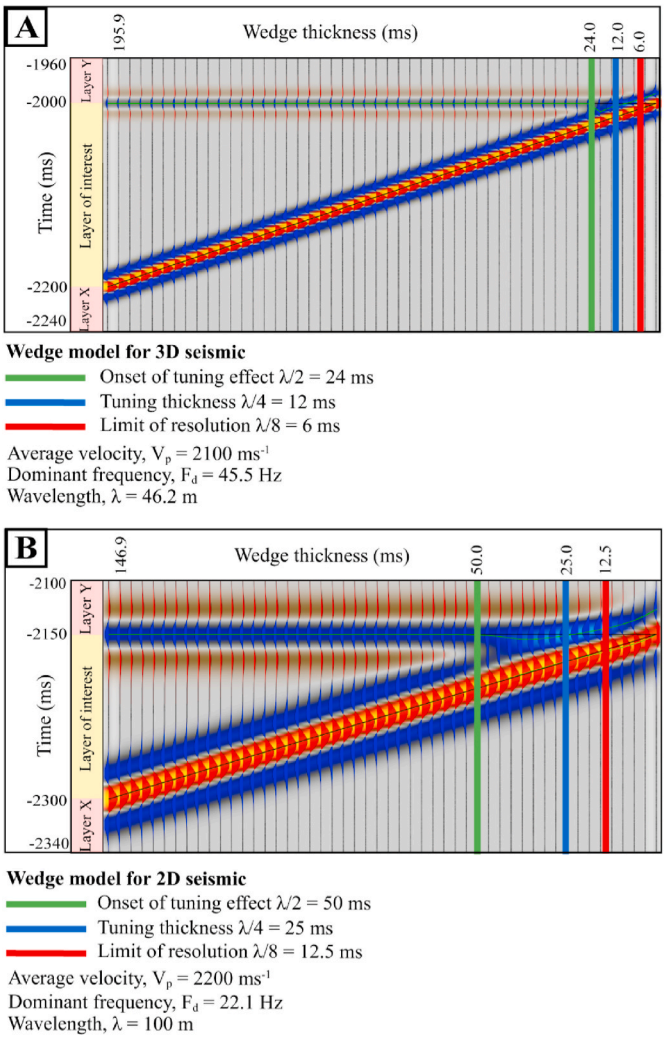

Fig. 5. Example wedge models for (A) 2D seismic data and (B) 3D seismic data from Taranaki Basin. Each example model uses a different velocity and frequency. The models show the thickness at the onset of the tuning effect (24 ms in A and 50 ms in B), the tuning thickness (12 ms in A and 25 ms in B), and the limit of resolution (6 ms in A and 12.5 ms in B). Calculations are based on Widess (1973).

Moki and Mount Messenger formations was undertaken by King and Thrasher (1996). They reported that these two sandstone formations were characterised by high amplitude signals in seismic reflection profiles, and based on this feature and wireline log interpretations, mapped the distribution of channels and fans. King and Thrasher's (1996) interpretations were strongly informed by down-hole tabular or blocky SP and gamma-ray log motifs (e.g., in Maui-4 and Te Whatu-2 records). Their extensive Moki and Mount Messenger fan interpretations were reported in a series of paleogeographic maps. A second generation of paleogeographic maps showing the extent of canyons, channels and fans in the Moki and Mount Messenger formations was reported by Strogen et al. (2011). Seven paleogeographic maps cover the interval from 16.5 to 7.2 Ma. These maps draw heavily upon the fan extents shown in King and Thrasher (1996), although they were modified to be consistent with new paleobathymetric data. Attribute mapping in selected areas and seismic facies mapping are claimed to have assisted in the remapping of these submarine fans (Strogen et al., 2011), although no details were given. The mapping of submarine fans and channels by Kroeger et al. (2019) is the most recent contribution and the first to have used amplitude extraction to map these depositional elements. Hence we refer to that work in relation to demonstrating the importance of

Table 1
List of stratal patterns used to identify fans in seismic data, as outlined by Posamentier and Erskine (1991).

1. Reflectors pinch out against high seafloor topography.
2. Continuous high-amplitude reflectors onlap basin margin.
3. Bidirectional downlap reflectors within the fans or lobes.
4. External mounding on the fan top bounding surface.

detuning seismic reflection data within the intervals ahead of amplitude extraction and mapping. The outcome is that we dismiss all of the lobes and fans in their upper Moki and Mount Messenger formation palaeogeographic maps (Fig. 4). Separately, we have mapped the occurrence and character of two new distal deep-water fans in offshore western Taranaki Basin, which we attribute to lying within the lower and uppermost Mount Messenger Formation. Strogen et al. (2011) also reported the distribution of submarine fans beneath on land Taranaki Peninsula and in offshore North Taranaki Basin. They were not considered in the Kroeger et al. (2019) study. Neither have we re-assessed those "fans" here, although our investigations in eastern parts of offshore North Taranaki Basin and the well known coastal outcrop section so far do not support their occurrence in those areas; rather, we regard the sandstone beds as slope deposits, including as channels and gully fills.

4. Data and methods

This study utilises 6550 km^2 of 3D and 24,000 km of 2D seismic reflection data as well as petrophysical well log data for 14 drill holes (see Table ii in Supplementary Data) accessed through the New Zealand Petroleum and Minerals database (https://www.data.nzpam.govt.nz) (Fig. 1). The quality of the 2D and 3D seismic data (see Table iii in Supplementary Data) is good to excellent. These data were examined using integrated methodologies that leverage several key disciplines, including seismic interpretation, seismic stratigraphy, seismic attributes analysis, well log interpretation and seismic geomorphology.

Coloured inversion was implemented to the 3D seismic volumes to boost the low-frequency seismic response, thereby increasing the resolution of the seismic data in the intervals of interest (Lancaster and Whitcombe, 2000; Maurya and Singh, 2017; Assis et al., 2018). Synthetic seismographs were then aligned with the seismic data to guide the mapping of regional horizons, while incorporating biostratigraphy markers from Roncaglia et al. (2013). For time-depth conversion, a regional velocity model was constructed using borehole checkshot data. The average seismic velocity of the Miocene interval ranged from 1200 to 3000 ms^{-1}, with a mean value of 2200 ms^{-1}.

The effects of thin-bed tuning on seismic data due to constructive and destructive interference (Simm and Bacon, 2014), were assessed using wedge models analysed in the Cegal Blueback plugin for Petrel (https://www.cegal.com/en/software) (Fig. 5). A process of seismic amplitude detuning was carried out to leave only meaningful seismic amplitudes in the data (Brown et al., 1986; Bunt, 2015; Francis, 2015; Guo et al., 2015; Ab Fatah et al., 2016).

Mapping geomorphological elements began with identifying and mapping major canyon and channel networks because they are the sediment conduits necessary to build submarine fans. Their mouths are where fans are expected to develop (Posamentier and Erskine, 1991; Covault et al., 2012; Deptuck and Sylvester, 2018; Fildani et al., 2021). Next, we compared the seismic reflection patterns in the interval of interest against specific seismic stratal pattern criteria developed by previous workers for identifying submarine fans (e.g., Sarg and Skjold, 1982; Mitchum et al., 1985; Posamentier and Erskine, 1991) (Table 1). These criteria include: (i) pinch out of reflectors against high paleo-seafloor topography, (ii) continuous high-amplitude reflectors that onlap basin margins, (iii) the occurrence of bidirectional downlapping reflectors within fans or lobes, and (iv), subtle low-relief

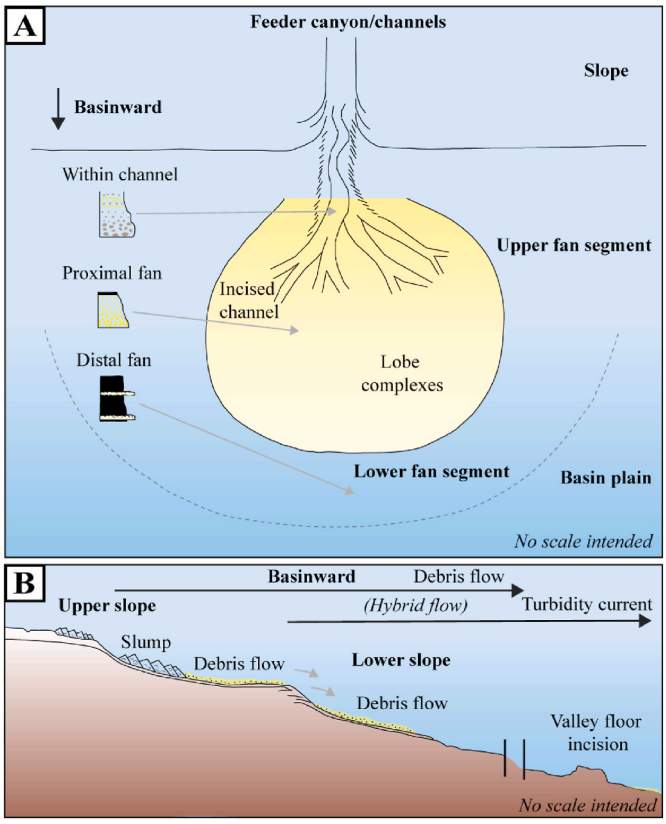

Fig. 6. (A) Conceptual model of an ancient fan system used in this study that demonstrates the fan system comprises an upper fan segment, including feeder and distributary channels and a lower fan segment on a shallower slope gradient of the basin plain (modified from Walker, 1978). This study adapted this fan model to map the Miocene fans' divisions and the associate feeder canyons and/or channel networks on continental slope. (B) Conceptual model of sandy debris flows that develop on slope margins. Debris flows occur due to the down-slope evolution of a mass-slumping event, i.e., the 1929 Grand Banks earthquake (modified from Piper et al., 1999).

external mounding of any upper bounding surface/reflector of a fan. During this comparison we considered both Widess' (1/4 λ; Chopra et al., 2006) and Rayleigh's (1/2 λ; Kallweit and Wood, 1982) vertical seismic resolution limits to determine the range of geobody thickness that would be resolvable in our data. This is because seismic stratal pattern recognition depends upon vertical seismic resolution as a function of velocity, frequency, and wavelength (Widess, 1973; Kallweit and Wood, 1982; Posamentier et al., 2022).

In addition to mapping seismic reflector geometry, we also applied seismic geomorphological concepts to seismic attributes extracted from the interpreted horizons using the Root Mean Square (RMS) amplitude and variance (e.g., coherence and curvature) attributes (Miller and Stuart, 1992; Sømme et al., 2013; Bunt, 2015). These attributes are important for distinguishing Moki and Mount Messenger formation sandstone beds from the background mudstone of the Manganui Formation.

Detuned seismic attribute analysis was based on the concepts of Connolly (2007) and Simm (2009). During analysis of seismic amplitude attribute maps, we picked base and top horizons for each interval as well as additional horizons within the interval to sub-divided our analysis. Extra horizons were inspected to constrain amplitude analysis using relatively small time-windows (i.e., ~30 ms for the upper Moki Formation and ~40 ms for the lower Mount Messenger Formation). To constrain the amplitude in the upper Moki Formation we used two sub-intervals (i.e., UMK 1 and UMK 2) and in the lower Mount Messenger we used three sub-intervals (i.e., LMM 1, LMM 2 and LMM 3). Finally, horizons were flattened and structural balancing was applied to the 3D seismic data to measure the gradient of the slope. Slope gradient was smoothed using a window of roughly 10–50 km^2 to remove the effects of seafloor irregularities.

5. Terminology

5.1. Submarine-fan subdivisions

There are numerous models of submarine fans in the literature (Bouma, 1962; Walker, 1978; Mitchum et al., 1985; Vail, 1987). These models generally subdivide fans into feeder canyon-channels, upper fan, middle fan, and lower fan components (Fig. 6A), based on the following criteria: (i) geometry, morphology and organisation of channel complexes within a fan, (ii) longitudinal (i.e., down dip) seismic facies variations, (iii) channel depth and fan thickness, and (iv), seafloor slope gradient where a fan may have developed (Mutti and Ricci-Lucchi, 1972; Walker, 1978; Droz and Bellaiche, 1991; Weimer and Link, 1991; Escutia et al., 2000; Curray et al., 2002). However, due to limitations in the interpretation of fan elements in 2D seismic data, we describe Taranaki Basin Miocene fans using a simplified tripartite scheme consisting of (i) feeder canyon and distributary channels, (ii) upper fan segment, and (iii), lower fan segment.

With regard to the findings of previous studies, submarine fan divisions can be distinguished by their key characteristics, and in parts, we use these key characteristics to guide our fan system interpretation. On the continental slope at gradients of ~2–5°, feeder canyon-channels are generally narrow with steep walls (Droz and Bellaiche, 1991; Cronin et al., 2005; Kamaruzaman et al., 2023). They widen significantly as they become less confined towards the basin plain, where depositional gradients decrease to the range ~0–2°. The upper fan segment typically shows low-relief external mounding on upper seismic reflectors compared with lower fan segments (Posamentier and Erskine, 1991; Lee et al., 1996). Seismic facies of the upper fan show medium to high-amplitude reflectors indicative of the presence of sand-prone strata (Walker, 1978; Weimer, 1990; McHargue, 1991; Deptuck et al., 2003).

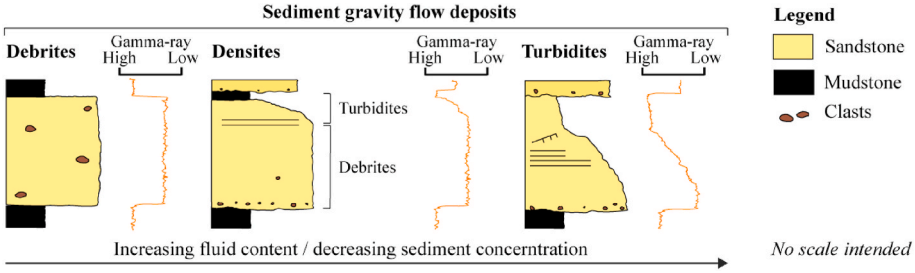

Fig. 7. Example facies characteristics of debrites, densites and turbidites, alongside typical gamma-ray lot motifs. Debrites are characterised by blocky sandstone bodies with abrupt lower and upper contacts, densites show a more subtly transitional upper contact, and turbidites have a very gradational profile from their base to top. Note the presence of mud clasts in debrites and their absence from turbidites (modified from Gani, 2004).

Table 2
Seismic data parameters and their calculated resolution. Parameters are based on Widess (1973).

Seismic data type	Dominant frequency within interval of interest (Hz)	Thickness at onset of tuning effect λ/2 (ms)	Tuning thickness λ/4 (ms)	Resolution limit λ/8 (ms)
2D	20 to 35	50 to 64	25 to 32	12.5 to 16
3D	40 to 50	24 to 40	12 to 20	6 to 10

In contrast, the lower fan region typically displays mainly low-amplitude reflectors representing mud-prone deposits. The basal bounding surface of the upper fan exhibits prominent erosional effects, while the erosional basal bounding surface in the lower fan is hardly recognisable on seismic data. The upper fan is narrower than the lower fan as the fan widens towards the lower slope and basin plain (Fig. 6A) (Walker, 1978). The number of distributary channels also differs between the upper fan and lower fan segments; there are more channels in upper versus lower parts of a fan (Normark and Gutmacher, 1983; Flood and Damuth, 1987). This study focuses on mapping the fan systems rather than describing their internal hierarchy and therefore we have chosen to refrain from applying any fan hierarchical models.

5.2. Sedimentary processes and deposits

A range of depositional mechanisms are inferred for continental slopes and on basin floors, resulting in a confusing lexicon in the literature (Talling, 2013; Shanmugam, 2016). To standardize our terminology we have adopted the Gani (2004) model of gravity flow deposits (Fig. 7). We have applied this model to the interpretation of wireline log records for drill holes investigated in the study area, following (Bernhardt et al., 2012; Shanmugam and Wang, 2015; Fudol et al., 2019). This has involved focussing on differentiating blocky gamma-ray log motifs with sharp upper and lower contacts (debris flow deposits) from bell-shaped (i.e., gamma-ray increasing upwards) log motifs (turbidity current deposits). A conceptual example is shown in Fig. 7 exhibiting debrites, densites and turbidites. Densites in particular, represent hybrid deposits consisting commonly of a lower debrite and an upper turbidite without developing any bedding plane in between, originated by bipartite sediment gravity flows (Gani, 2004). These deposits originated by flow transformation, or simultaneous or retrogressive release of co-genetic debris flows and turbidity currents, and belong to the class of hybrid event beds (Davis et al., 2009; Haughton et al., 2009; Talling, 2013). We chose this model (Fig. 7) in our study because we want to objectively distinguish the resultant sandstone bodies of sediment gravity flow processes. These processes can also produce mud-dominated deposits such as muddy debrites and turbidites (Amy and Talling, 2006; Shan et al., 2019; Patacci et al., 2020), however they are not the focus of this study. Where available, we have used drill cores to distinguish amongst gravity flow deposits.

While submarine fans can be constructed by a variety of sediment gravity flow deposit types, including debrites, densites and turbidites (Middleton and Hampton, 1973; Lowe, 1982; Shanmugam, 2000; Davis et al., 2009; Haughton et al., 2009), these deposits are not exclusive to fan systems. For example, sediment gravity flow deposits also occur in relation to submarine mass movement such as on the continental slope (Lee et al., 2007; Micallef et al., 2007; Parsons et al., 2007; Talling et al., 2007; Shanmugam, 2009; Fudol et al., 2019) (Fig. 6B). This distinction is relevant to the arguments we set forth later in this paper.

6. Results and interpretations

6.1. Resolution of seismic data

Calculation of the Widess and Rayleigh seismic resolution limits yielded a vertical resolution ranging from 6 to 16 ms within the stratigraphic intervals of interest on both 2D and 3D seismic data, respectively, from the study area, depending on the dominant frequency range (Table 2). This calculation also gives the thin bed tuning thickness and the thickness at which the onset of tuning occurs. Calculation of seismic

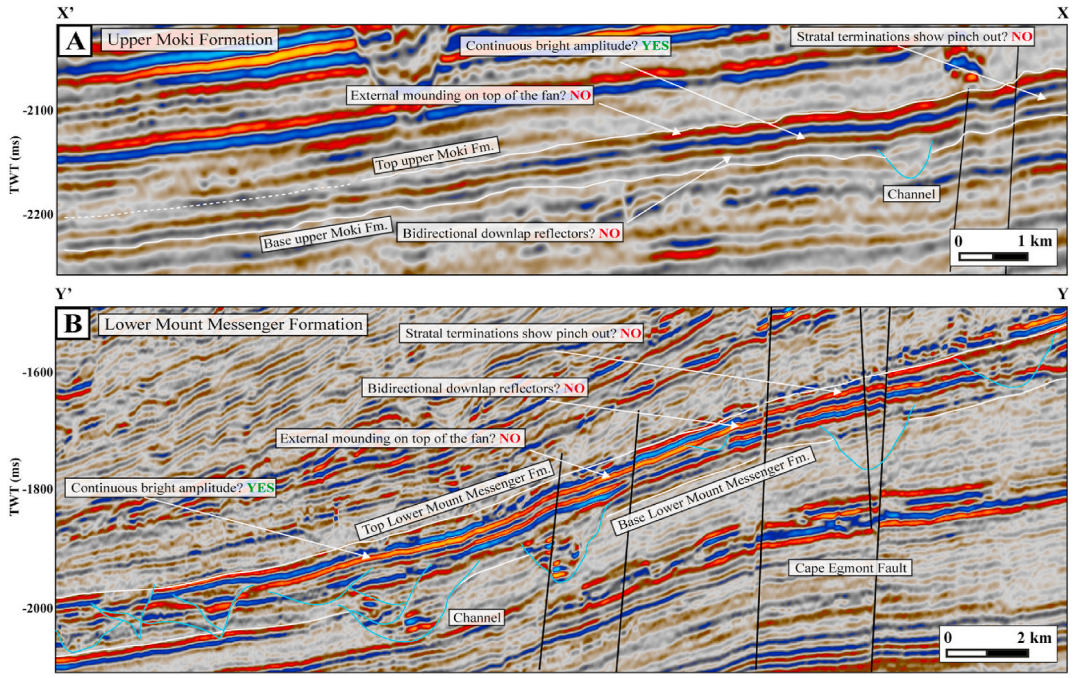

Fig. 8. Seismic cross-sections intersecting the interpreted "fans" of Kroeger et al. (2019) compared with the recognition parameters outlined in Posamentier and Erskine (1991) (Table 1). (A) Upper Moki Formation showing continuous high amplitude reflectors but (i) without pinchout of reflectors against the paleo-sea floor, (ii) bidirectional downlap of reflectors within fans, or (iii), external mounding of reflectors at the top of the fan. (B) Lower Mount Messenger Formation that does show continuous high amplitude reflectors but does not show pinchout of reflectors against the paleo-sea floor, bidirectional downlap of reflectors within fans, or external mounding of reflectors at the top of the fan. Refer Fig. 4 for transect line location.

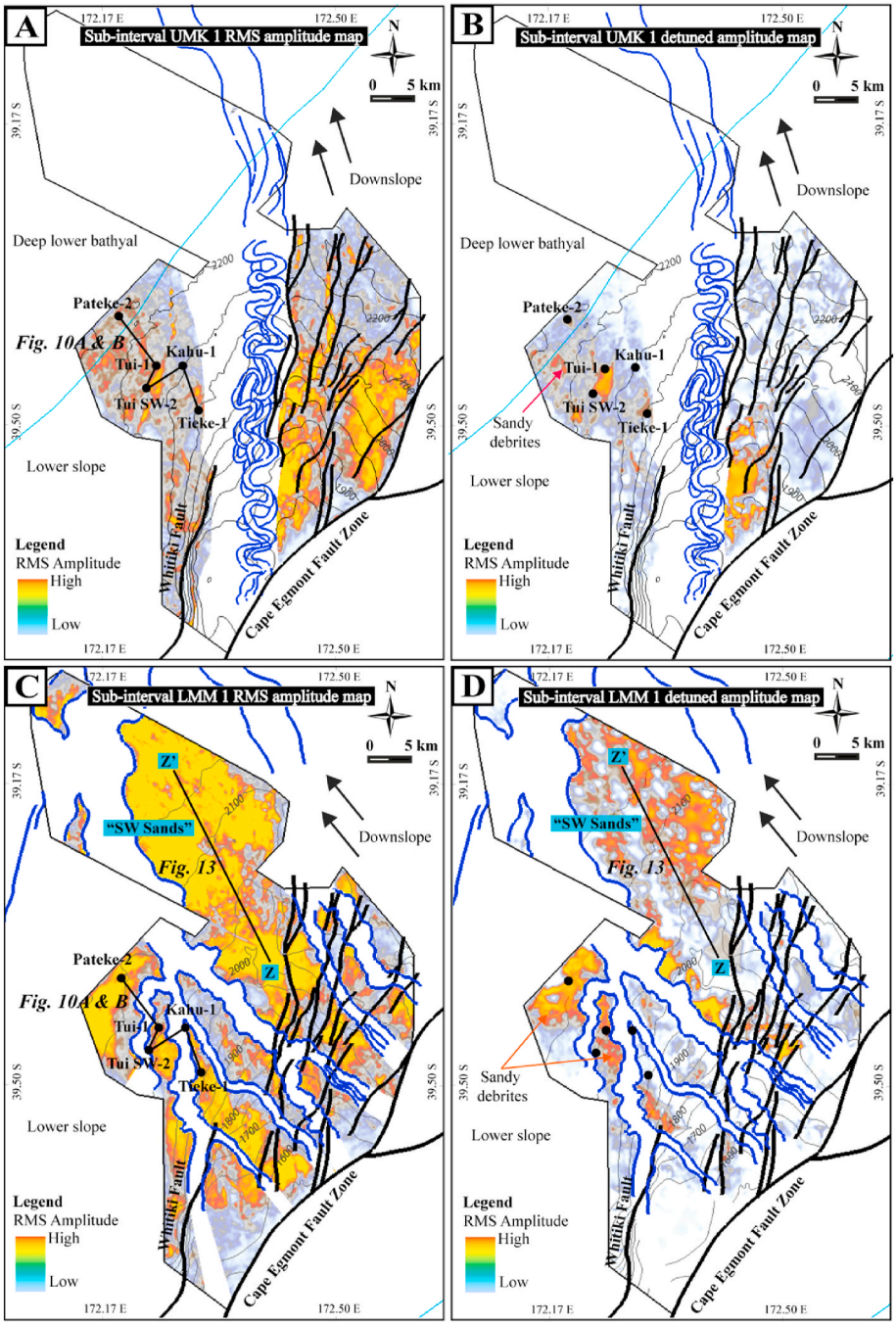

Fig. 9. Root mean squared (RMS) amplitude and detuned amplitude maps for the Moki and Mount Messenger formations (A) upper Moki Formation RMS amplitude and B) upper Moki Formation detuned amplitude. (C) Lower Mount Messenger Formation RMS amplitude and (D) lower Mount Messenger Formation detuned amplitude. Note how much of the high amplitude area was reduced during the detuning process. Most of the remaining high amplitude areas are interpreted as sandy debris flow deposits, although there is uncertainty in interpreting high amplitude areas away from well control. The underlain contour maps are in TWT (ms). Refer to Supplementary Data for complete set of maps for each sub-interval.

resolution limits of the data mean that not all fan elements are detectable. For example, individual lobes and/or lobe complexes may not be resolvable.

6.2. Part I: objective evaluation of previous interpretations of Moki and Mount Messenger formation submarine fans

6.2.1. Upper Moki Formation

Objective comparison of the parameters outlined in Table 1 against the Kroeger et al. (2019) map for the upper Moki Formation (their Figure 6C) demonstrates that (1) only one of the five Posamentier and Erskine (1991) seismic reflection criteria for submarine fans is met; specifically, the presence of continuous high amplitude reflectors throughout the interval. Seismic section Fig. 8A, which crosses the Kroeger et al. (2019) upper Moki Formation fan, shows this point. (2) Further interrogation of the locations of high seismic amplitude locations on the map in Fig. 9 shows that there are significant differences between the RMS amplitude attribute extraction and the detuned amplitude attribute extraction. The amplitude extraction maps of Kroeger et al. (2019) (their Figures 12A and B) used proportional slices. They did not specify if the maps show RMS or average amplitude, and therefore, we could not reproduce the maps exactly. As a result, in this

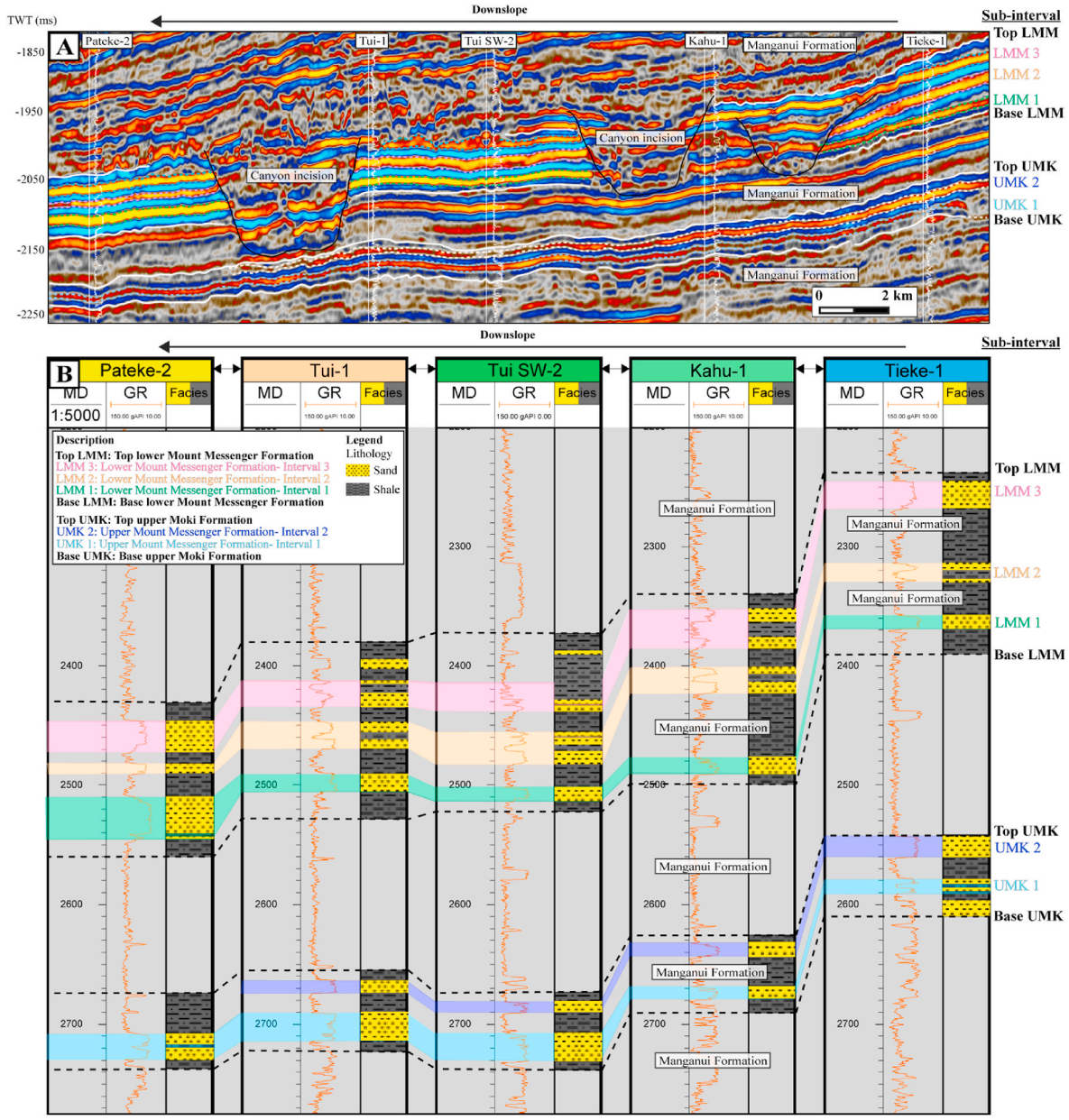

Fig. 10. (A) Seismic cross-section and (B) well correlation panel showing the sub-intervals within the upper Moki Formation and lower Mount Messenger Formation used during the seismic detuning process. The upper Moki Formation is split into the UMK 1 and UMK 2 intervals. The lower Mount Messenger Formation is divided into the LMM 1, LMM 2 and LMM 3 intervals). Refer to Fig. 9A and C for the location of the cross-section and drill holes.

study we take the maps as RMS amplitude and demonstrate the effect of seismic tuning on it. Comparison between their amplitude extraction and our detuned amplitude attribute extraction for one of the sub-intervals (Fig. 10) shows a significant reduction in the area of high-amplitude (Fig. 9A and B; see Figure iii in Supplementary Data for complete sub-intervals). Furthermore, the distribution of high amplitude in the detuned map does not show a lobate morphology as would be expected of fans, but instead displays a patchy (isolated) pattern. (3) A third aspect of the Kroeger et al. (2019) submarine fan interpretation for the upper Moki Formation is the presence of low gamma-ray signatures in drill hole logs. The gamma-ray log motifs show blocky profiles with sharp basal and upper contacts (Fig. 10B), which they interpreted as imaging turbidites. However, we note that such gamma-ray log motifs are equivocal and may also be interpreted as amalgamated sandy debris flow deposits (see examples in Bernhardt et al., 2012; Shanmugam and Wang, 2015; Fudol et al., 2019). (4) A final aspect that questions the interpretation made by Kroeger et al. (2019) for the fan-like character of the upper Moki Formation, is that they did not clearly define a fan morphology (i.e., the upper, middle and lower fan regions), which precludes objective seismic interrogation of their mapped fan systems. When taken together and in context, our results demonstrate that there is insufficient evidence to support the interpretation and occurrence of widespread submarine fan systems in the upper Moki Formation within southern Taranaki Basin.

6.2.2. *Lower Mount Messenger Formation*

As with the upper Moki Formation interval, we compared the parameters outlined in Table 1 against the lower Mount Messenger Formation fans mapped by Kroeger et al. (2019; that is, their Figure 6D). Our results show that the only Posamentier and Erskine (1991) criteria possibly defining their inferred submarine fan system is the occurrence of continuous high amplitude reflectors throughout the lower Mount

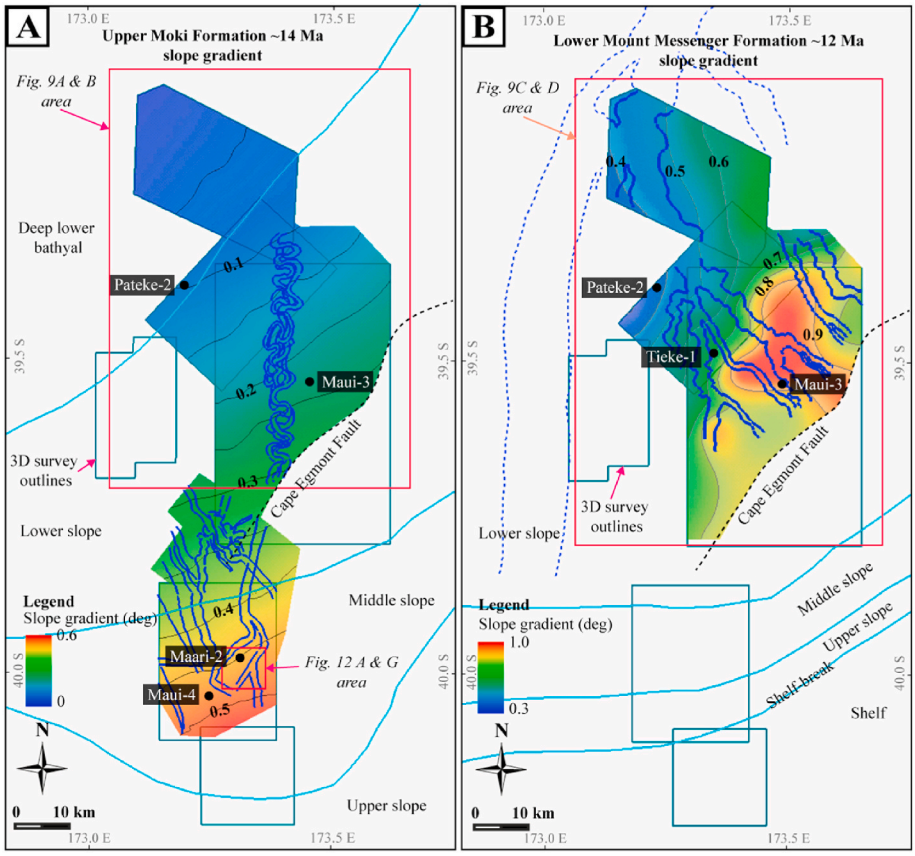

Fig. 11. Slope gradient map of (A) upper Moki Formation and (B) lower Mount Messenger Formation in South Taranaki Basin showing a trend of decreasing gradient to the north and northwest. Slope gradients range from 0.6 to <0.1° in the upper Moki Formation and from 1.0 to 0.3° in the lower Mount Messenger Formation. The lower Mount Messenger slope gradient is adapted from Kamaruzaman et al. (2023).

Messenger Formation interval (Fig. 8B). Comparison between their RMS amplitude extraction versus our detuned amplitude extraction shows a significant reduction in the area of high amplitude (Fig. 9C and D; see Figure iv in Supplementary Data for complete sub-intervals). However, in the detuned amplitude map an area of high amplitude remains in the northern part of the map, which Kroeger et al. (2019) referred to as the "SW Sands".

Finally, gamma-ray log motifs of the sandstone bedsets in the lower Mount Messenger Formation display mainly blocky profiles with sharp basal and top contacts (Fig. 10B), which, Kroeger et al. (2019) infer to be turbidite fans. However, the morphology of their mapped fans is not clearly defined in terms of upper, middle, and lower fan zones and their inferred fans (high amplitude areas) are located marginal to what we map as through-going channel margins (but which Kroeger et al. (2019) map as fans atop channels). Based on these observations, we simply do not find enough evidence to support the interpretation of fan systems occurring within the lower Mount Messenger Formation interval where they have been mapped by Kroeger et al. (2019).

6.3. Revised mapping of Moki and Mount Messenger formations

In this section we revisit the same dataset used by Kroeger et al. (2019) and more seismic data to the north of it, and propose an alternate interpretation for the deep-water sedimentary systems in the Moki and Mount Messenger formations in offshore southern Taranaki Basin.

6.3.1. Upper Moki Formation

6.3.1.1. Channel complex networks. Mapping of the channel complex in the upper Moki Formation in southern Taranaki Basin demonstrates that it is oriented south to north (Fig. 11A), crossing middle and lower slope regions, roughly 30 km north of the shelf edge and about 50 km north of the contemporary (Lillburnian, ~14 Ma) shoreline. Incised channel complexes drained northward normal to obliquely across a smooth slope with gradients ranging from 0.2 to 0.5° (Fig. 11A). The channel complexes within the middle slope region (mean slope gradient: 0.4°) are mainly aggradational, straight to slightly sinuous (mean sinuosity index: 1.1), with a maximum width of 2.5 km. In contrast, on the lower slope region (mean slope gradient: 0.2°), individual channels within the prominent channel complex are highly sinuous (mean sinuosity index: 2.4) and their maximum width decreased to approximately 1.2 km (Kamaruzaman et al., 2023) (Fig. 11A).

6.3.1.2. Gravity flow deposits on the slope. As shown in the previous section, detuned seismic amplitude maps display high amplitudes mainly within the slope region and they have a patchy distribution (Fig. 9B). The gamma-ray log response in the drill holes that intersect the high-amplitude area have blocky log motifs with sharp basal and upper contacts (Figs. 10B and 12A). Furthermore, these low gamma-ray intervals (sandstone bedsets) are not readily correlated between neighbouring drill holes (i.e., distance between drill holes ranges from ~1 to 6 km). The thickest sandstone intervals are up to 40 m thick in the Maari-2 drill hole located within the middle slope (Fig. 12A). In the Tui-1 drill hole, situated within the lower slope region, sandstone intervals get as thick as 28 m (Fig. 10B). Analysis of core data extracted from these intervals shows that they consist of massive (predominantly fine-grained) sandstone beds with mud clasts with long axes of up to 10 cm (Fig. 12B–F).

We interpret the patchy high (detuned) amplitude seismic distributions (Fig. 9B) to represent localised slope sandstone deposits (i.e., not

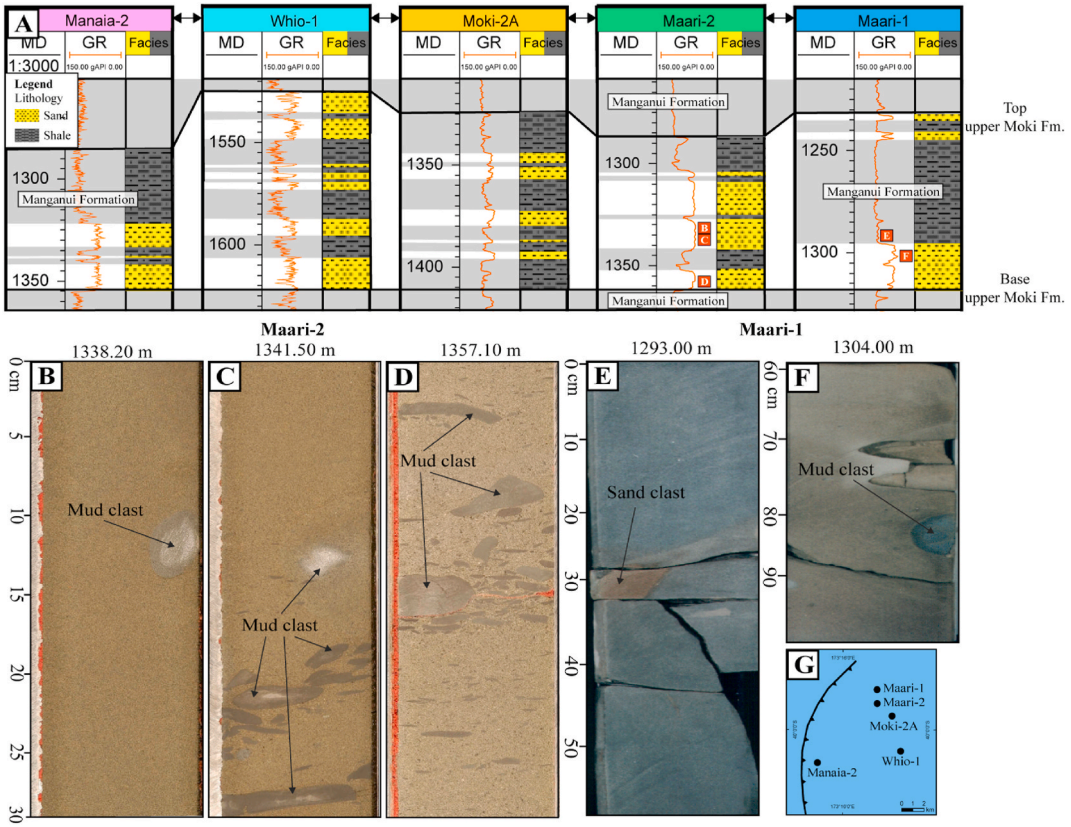

Fig. 12. (A) Gamma-ray log motifs for the upper Moki Formation interval in the upper slope region from selected drill holes. (B) To (D) core photographs from Maari-2 through interpreted sandy debris flow deposits showing floating mudstone clasts. (E) Core photograph from Maari-1 showing sandstone within mudstone. (F) Core photograph from Maari-1 showing a mudstone clast within an ungraded sandstone. The sandy deposits are considered debrites. (G) Location of drill holes, refer Fig. 11A for the location of the area.

lobate fans), and this is supported by the fact that sandstone intervals cannot be correlated on wireline logs between neighbouring drill holes (Figs. 9B and 12A). Nevertheless, due to the complexity of deep-water sedimentary systems (Stow and Mayall, 2000; Shanmugam, 2013), the localised sandstone deposits could also be reworked by contourite drifts (Kroeger et al., 2019). In addition, blocky gamma-ray log motifs, the massive internal nature of sandstone beds, including the presence of mud clasts (Fig. 12B–F), suggests that these deposits were generated by gravity flows with high sediment concentrations, low Reynolds numbers (i.e., laminar), and a relatively strong matrix strength (Gani, 2004). Hence, the deposits of the upper Moki Formation on the depositional slope margin are interpreted here to be amalgamated sandy debrites following Gani (2004) and other publications (e.g., Talling et al., 2007; Haughton et al., 2009; Shanmugam et al., 2009; Jin et al., 2021) (Fig. 7).

6.3.2. *Lower Mount Messenger Formation*

6.3.2.1. Canyon-channel complex network. The lower Mount Messenger Formation canyon-channel networks originated from, and lie within, southern Taranaki Basin, roughly 16–22 km from the contemporary (Waiauan, ~12 Ma) shoreline (Fig. 11B). The canyons reached 9 km wide on the lower slope (Fig. 9C and D). The canyon-channels directed sediment in a SE-NW direction, incising into the lower slope margin in the vicinity of the Maui Field (Fig. 1).

Numerous lower Mount Messenger Formation canyon-channels are observed incised into thick sandy strata forming a network. The canyon-channels developed on a smooth slope gradient of 0.4° to 1° (Fig. 11B) along the bottomset of sigmoidal clinoforms (Kamaruzaman et al., 2023). Seismic profiles reveal that asymmetrical v- and u-shaped incisions, which are narrow at their base, are the dominant type of canyon incision (Fig. 10A). Internal seismic configuration within the canyons

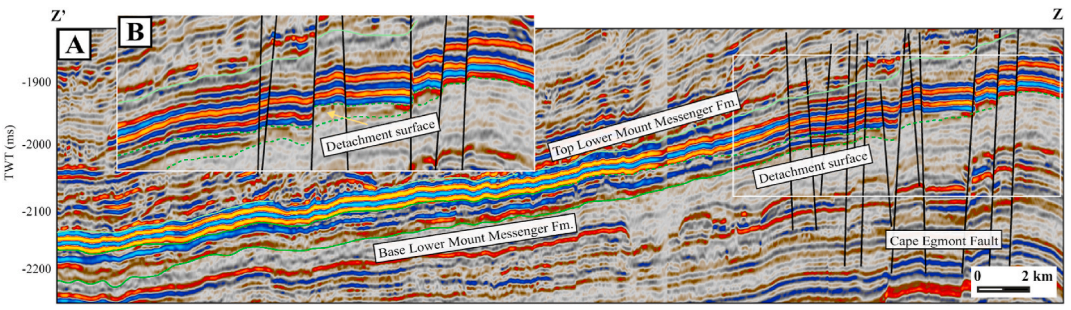

Fig. 13. (A) Seismic cross-section showing a detachment surface at the base of sandy debris flow deposits in the lower Mount Messenger Formation. (B) A close-up view of the detachment surface. See Fig. 9D for location.

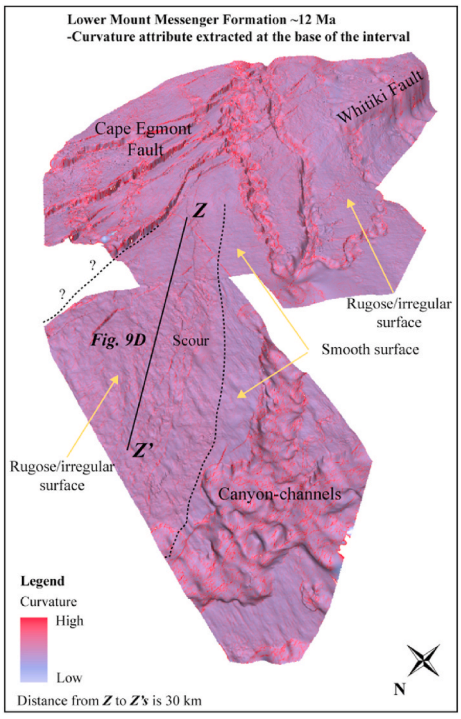

Fig. 14. Curvature seismic attribute extraction from the base of an interval characterised by sandy debris flows in the lower Mount Messenger Formation. The surface is characterised by rugose, topopgraphy, and is interpreted as a debris flow detachment surface (+10 ms).

shows high amplitude discordant seismic reflectors at the base. The canyons are filled with vertical and lateral stacked u-shaped channel complexes of 50–200 m thickness (Kamaruzaman et al., 2023). These channel complexes are manifest as a combination of parallel to sub-parallel and divergent low to medium amplitude seismic reflectors, dipping at low angles toward channel thalwegs.

6.3.2.2. Gravity flow deposits on the slope. The detuned seismic amplitude map for the lower Mount Messenger Formation shows high amplitude patches on the lower slope (Fig. 9C and D; SW Sands). Further investigation of the seismic facies occurring within these patches show sudden changes from continuous, parallel and high amplitude reflectors to discontinuous, discordant and mixed low to medium amplitude reflectors at the base of the interval (Fig. 13A and B). Notably, no feeder channels are observed at the stratigraphic interval where these seismic facies change as described above. Furthermore, extraction of the curvature seismic attribute along the base horizon (i.e., detachment surface) displays a rugose pattern within the area where the "SW Sands" occur as opposed to a smooth surface in other areas on the map (Fig. 14).

Wireline log cross-sections show a general basinward thickening of sandstone bedsets represented by overall blocky and narrow-spiky gamma-ray log motifs (Fig. 9B). The sandstone beds are poorly consolidated and comprised of very fine to fine sand (New Zealand Overseas Petroleum Ltd, 2004). The thickest sandstone interval is ~50 m, recorded in the Pateke-2 drill hole. However, these sandstone intervals cannot be individually correlated down dip.

Based on the distribution of high-amplitude regions in detuned amplitude maps, the lack of feeder channel mouths and the blocky gamma-ray log characteristics with poor lateral and down-dip continuity, we interpret the Mount Messenger Formation interval in the area, as analysed by Kroeger et al. (2019), to be dominated by amalgamated sandy debris flow beds separated by mudstone. These debrites would have been deposited on the lower slope by flows with high sediment concentration, a low Reynolds number (i.e., laminar flow), and a relatively high matrix strength (Fig. 7). This interpretation is further supported by seismic reflection profiles that show down-dip (towards the NW, parallel to slope orientation) changes in their coherence, amplitude and vertical stacking, which we take to represent a detachment surface at the base of a sandy debris flow interval (Fig. 13). The rough surface identified at the base of the lower Mount Messenger Formation (Fig. 14) is attributed to the scouring of debris flows into the underlying mudstone strata ahead of the actual deposition from the debris flow (Fig. 13). The analogue to this interpretation (debris flows) is presented in publications (e.g., Piper et al., 1985; Sohn, 2000; Pareschi et al.,

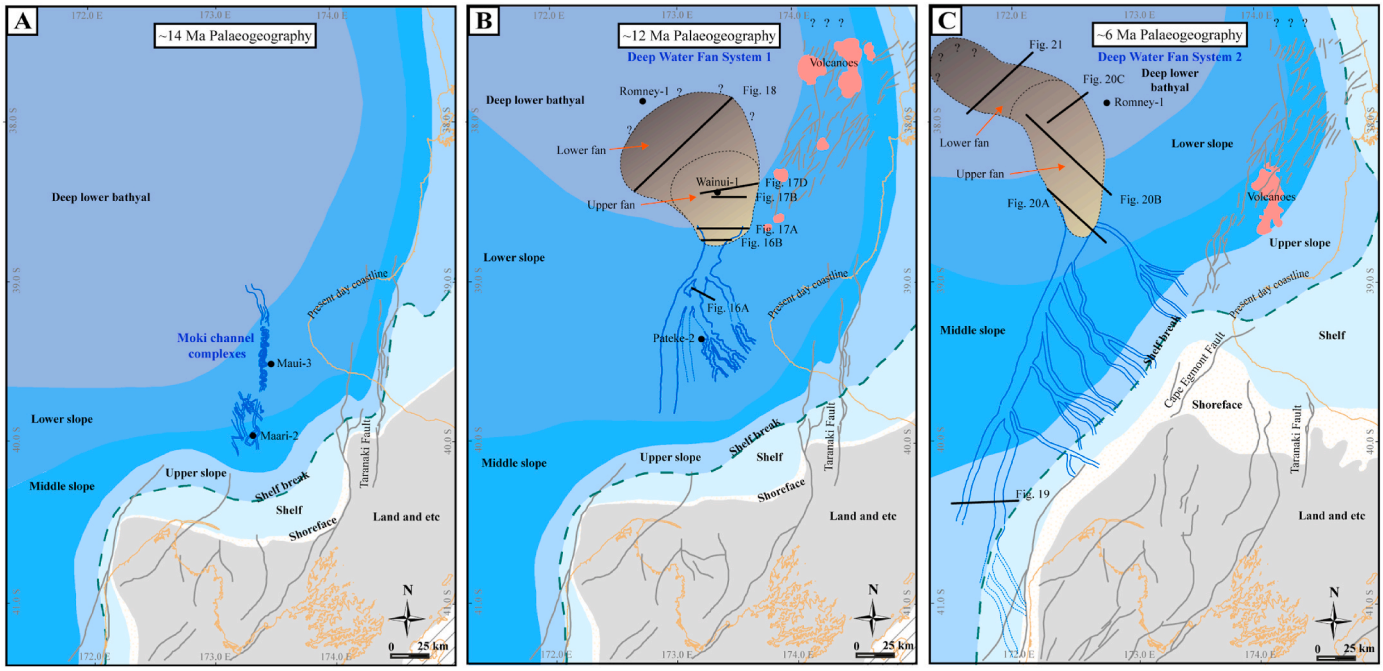

Fig. 15. Revised paleogeography maps of: (A) upper Moki Formation (~14 Ma), Mount Messenger Formation (B) Deep Water Fan System 1 (labelled DWF1 in Fig. 2) and (C) Deep Water Fan System 2 (labelled DWF2 in Fig. 2). Note that we remove fans from the paleogeography maps in South and central Taranaki Basin entirely in all intervals, but depict new fans in deep Taranaki Basin in B and C. The paleobathymetry, active faults and volcanoes are adapted from Strogen et al. (2011).

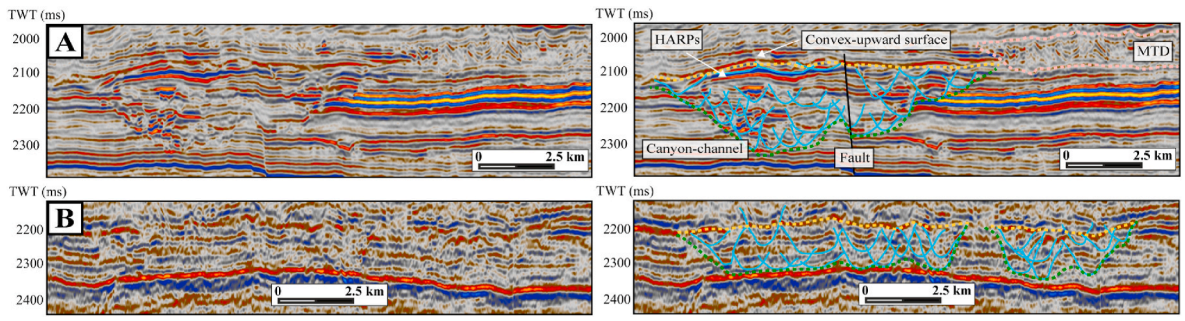

Fig. 16. Uninterpreted and interpreted (A) upper (inline 1080, Kokako 3D) and (B) lower (2D seismic line BO_81 nm-204–1018) parts of feeder canyon-channels in the Mount Messenger Formation Deep Water Fan System 1 (~12 Ma). Refer to Fig. 15B for cross-section location.

2000).

6.4. Part II: new insights into the Taranaki Basin deep-water fan systems

We further investigated here the Mount Messenger Formation fan systems in deep-water Taranaki Basin beyond the contemporary depositional slope. This mapping and interpretation were carried out using the fan criteria of Posamentier and Erskine (1991), as outlined in Table 1. The results show that in offshore western Taranaki Basin there are two main deep-water fan systems: (i) a Middle Miocene Deep Water Fan System 1 (~13–12 Ma; Waiauan Stage), and (ii) a Late Miocene Deep Water Fan System 2 (~7–6 Ma; Kapitean Stage), both of which are characterised by a terminal submarine fan (Fig. 15). The pathway for the older of the two fan systems originated from the southeast part of the basin and propagated through the Maui Field area, routing sediment in a southeast to northwest direction to deep Taranaki Basin. The younger sediment pathway (Late Miocene Deep Water Fan System) originated in the south and flowed directly northward to the deep-water basin plain. Here, we describe both deepwater fan systems appealing to a simplified tripartite scheme consisting of (i) feeder canyon-channel networks, (ii) upper fan segment, and (iii) lower fan segment.

6.4.1. Deep water fan system 1 (Middle Miocene)

6.4.1.1. Feeder canyon-channel networks. The Mid-Miocene feeder canyon-channel is located on the lower slope and can be divided into upper and lower parts, which together form a network. The upper part of the feeder canyon-channel displays prominent convex-upward bulges with highly asymmetry canyon walls (Fig. 16A). The canyons contain dense multi-storey (stacked) lateral channel complexes. The canyons have an average width of 8 km and an average depth of 215 m. The confined channel complexes have lesser widths and depths that range from 0.5 to 2 km and 20 to120 m, respectively (Kamaruzaman et al., 2023). In map view, these internal channels are linear to sinuous. The slope gradient in the region ranges from 0.3 to 0.5°.

The lower part of this canyon-channel network passes basinward into the main feeder channel where it becomes less confined and has nearly symmetric walls (Fig. 16B). Wall steepness decreases significantly as the main channel broadens across the lower slope with a gradient less than 0.2°. A convex-up surface at the top of the channel complex is observed throughout the region, even though the convex-up surface is less conspicuous than in the upper feeder canyon-channel region. The width of the main channel increases from ~12.5 to ~15 km basinward. As with the upper feeder canyon-channel (Fig. 16A), the lower feeder channel (Fig. 16B) is also composed of numerous superimposed channels within the complex with average widths between 1.0 and 2.5 km and average depths between 40 and 80 m. In contrast to the densely stacked channel complex in the upper feeder canyon-channel region, the channel complex of the lower feeder channel region displays less multi-storey stacking and has a more lateral (adjacent) offlapping arrangement. Channel networks in this region are sinuous to meandering.

6.4.1.2. Upper fan segment. An upper fan segment can be observed immediately basinward of the mouth of the primary feeder channel, and it extends outward across a slope of approximately 0.4°, with a width ranging from 32.5 to 50 km (Fig. 17). The upper surface of the fan exhibits subtle low-relief mounding, characterized by a convex-up morphology and high-amplitude reflections along its upper bounding surface. Above this top surface, the fan is overlain by an interval of chaotic and low-amplitude reflectors.

Within the upper fan, a combination of stratified and discontinuous medium to high-amplitude reflections can be distinguished from the low-amplitude reflections in underlying strata (Fig. 17D). Subtle bidirectional pinch-out of reflectors and multiple channel incisions with concave-upward infill patterns are also observed. The maximum width of channel systems within the region is approximately 2.5 km. The basal bounding surface of the fan is identified by truncation of reflectors against the underlying strata, and the surface is depressed at the centre of the fan and rises towards the flanks before pinching out beneath overlying strata (Fig. 17B). Gamma-ray log responses from the appropriate Wainui-1 drill hole level reveals that the fan is approximately 100 m thick with the gamma-ray log showing an alternate increasing and decreasing signal upward through the fan succession (Fig. 17C).

We interpret the presence of a subtle low-relief mounding surface at the top of the fan to indicate rapid sedimentation and associated fan build up within the vicinity of the mouth of feeder channels, generally in the centre of the fan (Fig. 17A). This feature is subtle in cross-sectional images. However, well completion reports for the Wainui-1 drill hole indicate that the fan strata are overlain by Mohakatino Formation strata (Shell BP Todd Oil Services Ltd, 1982) (Fig. 17C), which we interpret as a 250–350 m thick mass transport deposit (MTD) because of its chaotic and low amplitude reflectors. The occurrence of bidirectional reflector pinch-out and concave-upward channel incision suggests lateral migration of channels and switching of lobe complexes (Fig. 17B). Bidirectional downlapping reflectors at the edge of the fan are not clearly observed, as the late-Middle Miocene seafloor slope in the region was very low, with a mean gradient of only 0.4°. Depression at the base and centre of the fan complex is attributed to compaction subsidence of the fan into the underlying Manganui Formation mudstone (Fig. 17B). The gamma-ray log motif corresponds to alternating coarsening (very fine sand) upward and fining (mud) upward successions indicating switching of lobe complexes as the fan built upward (Fig. 17C).

6.4.1.3. Lower fan segment. The lower fan segment is situated on the basin floor where the slope is ~0.2°. This portion of the fan extends for approximately 75 km laterally (Fig. 18). While high amplitude continuous reflectors mark its upper bounding surface, stratal truncation along the basal bounding surface is not observed. Fan strata primarily onlap the high sloping margins of the basin floor along its southwestern side, which demarcates the southwestern boundary of the fan. There is no

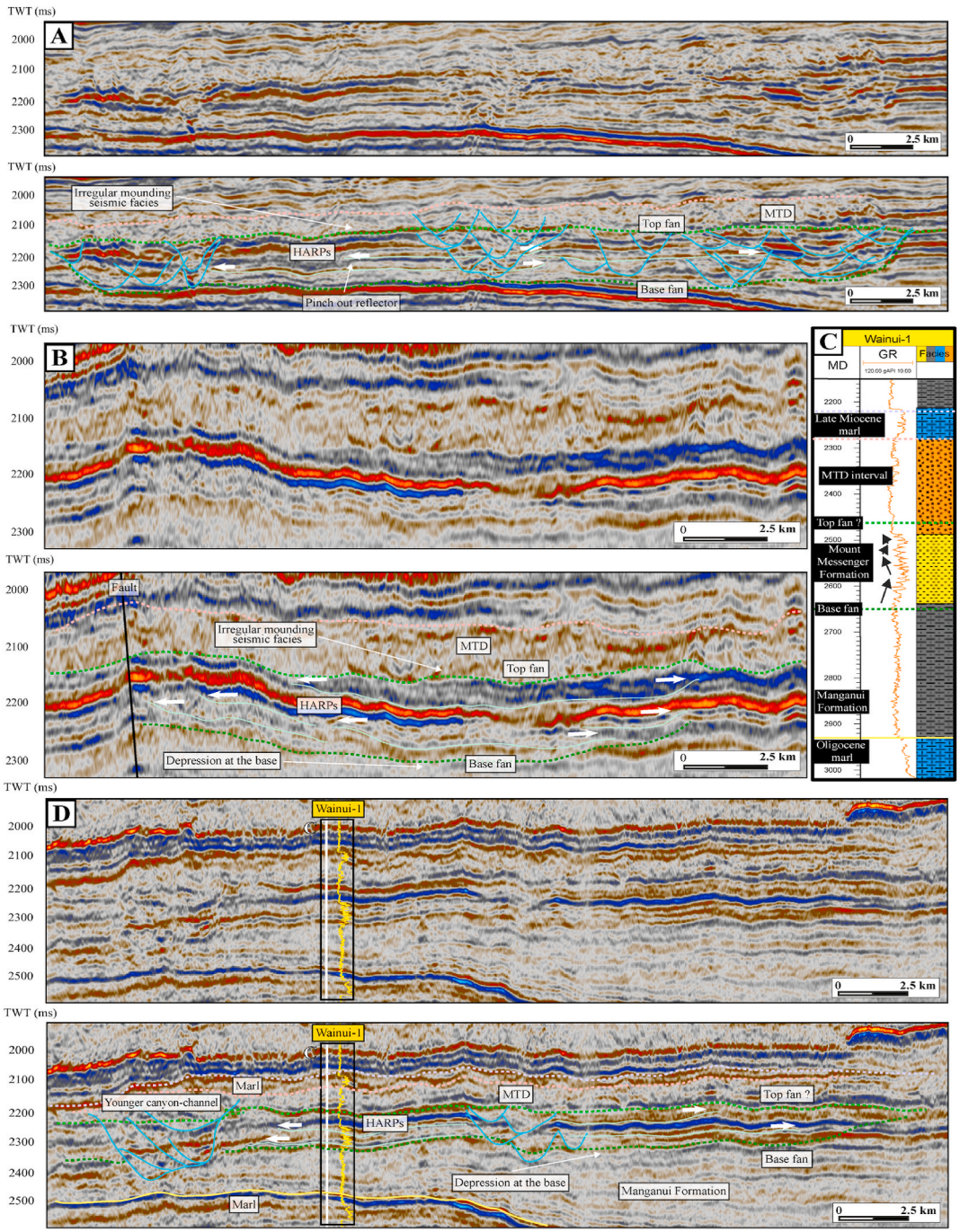

Fig. 17. Uninterpreted and interpreted seismic sections of upper fan segment in the Mount Messenger Formation Deep Water Fan System 1 (~12 Ma): 2D seismic (A) line BO_ar90-445-110-1628, (B) line BO_ar89-446-106-1475 and (D) line ar89-446-108-1475. Refer to Fig. 15B for cross-sections location. (C) Gamma-ray motifs and associated lithology from Wainui-1 drill hole.

channel incision into the lower fan segment originating from the southeast.

The lower fan blanketed the prior flat seafloor profile with sheet-like deposits. There may be a volcanic ash component within the upper part of the fan as Mohakatino volcanic edifices occur nearby to the northwest (Fig. 15B). The base of the fan is identified by a contrast in seismic facies with low amplitude reflectors of Manganui Formation mudstone, contrasting with medium amplitude reflectors of the lowermost fan facies. Stratal onlap of sloping portions of the basin floor implies that pre-existing seafloor topography influenced the distribution of the fan and its depositional trajectory towards the head of the New Caledonia Basin (also known as the Aotea Basin). A northern boundary of the fan has not been identified. A channel system that incises this fan segment from the west is associated with a younger sediment routing system.

6.4.2. *Deep water fan system 2 (Late Miocene)*

6.4.2.1. Feeder canyon-channel networks. The sediment pathway system at ~7–6 Ma includes a feeder canyon-channel network that supplied sediment to a fan in lower bathyal water depths (Fig. 15C). The canyon network originated from the south, with the main branch having a width of 4.2 km and symmetrical walls and the other branch being 8 km wide with asymmetrical walls (Fig. 19). The average depth of both channels was about 260 m. Both channels were directed basinward across a slope

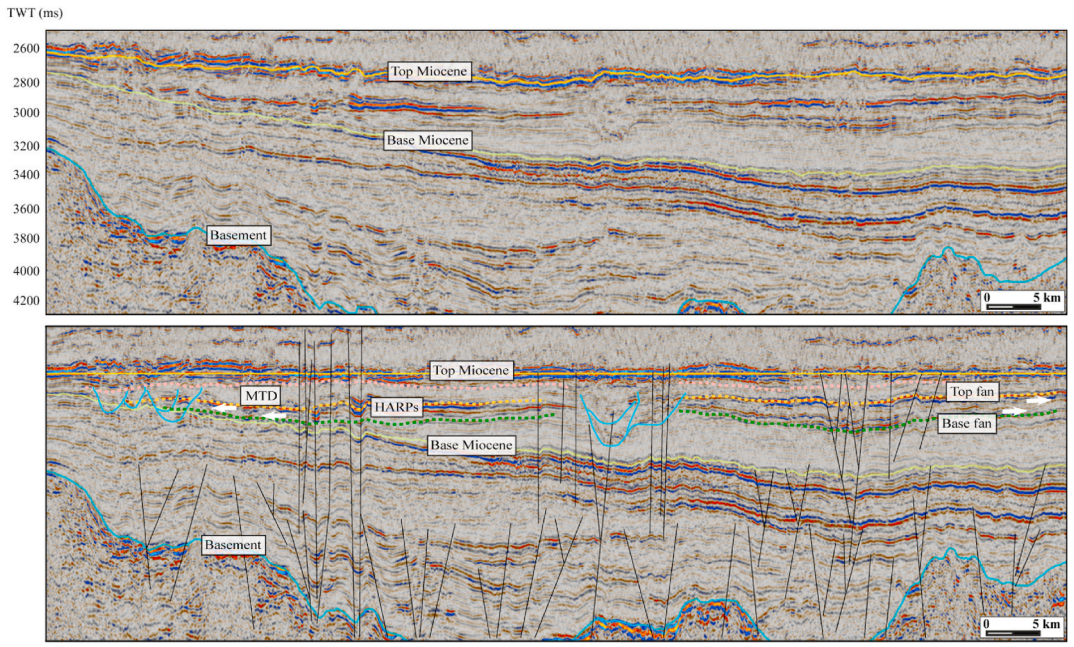

Fig. 18. Uninterpreted and interpreted lower fan segment in the Mount Messenger Formation Deep Water Fan System 1 (~12 Ma), 2D seismic line BO_DTB01-26-2847. Refer to Fig. 15B for cross-section location.

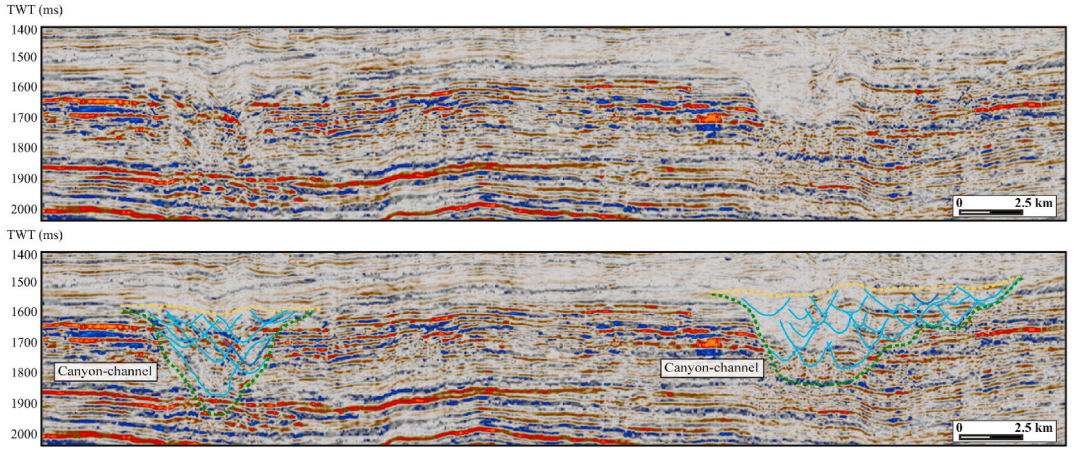

Fig. 19. Uninterpreted and interpreted canyon-channel networks in the Mount Messenger Formation Deep Water Fan System 2 (~6 Ma), 2D seismic line BO_HZT82C_AWE_1_106. Refer to Fig. 15C for cross-section location.

with an average gradient of ~1.5°. The infill of the channels is a combination of stratified and discordant low to medium-amplitude reflectors and they display a predominantly concave-upward pattern. The internal organisation of the channel systems is one of predominantly multi-storey (i.e., stacked) sediment accumulation.

6.4.2.2. Upper fan segment. The upper fan occurs immediately basinward of the feeder canyon-channel network, on a slope gradient of ~1° (Figs. 15C and 20). The upper fan is approximately 40 km wide in the immediate vicinity of the feeder canyon-channel mouth and 70 km wide where it transitions into the lower fan segment. The base of the fan is recognized by the contrast between low amplitude reflectors of Manganui Formation mudstone and higher amplitude reflectors of the overlying fan (Fig. 20B). The top of the fan is demarcated by high-amplitude reflectors. The lateral boundaries of the fan are identified by stratal onlap onto the underlying topography (Fig. 20A). A channel system across the upper fan segment has an average width of 3.5 km and an average depth of 100 m.

The upper fan developed outside and west of the canyon-channel network due to it being less confined on the lower slope and basin plan region. Bidirectional pinch-out of reflectors and concave-upward channel incisions have been identified (Fig. 20), indicative of lateral migration of the channel and switching of the lobe complex across the fan. However, evidence for bidirectional downlapping of fan reflectors against the seafloor is difficult to identify because the seafloor was so flat (~0.1°). One challenge to clearly identifying the upper bounding surface of the fan was to differentiate its continuous high-amplitude reflectors from similar reflectors of the overlying Ariki Formation marl, which has similar characteristics.

6.4.2.3. Lower fan segment. The lower fan segment is marked by stratified medium to high-amplitude reflectors that onlap the underlying topography (Fig. 21). Away from these margins, and in the middle of the lower fan segment, reflectors are more or less continuous and have low amplitude.

The underlying topography expressed as structural highs in the

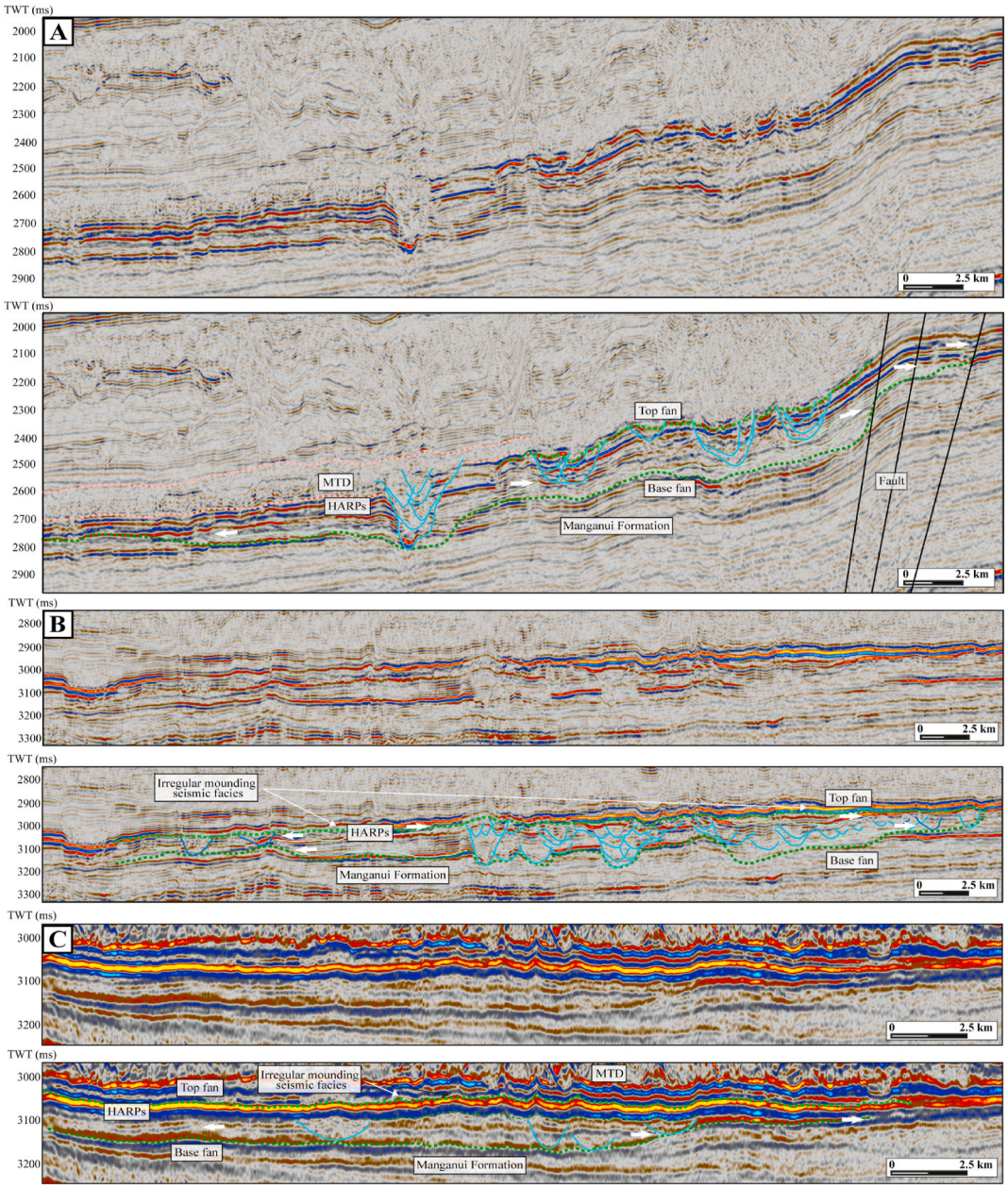

Fig. 20. (A) 2D seismic line BO_DTB01-21-2847, (B) 2D seismic line BO_DTB01-19-2847 and (C) Inline 2150, Romney 3D, Uninterpreted and interpreted upper fan segment in the Mount Messenger Formation Deep Water Fan System 2 (~6 Ma). Refer to Fig. 15C for cross-section location.

region extend into the New Caledonia Basin. These highs controlled the initial morphology of the fan and its depositional trajectory. However, in the lower fan segment it is challenging to differentiate the fan from background Manganui Formation mudstone strata due to both being expressed as amplitude reflectors, possibly signifying that the lower fan is mud-prone. Incising into the top of the fan are younger canyon-channels heading towards New Caledonia Basin.

7. Discussion

7.1. Dismissal of middle Miocene fan systems in southern and central Taranaki Basin

Submarine channels in southern and central Taranaki Basin have been described in several papers (e.g., King and Thrasher, 1996; Baur et al., 2010; Strogen et al., 2011; Kroeger et al., 2019), but in none of them provided explicit documentation of where the mouth of a feeder channel has transitioned into a fan. For example, in the paleogeographic maps in Kroeger et al. (2019) (see Fig. 4) most of the submarine channels cross fans along their whole down-slope length; that is, the mouths of feeder channels do not transition into fans, but rather pass through them. We think that this highly atypical stratal arrangement is incorrect and arises from two incorrect interpretations. (1) The high amplitude slope strata adjacent to channels have been interpreted to represent turbidite beds or bedsets and hence are considered to have accumulated as submarine fans. (2) High amplitude continuous reflectors on the flanks of channels define submarine fan geometry. Our detuning of the southern and central Taranaki Basin seismic reflection within the interval of interest ahead of amplitude extraction, has resulted in removal of the high amplitude signal in most areas where fans have previously been defined (Fig. 9), including adjacent to channels, meaning that the inferred fan geometry is an artifact of bed thickness; that is, those fans do not exist in reality. In the one area where high-amplitude remained after detuning, which was named the "SW Sands" by Kroeger et al. (2019)

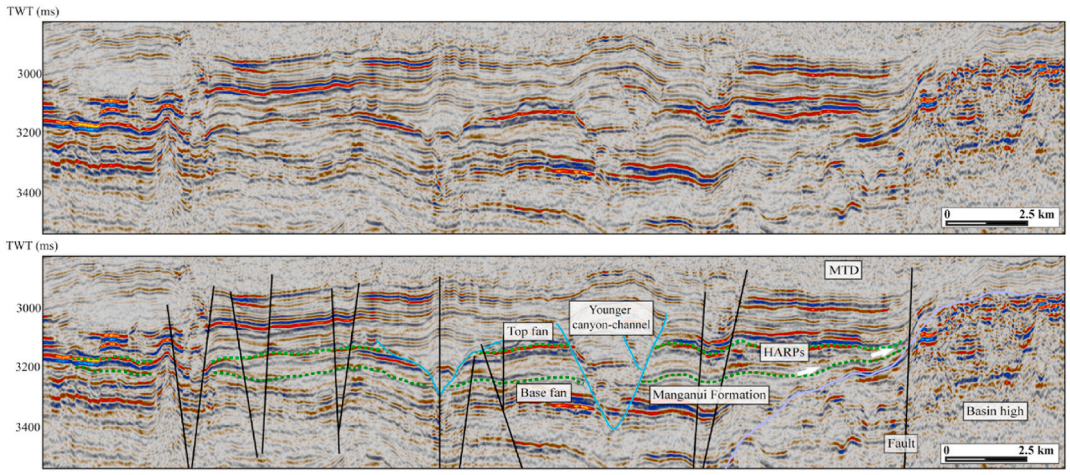

Fig. 21. Uninterpreted and interpreted lower fan segment in the Mount Messenger Formation Deep Water Fan System 2 (~6 Ma), 2D seismic line BO_DTB01-08-2847. Refer to Fig. 15C for cross-section location.

(Fig. 9C and D), curvature seismic attribute extraction shows a rugose surface at its base (Fig. 14), which resulted from seafloor scouring typical of the base of debris flows (Costard et al., 2001; Micallef et al., 2007; Nomikou et al., 2009; Posamentier et al., 2011). Hence, the patchy amplitude distribution in the area of "SW Sands" better fits a model of patchy base of slope deposition of thick isolated and discontinuous sandy debris flows amongst muddy strata (Zampetti et al., 2004; Bernhardt et al., 2012; Liu et al., 2023), rather than the deposition of lowstand turbidite fans as in Kroeger et al. (2019). Accordingly, we have interpreted the upper Moki and lower Mount Messenger formation strata showing high amplitude reflections adjacent to channels as representing upper to middle slope debris flow deposits (debrites). In addition, the fans inferred by Kroeger et al. (2019) and others do not meet the criteria for fan systems as outlined in Tables 1 and 3, which are widely applied to (fully or partially) recognise fan systems in deep water settings using seismic reflection data (Mitchum et al., 1985; Posamentier and Erskine, 1991; Jager et al., 1993; Radovich et al., 2002; Pickering and Corregidor, 2005; Saller et al., 2008; Covault and Romans, 2009; Vesely, 2016; Park et al., 2021). In seismic reflection lines across the inferred Kroeger et al. (2019) fans, the only seismic criteria that could potentially support them is the presence of high amplitude reflectors (Fig. 8; Table 3). However, the continuous high amplitude reflectors adjacent to channels are repeated in sections with thicknesses of 20–40 ms, rather than being limited to the upper bounding surface. This contradicts observations of fan systems by other workers (e.g., McHargue, 1991; Flood et al., 1991; Gong et al., 2022; Maier et al., 2020). Hence, we have dismissed interpretations about the occurrence of submarine fans in the Moki and Mount Messenger formations in southern and central Taranaki Basin as reported in King and Thrasher (1996), Grain (2008), Baur et al. (2010), Strogen et al. (2011) and Kroeger et al. (2019).

7.2. New deep water fan systems in the Mount Messenger formation

Mapping of canyon and channel networks in offshore western Taranaki Basin reveals two major Mount Messenger Formation fan systems (i.e., a Middle Miocene Deep Water Fan System 1: DWF1 and a Late Miocene Deep Water Fan System 2: DWF2 in Fig. 2) and associated sediment routing pathways (Fig. 15B and C). We have included both of these fan systems in the Mount Messenger Formation, even though the older one is of Waiauan age (about 13–11 Ma) and about 1–2 million years older than the 11 Ma age of the base of this formation as defined in the coastal North Taranaki outcrop section (King et al., 1993). The Middle Miocene Deep Water Fan System 1 fan has previously been attributed to the Mohakatino Formation in the well completion report for Wainui-1 (Shell BP Todd Oil Services Ltd, 1982). While some volcanic ash is recorded in the fan interval, this fan is best included in the Mount Messenger Formation as it represents diachronous outbuilding of sediment sourced from the south, as for other parts of this formation.

These two newly identified fan systems were identified from analysis of seismic reflection data using the stratal patterns summarised in Table 1. They also fulfil most of the submarine fan criteria presented in Table 3. Both of these submarine fans occur at the terminus of channel mouths and lie on the outer parts of the lower slope and basin plain. This contrasts with the King and Thrasher (1996), Strogen et al. (2011) and Kroeger et al. (2019) fan locations higher up on the continental slope. New paleogeographic maps including the two new fans are shown in Fig. 15B and C.

7.2.1. Factors controlling fan development

A revised southern Taranaki paleogeographic map for the 14 Ma interval (Fig. 15A) shows the main channel of the Moki Formation does not connect with a submarine fan. This arises because there was insufficient terrigenous sediment supply to form a fan. Sandstone is markedly subordinate to mudstone in the Early and Middle Miocene succession of Taranaki Basin. Sandstone became more common during the Late Miocene when uplift and erosion of the basement underlying the Southern Alps started along the continent-continent plate boundary in South Island (Kamp et al., 1989; Tippett and Kamp, 1993; Ring et al., 2019). Zircon U-Pb ages for two samples from the Moki Formation in Kea-1 (southern Taranaki Basin) have age distributions suggesting a source from Cretaceous basement in northwest Nelson immediately south of Taranaki Basin (unpublished data, 2023). The zircon ages are not similar to the distinctive age distribution of the Permian and Triassic age peaks in Torlesse Complex sandstone and schist that underlies the Southern Alps. Insufficient sand was supplied to the Moki channels to build a submarine fan beyond the sand that accumulated within the channels. A revised paleogeography is shown in Fig. 15A.

The rate of terrigenous sediment supply to Taranaki Basin increased rapidly from about 12 Ma and particularly from 11 Ma (Tongaporutuan Stage), as expressed in the voluminous accumulation (e.g., 510 m thick in Tuhua-1; Fig. 1) of the Mount Messenger Formation, both in Taranaki Basin and across the King Country Basin to the east of Taranaki Basin (Kamp et al., 2004), which markedly prograded the shelf-slope margin to the northwest within the Taranaki foreland basin (Bull et al., 2019). This coincides with the age of early uplift of the Southern Alps (Kamp et al., 1989; Tippett and Kamp, 1993; Ring et al., 2019), and with the start of inversion in southern Taranaki Basin (Kamp and Green, 1990; Crowhurst et al., 2002), which enhanced progradation of the shelf-slope margin to the north into the Taranaki Peninsula area and northwest into

Table 3
Assessment of recognition criteria for fans in southern and central Taranaki Basin versus North Taranaki Basin for the upper Moki and lower Mount Messenger formations based on seismic and well log data. Criteria after Posamentier and Erskine (1991) but expanded upon.

Aspect	Criteria	Southern Taranaki Basin		Western Taranaki Basin	
		Upper Moki Fm. (~14 Ma)	Lower Mt. Messenger Fm. (~12 Ma)	Mt. Messenger Fm. Deep Water Fan System 1 (~12 Ma)	Mt. Messenger Fm. Deep Water Fan System 2 (~6 Ma)
Physiography of fan systems	The mouth of the feeder canyon-channels can be located				
	The segments of the fans (i.e., upper and lower) can be identified				
Seismic stratigraphic interpretation	Continuous high-amplitude reflectors (usually at top fans) onlap basin margin				
	Bidirectional downlap reflectors within fan				
	Stratal terminations show pinch out				
	External mounding on the fan upper bounding surface				
Seismic amplitude analysis	Detuned seismic maps show regions of high amplitude that resemble fans				
Gamma-ray log signature	Overall trend of Gamma-ray log leaning towards fan depositions				

Legend
High confidence | Low confidence | No confidence | Cannot be accessed

deeper parts of the basin. These factors help explain why there is no submarine fan associated with the Moki channels, yet fans accumulated in deep water to the west and north in the Mount Messenger Formation.

The Middle Miocene Deep Water Fan System 1 (~13–12 Ma) coincides with the timing of a global drop in sea level (sea-level curve of Miller et al., 2020, Fig. 3B). While sea level change is considered to influence deep water sedimentation processes (e.g., Posamentier and Erskine, 1991; Xiong et al., 2004; Saller et al., 2004) the mechanism by which this occurs in the case of channel and fan development in Taranaki Basin is difficult to substantiate. The Late Miocene Deep Water Fan System 2 (~7–6 Ma) in deep water Taranaki Basin shows little correlation with a fall in sea level (less than 10 m) on the Miller et al. (2020) sea-level curve (Fig. 3B). Many workers (e.g., Covault and Graham, 2010; Dixon et al., 2012; Harris et al., 2018) have argued that deep water sedimentation can occur at any phase of a sea level cycle where submarine sediment routing systems remain connected to their sediment source areas, which may also have been the case for Taranaki Basin (Maier et al., 2013).

Research efforts to date have shown that the Moki Formation channels were relatively stable in their locations. From the late-Middle Miocene (Waiauan Stage) onwards, the shelf-slope margin in Taranaki Basin became increasingly rich in gullies as the depositional slope became steeper (Kamaruzaman et al., 2023). In the Mount Messenger Formation, the gullies were captured by feeder canyon-channels, which in turn fed sediment to two fans of different age (~13–12 Ma and ~7–6 Ma). However the rate of sediment supply to the depositional slope during the Late Miocene also resulted in the retention of a proportion of the material in the gully network, with frequent burial of gullies and formation of new ones as the slope rapidly prograded to the north and west (Kamaruzaman et al., 2023). The retention of material on the slope can partly explain the enigma that although there was copious supply of sediment to the basin during the Late Miocene, so far only two Mount Messenger Formation submarine fans have been documented outboard of the depositional slope (c.f., Fisher et al., 2021).

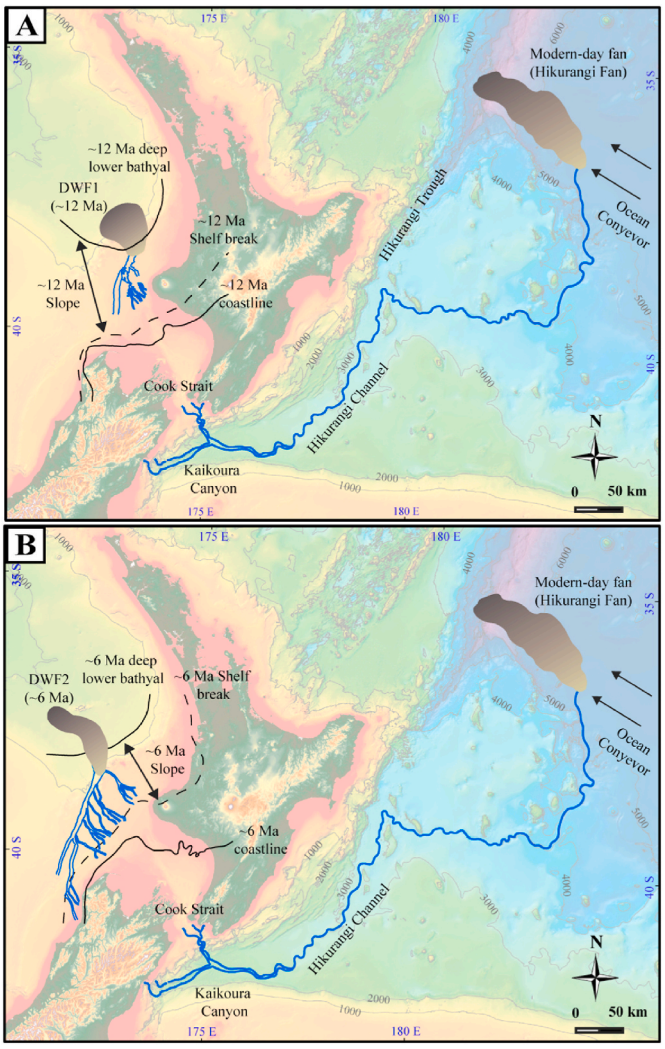

Fig. 22. Comparison between the newly interpreted (A) the Mount Messenger Formation Deep Water Fan System 1: DWF1 (~12 Ma) and (B) the Mount Messenger Formation Deep Water Fan System 2: DWF2 (~6 Ma) with the late Neogene fan (Hikurangi Fan) at the terminus of the Hikurangi Channel. Subdivision between the paleo-coastline, shelf-break (at 200 m water depth) and deep lower bathyal (>1500 m water depth) for ~12 Ma and ~6 Ma are also shown. The modern Hikurangi Channel and fan outlines are adapted from (Lewis et al., 2013), and modern seafloor bathymetry data (water depth in meter) are from NZP&M (2018).

7.2.2. Modern analogue

As noted above, the newly mapped Middle and Late Miocene deep-water fans in western Taranaki Basin are mudstone-dominated. Despite the Wainui-1 drill hole containing intervals of sandstone in the upper fan part of the ~13–12 Ma fan (Fig. 17C), the maximum width (10 km) of the main feeder canyon-channels and the distance of the fans from the contemporary shelf-slope break (~150 km) support this notion. The principal source rock area (Torlesse Complex in the Southern Alps) for the two fans is comprised of greywacke and schist, which breaks down by weathering and attrition to fine sand and mud. The closest analogue to the conditions that led to the Late Miocene fan accumulations in Taranaki Basin is the fan that has formed at the mouth of the Hikurangi Channel east of North Island (Fig. 22) (Grahame, 2015). Sediment entering the Hikurangi Channel is fed by the very steep Kaikoura Canyon offshore of the northern end of the Southern Alps and by canyons at the eastern end of Cook Strait (Fig. 22). The sediment routed via the Cook Strait canyons followed a pathway from the western face of the Southern Alps via longshore drift to the northwestern tip of South Island (Farewell Spit) and hence into Cook Strait. The Hikurangi Channel mostly lies at 3000–5000 m water depth east of the Hikurangi subduction zone. It traverses the Hikurangi Plateau (thickened oceanic crust) northward before turning sharply east and then north upon reaching the Southwest Pacific Abyssal Plain, where sediment transport and the depositional trajectory are strongly controlled by the Ocean Conveyor Current (Hikurangi Fan-drift; Lewis, 1994; Carter et al., 2004). At the terminus of the channel the sediment has accumulated in a mud-dominated basin floor fan called the Hikurangi Fan, which started accumulating during the late Neogene (Fig. 22) (Lewis et al., 2013; Mountjoy et al., 2018). Common features of the Hikurangi Fan and the Late Miocene fans in the Mount Messenger Formation are, (i) that their sediments derived from the same source area, (ii) they lie at the mouths of prominent channels, (iii) the sediments comprising the fans are mudstone, and (iv), they have similar plan shapes. In addition, the respective fans are small in size and volume compared with the volumes of material eroded from the Southern Alps during the late Neogene.

7.2.3. Significance of newly mapped deep water Mount Messenger formation fan systems for resource exploration

The significance of Moki Formation channels for petroleum exploration and production has been well described by Engbers et al. (2000) and Engbers (2002). The two newly mapped Mount Messenger submarine fans occur on the Western Stable Platform, a structural province built upon Palaeozoic basement, overlain in places by Late Cretaceous-Paleocene sediments, sometimes in half-grabens. The province is onlapped by Eocene-Recent strata disrupted by few faults (King and Thrasher, 1996). The Top Eocene surface forms a monocline dipping east, in part arising from flexure associated with Oligocene-Miocene foreland basin subsidence to the east (Holt and Stern, 1994). Oligocene and Miocene sediments onlap the monocline, including the two new fans described here. This structural and stratigraphic setting differs from that in the Taranaki oil and gas fields, which arises from structural traps. These either formed through shortening within the Taranaki Fault System or shortening in the southern Taranaki Inversion Zone, where antiforms formed from the inversion on pre-existing normal faults. The antiforms represent migration of shortening from the Taranaki Fault System into the foreland basin during the Late Miocene. Hence the two fans lie in frontier parts of Taranaki Basin and should oil and/or gas occur there, it is likely to be in stratigraphic traps. The presence of high-amplitude reflectors within the proximal upper fan segments, probably image continuous sheet sandstone beds (Shanmugam and Moiola, 1988; Nagatomo and Archer, 2015; Mayall and Kneller, 2021). This differs from the distal lower fan segments, which appear to be muddier, as shown by lower seismic amplitude (Reading and Richards, 1994; Bouma and Stone, 2000; Fildani et al., 2021). The mud-rich sediment calibre of the two fans and the inclusion of volcanic ash in the younger one will likely be challenges for reservoir quality. Seal may not be an issue. Given that only one drill hole (Wainui-1) has been located over one of the fans means that source rock distribution and composition are poorly known. Maturation of organic matter in either of the two fans will be an issue (VR of 0.58% in the coal measure beds in Wainui-1) to charge stratigraphic traps within the fans. Hence migration pathways from deeper organic horizons will need to be considered in any exploration proposal. To further access the petroleum potential of the fans, high-resolution 3D seismic volumes and seep analysis will likely be required ahead of drilling to gain some confidence about the presence or otherwise of mobile thermogenic hydrocarbons in the Mount Messenger Formation within the vicinity of the documented fans.

8. Conclusions

1) Submarine channels in the Middle Miocene Moki Formation are standalone features on the continental slope in southern Taranaki Basin and do not transition down-slope into submarine fans. Detuning of 3D seismic data coverage has removed the RMS high

amplitude extracted attribute signal from which the previously published Moki fans have been inferred. Published late-Middle Miocene submarine fans located on the continental slope in the Lower Mount Messenger Formation (southern and central Taranaki Basin) have also been dismissed on the same basis as well as not displaying well established stratal criteria for the identification of fan systems (Table 3).

2) Two new submarine fan systems in the Mount Messenger Formation do, however, occur in deeper parts of western Taranaki Basin, one of late-Middle Miocene age and the other of Late Miocene age. They have been mapped and verified on established submarine fan stratal criteria.
3) A marked increase in terrigenous sediment supply at about 12 Ma, sourced from uplift and erosion of the Southern Alps, resulted in rapid progradation of the Late Middle to Late Miocene continental slope in Taranaki Basin. Most sediment rapidly accumulated on the slope. Consequently, its angle increased and gullies became prolific, incising, infilling, re-incising and being buried. A few channels are mapped on the lower slope passing into a fan on the basin plain. A second fan with similar attributes and 7–6 Ma age accumulated above the first, extending farther out towards the New Caledonia Basin. Both fans are mud-dominated. Their volume is minor compared with the volume of sediment delivered to the basin during the Late Miocene and hence submarine fans are much less volumetrically significant than the slope as depositional surfaces. The Hikurangi Fan outboard of the Hikurangi subduction zone is a modern analogue for the two new fans documented here for western Taranaki Basin.

CRediT authorship contribution statement

Erman H. Kamaruzaman: Conceptualization, Investigation, Methodology, Software, Validation, Visualization, Writing - original draft. **Andrew D. La Croix:** Conceptualization, Methodology, Supervision, Writing - review & editing. **Peter J.J. Kamp:** Conceptualization, Methodology, Supervision, Writing - review & editing.

Declaration of competing interest

The authors declare that they have no known competing financial interests or personal relationships that could have appeared to influence the work reported in this paper.

Data availability

Data will be made available on request.

Acknowledgements

We thank Schlumberger for provision of academic licenses for Petrel software to the University of Waikato. We also thank Cegal for access to their Marina “Blueback” plugin, which was used in our seismic and well log interpretations. New Zealand Petroleum and Minerals (Ministry of Business, Innovation and Employment) is acknowledged as the source of seismic reflection and well data for Taranaki Basin. This paper was greatly improved by the reviews of Dr Xin Shan and an anonymous reviewer. We also thank Associate Editor Dr Eleonora Martorelli.

Appendix A. Supplementary data

Supplementary data to this article can be found online at https://doi.org/10.1016/j.marpetgeo.2023.106664.

References

Ab Fatah, A., Mohamed, H., Hee, R.P., Tukimin, N., 2016. Horizon Independent Detuning of Seismic Volume from Sarawak Field, pp. 1–5. https://doi.org/10.3997/2214-4609.201602407, 2016(1).

Amy, L.A., Talling, P.J., 2006. Anatomy of turbidites and linked debrites based on long distance (120 × 30 km) bed correlation, Marnoso Arenacea Formation, Northern Apennines, Italy. Sedimentology 53 (1), 161–212. https://doi.org/10.1111/j.1365-3091.2005.00756.x.

Assis, C., Santos, H., Schleicher, J., 2018. Colored and linear inversions to relative acoustic impedance. Geophysics 84 (2).

Baur, J.R., King, P.R., Stern, T., Leitner, B., Wood, L.J., Simo, T.T., Rosen, N.C., 2010. Development and seismic geomorphology of a Miocene slope channel megasystem, offshore Taranaki Basin, New Zealand. In: Seismic Imaging of Depositional and Geomorphic Systems (Vol. 30, pp. 0). SEPM Society for Sedimentary Geology. https://doi.org/10.5724/gcs.10.30.0618.

Bernhardt, A., Stright, L., Lowe, D.R., 2012. Channelized debris-flow deposits and their impact on turbidity currents: the Puchkirchen axial channel belt in the Austrian Molasse Basin. Sedimentology 59 (7), 2042–2070. https://doi.org/10.1111/j.1365-3091.2012.01334.x.

Bierbrauer, K., Herdy, T., Rek, A., Mills, K., 2008. Exploring the Greater Taranaki Basin North of the Established Hydrocarbon Fairway.

Bouma, A.H., 1962. Sedimentology of Some Flysch Deposits: A Graphical Approach to Facies Interpretation. Elsevier, New York.

Bouma, A.H., Stone, C., 2000. Fine-Grained, Mud-Rich Turbidite Systems: Model and Comparison with Coarse-Grained, Sand-Rich Systems, vol. 68. Special Publication-SEPM, pp. 9–20.

Brown, A.R., Wright, R.M., Burkart, K.D., Abriel, W.L., McBeath, R.G., 1986. Tuning effects, lithological effects and depositional effects in the seismic response of gas reservoirs. Geophys. Prospect. 34 (5), 623–647. https://doi.org/10.1111/j.1365-2478.1986.tb00485.x.

Bull, S., Nicol, A., Strogen, D., Kroeger, K., Seebeck, H.S., 2019. Tectonic controls on Miocene sedimentation in the Southern Taranaki Basin and implications for New Zealand plate boundary deformation. Basin Research 31 (2), 253–273. https://doi.org/10.1111/bre.12319.

Bunt, R.J.W., 2015. The use of seismic attributes for fan and reservoir definition in the Sea Lion Field, North Falkland Basin. Petrol. Geosci. 21 (2–3), 137–149. https://doi.org/10.1144/petgeo2014-055.

Bussell, M.R., 1994. Seismic Interpretation of the Moki Formation on the Maui 3D Survey, Taranaki Basin. New Zealand Petroleum Conference, Wellington.

Campbell, H.J., Mortimer, N., Turnbull, I.M., 2003. Murihiku supergroup, New Zealand: redefined. J. Roy. Soc. N. Z. 33 (1), 85–95. https://doi.org/10.1080/03014223.2003.9517722.

Carter, L., Carter, R.M., McCave, I.N., 2004. Evolution of the sedimentary system beneath the deep Pacific inflow off eastern New Zealand. Mar. Geol. 205 (1), 9–27. https://doi.org/10.1016/S0025-3227(04)00016-7.

Chopra, S., Castagna, J., Portniaguine, O., 2006. Thin bed reflectivity inversion. In: SEG Technical Program Expanded Abstracts 2006. Society of Exploration Geophysicists, pp. 2057–2061.

Connolly, P., 2007. A simple, robust algorithm for seismic net pay estimation. Lead. Edge 26 (10), 1278–1282. https://doi.org/10.1190/1.2794386.

Cooper, R., Agterberg, F.P., Alloway, B., Beu, A., Campbell, H., Crampton, J.S., Crouch, E., Crundwell, M., Graham, I.J., Hollis, C., Jones, C., Kamp, P., Mildenhall, D.C., Morgans, H., Naish, T.R., Raine, J.I., Roncaglia, L., Sadler, P.M., Schiøler, P., Wilson, G., 2004. The New Zealand Geological Timescale. Institute of Geological and Nuclear Sciences. Monograph, pp. 22–284.

Costard, F., Forget, F., Mangold, N., Mercier, D., Peulvast, J.-P., 2001. Debris Flows on Mars: Analogy with Terrestrial Periglacial Environment and Climatic Implications.

Covault, J.A., Graham, S.A., 2010. Submarine fans at all sea-level stands: tectono-morphologic and climatic controls on terrigenous sediment delivery to the deep sea. Geology 38 (10), 939–942. https://doi.org/10.1130/g31081.1.

Covault, J.A., Romans, B.W., 2009. Growth patterns of deep-sea fans revisited: turbidite-system morphology in confined basins, examples from the California Borderland. Mar. Geol. 265 (1), 51–66. https://doi.org/10.1016/j.margeo.2009.06.016.

Covault, J.A., Shelef, E., Traer, M., Hubbard, S.M., Romans, B.W., Fildani, A., 2012. Deep-water channel run-out length: insights from seafloor geomorphology. J. Sediment. Res. 82 (1), 21–36. https://doi.org/10.2110/jsr.2012.2.

Cronin, B.T., Akhmetzhanov, A.M., Mazzini, A., Akhmanov, G., Ivanov, M., Kenyon, N. H., 2005. Morphology, evolution and fill: implications for sand and mud distribution in filling deep-water canyons and slope channel complexes. Sediment. Geol. 179 (1), 71–97. https://doi.org/10.1016/j.sedgeo.2005.04.013.

Crowhurst, P., Green, P., Kamp, P., 2002. Appraisal of (U-Th)/He apatite thermochronology as a thermal history tool for hydrocarbon exploration: an example from the Taranaki Basin, New Zealand. AAPG (Am. Assoc. Pet. Geol.) Bull. 86 https://doi.org/10.1306/61EEDD82-173E-11D7-8645000102C1865D.

Curray, J.R., Emmel, F.J., Moore, D.G., 2002. The Bengal Fan: morphology, geometry, stratigraphy, history and processes. Mar. Petrol. Geol. 19 (10), 1191–1223. https://doi.org/10.1016/S0264-8172(03)00035-7.

Davis, C., Haughton, P., McCaffrey, W., Scott, E., Hogg, N., Kitching, D., 2009. Character and distribution of hybrid sediment gravity flow deposits from the outer Forties Fan, Palaeocene Central North Sea, UKCS. Mar. Petrol. Geol. 26 (10), 1919–1939. https://doi.org/10.1016/j.marpetgeo.2009.02.015.

De Bock, J.F., 1994. Moki Formation, a Miocene reservoir sequence, its facies distribution and source in offshore, southern Taranaki Basin. New Zealand Petroleum.

Deptuck, M.E., Sylvester, Z., 2018. Submarine fans and their channels, levees, and lobes. In: Submarine Geomorphology, pp. 273–299. https://doi.org/10.1007/978-3-319-57852-1_15.

Deptuck, M.E., Steffens, G.S., Barton, M., Pirmez, C., 2003. Architecture and evolution of upper fan channel-belts on the Niger Delta slope and in the Arabian Sea. Mar. Petrol. Geol. 20 (6–8), 649–676. https://doi.org/10.1016/j.marpetgeo.2003.01.004.

Dixon, J.F., Steel, R.J., Olariu, C., 2012. Shelf-edge delta regime as A predictor of deep-water deposition. J. Sediment. Res. 82 (9), 681–687. https://doi.org/10.2110/jsr.2012.59.

Droz, L., Bellaiche, G., 1991. Seismic facies and geologic evolution of the central portion of the indus fan. In: Weimer, P., Link, M.H. (Eds.), Seismic Facies and Sedimentary Processes of Submarine Fans and Turbidite Systems. Springer New York, pp. 383–402. https://doi.org/10.1007/978-1-4684-8276-8_21.

Engbers, P., 2002. Evaluation of Moki sands prospectivity. In: Maui PML. 1989 New Zealand Oil Exploration Conference Proceedings.

Engbers, P., Adams, S., Farmer, R., Mathers, R., Soek, H., 2000. Whaarangi; Prospect Potential Resolved. SPE Asia Pacific Oil and Gas Conference and Exhibition.

Escutia, C., Eittreim, S.L., Cooper, A.K., Nelson, C.H., 2000. Morphology and acoustic character of the antarctic wilkes land turbidite systems: ice-sheet-sourced versus river-sourced fans. J. Sediment. Res. 70 (1), 84–93. https://doi.org/10.1306/2dc40900-0e47-11d7-8643000102c1865d.

Fildani, A., Kostic, S., Covault, J.A., Maier, K.L., Caress, D.W., Paull, C.K., 2021. Exploring a new breadth of cyclic steps on distal submarine fans. Sedimentology 68 (4), 1378–1399. https://doi.org/10.1111/sed.12803.

Fisher, W.L., Galloway, W.E., Steel, R.J., Olariu, C., Kerans, C., Mohrig, D., 2021. Deep-water depositional systems supplied by shelf-incising submarine canyons: 2 recognition and significance in the geologic record. Earth Sci. Rev. 214 https://doi.org/10.1016/j.earscirev.2021.103531.

Flood, R.D., Damuth, J.E., 1987. Quantitative characteristics of sinuous distributary channels on the Amazon Deep-Sea Fan. GSA Bulletin 98 (6), 728–738.

Flood, R.D., Manley, P.L., Kowsmann, R.O., Appi, C.J., Pirmez, C., 1991. Seismic facies and late quaternary growth of amazon submarine fan. In: Weimer, P., Link, M.H. (Eds.), Seismic Facies and Sedimentary Processes of Submarine Fans and Turbidite Systems. Springer New York, pp. 415–433. https://doi.org/10.1007/978-1-4684-8276-8_23.

Francis, A., 2015. Geophysics: A Simple Guide to Seismic Amplitudes and Detuning, vol. 12. GeoExPro. https://www.geoexpro.com/articles/2015/11/geophysics-a-simple-guide-to-seismic-amplitudes-and-detuning.

Francis, A., 2016. Seismic amplitudes benefit from seismic trace detuning. https://www.hartenergy.com/exclusives/seismic-amplitudes-benefit-seismic-trace-detuning-176002#:~:text=In%20summary%2C%20seismic%20trace%20detuning%20is%20a%20significant,and%20direct%20hydrocarbon%20detection%20from%20seismic%20data.%2018.

Fudol, Y.A.H., Zhao, Y., Liu, H., Zhou, S., Li, Y., Li, X., 2019. Origin and reservoir properties of deep-water gravity flow sediments in the upper Triassic Ch6–Ch7 members of the Yanchang Formation in the Jinghe Oilfield, the southern Ordos basin, China. Energy Explor. Exploit. 37 (4), 1227–1252. https://doi.org/10.1177/0144598719832066.

Gaina, C., Müller, D.R., Royer, J.-Y., Stock, J., Hardebeck, J., Symonds, P., 1998. The tectonic history of the Tasman Sea: a puzzle with 13 pieces. J. Geophys. Res. Solid Earth 103 (B6), 12413–12433. https://doi.org/10.1029/98JB00386.

Gani, M.R., 2004. From turbid to lucid: a straightforward approach to sediment gravity flows and their deposits. Sediment. Rec. 2 (3), 4–8. https://doi.org/10.2110/sedred.2004.3.4.

Gong, C., Wang, H., Shao, D., Wang, H., Qi, K., Xu, X., 2022. How did the world's largest submarine fan in the Bay of Bengal grow and evolve at the subfan scale? AAPG (Am. Assoc. Pet. Geol.) Bull. 106 (7), 1431–1451. https://doi.org/10.1306/02072219107.

Grahame, J., 2015. Deepwater Taranaki Basin, New Zealand - New Interpretation and Modelling Results for Large Scale Neogene Channel and Fan Systems: Implications for Hydrocarbon Prospectivity. In: AAPG/SEG International Conference & Exhibition, Melbourne, Australia.

Grain, S.L., 2008. Paleogeography of a Mid Miocene Turbidite Complex. New Zealand Victoria University of Wellington, Moki Formation, Taranaki Basin.

Guo, Q., Islam, N., Pennington, W.D., 2015. Tuning of flat spots with overlying bright spots, dim spots, and polarity reversals. Interpretation: SEG 3 (3), SS37–SS48.

Hansen, R.J., Kamp, P.J., 2002. Evolution of the Giant Foresets Formation, Northern Taranaki Basin, New Zealand. In: New Zealand Petroleum Conference Proceedings, New Zealand, 24th–27th February.

Harris, A.D., Baumgardner, S.E., Sun, T., Granjeon, D., 2018. A poor relationship between sea level and deep-water sand delivery. Sediment. Geol. 370, 42–51. https://doi.org/10.1016/j.sedgeo.2018.04.002.

Haughton, P., Davis, C., McCaffrey, W., Barker, S., 2009. Hybrid sediment gravity flow deposits – classification, origin and significance. Mar. Petrol. Geol. 26 (10), 1900–1918. https://doi.org/10.1016/j.marpetgeo.2009.02.012.

Holt, W.E., Stern, T., 1994. Subduction, platform subsidence, and foreland thrust loading: the late Tertiary development of Taranaki Basin, New Zealand. Tectonics 13, 1068–1092.

Jager, D.D.H., Giles, M.R., Griffiths, G.R., 1993. Evolution of Paleogene submarine fans of the North Sea in space and time. Geol. Soc., London, Petrol. Geol. Conf. Ser. 4 (1), 59–71.

Jin, L., Shan, X., Shi, X., Fonnesu, M., Qiao, S., Kandasamy, S., Wang, H., Liu, S., Fang, X., Zou, X., 2021. Hybrid event beds generated by erosional bulking of modern hyperpycnal flows on the Choshui River delta front, Taiwan Strait. Sedimentology. https://doi.org/10.1111/sed.12862.

Kallweit, R.S., Wood, L.C., 1982. The limits of resolution of zero-phase wavelets. Geophysics 47 (7), 1035–1046. https://doi.org/10.1190/1.1441367.

Kamaruzaman, E.H., La Croix, A.D., Kamp, P.J.J., 2023. Quantitative seismic geomorphology of sediment conduits on an evolving Miocene slope in Taranaki Basin (New Zealand): the influence of increasing slope gradient through time. Mar. Petrol. Geol. 152, 106233 https://doi.org/10.1016/j.marpetgeo.2023.106233.

Kamp, P.J.J., Green, P., 1990. Thermal and tectonic history of selected Taranaki Basin (New Zealand) wells assessed by apatite fission track analysis. AAPG Bull. 74, 1401–1419.

Kamp, P.J.J., Green, P., White, S., 1989. Fission track analysis reveals character of collisional tectonics in New Zealand. Tectonics 8, 169–195. https://doi.org/10.1029/TC008i002p00169.

Kamp, P.J.J., Vonk, A.J., Bland, K.J., Hansen, R.J., Hendy, A.J.W., McIntyre, A.P., Ngatai, M., Cartwright, S.J., Hayton, S., Nelson, C.S., 2004. Neogene stratigraphic architecture and tectonic evolution of Wanganui, King Country, and eastern Taranaki basins, New Zealand. N. Z. J. Geol. Geophys. 47, 625–644.

King, P., Thrasher, G.P., 1996. Cretaceous-Cenozoic geology and petroleum systems of the Taranaki Basin, New Zealand. Inst. Geol. Nucl. Sci. Monogr. 13. Part 1 and 2.

King, P.R., Scott, G.H., Robinson, P.H., 1993. Description, Correlation and Depositional History of Miocene Sediments Outcropping along North Taranaki Coast.

Kroeger, K.F., Thrasher, G.P., Sarma, M., 2019. The evolution of a middle Miocene deep-water sedimentary system in northwestern New Zealand (Taranaki Basin): depositional controls and mechanisms. Mar. Petrol. Geol. 101, 355–372. https://doi.org/10.1016/j.marpetgeo.2018.11.052.

Lancaster, S., Whitcombe, D., 2000. Fast-track 'coloured' inversion. In: SEG Technical Program Expanded Abstracts 2000, pp. 1572–1575. https://doi.org/10.1190/1.1815711.

Lee, G.H., Watkins, J.S., Bryant, W.R., 1996. Bryant canyon fan system: an unconfined, large river-sourced system in the northwestern gulf of Mexico1. AAPG (Am. Assoc. Pet. Geol.) Bull. 80 (3), 340–357. https://doi.org/10.1306/64ED87DC-1724-11D7-8645000102C1865D.

Lee, H.J., Locat, J., Desgagnés, P., Parsons, J.D., McAdoo, B.G., Orange, D.L., Puig, P., Wong, F.L., Dartnell, P., Boulanger, E., 2007. Submarine mass movements on continental margins. In: Continental Margin Sedimentation: from Sediment Transport to Sequence Stratigraphy, vol. 37. Citeseer, pp. 213–274.

Lewis, K.B., 1994. The 1500-km-long Hikurangi Channel: trench-axis channel that escapes its trench, crosses a plateau, and feeds a fan drift. Geo Mar. Lett. 14 (1), 19–28. https://doi.org/10.1007/BF01204467.

Lewis, K., Carter, L., Nodder, S.D., 2013. Sea Floor Geology: New Zealand Sea-Floor Sediment, Te Ara: the Encyclopedia of New Zealand. http://www.TeAra.govt.nz/en/map/5624/hikurangi-channel.

Liu, C., Xie, X., Yu, X., Huang, L., He, Y., Chen, H., Tian, D., Mi, H., Li, M., Zhang, H., 2023. Kinematics and Sediment Dispersal Pattern of Multi-Stage Mass Transport Deposits on a Stepped Slope with Numerous Elliptical Depressions, Northwestern South China Sea.

Lowe, D.R., 1982. Sediment gravity flows; II, Depositional models with special reference to the deposits of high-density turbidity currents. J. Sediment. Res. 52 (1), 279–297. https://doi.org/10.1306/212f7f31-2b24-11d7-8648000102c1865d.

Maier, K.L., M, A., S A, C., P K, G., B, G.H., A, M.J., C, M.P., 2013. Provenance and Paleogeographic Reconstruction of a Progradational Deep-Water Slope Succession in the Late Miocene Taranaki Basin, North Island, New Zealand. Geological Society of America Abstracts with Programs, p. 604 v. 45/7.

Maier, K.L., Paull, C.K., Caress, D.W., Anderson, K., Nieminski, N.M., Lundsten, E., Erwin, B.E., Gwiazda, R., Fildani, A., 2020. Submarine-fan development revealed by integrated high-resolution datasets from La Jolla Fan, offshore California, U.S.A. J. Sediment. Res. 90 (5), 468–479. https://doi.org/10.2110/jsr.2020.22.

Márquez, E., Berton, F., Stevanato, A.C., Chaves, F., Ojevan, N., Brasil, E., 2021. New Opportunities in a Mature Oil Field: Stretching Data Interpretation for Complex Reservoir Prediction.

Maurya, S.P., Singh, N.P., 2017. Seismic Colored Inversion: A Fast Way to Estimate Rock Properties from the Seismic Data Challenges in Petro-Physical Evaluation and Rock Physics Modelling of Carbonate Reservoirs. Likely Elucidations & Way Forward, Victor Menezes Convention Centre (VMCC), IIT Bombay, India, 30th November–01st December 2017.

Mayall, M., Kneller, B., 2021. Seismic interpretation workflows for deep-water systems: A practical guide for the subsurface. AAPG (Am. Assoc. Pet. Geol.) Bull. 105 (11), 2127–2157. https://doi.org/10.1306/05262120094.

McHargue, T.R., 1991. Seismic Facies, Processes, and Evolution of Miocene Inner Fan Channels, Indus Submarine Fan. In: Weimer, P., Link, M.H. (Eds.), Seismic Facies and Sedimentary Processes of Submarine Fans and Turbidite Systems. Springer New York, pp. 403–413. https://doi.org/10.1007/978-1-4684-8276-8_22.

Micallef, A., Berndt, C., Masson, D.G., Stow, D.A.V., 2007. A technique for the morphological characterization of submarine landscapes as exemplified by debris flows of the Storegga Slide. J. Geophys. Res.: Earth Surf. 112 (F2) https://doi.org/10.1029/2006JF000505.

Middleton, G.V., Hampton, M.A., 1973. Part I. Sediment Gravity Flows: Mechanics of Flow and Deposition.

Miller, L.R., Stuart, W.J., 1992. Seismic stratigraphic evaluation of a neocomian submarine fan system, browse basin, north west shelf. APPEA J. 32, 171–182.

Miller, K.G., Browning, J.V., Schmelz, W.J., Kopp, R.E., Mountain, G.S., Wright, J.D., 2020. *Smoothed Cenozoic Sea-level Relative to Modern from Deep-Sea Geochemical and Continental Margin Records* PANGAEA. https://doi.org/10.1594/PANGAEA.923139.

Mitchell, W.H., Whittaker, A.C., Mayall, M., Lonergan, L., 2023. Reconciling bathymetric and stratigraphic expressions of submarine channel geometry. Mar. Geol. 459, 107025 https://doi.org/10.1016/j.margeo.2023.107025.

Mitchum Jr., R.M., Berg, O.R., Woolverton, D.G., 1985. Seismic Stratigraphic Expression of Submarine Fans. In: Seismic Stratigraphy II: an Integrated Approach to

Hydrocarbon Exploration. American Association of Petroleum Geologists. https://doi.org/10.1306/m39449c7.
Mountjoy, J.J., Howarth, J.D., Orpin, A.R., Barnes, P.M., Bowden, D.A., Rowden, A.A., Schimel, A.C.G., Holden, C., Horgan, H.J., Nodder, S.D., Patton, J.R., Lamarche, G., Gerstenberger, M., Micallef, A., Pallentin, A., Kane, T., 2018. Earthquakes drive large-scale submarine canyon development and sediment supply to deep-ocean basins. Sci. Adv. 4 (3), eaar3748.
Mutti, E., Ricci-Lucchi, F., 1972. Turbidites of the northern Apennines. A.G.I. Reprint Ser 3, 125–166. https://www.scopus.com/inward/record.uri?eid=2-s2.0-84912716413&partnerID=40&md5=21f6ea550aad24f5bc0104da731a25b6.
Nagatomo, A., Archer, S., 2015. Termination geometries and reservoir properties of the Forties Sandstone pinch-out, East Central Graben, UK North Sea. Geol. Soc. London, Special Pub. 403 (1), 133–155.
New Zealand Overseas Petroleum Ltd, 2004. Pateke-2 Well Completion Report.
Nomikou, P., Tibaldi, A., Pasquaré Mariotto, F., Papanikolaou, D., 2009. Submarine morphological analysis based on multibeam data of a huge collapse at the SE flank of Nisyros volcano. Rendiconti Online Societa Geologica Italiana 7, 177–179.
Normark, W.R., Gutmacher, C.E., 1983. Delgada Fan: Preliminary interpretation of channel development. Geo Mar. Lett. 3 (2), 79–83. https://doi.org/10.1007/BF02462451.
NZP&M, 2018. *New Zealand Petroleum Exploration Data Pack,* New Zealand Petroleum and Minerals.
Pareschi, M.T., Favalli, M., Giannini, F., Sulpizio, R., Zanchetta, G., Santacroce, R., 2000. 1998, debris flows in circum-Vesuvian areas (southern Italy): insights for hazard assessment. Geology 28 (7), 639–642. https://doi.org/10.1130/0091-7613(2000)28<639:MDFICA>2.0.CO;2.
Park, Y., Yoo, D., Kang, N., Yi, B., Kim, B., 2021. Tectonic control on mass-transport deposit and canyon-fed fan system in the Ulleung Basin, East Sea (Sea of Japan). Basin Res. 33 (2), 991–1016. https://doi.org/10.1111/bre.12501.
Parsons, J.D., Friedrichs, C.T., Traykovski, P.A., Mohrig, D., Imran, J., Syvitski, J.P.M., Parker, G., Puig, P., Buttles, J.L., García, M.H., 2007. The Mechanics of Marine Sediment Gravity Flows. In: *Continental Margin Sedimentation*, pp. 275–337. https://doi.org/10.1002/9781444304398.ch6.
Patacci, M., Marini, M., Felletti, F., Di Giulio, A., Setti, M., McCaffrey, W., 2020. Origin of mud in turbidites and hybrid event beds: Insight from ponded mudstone caps of the Castagnola turbidite system (north-west Italy). Sedimentology 67 (5), 2625–2644. https://doi.org/10.1111/sed.12713.
Pickering, K.T., Corregidor, J., 2005. Mass-Transport Complexes (MTCs) and Tectonic Control on Basin-Floor Submarine Fans, Middle Eocene, South Spanish Pyrenees. J. Sediment. Res. 75 (5), 761–783. https://doi.org/10.2110/jsr.2005.062.
Piper, D.J.W., Cochonat, P., Morrison, M.L., 1999. The sequence of events around the epicentre of the 1929 Grand Banks earthquake: initiation of debris flows and turbidity current inferred from sidescan sonar. Sedimentology 46 (1), 79–97. https://doi.org/10.1046/j.1365-3091.1999.00204.x.
Piper, D.J.W., Farre, J.A., Shor, A., 1985. Late Quaternary slumps and debris flows on the Scotian Slope. GSA Bull. 96 (12), 1508–1517.
Posamentier, H.W., Erskine, R.D., 1991. Seismic Expression and Recognition Criteria of Ancient Submarine Fans. In: Weimer, P., Link, M.H. (Eds.), Seismic Facies and Sedimentary Processes of Submarine Fans and Turbidite Systems. Springer, New York, pp. 197–222. https://doi.org/10.1007/978-1-4684-8276-8_10.
Posamentier, H.W., Martinsen, O.J., Shipp, R.C., Weimer, P., Posamentier, H.W., 2011. The Character and Genesis of Submarine Mass-Transport Deposits: Insights from Outcrop and 3D Seismic Data. In: Mass-Transport Deposits in Deepwater Settings (Vol. 96, pp. 0). SEPM Society for Sedimentary Geology. https://doi.org/10.2110/sepmsp.096.007.
Posamentier, H.W., Paumard, V., Lang, S.C., 2022. Principles of seismic stratigraphy and seismic geomorphology I: Extracting geologic insights from seismic data. Earth Sci. Rev. 228 https://doi.org/10.1016/j.earscirev.2022.103963.
Radovich, B.J., Armentrout, J.M., Rosen, N.C., 2002. Cyclic Attributes on Seismic Data and Sequence Stratigraphy—New Criteria for Exploration, New Interpretation Styles. In: Sequence Stratigraphic Models for Exploration and Production: Evolving Methodology, Emerging Models and Application Histories, vol. 22. SEPM Society for Sedimentary Geology.
Reading, H.G., Richards, M., 1994. Turbidite Systems in Deep-Water Basin Margins Classified by Grain Size and Feeder System 1. AAPG (Am. Assoc. Pet. Geol.) Bull. 78 (5), 792–822. https://doi.org/10.1306/a25fe3bf-171b-11d7-8645000102c1865d.
Ring, U., Glodny, J., Angiboust, S., Little, T., Lang, K.A., 2019. Middle to Late Miocene Age for the End of Amphibolite-Facies Mylonitization of the Alpine Schist, New Zealand: Implications for Onset of Transpression Across the Alpine Fault. Tectonics 38 (12), 4335–4359. https://doi.org/10.1029/2019TC005577.
Roncaglia, M., P, M., M, C., Miko, F., M, G., E, H., 2013. Well Log Stratigraphy in the Central and Southern Offshore Area of the Taranaki Basin, New Zealand. Lower Hutt : GNS Science.
Saller, A.H., Noah, J.T., Ruzuar, A.P., Schneider, R., 2004. Linked lowstand delta to basin-floor fan deposition, offshore Indonesia: An analog for deep-water reservoir systems. AAPG (Am. Assoc. Pet. Geol.) Bull. 88 (1), 21–46. https://doi.org/10.1306/09030303003.
Saller, A., Werner, K., Sugiaman, F., Cebastiant, A., May, R., Glenn, D., Barker, C., 2008. Characteristics of Pleistocene deep-water fan lobes and their application to an upper Miocene reservoir model, offshore East Kalimantan, Indonesia. AAPG (Am. Assoc. Pet. Geol.) Bull. 92 (7), 919–949. https://doi.org/10.1306/03310807110.
Sarg, J.F., Skjold, L.J., 1982. Stratigraphic traps in Paleocene sands in the Balder area, North Sea. The Deliberate Search for the Subtle Trap 32, 197–206. https://www.scopus.com/inward/record.uri?eid=2-s2.0-0013282272&partnerID=40&md5=6b708ac5cc42e6dc16a3dbfaf7d6849a.
Shan, X., Shi, X., Qiao, S., Jin, L., Otharán, G.A., Zavala, C., Liu, J., Zhang, Y., Zhang, D., Xu, T., Fu, C., 2019. The fluid mud flow deposits represent mud caps of Holocene hybrid event beds from the widest and gentlest shelf. Marine Geology 415, 105959. https://doi.org/10.1016/j.margeo.2019.06.004.
Shanmugam, G., 2000. 50 years of the turbidite paradigm (1950s—1990s): deep-water processes and facies models—a critical perspective. Mar. Petrol. Geol. 17 (2), 285–342. https://doi.org/10.1016/S0264-8172(99)00011-2.
Shanmugam, G., 2009. Slides, Slumps, Debris Flows, and Turbidity Currents. In: Steele, J. H. (Ed.), Encyclopedia of Ocean Sciences, second ed. Academic Press, pp. 447–467. https://doi.org/10.1016/B978-012374473-9.00669-X.
Shanmugam, G., 2013. New perspectives on deep-water sandstones: Implications. Petrol. Explor. Dev. 40 (3), 316–324. https://doi.org/10.1016/S1876-3804(13)60038-5.
Shanmugam, G., 2016. Submarine fans: A critical retrospective (1950–2015). J. Palaeogeogr. 5 (2), 110–184. https://doi.org/10.1016/j.jop.2015.08.011.
Shanmugam, G., Moiola, R.J., 1988. Submarine fans: Characteristics, models, classification, and reservoir potential. Earth Sci. Rev. 24 (6), 383–428. https://doi.org/10.1016/0012-8252(88)90064-5.
Shanmugam, G., Wang, Y., 2015. The landslide problem. J. Palaeogeogr. 4 (2), 109–166. https://doi.org/10.3724/SP.J.1261.2015.00071.
Shanmugam, G., Shrivastava, S.K., Das, B., 2009. Sandy Debrites and Tidalites of Pliocene Reservoir Sands in Upper-Slope Canyon Environments, Offshore Krishna-Godavari Basin (India): Implications. J. Sediment. Res. 79 (9), 736–756. https://doi.org/10.2110/jsr.2009.076.
Shell BP Todd Oil Services Ltd, 1982. Well Resume, Wainui-1. Taranaki Offshore. *PPL 38049*.
Simm, R.W., 2009. Simple net pay estimation from seismic: a modelling study. First Break 27, 45–53.
Simm, R., Bacon, M., 2014. Seismic Amplitude: an Interpreter's Handbook. Cambridge University Press.
Sohn, Y.K., 2000. Depositional Processes of Submarine Debris Flows in the Miocene Fan Deltas, Pohang Basin, SE Korea with Special Reference to Flow Transformation. J. Sediment. Res. 70 (3), 491–503. https://doi.org/10.1306/2DC40922-0E47-11D7-8643000102C1865D.
Sømme, T.O., Jackson, C.A.L., Vaksdal, M., 2013. Source-to-sink analysis of ancient sedimentary systems using a subsurface case study from the Møre-Trøndelag area of southern Norway: Part 1 – depositional setting and fan evolution. Basin Res. 25 (5), 489–511. https://doi.org/10.1111/bre.12013.
Stagpoole, V., Nicol, A., 2008. Regional structure and kinematic history of a large subduction back thrust: Taranaki Fault, New Zealand. J. Geophys. Res. Solid Earth 113 (B1).
Stow, D.A.V., Mayall, M., 2000. Deep-water sedimentary systems: New models for the 21st century. Mar. Petrol. Geol. 17 (2), 125–135. https://doi.org/10.1016/S0264-8172(99)00064-1.
Strogen, D.P., Baur, J.R., Bland, K.J., King, P.R., Vonk, A.J., Kamp, P.J.J., 2011. Updated Paleogeographic Maps for the Taranaki Basin and Surrounds (GNS Science Report 2010/53, Issue).
Strogen, D.P., Bland, K.J., Nicol, A., King, P.R., 2014. Paleogeography of the Taranaki Basin Region during the Latest Eocene–Early Miocene and Implications for the 'Total Drowning' of Zealandia. N. Z. J. Geol. Geophys. 57 (2), 110–127. https://doi.org/10.1080/00288306.2014.901231.
Strogen, D., Seebeck, H., Nicol, A., King, P., 2017. Two-phase Cretaceous–Paleocene rifting in the Taranaki Basin region, New Zealand; implications for Gondwana breakup. GNS Science.
Strogen, D.P., Seebeck, H., Hines, B.R., Bland, K.J., Crampton, J.S., 2022. Palaeogeographic evolution of Zealandia: mid-Cretaceous to present. N. Z. J. Geol. Geophys. 1–30. https://doi.org/10.1080/00288306.2022.2115520.
Talling, P.J., 2013. Hybrid submarine flows comprising turbidity current and cohesive debris flow: Deposits, theoretical and experimental analyses, and generalized models. Geosphere 9 (3), 460–488. https://doi.org/10.1130/ges00793.1.
Talling, P.J., Wynn, R.B., Masson, D.G., Frenz, M., Cronin, B.T., Schiebel, R., Akhmetzhanov, A.M., Dallmeier-Tiessen, S., Benetti, S., Weaver, P.P.E., Georgiopoulou, A., Zühlsdorff, C., Amy, L.A., 2007. Onset of submarine debris flow deposition far from original giant landslide. Nature 450 (7169), 541–544. https://doi.org/10.1038/nature06313.
Tippett, J.M., Kamp, P.J.J., 1993. Fission track analysis of the late Cenozoic vertical kinematics of continental Pacific crust, South Island, New Zealand. J. Geophys. Res. Solid Earth 98 (B9), 16119–16148.
Vail, P.R., 1987. Seismic Stratigraphy Interpretation Using Sequence Stratigraphy: Part 1: Seismic Stratigraphy Interpretation Procedure.
Vesely, F.F., 2016. Seismic expression of depositional elements associated with a strongly progradational shelf margin: northern Santos Basin, southeastern Brazil. Braz. J. Genet. 46, 585–603.
Walker, R.G., 1978. Deep-water sandstone facies and ancient submarine fans: Models for exploration for stratigraphic trap. AAPG Bull. 62 (6).
Weimer, P., 1990. Sequence Stratigraphy, Facies Geometries, and Depositional History of the Mississippi Fan, Gulf of Mexico1. AAPG (Am. Assoc. Pet. Geol.) Bull. 74 (4), 425–453. https://doi.org/10.1306/0C9B2321-1710-11D7-8645000102C1865D.
Weimer, P., Link, M.H., 1991. Global Petroleum Occurrences in Submarine Fans and Turbidite Systems. In: Weimer, P., Link, M.H. (Eds.), Seismic Facies and Sedimentary Processes of Submarine Fans and Turbidite Systems. Springer New York, pp. 9–67. https://doi.org/10.1007/978-1-4684-8276-8_2.

Widess, M.B., 1973. How thin is a thin bed? Geophysics 38 (6), 1176–1180. https://doi.org/10.1190/1.1440403.

Xiong, P., Shaokun, Y., Ming, Z., Jinsong, L., 2004. Deep-water Fan Systems and Petroleum Resources on the Northern Slope of the South China Sea. Acta Geologica Sinica - Eng. Ed. 78 (3), 626–631. https://doi.org/10.1111/j.1755-6724.2004.tb00175.x.

Zampetti, V., Schlager, W., van Konijnenburg, J.-H., Everts, A.-J., 2004. 3-D Seismic Characterization of Submarine Landslides on a Miocene Carbonate Platform (Luconia Province, Malaysia). J. Sediment. Res. 74 (6), 817–830. https://doi.org/10.1306/040604740817.

Data in Brief 52 (2024) 110035

Contents lists available at ScienceDirect

Data in Brief

journal homepage: www.elsevier.com/locate/dib

Data Article

Dataset of 3D computer models of Late Miocene Mount Messenger Formation outcrops in New Zealand, built with UAV drones

Erman H. Kamaruzaman*, Andrew D. La Croix, Peter J.J. Kamp

Sedimentary Environments and Analogues Research Group, Earth and Environmental Sciences, School of Science, University of Waikato, Private Bag 3105, Hamilton 3240, New Zealand

ARTICLE INFO

Article history:
Received 19 November 2023
Revised 31 December 2023
Accepted 3 January 2024
Available online 9 January 2024

Dataset link: 3D drone outcrop models of the Mount Messenger Formation, New Zealand (Original data)

Keywords:
Taranaki Basin
Late Miocene
Virtual fieldwork
Deep-water sedimentary systems
Mount Messenger Formation

ABSTRACT

The aim of constructing 3D computer models of outcrops of the Mount Messenger Formation using unmanned aerial vehicle (UAV) drone technology was to enable better visualization and potential for analysis of deep-water sedimentary systems in Taranaki Basin, New Zealand. The Late Miocene-aged strata crop out along the north Taranaki coast of western North Island, New Zealand. The Mount Messenger Formation sandstone and siltstone beds are outstanding examples of deep-water sedimentary strata. These strata can be observed in outcrop sections, as well as in offshore drillholes (wireline logs) and in seismic reflection data acquired immediately offshore of the north Taranaki coastal section. In previous research undertaken on the Mount Messenger Formation in North Taranaki Basin, geologists used photographs and coupled these with observations and descriptions of strata in the field. Modern UAV drone technology now enables 3D perspectives to be obtained of outcrop sections, which greatly improves geometrical analysis of the rocks. This type of analysis, coupled with mapping of seismic reflection data in the immediate offshore area has enabled us to better understand the nature of Mount Messenger Formation deep-water sedimentary strata and to interpret the asso-

* Corresponding author.
E-mail address: ek100@students.waikato.ac.nz (E.H. Kamaruzaman).

https://doi.org/10.1016/j.dib.2024.110035

ciated paleogeography with implications for energy resource exploration and evaluation.
Using UAV drone photogrammetry, we acquired ~3000 images of the Mount Messenger Formation outcrop at four locations along the north Taranaki coast. Drone surveys were conducted using a real-time kinetic (RTK) global positioning system (GPS) for accurate geolocation. The surveys were conducted on a DJI Phantom 4 drone, with a focal length of 24 mm with a 20-megapixel resolution. Survey images overlapped by 80–90%. The drone work adhered to the rules and regulations of the Aviation Security Service and the University of Waikato, New Zealand. Images were captured using programmed flight paths where the drone faced the outcrops at distances ranging from ~3–7 m.
3D computer models were constructed using Pix4Dmapper version 4.4.12 to generate dense 3D point clouds, digital surface models (DSMs), triangle meshes, and orthomosaic images of the outcrops (i.e., 3D models). Once the 3D computer models of the outcrops were constructed, they were exported out of Pix4Dmapper as ArcGIS Scene Layer Package format (.slpk) and loaded into ArcGIS Pro version 3.0.3 for further analysis.
The 3D computer models comprise a rich and valuable scientific dataset that can enhance geological analysis of sedimentary strata beyond the capabilities of photographs and manual fieldwork. These models allow desktop analysis of the geology and "virtual fieldwork" by imaging areas that are commonly inaccessible on foot due to their high elevation above ground level, location in rugged and steep terrane, as well as periodic intertidal flooding. This electronic geological dataset is stored in commonly used spatial format and plain-text ASCII files, allowing the preservation of geological data in digital records, especially when the outcrops are prone to erosion and cover by vegetation. The drone model dataset can be reused by the scientific community for virtual geological fieldwork, as petroleum and water reservoir analogues, as well as for research on coastal, environmental and geotechnical topics.

Specifications Table

Subject	Earth and Planetary Sciences / Geology
Specific subject area	Construction of 3D computer model dataset based on geolocated UAV drone images of Mount Messenger Formation outcrops on coastal sections of Taranaki Basin, North Island, New Zealand
Data format	Raw
Type of data	.slpk files (Scene Layer Packages) .xyz files (ASCII data with X,Y and Z coordinates) .ppkx files (ArcGIS Pro Project Packages)
Data collection	Approximately three thousand photographs were captured using UAV drones at four geological outcrop locations along the North Taranaki coast, North Island, New Zealand (Figs. 1 and 2). Images were captured using a DJI Phantom 4 drone connected to a real-time kinetic (RTK) global positioning system (GPS)

(*continued on next page*)

	for accurate geolocation. In addition to the RTK GPS, we also used a Leica GPS system for precise ground geolocation. Drone surveys of the four sites used programmed flight paths operating on the WGS 84 coordinate reference system and EGM 2008 Geoid. The focal length of the drone camera was 24 mm with a 20-megapixel resolution. The images captured outcrop at an average of 3–10 cm Ground Sampling Distance (GSD). Survey images were overlapped by 80–90%. Once the surveys were completed, drone images were processed using Pix4Dmapper version 4.4.12 to generate dense 3D point clouds, digital surface models (DSMs), triangle meshes, and orthomosaic images of the outcrops (i.e., 3D models). Once 3D outcrop models were built, they were exported out of Pix4Dmapper in Scene Layer Package format, and then imported into ArcGIS Pro-version 3.0.3. Drone surveys were conducted on relatively fair-weather days where cloud cover was minimal and with wind speeds below 32 kms per hour to ensure sufficient exposure on the outcrops for good quality photographs. Permission from the Department of Conservation (New Zealand Government) and a private landowner were obtained prior to conducting the surveys. Licensed drone operators were in charge of surveys, which were flown on the 16th- 17th of June, 12th of August, and 28th-29th of October 2023.
Data source location	The location of the sites where drone surveys were conducted are as follow: 1. Site 1 - Latitude: 38°39′56.49″S, Longitude: 174°37′48.01″E 2. Site 2 - Latitude: 38°42′27.39″S, Longitude: 174°37′1.52″E 3. Site 3 - Latitude: 38°46′9.60″S, Longitude: 174°36′0.00″E 4. Site 4 - Latitude: 38°49′0.24″S, Longitude: 174°35′9.04″E These locations are situated on the west coast of New Zealand's North Island (Figs. 1 and 2).
Data accessibility	Repository name: Harvard Dataverse 2023 Data identification number: https://doi.org/10.7910/DVN/I0C6 × 3 Direct URL to data: 3D drone outcrop models of the Mount Messenger Formation, New Zealand - Harvard Dataverse Instructions for accessing these data: Log in to the database using your credentials and download the data.
Related research article	

1. Value of the Data

- This dataset is valuable because it can be used to enhance visualization of large-scale geological layers. The 3D models provide a more precise and detailed representation of geological strata compared with photographs and hand-drawn sketches, which are historically how geological field observations have been recorded. This enhanced vizualisation helps geologists, geophysicists and engineers better understand the stratigraphic and structural characteristics of strata in outcrops that were deposited in ancient deep-water sedimentary environments.
- The value of the data also lies in its capacity to facilitate virtual fieldwork or field trips. The 3D models enable researchers and students to conduct digital field analysis of the geological layers. Many sections of the Mount Messenger Formation outcrop are inaccessible due to their location at high elevation above ground level, occurrence in rugged and steep terrane, as well as coastal areas that may be periodically submerged during high tides. Moreover, UAV drone surveys require permission from landowners, which may limit access to field locations. The 3D models of rock outcrops are of particular use for scientists and students conducting research when travel is not permitted (e.g., during the COVID-19 lockdown), or if they are physically unable to undertake fieldwork.
- This dataset is valuable because it digitally preserves geological data and observations. The 3D computer models are digital records of the geological outcrops and preserve this for use indefinitely into the future. This is particularly important for the Mount Messenger

Formation outcrops along the west coast of the North Island of New Zealand because they are prone to coastal erosion and significant vegetation cover.

- This dataset can be used by other scientists and students for research and education relating to sedimentology, stratigraphy, and sedimentary basin analysis of paleo deep-water sedimentary systems.
- This dataset can be used by researchers and industry practitioners for flow modelling of aquifers, petroleum reservoirs, and carbon capture and geostorage intervals. The 3D computer models are analogues to other reservoir systems globally that were deposited by deep-water sedimentary systems and can be used to estimate flow properties such as porosity and permeability distributions.
- This dataset can be used for coastal geological and geomorphological research. The models will help us understand how coastal erosion develops over time. For instance, outcrops at Sites 3 and 4 are situated along the coast and are subject to constant erosion from marine processes (Fig. 2C and D). Throughout our multiple visits to the sites to conduct drone surveys, we noticed parts of the outcrops had collapsed and eroded between visits. Apart from coastal studies, this dataset can be used by other researchers for environmental and geotechnical analysis. The outcrop models can assist researchers in studies of landslides. For example, the outcrop at Site 2 (Fig. 2B) is adjacent to State Highway 3 (i.e., Mokau Road). Landslides and rock falls are common in this area and cause serious environmental and safety issues and road closures.

2. Background

The aim of constructing 3D computer models of geological outcrops of the Mount Messenger Formation was to better understand ancient deep-water sedimentary systems in Taranaki Basin. The Late Miocene-aged sedimentary strata that outcrop along the north Taranaki coast (Figs. 1 and 2) are excellent examples of deep-water sandstone and siltstone layers that are also present in offshore drill hole materials are imaged in seismic reflection data [1,4]. While previous studies [2,6] of these outcrops mainly used photographs, this study is the first to introduce UAV drones imagery to capture their sedimentary characteristics. Incorporating drones in this study allowed a broader coverage of areas than previously possible, including areas inaccessible by foot. Therefore, geological analysis of these deep-water sedimentary systems is improved, especially when viewed from a 3D perspective. This analysis yields a more holistic understanding of the ancient sedimentary system in the region, surpassing the insights provided by earlier studies. The drone images were processed in Pix4Dmapper version 4.4.12 with precise geolocation to generate the 3D computer models. Then, qualitative and quantitative stratigraphic analyses of the outcrops were carried out using ArcGIS Pro version 3.0.3 [5].

3. Data Description

The 3D computer models of rock outcrops along the north Taranaki coast, New Zealand, were built using UAV drones to capture images of the sedimentary characteristics of the Late Miocene Mount Messenger Formation beds. Each 3D computer model allows the geometric analysis of sandstone and siltstone layers to be calculated, including bed thickness, bed orientation, as well as stratal stacking patterns (e.g., comfortable and erosional) and related structural deformation (e.g., faulting and folding). The present-day elevation, aerial extent, length and camera-facing direction of the outcrops are displayed in Table 1. The dataset are stored in a public research database: doi:10.7910/DVN/I0C6 × 3 [3]

Seven 3D computer models of geological outcrops are stored in ArcGIS Scene Layer Package format (i.e., Site 1 Battleship Promontory.slpk, Site 2 Ferry Sandstone.slpk, Site 3 Jam Roll Part 1.slpk, Site 3 Jam Roll Part 2.slpk, Site 4 Tongaporutu River Mouth Part 1.slpk and Site 4 Tongaporutu River Mouth Part 2.slpk). Scene layer package (.slpk) format was chosen to optimize

Fig. 1. Overview map of the drone survey areas. The inset map shows the locations along the north Taranaki Coast, North Island, New Zealand (red polygon). (For interpretation of the references to color in this figure legend, the reader is referred to the web version of this article.)

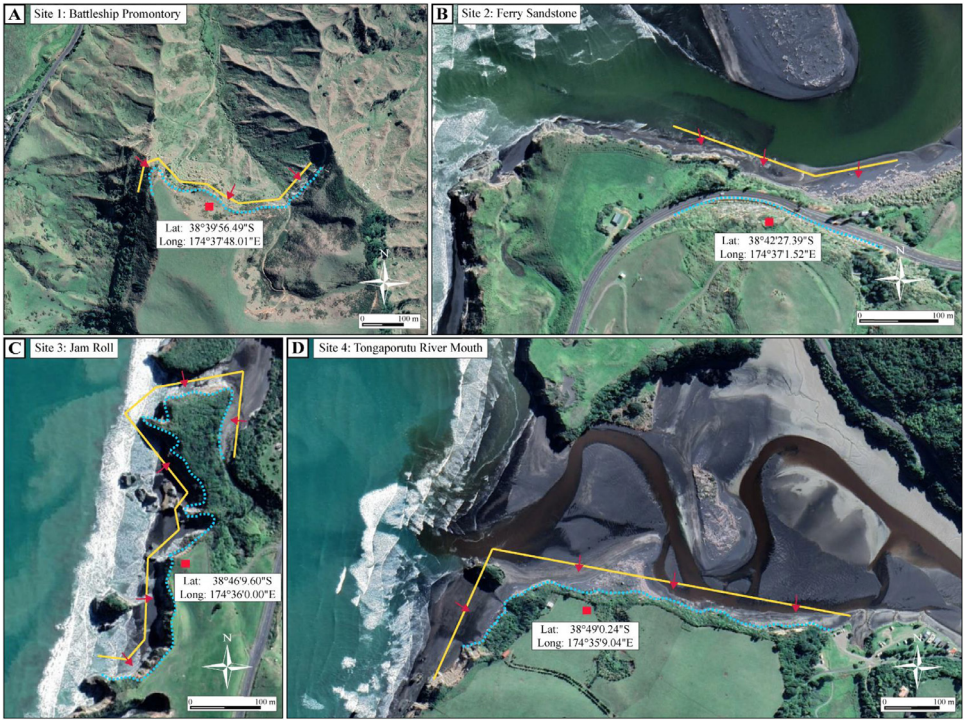

Fig. 2. Close-up of the study areas: (A) Site 1 Battleship Promontory, (B) Site 2 Ferry Sandstone, (C) Site 3 Jam Roll and (D) Site 4 Tongaporutu River Mouth. The yellow lines are the drone flight paths, and the red arrows represent the direction that drone cameras were facing. (For interpretation of the references to color in this figure legend, the reader is referred to the web version of this article.)

Table 1
Outcrop site elevation ranges and estimated length and aerial extent.

Site	Elevation range (mean sea level)	~ Length	~ Aerial extent
Site 1	145–210 m	900 m	0.20 km^2
Site 2	7–80 m	370 m	0.035 km^2
Site 3	0.5–22 m	800 m	0.092 km^2
Site 4	2 to 25 m	900 m	0.052 km^2

the large file size of these 3D models. The corresponding ASCII files (.xyz format) of the computer models have the coordinates (horizontal) and elevation (vertical) information originating from the Digital Surface Model (DSM). The application of these ASCII files is extremely flexible and can be imported into many standard spatial-based software. The resolution of the 3D models and the DSM are based on the density of the point cloud during their generation in Pix4Dmapper software, which ranged from 20 to 50 cm.

The companion ArcGIS Pro project package (.ppkx format) contains all four 3D computer models. Scientists and students, primarily geologists, can import individual models (.slpk) into their own ArcGIS Pro project, or can directly use the companion ArcGIS Pro project. The summary of the dataset is presented in Table 2. The drone models use the WGS 84 UTM 60S coordinate reference system. When opening the ArcGIS project, users must have sufficient high-end computer capacity to display the drone models and import the ASCII files for Digital Surface Model generation.

Table 2
Description of the dataset.

Item	Description
3D computer models – scene layer packages	
1. Site 1 Battleship Promontory Close up.slpk	3D computer model of Site 1 – close up view
2. Site 1 Battleship Promontory Overview.slpk	3D model of Site 1 - overview
3.Site 2 Ferry Sandstone.slpk	3D model of Site 2
4.Site 3 Jam Roll part 1.slpk	3D model of Site 3 - first part
5. Site 3 Jam Roll part 2.slpk	3D model of Site 3 - second part
6. Site 4 Tongaporutu River Mouth part 1.slpk	3D model of Site 4 - first part
7. Site 4 Tongaporutu River Mouth part 2.slpk	3D model of Site 4 - second part
Digital Surface Model (DSM) – ASCII xyz	
1. Site 1 Battleship Promontory Close up_i.xyz	DSM for Site 1 - close up view part 1
2. Site 1 Battleship Promontory Close up_ii.xyz	DSM for Site 1 - close up view part 2
3. Site 1 Battleship Promontory Overview.xyz	DSM for Site 1 - overview
4. Site 2 Ferry Sandstone.xyz	DSM for Site 2
5. Site 3 Jam Roll part 1_i.xyz	DSM for Site 3 - part 1
6. Site 3 Jam Roll part 1_ii.xyz	DSM for Site 3 - part 1 continue
7. Site 3 Jam Roll part 2.xyz	DSM for Site 3 - part 2
8. Site 4 Tongaporutu River Mouth part 1_i.xyz	DSM for Site 4 – part 1
9. Site 4 Tongaporutu River Mouth part 1_ii.xyz	DSM for Site 4 - part 1 continue
10.Site 4 Tongaporutu River Mouth part 2.xyz	DSM for Site 4 - part 2
ArcGIS Pro (version 3.0.3) project packages	
1. Sites 1 and 2 3D computer models	ArcGIS Pro project of the 3D computer model for Sites 1 and 2
2. Sites 3 and 4 3D computer models	ArcGIS Pro project of the 3D computer model for Sites 3 and 4

The 3D computer models generated herein are extremely valuable as they enhance the analysis potential of large-scale geological layers, which offers more precise and detailed representations of strata compared to traditionalphotographs and field observations. This will aid geologists, geophysicists, and engineers in gaining a better understanding of the stratigraphic and structural characteristics of formations deposited by ancient deep-water sedimentary systems. Furthermore, the data's utility extends to facilitating virtual fieldwork and field trips by researchers and students, which is advantageous for analyzing areas that are challenging to access due to high elevation, rugged terrain, or locations prone to periodic submersion during high tides. Particularly, these 3D models become invaluable in situations where travel restrictions, such as due to COVID-19, or physical constraints prevent traditional fieldwork from being undertaken.

In addition to the dataset's value for analysis and access, it is also especially important for the digital preservation of geological data and observations. The 3D computer models serve as enduring digital records of these globally significant geological outcrops, which is crucial for the Mount Messenger Formation along the west coast of the North Island of New Zealand, given their vulnerability to coastal erosion and substantial vegetation cover.

Beyond the primary users, this dataset also proves beneficial for other scientists and students engaged in sedimentology, stratigraphy, and sediment basin analysis of paleo deep-water sedimentary deposits. Researchers and industry practitioners may also find utility in this dataset for flow modeling of aquifers, petroleum reservoirs, and carbon capture and geostorage intervals. The 3D computer models function as analogs to similar reservoir systems globally, aiding in estimating flow properties such as porosity and permeability distributions.

Finally, this dataset can be used to support coastal geological and geomorphological research, offering insights into the development of coastal erosion over time. For example, outcrops at specific sites along the coast experience constant erosion from marine processes, impacting the landscape between visits. Beyond coastal studies, the dataset is versatile, applying to environmental and geotechnical analyses. The outcrop models contribute to studies of landslides, exemplified by the outcrop at a specific site adjacent to State Highway 3, an area prone to landslides and rock falls with consequential environmental, safety, and road closure implications.

4. Experimental Design, Materials and Methods

The acquisition of the dataset was divided into three stages:

1. Planning:

Planning the drone surveys involved a pre-survey reconnaissance trip to the outcrop sites to assess the feasibility of conducting drone survey operations at the proposed locations. The reconnaissance was carried out in April 2023. Once the drone survey operations were deemed feasible, the drone survey routes and specific locations were planned and necessary permissions from the Department of Conservation, the New Zealand Government, and a private landowner were sought. Once permissions were granted, drone operations were scheduled to account for weather, daylight, and tidal conditions at coastal locations (Sites 3 and 4).

2. Drone survey:

Drone surveys were conducted on the 16th and 17th of June, 12th of August, and 28th and 29th of October 2023. Drone images were captured using programmed flight paths operating on the WGS 84 UTM coordinate reference system and EGM 96 Geoid. RTK and Leica GPS systems were linked to the drone for precise geolocation. The GPS accuracy ranged from 10 to 30 cm. The flight paths were planned to front-face the outcrops, and the distance from the outcrops at Sites 1, 3 and 4 was kept in the range of approximately 3–7 m. However, the drone distance from the outcrop at Site 2 (Fig. 2B) was kept at approximately 15–20 m due to proximity to the road. Due to access permissions, at Site 3, the drone was not allowed to fly over the outcrops, except along the beach section (Fig. 2C). The focal length of the drone camera is 24 mm and images have 20-megapixel resolution. Survey images overlap by 80–90%. Drone survey operations were conducted per the rules and regulations of the Aviation Security Service, New Zealand, and the University of Waikato.

3. 3D outcrop model construction

Approximately three thousand drone images (in jpeg format) were captured during drone surveys. Quality checks of the images ensured that they adequately captured the areas of interest. Minimum preprocessing of images was undertaken, such as colour correction and contrast enhancement. However, 95% of the drone images did not require preprocessing.

The 3D outcrop drone models were constructed in Pix4Dmapper (version 4.4.12) (Fig. 3). At each outcrop site, the software was used to generate dense 3D point clouds, digital surface models (DSMs), digital terrain models (DTMs), triangle meshes, and orthomosaic images of the outcrops (i.e., 3D models). Constructing individual 3D models took roughly 3–5 h to complete, and the processing reports are attached in the Supplementary Data. Once the 3D outcrop models were constructed, they were exported out of Pix4Dmapper in ArcGIS Pro (version 3.0.3) Scene Layer Package format (.slpk) and loaded into ArcGIS Pro for further geological analysis. An example of the 3D outcrop model is shown in Fig. 4. Accordingly, the corresponding Digital Surface Models are exported to ASCII (.xyz format).

Limitations

Limitations of 3D computer models built using UAV drone imagery are primarily a function of drone image resolution and their associated models (which in this case ranges from 20 to 50 cm), based on the density of point clouds at certain locations within the models. The GPS accuracy recorded in the field ranged from 10 to 30 cm.

Weather conditions were another limiting factor, especially in terms of adequate sun exposure to capture clear imagery. For example, small parts of the outcrop were not illuminated by the sun to a satisfactory level. However, this did not hinder our objective to conduct geological analysis because the sandstone beds are relatively easy to identify, even under low lighting.

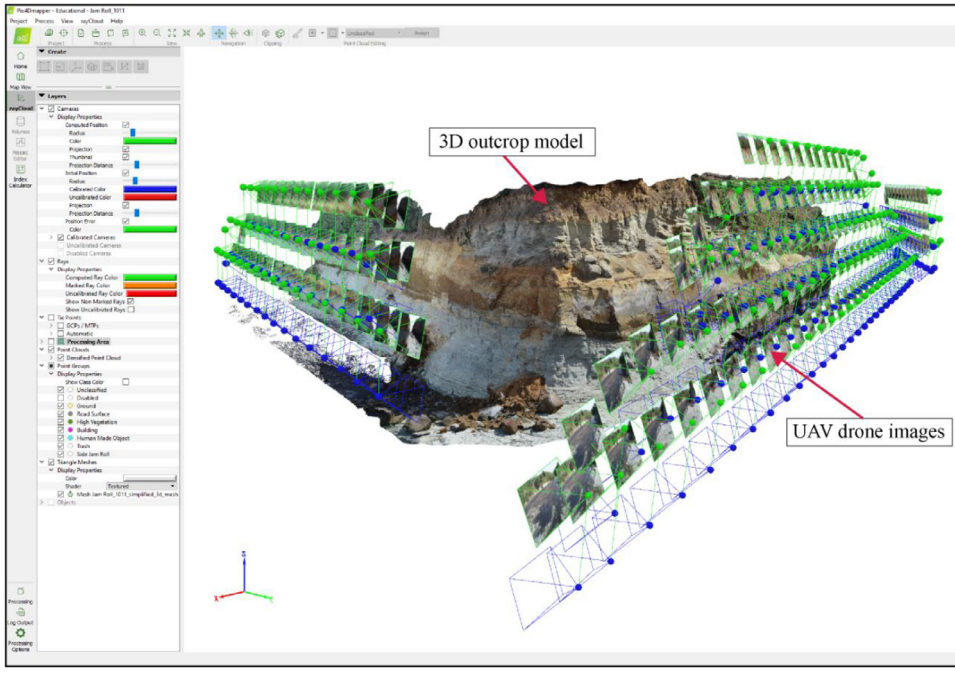

Fig. 3. Outcrop 3D computer model generation in Pix4Dmapper. The geolocated UAV drone images overlap by >80% to create a dense point cloud to generate the outcrop model.

Fig. 4. An example of the 3D outcrop model for a part of Site 3: Jam Roll section.

Other limitations for drone images resulted from them being captured on different days and times of day, leaving sun-exposure intensity sometimes inconsistent.

Ethics Statement

We have read and followed the ethical requirements for publication in Data in Brief, and this work did not involve human subjects, animal experiments, or any data collected from social media platforms.

CRediT Author Statement

Erman Kamaruzaman, Andrew La Croix and Peter Kamp: Conceptualisation, Methodology, Writing and Editing. Erman Kamaruzaman: Software, Data Investigation and Visualisation. Erman Kamaruzaman and Andrew La Croix: Data acquisition.

Data Availability

3D drone outcrop models of the Mount Messenger Formation, New Zealand (Original data) (Dataverse)

Acknowledgements

We thank Vicki Moon for helping fund the drone survey operations. We also thank Ben Roche, Cole Dawson and Tom Robertson for field assistance in conducting drone surveys. Thank you David and Megan Black for land access at Site 1, as well as the Department of Conservation, New Zealand, for permission to fly drones near reserve areas. Pix4D is acknowledge for provision of educational licenses to their software.

Declaration of Competing Interest

The authors declare that they have no known competing financial interests or personal relationships that could have appeared to influence the work reported in this paper.

Supplementary Materials

Supplementary material associated with this article can be found, in the online version, at doi:10.1016/j.dib.2024.110035.

References

[1] G.H. Browne, R.M. Slatt, Outcrop and behind-outcrop characterization of a late Miocene slope fan system, Mt. Messenger Formation, New Zealand, Am. Assoc. Pet. Geol. Bull. 86 (5) (2002) 841–862, doi:10.1306/61eedbb6-173e-11d7-8645000102c1865d.
[2] R.J. Hansen, Stratigraphy, Sedimentology, and Palaeomagnetism of a Late Miocene Succession, Eastern Taranaki Basin Margin University of Waikato, 1996.
[3] E. Kamaruzaman, A. La Croix, P.J.J. Kamp, 3D Drone Outcrop Models of the Mount Messenger Formation, New Zealand, 2023 Retrieved from:, doi:10.7910/DVN/I0C6X3.
[4] P.R. King, G.H. Scott, P.H. Robinson, Description, Correlation and Depositional History of Miocene Sediments Outcropping Along North Taranaki Coast, Institute of Geological & Nuclear Sciences Ltd, Lower Hutt, 1993.
[5] A. Marques, R.K. Horota, E.M. de Souza, L. Kupssinskü, P. Rossa, A.S. Aires, L. Bachi, M.R. Veronez, L. Gonzaga, C.L. Cazarin, Virtual and digital outcrops in the petroleum industry: a systematic review, Earth-Sci. Rev. 208 (2020), doi:10.1016/j.earscirev.2020.103260.
[6] L.U. Masalimova, D.R. Lowe, G.R. Sharman, P.R. King, M.J. Arnot, Outcrop characterization of a submarine channel-lobe complex: the Lower Mount Messenger Formation, Taranaki Basin, New Zealand, Mar. Pet. Geol. 71 (2016) 360–390, doi:10.1016/j.marpetgeo.2016.01.004.

Appendix B

Appendix B consists of tables and figures related to Chapter 3.

Table i - Appendix B: Paleobathymetry framework used in this study

Region (Strogen et al., 2011)	Depth (m) (Strogen et al., 2011)	Region and depth (Simplified in this study)
Inner shelf	0-50	Shelf (0-200 m)
Middle shelf	50-100	
Outer shelf	100-200	
Uppermost slope	200-400	Upper slope (200-600m)
Upper slope	400-600	
Middle slope	600-1000	Middle slope (600-1000m)
Lower slope	1000-1500	Lower slope (1000-1500m)
Deep lower bathyal	1500-2000	Deep lower bathyal (1500-2000 m)

Table ii - Appendix B: List of drill holes used in this study and their locations

Drill hole	Latitude	Longitude
Manaia-2	-40.026739	173.240219
Whio-1	-40.017357	173.327456
Moki-2A	-39.988918	173.318331
Maari-2	-39.978955	173.30268
Maari-1	-39.96778	173.302601
Pateke-2	-39.379396	173.19348
Tui-1	-39.434701	173.246594
Tui-SW-2	-39.461347	173.231344
Kahu-1	-39.432422	173.290097
Tieke-1	-39.484839	173.307075
Maui-3	-39.534633	173.451588
Wainui-1	-38.462685	173.308525
Romney-1	-37.894261	172.731311
Maui - 4	-40.038334	173.241022

Table iii - Appendix B: List of 3D seismic surveys used in this study

3D seismic survey	Year acquired	Area (km^2)	Vertical length (s)
Matariki	2010	290	6.0
Maari	1999	590	6.0
Maui	1991	1562	6.0
Matuku	2012	323	7.1
Tui	2003	560	6.1
Kokako	2013	600	6.1
Romney	2012	2622	8.2

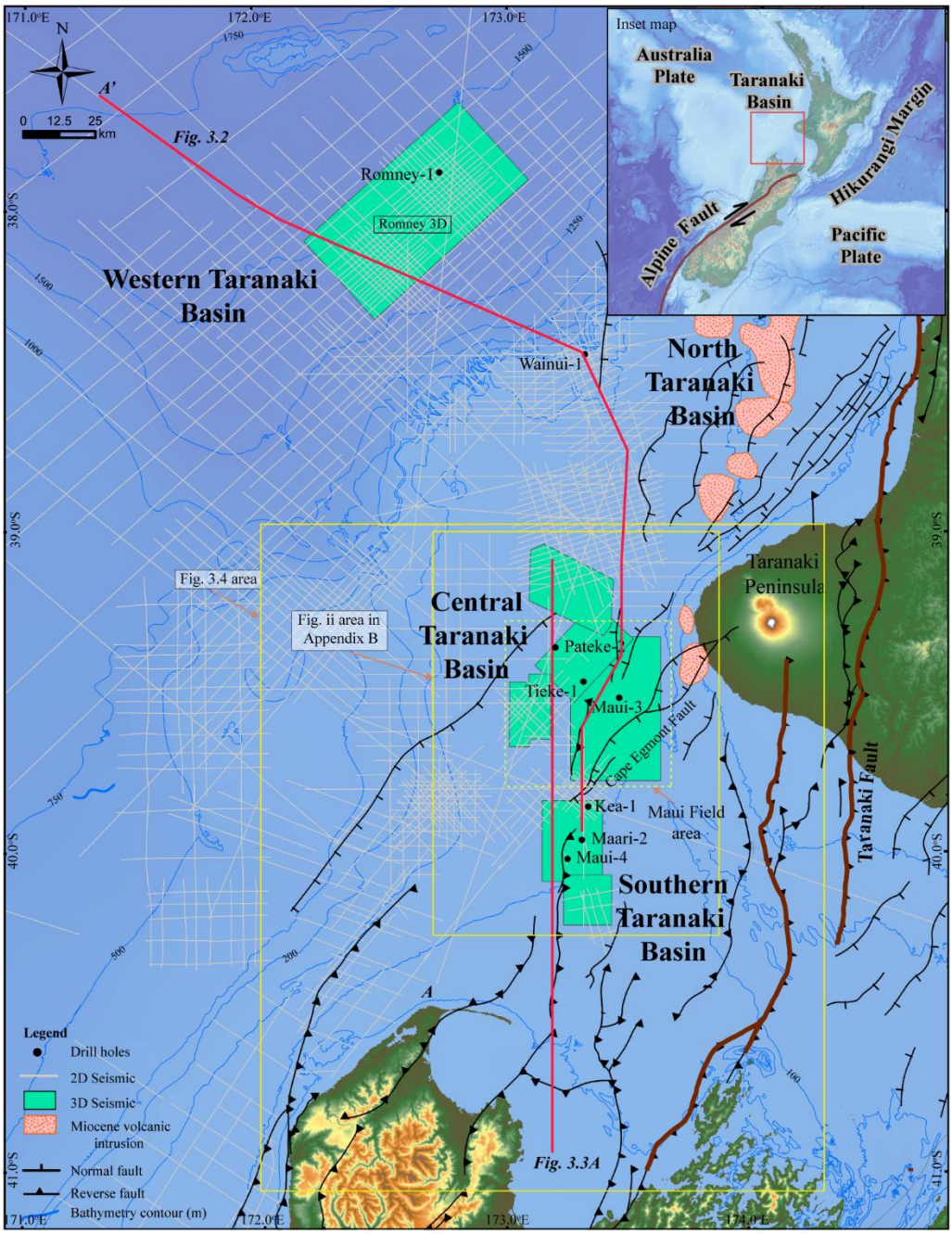

Figure i - Appendix B: Map of the study area in Taranaki Basin, New Zealand, showing the location of 2D and 3D seismic surveys and some drill holes relevant to this study. GIS data from NZP&M (2018).

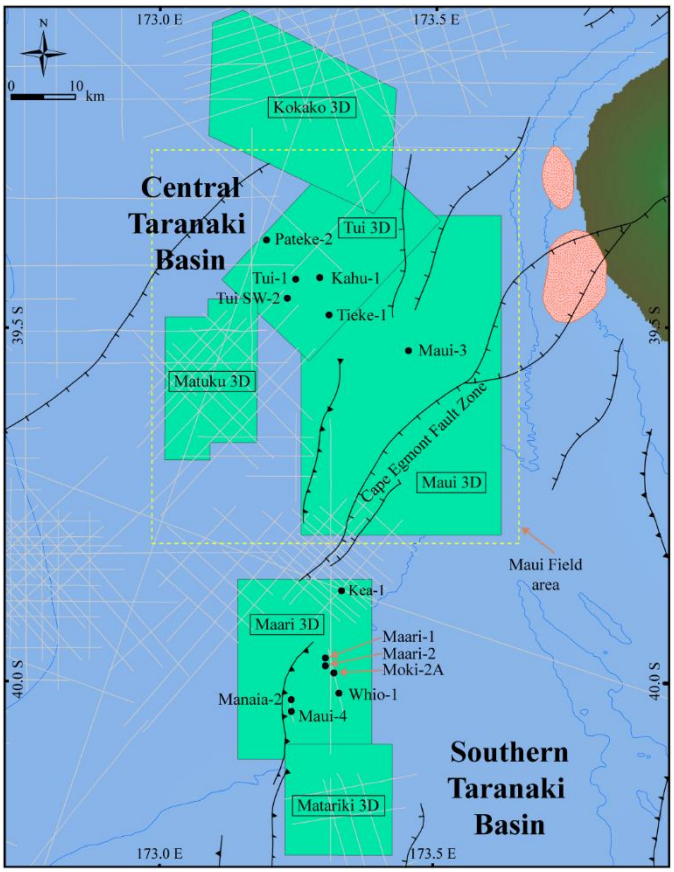

Figure ii - Appendix B: Close-up map of the southern and central Taranaki Basin showing the location of 3D seismic surveys and drill holes. GIS data from NZP&M (2018). The area is shown in Figure i-Appendix B.

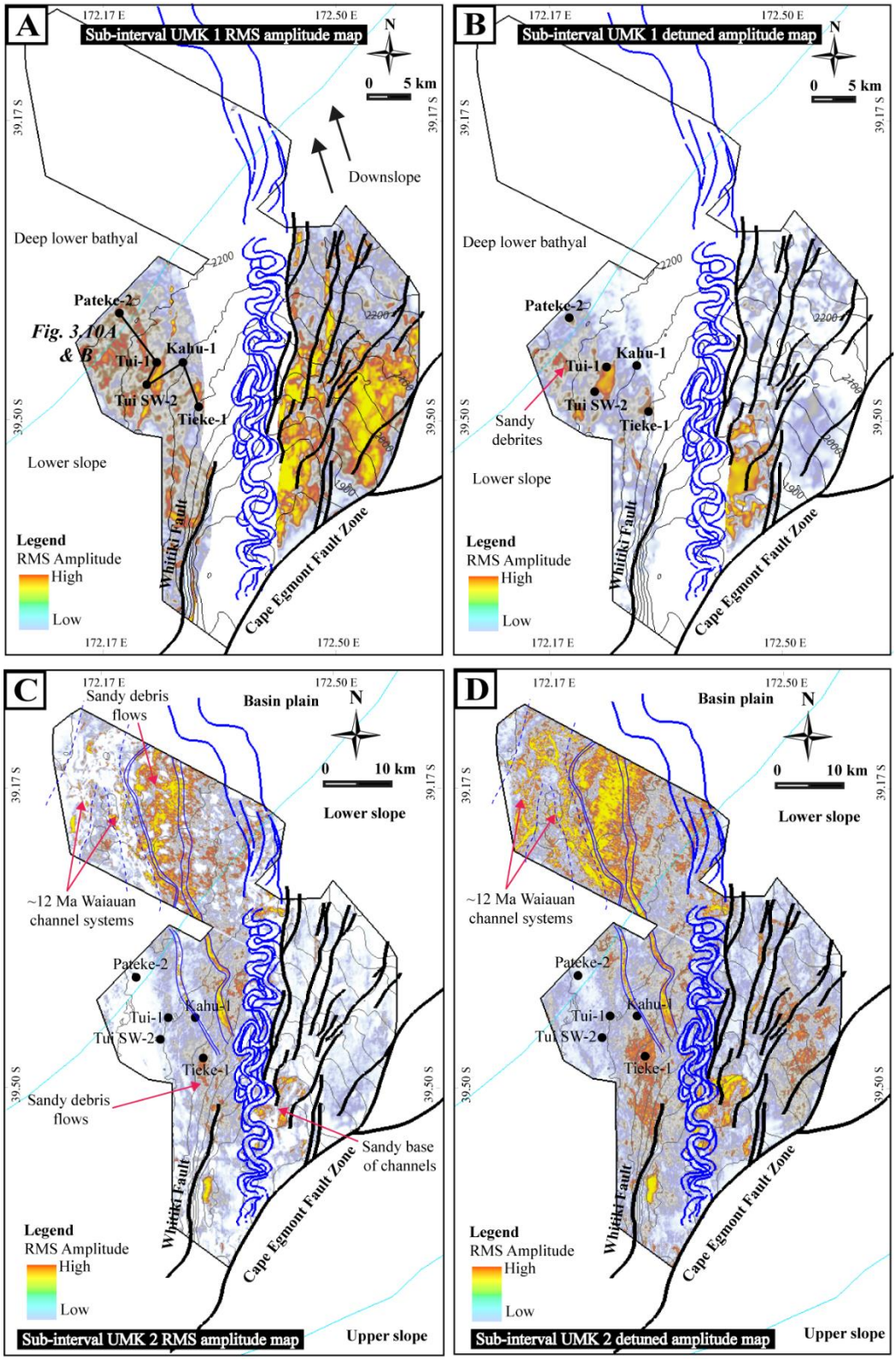

Figure iii - Appendix B: Upper Moki Formation amplitude and detuned amplitude maps. Sub-interval UMK 1: (A) Amplitude (B) detuned amplitude maps. Sub-interval UMK 2: (D) Amplitude (C) detuned amplitude maps

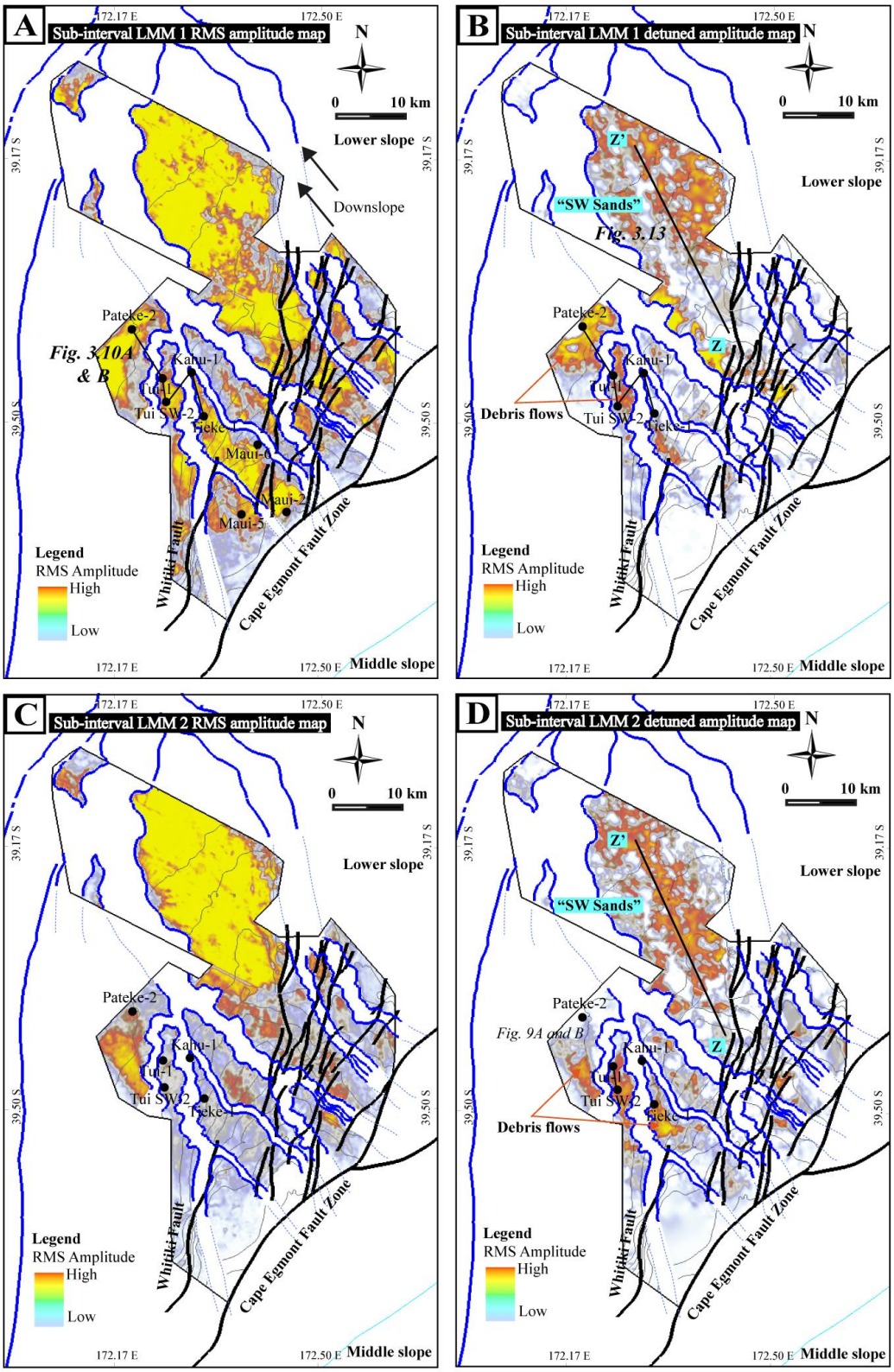
A
Sub-interval LMM 1 RMS amplitude map
B
Sub-interval LMM 1 detuned amplitude map
C
Sub-interval LMM 2 RMS amplitude map
D
Sub-interval LMM 2 detuned amplitude map
172.17 E
172.50 E
39.17 S
39.50 S
N
0
10 km
Lower slope
Downslope
Middle slope
Pateke-2
Kahu-1
Tui-1
Tui SW-2
Pateke-1
Maui-6
Maui-2
Maui-5
Fig. 3.10A & B
Z'
Z
"SW Sands"
Fig. 3.13
Debris flows
Fig. 9A and B
Whitiki Fault
Cape Egmont Fault Zone
Legend
RMS Amplitude
High
Low

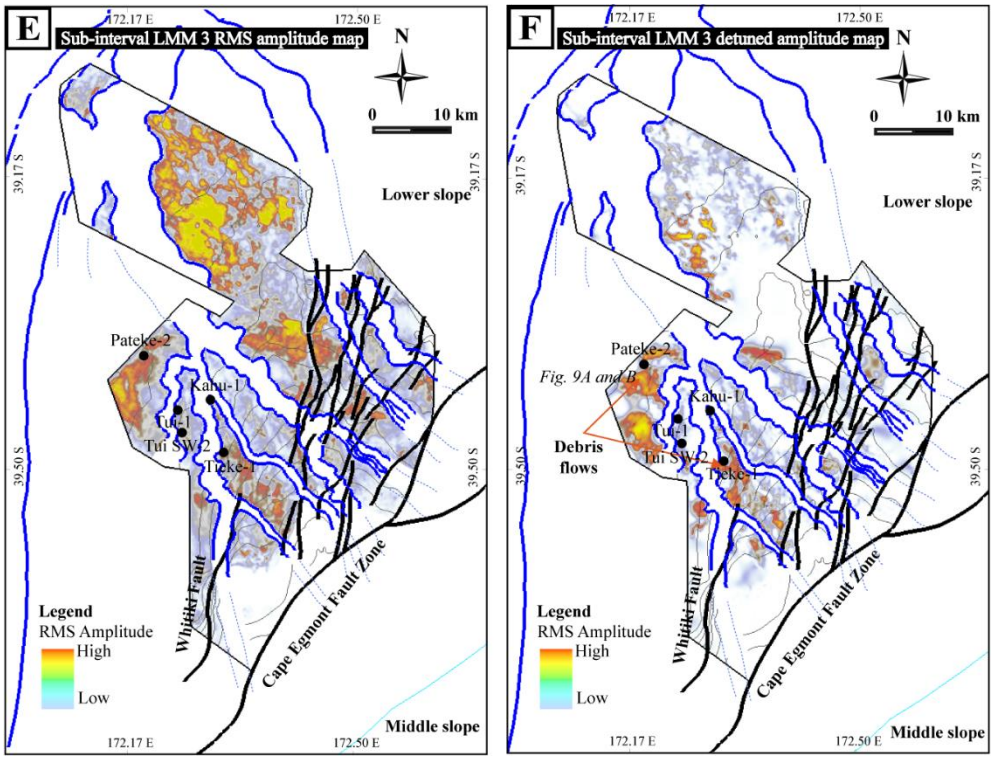

Figure iv - Appendix B: Lower Mount Messenger Formation amplitude and detuned amplitude maps. Sub-interval LMM 1: (A) Amplitude (B) detuned amplitude maps. Sub-interval LMM 2: (C) Amplitude (D) detuned amplitude maps. Sub-interval LMM 3: (E) Amplitude (F) detuned amplitude maps.

Appendix C

Appendix C consists of figures related to Chapter 4.

Table i: Mercury-Mokau 3D seismic survey reprocessing parameters. The 3D seismic data was downloaded from the NZP&M Exploration Database (https://www.nzpam.govt.nz)

Basic information	
Processor	Loyz Energy Limited and Kea Petroleum Group
Operator	Kea Petroleum Group
Year	2013
Key migration processing parameters	
Input Trace Length	6194 ms
Input Sampling	2 ms
Input Bin Spacing (inline x xline)	25.0m x 12.5m
Input Offset Range	112 m – 5062 m, inc 75 m
Input Fold	67
Migration Aperture	5000 m
Output Trace Length	6144 ms
Output Sampling	4 ms
Output Bin Spacing (inline x xline)	25.0m x 12.5m
Output Offset Range	112 m – 5062 m, inc 75 m
Output Fold	67

Table ii: Information related 2D seismic lines used in this study. The 2D seismic lines were downloaded from the NZP&M Exploration Database (https://www.nzpam.govt.nz).

2D line name	Survey name	Survey year	Domain
BO_p90-05-1765_matched	P90	1990	Time
BO_p90-06-fugro_matched	P90	1990	Time
BO_p90-11-1765_matched	P90	1990	Time
BO_p90-12_a_r-fugro_matched	P90	1990	Time
BO_p90-13-1765_matched	P90	1990	Time
BO_p90-16-1765_matched	P90	1990	Time
BO_p90-18-1765_matched	P90	1990	Time
BO_p90-31-1765_matched	P90	1990	Time
BO_p90-32-1765_matched	P90	1990	Time
BO_p90-33-1765_matched	P90	1990	Time
BO_p90-34-1765_matched	P90	1990	Time
BO_p90-35-1765_matched	P90	1990	Time
BO_p90-36-1765_matched	P90	1990	Time
BO_p90-37-1765_matched	P90	1990	Time
BO_p90-38-fugro_matched	P90	1990	Time
BO_p90-39-1765_matched	P90	1990	Time
BO_p90-40-1765_matched	P90	1990	Time
BO_p90-41-1765_matched	P90	1990	Time
BO_pt2k-032-2484_matched	PT00	2000	Time
BO_pt2k-033-2484_matched	PT00	2000	Time
BO_pt2k-034-2484_matched	PT00	2000	Time
BO_pt2k-035-2484_matched	PT00	2000	Time
BO_pt2k-036-2484_matched	PT00	2000	Time
SBPT098-85-PR1123-T-MIG_Filtered_Migration_2D_T-109	SBPT098_85	1985	Time
SBPT098-85-PR1123-T-MIG_Filtered_Migration_2D_T-110-5	SBPT098_85	1985	Time
SBPT098-85-PR1123-T-MIG_Filtered_Migration_2D_T-111-5	SBPT098_85	1985	Time
SBPT098-85-PR1123-T-MIG_Filtered_Migration_2D_T-112	SBPT098_85	1985	Time
SBPT098-85-PR1123-T-MIG_Filtered_Migration_2D_T-116	SBPT098_85	1985	Time
SBPT098-85-PR1123-T-MIG_Filtered_Migration_2D_T-116A	SBPT098_85	1985	Time
SBPT098-85-PR1123-T-MIG_Filtered_Migration_2D_T-119	SBPT098_85	1985	Time
SBPT098-85-PR1123-T-MIG_Filtered_Migration_2D_T-122	SBPT098_85	1985	Time
SBPT098-85-PR1123-T-MIG_Filtered_Migration_2D_T-123	SBPT098_85	1985	Time

SBPT098-85-PR1123-T-MIG_Filtered_Migration_2D_T-126	SBPT098_85	1985	Time
SBPT098-85-PR1123-T-MIG_Filtered_Migration_2D_T-126-5	SBPT098_85	1985	Time
SBPT098-85-PR1123-T-MIG_Filtered_Migration_2D_T-126-5A	SBPT098_85	1985	Time
SBPT098-85-PR1123-T-MIG_Filtered_Migration_2D_T-126A	SBPT098_85	1985	Time
SBPT098-85-PR1123-T-MIG_Filtered_Migration_2D_T-128-5	SBPT098_85	1985	Time
SBPT098-85-PR1123-T-MIG_Filtered_Migration_2D_T-128-5-2	SBPT098_85	1985	Time
SBPT098-85-PR1123-T-MIG_Filtered_Migration_2D_T-128-5A	SBPT098_85	1985	Time
SBPT098-85-PR1123-T-MIG_Filtered_Migration_2D_T-203	SBPT098_85	1985	Time
SBPT098-85-PR1123-T-MIG_Filtered_Migration_2D_T-203A	SBPT098_85	1985	Time
SBPT098-85-PR1123-T-MIG_Filtered_Migration_2D_T-206	SBPT098_85	1985	Time
SBPT098-85-PR1123-T-MIG_Filtered_Migration_2D_T-206A	SBPT098_85	1985	Time
SBPT098-85-PR1123-T-MIG_Filtered_Migration_2D_T-206B	SBPT098_85	1985	Time
SBPT098-85-PR1123-T-MIG_Filtered_Migration_2D_T-206C	SBPT098_85	1985	Time
SBPT098-85-PR1123-T-MIG_Filtered_Migration_2D_T-209	SBPT098_85	1985	Time
SBPT098-85-PR1123-T-MIG_Filtered_Migration_2D_T-209A	SBPT098_85	1985	Time
SBPT098-85-PR1123-T-MIG_Filtered_Migration_2D_T-209B	SBPT098_85	1985	Time
SBPT098-85-PR1123-T-MIG_Filtered_Migration_2D_T-211	SBPT098_85	1985	Time
SBPT098-85-PR1123-T-MIG_Filtered_Migration_2D_T-215B	SBPT098_85	1985	Time

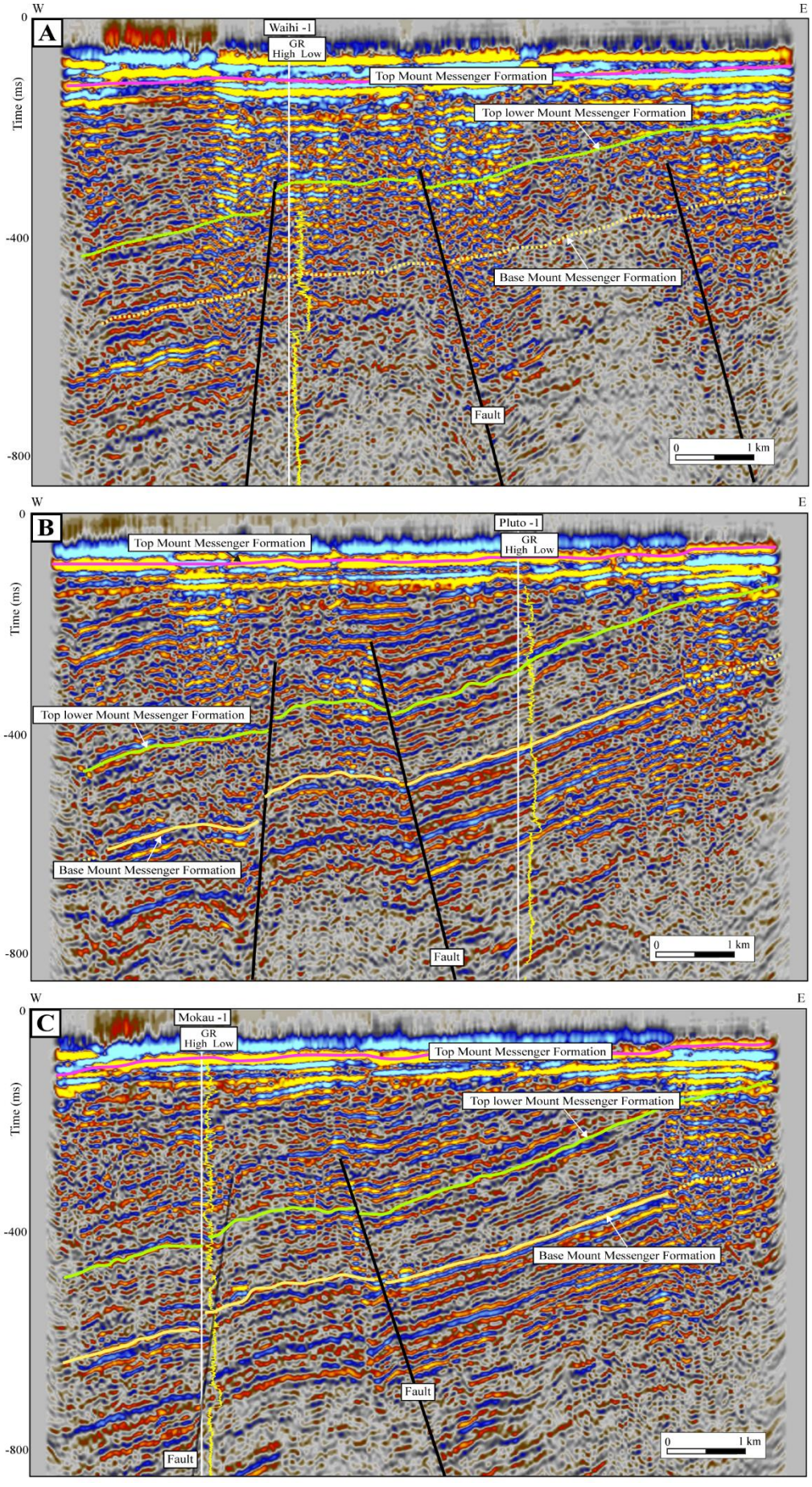
W
E
0
A
Waihi -1
GR
High Low
Top Mount Messenger Formation
Top lower Mount Messenger Formation
Time (ms)
-400
Base Mount Messenger Formation
Fault
-800
0
1 km
W
E
0
B
Pluto -1
GR
High Low
Top Mount Messenger Formation
Time (ms)
Top lower Mount Messenger Formation
-400
Base Mount Messenger Formation
Fault
-800
0
1 km
W
E
0
C
Mokau -1
GR
High Low
Top Mount Messenger Formation
Top lower Mount Messenger Formation
Time (ms)
-400
Base Mount Messenger Formation
Fault
Fault
-800
0
1 km

Figure i: Interpreted (A) Crossline 1942 Mercury-Mokau 3D seismic section intersects with Waihi-1, (B) Crossline 1472 Mercury-Mokau 3D seismic section intersects with Pluto-1, and (C) Crossline 1412 Mercury-Mokau 3D seismic section intersects with Mokau-1. Gamma-ray log is shown alongside each borehole. Refer Figure ii for the uninterpreted seismic sections.

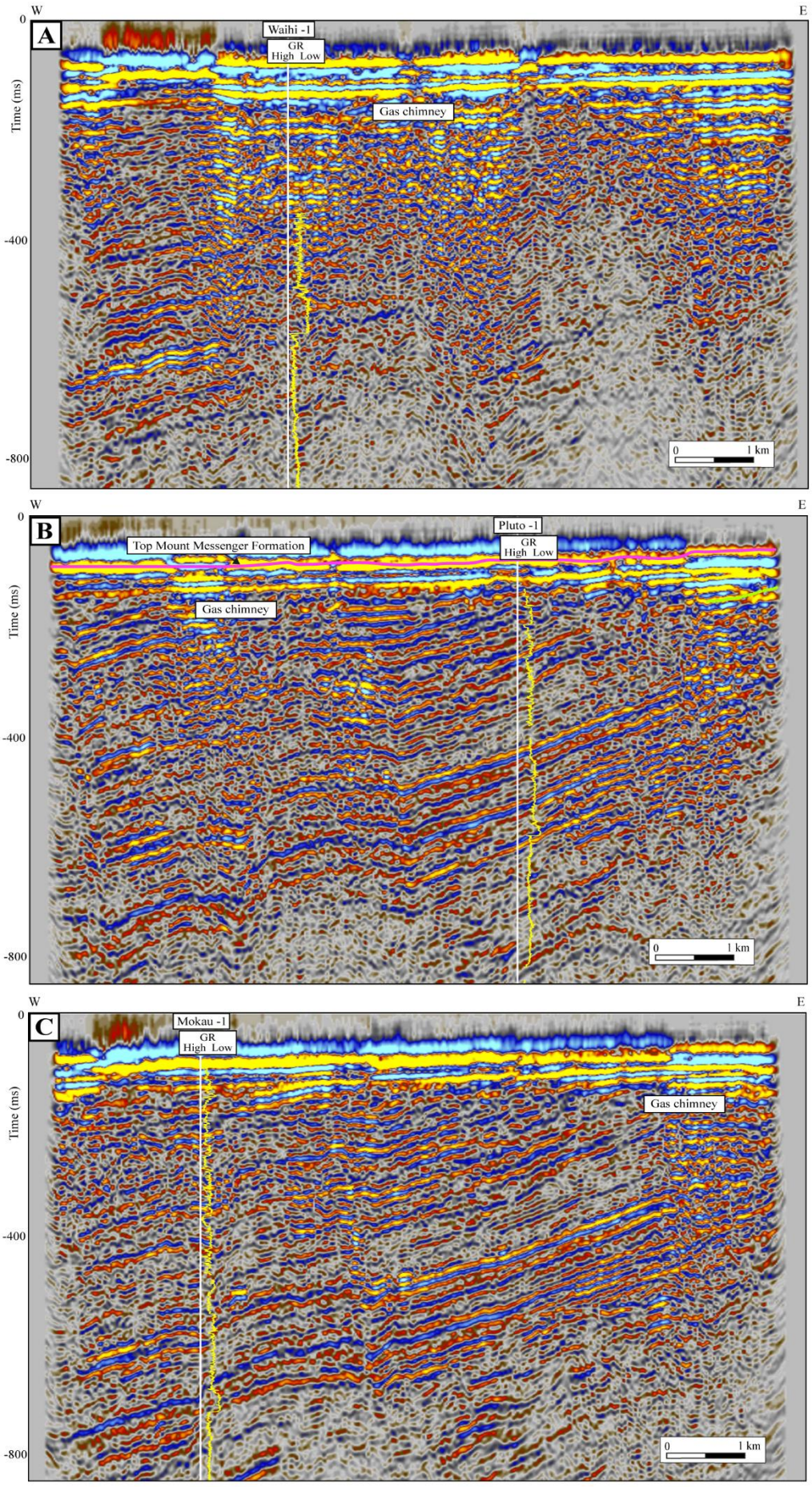
W
E
0
A
Waihi -1
GR
High Low
Gas chimney
Time (ms)
-400
-800
0
1 km
W
E
0
B
Pluto -1
GR
High Low
Top Mount Messenger Formation
Gas chimney
Time (ms)
-400
-800
0
1 km
W
E
0
C
Mokau -1
GR
High Low
Gas chimney
Time (ms)
-400
-800
0
1 km

Figure ii: Uninterpreted (A) Crossline 1942 Mercury-Mokau 3D seismic section intersects with Waihi-1, (B) Crossline 1472 Mercury-Mokau 3D seismic section intersects with Pluto-1, and (C) Crossline 1412 Mercury-Mokau 3D seismic section intersects with Mokau-1. Gamma-ray log is shown alongside each borehole.

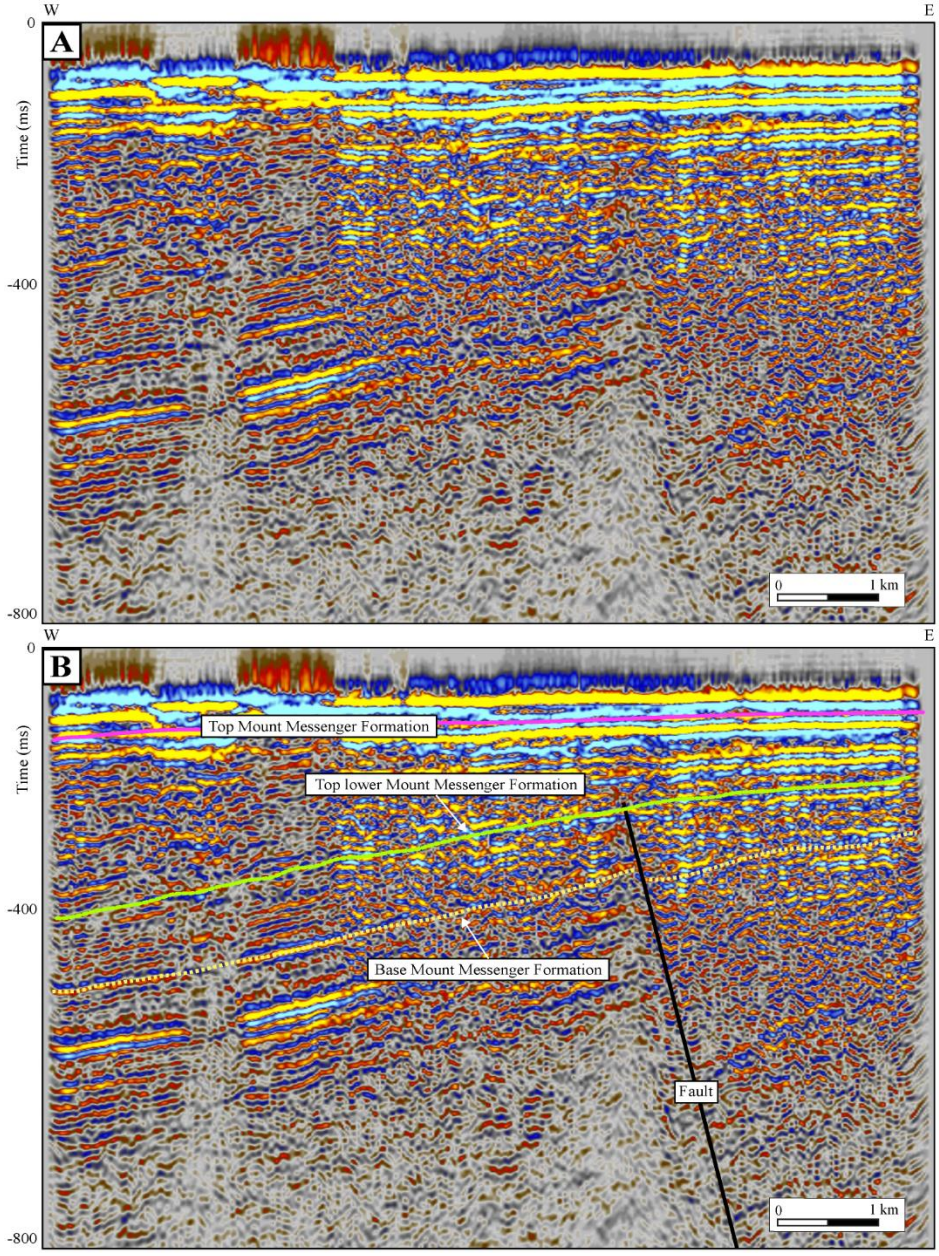

Figure iii: Uninterpreted (A) and (B) interpreted seismic section, crossline 2242 Mercury-Mokau 3D.

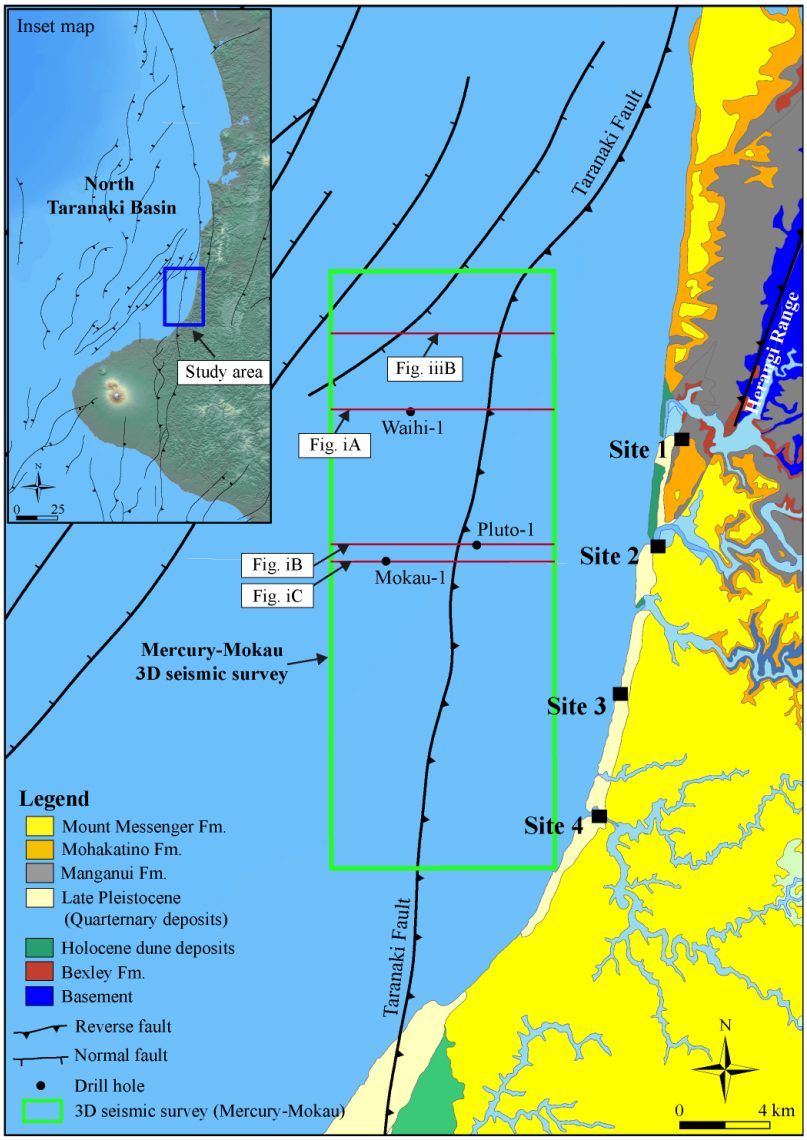

Figure iv: Overview map that shows the location of seismic sections from the Mercury-Makau 3D seismic.

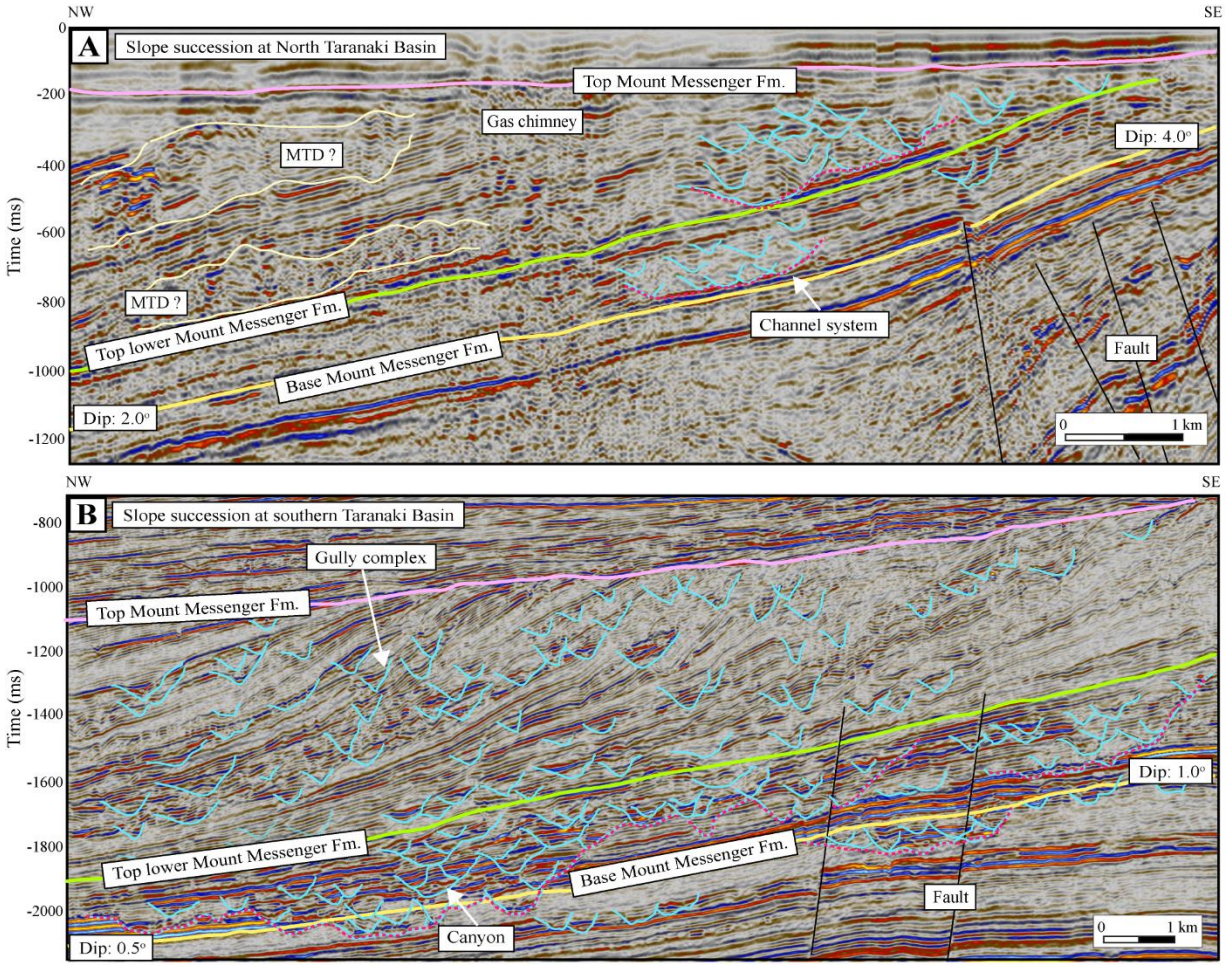

Figure v: Seismic reflection profiles show the slope succession with major regional horizons for (A) North Taranaki Basin (study area) with slope angles ranging from 2 to 4°, and (B) southern Taranaki Basin with slope angles ranging from 0.5 to 1° for a succession immediately above the base of the Mount Messenger Formation horizon. The seismic cross sections also show channelform features (i.e., canyons, channels and gullies) within the continental slope succession in both areas. The light green horizon is a horizon that approximately separates the lower and upper parts of the Mount Messenger Formation. Refer to Figure 2A for the seismic line locations (A: 2D seismic line BO_hzt82b-114 and B: arbitrary line from Maui – Kokako 3D merge seismic surveys). Refer Figure vi for the uninterpreted seismic sections.

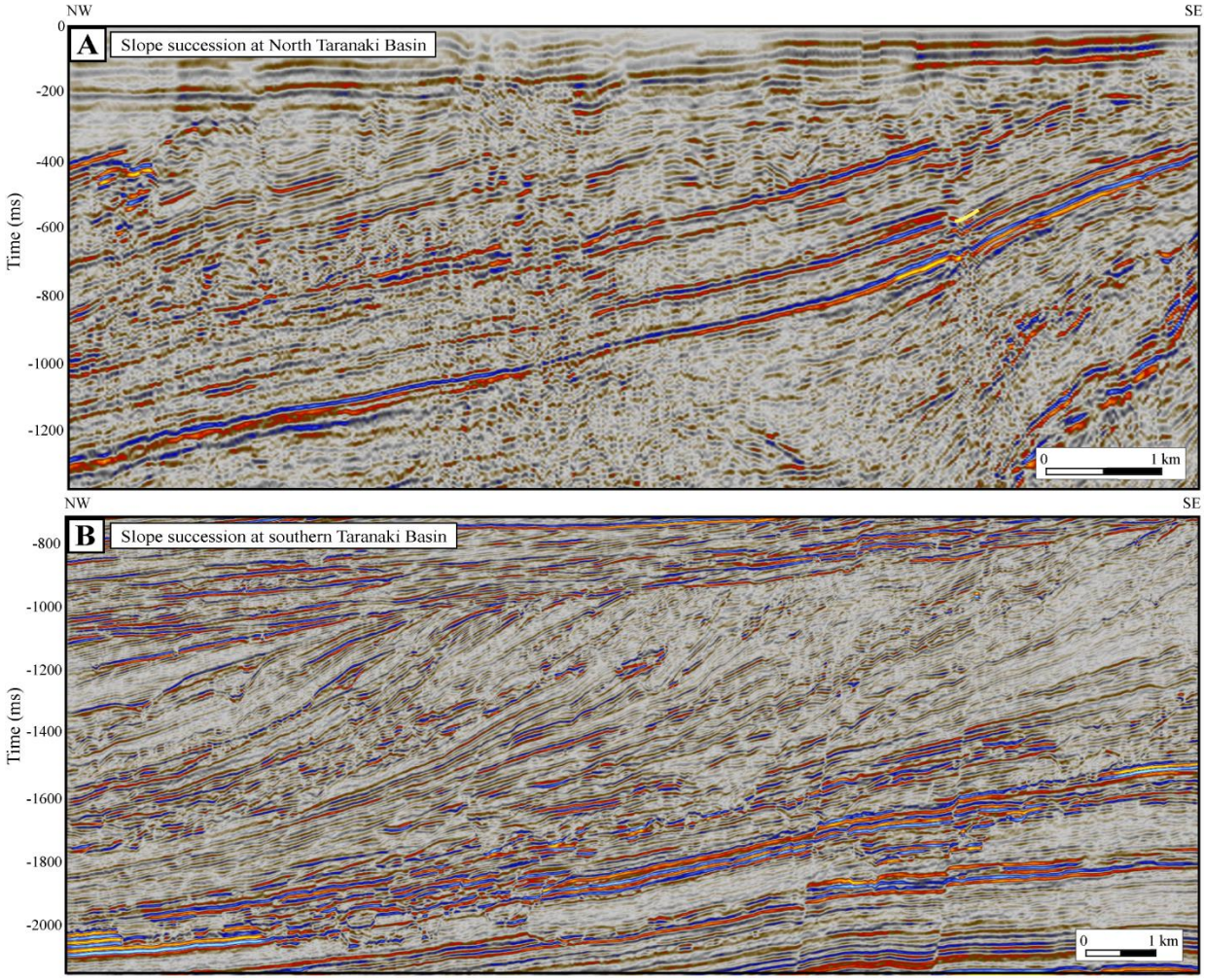

Figure vi: Uninterpreted seismic sections for (A) North Taranaki Basin (study area) and (B) southern Taranaki Basin.

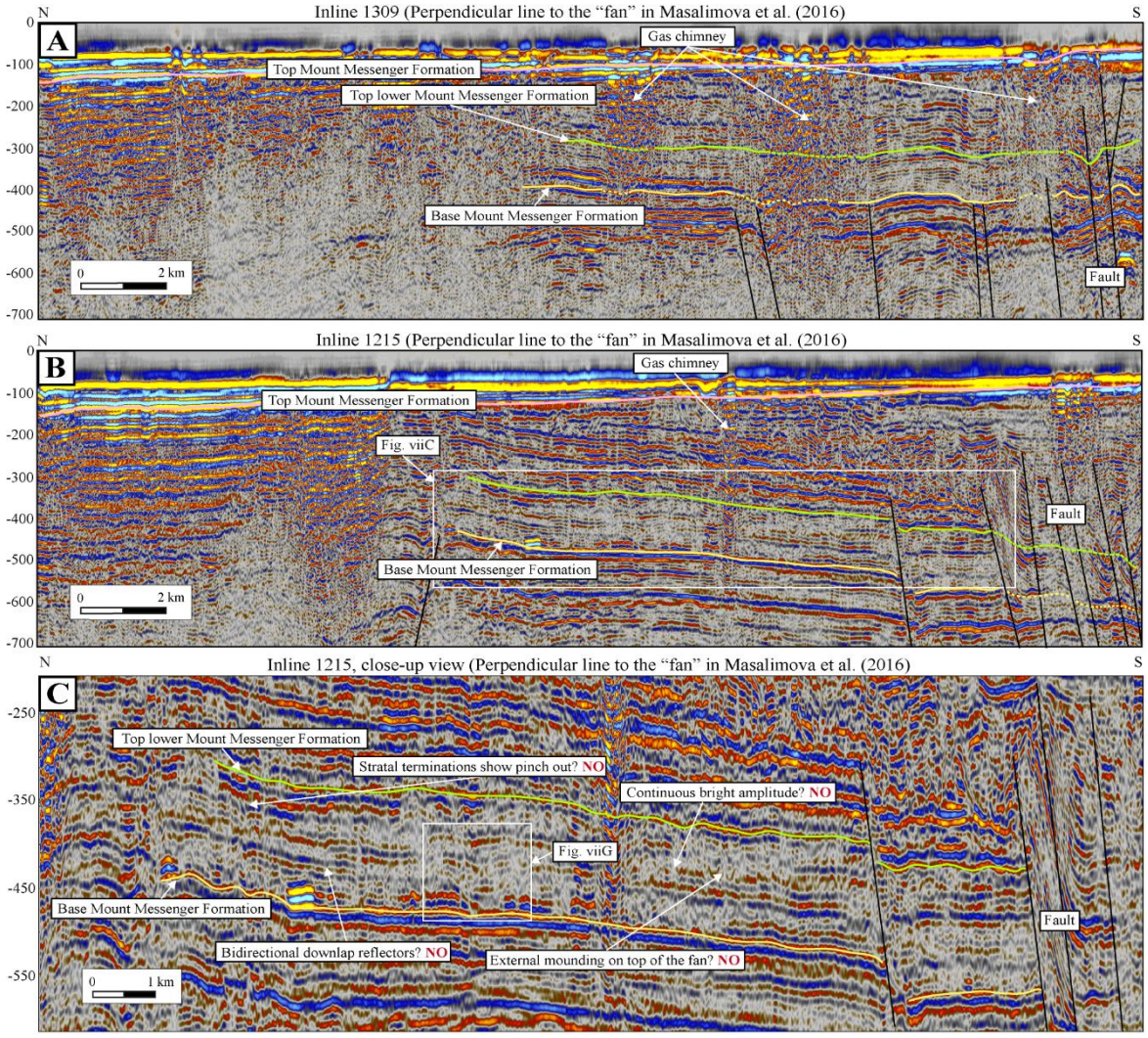
N
Inline 1309 (Perpendicular line to the "fan" in Masalimova et al. (2016)
S
A
Gas chimney
Top Mount Messenger Formation
Top lower Mount Messenger Formation
Base Mount Messenger Formation
Fault
0
2 km
N
Inline 1215 (Perpendicular line to the "fan" in Masalimova et al. (2016)
S
B
Gas chimney
Top Mount Messenger Formation
Fig. viiC
Fault
Base Mount Messenger Formation
0
2 km
N
Inline 1215, close-up view (Perpendicular line to the "fan" in Masalimova et al. (2016)
S
C
Top lower Mount Messenger Formation
Stratal terminations show pinch out? NO
Continuous bright amplitude? NO
Fig. viiG
Base Mount Messenger Formation
Fault
Bidirectional downlap reflectors? NO
External mounding on top of the fan? NO
0
1 km

……continue

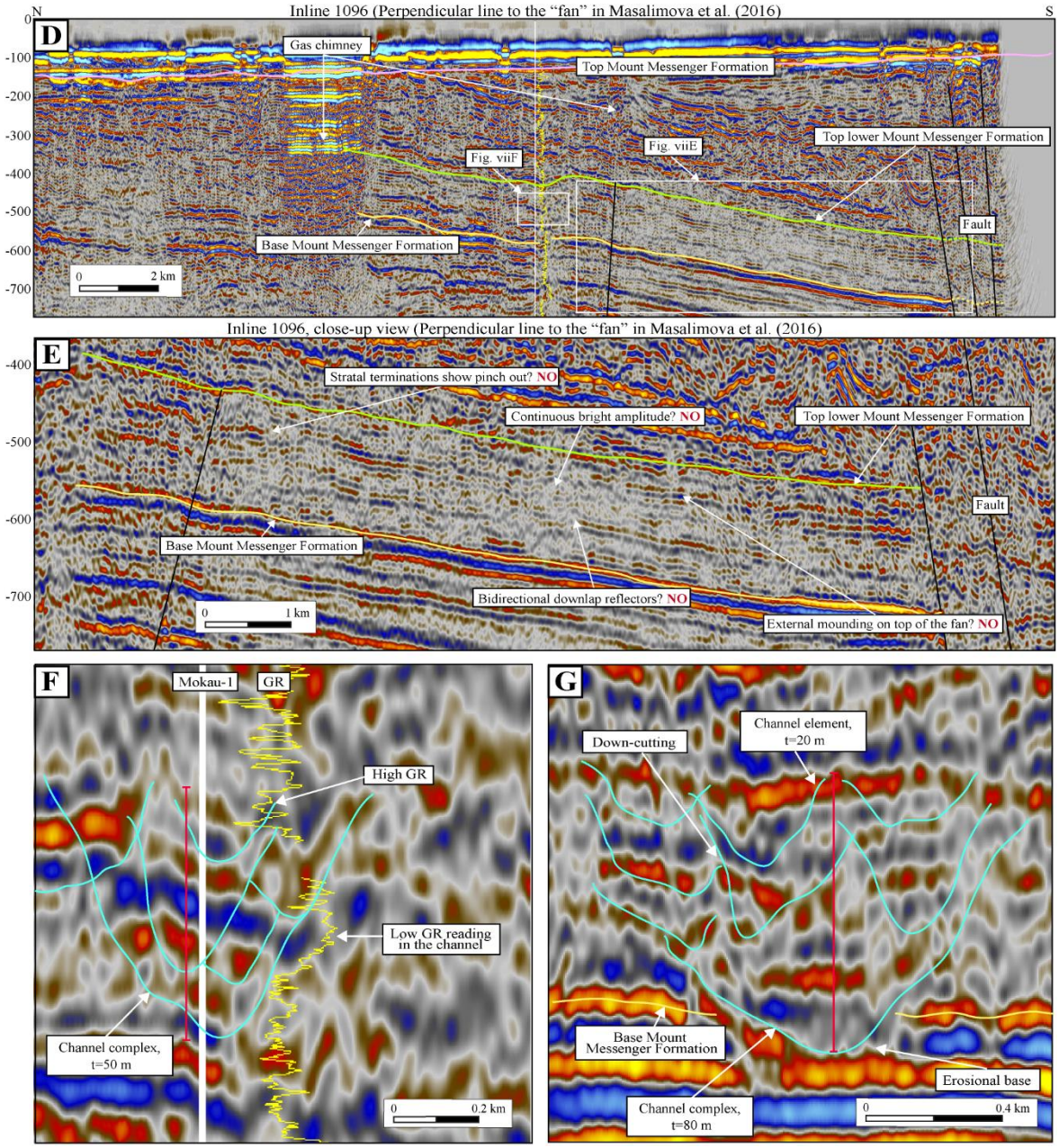

Figure vii: Interpreted seismic section from the Mercury-Mokau 3D seismic (A) inline 1309, (B) inline 1215, (C) close-up view of inline 1215, (D) inline 1096 and (E) close-up view of inline 1096. These inlines are perpendicular to the inferred "fan" in Masalimova et al. (2016). The seismic section shows no evidence of fan occurrence when compared to the Posamentier and Erskine (1991) criteria of recognising fan in seismic reflection data. Refer Figure xi for the inline locations. (F) and (G) close-up view of seismic sections. The uninterpreted seismic sections are shown in Figure viii.

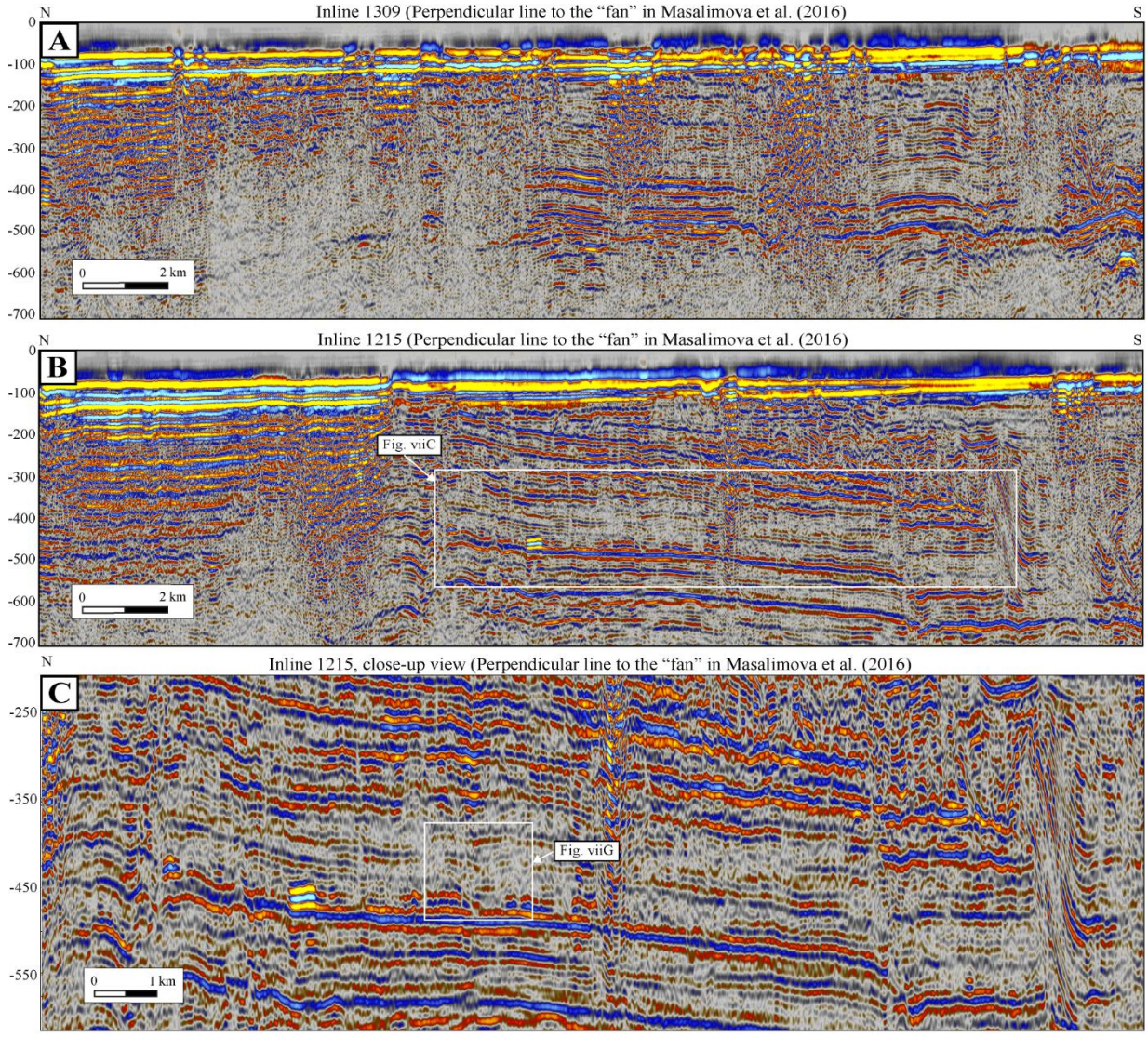
N
Inline 1309 (Perpendicular line to the "fan" in Masalimova et al. (2016)
S
A
0
-100
-200
-300
-400
-500
-600
-700
0
2 km
N
Inline 1215 (Perpendicular line to the "fan" in Masalimova et al. (2016)
S
B
Fig. viiC
0
2 km
N
Inline 1215, close-up view (Perpendicular line to the "fan" in Masalimova et al. (2016)
C
-250
-350
-450
-550
Fig. viiG
0
1 km

……continue

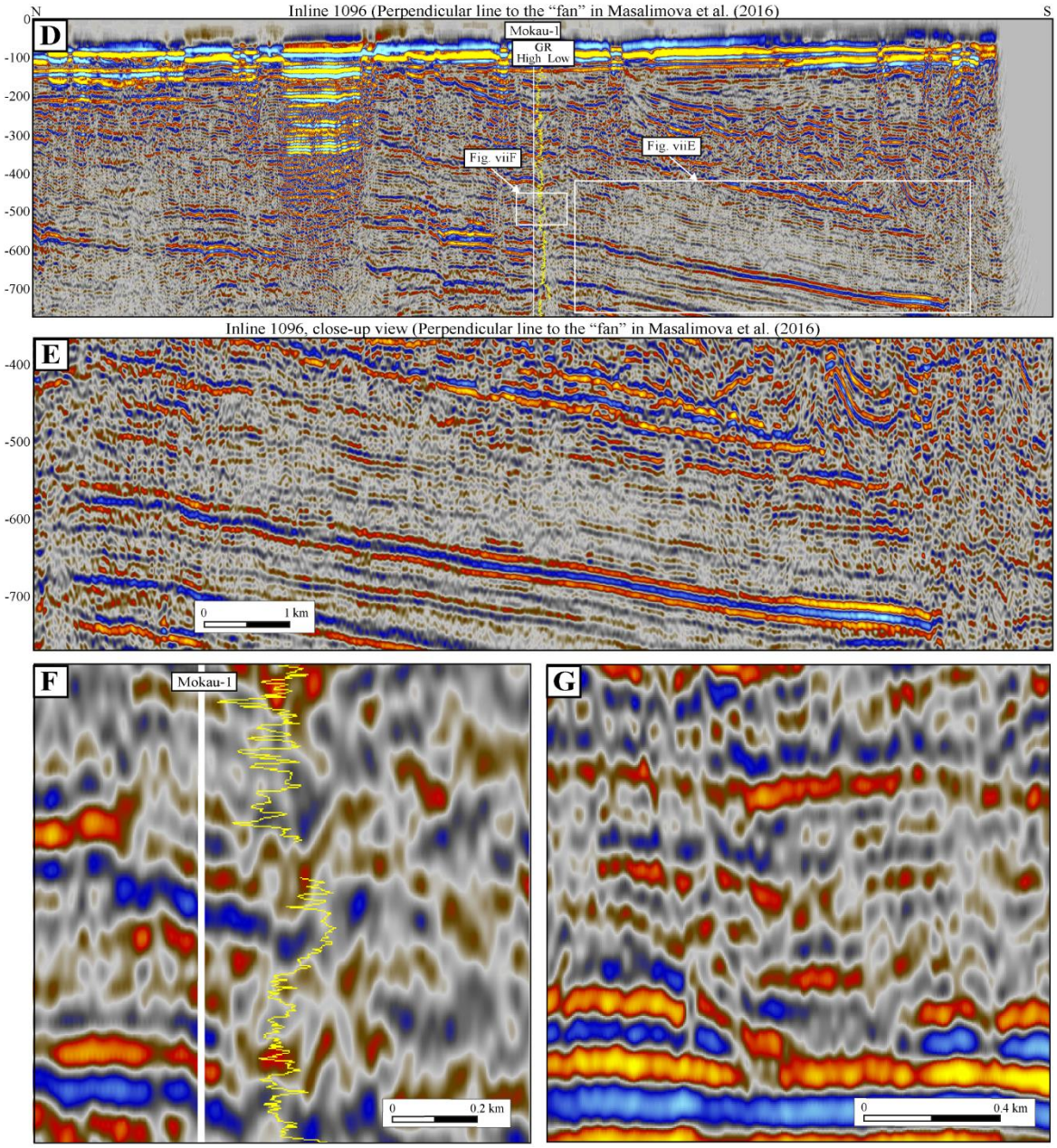

Figure viii: Uninterpreted seismic sections related to Figure vii.

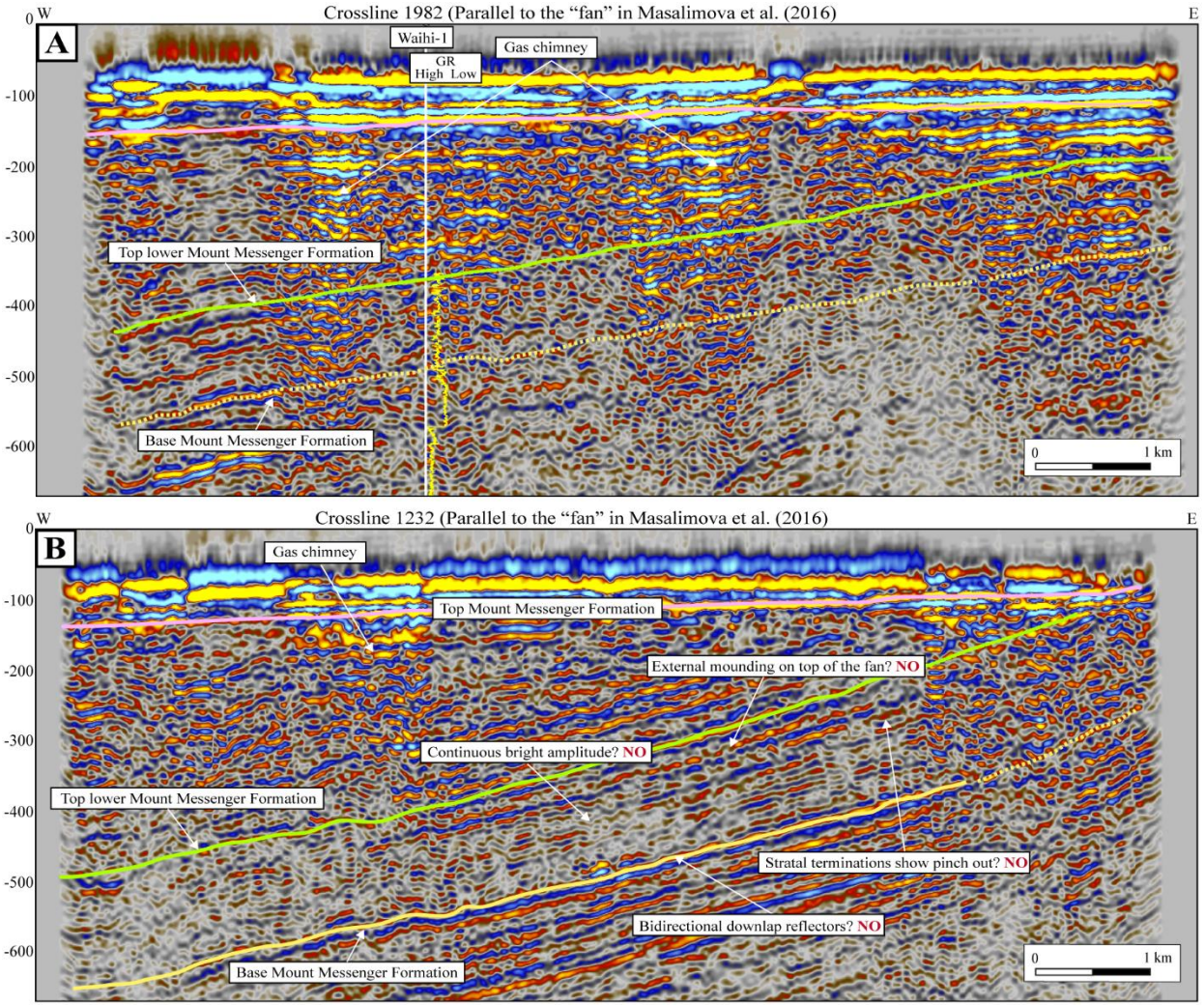
W
Crossline 1982 (Parallel to the "fan" in Masalimova et al. (2016)
E
A
Waihi-1
GR
High Low
Gas chimney
Top lower Mount Messenger Formation
Base Mount Messenger Formation
0
-100
-200
-300
-400
-500
-600
0
1 km
W
Crossline 1232 (Parallel to the "fan" in Masalimova et al. (2016)
E
B
Gas chimney
Top Mount Messenger Formation
External mounding on top of the fan? NO
Continuous bright amplitude? NO
Top lower Mount Messenger Formation
Stratal terminations show pinch out? NO
Bidirectional downlap reflectors? NO
Base Mount Messenger Formation
0
-100
-200
-300
-400
-500
-600
0
1 km

……continue

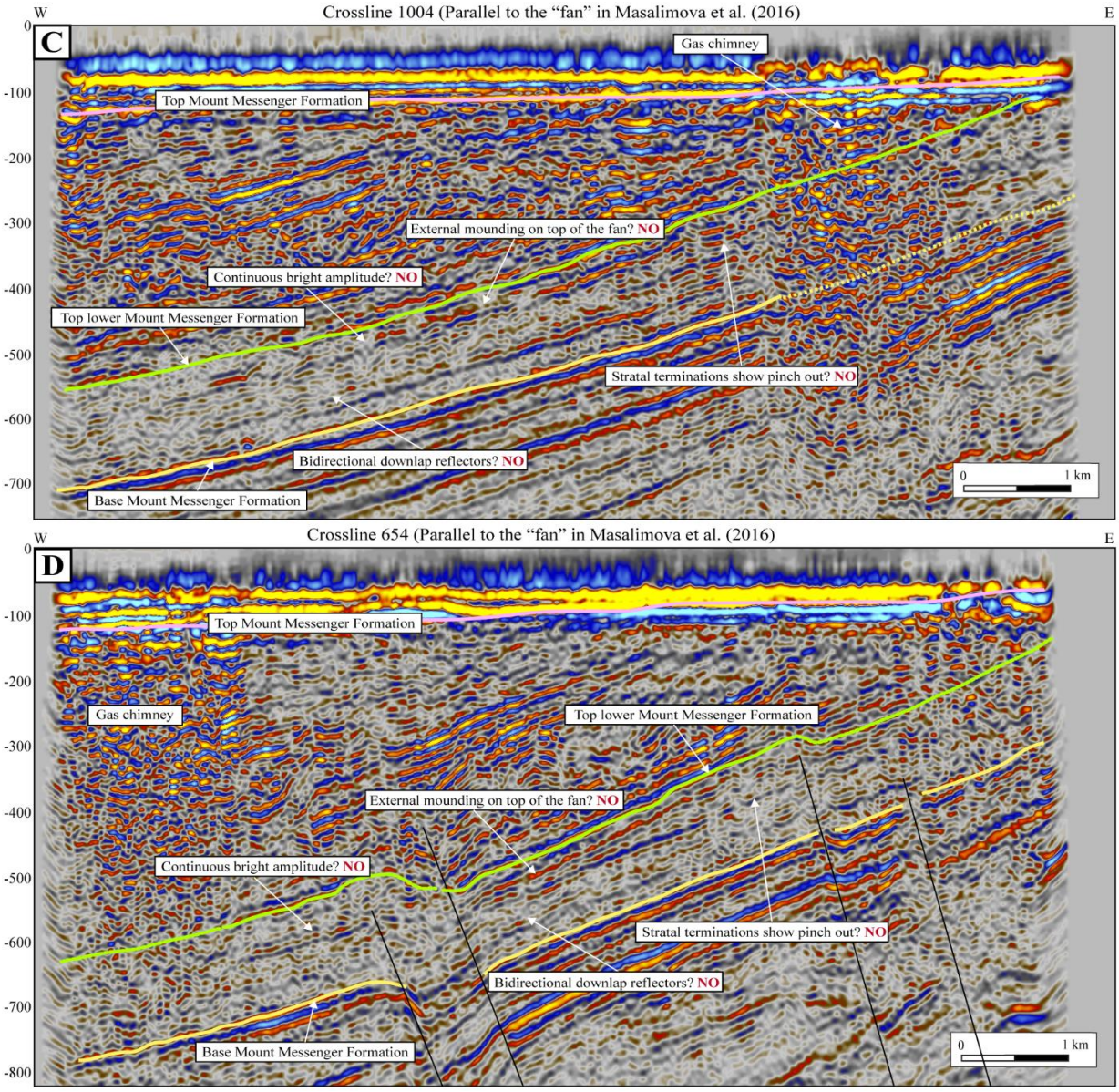

Figure ix: Interpreted seismic section from the Mercury-Mokau 3D seismic (A) crossline 1982, (B) inline 1232, (C) crossline 1004 and (D) inline 654. These inlines are parallel to the inferred "fan" in Masalimova et al. (2016). The seismic section shows no evidence of fan occurrence when compared against the Posamentier and Erskine (1991) criteria of recognising fan in seismic reflection data. Refer Figure xi for the inline locations. The uninterpreted seismic sections are shown in Figure x.

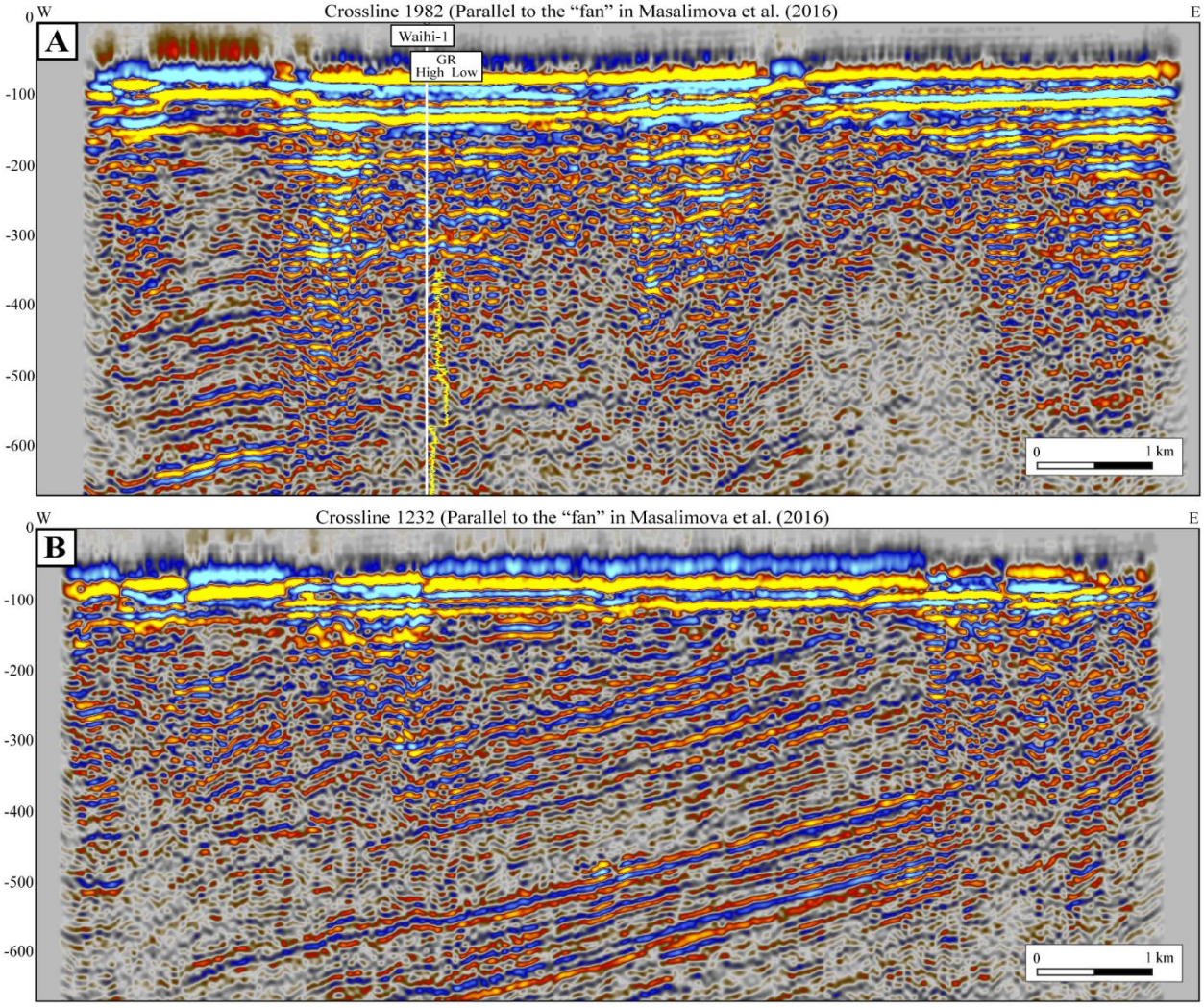
W
Crossline 1982 (Parallel to the "fan" in Masalimova et al. (2016)
E
A
Waihi-1
GR
High Low
0
-100
-200
-300
-400
-500
-600
0
1 km
W
Crossline 1232 (Parallel to the "fan" in Masalimova et al. (2016)
E
B
0
-100
-200
-300
-400
-500
-600
0
1 km

……continue

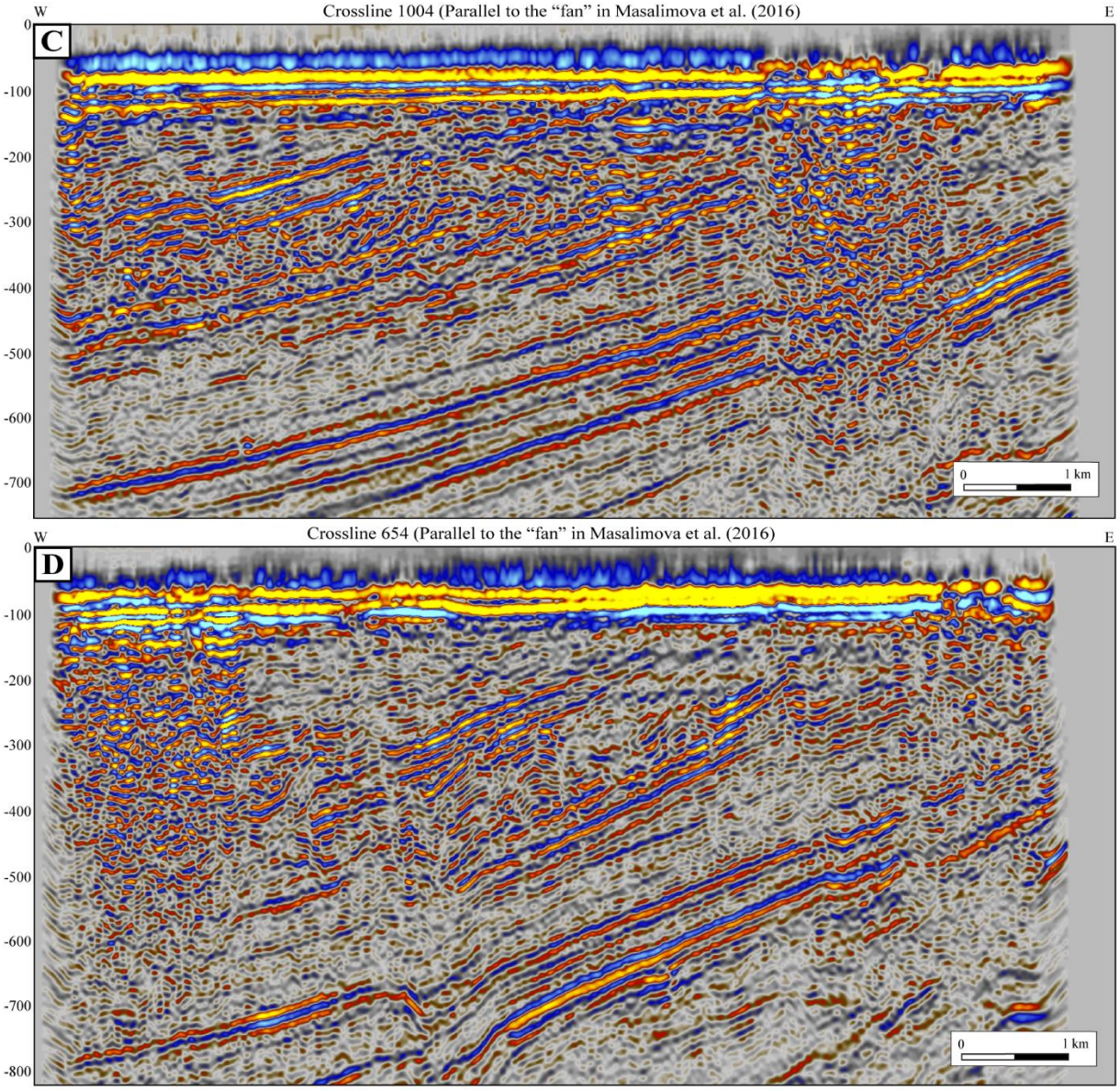

Figure x: Uninterpreted seismic sections related to Figure ix.

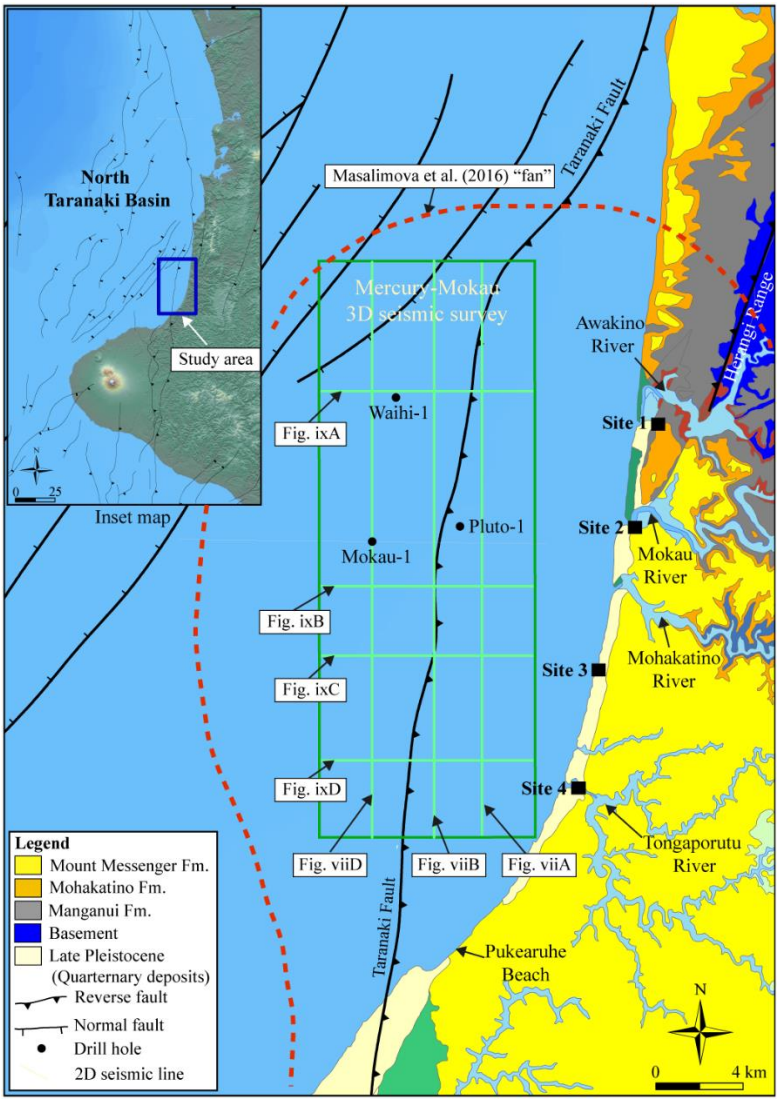

Figure xi: Location of seismic sections for Figures vii, viii, ix and x, shown in light green. The Mercury-Mokau 3D seismic survey shown if dark green box. The inferred "fan" in Masalimova et al. 2016 shown in dash red line.

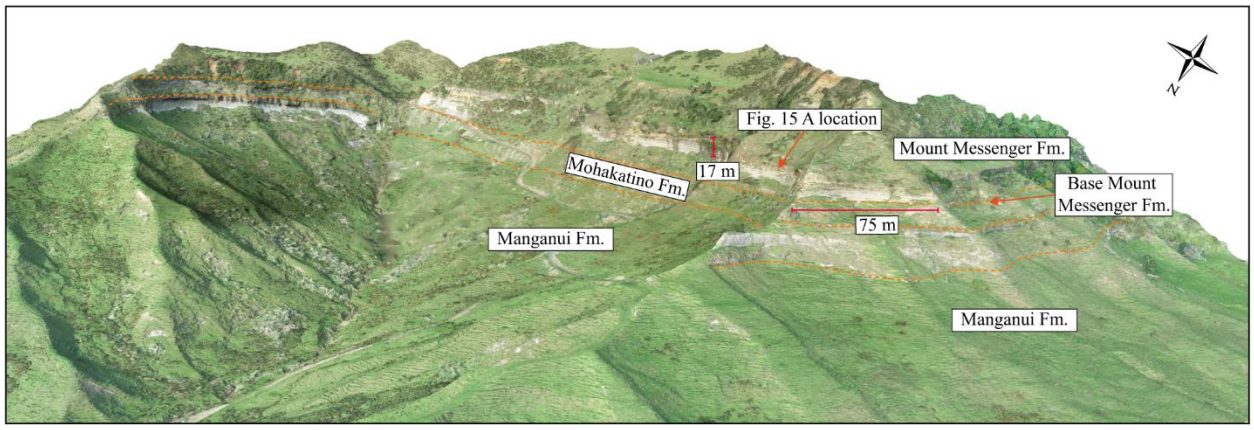

Figure xii: Overview of the lower Mount Messenger Formation outcrops at Site 1: Battleship Promontory. The lower Mount Messenger Formation outcrop overlies the Mohakatino Formation and Manganui Formation outcrops.

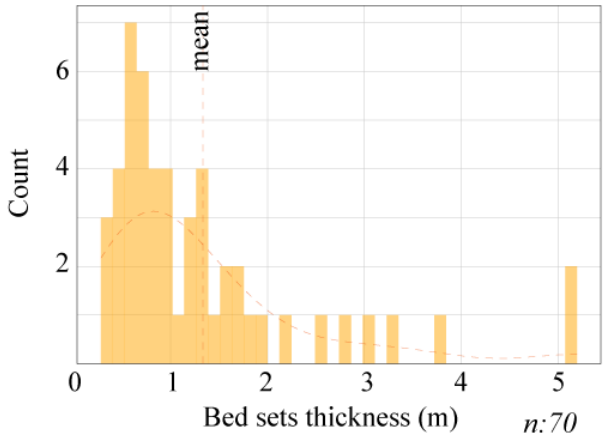

Figure xiii : Lower Mount Messenger Formation outcrop bedset thickness distribution at Site 1: Battleship Promontory.

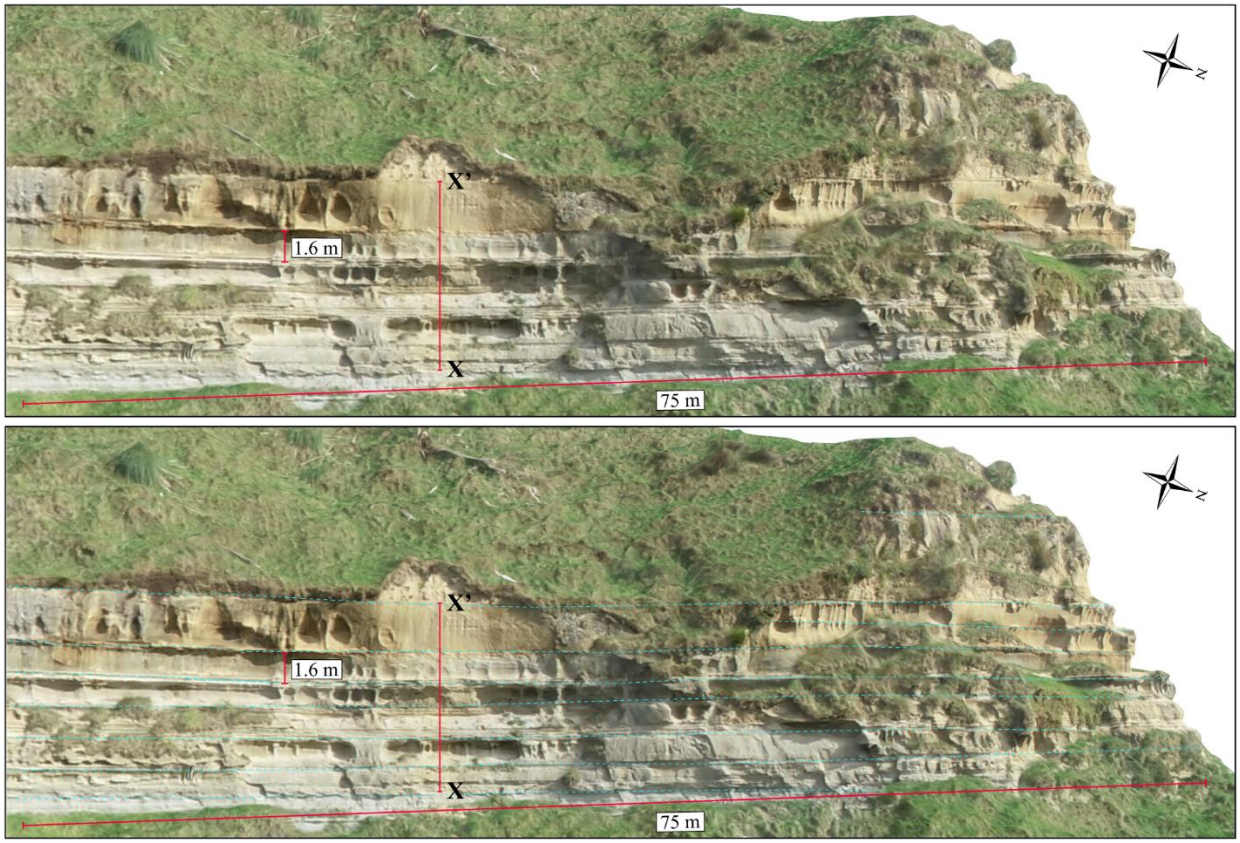

Figure xiv : Uninterpreted and interpreted lower Mount Messenger Formation outcrop at Site 1: Battleship Promontory.

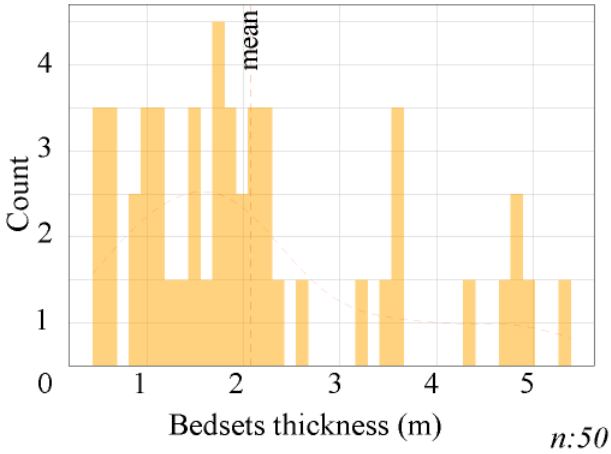

Figure xv : Lower Mount Messenger Formation outcrop bedset thickness distribution at Site 2: Ferry Sandstone.

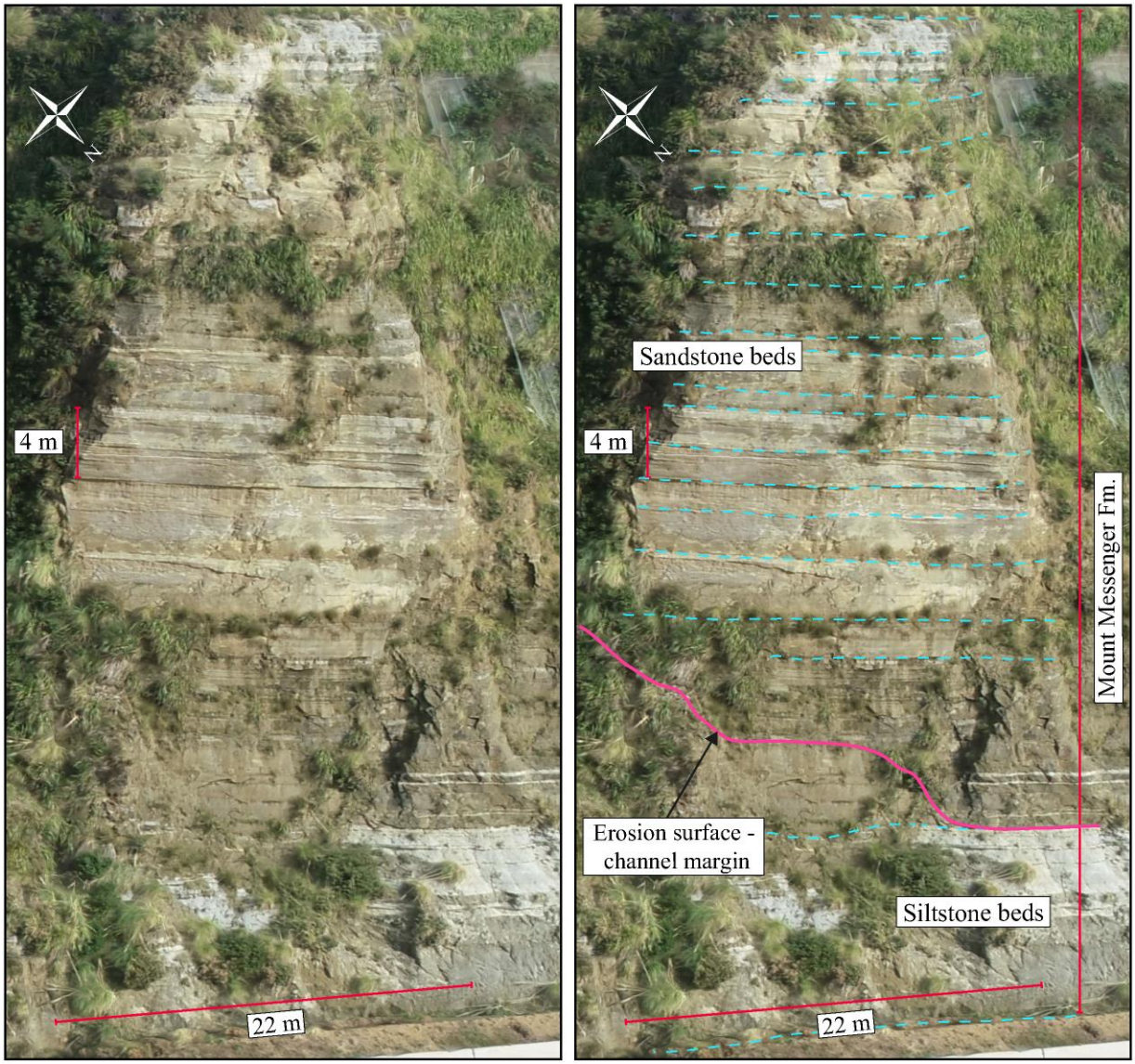

Figure xvi : Uninterpreted and interpreted lower Mount Messenger Formation outcrop at Site 2: Ferry Sandstone.

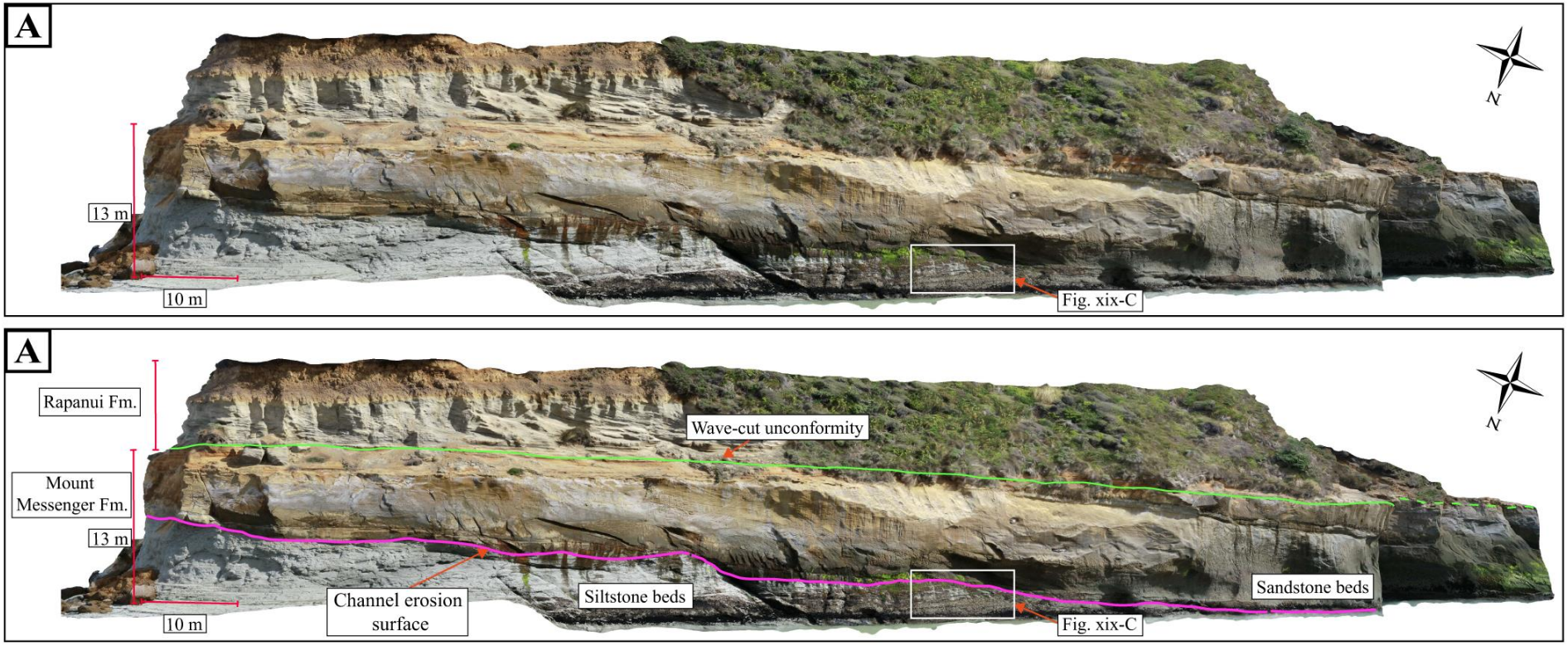

Figure xvii : (A) Uninterpreted and interpreted lower Mount Messenger Formation outcrop at the area near Kawau Pa; Site 3: Jam Roll.

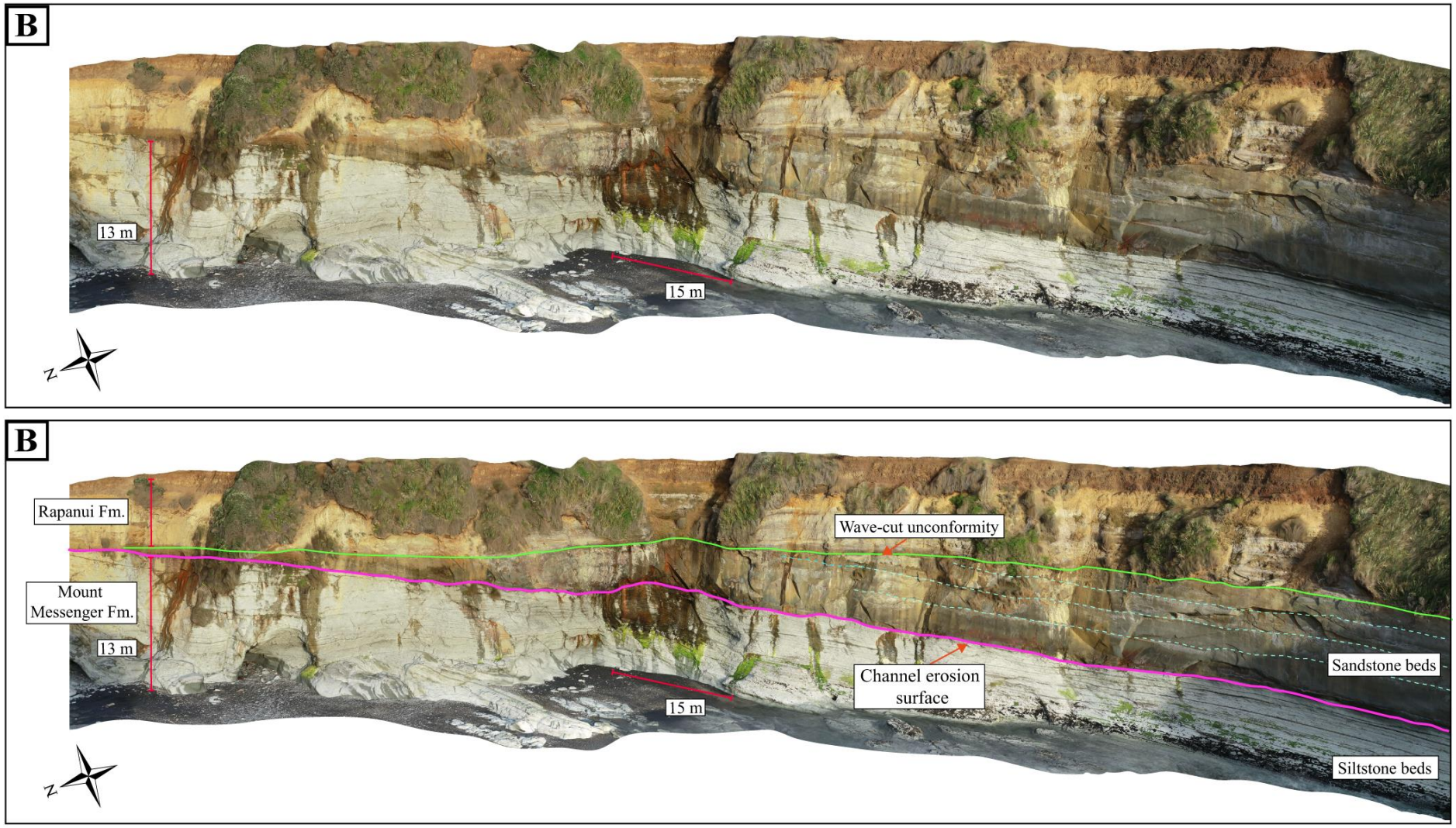

Figure xviii : (B) Uninterpreted and interpreted lower Mount Messenger Formation outcrop at southern part area; Site 3: Jam Roll.

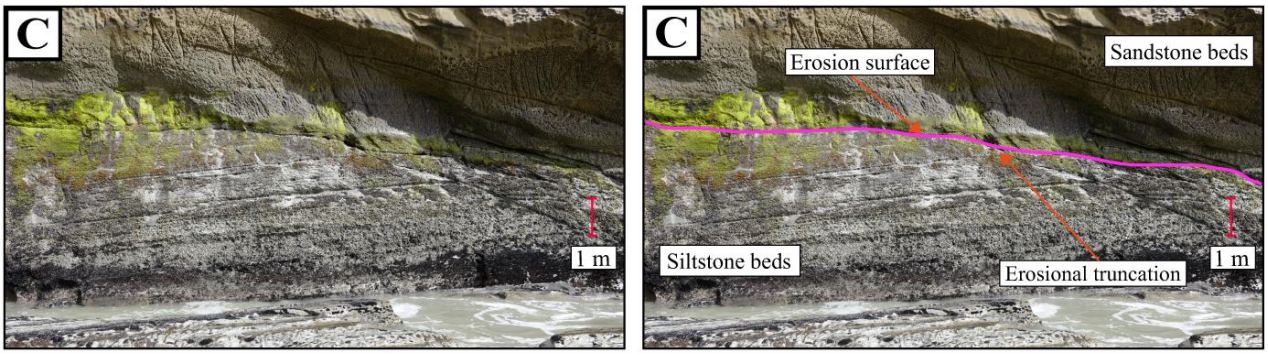

Figure xix : (C) Uninterpreted and interpreted close-up section shows sharp erosion surface.

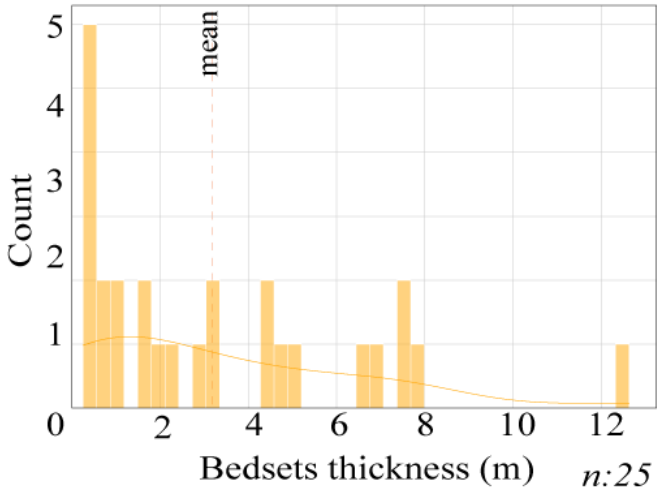

Figure xx : Lower Mount Messenger Formation outcrop bedsets thickness distribution at Site 3: Jam Roll.

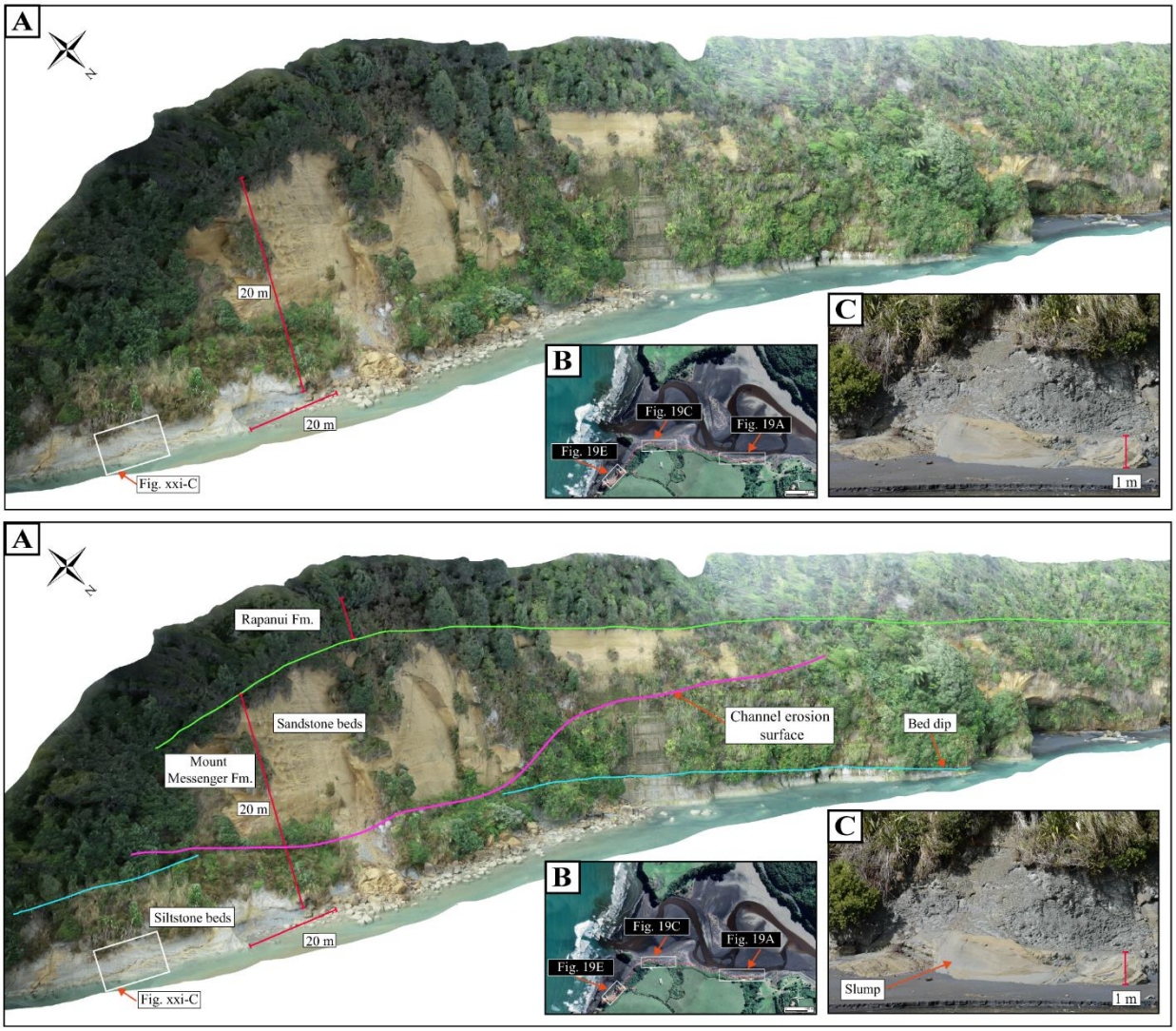

Figure xxi : (A) Uninterpreted and interpreted lower Mount Messenger Formation outcrop at the eastern end of the outcrop; Site 4: Tongaporutu River Mouth. (B) Overview of the outcrop section. (C) Close-up of the slump deposits.

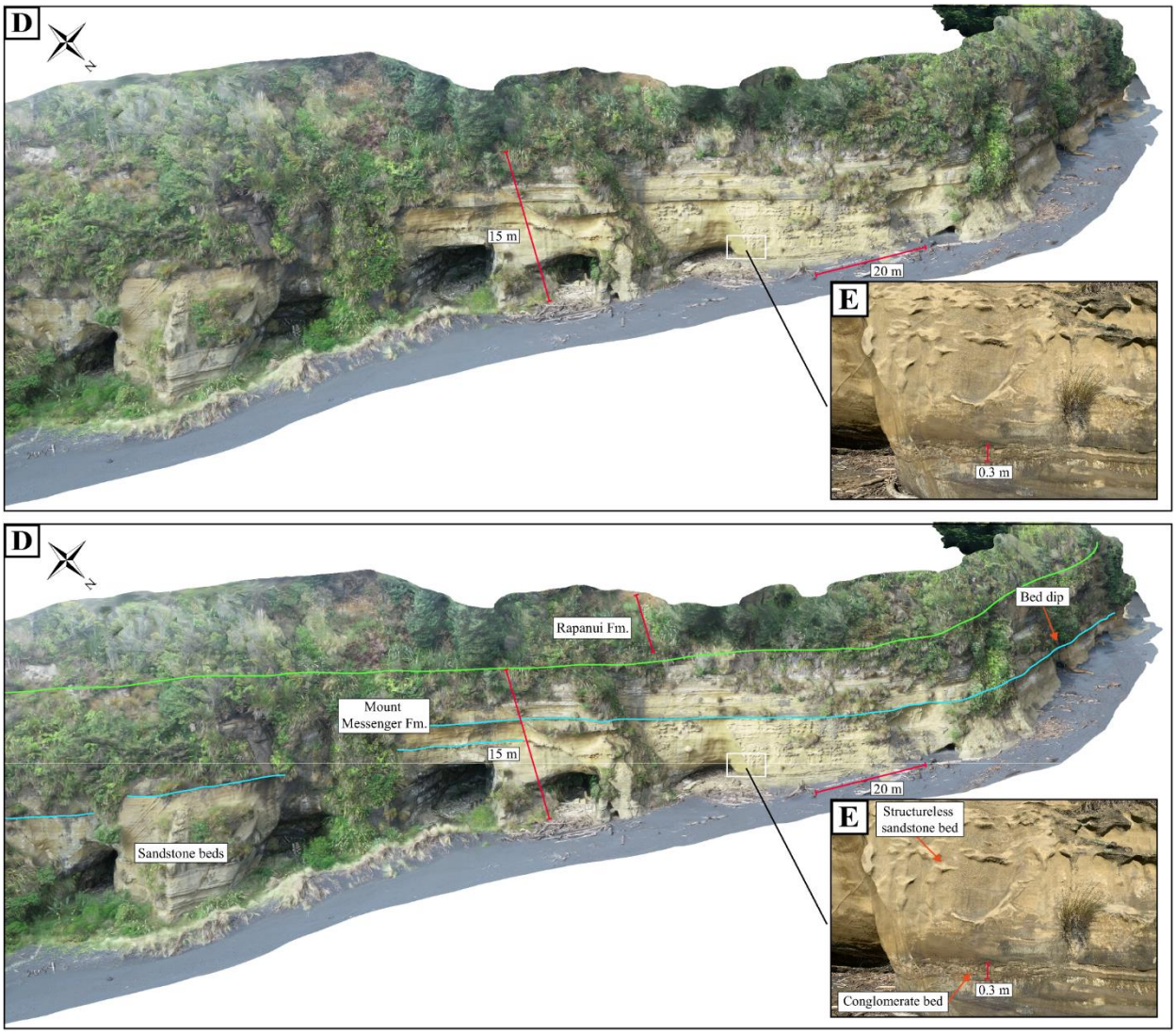

Figure xxii : (D) Uninterpreted and interpreted lower Mount Messenger Formation outcrop at the middle part of the outcrop; Site 4: Tongaporutu River Mouth. (E) Close-up of the sandstone deposits.

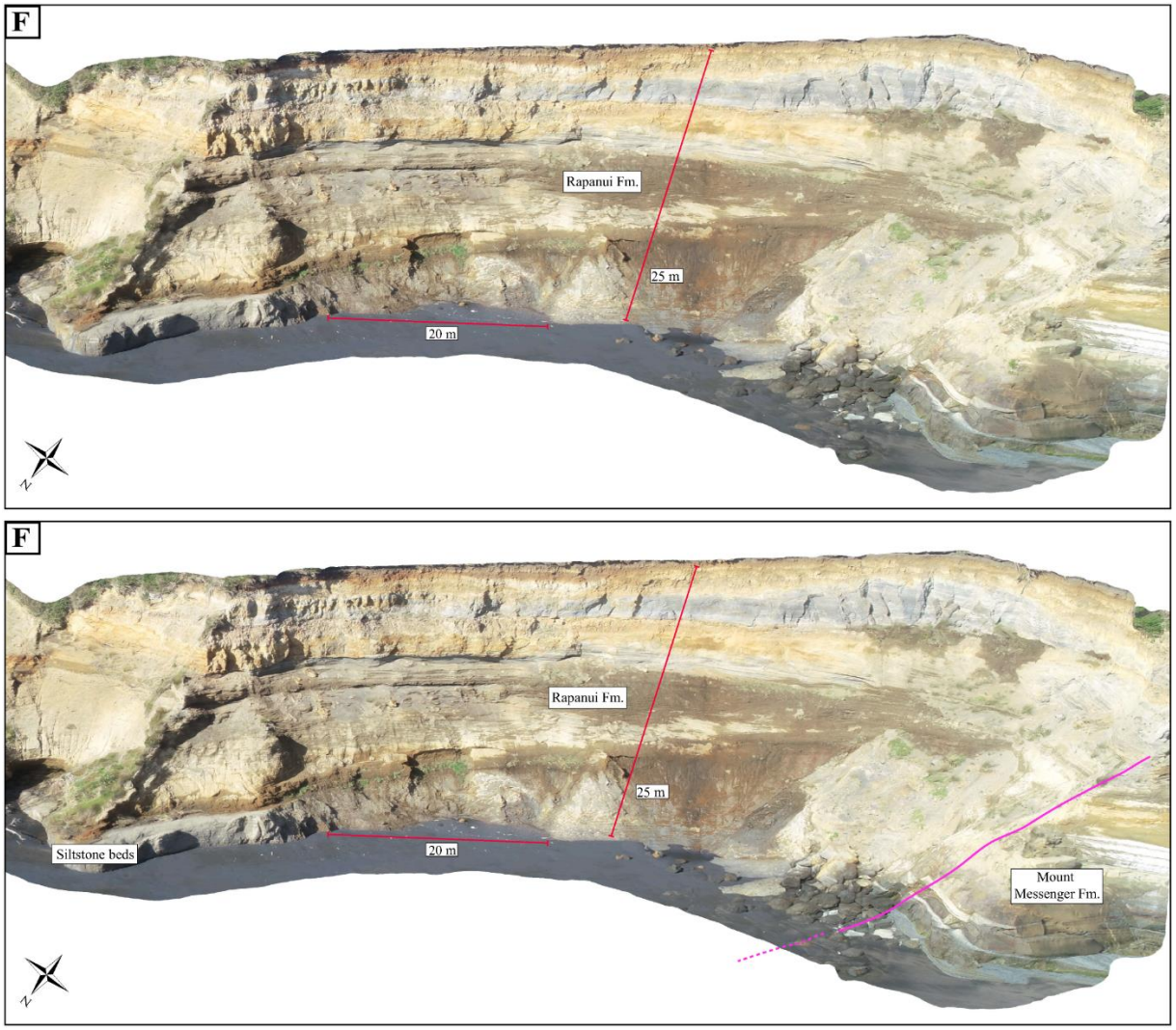

Figure xxiii : (F) Uninterpreted and interpreted lower Mount Messenger Formation outcrop at the western end of the outcrop; Site 4: Tongaporutu River Mouth.

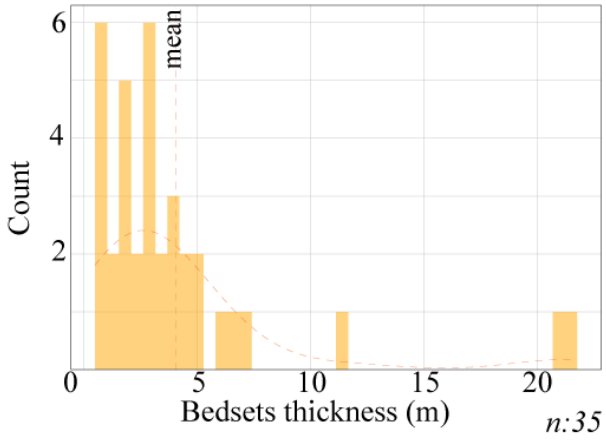

Figure xiv – Appendix C: Lower Mount Messenger Formation outcrop bedset thickness distribution at Site 4: Tongaporutu River Mouth.

Appendix D

Appendix D consists of the signed co-authorship forms for the three published and one unpublished chapter from the thesis:

i. Chapter 2: Quantitative seismic geomorphology of sediment conduits on an evolving Miocene slope in Taranaki Basin (New Zealand): The influence of increasing slope gradient through time.
   Published in Marine and Petroleum Geology Journal, March 2023

ii. Chapter 3: Critical re-assessment of Middle and Late Miocene submarine fans in offshore southern and western Taranaki Basin, New Zealand, to update the paleogeography.
   Published in Marine and Petroleum Geology Journal, Jan 2004

iii. Chapter 4: Interpreting Environments of Deposition from Facies Analysis of Outcrop Versus Seismic Reflection Data: A Cautionary Tale from the Mount Messenger Formation, Taranaki Basin (New Zealand).
   Unpublished: The paper has been peer-reviewed by the Marine and Petroleum Geology Journal, and corrections have been made accordingly. The paper has been resubmitted to the journal in May 2024.

iv. Chapter 5: Dataset of 3D computer models of Late Miocene Mount Messenger Formation outcrops in New Zealand, built with UAV drones
   Published in Data In Brief Journal, Jan 2024

THE UNIVERSITY OF WAIKATO
Te Whare Wānanga o Waikato

Postgraduate Studies Office
Student and Academic Services Division
Wahanga Ratonga Matauranga Akonga
The University of Waikato
Private Bag 3105
Hamilton 3240, New Zealand
Phone +64 7 838 4439
Website: http://www.waikato.ac.nz/sasd/postgraduate/

Co-Authorship Form

This form is to accompany the submission of any PhD that contains research reported in published or unpublished co-authored work. **Please include one copy of this form for each co-authored work**. Completed forms should be included in your appendices for all the copies of your thesis submitted for examination and library deposit (including digital deposit).

Please indicate the chapter/section/pages of this thesis that are extracted from a co-authored work and give the title and publication details or details of submission of the co-authored work.

Chapter 2: Quantitative seismic geomorphology of sediment conduits on an evolving Miocene slope in Taranaki Basin (New Zealand): The influence of increasing slope gradient through time
Published in Marine and Petroleum Geology Journal, March 2023

Nature of contribution by PhD candidate	Conceptualization, Investigation, Methodology, Software, Validation, Visualization, Writing - original draft.
Extent of contribution by PhD candidate (%)	90

CO-AUTHORS

Name	Nature of Contribution
Andrew La Croix	Conceptualization, Methodology, Supervision, Writing - review & editing.
Peter Kamp	Conceptualization, Methodology, Supervision, Writing - review & editing.

Certification by Co-Authors

The undersigned hereby certify that:

- the above statement correctly reflects the nature and extent of the PhD candidate's contribution to this work, and the nature of the contribution of each of the co-authors; and

Name	Signature	Date
Andrew La Croix		January 31, 2024
Peter Kamp	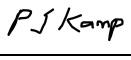	February 2, 2024

THE UNIVERSITY OF WAIKATO
Te Whare Wānanga o Waikato

Postgraduate Studies Office
Student and Academic Services Division
Wahanga Ratonga Matauranga Akonga
The University of Waikato
Private Bag 3105
Hamilton 3240, New Zealand
Phone +64 7 838 4439
Website: http://www.waikato.ac.nz/sasd/postgraduate/

Co-Authorship Form

This form is to accompany the submission of any PhD that contains research reported in published or unpublished co-authored work. **Please include one copy of this form for each co-authored work**. Completed forms should be included in your appendices for all the copies of your thesis submitted for examination and library deposit (including digital deposit).

Please indicate the chapter/section/pages of this thesis that are extracted from a co-authored work and give the title and publication details or details of submission of the co-authored work.

Chapter 3: Critical re-assessment of Middle and Late Miocene submarine fans in offshore southern and western Taranaki Basin, New Zealand, to update the paleogeography.
Published in Marine and Petroleum Geology Journal, Jan 2004

Nature of contribution by PhD candidate	Conceptualization, Investigation, Methodology, Software, Validation, Visualization, Writing - original draft.
Extent of contribution by PhD candidate (%)	90

CO-AUTHORS

Name	Nature of Contribution
Andrew La Croix	Conceptualization, Methodology, Supervision, Writing - review & editing.
Peter Kamp	Conceptualization, Methodology, Supervision, Writing - review & editing.

Certification by Co-Authors

The undersigned hereby certify that:

- the above statement correctly reflects the nature and extent of the PhD candidate's contribution to this work, and the nature of the contribution of each of the co-authors; and

Name	Signature	Date
Andrew La Croix		January 31, 2024
Peter Kamp		February 2, 2024

Co-Authorship Form

School of Graduate Research
The University of Waikato
Private Bag 3105
Hamilton 3240, New Zealand
Phone +64 7 838 5096
Email: SGR@waikato.ac.nz
Website: http://www.waikato.ac.nz/students/research-degree

This form is to accompany the submission of any PhD that contains research reported in published or unpublished co-authored work. **Please include one copy of this form for each co-authored work**. Completed forms should be included in your appendices for all the copies of your thesis submitted for examination and library deposit (including digital deposit).

Please indicate the chapter/section/pages of this thesis that are extracted from a co-authored work and give the title and publication details or details of submission of the co-authored work.

Chapter 4: Interpreting Environments of Deposition from Facies Analysis of Outcrop Versus Seismic Reflection Data: A Cautionary Tale from the Mount Messenger Formation, Taranaki Basin (New Zealand).
The paper has been peer-reviewed, revised, and submitted to the Marine and Petroleum Geology Journal in May 2024

Nature of contribution by PhD candidate	Conceptualization, Investigation, Methodology, Software, Validation, Visualization, Writing - original draft.
Extent of contribution by PhD candidate (%)	90

CO-AUTHORS

Name	Nature of Contribution
Andrew La Croix	Conceptualization, Methodology, Supervision, Writing - review & editing.
Peter Kamp	Conceptualization, Methodology, Supervision, Writing - review & editing.

Certification by Co-Authors

The undersigned hereby certify that:

- the above statement correctly reflects the nature and extent of the PhD candidate's contribution to this work, and the nature of the contribution of each of the co-authors; and
- that the candidate wrote all or the majority of the text.

Name	Signature	Date
Andrew La Croix	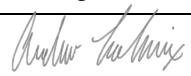	May 31, 2024
Peter Kamp	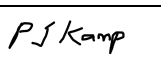	May 31, 2024

THE UNIVERSITY OF WAIKATO
Te Whare Wānanga o Waikato

Postgraduate Studies Office
Student and Academic Services Division
Wahanga Ratonga Matauranga Akonga
The University of Waikato
Private Bag 3105
Hamilton 3240, New Zealand
Phone +64 7 838 4439
Website: http://www.waikato.ac.nz/sasd/postgraduate/

Co-Authorship Form

This form is to accompany the submission of any PhD that contains research reported in published or unpublished co-authored work. **Please include one copy of this form for each co-authored work**. Completed forms should be included in your appendices for all the copies of your thesis submitted for examination and library deposit (including digital deposit).

Please indicate the chapter/section/pages of this thesis that are extracted from a co-authored work and give the title and publication details or details of submission of the co-authored work.

Chapter 5: Dataset of 3D computer models of Late Miocene Mount Messenger Formation outcrops in New Zealand, built with UAV drones
Published in Data In Brief Journal, Jan 2024

Nature of contribution by PhD candidate	Conceptualization, Investigation, Methodology, Software, Validation, Visualization, Writing - original draft.
Extent of contribution by PhD candidate (%)	90

CO-AUTHORS

Name	Nature of Contribution
Andrew La Croix	Conceptualization, Methodology, Supervision, Writing - review & editing.
Peter Kamp	Conceptualization, Methodology, Supervision, Writing - review & editing.

Certification by Co-Authors

The undersigned hereby certify that:

- the above statement correctly reflects the nature and extent of the PhD candidate's contribution to this work, and the nature of the contribution of each of the co-authors; and

Name	Signature	Date
Andrew La Croix		January 31, 2024
Peter Kamp		February 2, 2024